

**EVALUATION OF COMPUTATIONAL METHODS OF
PALEOSTRESS ANALYSIS USING FAULT-STRIATION DATA**

Abstract of
a thesis presented to the Faculty
of the State University of New York
at Albany
in partial fulfillment of the requirements
for the degree of
Master of Science

College of Science and Mathematics
Department of Geological Sciences

Steven Henry Schimmrich

1991

ABSTRACT

Over the past 12 years, many different computational methods or variations of existing methods have been proposed for determining paleostress tensors from fault populations and their slip directions. These methods are all based upon well-known relationships between stress and shear and use iterative, non-linear mathematical algorithms which seek to minimize the angles between the calculated maximum shear stress direction and the observed movement directions on each fault plane in a population. The solution returned is the best-fit paleostress tensor for the population.

By taking the Coulomb failure criterion into account, several paleostress analysis programs have been able to use linear, rather than non-linear, methods to solve for a paleostress tensor. The advantages of using linear equations is that they are less computationally-intensive and are far easier to solve.

A major problem with computational methods of paleostress analysis is that very little work has been done on evaluating their effectiveness and/or possible limitations. If the techniques return results consistent with other methods of estimating paleostress directions, or with various kinematic analysis methods, they are often used by geologists. If not, an attempt may be made to explain why, but geological explanations are usually sought rather than criticizing the paleostress analysis methods. This study is an attempt to formulate the problem and to begin systematically examining it.

For my thesis project, I obtained several working versions of paleostress analysis computer programs. After much work, I decided to test two of the methods -- those developed by Angelier and Reches. Artificial fault populations were created for these tests with a slip vector calculation program which I wrote specifically for that purpose. The artificial fault populations were created using exactly the same initial assumptions that the paleostress analysis programs used.

An artificial fault population is a set of fault orientations and their associated slip directions consistent with a predetermined stress field. For all of the fault populations created, the most compressive principal stress axis was vertical with a relative magnitude of +1.0 and the least compressive principal stress axis was oriented north-south with a relative magnitude of -1.0. Entering these populations into a paleostress analysis program should have, theoretically, returned the same orientations for the principal stress axes.

With this in mind, I chose to create several different types of artificial fault populations to test possible limitations in paleostress analysis. I used randomly-oriented fault populations, special-case fault populations, and fault populations which had data added or removed from them.

The results of these tests are that the two paleostress analysis programs I examined may work sufficiently well for certain types of well-constrained fault populations, but often give large errors when examining special types of fault sets such as conjugate faults, orthorhombic symmetry faults, and fault populations where all of the faults have very similar orientations. The paleostress analysis programs may also be sensitive to measurement errors and/or extraneous data depending upon several factors, including the orientations of the faults in question.

In conclusion, much more work is currently needed to further examine this topic and to begin to formulate general guidelines for applying paleostress analysis methods to fault populations gathered by geologists in the field.

**EVALUATION OF COMPUTATIONAL METHODS OF
PALEOSTRESS ANALYSIS USING FAULT-STRIATION DATA**

A thesis presented to the Faculty
of the State University of New York
at Albany
in partial fulfillment of the requirements
for the degree of
Master of Science

College of Science and Mathematics
Department of Geological Sciences

Steven Henry Schimmrich

1991

ACKNOWLEDGEMENTS

I owe my greatest debt to my thesis advisor, Dr. Winthrop D. Means of the State University of New York at Albany. Without his constant assistance, encouragement, and patience this project would not have been possible. I greatly benefited from my association with him.

I am also indebted to the following people for their assistance...

Jacque Angelier of the Tectonique Quantitative, Université Pierre et Marie Curie at Paris for allowing me to use his paleostress analysis programs and to Christopher Barton of Lamont-Doherty Geological Observatory for supplying me with copies of them.

Arnaud Etchecopar of the Laboratoire de Géologie Structurale, Université des Sciences et Techniques du Languedoc, Montpellier, France for allowing me to use his paleostress analysis programs and to Richard Plumb of Schlumberger Doll Research in Ridgefield, Connecticut for supplying me with copies of them.

Kenneth Hardcastle of the Department of Geology, University of Massachusetts at Amherst (now at Emery and Garrett Groundwater, Meredith, New Hampshire) for supplying me with copies of his paleostress analysis programs which utilize algorithms developed by Ze'ev Reches of the Department of Geology, Hebrew University, Jerusalem.

John Gephart of the Institute for the Study of Continents, Cornell University for supplying me with copies of his paleostress analysis program.

Richard Allmendinger of the Department of Geological Sciences, Cornell University for supplying me with paleostress analyses and field data he collected from the Chilean Andes.

Steven Wojtal of the Department of Geology, Oberlin College, Ohio for supplying me with English translations of several French paleostress papers.

William Kelly of the New York State Geological Survey in Albany for allowing me to take some time off to finish writing this thesis.

The numerous people, here at SUNY Albany and elsewhere, who graciously gave me preprints of their papers, explained their research to me, and took the time to make helpful suggestions and criticisms of my work.

Last, but certainly not least, I would like to thank Debra Lenard. Her constant encouragement (*i.e.* "Write your damn thesis already!") kept me going at times when I would rather have quit. She provided me with invaluable assistance by helping me translate paleostress program documentation from French into English, by being incredibly supportive, and by being one of the few people who actually listened to me when I talked about paleostress analysis.

Research leading to this thesis was partially supported by National Science Foundation Grant EAR-8606961 to Winthrop D. Means, a two-year teaching assistantship from the State University of New York at Albany, and by occasional loans of cash (which, unfortunately, have yet to be repaid) from both parents and grandparents.

I have yet to see any problem, however complicated, which, when looked at in the right way, did not become still more complicated.

Poul Anderson

(Thorpe, 1969)

TABLE OF CONTENTS

	Page
Abstract	ii
Acknowledgements	v
Table of Contents	vii
List of Figures	x
List of Tables	xxi
CHAPTER 1: INTRODUCTION	1
1.1 Purpose of this Study	1
1.2 Scope of this Study	3
1.3 Testing Procedures	4
1.4 Thesis Organization	6
CHAPTER 2: PALEOSTRESS ANALYSIS	7
2.1 Andersonian Fault Classification	8
2.2 Bott's Formula	13
2.3 Graphical Methods of Fault-Striation Paleostress Analysis	16
2.4 Right-Dihedra Methods of Fault-Striation Analysis	24
CHAPTER 3: COMPUTATIONAL PALEOSTRESS ANALYSIS OF FAULT POPULATIONS	39
3.1 Early Attempts at Computational Paleostress Analysis	39
3.2 Etchecopar's Method of Paleostress Analysis	40
3.3 Michael's Method of Paleostress Analysis	41
3.4 Gephart and Forsyth's Method of Paleostress Analysis	43
3.5 Recent Trends in Paleostress Analysis	44
CHAPTER 4: PROBLEMS IN PALEOSTRESS ANALYSIS	46
4.1 Measurement Errors	46

4.2	Determining Fault Slip	50
4.3	Fault Morphology	53
4.4	The Relationship of Shear Stress to Fault Slip Directions	55
4.5	Faulting Phase Differentiation	63
4.6	Determining a Paleostress Tensor	65
4.7	Discussion	66
CHAPTER 5:	GENERATING ARTIFICIAL FAULT POPULATIONS	69
5.1	Theory	69
5.2	Deriving Bott's Formula	72
5.3	Program Input	78
5.4	Program Procedures	79
5.5	Program Output	83
5.6	Creating Fault Populations	84
CHAPTER 6:	ANGELIER'S METHOD OF PALEOSTRESS ANALYSIS	90
6.1	Program Assumptions	90
6.2	Theory	91
6.3	Program Input	97
6.4	Program Procedures	99
6.5	Program Output	99
6.6	Discussion	101
CHAPTER 7:	RECHES' METHOD OF PALEOSTRESS ANALYSIS	102
7.1	Program Assumptions	102
7.2	Theory	103
7.3	Program Input	107
7.4	Program Procedures	109
7.5	Program Output	110

7.6	Discussion	112
CHAPTER 8:	PALEOSTRESS ANALYSIS TEST DATA	114
8.1	Creating the Artificial Fault Populations	114
8.2	Random Fault-Slip Populations	115
8.3	Creating Special-Case Fault Populations	133
8.4	Andersonian Conjugate Fault Populations	133
8.5	Orthorhombic Fault Populations	140
8.6	Radial Symmetry Fault Populations	151
8.7	Fault Populations of a Similar Orientation	151
8.8	Final Fault Population Tests	173
CHAPTER 9:	TESTING PROCEDURES AND RESULTS	176
9.1	Testing Procedures	176
9.2	Random-Pole Fault Population Results	176
9.3	Special-Case Fault Population Results	213
9.4	Other Test Results	297
CHAPTER 10:	CONCLUSIONS	300
10.1	What do the Results Mean?	300
10.2	Practical Problems in Evaluating Paleostress Analysis Programs ...	301
10.3	Suggestions for Future Work	306
APPENDIX A:	GLOSSARY OF SYMBOLS	308
APPENDIX B:	ARTIFICIAL FAULT POPULATION DATA	311
APPENDIX C:	SLIP VECTOR CALCULATION PROGRAM	322
APPENDIX D:	FAULT PLANE PLOTTING PROGRAM	374
APPENDIX E:	VECTOR ANGLE CALCULATION PROGRAM	384
References	388

LIST OF FIGURES

		Page
2-1	An infinitesimal prism <opqrst> situated within a right-handed XYZ coordinate system	9
2-2	The three Andersonian classes of conjugate fault sets	14
2-3	A plot of the shear stresses and normal stresses acting upon a plane	18
2-4	Stereographic projection showing 24 conjugate normal faults and their associated slip vectors	19
2-5	Stereographic projection showing the relationship between a fault plane, the normal and slip vectors, and the m-plane	20
2-6	Stereographic projection showing the m-plane method of locating a principal strain axis	22
2-7	Analyzing a common intersection point (CIP) of m-planes	23
2-8	Schematic diagram and stereographic projection illustrating the relationship between a normal fault plane, its associated auxiliary plane, the zones of compression and dilation, and the axes of compression and tension	25
2-9	Stereographic projections showing the relationship between a fault plane, its auxiliary plane, and its movement plane	27
2-10	Stereographic projections showing how the region containing σ_1 is constrained by normal fault populations	28
2-11	Stereographic projection showing 20 slip vectors representing Φ values ranging from 0.0 to 1.0 on a fault plane with a normal vector oriented at 70/030 degrees	30
2-12	Stereographic projection showing the right dihedral defined by Lisle (1987) as A and B	31

2-13	Stereographic projection of three faults with slip vectors S and fault normals N	32
2-14	Stereographic projection showing the σ_1 and σ_3 fields constructed by superimposing the fault data from figure 2-13	33
2-15	Stereographic projection showing the regions constructed by superimposing the A and B dihedral from the fault data in figure 2-13	34
2-16	Stereographic projection showing the σ_1 and σ_3 fields constructed by utilizing Lisle's (1987) constraint on the fault data from figure 2-13	36
2-17	Stereographic projection showing the σ_1 and σ_3 regions derived using Lisle's (1987) method on four thrust faults	37
2-18	Stereographic projection showing the σ_1 and σ_3 regions derived using Lisle's (1987) method on a conjugate set of four normal faults and an orthorhombic set of four normal faults	38
3-1	Northeast quadrant of a stereographic projection showing the relative magnitudes of shear stresses on fault planes represented by their poles	42
4-1	Graph of the maximum strike error of a fault plane as a function of the dip angle	48
4-2	Graph of the maximum trend error of a slickenline on a fault plane as a function of the pitch of the slickenline and the dip angle of the fault	49
4-3	Diagram demonstrating how the net slip vector on a fault plane may be the result of several distinct slip events with differing slip directions	51
4-4	Cross-sectional view of a fault plane showing how steps may be used as sense-of-slip indicators on fault surfaces	52
4-5	Diagram demonstrating the difference between a fault's slip plane and the actual fault surface which may not be planar	56

4-6	Two fault types with a rotational component of slip	58
4-7	Cross-sectional view of a fault surface parallel to shearing with an asperity A creating an angle ϕ with the fault	59
4-8	An undulating fault plane with the maximum shear stress direction making an angle α with the long axis of the undulations	61
4-9	Graph of the change in phi (Φ) as alpha (α) varies from 0° to 90°	64
4-10	Mohr circles demonstrating how two faults of slightly different orientations will slip at different times as σ_1 increases	67
5-1	Relationship between a plane XYZ situated within a geographic coordinate system and the principal stress axes σ_1 , σ_2 , and σ_3	70
5-2	Determining the shear stress and normal stress magnitudes acting upon a fault plane	73
5-3	Relationship between a plane XYZ situated in a geographic coordinate system, the principal stress axes σ_1 , σ_2 , and σ_3 , and the direction cosines l_1 , l_2 , and l_3	74
5-4	Stereographic projection showing three arbitrarily oriented principal stresses in relation to an arbitrarily oriented fault plane	80
5-5	Interactive screen displayed by the slip vector calculation program as the user enters the initial data	81
5-6	Simplified flow chart demonstrating the mathematical algorithm used by the slip vector calculation program	85
5-7	Graph of 21 Φ values for each slip vector as they range from 0.0 to 1.0 versus the pitch of the slip vectors	87
5-8	Stereographic projection of 21 slip vectors representing values ranging from 0.0 to 1.0 on a fault plane	88

6-1	Geometry of the stresses on a striated fault plane	92
6-2	Diagram of a fault plane looking down the plunge of the normal vector at the footwall block	94
6-3	Stereographic projection showing a conjugate set of two normal faults	100
7-1	Stereographic projection showing a conjugate set of two normal faults	108
7-2	Figure showing the graphical output from Reches' method of paleostress analysis	111
8-1	Stereographic projection of fault population RP-01 where $\Phi = 0.00$	118
8-2	Stereographic projection of fault population RP-01 where $\Phi = 0.25$	119
8-3	Stereographic projection of fault population RP-01 where $\Phi = 0.50$	120
8-4	Stereographic projection of fault population RP-01 where $\Phi = 0.75$	121
8-5	Stereographic projection of fault population RP-01 where $\Phi = 1.00$	122
8-6	Stereographic projection of fault population RP-02 where $\Phi = 0.00$	123
8-7	Stereographic projection of fault population RP-02 where $\Phi = 0.25$	124
8-8	Stereographic projection of fault population RP-02 where $\Phi = 0.50$	125
8-9	Stereographic projection of fault population RP-02 where $\Phi = 0.75$	126
8-10	Stereographic projection of fault population RP-02 where $\Phi = 1.00$	127
8-11	Stereographic projection of fault population RP-03 where $\Phi = 0.00$	128
8-12	Stereographic projection of fault population RP-03 where $\Phi = 0.25$	129
8-13	Stereographic projection of fault population RP-03 where $\Phi = 0.50$	130
8-14	Stereographic projection of fault population RP-03 where $\Phi = 0.75$	131
8-15	Stereographic projection of fault population RP-03 where $\Phi = 1.00$	132
8-16	Stereographic projection of fault population AC-01 where $\Phi = 0.00$	135

8-17	Stereographic projection of fault population AC-01 where $\Phi = 0.25$	136
8-18	Stereographic projection of fault population AC-01 where $\Phi = 0.50$	137
8-19	Stereographic projection of fault population AC-01 where $\Phi = 0.75$	138
8-20	Stereographic projection of fault population AC-01 where $\Phi = 1.00$	139
8-21	Stereographic projection of fault population AC-02 where $\Phi = 0.00$	141
8-22	Stereographic projection of fault population AC-02 where $\Phi = 0.25$	142
8-23	Stereographic projection of fault population AC-02 where $\Phi = 0.50$	143
8-24	Stereographic projection of fault population AC-02 where $\Phi = 0.75$	144
8-25	Stereographic projection of fault population AC-02 where $\Phi = 1.00$	145
8-26	Stereographic projection of fault population OS-01 where $\Phi = 0.00$	146
8-27	Stereographic projection of fault population OS-01 where $\Phi = 0.25$	147
8-28	Stereographic projection of fault population OS-01 where $\Phi = 0.50$	148
8-29	Stereographic projection of fault population OS-01 where $\Phi = 0.75$	149
8-30	Stereographic projection of fault population OS-01 where $\Phi = 1.00$	150
8-31	Stereographic projection of fault population RS-01 where $\Phi = 0.00$	153
8-32	Stereographic projection of fault population RS-01 where $\Phi = 0.25$	154
8-33	Stereographic projection of fault population RS-01 where $\Phi = 0.50$	155
8-34	Stereographic projection of fault population RS-01 where $\Phi = 0.75$	156
8-35	Stereographic projection of fault population RS-01 where $\Phi = 1.00$	157
8-36	Stereographic projection of fault population SO-01 where $\Phi = 0.00$	158
8-37	Stereographic projection of fault population SO-01 where $\Phi = 0.25$	159
8-38	Stereographic projection of fault population SO-01 where $\Phi = 0.50$	160

8-39	Stereographic projection of fault population SO-01 where $\Phi = 0.75$	161
8-40	Stereographic projection of fault population SO-01 where $\Phi = 1.00$	162
8-41	Stereographic projection of fault population SO-02 where $\Phi = 0.00$	163
8-42	Stereographic projection of fault population SO-02 where $\Phi = 0.25$	164
8-43	Stereographic projection of fault population SO-02 where $\Phi = 0.50$	165
8-44	Stereographic projection of fault population SO-02 where $\Phi = 0.75$	166
8-45	Stereographic projection of fault population SO-02 where $\Phi = 1.00$	167
8-46	Stereographic projection of fault population SO-03 where $\Phi = 0.00$	168
8-47	Stereographic projection of fault population SO-03 where $\Phi = 0.25$	169
8-48	Stereographic projection of fault population SO-03 where $\Phi = 0.50$	170
8-49	Stereographic projection of fault population SO-03 where $\Phi = 0.75$	171
8-50	Stereographic projection of fault population SO-03 where $\Phi = 1.00$	172
8-51	Stereographic projection of Angelier's (1979) fault population FD-01	174
9-1	Reches' method results for fault population RP-01 at $\Phi = 0.00$	177
9-2	Reches' method results for fault population RP-01 at $\Phi = 0.25$	178
9-3	Reches' method results for fault population RP-01 at $\Phi = 0.50$	179
9-4	Reches' method results for fault population RP-01 at $\Phi = 0.75$	180
9-5	Reches' method results for fault population RP-01 at $\Phi = 1.00$	181
9-6	Reches' method results for fault population RP-02 at $\Phi = 0.00$	182
9-7	Reches' method results for fault population RP-02 at $\Phi = 0.25$	183
9-8	Reches' method results for fault population RP-02 at $\Phi = 0.50$	184
9-9	Reches' method results for fault population RP-02 at $\Phi = 0.75$	185

9-10	Reches' method results for fault population RP-02 at $\Phi = 1.00$	186
9-11	Reches' method results for fault population RP-03 at $\Phi = 0.00$	187
9-12	Reches' method results for fault population RP-03 at $\Phi = 0.25$	188
9-13	Reches' method results for fault population RP-03 at $\Phi = 0.50$	189
9-14	Reches' method results for fault population RP-03 at $\Phi = 0.75$	190
9-15	Reches' method results for fault population RP-03 at $\Phi = 1.00$	191
9-16	Angelier's method results for fault population RP-01 at $\Phi = 0.00$	192
9-17	Angelier's method results for fault population RP-01 at $\Phi = 0.25$	193
9-18	Angelier's method results for fault population RP-01 at $\Phi = 0.50$	194
9-19	Angelier's method results for fault population RP-01 at $\Phi = 0.75$	195
9-20	Angelier's method results for fault population RP-01 at $\Phi = 1.00$	196
9-21	Angelier's method results for fault population RP-02 at $\Phi = 0.00$	197
9-22	Angelier's method results for fault population RP-02 at $\Phi = 0.25$	198
9-23	Angelier's method results for fault population RP-02 at $\Phi = 0.50$	199
9-24	Angelier's method results for fault population RP-02 at $\Phi = 0.75$	200
9-25	Angelier's method results for fault population RP-02 at $\Phi = 1.00$	201
9-26	Angelier's method results for fault population RP-03 at $\Phi = 0.00$	202
9-27	Angelier's method results for fault population RP-03 at $\Phi = 0.25$	203
9-28	Angelier's method results for fault population RP-03 at $\Phi = 0.50$	204
9-29	Angelier's method results for fault population RP-03 at $\Phi = 0.75$	205
9-30	Angelier's method results for fault population RP-03 at $\Phi = 1.00$	206
9-31	Reches' method results for fault population AC-01 at $\Phi = 0.00$	215

9-32	Reches' method results for fault population AC-01 at $\Phi = 0.25$	216
9-33	Reches' method results for fault population AC-01 at $\Phi = 0.50$	217
9-34	Reches' method results for fault population AC-01 at $\Phi = 0.75$	218
9-35	Reches' method results for fault population AC-01 at $\Phi = 1.00$	219
9-36	Angelier's method results for fault population AC-01 at $\Phi = 0.00$	220
9-37	Angelier's method results for fault population AC-01 at $\Phi = 0.25$	221
9-38	Angelier's method results for fault population AC-01 at $\Phi = 0.50$	222
9-39	Angelier's method results for fault population AC-01 at $\Phi = 0.75$	223
9-40	Angelier's method results for fault population AC-01 at $\Phi = 1.00$	224
9-41	Reches' method results for fault population AC-02 at $\Phi = 0.00$	225
9-42	Reches' method results for fault population AC-02 at $\Phi = 0.25$	226
9-43	Reches' method results for fault population AC-02 at $\Phi = 0.50$	227
9-44	Reches' method results for fault population AC-02 at $\Phi = 0.75$	228
9-45	Reches' method results for fault population AC-02 at $\Phi = 1.00$	229
9-46	Angelier's method results for fault population AC-02 at $\Phi = 0.00$	230
9-47	Angelier's method results for fault population AC-02 at $\Phi = 0.25$	231
9-48	Angelier's method results for fault population AC-02 at $\Phi = 0.50$	232
9-49	Angelier's method results for fault population AC-02 at $\Phi = 0.75$	233
9-50	Angelier's method results for fault population AC-02 at $\Phi = 1.00$	234
9-51	Reches' method results for fault population OS-01 at $\Phi = 0.00$	238
9-52	Reches' method results for fault population OS-01 at $\Phi = 0.25$	239
9-53	Reches' method results for fault population OS-01 at $\Phi = 0.50$	240

9-54	Reches' method results for fault population OS-01 at $\Phi = 0.75$	241
9-55	Reches' method results for fault population OS-01 at $\Phi = 1.00$	242
9-56	Angelier's method results for fault population OS-01 at $\Phi = 0.00$	243
9-57	Angelier's method results for fault population OS-01 at $\Phi = 0.25$	244
9-58	Angelier's method results for fault population OS-01 at $\Phi = 0.50$	245
9-59	Angelier's method results for fault population OS-01 at $\Phi = 0.75$	246
9-60	Angelier's method results for fault population OS-01 at $\Phi = 1.00$	247
9-61	Reches' method results for fault population RS-01 at $\Phi = 0.00$	251
9-62	Reches' method results for fault population RS-01 at $\Phi = 0.25$	252
9-63	Reches' method results for fault population RS-01 at $\Phi = 0.50$	253
9-64	Reches' method results for fault population RS-01 at $\Phi = 0.75$	254
9-65	Reches' method results for fault population RS-01 at $\Phi = 1.00$	255
9-66	Angelier's method results for fault population RS-01 at $\Phi = 0.00$	256
9-67	Angelier's method results for fault population RS-01 at $\Phi = 0.25$	257
9-68	Angelier's method results for fault population RS-01 at $\Phi = 0.50$	258
9-69	Angelier's method results for fault population RS-01 at $\Phi = 0.75$	259
9-70	Angelier's method results for fault population RS-01 at $\Phi = 1.00$	260
9-71	Reches' method results for fault population SO-01 at $\Phi = 0.00$	263
9-72	Reches' method results for fault population SO-01 at $\Phi = 0.25$	264
9-73	Reches' method results for fault population SO-01 at $\Phi = 0.50$	265
9-74	Reches' method results for fault population SO-01 at $\Phi = 0.75$	266
9-75	Reches' method results for fault population SO-01 at $\Phi = 1.00$	267

9-76	Angelier's method results for fault population SO-01 at $\Phi = 0.00$	268
9-77	Angelier's method results for fault population SO-01 at $\Phi = 0.25$	269
9-78	Angelier's method results for fault population SO-01 at $\Phi = 0.50$	270
9-79	Angelier's method results for fault population SO-01 at $\Phi = 0.75$	271
9-80	Angelier's method results for fault population SO-01 at $\Phi = 1.00$	272
9-81	Reches' method results for fault population SO-02 at $\Phi = 0.00$	275
9-82	Reches' method results for fault population SO-02 at $\Phi = 0.25$	276
9-83	Reches' method results for fault population SO-02 at $\Phi = 0.50$	277
9-84	Reches' method results for fault population SO-02 at $\Phi = 0.75$	278
9-85	Reches' method results for fault population SO-02 at $\Phi = 1.00$	279
9-86	Angelier's method results for fault population SO-02 at $\Phi = 0.00$	280
9-87	Angelier's method results for fault population SO-02 at $\Phi = 0.25$	281
9-88	Angelier's method results for fault population SO-02 at $\Phi = 0.50$	282
9-89	Angelier's method results for fault population SO-02 at $\Phi = 0.75$	283
9-90	Angelier's method results for fault population SO-02 at $\Phi = 1.00$	284
9-91	Reches' method results for fault population SO-03 at $\Phi = 0.00$	285
9-92	Reches' method results for fault population SO-03 at $\Phi = 0.25$	286
9-93	Reches' method results for fault population SO-03 at $\Phi = 0.50$	287
9-94	Reches' method results for fault population SO-03 at $\Phi = 0.75$	288
9-95	Reches' method results for fault population SO-03 at $\Phi = 1.00$	289
9-96	Angelier's method results for fault population SO-03 at $\Phi = 0.00$	290
9-97	Angelier's method results for fault population SO-03 at $\Phi = 0.25$	291

9-98	Angelier's method results for fault population SO-03 at $\Phi = 0.50$	292
9-99	Angelier's method results for fault population SO-03 at $\Phi = 0.75$	293
9-100	Angelier's method results for fault population SO-03 at $\Phi = 1.00$	294
9-101	Reches' method results for fault population FD-01	298
9-102	Angelier's method results for fault population FD-01	299

LIST OF TABLES

	Page
5-1 Table of data generated by the calculation of 21 slip vectors	86
8-1 Table of data listing Angelier's (1979) population of 38 normal faults	175
9-1 Reches' and Angelier's results for fault population RP-01	210
9-2 Reches' and Angelier's results for fault population RP-02	211
9-3 Reches' and Angelier's results for fault population RP-03	212
9-4 Reches' and Angelier's results for fault population AC-01	235
9-5 Reches' and Angelier's results for fault population AC-02	236
9-6 Reches' and Angelier's results for fault population OS-01	248
9-7 Reches' and Angelier's results for fault population RS-01	261
9-8 Reches' and Angelier's results for fault population SO-01	273
9-9 Reches' and Angelier's results for fault population SO-02	295
9-10 Reches' and Angelier's results for fault population SO-03	296

CHAPTER 1

INTRODUCTION

A numerical algorithm for paleostress analysis using fault populations was first proposed by Carey and Brunier (1974) sixteen years ago (Angelier and Goguel, 1979; Etchecopar, *et. al.*, 1981; Angelier, *et. al.*, 1982; Célérrier, 1988; Angelier, 1989). Since that time, several different computational methods have been proposed (Carey and Brunier, 1974; Armijo and Cisternas, 1978; Angelier, 1979; Etchecopar, *et. al.*, 1981; Angelier, *et. al.*, 1982; Vasseur, *et. al.*, 1983; Angelier, 1984; Gephart and Forsyth, 1984; Michael, 1984; Reches, 1987; Angelier, 1989), each having distinct advantages over the preceding ones. These numerical methods are all based upon the theoretical relationships between stress and shear described by Wallace (1951) and Bott (1959) and use iterative methods to seek a best-fit between the observed slip directions of faults and the directions of maximum shear stress on each fault plane for different paleostress tensors (Etchecopar, *et. al.*, 1981; Angelier, 1984; Gephart and Forsyth, 1984; Michael, 1984; Reches, 1987; Angelier, 1989).

Paleostress analysis programs require an initial data set of faults assumed, or known, to have been activated during a single tectonic event within a homogeneous stress field. A fault datum consists of the fault's orientation, slip direction, and sense of slip. This fault population data is used to calculate the orientation of the three principal stress axes σ_1 , σ_2 , and σ_3 and a value signifying some ratio of their relative magnitudes, commonly denoted as Φ (Angelier, 1979; Michael, 1984).

1.1 Purpose of this Study

Paleostress analysis techniques have recently been applied by many geologists to

regional fault populations (Angelier and Mechler, 1977; Angelier, 1979; Angelier and Goguel, 1979; Aydin, 1980; Etchecopar, *et. al.*, 1981; Angelier, *et. al.*, 1982; Angelier, 1984; Michael, 1984; Aleksandrowski, 1985; Angelier, *et. al.*, 1985; Frizzell and Zoback, 1987; Hancock, *et. al.*, 1987; Julien and Cornet, 1987; Lisle, 1987; Pfiffner and Burkhard, 1987; Reches, 1987; Sassi and Carey-Gailhardis, 1987; Caputo and Caputo, 1988; Célérier, 1988; Larroque and Laurent, 1988; Lisle, 1988; Angelier, 1989; Hardcastle, 1989; Hatzor and Reches, 1989; Manning and de Boer, 1989; Wallbrecher and Fritz, 1989; Umhoefer, 1990) in order to derive regional paleostress tensors. A close examination of published studies indicate that numerical paleostress analysis techniques are commonly applied to fault populations only when the results are consistent with other methods of estimating paleostresses (Frizzell and Zoback, 1987; Hancock, *et. al.*, 1987; Pfiffner and Burkhard, 1987; Larroque and Laurent, 1988; Hardcastle, 1989; Manning and de Boer, 1989; Wallbrecher and Fritz, 1989; Hatzor and Reches, 1990). Unfortunately, very little work has been published on the possible limitations of individual paleostress analysis programs currently in use (Angelier, *et. al.*, 1982; Angelier, 1984; Célérier, 1988) and I am not aware of any published papers providing a detailed study of the limitations of paleostress analysis programs in general. This implies that some researchers may be applying paleostress analysis to regional fault populations without having a clear idea of how appropriate the application of such techniques to their data sets may be (Edelman, 1989) although, since work on this thesis has started, several researchers have begun to examine this important topic (Pershing, 1989; Pollard, 1990).

My study is an attempt to correct this problem by systematically examining two widely-used paleostress analysis programs and demonstrating that they both possess important limitations. Geologists should be made aware of these limitations before they use paleostress analysis techniques to determine a possible paleostress tensor from field data.

1.2 Scope of this Study

The two paleostress analysis programs I chose to examine for this study were those developed by Angelier (Angelier, 1979; Angelier, 1989) and Reches (Reches, 1987). These programs were chosen for testing because the literature indicated that they are the most commonly used paleostress analysis programs (Angelier, 1979; Angelier, *et. al.*, 1982; Angelier, 1984; Angelier, *et. al.*, 1985; Pfiffner and Burkhard, 1987; Reches, 1987; Angelier, 1989; Hardcastle, 1989; Hatzor and Reches, 1990). I have also begun examining other paleostress analysis programs including those developed by Etchecopar (Etchecopar, *et. al.*, 1981), Michael (Michael, 1984), Gephart (Gephart and Forsyth, 1984), and Lisle (Lisle., 1988) although the results from those programs are too preliminary to be included here and will be addressed in a future paper.

To evaluate the usefulness of the paleostress analysis programs tested, I will address the following three questions in this thesis.

1. Do the two paleostress analysis programs chosen for testing have significant limitations?
2. If so, what exactly are those limitations?
3. How does this information pertain to the geologist applying paleostress analysis techniques?

Several researchers have shown that each of the paleostress analysis programs I tested will yield geologically-reasonable, or expected, results for certain fault populations (Angelier, 1979; Angelier, *et. al.*, 1982; Angelier, 1984; Angelier, *et. al.*, 1985; Pfiffner and Burkhard, 1987; Reches, 1987; Angelier, 1989; Hardcastle, 1989; Hatzor and Reches, 1990). I specifically set out to find situations in which the methods would not yield the expected results.

In this way, I hoped to discover and evaluate any weaknesses inherent in these programs.

The hypothesis I wish to prove in this thesis is that *computational methods of paleostress analysis have several significant limitations that geologists must be aware of when using these techniques to derive a regional paleostress tensor from natural fault populations.*

1.3 Testing Procedures

All of the paleostress analysis programs tested make three very important initial assumptions.

1. The fault and slip orientations which comprise the data set are associated with a unique, homogeneous regional paleostress tensor.
2. The faults each behave independently of one another and do not interact mechanically.
3. The movement vector for each fault plane corresponds to the direction of maximum shear stress within that plane.

Artificial fault populations consistent with a known stress tensor were derived using these three simplifying assumptions. These artificial fault population data sets were then used to test the paleostress analysis programs in four different ways.

1. The accuracy of each paleostress analysis program was tested by creating random fault-slip populations consistent with a chosen stress tensor. The orientations of the fault planes were randomly chosen and their slip directions were coincident with the direction of maximum shear stress within each plane. These fault populations were used as input for the paleostress analysis programs and the results were compared to

the original stress tensor under which the fault-slip data were created.

2. The behavior of each paleostress analysis program when applied to special-case fault populations was tested by using the following fault populations associated with a known stress tensor.
 - A. Simple Andersonian conjugate fault sets (Anderson, 1951).
 - B. Orthorhombic, or rhombohedral, fault populations (Aydin and Reches, 1982; Krantz, 1986; Krantz, 1989).
 - C. Fault populations where all faults have approximately the same orientation.
 - D. Fault populations where some or all of the faults have approximately the same orientation as the principal stress planes.

3. The stability of the calculated paleostress tensors to insufficient data, extraneous data, and measurement errors was tested by applying the following procedures and noting the effect upon the calculated paleostress tensor.
 - A. Randomly removing one or more fault planes from a fault population.
 - B. Randomly adding one or more fault planes, with randomly chosen slip directions, to the fault population.
 - C. Giving a $\pm 5^\circ$ variability to the orientations of the fault plane normal and slip vectors.

4. Finally, the programs were compared to one another, using both natural and artificial fault populations, to see how consistent the results were given the same initial data sets. Since one assumption shared by all of the paleostress analysis programs is that

there exists a unique regional paleostress tensor for any given fault population arising from a single tectonic event, inconsistencies between the output of the various programs would indicate their unreliability given certain initial data sets.

1.4 Thesis Organization

I have organized this thesis into four main sections. Chapters 2 and 3 introduce the concept of paleostress analysis as it is applied to fault populations and give a review of previous work. The second section consists of chapter 4 which discusses problems inherent in paleostress analysis, chapter 5 which describes the program and methodology used to generate artificial fault populations, and chapters 6 and 7 which describe the two paleostress analysis programs tested. The third section, consisting of chapters 8 and 9, is the main body of the thesis and details the procedures used to test the paleostress analysis programs and presents the results of those tests. Finally, chapter 10 presents the conclusions of this study and suggestions for further work.

CHAPTER 2

PALEOSTRESS ANALYSIS

Paleostress analysis refers to various methods which attempt to determine a regional stress tensor consistent with existing geologic structures. Several different techniques for estimating stress tensors have been proposed. Principal stress directions and relative magnitudes have been determined from **fault populations** (Angelier and Mechler, 1977; Angelier, 1979; Angelier and Goguel, 1979; Aydin, 1980; Etchecopar, *et. al.*, 1981; Angelier, *et. al.*, 1982; Angelier, 1984; Michael, 1984; Alesandrowski, 1985; Angelier, *et. al.*, 1985; Frizzell and Zoback, 1987; Hancock, *et. at.*, 1987; Lisle, 1987; Pfiffner and Burkhard, 1987; Reches, 1987; Sassi and Carey-Gailhardis, 1987; Caputo and Caputo, 1988; Célérier, 1988; Larroque and Laurent, 1988; Lisle, 1988; Angelier, 1989; Hardcastle, 1989; Manning and de Boer, 1989; McBride, 1989; Wallbrecher and Fritz, 1989; Hatzor and Reches, 1990; Umhoefer, 1990), **earthquake focal mechanism data** (McKenzie, 1969; Ellsworth and Zhonghuai, 1980; Vasseur, *et. al.*, 1983; Gephart and Forsyth, 1984; Julien and Cornet, 1987; Pfiffner and Burkhard, 1987; Wahlstrom, 1987; Michael, 1987a; Michael, 1987b; Jones, 1988), **borehole elongation data** (Zoback and Zoback, 1980; Plumb and Cox, 1986; Suter, 1986; Hansen and Mount, 1990), **joint sets** (Price, 1966; Engelder and Geiser, 1980; Engelder, 1982; Hancock, 1985; Hancock, *et. al.*, 1987), **dike sets** (Berger, 1971; Muller and Pollard, 1977; Davidson and Park, 1978; Borradaile, 1986; Rice, 1986; Lisle, 1989; Manning and de Boer, 1989; Hansen and Mount, 1990), **calcite e-twins** (Spang, 1972; Spang and Van Der Lee, 1975; Laurent, *et. al.*, 1981; Pfiffner and Burkhard, 1987; Larroque and Laurent, 1988), **various microstructural features** (Friedman, 1964; Scott, *et. al.*, 1965; Carter and Raleigh, 1969; Spang and Van Der Lee, 1975; White, 1979; Plumb, *et. al.*, 1984; Pêcher, *et. al.*, 1985; Lespinasse and Pêcher, 1986; Kowallis, *et. al.*, 1987; Jang, *et. al.*, 1989; Laubach, 1989; Shepard, 1990), **folds** (Dieterich and Carter, 1969; Michael, 1984), **stylolites**

(Arthaud and Mattaeur, 1969; Buchner, 1981; Hancock, *et. al.*, 1987), **kink bands** (Gay and Weiss, 1974), and **fracture markings on joint surfaces** (Bahat and Rabinovich, 1988).

Fault-striation paleostress analysis, the topic of this thesis, is the subset of paleostress analysis which attempts to estimate the relative magnitudes and orientations of the three principal stresses σ_1 , σ_2 , and σ_3 (most compressive to least compressive respectively) from fault populations and their associated slip directions.

2.1 Andersonian Fault Classification

To determine the stress tensor associated with a displacement along a fault in a given slip direction, some hypothesis must be made about the failure mechanisms involved. The first, and simplest, hypothesis is that failure occurred within intact isotropic rock. In Anderson's classic work on faulting (Anderson, 1951, p. 7), Coulomb's failure criterion (Coulomb, 1776; Handin, 1969) was used to predict the orientations of the three principal stress axes σ_1 , σ_2 , and σ_3 resulting in the three common types of conjugate fault systems -- thrust, normal, and wrench.

Anderson began by examining an infinitesimal prism (or at least one small enough such that the stresses present are homogeneous throughout its volume) situated within a right-handed XYZ coordinate system where σ_1 , σ_2 , and σ_3 are parallel the X, Y, and Z directions respectively (figure 2-1). If face A is assumed to be of unit area and θ is defined as the angle between plane A and the X-axis, this would imply an area of $\sin(\theta)$ for face <opr> and an area of $\cos(\theta)$ for face <pqr>. If the system is in equilibrium, then a simple force balance shows that the force acting normal to plane A (which is equivalent to the normal stress σ_n upon the plane) is

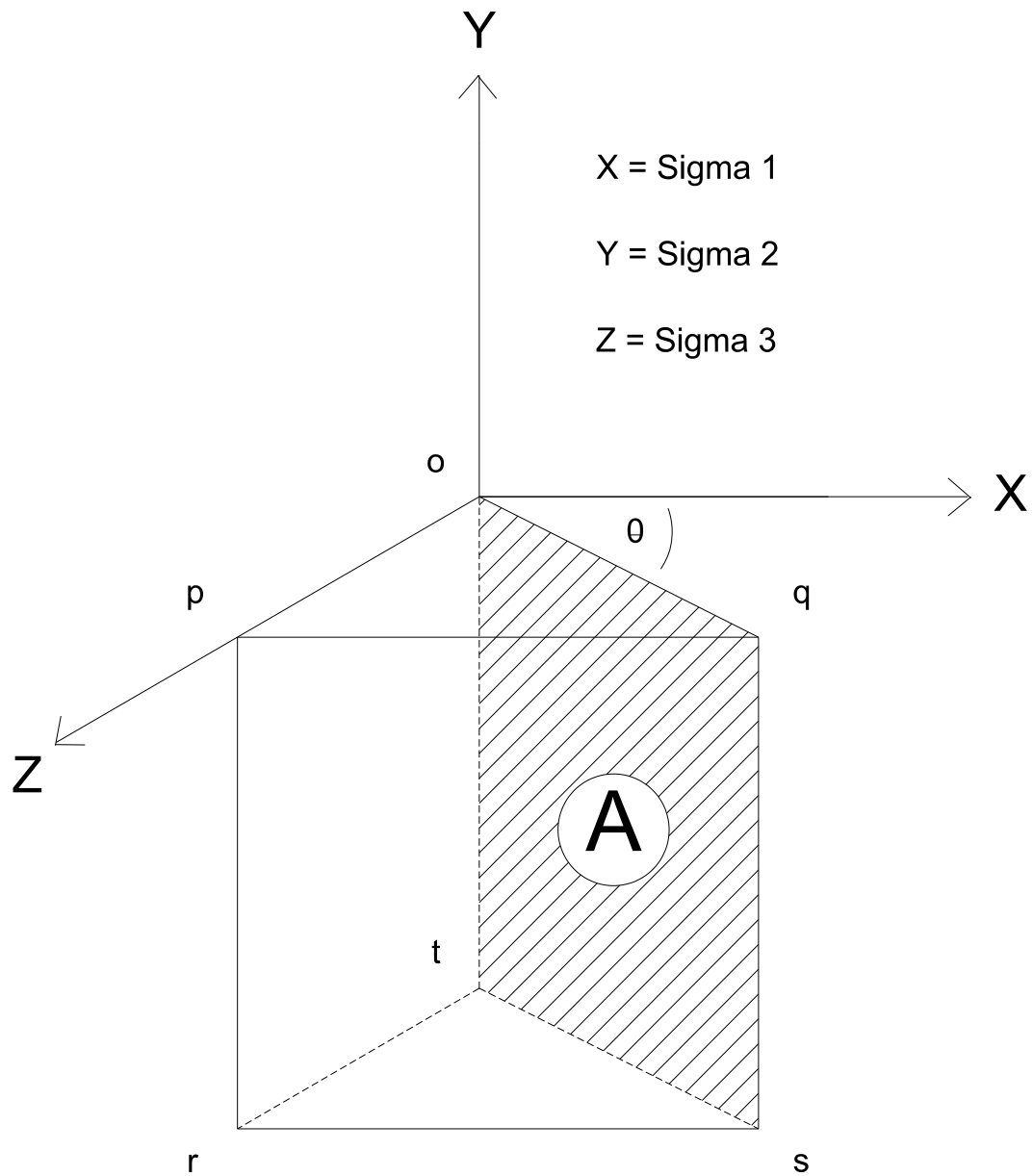


Figure 2-1 - An infinitesimal prism $\langle opqrst \rangle$ situated within a right-handed XYZ coordinate system. The three principal stresses σ_1 , σ_2 , and σ_3 parallel the X, Y, and Z-axes respectively and θ defines the angle between plane A and the X-axis. Plane A is defined to be of unit area.

$$\sigma_n = \sigma_1 \sin(\theta) \sin(\theta) + \sigma_3 \cos(\theta) \cos(\theta) \quad (1)$$

and the shear stress σ_s , which is found by resolving the forces parallel to the direction $\langle oq \rangle$, is

$$\sigma_s = \sigma_1 \sin(\theta) \cos(\theta) - \sigma_3 \sin(\theta) \cos(\theta) \quad (2)$$

which can be reduced using the trigonometric identity $2\sin(\theta)\cos(\theta) = \sin(2\theta)$ to yield

$$\sigma_s = [(\sigma_1 - \sigma_3) / 2] \sin(2\theta) \quad (3)$$

It is clear, for any given magnitudes of principal stresses present, that the shear stress will be greatest when $\sin(2\theta) = \pm 1$, or $\theta = \pm 45^\circ$. There are thus two planes at any point across which the shear stress magnitudes are at a maximum.

Anderson noted, however, that in natural and artificial conjugate faults, an acute and an obtuse angle are present with the acute angle bisected by σ_1 and the obtuse angle bisected by σ_3 (*i.e.* the principal stress axes are not oriented at 45° from the fault planes as equation (3) predicts). This principal is occasionally referred to as Hartmann's Rule (Hartmann, 1896; Dennis, 1987, p. 238) after the French metallurgist who first formulated it. The solution to this discrepancy between theory and observation is to take into account the Coulomb failure criterion

$$\sigma_s = C_0 + \mu \sigma_n \quad (4)$$

where C_0 is a constant denoting the cohesion of the fault surface and μ is the coefficient of

internal friction (Coulomb, 1776; Handin, 1969). This is needed because friction exists on real fault surfaces. Substituting in the normal stress from equation (1) results in

$$\sigma_s = C_0 + \mu[\sigma_1 \sin^2(\theta) + \sigma_3 \cos^2(\theta)] \quad (5)$$

and substituting the identities $\sigma_1 \equiv [(\sigma_1 + \sigma_3) / 2] + [(\sigma_1 - \sigma_3) / 2]$ and $\sigma_3 \equiv [(\sigma_1 + \sigma_3) / 2] - [(\sigma_1 - \sigma_3) / 2]$ into equation (5) and reducing it through suitable algebraic manipulations and the two trigonometric identities $[\sin^2(\theta) + \cos^2(\theta)] = 1$ and $[\cos^2(\theta) - \sin^2(\theta)] = \cos(2\theta)$ yields

$$\sigma_s = C_0 + \mu[((\sigma_1 + \sigma_3) / 2) - ((\sigma_1 - \sigma_3) / 2) \cos(2\theta)] \quad (6)$$

or

$$[(\sigma_1 - \sigma_3) / 2] \sin(2\theta) = C_0 + \mu[((\sigma_1 + \sigma_3) / 2) ((\sigma_1 - \sigma_3) / 2) \cos(2\theta)] \quad (7)$$

The problem is now to find the planes along which the shearing stress (which drives slip) will most likely overcome the normal stress (which acts to retard slip). Since the shear stress may have both positive and negative values, the problem reduces to finding the angles for which

$$[(\sigma_1 - \sigma_3) / 2] \sin(2\theta) + \mu[((\sigma_1 + \sigma_3) / 2) ((\sigma_1 - \sigma_3) / 2) \cos(2\theta)] \quad (8)$$

is at a maximum, and

$$[(\sigma_1 - \sigma_3) / 2] \sin(2\theta) - \mu[((\sigma_1 + \sigma_3) / 2) ((\sigma_1 - \sigma_3) / 2) \cos(2\theta)] \quad (9)$$

is at a minimum. Differentiating these two equations with respect to θ and setting them equal to zero yields

$$[(\sigma_1 - \sigma_3) / 2] \cos(2\theta) \pm \mu[(\sigma_1 - \sigma_3) / 2] \sin(2\theta) = 0 \quad (10)$$

which reduces to

$$\cos(2\theta) \pm \mu \sin(2\theta) = 0 \quad (11)$$

or, alternatively

$$\tan(2\theta) = \pm(1 / \mu) \quad (12)$$

Since the coefficient of friction in most rocks has been experimentally determined to range from 0.5 to 1.0 (Byerlee, 1968; Handin, 1969; Jaeger and Cook, 1979, p. 59; Brace and Kohlstedt, 1980), θ will be less than 45° and the angle between conjugate faults will be less than 90° where bisected by σ_1 and greater than 90° where bisected by σ_3 .

Anderson reasoned that in natural faults one of the principal stress orientations will be vertical since the surface of the earth may be thought of as a free surface unable to support shear stresses. The other two principal stresses are thus required to be horizontal. Assuming that the relative magnitudes of the principal stresses must change for faulting to occur, there are three possible relationships between the magnitudes of the horizontal principal stresses -- they are either both increasing in magnitude, both decreasing in magnitude, or one is increasing while the other is decreasing (Anderson, 1951, p. 13). These correspond, respectively, to the three common types of conjugate fault systems -- reverse faults, normal

faults, and wrench faults (figure 2-2). The success of Anderson's method is witnessed by the fact that it is still used today as a first approximation for determining the principal stress orientations from conjugate fault sets (Davis, 1984, p. 306; Ragan, 1985, p. 135; Suppe, 1985, p. 292; Rowland, 1986, p. 134; Dennis, 1987, p. 236; Marshak and Mitra, 1988, p. 261; Spencer, 1988, p. 199). Care must be used, however, since conjugate fault sets exist which do not fit the Andersonian classification (Oertel, 1965; Aydin, 1977; Aydin and Reches, 1982; Reches and Dieterich, 1983; Krantz, 1988; Krantz, 1989).

2.2 Bott's Formula

The next important steps in paleostress analysis were the determination of the relationship of shear stresses to the orientation of fault planes and their associated slip directions (Wallace, 1951) and the relationship of the principal stress magnitudes and orientations to the resulting directions of maximum shear stress within fault planes (Bott, 1959). These steps were motivated by the fact that rock in its natural state is rarely intact and isotropic (Anderson's assumption). The upper 5 to 10 kilometers of the earth's crust is riddled with preexisting fault planes, joints, and bedding surfaces with sliding often occurring on these planar discontinuities long before a state of stress high enough to cause fracture in an intact volume of rock is reached (Wallace, 1951; Bott, 1959; Jaeger, 1960; Donath, 1964; Handin, 1969; McKenzie, 1969).

Wallace (1951), using stereographic projections, plotted shear stress magnitudes for various orientations of planes within a stress system and the directions of maximum shearing stress in those same planes. Wallace's major contribution, however, was to show how a body has a tendency to shear in a plane which represents a compromise between experiencing a low normal stress and a high shear stress and that this plane will always be oriented at less than 45° from the σ_1 direction. This may be shown by solving for the minimum of the normal

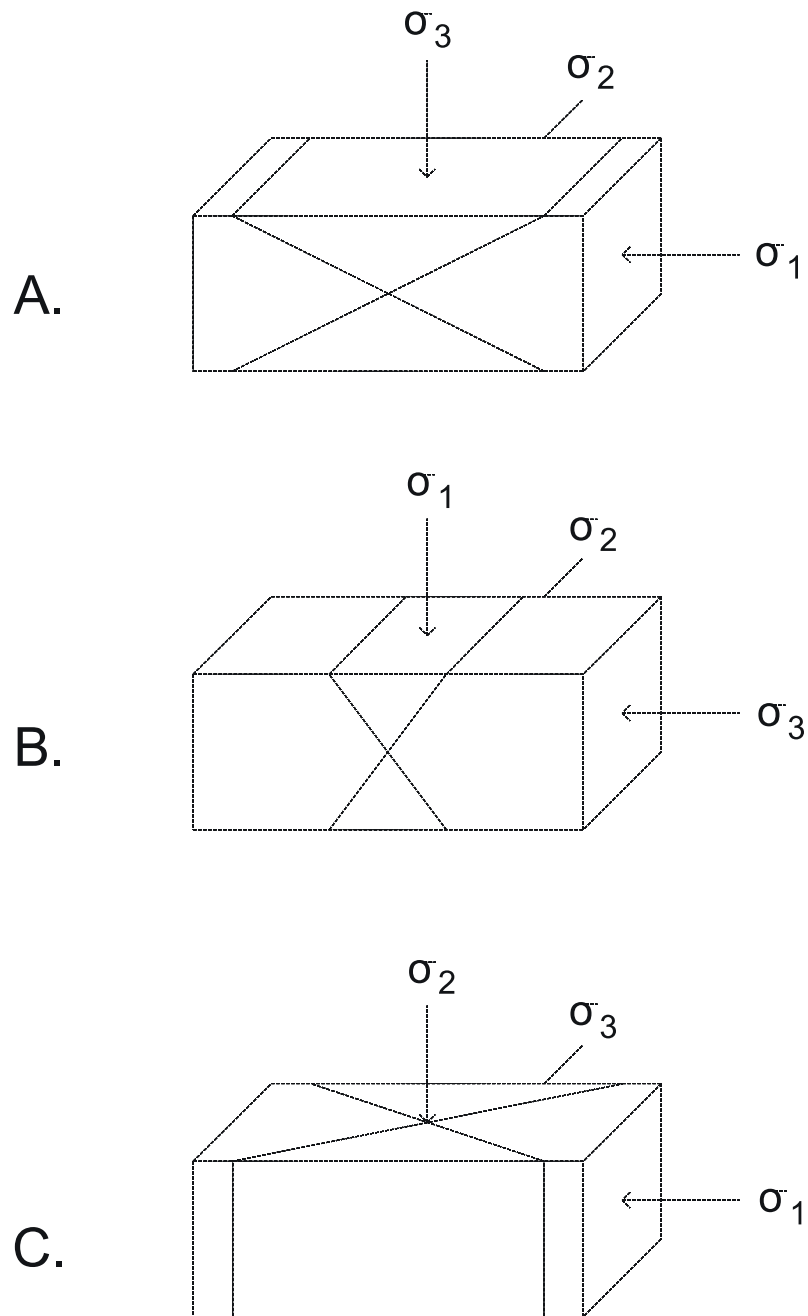


Figure 2-2 - The three Andersonian classes of conjugate fault sets. **A.** Conjugate thrust faults with horizontal σ_1 and vertical σ_3 . **B.** Conjugate normal faults with vertical σ_1 and horizontal σ_3 . **C.** Conjugate wrench faults with σ_1 and σ_3 both horizontal. In all three cases σ_2 parallels the intersection line of the two fault planes.

stress/shear stress difference in the following way

$$d[\sigma_n - \sigma_s] / d\theta = 0 \quad (13)$$

which, upon substitution of the standard formulas for σ_n and σ_s (Means, 1976, p. 72) becomes

$$d[((\sigma_1 + \sigma_3) / 2) + ((\sigma_1 - \sigma_3) / 2)\cos(2\theta) - ((\sigma_1 - \sigma_3) / 2)\sin(2\theta)] / d\theta = 0 \quad (14)$$

which, after differentiation, yields

$$(\sigma_1 - \sigma_3)[- \sin(2\theta) - \cos(2\theta)] = 0 \quad (15)$$

which implies $\tan(2\theta) = -1$ or $\theta = 67.5$ for any values of σ_1 and σ_3 (figure 2-3).

Wallace's work laid the groundwork for Bott (1959) who derived a formula relating the direction of maximum shear stress within the fault plane to the fault plane's orientation with respect to the principal stress axes and the relative magnitudes of these stresses which may be represented as follows

$$\theta = \tan^{-1}[(l_1^2 l_2 - \Phi l_2 + \Phi l_2^3) / (l_1 l_3)] \quad (16)$$

where θ is the pitch angle between the maximum shear stress direction and the strike of the fault plane, l_1 , l_2 , and l_3 are the three direction cosines of the normal vector to the fault plane, and Φ is defined as (Angelier, 1979; Michael, 1984)

$$\Phi = [(\sigma_2 - \sigma_3) / (\sigma_1 - \sigma_3)] \quad (17)$$

which ranges from 0.0 to 0.1 and represents the relative magnitudes of the three principal stresses (*i.e.* describes the shape of the stress ellipsoid). Other similar principal stress magnitude ratios have been defined, including the tensor aspect ratio δ (C  lerier, 1988)

$$\delta = [(\sigma_1 - \sigma_2) / (\sigma_1 - \sigma_3)] \quad (18)$$

where δ also ranges from 1.0 to 0.0 (*i.e.* $\delta = 1 - \Phi$) and the parameter R (called C by Aleksandrowski, 1985), which has been defined (Armijo and Cisternas, 1978; Etchecopar, *et al.*, 1981) as

$$R = [(\sigma_z - \sigma_x) / (\sigma_y - \sigma_x)] \quad (19)$$

R may have values from $-\infty$ to $+\infty$ since σ_x , σ_y , and σ_z may correspond to σ_1 , σ_2 , and σ_3 in any order although some confusion has resulted due to the use of the symbol R with definitions different than the original one of Armijo and Cisternas (Lisle, 1987; Gephart and Forstyth, 1984; Larroque and Laurent, 1988). An important implication of Bott's formula is that the slip direction of a fault plane is dependent upon the relative magnitudes of the three principal stresses σ_1 , σ_2 , and σ_3 (expressed by Φ) and not simply their orientations. A complete derivation of Bott's formula and its application in generating artificial fault populations is given in chapter 4.

2.3 Graphical Methods of Fault-Striation Paleostress Analysis

One of the simplest graphical methods of paleostress analysis using fault-striation data, is to plot the fault planes on a Schmidt or W  lff stereographic projection along with their

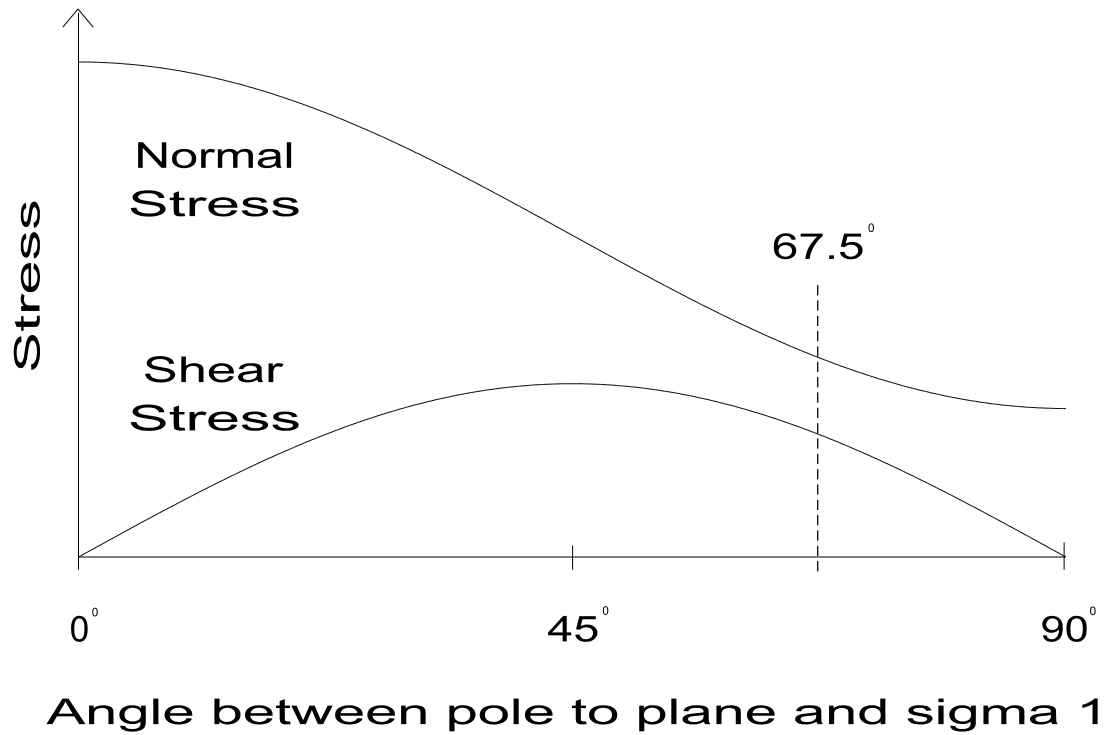


Figure 2-3 - A plot of the shear stresses and normal stresses acting upon a plane parallel to the σ_2 direction versus the inclination angle of the plane's normal from the σ_1 orientation. The upper curve represents the normal stresses and the lower curve represents the shear stresses. It may be seen by inspection that the normal stress/shear stress difference is at a minimum at 67.5° (denoted by the dashed line).

associated slip directions. If the fault population forms a conjugate set, the σ_1 axis is assumed to bisect the acute angle of the conjugate set, σ_3 the obtuse angle, and σ_2 is located at the intersection of the fault planes -- assuming, of course, that these placements are consistent with the slip directions on the fault planes present (figure 2-4). The drawback of this method is that it will only work on the simplest of conjugate fault sets (Ragan, 1985, p. 135; Suppe, 1985, p. 292; Rowland, 1986, p. 134; Marshak and Mitra, 1988, p. 261).

A somewhat different type of graphical paleostress analysis was developed from a postulated direct relationship between the regional strain ellipsoid and the regional stress ellipsoid associated with a fault population. Arthaud's method (Arthaud, 1969), and the modification of that method by Aleksandrowski (Aleksandrowski, 1985), used movement planes to determine the orientations of σ_1 , σ_2 , and σ_3 .

An M-plane, or movement plane, associated with a fault is the plane containing the fault's normal and slip vectors (figure 2-5). One of the important properties of m-planes is that these planes contain at least one of the principal strain axes. Assuming a fault population consisting of randomly-distributed, preexisting planes activated during one tectonic event, the following steps allow one to use m-planes to graphically locate the principal strain axes (Arthaud, 1969; Aleksandrowski, 1985):

1. Plot the fault plane normal and slip vectors on a stereonet.
2. Join each pole and its associated slip vector with a great circle. These great circles are the m-planes.
3. Plot the poles (π M-poles) to the m-planes.

All of the m-planes should intersect at one, two, or three generally diffuse points which are the normals of the same number of mutually perpendicular great circles of π M-

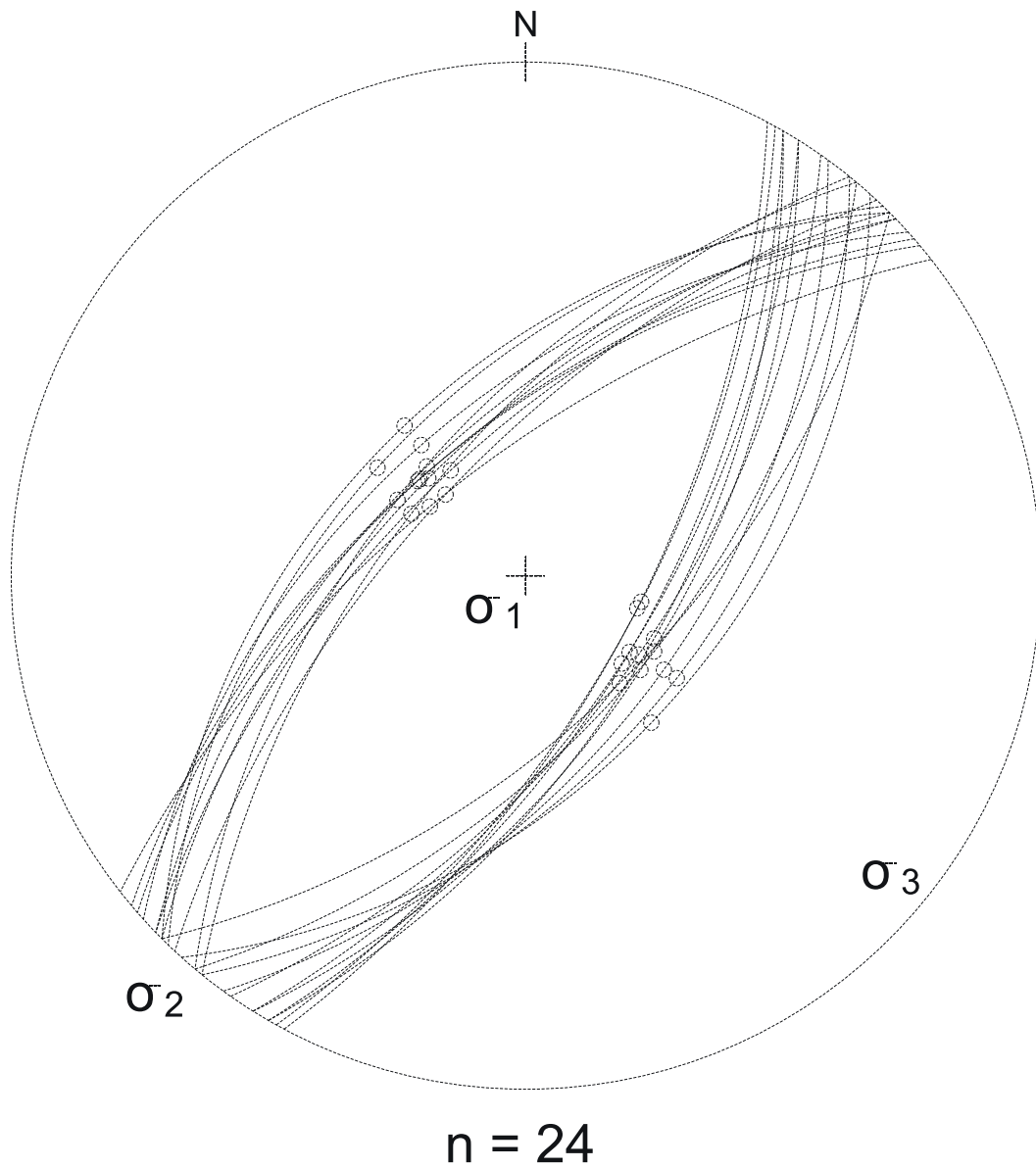


Figure 2-4 - Lower-hemisphere stereographic projection showing 24 conjugate normal faults and their associated slip vectors (small circles on fault planes). In this simple fault population, the σ_1 , σ_2 , and σ_3 axes may be assigned by inspection -- σ_1 bisecting the acute angle of the conjugate fault set, σ_3 bisecting the obtuse angle, and σ_2 at the intersection of the fault planes.

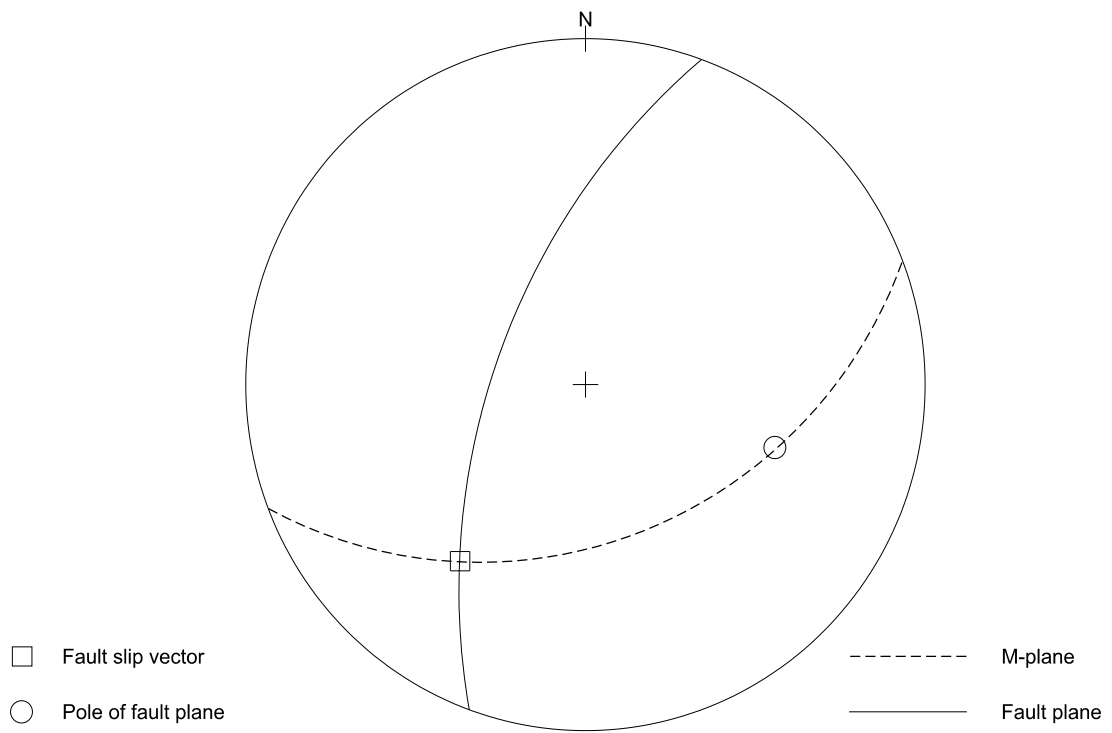


Figure 2-5 - Lower-hemisphere stereographic projection showing the relationship between a fault plane, the normal and slip vectors, and the m-plane. The m-plane is the plane perpendicular to the fault along which movement takes place.

poles (*i.e.* if m-planes intersect, their π M-poles lie on a great circle). Intersection points of the m-planes correspond to an orthogonal system of X, Y, and Z axes where X is the axis of maximum extension, Y in the intermediate axis, and Z is the axis of maximum shortening. These are the principal strain axes and are assigned according to the movement directions of the faults present and orientation of any stylolites or tension fractures present (figure 2-6).

This technique is known as Arthaud's method (Arthaud, 1969) and he contended that given the strain ellipsoid associated with a fault population, it was possible to place constraints upon the stress ellipsoid. A serious limitation in this method is that it can be successfully applied only to populations originating in radial stress fields (*i.e.* one defined by a Φ value of 0.0 where $\sigma_2 = \sigma_3$ or a Φ value of 1.0 where $\sigma_2 = \sigma_1$) and the only axis of deformation obtainable from such populations corresponds to the revolution axis of a prolate or oblate stress ellipsoid (Carey, 1976; Aleksandrowski, 1985).

Aleksandrowski (1985) modified Arthaud's method to make it applicable for a general, triaxial stress field (*i.e.* a stress field in which the three principal stress magnitudes are unequal). The procedure is the same as in Arthaud's method (steps 1 – 3 above) except that the final result consists of more than three common intersection points of m-planes. Each of these common intersection points must then be separately analyzed to ascertain whether or not the slip vectors corresponding to the m-planes lie on a great circle and at fairly large angular distances from one another; the intersection point of this great circle with the girdle of associated π M-poles is one of the three principal stress axes. The plane perpendicular to this principal stress axis which passes through the common intersection point contains the other two principal stresses (figure 2-7). If another common intersection point can be found which satisfies these conditions, the three principal stress axes may be located with varying degrees of precision (Aleksandrowski, 1985; Marshak and Mitra, 1988, p. 263). A Φ value may then also be calculated from the orientation of any one of the slip vectors and its associated fault

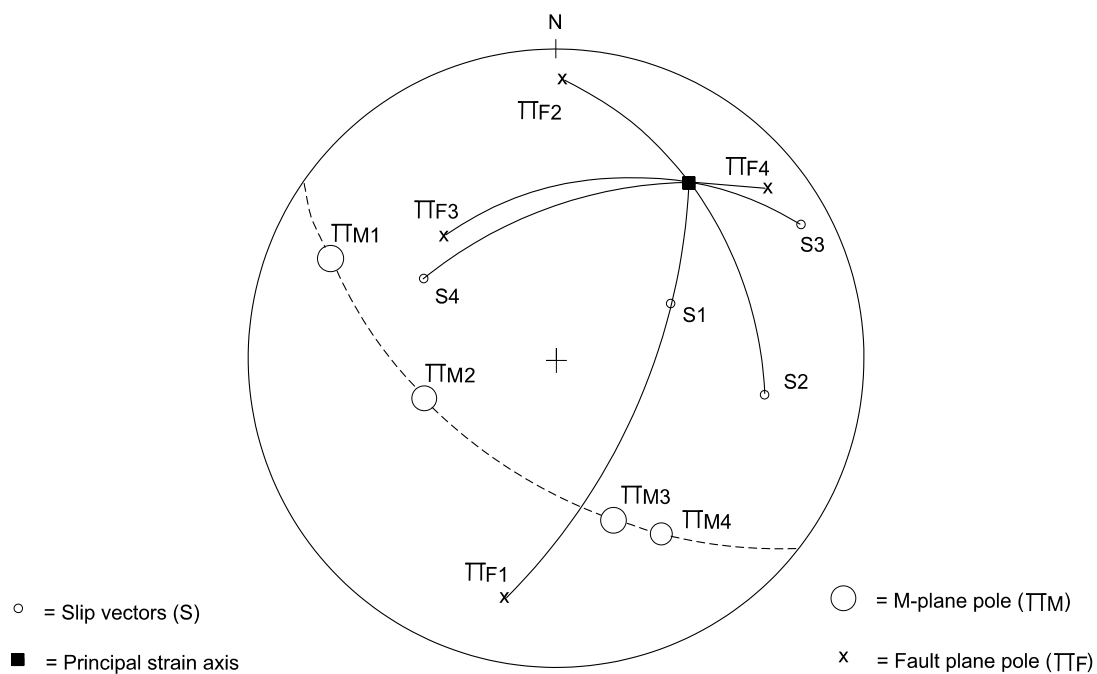


Figure 2-6 - Lower hemisphere stereographic projection demonstrating the m-plane method of locating a principal strain axis. Four fault planes are used, their poles ($\pi F1 \rightarrow \pi F4$) and slip vectors ($S1 \rightarrow S4$) are connected by great circles (m-planes) and the poles to the m-planes ($\pi M1 \rightarrow \pi M4$) are shown to form a girdle. The intersection of the m-planes (which is also the pole of the girdle) is one of the three principal strain axes (figure modified from Arthaud, 1969).

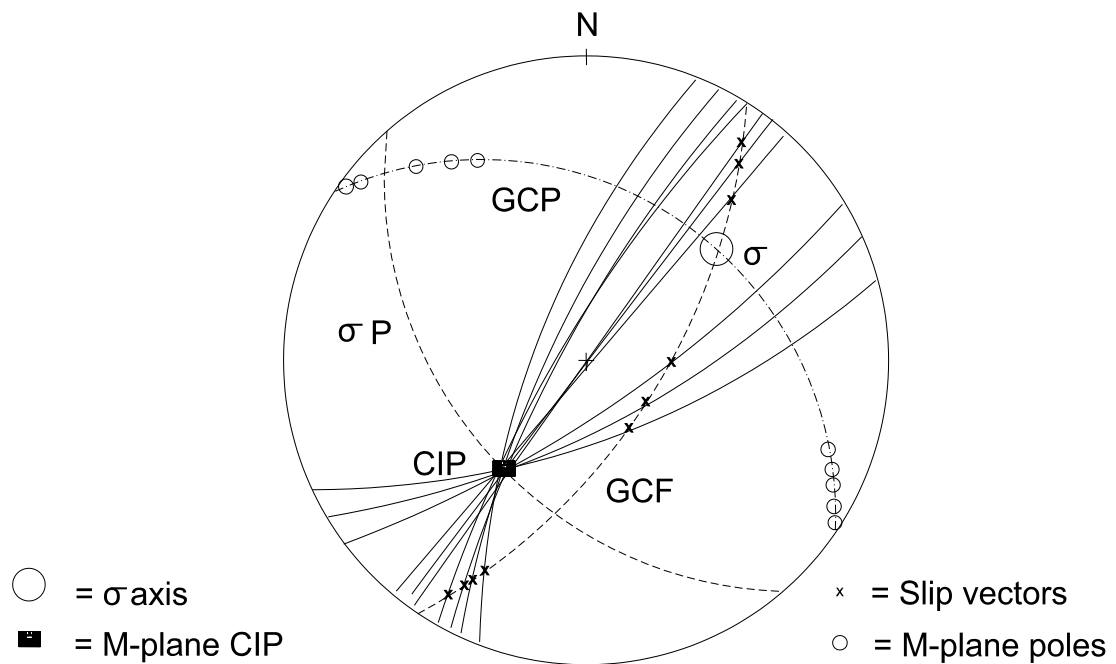


Figure 2-7 - Analyzing a common intersection point (CIP) of m-planes (solid great circles). The poles (π M-poles) to the m-planes (circles) define a great circle denoted by GCP (long dashed/short dashed line) and the pole of the GCP is the CIP. A great circle may be drawn through the slip vectors (x symbols) of each of the m-planes and is denoted by GCF (short dashed line). The intersection of the GCP and GCF is a principal stress axis σ . The plane perpendicular to σ , through the CIP, and denoted by σP (long dashed line) contains the other two principal stress axes (figure modified from Aleksandrowski, 1985).

plane using Bott's formula (equation 15).

2.4 Right-Dihedra Methods of Fault-Striation Analysis

Another graphical method of paleostress analysis has been developed by adapting the construction techniques of fault-plane solutions from seismic data to striated fault populations (McKenzie, 1969; Angelier and Mechler, 1977; Lisle, 1987; Lisle, 1988). The relationship between the fault plane solutions and the principal stress axes was first shown by McKenzie (1969), who rigorously demonstrated that the most compressive principal stress σ_1 must lie within the quadrant containing the axis of compression P for fault plane solutions of shallow earthquakes assumed to have occurred along preexisting planar discontinuities.

Fault-plane solutions are constructed from striated faults or from the seismic first motions of earthquakes and show the relationship between a fault and its corresponding auxiliary plane, the zones of compression and dilation, and the axes of compression and tension (figure 2-8). The auxiliary plane is the plane which is perpendicular to both the fault plane and the slip direction and, along with the fault plane, defines two compressional and two extensional right dihedra (Cox and Hart, 1986, p. 197). By constructing fault plane solutions for each datum of a population of faults, the overlapping quadrants containing the compression axis P will act to constrain the location of σ_1 . This technique has been called the right-dihedra method (*la méthode des dièdres droits*) by Angelier (Angelier and Mechler, 1977) and was later modified by Lisle (Lisle, 1987; Lisle, 1988) who added an additional constraint upon the location of σ_1 .

To utilize these methods, consider a fault plane with a normal vector \mathbf{N} , a slip vector \mathbf{S} , and a vector \mathbf{O} at right angles to both \mathbf{N} and \mathbf{S} . Three orthogonal planes may be defined by these vectors -- the fault plane which contains \mathbf{S} and \mathbf{O} , the auxiliary plane which contains

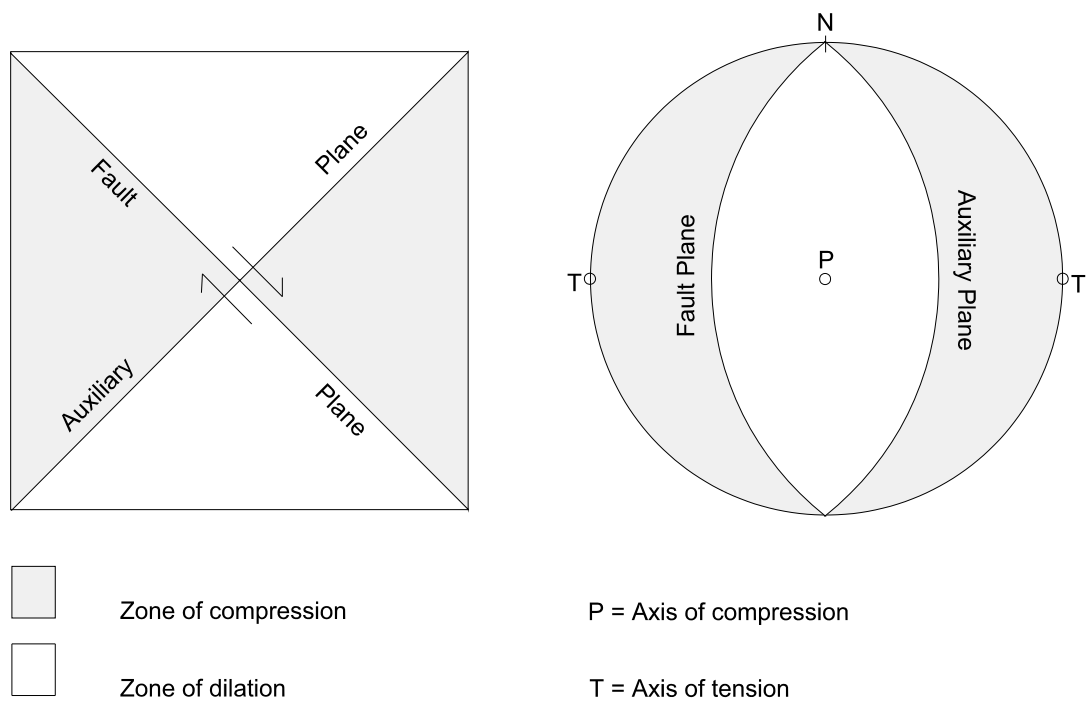


Figure 2-8 - Schematic diagram and lower-hemisphere stereographic projection illustrating the relationship between a normal fault plane dipping at 45° and its associated auxiliary plane, the zones of compression and dilation, and the axes of compression and tension in a fault plane solution.

\mathbf{N} and \mathbf{O} , and the movement plane (the m-plane of Aleksandrowski, 1985) which contains \mathbf{N} and \mathbf{S} (figure 2-9). The four right dihedral angles of Angelier and Mechler's method (Angelier and Mechler, 1977) are bounded by the fault plane and the auxiliary plane. By knowing the direction, and sense, of slip on the fault plane, two dihedral angles may be defined as compressional regions and two dihedral angles as extensional regions. If the assumption is made that the compressional regions contain σ_1 and that the extensional regions contain σ_3 (McKenzie, 1969), the position of the paleostress axes may thus be constrained for each fault datum. Superimposing the σ_1 and σ_3 regions for several faults, the possible positions for σ_1 and σ_3 may be constrained even further (figure 2-10).

Lisle (1987), introduced another constraint upon the orientations of σ_1 and σ_3 by considering how the orientation of the slip vector \mathbf{S} changes as the stress ratio Φ (equation 17) changes. If the normal vector \mathbf{N} of a fault plane has direction cosines of l , m , and n with respect to the σ_1 , σ_2 , and σ_3 axes respectively, it can be shown (Jaeger, 1969, p. 18) that the vector \mathbf{O} has direction cosines proportional to

$$\begin{aligned} & mn (\sigma_3 - \sigma_2), \\ & nl (\sigma_1 - \sigma_3), \text{ and} \\ & lm (\sigma_2 - \sigma_1). \end{aligned} \tag{20}$$

When the stress ratio Φ is equal to 0.0 (the case of axial compression), σ_2 is equal to σ_3 and the first direction cosine in equation (20) reduces to zero. This implies that the vector \mathbf{O} has no component parallel to the σ_1 axis, and σ_1 is thus parallel to the movement plane. The projection of σ_1 onto the fault plane will then be coincident with the slip vector \mathbf{S} . When the stress ratio is equal to 1.0 (the case of axial extension), σ_2 is equal to σ_1 and the third

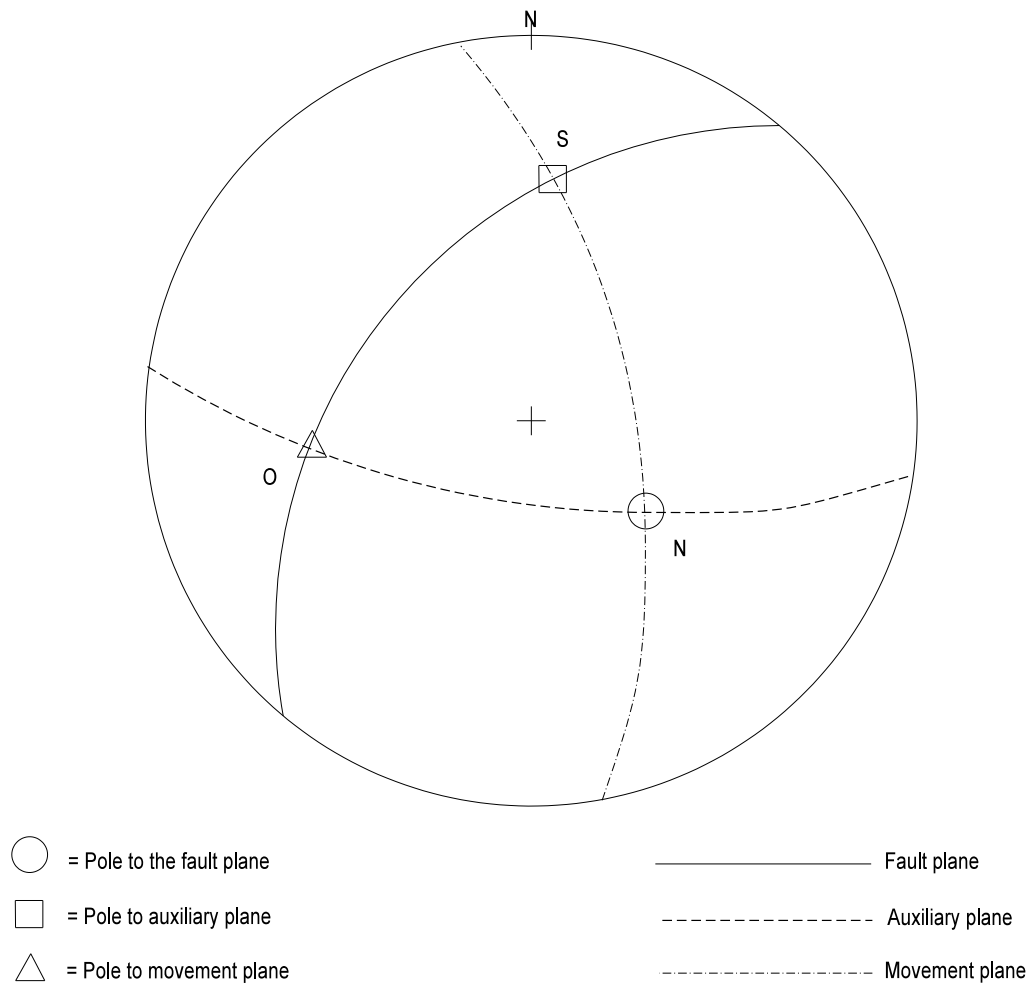


Figure 2-9 - Lower-hemisphere stereographic projection showing the relationship between a fault plane with a normal vector **N**, its associated auxiliary plane with a normal vector **S** (the fault's slip vector), and its associated movement plane (m-plane) with a normal vector **O**.

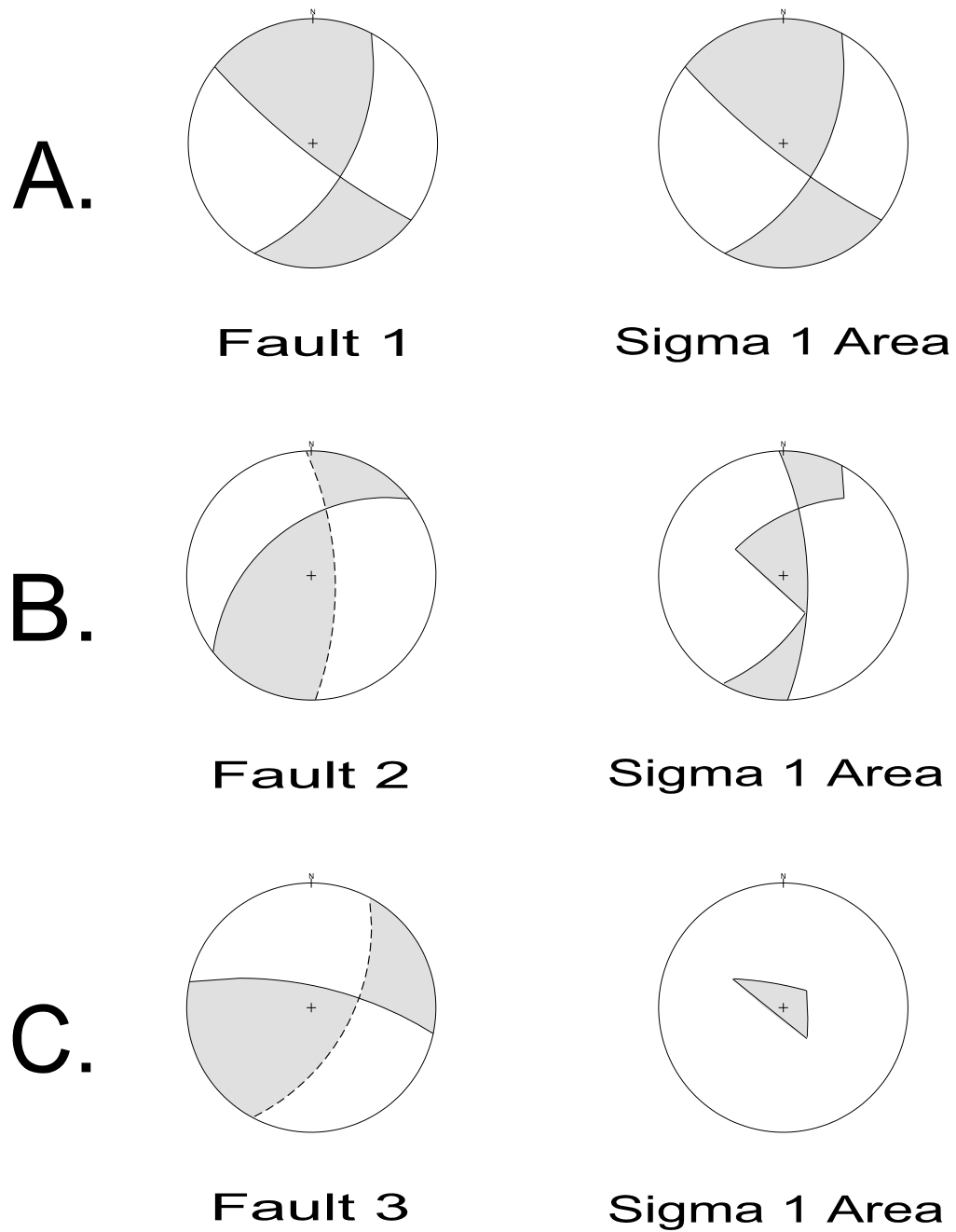


Figure 2-10 - Lower-hemisphere stereographic projections showing how the region containing σ_1 is constrained by normal fault populations consisting of **A.** one plane, **B.** two planes, and **C.** three planes.

direction cosine in equation (20) reduces to zero. This implies that the vector \mathbf{O} has no component parallel to the σ_3 direction, and σ_3 is thus parallel to the movement plane. The projection of σ_3 onto the fault plane will then be coincident with the slip vector \mathbf{S} . \mathbf{S} will be within the acute angle between these two extreme positions for intermediate values of Φ (figure 2-11). Given this constraint upon the position of \mathbf{S} , it can be inferred that the projections of σ_1 and σ_3 lie on opposite sides of \mathbf{S} and are both 90° or less from \mathbf{S} . Or, in three dimensions, σ_1 and σ_3 will be within separate right dihedral angles bounded by the fault's auxiliary and movement planes. Lisle (1987) arbitrarily labelled these dihedral angles A and B for convenience (figure 2-12) and, if σ_1 is known to lie in the A dihedral angle, then σ_3 must lie in the B and vice versa.

To use Lisle's method, auxiliary and movement planes are used to create A and B dihedral angles for each fault. Superimposing these dihedral angles, regions are obtained which may be labelled according to which dihedral angle it falls into for each fault. Thus, in a population of four superimposed faults, the region designated ABAA lies in the A dihedral angle with respect to fault 1, in the B dihedral angle with respect to fault 2, and in the A dihedral angles with respect to faults 3 and 4.

As an example, consider the data set of three faults represented in figure 2-13. Using Angelier and Mechler's (1977) method, fairly large σ_1 and σ_3 regions may be constructed (figure 2-14). Lisle's (1987) method begins by superimposing the A and B dihedral angles (figure 2-15) and comparing them to the σ_1 and σ_3 regions of Angelier and Mechler's (1977) method -- keeping in mind that σ_1 and σ_3 must be in separate A and B dihedral angles for each fault datum. The σ_1 region in figure 2-14 consists of the AAA, ABA, ABB, BAA, BAB, BBA, and BBB areas of figure 2-15. The presence of σ_1 in area BAB is compatible with σ_3 being in ABA. The same may be said for AAA, ABA, BAB, BBA, and BBB in the σ_1 region and AAA, AAB,

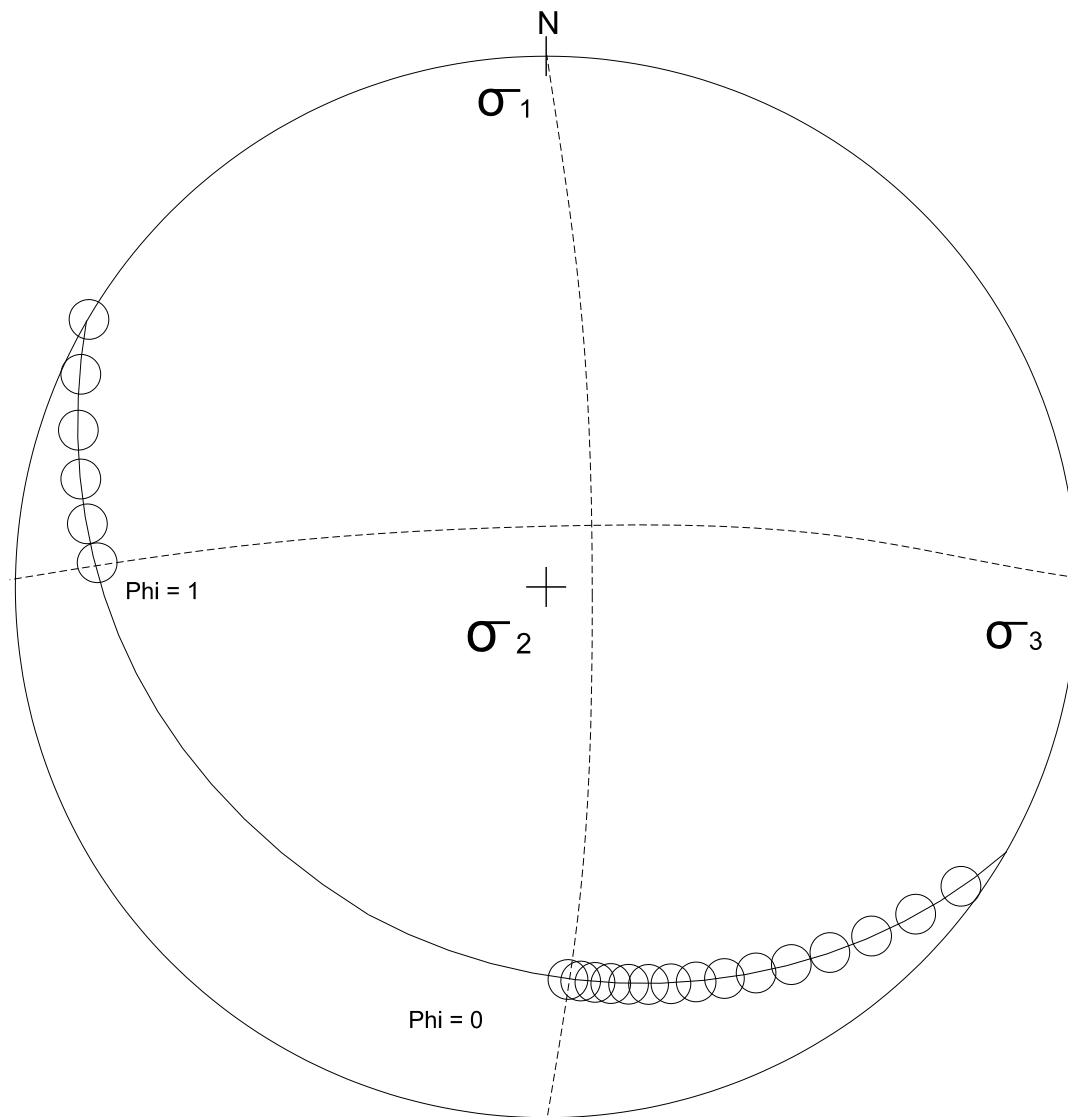


Figure 2-11 - Lower-hemisphere stereographic projection showing 20 slip vectors representing Φ values ranging from 0.0 to 1.0 on a fault plane with a normal vector oriented at 70/030 degrees. The σ_1 , σ_2 , and σ_3 axes correspond to the north, up, and east directions respectively. The dashed lines represent the projections of σ_1 and σ_3 onto the fault plane (figure modified from Schimmrich, 1990).

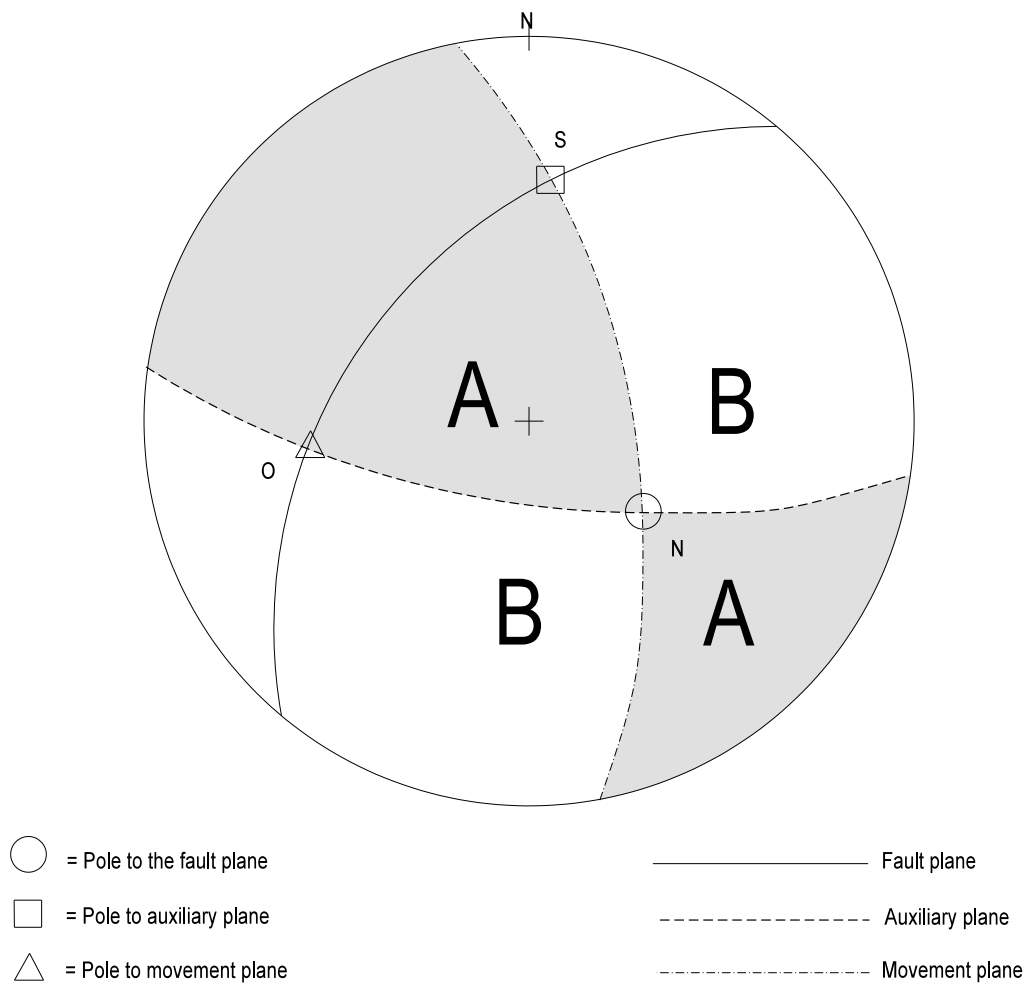


Figure 2-12 - Lower-hemisphere stereographic projection showing the right dihedral defined by Lisle (1987) as A (stippled) and B (unstippled). These right dihedral are bounded by the fault's auxiliary and movement planes. The pole to the fault plane is **N**, the pole to the movement plane is **O**, and the pole to the auxiliary plane is **S** (the fault's slip vector).

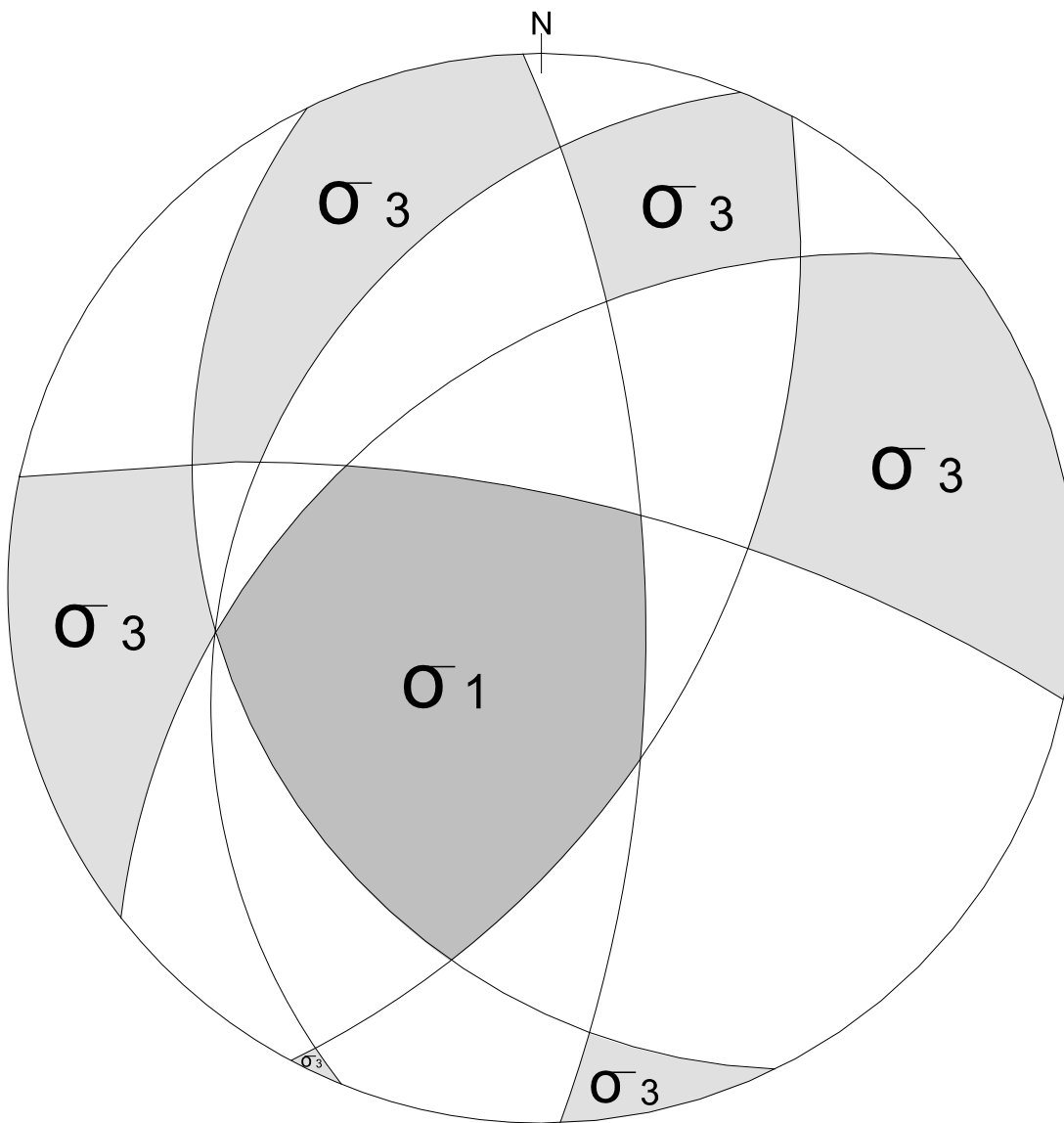


Figure 2-14 - Lower-hemisphere stereographic projection showing the σ_1 and σ_3 fields constructed by superimposing the fault data from figure 2-13. This is the Angelier and Mechler (1977) method (figure modified from Lisle, 1987).

ABA, BAB, and BBB in the σ_3 region. The BAA and ABB areas in the σ_1 region, however, have no counterparts in the σ_3 region (ABB or BAA) and may be eliminated as areas of possible σ_1 directions. For the same reason, BBA may be eliminated as an area containing the σ_3 direction. The resulting solution (figure 2-16) has noticeably smaller σ_1 and σ_3 regions.

It is easy to see that for these methods to give satisfactory results, one must have a population of faults sufficiently scattered to constrain the σ_1 and σ_3 regions to small areas. A population of faults where all of the faults have similar orientations will yield no more information than any subset of that population (figure 2-17). These methods will also not perform very well when dealing with certain types of symmetrical fault populations such as conjugate sets (Anderson, 1951) or orthorhombic sets (Aydin and Reches, 1982; Krantz, 1986; Krantz, 1989) of faults (figure 2-18).

The graphical methods of paleostress analysis developed by Angelier and Mechler (1977) and Lisle (1987) are extremely cumbersome to do on a stereonet when dealing with more than a handful of fault planes. For this reason, these methods are usually performed numerically by a computer program (Angelier and Mechler, 1977; Lisle, 1988). It should be kept in mind, however, that even though these methods are adapted for a computer, they are still essentially considered graphical methods and **not** computational methods.

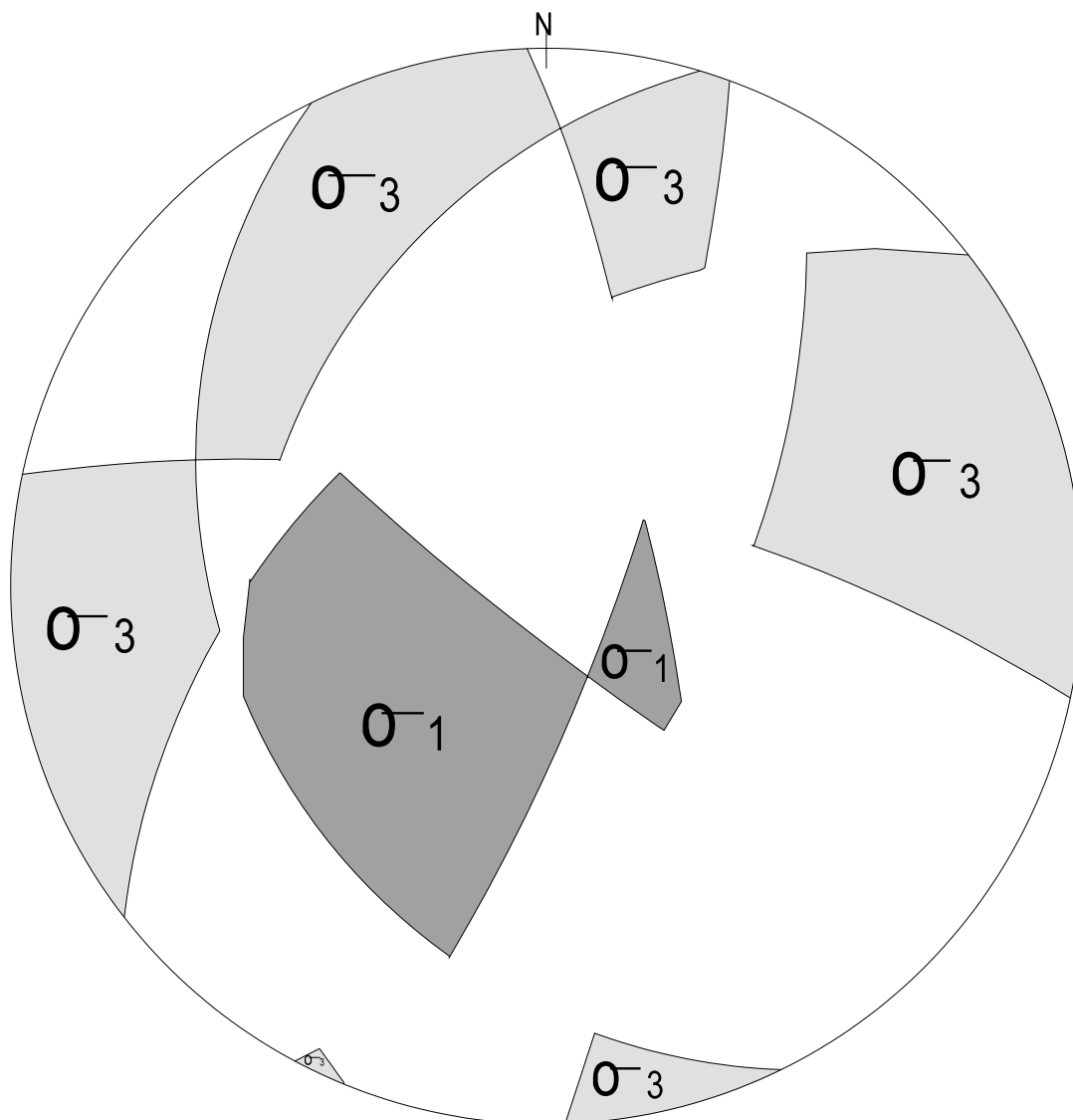


Figure 2-16 - Lower-hemisphere stereographic projection showing the σ_1 and σ_3 fields constructed by utilizing Lisle's (1987) constraint on the fault data from figure 2-13. Even with a small population of three faults, there is a noticeable improvement over Angelier and Mechler's (1977) method (figure modified from Lisle, 1987).

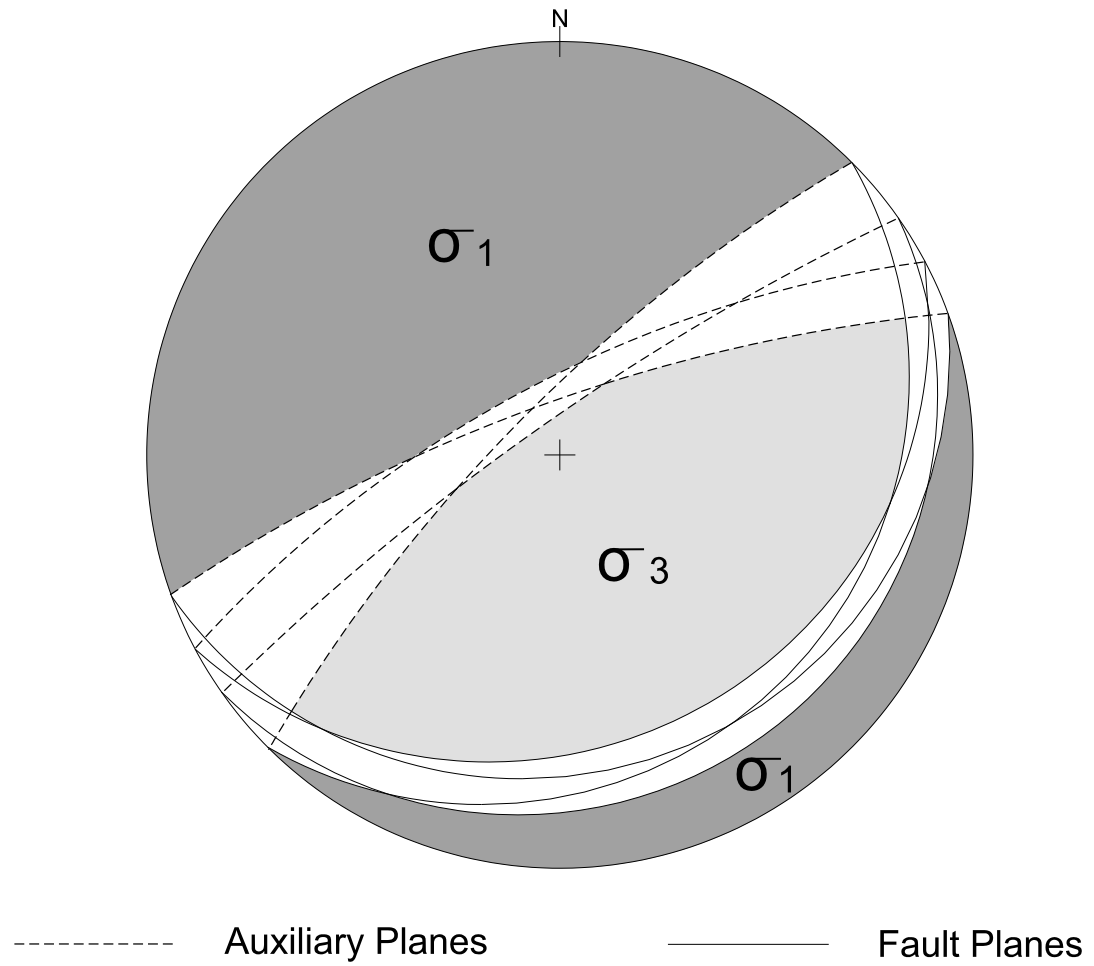


Figure 2-17 - Lower-hemisphere stereographic projection showing the σ_1 and σ_3 regions derived using Lisle's (1987) method on four thrust faults all having a similar orientation.

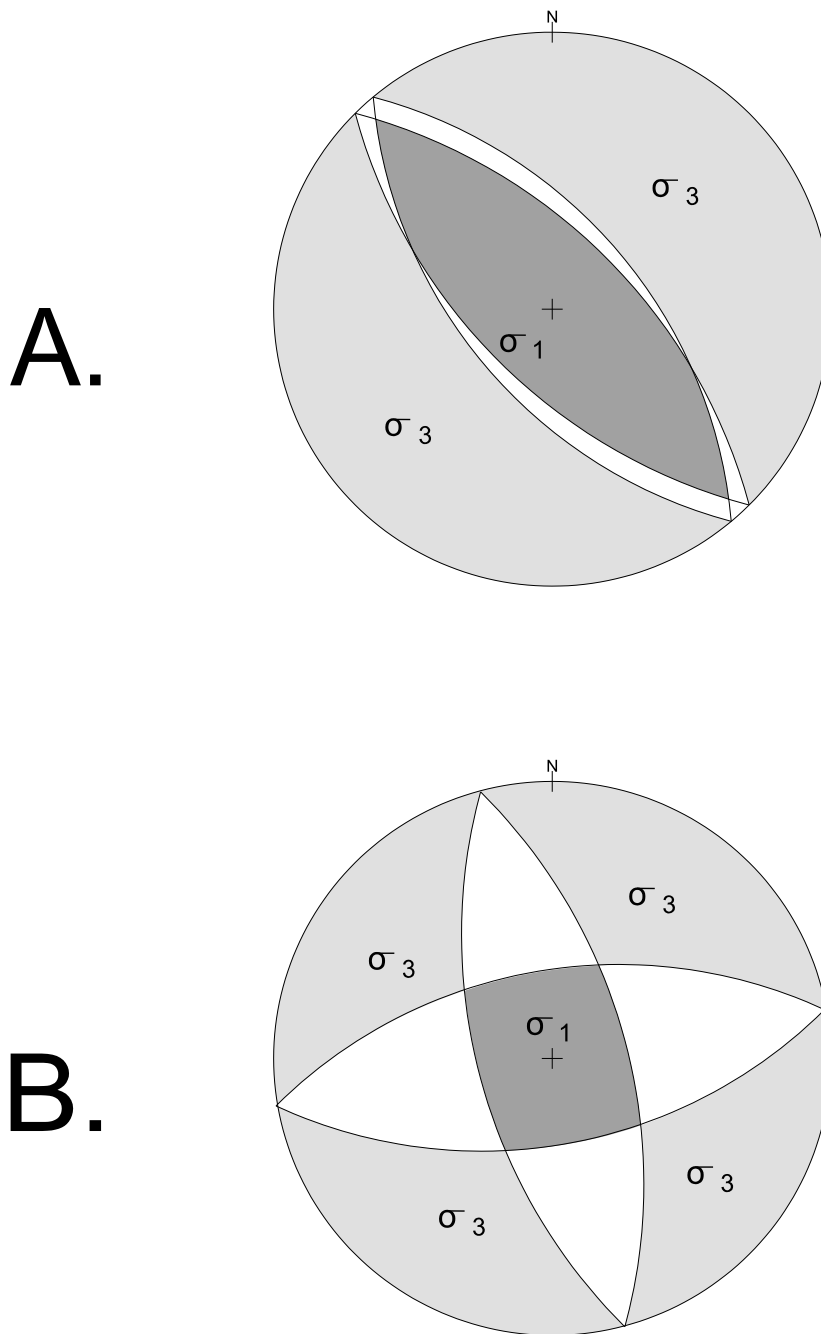


Figure 2-18 - Lower-hemisphere stereographic projection showing the σ_1 and σ_3 regions derived using Lisle's (1987) method on **A.** a conjugate set of four normal faults and **B.** an orthorhombic set of four normal faults.

CHAPTER 3

COMPUTATIONAL PALEOSTRESS ANALYSIS OF FAULT POPULATIONS

Given the assumption that faults will slip in the direction of their maximum resolved shear stress, determining the direction and sense of slip on a population of fault planes of known orientations for a given stress tensor σ is a trivial matter (Bott, 1959). The inverse of this problem -- finding a stress tensor σ satisfying known slip directions and orientations for a population of faults -- is much more difficult. This is termed the "inverse problem" and its solution is the goal of computational methods of paleostress analysis (Etchecopar, *et. al.*, 1981; Armijo, *et. al.*, 1982; Angelier, 1989).

All paleostress analysis methods assume that two items of information are known for each fault -- the fault plane's orientation in a geographic coordinate system and the fault's direction and sense of slip. In addition, two very important fundamental assumptions are made by all of the methods -- that the direction of slip on a fault plane is always parallel to the direction of resolved shear stress on that plane and that all of the faults are activated within a unique, static stress field.

3.1 Early Attempts at Computational Paleostress Analysis

In 1974, Carey and Brunier made the first attempt at formulating and solving the mathematics defining the inverse problem (Armijo, *et. al.*, 1982; Célérier, 1988; Angelier, 1989). Two years later, Carey (1976) developed the first paleostress analysis program which sought to minimize the angular deviations between measured fault striations and the calculated shear stress directions on each fault plane for a chosen paleostress tensor σ . Angelier also developed a similar method at approximately the same time (1975). Since then, Angelier has

developed several successive methods, each possessing slight improvements in the mathematical algorithms used to perform the analyses (chapter 6).

An important characteristic (some would say a problem) of methods of paleostress analysis such as Angelier's is that they set up non-linear iterative equations and thus have extremely complex mathematical solutions. These equations are termed non-linear because, for each step in the iteration, the output variable is changed (just as it is in a linear equation) and this new output variable will result in different input variables (which does not happen in a linear equation).

3.2 Etchecopar's Method of Paleostress Analysis

In 1981, Etchecopar (Etchecopar, *et. al.*, 1981) developed a method of paleostress analysis similar to that being developed at approximately the same time by Angelier (Angelier, 1979; Angelier, *et. al.*, 1982). This method was similar to Angelier's in that it sought to minimize the angular deviation of the maximum shear stress directions from the slip directions for a chosen paleostress tensor σ on each fault plane in the population examined. The only substantial difference was the use by Etchecopar of a slightly different iterative algorithm for performing the non-linear least-squares inversion.

After corresponding with Arnaud Etchecopar of the Université des Sciences et Techniques du Languedoc in Montpellier, France, I obtained a copy of his program through Richard Plumb of Schlumberger Doll Research in Ridgefield, Connecticut. The program source code was written in FORTRAN and sent on a magnetic tape, the contents of which I transferred to SUNY Albany's VAX-8650 mainframe computer. After translating the program documentation from the original French into English (with the assistance of Debra Lenard -- a SUNY Albany linguistics major), I was able to compile and run the program for several fault populations. Unfortunately, all of the results obtained were no different than

those given by Angelier's program and I abandoned further testing of this method in favor of Angelier's.

3.3 Michael's Method of Paleostress Analysis

Michael (1984) derived a method of paleostress analysis which made a new initial assumption -- that the magnitudes of the shear stress σ_s on each of the fault planes in a population at the time of slip are similar. Michael claimed this assumption was justified by observing that the fault planes all experienced slip, therefore the absolute magnitudes of the shear stresses on all of the planes were similar and minimizing the difference $|\sigma_s| - 1$ for all of the fault planes will allow one to determine $|\sigma_s|$ for each fault plane. This allows a fairly simple linear inversion to solve for the stress tensor σ .

I wrote a Turbo Pascal version 3.01 computer program for performing paleostress analyses using Michael's method in May, 1987. Unfortunately, I found that this method gave inconsistent results for many types of fault populations -- especially those with faults which are close to being parallel to the principal stress axes. This is probably due to the fact that the shear stress on such planes becomes quite low relative to those planes at 45° to the principal stress axes (figure 3-1). Michael's method also does not work well with too few faults (what constitutes "too few" is not well-defined and is dependent upon the fault's orientations) and faults which all have a very similar orientation. This is because the inversion matrix becomes close to being a singular matrix and the calculated confidence limits become very large as a result (Michael, 1984).

C  lerier (1988) severely criticized Michael's method and stated that the shear stress assumption does not correspond to a realistic failure criterion and the only rational for using it is that it results in a simplification for the inversion by linearizing the equations. Michael

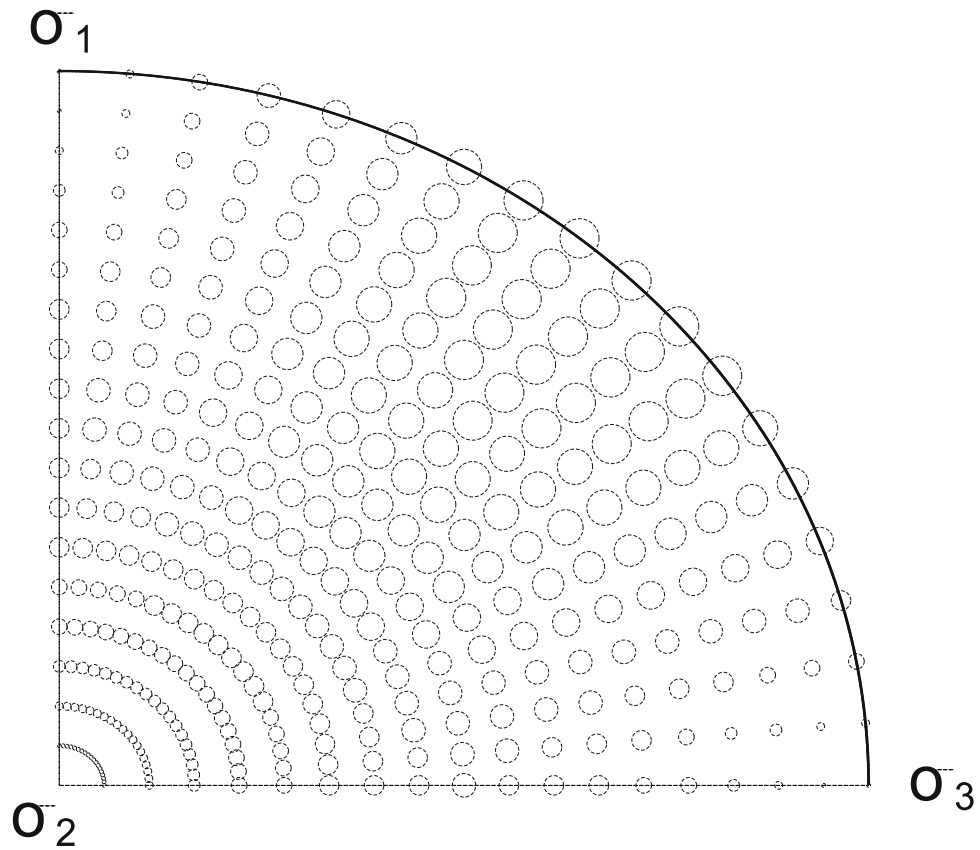


Figure 3-1 - Northeast quadrant of a lower-hemisphere stereographic projection showing poles to fault planes where the relative sizes of each pole reflect the relative magnitudes of the shear stresses on their associated planes. A Φ value of 0.5 and a ratio of the isotropic stress to the deviatoric stress of 4.5 (Michael, 1984) was used to calculate this data.

later modified his algorithm to use non-Gaussian rather than Gaussian statistics in the inversion (Michael, 1987a; Michael, 1987b) which improved the method but which also effectively rendered my program obsolete.

3.4 Gephart and Forsyth's Method of Paleostress Analysis

Also in 1984, Gephart and Forsyth proposed a slightly different method of paleostress analysis using earthquake focal mechanism data. This method begins by setting up a grid of points on a stereonet (Gephart recommends either 10° or 5° spacings) and then systematically orienting the most compressive principal stress axis σ_1 such that it is coincident with each of these grid points in turn while then systematically orienting the least compressive principal stress axis σ_3 such that it is coincident with all points 90° from σ_1 in turn and then varying the stress ratio Φ at each of the σ_3 locations. This obviously results in a very large number of stress tensors being defined for each fault population (dependent upon the number of grid points defined). For each stress tensor σ thus defined, the angle which the normal vector for each fault plane must be rotated through to have that fault's slip vector be consistent with the stress field is computed. The program seeks to minimize the sum of the squares of these angular divergences. The stress model which has the smallest sum is assumed to be the population's paleostress tensor.

I obtained a copy of this paleostress analysis program in February, 1989 from John Gephart at Cornell University. The program consisted of several subroutines all written in FORTRAN for the Macintosh II computer. A major characteristic of the program is that it is very computationally intensive and requires approximately a full 24-hour day to perform a search of 10,000 stress models for a relatively small data set of 20 focal mechanisms. While this is not too severe a limitation for a small number of analyses, a thorough testing of the

method would be extremely time consuming.

Gephart further modified this method and created a FORTRAN program called FMSI (an acronym for focal mechanism stress inversion) which has recently been submitted for publication (Gephart, 1990). This method does not differ much from earlier work and is primarily an attempt to speed up the computational procedures.

3.5 Recent Trends in Paleostress Analysis

In 1987, Reches derived a paleostress analysis method which used a linear least-squares inversion method rather than a non-linear one. This greatly simplifies the calculations involved by taking the Coulomb failure criterion into account (chapter 7). Célérier (1988) also derived mathematical algorithms for calculating paleostress tensors by introducing a frictional constraint upon the faults in the population. The advantage of being able to introduce an additional constraint is that the inverse problem equations become linear and thus much easier and faster to solve computationally.

The most recent papers on paleostress analysis are concerned with techniques to estimate absolute magnitudes for the principal stress axes σ_1 , σ_2 , and σ_3 rather than simply their relative magnitudes (expressed by the stress ratio Φ). To do this, two additional constraints must be placed upon the problem. Angelier (1989) attempted to do this by considering geologically-reasonable rupture and friction laws for the faults examined. Angelier also attempted to constrain the vertical stress by assuming it to be coincident with one of the three principal stresses and taking into account the thickness of the sedimentary overburden for faults in the Basin and Range Hoover Dam locality in Nevada-Arizona (Angelier, *et. al.*, 1985; Angelier, 1990).

Another important area of research is the attempt to relate fault geometry and kinematics to driving stresses. Dynamic (stress-based) and kinematic (strain-based) methods

of fault analysis are being used together in an attempt to learn more about the mechanics of faulting. A current leader in this field of study is Richard Allmendinger of Cornell University (Marrett and Allmendinger, 1990).

CHAPTER 4

PROBLEMS IN PALEOSTRESS ANALYSIS

Problems in computational methods of paleostress analysis using striated-fault populations arise in two areas -- in the gathering of data as input for the programs and in the fundamental simplifying assumptions made by these programs as they attempt to calculate a paleostress tensor. All of the paleostress analysis programs currently in use require, as numerical input, the orientation of each fault plane along with the fault's direction, and sense, of slip. Problems may arise in gathering this information from the field since inaccurate data may result in a program returning an incorrect paleostress tensor (sections 4.1 and 4.2). Paleostress analysis programs also make several simplifying assumptions about faults and the nature of faulting which may lead to resultant errors (sections 4.3 through 4.6). In order to understand the limitations of these programs, all of the assumptions inherent within them must be closely examined.

4.1 Measurement Errors

A careful field worker should be able to collect fairly accurate ($\pm 5^\circ$ or less) orientation data for a population of faults using only a compass and clinometer (Compton, 1962, p. 21-35; Ragan, 1985, p. 15). There are, however, conditions under which small measurement errors made while determining the strike of a fault plane or the trend of a lineation within that fault plane may become magnified.

When, in measuring the strike of a fault plane, the compass is not held exactly horizontal then a direction of strike will be measured other than the true strike. If the angular departure in degrees of this apparent strike from the true strike is denoted as ϵ_0 and the dip of the fault plane as δ , then the resultant strike error (ϵ_s) may be calculated by

$$\epsilon_s = \sin^{-1}[\tan \epsilon_0 / \tan \delta] \quad (1)$$

From this equation (Ragan, 1985, p. 16), it may be seen that for shallow-dipping fault planes, the resultant strike errors may be quite large given fairly small measurement errors (figure 4-1).

When measuring the trend of a lineation on a fault plane, it is a common practice to align the compass in the direction of a projection of that lineation onto a horizontal plane. If an error is made in this alignment, as measured by the angle ϵ , for a lineation of pitch r on a fault plane of dip δ , then the resultant trend error (ϵ_T) may be calculated by

$$\epsilon_T = \tan^{-1}\{[\tan(r+\epsilon) - \tan(r)]\cos \delta / 1 + [\tan(r)\tan(r+\epsilon) \cos^2 \delta]\} \quad (2)$$

From this equation¹, it may be seen that for lineations with large pitch angles on steeply-dipping fault planes, a large trend error for those lineations may occur (figure 4-2). In addition, the maximum error associated with $(r-\epsilon)$ is less than it is for $(r+\epsilon)$ and repeated measurements will not be symmetrically distributed around the true trend (Ragan, 1985, p. 56).

Given the above information, it would be useful to know how sensitive paleostress analysis programs are to small variations in the orientations of the fault planes and their slip directions. If small measurement errors gave significantly different results for the calculated paleostress tensors, these programs would lose some of their usefulness given geologically realistic fault population data.

¹ Equation 4.8 in Ragan (1985, p. 56) is given as: $\tan \epsilon_T = [\tan(r+\epsilon) - \tan \delta]\cos \delta / 1 + [\tan r \tan(r+\epsilon)\cos^2 \delta]$ which is incorrect and has been corrected here in equation (2).

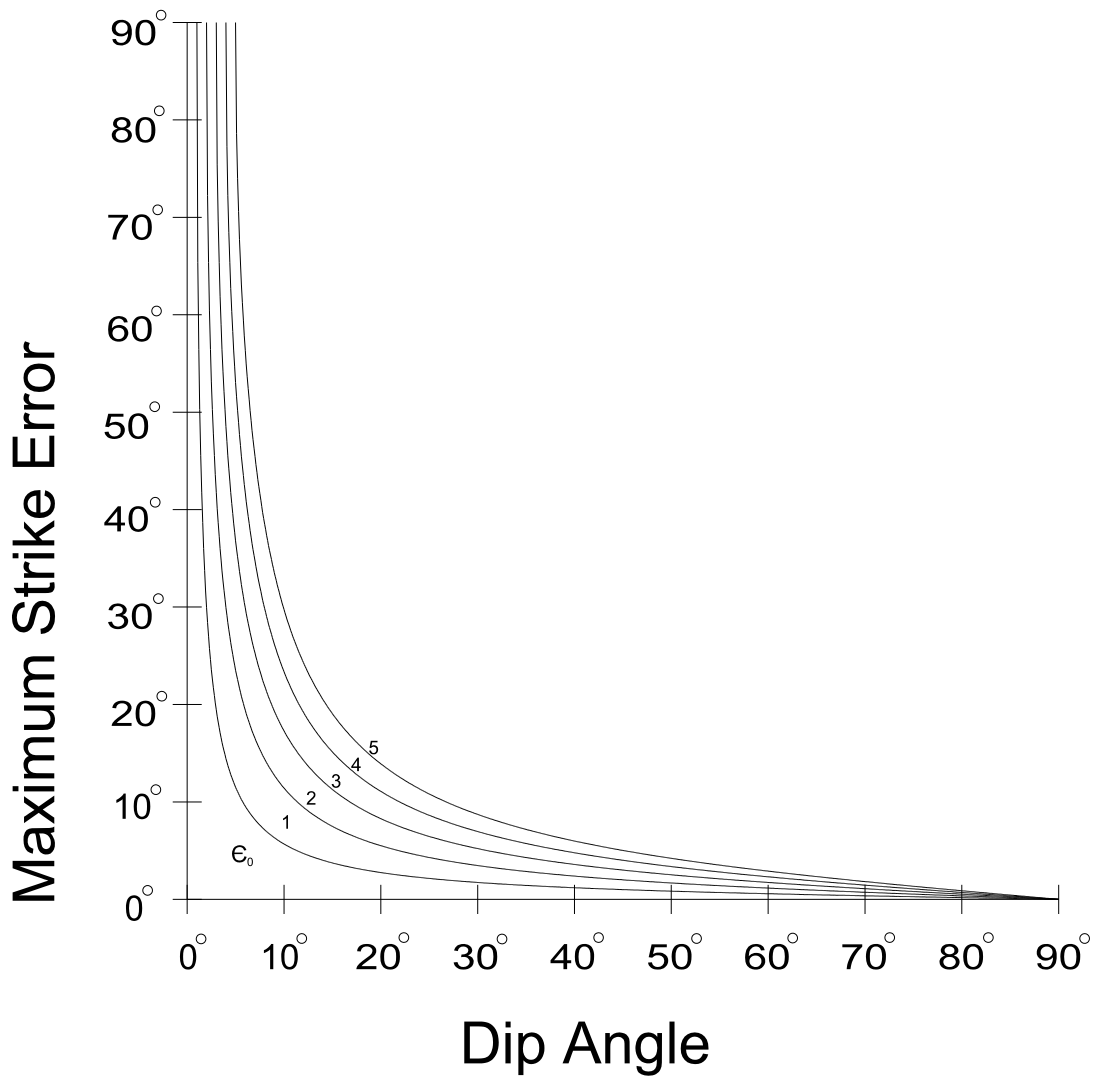


Figure 4-1 - Graph of the maximum strike error for a fault plane arising from a strike measurement error (ϵ_0) of 1° to 5° as a function of the dip of the fault plane (figure modified from Ragan, 1985, p. 16).

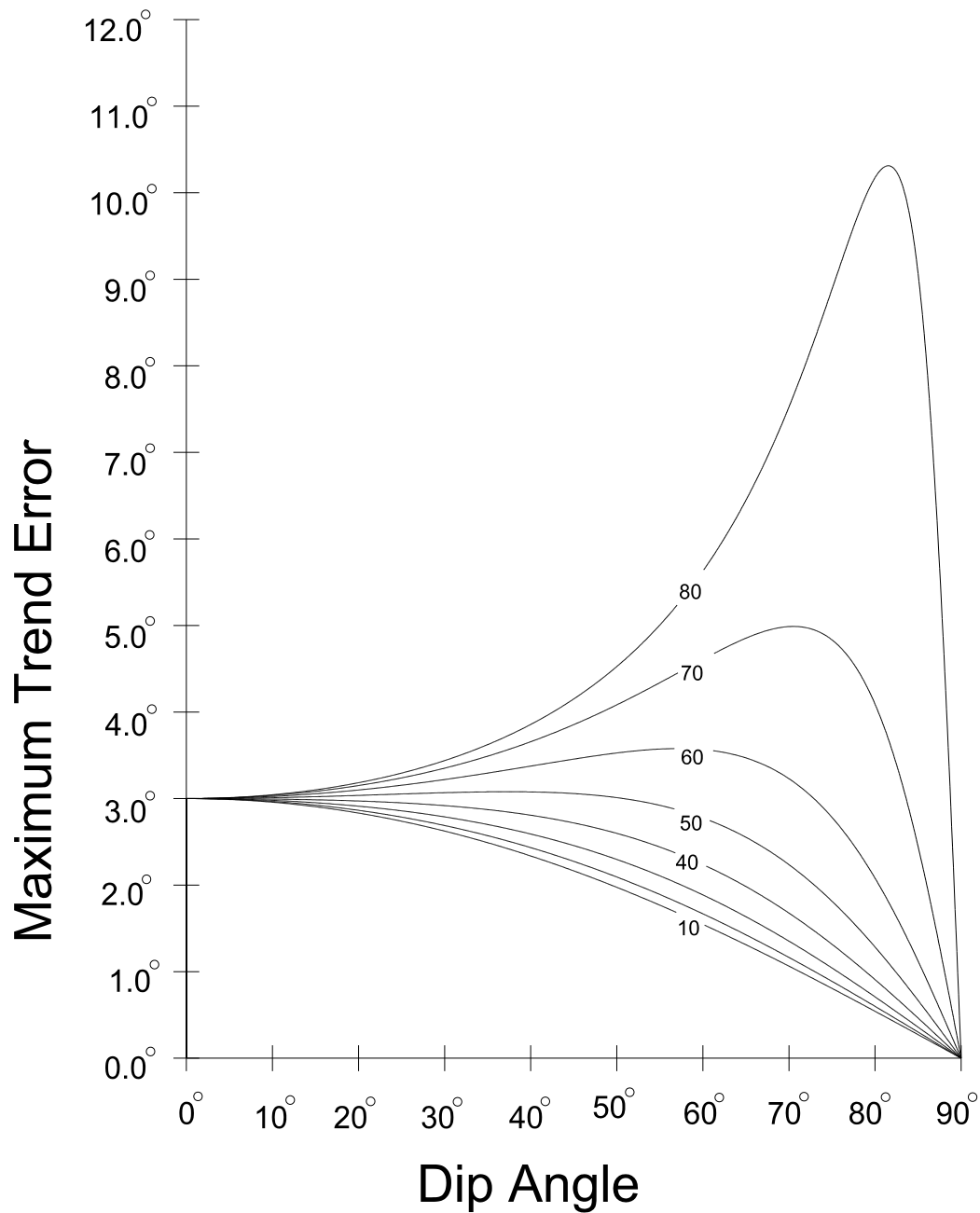


Figure 4-2 - Graph of the maximum trend error of a slickenline on a fault plane arising from a trend measurement error (ϵ) of 3° as a function of the pitch of the slickenline (10° to 80° in 10° increments) and the dip of the fault plane (figure modified from Ragan, 1985, p. 57).

4.2 Determining Fault Slip

The direction of slip on a fault is commonly obtained by examining lineations known as slickenlines on the fault's surface (Tjia, 1964; Means, 1987). Slickenlines are linear striations, or grooves, resulting from friction or shear strain on fault surfaces and indicating the last direction of movement on that fault (Fleuty, 1975). It is possible for fault surfaces to contain more than one set of slickenlines and careful examination may be needed to distinguish the latest slip direction from earlier ones. Also, slickenlines are axial data (Cheeney, 1983, p. 10-11), giving two possible slip directions 180° apart, and some other criteria are thus needed to establish the sense of slip of the fault (*i.e.* which end of a slickenline points in the direction of movement of the opposing fault block). The best sense-of-slip indicators are geometric or physical lines which have been offset by faulting (Davis, 1984, p. 268; Ragan, 1985, p. 92-93). These features must be used cautiously as slip direction indicators, however, since they record the net slip on the fault which may be the result of several distinct slip events with differing slip directions (figure 4-3).

Before 1958, it was considered axiomatic that step-like features on fault planes could be used as sense-of-slip indicators (Hobbs, *et. al.*, 1976, p. 304). By running your hand over the fault surface, the direction of least resistance (*i.e.* the direction where your hand jumps over the risers of the steps rather than slamming into them) is the direction of movement of the opposing fault block (figure 4-4). A problem with this method is that other workers have since claimed that steps are an unreliable sense-of-slip indicator since steps with an incongruous sense-of-slip are known from the field and the laboratory (Paterson, 1958; Tjia, 1964; Riecker, 1965; Tjia, 1967; Norris and Barron, 1969; Gay, 1970; Hobbs, *et. al.*, 1976, p. 303-305). In 1969, Norris and Barron distinguished between two different types of steps found on fault planes -- accretion steps and fracture steps. Accretion steps are formed by the adhesion of mineralized gouge onto the slip surface and fracture steps are steps which have

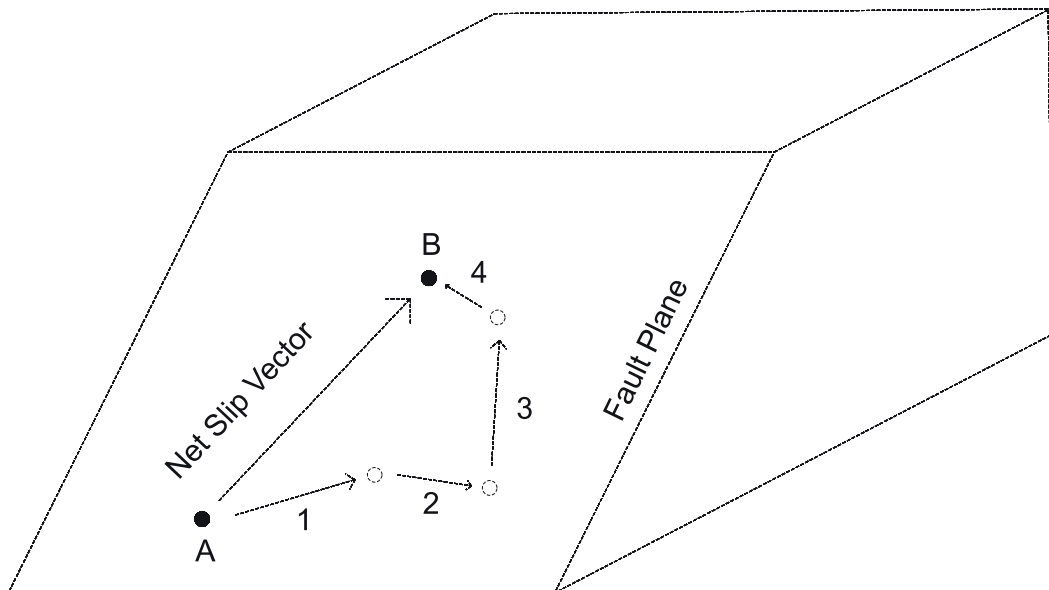


Figure 4-3 - Diagram demonstrating how the net slip vector on a fault plane may be the result of several distinct slip events with differing slip directions (slip vectors 1 through 4).

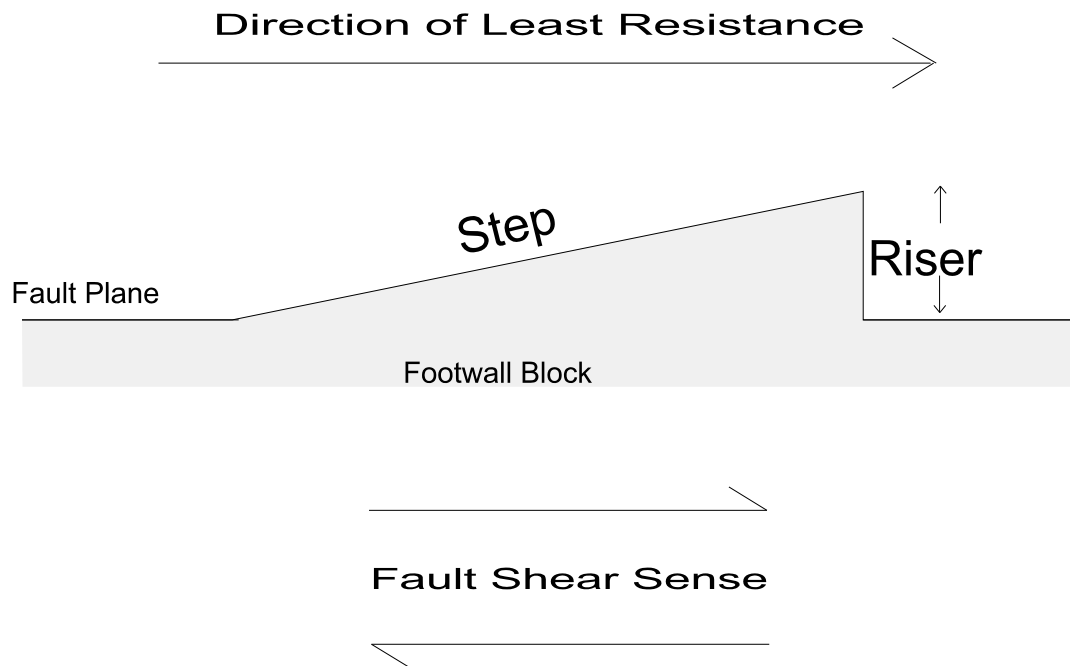


Figure 4-4 - Cross-sectional view of a fault plane showing how steps may be used as sense-of-slip indicators on fault surfaces. The direction of least resistance is taken to be the direction of motion for the opposing fault block.

been cut into the solid rock. Accretion steps are formed as the slip surface is parted with the step's risers facing preferentially in the direction of movement of the opposing block. Accretion steps are therefore usually congruous with the fault's sense-of-slip. Fracture steps may face in either direction and thus may give either a congruous or an incongruous sense-of-slip. Durney and Ramsay (1973) claimed that a third type of steps formed from layers of fibrous minerals on the slip surface always gave a congruous sense-of-slip. Therefore, with care, steps may be used as sense-of-slip indicators on some faults (Rod, 1966; Tjia, 1967; Tjia, 1972; Norris and Barron, 1969; Durney and Ramsay, 1973; Petit, *et. al.*, 1983; Petit, 1987).

Other possible sense-of-slip indicators are structural features such as prod marks, crescentic gouges, pluck marks, chattermarks, protuberances resembling *roches moutonnées*, spalls, bruised step risers (Tjia, 1967; Tjia, 1972; Gamond, 1983), drag folds (Davis, 1984, p. 270-272; Hobbs, *et. al.*, 1976, p. 305-306), *en échelon* tension gashes, and the orientation of any secondary shear fractures (Gamond, 1983; Petit, *et. al.*, 1983; Hancock, 1985; Gamond, 1987; Petit, 1987). Fault gouge (Byerlee, *et. al.*, 1978) and slickensides (Lee, 1990) may also contain microstructural sense-of-slip indicators when examined petrographically.

When collecting fault population data for paleostress analysis programs, a recommended final check on the sense-of-slip data is to see whether they are all consistent with one another -- a single reverse fault in a population of normal faults should signal caution since it is unlikely to belong to the same stress field as the others.

4.3 Fault Morphology

An implicit assumption in paleostress analysis is that faults are planar (*i.e.* they may be described by a unique strike, dip, and dip direction). In reality, however, faults are not perfectly planar on any scale (Scholz, 1990, p. 146-147).

Most faults show a degree of curvature in dip sections or in plan view (Mandl, 1988,

p. 24). Listric (shovel-shaped) normal and thrust faults are extreme examples of this and are quite common in areas of thin-skinned tectonics. Subsurface stress distributions have been used to account for the development of listric faults (Hafner, 1951; Jaroszewski, 1984, p. 215-217) and factors which may affect the curvature of a developing fault include anisotropies in the shearing strength of the rock mass, compaction by the overburden, abnormally high pore fluid pressures, and changes in the tectonic stress field (Mandl, 1988, p. 24). Faults may also be curved, or wavy, on a smaller scale (Gamond, 1983; Jaroszewski, 1984, p. 218; Hancock, 1985) due primarily to anisotropies of the rock mass or changes in the tectonic stress field during their formation.

Curved faults will yield different strike and dip orientations, depending upon where on the fault's surface the measurements are made, resulting in problems for paleostress analysis programs similar to those presented by measurement errors. Another problem with curved faults (dealt with in more detail in section 4.4) is that fault curvature, more so than the maximum resolved shear stress, may determine the fault's slip direction when the fault is reactivated.

Another characteristic of faults is their discontinuity. Field studies have shown that faults, at all scales, are discontinuous and consist of numerous discrete segments (Wallace, 1973; Segall and Pollard, 1980; Mandl, 1987; Mandl, 1988, p. 43-47; Scholz, 1990, p. 151). Discontinuous faults have been modelled as arrays of right- or left-stepping pairs of *en échelon* segments (Segall and Pollard, 1980) which have pronounced differences in mechanical behavior from continuous faults and which influence their slip directions when subjected to a given stress field.

In 1970, Tchalenko demonstrated that the formation and evolution of shear zones involved identical characteristic stages independent of their size. Shear zones were thus shown to be self-similar from the scale of shear-box experiments (tens of millimeters) to earthquake-producing faults (hundreds of meters). Self-similarity at different scales is an important

characteristic of a class of fractals (Mandelbrot, 1977; Mandelbrot, 1983), and several workers have since demonstrated that fault surfaces may be described by fractal geometry (Brown and Scholz, 1985; Scholz and Aviles, 1986; Okubo and Aki, 1987; Power, *et. al.*, 1987; Scholz, 1990, p. 147).

Faults whose surface roughness is best described by a fractal, or Hausdorff-Besicovitch, dimension may be used in paleostress analysis if the orientation of the fault's slip plane, rather than the fault plane itself, is used (Scholz, 1990, p. 147). The slip plane is defined as the idealized plane upon which the slip vector lies and may be viewed as the regional mean of the actual fault plane (figure 4-5). Determining this slip plane from a small exposure of the fault plane in an outcrop may not always be possible.

Antithetic faults also pose a problem for paleostress analysis. Antithetic faults (Jaroszewski, 1984, p. 212; Mandl, 1988, p. 47) are minor faults with a sense-of-shear which is opposite to the general direction of an externally imposed shear. When movement occurs on a normal listric fault, for example, the increased curvature of the upper part of the fault causes the fault walls to separate. Second-order antithetic faults arise to accomodate this change in geometry. Since these faults arise due to a secondary stress field developing around the main fault, careful field work must be performed to be sure that antithetic faults are not included in fault populations used for paleostress analysis.

Finally, there are a special class of faults with a rotational component of slip (Donath, 1962; Davis, 1984, p. 266; Jaroszewski, 1984, p. 146; Ragan, 1985, p. 89; Mandal and Chakraborty, 1989; Twiss and Gefell, 1990). Such faults do not have a constant slip direction, or sense-of-slip, and cannot be used in paleostress analysis programs (figure 4-6).

4.4 The Relationship of Shear Stress to Fault Slip Directions

A fundamental assumption of all paleostress analysis programs is that fault slip always

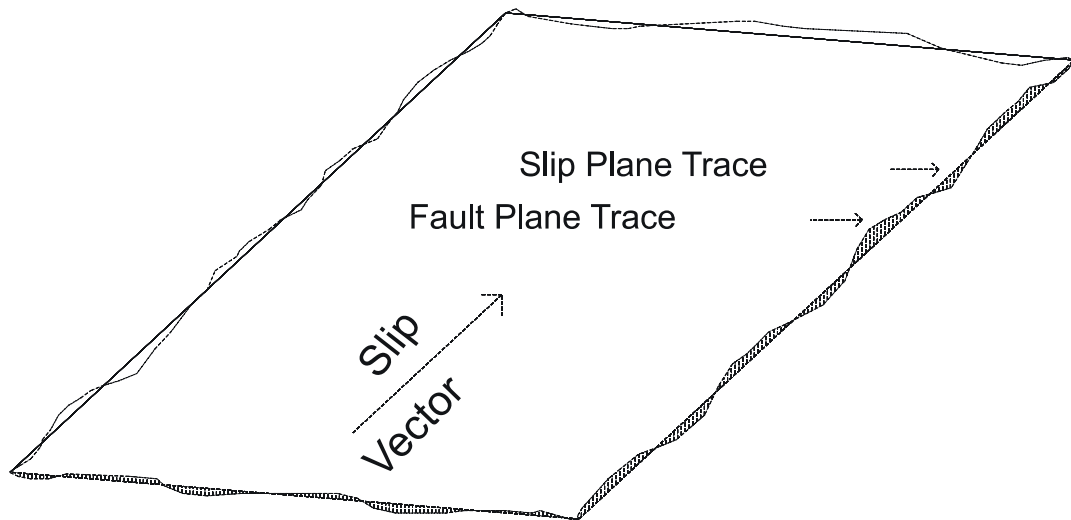


Figure 4-5 - Diagram demonstrating the difference between a fault's slip plane and the actual fault surface which may not be planar (figure modified from Scholz, 1990, p. 148).

occurs in the maximum resolved shear stress direction on the fault plane (Carey and Brunier, 1974; Armijo and Cisternas, 1978; Angelier, 1979; Etchecopar, *et. al.*, 1981; Angelier, *et. al.*, 1982; Vasseur, *et. al.*, 1983; Angelier, 1984; Gephart and Forsyth, 1984; Michael, 1984; Reches, 1987; Angelier, 1989). It may be shown, however, that under certain conditions faults may not always slip in the direction of the maximum resolved shear stress.

For fault surfaces with long-wavelength asperities (*i.e.* wavy or curved faults), sliding will occur at some small angle ϕ to a slip plane with a normal force of N , a shearing force of S , and a coefficient of friction of μ (Jaeger and Cook, 1979, p. 55; Scholz, 1990, p. 52). Two equations may be derived relating N and S to the normal force (n) and the shear force (s) acting upon the ramp of the asperity as follows (figure 4-7)

$$n = N \cos(\phi) + S \sin(\phi) \quad (3)$$

and

$$s = S \cos(\phi) - N \sin(\phi) \quad (4)$$

Assuming a Coulomb failure criterion such that

$$s = \mu n \quad (5)$$

the following equation results upon the substitution of equations (3) and (4) into equation (5)

$$S \cos(\phi) - N \sin(\phi) = \mu [N \cos(\phi) + S \sin(\phi)] \quad (6)$$

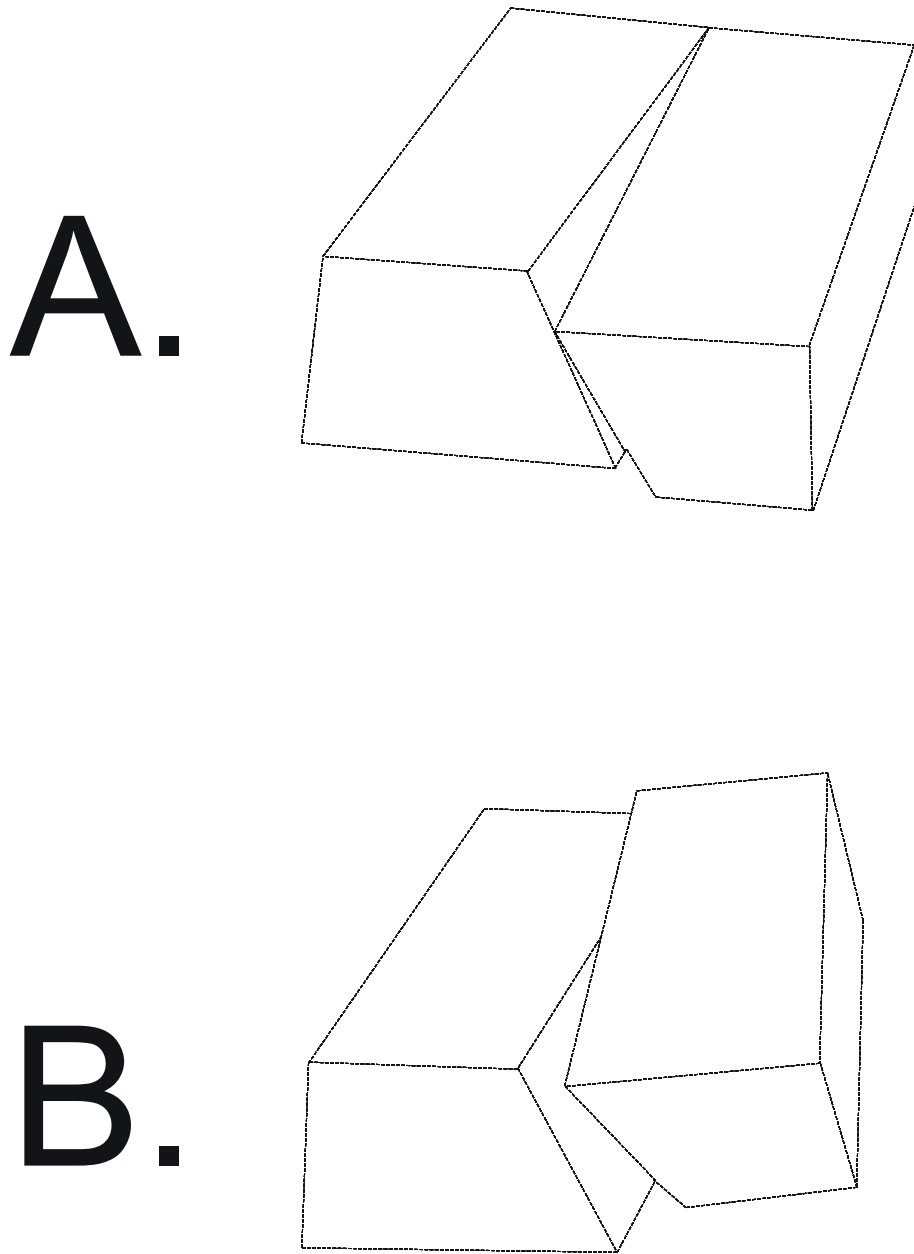


Figure 4-6 - Two fault types with a rotational component of slip. **A.** Hinge faults and **B.** Pivotal faults (figure modified from Ragan, 1985, p. 89).

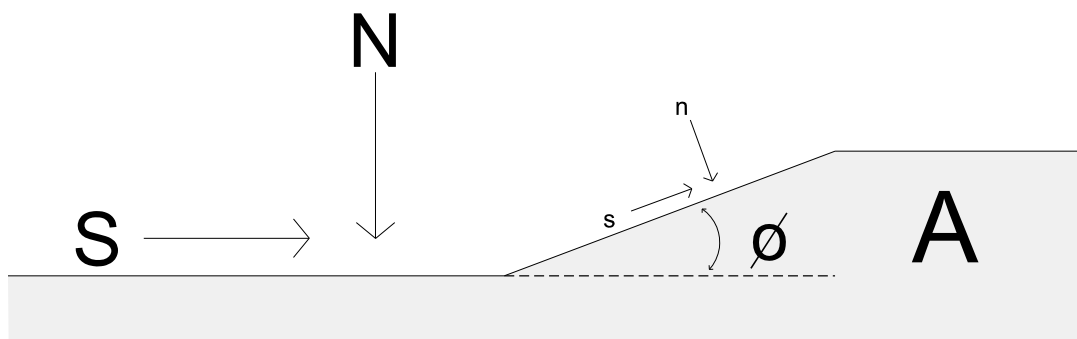


Figure 4-7 - Cross-sectional view of a fault surface parallel to shearing with an asperity A creating an angle ϕ with the fault subjected to a total shearing force of S and a total normal force of N. The ramp of asperity A is subjected to the resolved normal force (n) and shearing force (s).

Multiplying equation (6) by $[1 / \cos(\phi)]$ and algebraically rearranging yields

$$S = [\mu + \tan(\phi)] / [1 - \mu \tan(\phi)] N \quad (7)$$

which reduces to

$$S = \mu N \quad (8)$$

when there are no asperities in the shearing direction ($\phi = 0$). Therefore, shearing on a fault surface with asperities will require a larger shearing force (S) than shearing on a fault surface without asperities for sufficiently small values of ϕ . The difference is a result of the increase in the frictional coefficient term of equation (8) from μ to $[\mu + \tan(\phi)] / [1 - \mu \tan(\phi)]$ of equation (7) provided that $\phi < \tan^{-1}(1 / \mu)$ since at $\phi = \tan^{-1}(1 / \mu)$ the equation changes sign.

Assume an undulating fault plane (figure 4-8) such that

$$S = \mu' N \quad (9)$$

represents shearing in the maximum resolved shear stress direction at some acute angle α to the long axis of the undulations where

$$\mu' = [\mu + \tan(\phi)] / [1 - \mu \tan(\phi)] \quad (10)$$

The equation

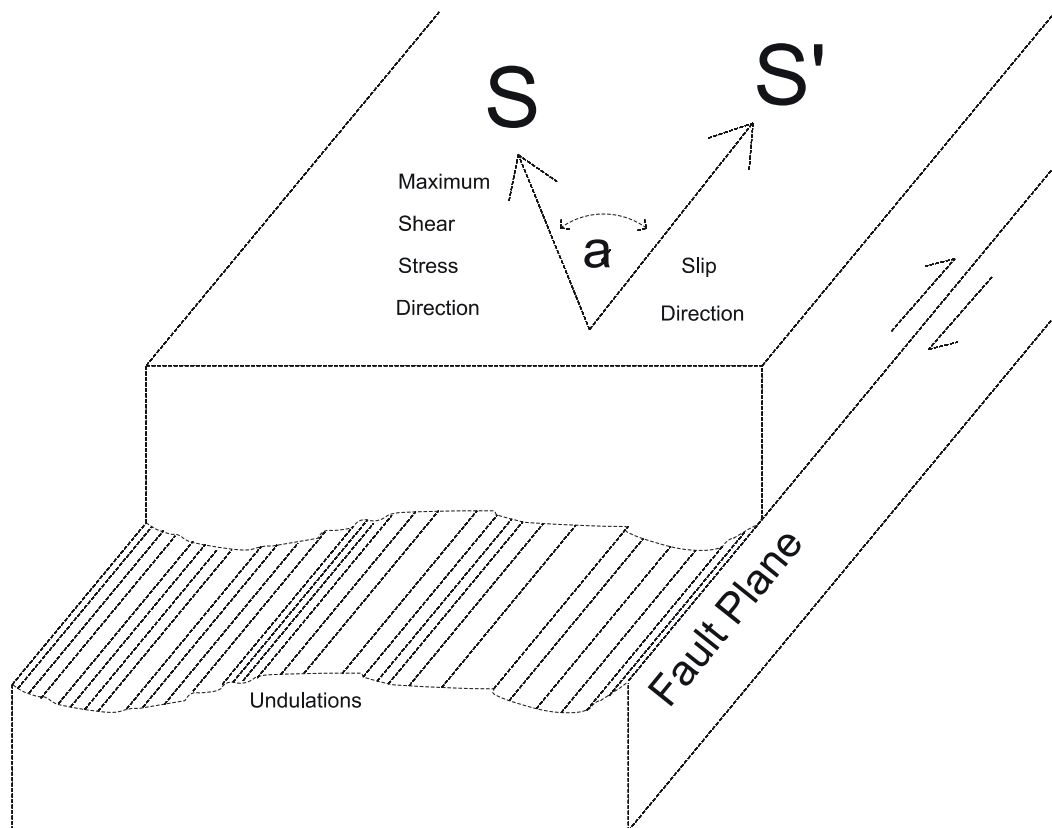


Figure 4-8 - An undulating fault plane with the maximum resolved shear stress direction (vector S) making an angle α with the slip direction which corresponds to the long axis of the undulations (vector S'). It is assumed that only sliding parallel to the long axis of the undulations encounters no asperities.

$$S \cos(\alpha) = \mu N \quad (11)$$

or

$$S = \mu N / \cos(\alpha) \quad (12)$$

will then represent shearing parallel to the long axis of the undulations.

Setting equation (9) equal to equation (12) yields

$$\mu' N = \mu N / \cos(\alpha) \quad (13)$$

which reduces to

$$\mu' = \mu / \cos(\alpha) \quad (14)$$

Substituting equation (10) into equation (14) yields

$$[\mu + \tan(\phi)] / [1 - \mu \tan(\phi)] = \mu / \cos(\alpha) \quad (15)$$

which reduces, through algebraic manipulation, to

$$\phi = \tan^{-1} [\mu - \mu \cos(\alpha)] / [\cos(\alpha) + \mu^2] \quad (16)$$

Assuming a geologically reasonable coefficient of friction (μ) of 0.85 for upper crustal rocks (Barton and Choubey, 1977; Byerlee, 1978), equation (16) may be rewritten as

$$\phi = \tan^{-1} [0.85 - 0.85 \cos(\alpha)] / [\cos(\alpha) + 0.7225] \quad (17)$$

and the relationship between the angles α and ϕ may be graphed as α varies from 0° to 90° (figure 4-9).

From the above, it may be seen that non-planar faults (*i.e.* most faults) with favorably-aligned asperities do not always slip in the direction of their maximum resolved shear stress.

4.5 Faulting Phase Differentiation

An important problem in paleostress analysis using striated-fault populations is determining if each of the faults in the population were activated within a single stress field. Careful field work can often distinguish the relative ages of faults using cross-cutting relationships but there is no guarantee that contemporaneously-formed faults all belong to the same faulting phase since a fault is created at one time and may then be reactivated many times during its existence. Paleostress analysis programs assume that faulting will occur on pre-existing planes of weakness (Angelier, 1979; Etchecopar, *et. al.*, 1981; Angelier, *et. al.*, 1982; Vasseur, *et. al.*, 1983; Angelier, 1984; Gephart and Forsyth, 1984; Michael, 1984; Reches, 1987; Angelier, 1989). Therefore, faults of widely disparate initiation ages may be reactivated when subjected to a given paleostress field. Observing geometric relationships between faults and the presence of any successive striations of different attitudes on faults indicates that two or more paleostress fields have been recorded but, in general, distinguishing which faults have been reactivated at the same time is a difficult problem which has not been widely addressed.

In the past ten years, numerical algorithms have been proposed which separate faults into different faulting phases (Angelier and Manoussis, 1980; Huang and Angelier, 1987;

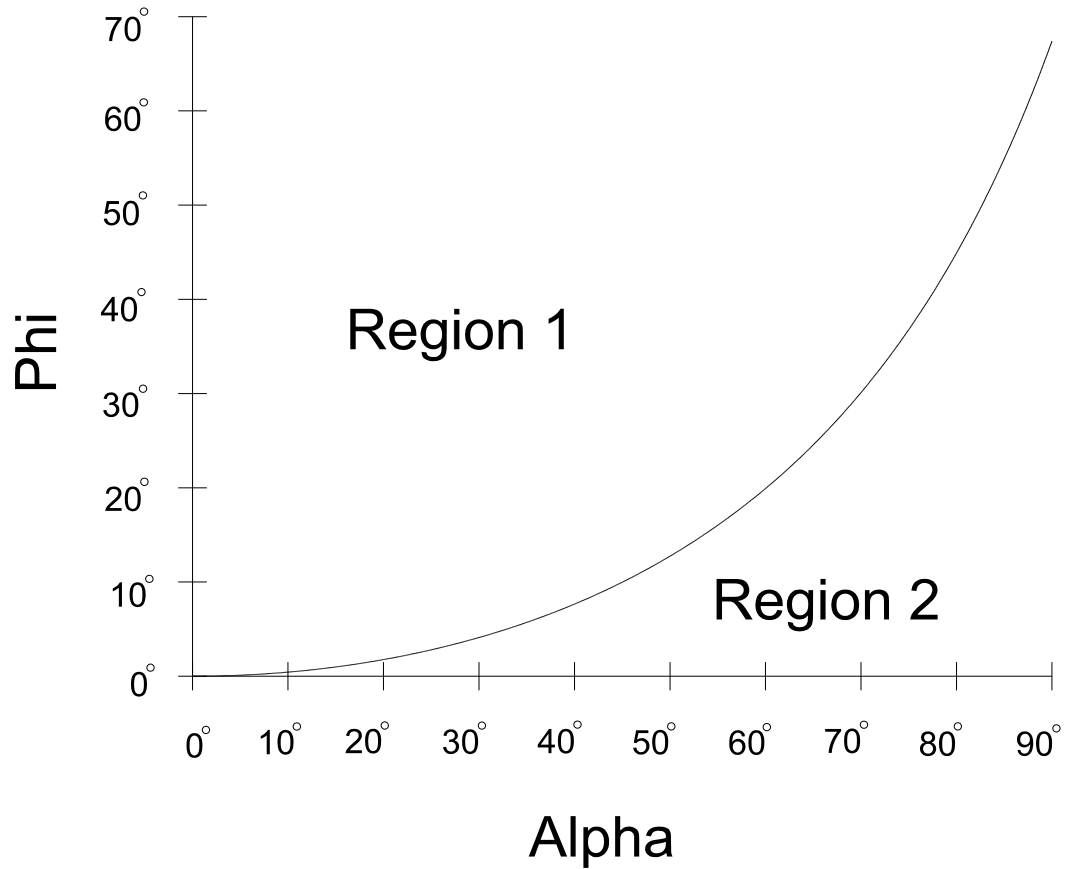


Figure 4-9 - Graph of the change in alpha (α) from 0° to 90° for differing angles of phi (ϕ).

Region 1 contains the angles of α and ϕ for which sliding will occur parallel to the long axis of the undulations and region 2 contains the angles of α and ϕ for which sliding will occur parallel to the maximum resolved shear stress direction. For small angles of α , even very small long-wavelength asperities will act as barriers to slip in the maximum resolved shear stress direction.

Galindo-Zaldivar and Gonzalez-Lodeiro, 1988; Huang, 1988). Unfortunately, these methods all rely on the same computational methods used to determine paleostress axes from fault populations (chapters 6 and 7). Separating faults into homogeneous faulting phase subsets with these programs will therefore guarantee an excellent fit for a paleostress tensor when these subsets are run through an analysis program. The results may not be very useful, however, since the subsets are essentially created by how well they will constrain a paleostress tensor.

4.6 Determining a Paleostress Tensor

Paleostress analysis programs attempt to define a paleostress field which is consistent with a population of striated faults. The implication of this is that a single, unique paleostress tensor is recorded in the faulting rocks at a specific point in time. A major problem with this implication is that stress fields are not always static -- they may evolve with time (Mandl, 1988, p. 15-16).

Consider two thrust faults situated within a stress field where the least compressive principal stress axis (σ_3) is vertical and constant in magnitude, the intermediate principal stress axis (σ_2) is horizontal and constant in magnitude, while the most compressive principal stress axis (σ_1) is horizontal and steadily increasing in magnitude. If the two faults have a strike direction perpendicular to σ_1 and differ only in their dip angles, it is quite possible for them both to be activated by essentially the same stress field at two different times and with two different slip directions. The different slip directions arise since, according to Bott (1959), the slip direction is a function of the ratios of the principal stresses and this ratio changes as σ_1 increases in magnitude (figure 4-10).

Faults may also totally switch style during a single tectonic event (Mandl, 1988, p. 15-

16). As the principal stress axes increase or decrease in magnitude, they may exchange orientations (*i.e.* a horizontal σ_3 increases in magnitude until it becomes σ_2 and then σ_1 while σ_2 and σ_1 become σ_3 and σ_2 respectively). As the principal stress axes change orientations, faulting styles may switch between normal, wrench, or thrust faults.

Another way in which faults may change in style is by gravitational re-equilibration. A thrust fault may, when the horizontal compressive stress begins lessening, behave like a normal fault (Beutner, 1972; Jaroszewski, 1984, p. 172).

According to Edelman (1989), while reasonable estimates may be made for paleostress states using small faults, large faults are indicative of large, finite, nonelastic strains and there are no constitutive equations relating stress and permanent strain. If the strain rate, coaxiality, and viscosity tensor were known for some instant in time in the deformation history of a rock mass, calculation of the stress would be trivial and contain the propagated errors of the other measurements. In other words, a single paleostress determination is a derived, unverifiable quantity. This is important since paleostress analysis programs are often used to determine the paleostress orientations for very large-scale faults such as the San Andreas and Coalinga fault systems (Michael, 1987b; Jones, 1988).

4.7 Discussion

To evaluate the performance of paleostress analysis algorithms, I created artificial fault populations using the same initial assumptions that are used by the programs. The artificial fault populations consist of perfectly planar normal faults with an exact strike and dip situated within a static stress field with the principal stress axes σ_1 , σ_2 , and σ_3 having orientations of north, up, or east. The slip vectors for each fault in the population are calculated using the same initial assumptions that paleostress analysis programs use when calculating paleostress tensors -- Bott's formula (Bott, 1959) is utilized to find the maximum

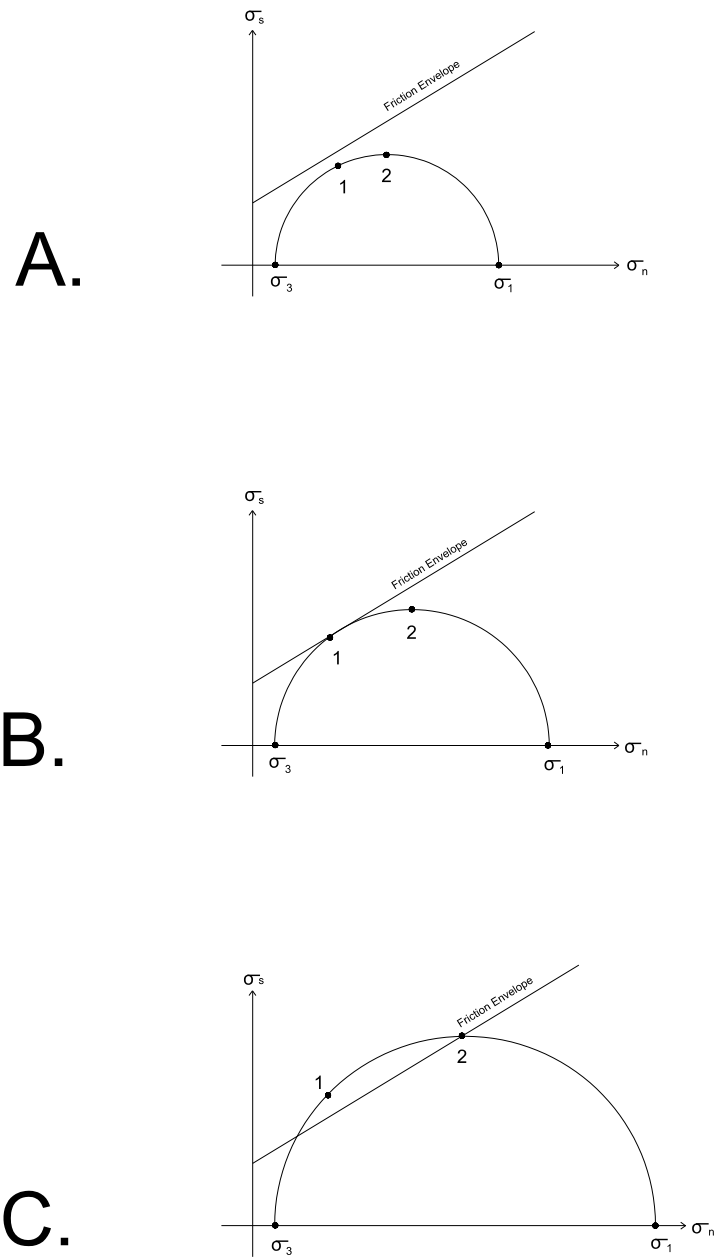


Figure 4-10 - Mohr circles demonstrating how two faults of slightly different orientations (graphed as 1 and 2 on the diagrams) will slip at different times as σ_1 increases. **A.** No slip occurs initially. **B.** Fault 1 begins to slip as σ_1 increases. **C.** Both faults 1 and 2 slip as σ_1 reaches a maximum value.

shear stress direction and this is assumed to be identical to the fault's slip direction. Running these fault populations through a paleostress analysis program should thus give the exact orientations of the principal stress axes used to create them. If the paleostress analysis programs examined return different results, the magnitude of their errors may be examined.

Systematically altering the orientations of the individual faults within the artificial fault populations allows one to test the sensitivity of the various paleostress analysis programs. As an example, increasing the dip of one of the fault planes in the population by a few degrees may be viewed as equivalent to using a real population where the dip of one of the faults is incorrect -- due either to a measurement error or possibly to the fact that the fault surface is non-planar. By placing a new fault plane into a population with an arbitrarily chosen orientation for its normal and slip vectors, the sensitivity of the paleostress analysis programs to the accidental inclusion of faults from separate tectonic phases may be examined.

Through careful selection of the artificial fault populations used to test the paleostress analysis programs, the effect of the various problems in paleostress analysis discussed in this chapter may be demonstrated and even quantified to some extent. That is the aim of this thesis.

CHAPTER 5

GENERATING ARTIFICIAL FAULT POPULATIONS

To develop synthetic data sets for testing computational methods of paleostress analysis, I wrote a Pascal program to calculate the slip vectors and the shear stress to normal stress ratios on any arbitrarily oriented fault plane situated within a stress field of varying principal stress magnitudes. This allowed me to derive artificial data sets of faults and their slip directions for a given stress tensor. A complete listing of this program is given in Appendix C.

5.1 Theory

It can be shown that for a given stress tensor, the total stress acting upon a plane in any orientation within that stress field may be calculated by a relationship described by Means (1976, p. 103) as Cauchy's formula, which may be written in tensor notation as

$$T_i = \sigma_{ij}l_j \quad (1)$$

where T_i represents the north, up, or east components of the total stress vector, l_j represents the north, up, or east direction cosines (Cheeney, 1983, p. 112), and σ_{ij} represents each of the nine components of the stress tensor. The north, up, and east direction cosines are defined here as the cosines of the angles between the fault plane normal vector and the north, up, and east coordinate axes which will correspond, for purposes of this section, to the three principal stresses σ_1 , σ_2 , and σ_3 respectively (figure 5-1).

When the direction cosines are calculated from the orientation of the normal vector to the fault plane, Cauchy's formula may be used to determine the components of the total

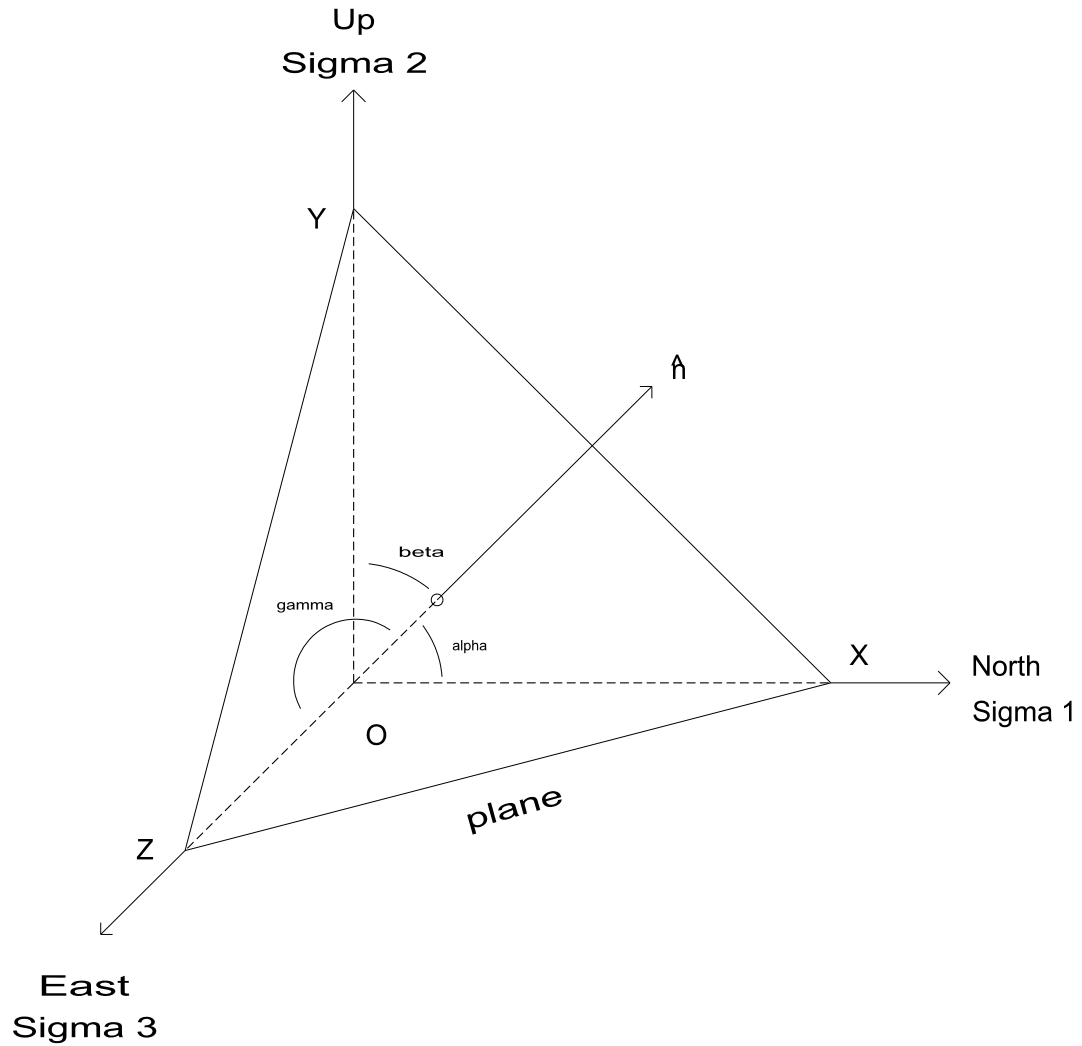


Figure 5-1 - Relationship between a plane XYZ situated within a geographic coordinate system where the north, up, and east coordinate axes correspond to the principal stress axes σ_1 , σ_2 , and σ_3 respectively. The direction cosines are the cosines of the angles between the plane's normal vector (n) and the three coordinate axes (*i.e.* $l_1 = \cos(\alpha)$, $l_2 = \cos(\beta)$, and $l_3 = \cos(\gamma)$).

stress vector acting upon that fault plane. Since the principal stress axes have the same orientation as the north, up, and east coordinate axes, the shear stress terms vanish from the stress tensor and Cauchy's formula (equation 1) reduces to

$$\begin{aligned} T_1 &= \sigma_1 l_1 \\ T_2 &= \sigma_2 l_2 \\ T_3 &= \sigma_3 l_3 \end{aligned} \tag{2}$$

where the 1, 2, and 3 components are the north, up, and east components respectively.

To calculate the normal stress and shear stress magnitudes acting upon the fault plane, the angle between the total stress vector and the normal vector to the fault plane must be found. A simple relationship exists between any two vectors in space and the angle (θ) between them such that

$$\theta = \cos^{-1}[(\mathbf{a} \cdot \mathbf{b}) / (\|\mathbf{a}\| \|\mathbf{b}\|)] \tag{3}$$

where $\mathbf{a} \cdot \mathbf{b}$ is the inner, or dot, product and $\|\mathbf{a}\|$ and $\|\mathbf{b}\|$ are the magnitudes of vectors \mathbf{a} and \mathbf{b} respectively (Marsden and Tromba, 1981, p. 20). The inner product between any two vectors is defined as

$$\mathbf{a} \cdot \mathbf{b} = a_1 b_1 + a_2 b_2 + a_3 b_3 \tag{4}$$

and the magnitude of any vector is defined as

$$\|\mathbf{a}\| = (a_1^2 + a_2^2 + a_3^2)^{1/2} \tag{5}$$

Once the angle between the two vectors has been calculated, it can be shown by simple trigonometry (figure 5-2) that the normal stress (σ_n) and shear stress (σ_s) magnitudes are

$$\sigma_n = \|\mathbf{T}\| \cos(\theta) \quad (6)$$

$$\sigma_s = \|\mathbf{T}\| \sin(\theta) \quad (7)$$

Once the normal stress and shear stress magnitudes acting upon the fault plane are calculated, the fault plane's shear stress to normal stress ratio (σ_s / σ_n) may be determined.

5.2 Deriving Bott's Formula

For a fault plane of any orientation within a stress field, there will be a maximum shear stress direction along which slip may occur. Bott (1959) showed that different relative magnitudes of the principal stresses will result in different directions of maximum shear stress. If the orientation of the fault plane relative to the principal stress axes is known, the relative magnitudes of the principal stresses can be used to determine the maximum shear stress direction within the fault plane.

To derive this equation, assume a plane XYZ of unit area situated within a north, up, and east coordinate system (figure 5-3). The principal stress axes σ_1 , σ_2 , and σ_3 and their associated direction cosines l_1 , l_2 , and l_3 coincide with the north, up, and east directions respectively. Since the XYZ plane is of unit area,

$$l_1^2 + l_2^2 + l_3^2 = 1 \quad (8)$$

and l_1 is the area of the OYZ plane, l_2 is the area of the OXZ plane, and l_3 is the area of the

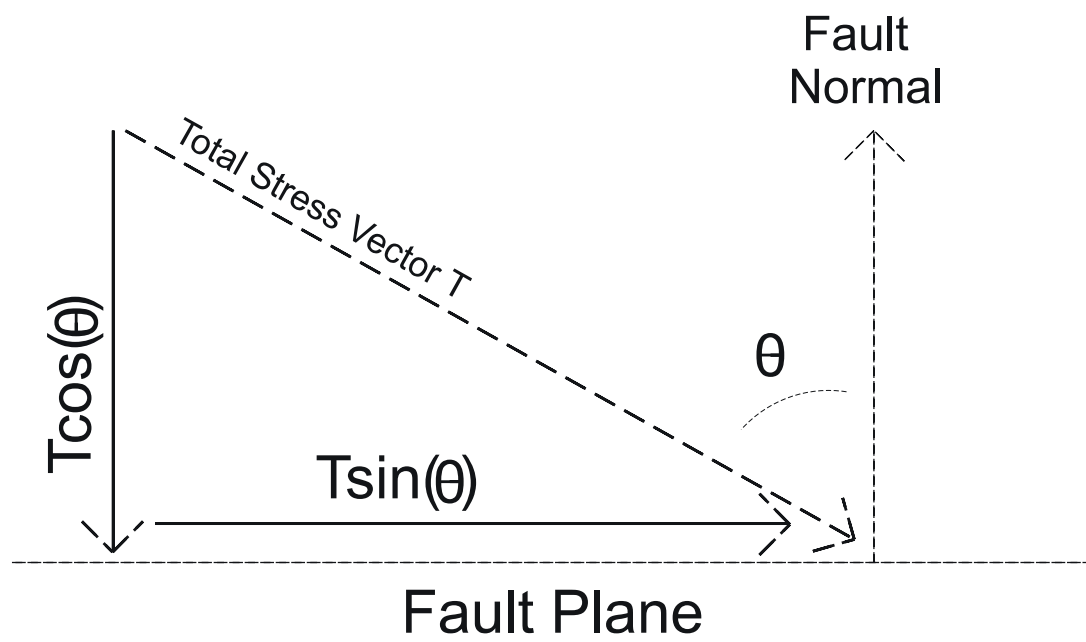


Figure 5-2 - Determining the shear stress and normal stress magnitudes from the angle between the total stress vector acting upon a fault plane and the fault plane's normal vector.

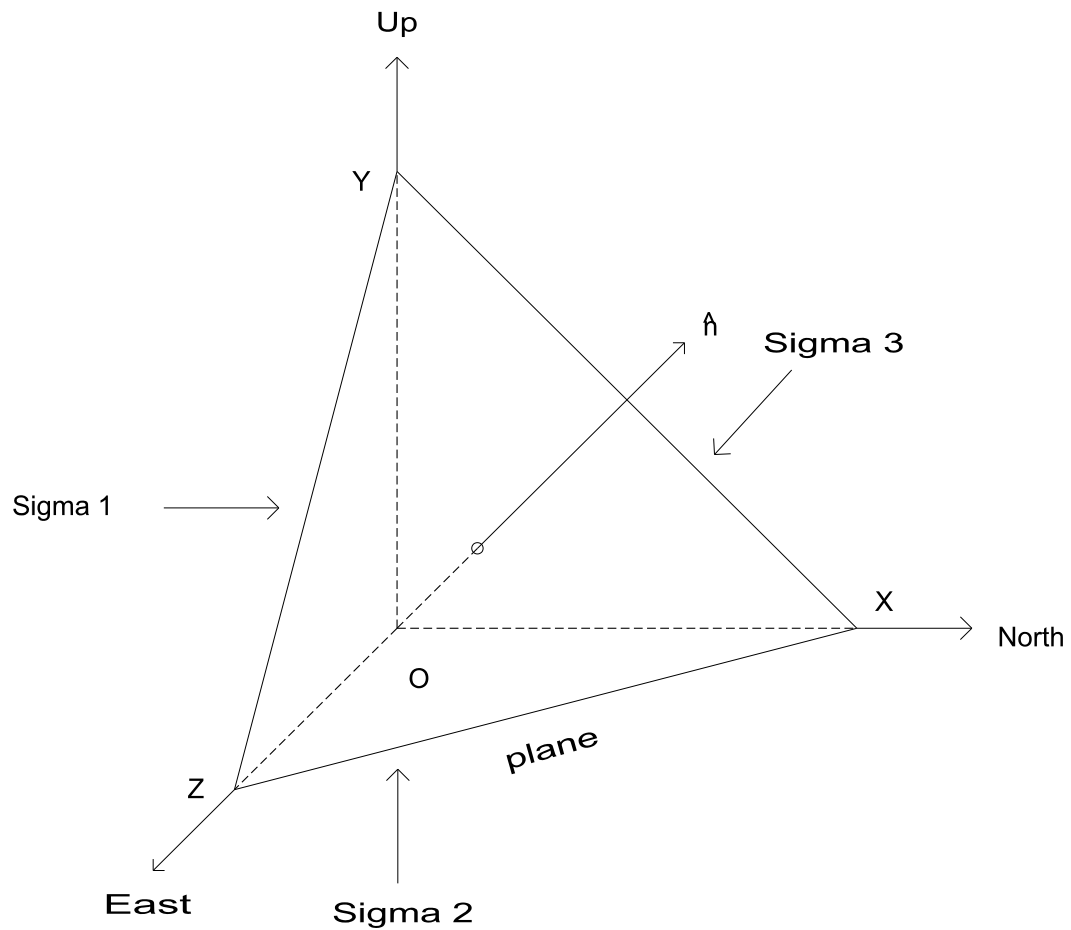


Figure 5-3 - Relationship between a plane XYZ situated within a geographic coordinate system where the principal stress axes σ_1 , σ_2 , and σ_3 and their associated direction cosines l_1 , l_2 , and l_3 correspond to the north, up, and east coordinate axes respectively.

OXY plane. Therefore, the normal force on the OYZ plane is $l_1\sigma_1$, the normal force on the OXZ plane is $l_2\sigma_2$, and the normal force on the OXY plane is $l_3\sigma_3$.

Since the system is in equilibrium, the three components of force acting upon the XYZ plane are $(-l_1\sigma_1, -l_2\sigma_2, -l_3\sigma_3)$. The total resultant force (F_T) on the XYZ plane is therefore

$$F_T = -(l_1^2\sigma_1^2 + l_2^2\sigma_2^2 + l_3^2\sigma_3^2)^{1/2} \quad (9)$$

and the normal force (F_N) acting upon the XYZ plane, which may be determined by resolving each component along the normal direction, is

$$F_N = -(l_1^2\sigma_1 + l_2^2\sigma_2 + l_3^2\sigma_3) \quad (10)$$

The maximum shear force (F_S) acting upon the XYZ plane may then be calculated using the relationship

$$F_T^2 = F_N^2 + F_S^2 \quad (11)$$

which, upon substitution of equations (9) and (10) into equation (11), is

$$F_S = [l_1^2\sigma_1^2 + l_2^2\sigma_2^2 + l_3^2\sigma_3^2 - (l_1^2\sigma_1 + l_2^2\sigma_2 + l_3^2\sigma_3)^2]^{1/2} \quad (12)$$

which yields

$$F_S = l_1^2(\sigma_1 - \sigma_3)^2 + l_2^2(\sigma_2 - \sigma_3)^2 - [l_1^2(\sigma_1 - \sigma_3) + l_2^2(\sigma_2 - \sigma_3)]^2 \quad (13)$$

after using the identity in equation (8) and algebraically rearranging.

The next step is to calculate the resolved components of the maximum shear force (F_S) along the strike direction ($F_{S\text{-strike}}$) and the dip direction ($F_{S\text{-dip}}$) using the relationship

$$F_S^2 = F_{S\text{-strike}}^2 + F_{S\text{-dip}}^2 \quad (14)$$

Resolving the components of shear force along the north-east direction yields

$$F_{S\text{-strike}} = [l_1 l_3 \sigma_1 / (l_1^2 + l_3^2)^{1/2}] - [l_1 l_3 \sigma_3 / (l_1^2 + l_3^2)^{1/2}] \quad (15)$$

which reduces to

$$F_{S\text{-strike}} = [l_1 l_3 (\sigma_1 - \sigma_3) / (l_1^2 + l_3^2)^{1/2}] \quad (16)$$

Substituting equations (13) and (16) into equation (14) results in

$$F_{S\text{-dip}} = \{l_1^2(\sigma_1 - \sigma_3)^2 + l_2^2(\sigma_2 - \sigma_3)^2 - [l_1^2(\sigma_1 - \sigma_3) + l_2^2(\sigma_2 - \sigma_3)]^2\}^{1/2} - [l_1 l_3 (\sigma_1 - \sigma_3) / (l_1^2 + l_3^2)^{1/2}]^2 \quad (17)$$

which yields

$$F_{S\text{-dip}} = l_2 [l_1^2 (\sigma_1 - \sigma_3) - (1 - l_2^2)(\sigma_2 - \sigma_3)] / (1 - l_2^2)^{1/2} \quad (18)$$

after using the identity in equation (8) and algebraically rearranging.

The pitch (α) of the maximum shear stress vector within the XYZ plane (*i.e.* the angle between the strike of the XYZ plane and the maximum shear stress direction) is given by

$$\tan(\alpha) = F_{S-dip} / F_{S-strike} \quad (19)$$

which, upon substitution of equations (16) and (18), yields

$$\tan(\alpha) = \{l_2 [l_1^2 (\sigma_1 - \sigma_3) - (1 - l_2^2)(\sigma_2 - \sigma_3)] / (1 - l_2^2)^{1/2}\} / [l_1 l_3 (\sigma_1 - \sigma_3) / (l_1^2 + l_3^2)^{1/2}] \quad (20)$$

Suitable algebraic rearrangement of equation (20) will result in

$$\alpha = \tan^{-1}[l_1^2 l_2 - \Phi l_2 + \Phi l_2^3] / (l_1 l_3) \quad (21)$$

where Φ is a useful value defined by Angelier (1979) as

$$\Phi = (\sigma_2 - \sigma_3) / (\sigma_1 - \sigma_3) \quad (22)$$

which ranges from 0.0 to 1.0 and represents the relative magnitudes of the principal stresses (*i.e.* represents the shape of the stress ellipsoid).

Bott's formula (equation 21) yields the pitch angle of the slip vector on the fault plane. For plotting on a stereographic projection, it may be more convenient to represent the slip vector simply by its plunge and trend. This may be done utilizing the three formulas

$$\text{beta} = \tan^{-1}[\tan(\text{pitch}) \cos(\text{dip})] \quad (23)$$

$$\text{trend} = \text{strike} + \text{beta} \quad (24)$$

$$\text{plunge} = \cos^{-1}[\cos(\text{pitch}) / \cos(\text{beta})] \quad (25)$$

where the pitch angle of the slip vector in the fault plane and the dip of the fault plane are used to calculate a value for beta which is the horizontal angle between the trend of the slip vector and the strike of the fault plane. The plunge of the slip vector is then calculated from the pitch angle and beta (Ragan, 1985, p. 51).

With some modifications of the above equations, the σ_1 , σ_2 , and σ_3 axes may have any arbitrary orientations other than the north, up, and east ones assigned to them. To do so, the l_1 , l_2 , and l_3 direction cosines must represent the cosines of the angles between the normal vector to the fault plane and the σ_1 , σ_2 , and σ_3 axes respectively. Through Cauchy's formula, the T_1 , T_2 , and T_3 total stress vector components will be resolved parallel to the σ_1 , σ_2 , and σ_3 axes. Bott's formula (equation 21) must be modified accordingly and each of the special cases where the fault plane may be parallel to one of the principal planes must be dealt with individually. The resultant pitch angle will then be the angle between the intersection of the plane containing σ_1 and σ_3 with the fault plane and the slip vector within that fault plane (figure 5-4).

5.3 Program Input

A program was written in Turbo Pascal version 3.01 to perform the above calculations and graphically display the results. The program requires nine items of information to perform the calculations -- the orientations of σ_1 and σ_3 relative to the north, east, and up coordinate axes, the magnitudes of σ_1 and σ_3 , the coefficient of friction (μ) of the fault

plane, the cohesion (C_0) of the fault plane, the plunge and trend of the fault plane's normal vector in degrees, and the number of Φ values to examine.

This information is obtained interactively by the program as the user enters each value when prompted (figure 5-5).

The entered magnitudes of σ_1 and σ_3 have arbitrary units since only their relative values are important, not their absolute values. The program also requires the σ_1 , σ_2 , and σ_3 axes to correspond to either the north, up, or east coordinate axes. This is done only to simplify the mathematics involved in calculating the slip vector orientations and does not significantly limit the program.

The user is required to enter the alphanumeric characters "N", "E", or "U" for the principal stress orientations, a real number between -100.0 and +100.0 for the principal stress magnitudes, a real number between 0.0 and 100.0 for the coefficient of friction and the cohesion, a real number between 0.0 and 90.0 for the plunge of the normal to the fault plane, a real number between 0.0 and 360.0 for the trend of the normal to the fault plane, and an integer between 2 and 50 for the number of σ_2 intervals to examine.

Once the initial data has been entered, the program may begin to calculate slip vector orientations for the specified fault plane.

5.4 Program Procedures

The slip vector calculation program consists of many procedures to interactively input, calculate, and output data. Most of the program procedures in Appendix C are there simply to enable the program to function interactively, to graphically display the results of the calculations, and to create the AutoCAD DXF files. The only procedures I will discuss here are those directly involved with mathematically calculating the slip vector orientations.

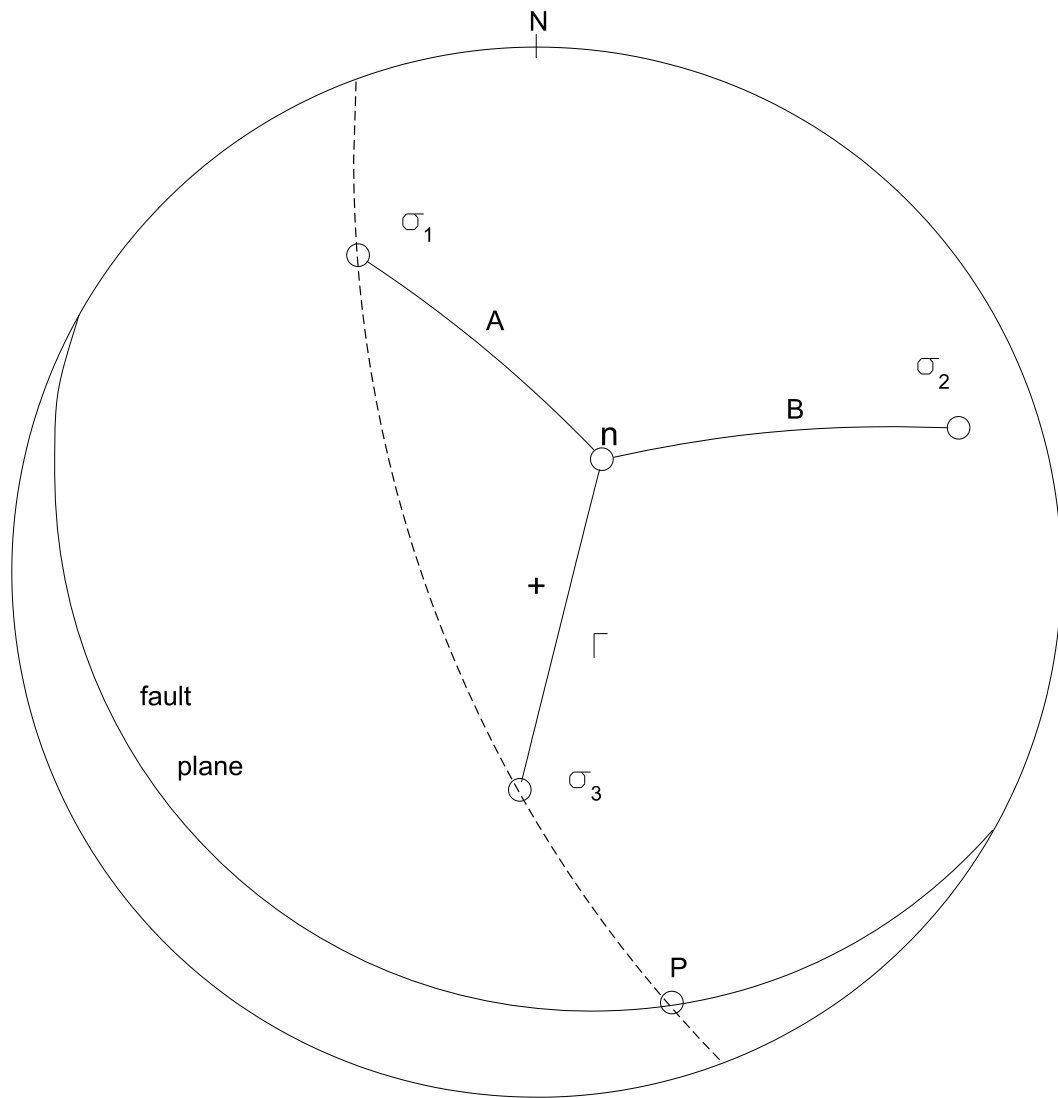


Figure 5-4 - Lower-hemisphere stereographic projection showing three arbitrarily oriented principal stresses σ_1 , σ_2 , and σ_3 in relation to an arbitrarily oriented fault plane with a normal vector \mathbf{n} . **A**, **B**, and Γ are the angles between the normal vector and σ_1 , σ_2 , and σ_3 respectively. The pitch angles of any slip vectors will be measured from the intersection **P** of the plane containing σ_1 and σ_3 with the fault plane (figure modified from Schimmrich, 1990).

```

SLIP VECTOR PLOTTING PROGRAM

What is the orientation of the maximum compressive
principal stress axis  $\sigma_1$  (North, East, or Up) ? N

What is the orientation of the minimum compressive
principal stress axis  $\sigma_3$  (North, East, or Up) ? E

Enter the value for  $\sigma_1$  : 1.0
Enter the value for  $\sigma_3$  : -1.0

Enter the coefficient of friction ( $\mu$ ) : 0.85
Enter the cohesion (C) : 0.0

Now enter the plunge and trend of the normal
vector to the fault plane you wish to examine

Enter the plunge : 70
Enter the trend : 030

How many values of  $\sigma_2$  between  $\sigma_1$ 
and  $\sigma_3$  do you wish to examine ? 20

```

Figure 5-5 - Interactive screen displayed by the slip vector calculation program as the user enters the initial data. In this example, the orientation of σ_1 is north with a magnitude of +1.0, the orientation of σ_3 is east with a magnitude of -1.0, the coefficient of friction is 0.85, the cohesion is 0.0, the fault plane has a normal vector oriented at 70/030, and 21 Φ values will be examined (since 20 σ_2 intervals equals 21 Φ values).

Once the data has been interactively entered through the program procedure *AskData*, the orientation of the σ_1 and σ_3 principal stress axes and the plunge and trend of the fault plane's normal vector are passed to procedure *DirCosines* which calculates the three direction cosines l_1 , l_2 , and l_3 using the equations

$$\begin{aligned} l_n &= [\cos(\text{plunge}) \cos(\text{trend})] \\ l_u &= \sin(\text{plunge}) \\ l_e &= [\cos(\text{plunge}) \sin(\text{trend})] \end{aligned} \tag{26}$$

where l_n , l_u , and l_e are the direction cosines relating the fault plane's normal vector to the north, up, and east coordinate axes respectively (Cheeney, 1983, p. 112). These must be converted to the proper l_1 , l_2 , and l_3 direction cosines depending upon the given orientations of the σ_1 , σ_2 , and σ_3 principal stress axes.

The direction cosines are used, along with the σ_1 and σ_3 magnitudes, to calculate the three components of the total stress vector acting upon the fault plane by procedure *Cauchy*. This procedure initially sets the magnitude of σ_2 equal to the magnitude of σ_3 and then increases it through the user-specified number of steps until it is equal in magnitude to σ_1 . For each of these steps, the magnitudes of σ_1 , σ_2 , and σ_3 are used to calculate a value for Φ (equation 22) and Cauchy's formula is used to calculate the total stress vector (equation 2) for each Φ value. This data is stored in two-dimensional arrays.

All of the data is then passed to procedure *CalculateStresses* which calculates the slip vector pitch angle and the shear stress to normal stress ratio for each Φ value. The principal stress σ_2 is once again set equal to the magnitude of σ_3 and increased by steps until it is equal in magnitude to σ_1 . Calculations are then performed for each Φ value.

The three direction cosines and components of the total stress vector are first used to calculate the angle between the fault plane's normal vector and the total stress vector acting upon the fault using equations (3), (4), and (5). From this angle, the shear stress and normal stress acting upon the fault plane may be calculated using equations (6) and (7). The effective shear stress to normal stress ratio (σ_s' / σ_n') is then determined using the following equation

$$(\sigma_s' / \sigma_n') = \sigma_s / [(\mu \sigma_n) + C_0] \quad (27)$$

provided that μ or σ_n are not equal to zero. This equation is used since a Coulomb failure criterion is assumed (Coulomb, 1776; Handin, 1969).

The program next checks for the special cases where the fault plane is parallel to one of the principal stress axes since this will result in a division by zero in procedure *CalculateStresses* (a fault plane parallel to a principal stress axis will have a direction cosine equal to zero).

Finally, Bott's formula (equation 21) is used to calculate the pitch angle of the fault's slip vector for each Φ value. A simplified flow-chart of these procedures is shown in figure 5-6.

The results of these calculations are then numerically or graphically displayed showing the slip vector orientations on the user-specified fault plane for each value of Φ calculated and the associated shear stress to normal stress ratios.

5.5 Program Output

There are several ways in which the results of the calculations may be displayed. The easiest way is to display them as a numerical listing (table 5-1). It is often difficult, however,

to see the relationships between numbers in a table of data, so a better method is to display the results as a graph of the Φ values versus the pitch angles of the slip vectors (figure 5-7). Alternatively, the same slip vectors may be plotted in a lower-hemisphere stereographic projection (figure 5-8). Using different symbols for slip vectors on planes with a shear stress to normal stress ratio above or below a certain chosen value may indicate which slip directions would have a higher chance of experiencing slip since this ratio is directly proportional to the coefficient of internal friction (Coulomb, 1776; Handin, 1969).

The slip vector calculation program will display, on the computer's screen, the results as a table of data, a graph of the Φ values versus the pitch angles of the slip vectors, or as a lower-hemisphere stereographic projection. The data may also be written to an ASCII file or be used to create AutoCAD-compatible drawing interchange files (DXF files) for plotting the graphs and stereographic projections via AutoCAD.

5.6 Creating Fault Populations

The slip vector calculation program was used to generate artificial fault populations for testing paleostress analysis programs. These populations were created using the following steps:

1. Deciding upon the type of fault population to test (*i.e.* conjugate faults, orthorhombic symmetry faults, randomly oriented faults).
2. Deciding upon the number of faults to test. Too few or too many faults will adversely affect the paleostress analysis.
3. Deciding upon the type of stress field in which to situate the fault population. The

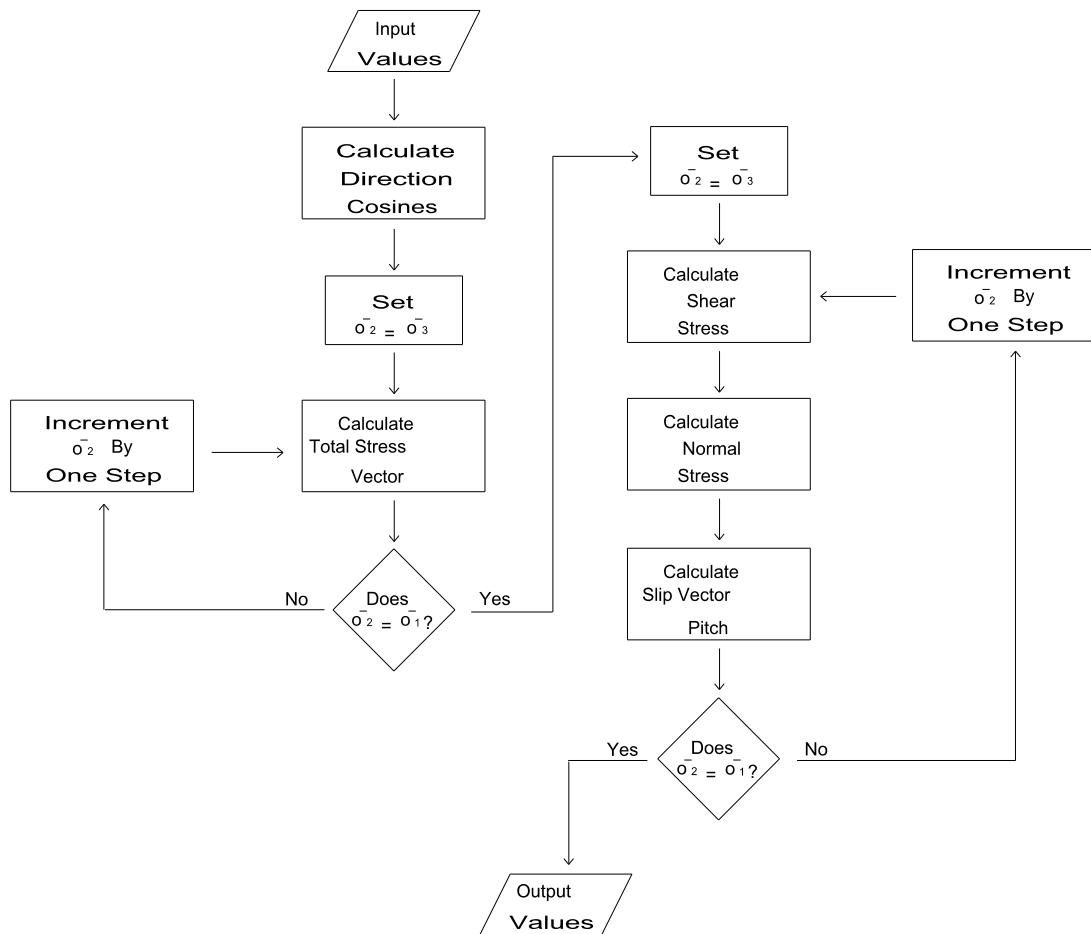


Figure 5-6 - Simplified flow chart demonstrating the mathematical algorithm used by the slip vector calculation program.

Sigma 1	Sigma 2	Sigma 3	Phi	Pitch	σ_s/σ_n
1.00	-1.00	-1.00	0.00	58.43°	0.69
1.00	-0.90	-1.00	0.05	56.64°	0.73
1.00	-0.80	-1.00	0.10	54.67°	0.79
1.00	-0.70	-1.00	0.15	52.48°	0.87
1.00	-0.60	-1.00	0.20	50.04°	0.98
1.00	-0.50	-1.00	0.25	47.34°	1.14
1.00	-0.40	-1.00	0.30	44.32°	1.40
1.00	-0.30	-1.00	0.35	40.96°	1.90
1.00	-0.20	-1.00	0.40	37.22°	3.15
1.00	-0.10	-1.00	0.45	33.07°	11.86
1.00	0.00	-1.00	0.50	28.48°	5.76
1.00	0.10	-1.00	0.55	23.46°	2.20
1.00	0.20	-1.00	0.60	18.03°	1.32
1.00	0.30	-1.00	0.65	12.24°	0.94
1.00	0.40	-1.00	0.70	6.19°	0.72
1.00	0.50	-1.00	0.75	0.00°	0.50
1.00	0.60	-1.00	0.80	-6.19°	0.51
1.00	0.70	-1.00	0.85	-12.24°	0.45
1.00	0.80	-1.00	0.90	-18.03°	0.41
1.00	0.90	-1.00	0.95	-23.46°	0.38
1.00	1.00	-1.00	1.00	-28.48°	0.36

Table 5-1 - Table of data generated by the calculation of 21 slip vectors representing a Φ value ranging from 0.0 to 1.0 on a fault plane with a normal vector oriented at 70/030 degrees. The σ_1 , σ_2 , and σ_3 values are in any arbitrary stress units, the pitch is defined as the angle between the strike of the fault plane and the slip vector in degrees, and the shear stress to normal stress ratio (σ_s / σ_n) is dimensionless (table modified from Schimmrich, 1990).

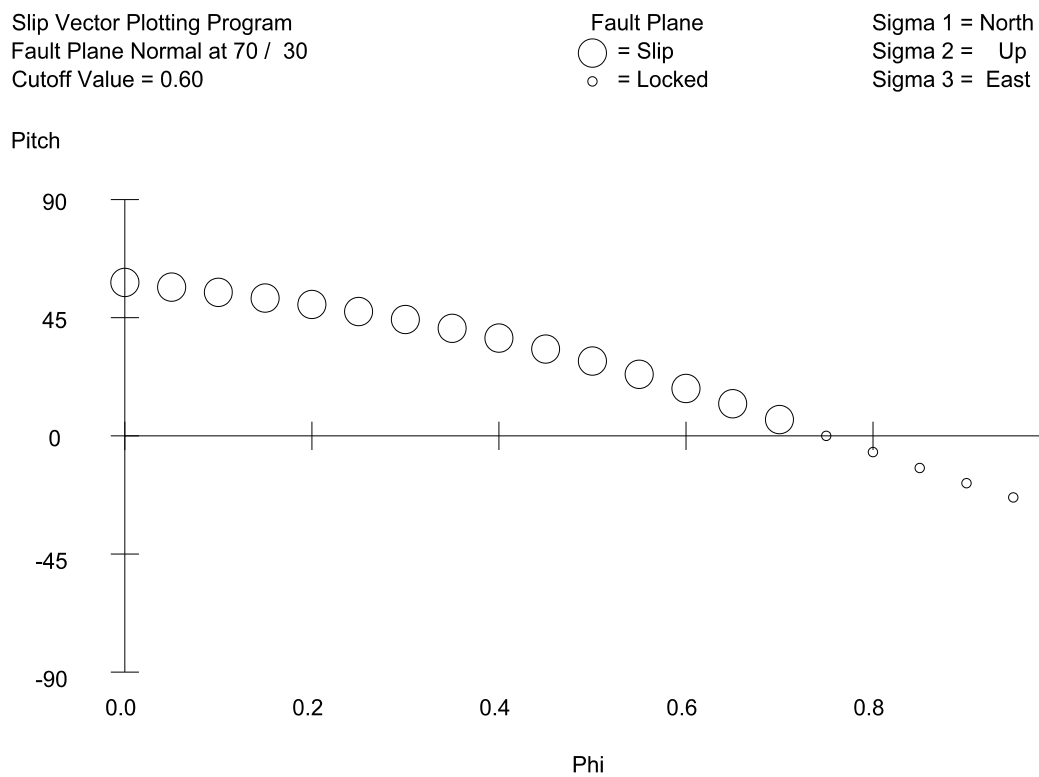


Figure 5-7 - Graph of 21 Φ values for each slip vector as they range from 0.0 to 1.0 versus the pitch of the slip vectors from the strike of the fault plane with a normal vector oriented at 70/030 degrees. The large circles represent slip vectors with a shear stress to normal stress ratio of 0.6 or greater and the small circles represent slip vectors with a shear stress to normal stress ratio of less than 0.6.

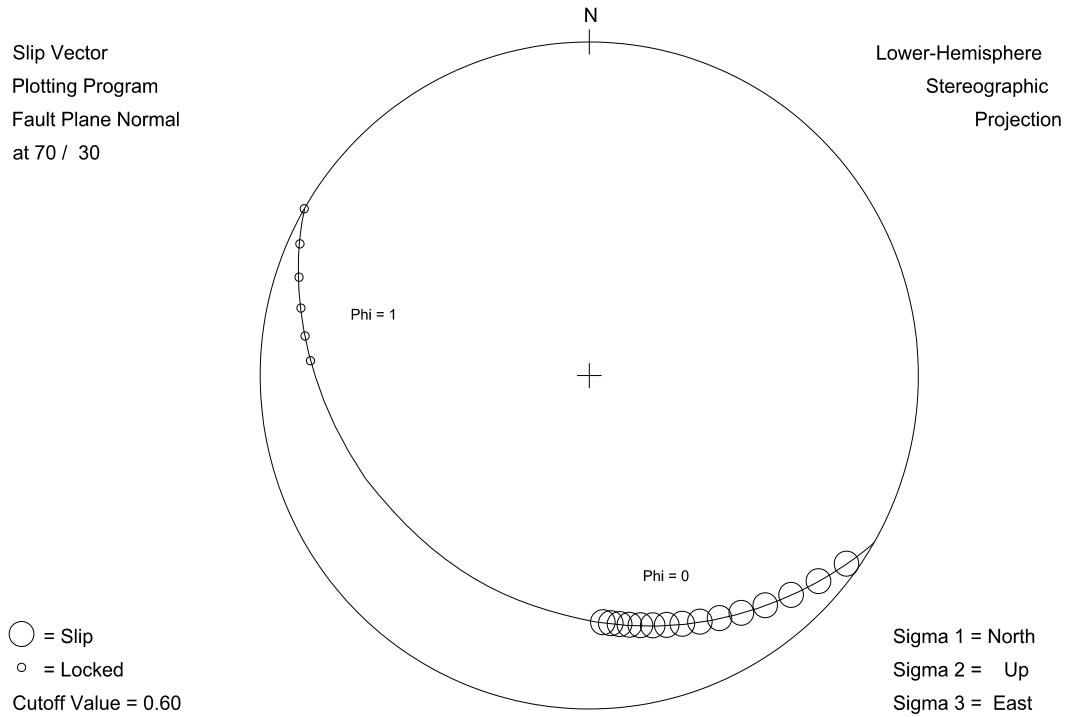


Figure 5-8 - Lower-hemisphere stereographic projection of 21 slip vectors representing values ranging from 0.0 to 1.0 on a fault plane with a normal vector oriented at 70/030 degrees. The large circles represent slip vectors with a shear stress to normal stress ratio of 0.6 or greater and the small circles represent slip vectors with a shear stress to normal stress ratio of less than 0.6.

orientations of σ_1 , σ_2 , and σ_3 relative to the north, up, and east coordinate axes and their ratio Φ must be determined.

4. Deciding upon values to use for the coefficient of friction (μ) and cohesion (C_0).
5. Determining the plunge and trend of the normal vector for each fault plane within the population which will be tested.
6. Using the slip vector calculation program to determine the pitch of the slip vector and the shear stress to normal stress ratio for each fault plane at the decided upon value of Φ .
7. Deciding upon a shear stress to normal stress ratio cutoff value to use since faults with a sufficiently low ratio will not experience slip under realistic geologic conditions and tossing out those faults which have a ratio below that cutoff.
8. Creating data files of the fault's orientations and slip directions in the proper format for entry into the various paleostress analysis programs.

The artificial fault populations generated in this manner were then run through several paleostress analysis programs to determine if the calculated paleostress tensors corresponded to the initial stress fields used to create the populations. This provides an independent means of assessing the accuracy of computational methods of paleostress analysis since the populations were created using the same initial mathematical assumptions as those used by the analysis programs.

CHAPTER 6

ANGELIER'S METHOD OF PALEOSTRESS ANALYSIS

In 1975, Jacques Angelier of the Université Pierre et Marie Curie in Paris proposed a new computational method for paleostress analysis which he subsequently modified over time (Angelier, 1975; Angelier, 1979; Angelier, *et. al.*, 1982; Angelier, 1984; Angelier, 1989). Angelier's method attempts to iteratively determine a paleostress tensor for a given fault population such that the angular divergence between the observed striations in the fault planes and the predicted slip directions are minimized (Angelier, *et. al.*, 1982).

I obtained a compiled version of Angelier's program from Christopher Barton of the Lamont-Doherty Geological Observatory in June, 1990. The program was written by Angelier in FORTRAN for an IBM PC or compatible computer with an 80287 math coprocessor.

I determined that this program was operating correctly by examining several published fault populations for which Angelier's method paleostress tensors were given and comparing my results to the published ones (Angelier, *et. al.*, 1982; Angelier, 1984). This done, I began to evaluate the performance of Angelier's method using artificial fault populations.

6.1 Program Assumptions

Angelier's method of paleostress analysis is based upon the following two very important initial assumptions (Angelier, 1989).

1. All faults which moved during a single tectonic event moved independently of one another and in a manner consistent with a unique, static stress tensor.

2. Faults are assumed to slip on pre-existing planar discontinuities in the direction of the maximum resolved shear stress within the fault plane (*i.e.* at right angles to the direction of zero shear stress).

6.2 Theory

The mathematics in this section roughly follow the derivations given in Angelier, *et al.* (1982).

Allow σ to be the unknown regional stress tensor acting upon a fault plane with a unit normal vector \mathbf{N} and a unit slip vector \mathbf{S} (figure 6-1). The stress vector \mathbf{T} acting upon the fault plane may be defined by

$$\mathbf{T} = \sigma \cdot \mathbf{N} \quad (1)$$

where $(\sigma \cdot \mathbf{N})$ is the inner, or dot, product of tensor σ and vector \mathbf{N} (Marsden and Tromba, 1981, p. 20) and the components of \mathbf{T} on \mathbf{N} and \mathbf{S} are

$$\mathbf{N} \cdot \mathbf{T} = \mathbf{N} \cdot \sigma \cdot \mathbf{N} \quad (2)$$

and

$$\mathbf{S} \cdot \mathbf{T} = \mathbf{S} \cdot \sigma \cdot \mathbf{N} \quad (3)$$

respectively.

Since the direction of the striations in the fault plane is taken to be the maximum

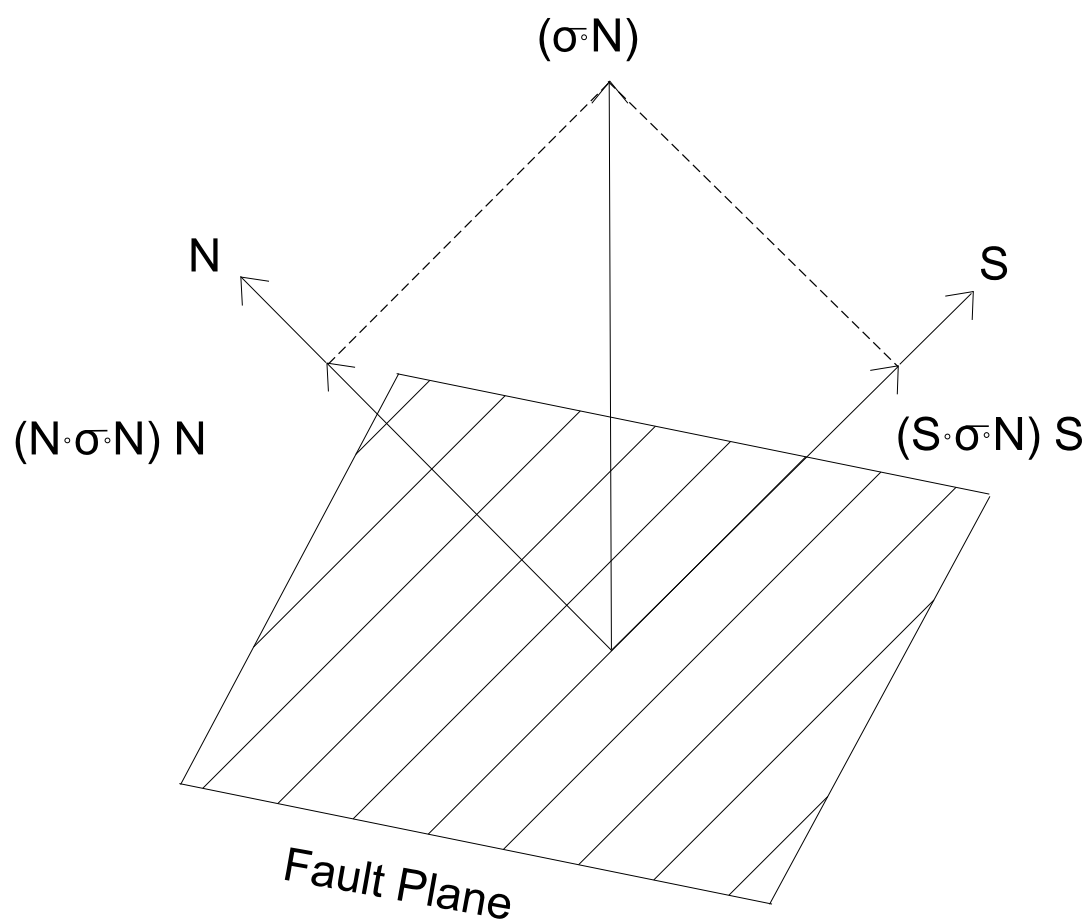


Figure 6-1 - Geometry of the stresses on a striated fault plane with a unit normal vector (\mathbf{N}), a unit slip vector (\mathbf{S}), and a stress vector ($\boldsymbol{\sigma} \cdot \mathbf{N}$) acting upon it (figure modified from Angelier, *et. al.*, 1982).

resolved shear stress direction, the following two equations may be written

$$\boldsymbol{\sigma} \cdot \mathbf{N} = (\mathbf{N} \cdot \boldsymbol{\sigma} \cdot \mathbf{N}) \mathbf{N} + (\mathbf{S} \cdot \boldsymbol{\sigma} \cdot \mathbf{N}) \mathbf{S} \quad (4)$$

$$\mathbf{S} \cdot \boldsymbol{\sigma} \cdot \mathbf{N} \geq 0 \quad (5)$$

Equation (4) may be simplified through the following steps

$$(\mathbf{S} \cdot \boldsymbol{\sigma} \cdot \mathbf{N}) \mathbf{S} = \boldsymbol{\sigma} \cdot \mathbf{N} - (\mathbf{N} \cdot \boldsymbol{\sigma} \cdot \mathbf{N}) \mathbf{N} \quad (6)$$

$$(\mathbf{S} \cdot \boldsymbol{\sigma} \cdot \mathbf{N})^2 = \| \boldsymbol{\sigma} \cdot \mathbf{N} - (\mathbf{N} \cdot \boldsymbol{\sigma} \cdot \mathbf{N}) \mathbf{N} \|^2 \quad (7)$$

$$(\mathbf{S} \cdot \boldsymbol{\sigma} \cdot \mathbf{N})^2 = \| \boldsymbol{\sigma} \cdot \mathbf{N} \|^2 - (\mathbf{N} \cdot \boldsymbol{\sigma} \cdot \mathbf{N})^2 \quad (8)$$

$$\mathbf{S} \cdot \boldsymbol{\sigma} \cdot \mathbf{N} = \pm [\| \boldsymbol{\sigma} \cdot \mathbf{N} \|^2 - (\mathbf{N} \cdot \boldsymbol{\sigma} \cdot \mathbf{N})^2]^{1/2} \quad (9)$$

and combining equations (5) and (9) yields

$$\mathbf{S} \cdot \boldsymbol{\sigma} \cdot \mathbf{N} = +[\| \boldsymbol{\sigma} \cdot \mathbf{N} \|^2 - (\mathbf{N} \cdot \boldsymbol{\sigma} \cdot \mathbf{N})^2]^{1/2} \quad (10)$$

a mathematical relationship which will be used later in this analysis.

In describing the orientation of the fault planes and their associated striations used in the paleostress analysis, three independent angles are defined in a north, up, and east geographic coordinate system. The trend of the fault's dip direction (d), the fault's dip angle (p), and the pitch angle of the fault's slip vector (i). The pitch angle (i) is defined as the clockwise angle (looking down the fault normal's plunge at the footwall block) between the slip vector and the fault's strike direction (the trend of the pole to the fault plane + $\pi/2$) such that $0 < i < \pi$ for a normal fault and $\pi < i < 2\pi$ for a reverse fault (figure 6-2).

The angles d , p , and i are those commonly measured in the field by geologists with a

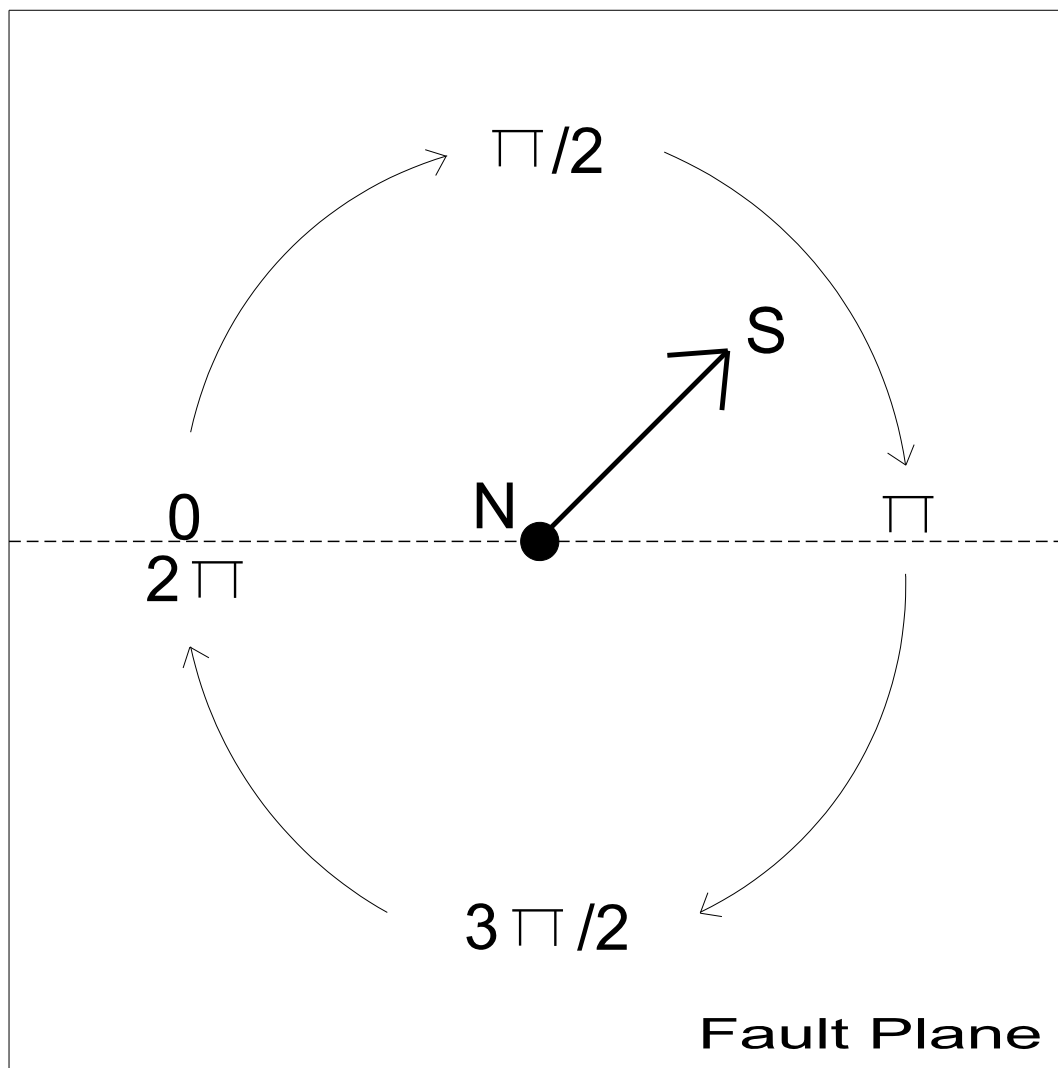


Figure 6-2 - Diagram of a fault plane looking down the plunge of the normal vector (N) to the fault at the footwall block showing a slip vector aligned at $3\pi/4$. In Angelier's (Angelier, *et. al.*, 1982) notational system, this implies a normal fault (the slip vector points in the direction of movement of the lower block).

compass and clinometer. The advantage in using these angles is that they are all independent of one another so an error in measuring one angle will not affect the other two.

The three components of the unit normal vector to the fault plane may thus be defined in terms of d , p , and i as

$$\begin{aligned} N_1 &= [\sin(d) \sin(p)] \\ N_2 &= [\cos(d) \sin(p)] \\ N_3 &= \cos(p) \end{aligned} \tag{11}$$

and, similarly, for the slip vector components

$$\begin{aligned} S_1 &= - [\sin(i) \cos(p) \sin(d)] + [\cos(i) \cos(d)] \\ S_2 &= - [\sin(i) \cos(p) \cos(d)] - [\cos(i) \sin(d)] \\ S_3 &= [\sin(i) \sin(p)] \end{aligned} \tag{12}$$

If $\boldsymbol{\sigma}$ is the unknown regional stress tensor for a given fault, a tensor $\boldsymbol{\sigma}'$ may be defined such that

$$\boldsymbol{\sigma} = t_1 \boldsymbol{\sigma}' + t_2 \mathbf{I} \tag{13}$$

where t_1 and t_2 are any positive constants and \mathbf{I} is any isotropic 3 x 3 tensor. It can be demonstrated that multiplying $\boldsymbol{\sigma}'$ by a positive constant and adding an isotropic tensor \mathbf{I} to it will not change the sense or direction of the predicted striations on the fault plane.

Since $\boldsymbol{\sigma}$ is a 3 x 3 symmetric tensor, it has six degrees of freedom (*i.e.* $\boldsymbol{\sigma}_{1,2} = \boldsymbol{\sigma}_{2,1}$, $\boldsymbol{\sigma}_{1,3} = \boldsymbol{\sigma}_{3,1}$, and $\boldsymbol{\sigma}_{2,3} = \boldsymbol{\sigma}_{3,2}$). The tensor $\boldsymbol{\sigma}'$ is thus termed the reduced deviatoric stress tensor

(Angelier, 1979; Angelier, *et. al.*, 1984) and has four degrees of freedom since t_1 and t_2 may have any arbitrary positive values. Furthermore, it is always possible to choose positive values for t_1 and t_2 such that

$$\sigma_{1,1} + \sigma_{2,2} + \sigma_{3,3} = 0 \quad (14)$$

and

$$\sigma_{1,1}^2 + \sigma_{2,2}^2 + \sigma_{3,3}^2 = (3/2) \quad (15)$$

For numbers satisfying equations (14) and (15), a unique number Ψ (modulo 2π) can be found such that

$$\begin{aligned} \sigma_{1,1} &= \cos(\Psi) \\ \sigma_{2,2} &= \cos[\Psi + (2\pi/3)] \\ \sigma_{3,3} &= \cos[\Psi + (4\pi/3)] \end{aligned} \quad (16)$$

which yields the reduced stress tensor σ'

$$\left[\begin{array}{ccc} \cos(\Psi) & \alpha & \gamma \\ \alpha & \cos[\Psi + (2\pi/3)] & \beta \\ \gamma & \beta & \cos[\Psi + (4\pi/3)] \end{array} \right] \quad (17)$$

where α , β , and γ are the shear stress terms ($\sigma_{1,2}$, $\sigma_{2,1}$, $\sigma_{2,3}$, $\sigma_{3,2}$, $\sigma_{1,3}$, and $\sigma_{3,1}$) of the tensor.

All tensors σ' and σ which satisfy equation (13) yield the same eigenvectors and eigenvalues and thus the principal stress axes orientations and magnitudes are the same for each.

Let ψ_0 , α_0 , β_0 , and γ_0 be values for the *a priori* estimate of σ' and σ^ψ , σ^α , σ^β , and σ^γ be their standard deviations. If there is no *a priori* estimate of σ' , the standard deviations must be made very large. Also, let $(d_0, p_0, i_0)_n$ be data and $(\sigma^d, \sigma^p, \sigma^i)$ be the standard deviations of that data for each fault n.

In the general case, **no** tensor σ' exactly satisfies equation (10) on each fault. Therefore, what is needed is a tensor σ' and a new set of data $(d, p, i)_n$ which exactly satisfies the equation. Since there are an infinite number of such solutions, the solution which minimizes the following sum (s) for a population of n faults is used.

$$s = \sum_{k=1}^n \{ [(d-d_0)/\sigma^d]_k^2 + [(p-p_0)/\sigma^p]_k^2 + [(i-i_0)/\sigma^i]_k^2 \} + [(\psi-\psi_0)/\sigma^\psi]^2 + [(\alpha-\alpha_0)/\sigma^\alpha]^2 + [(\beta-\beta_0)/\sigma^\beta]^2 + [(\gamma-\gamma_0)/\sigma^\gamma]^2 \quad (18)$$

This is a non-linear least-squares problem whose solution is obtained by a complicated iterative algorithm which may be found in Angelier, *et. al.* (1982).

6.3 Program Input

The program utilizing Angelier's method of paleostress analysis requires five items of information to run -- a two letter code (described in more detail below) describing the type of structure which will be analyzed, the fault's strike ($0^\circ \rightarrow 360^\circ$), the fault's dip angle ($0^\circ \rightarrow$

90°), the fault's dip direction (N, E, S, or W for north, east, south, or west respectively), and the trend (0° → 360°) of the striations on the fault surface.

The two letter code used by Angelier is to allow a wide variety of geologic structures such as faults, joints, tension gashes, dikes, bedding planes, mylonitic foliations, cleavages, mineral lineations, folds, etc. to be subjected to paleostress analysis. The codes used in my analyses are *CN*, *CI*, *CD*, and *CS* for, respectively, striated normal, reverse (inverse), dextral, or sinistral faults with a known sense of shear.

This information must be written to an ASCII data file in a special format so that it may be correctly read by Angelier's program. A data file creation program exists which creates these formatted files when the initial data is interactively entered. Each fault datum must be entered as a single line of characters and integers separated by a single blank space.

As an example, a conjugate set of two normal faults with an east-west strike and a dip of 45° (figure 6-3) would be entered into the data file creation program as

```
CN 090 45S 180  
CN 270 45N 000
```

since the first fault is normal, has a strike of 090°, is dipping 45° to the south, and has striations with a trend of 180°. The second fault is also normal, has a strike of 270°, is dipping 45° to the north and has striations with a trend of 000°. The data file creation program also asks for the magnetic deviation of the measurements in degrees, a value for the instrument error in degrees, the author's name, the site name, the date, and comments about the geology of the site.

Once the properly-formatted ASCII data file has been created and read into the program, the calculations are performed.

6.4 Program Procedures

When all of the data has been entered into the program, the three angles d_0 , p_0 , and i_0 are determined for each fault in the population. The standard deviations σ^d , σ^p , and σ^i of these angles are also determined from the entered measurement error term.

The next step in the program is to set the *a priori* constraints for the four parameters (ψ_0 , α_0 , β_0 , and γ_0) describing the reduced stress tensor σ' (equation 17) to zero and to set the *a priori* standard deviations to 4π for σ^ψ and to 100 for σ^α , σ^β , and σ^γ .

An iterative algorithm (Angelier, *et. al.*, 1982) is then used to determine values for [ψ , α , β , γ , (d, p, i)₁, ... (d, p, i)_n] such that equation (18) is minimized.

Once a reduced stress tensor σ' has been calculated, the three eigenvalues and eigenvectors of σ' may be determined using standard linear algebra techniques (Anton, 1981, p. 261-284; Fröberg, 1985, p. 22-26). These eigenvalues and eigenvectors correspond to the magnitudes and orientations of the three principal stress axes σ_1 , σ_2 , and σ_3 respectively.

6.5 Program Output

The program results are displayed on the computer's screen when the calculations have finished and the user has the option of saving them to an ASCII data file or performing another analysis.

The output data consists of the plunges and trends of the three principal stress axes σ_1 , σ_2 , and σ_3 and their relative magnitudes. The stress ratio Φ , defined as $[(\sigma_2 - \sigma_3) / (\sigma_1 - \sigma_3)]$, is also displayed.

The data for each paleostress analysis I obtained was plotted on lower-hemisphere

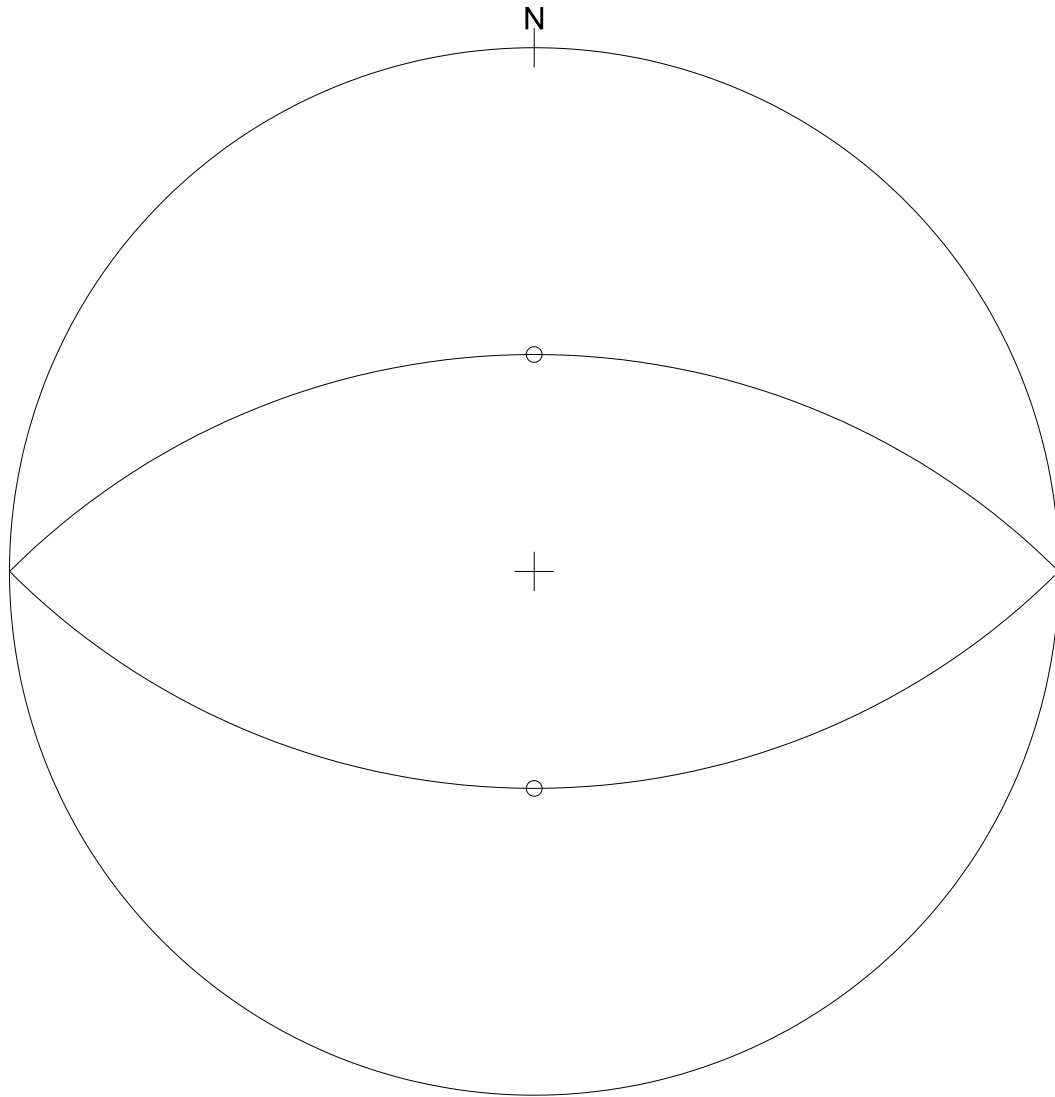


Figure 6-3 - Lower-hemisphere stereographic projection showing a conjugate set of two normal faults with an east-west strike and a dip of 45°

stereographic projections by a Turbo Pascal version 3.01 program I wrote for that purpose (Appendix D). The program read the fault population data and the predicted principal stress axes orientations and created AutoCAD script files for plotting stereonet via AutoCAD.

6.6 Discussion

Angelier's method of paleostress analysis was chosen for testing for several reasons. I had a working copy of the program for an IBM PC or compatible computer, the program performed calculations for reasonably-sized fault populations in relatively short amounts of time, Angelier's method of paleostress analysis is widely-used and is the standard by which most others are judged, and the method has been used in several published field studies (Angelier, 1984; Angelier, *et. al.*, 1985; Angelier, 1990).

CHAPTER 7

RECHES' METHOD OF PALEOSTRESS ANALYSIS

In 1987, Ze'ev Reches of the Hebrew University in Jerusalem proposed what he claimed to be a new and improved method of computational paleostress analysis (Reches, 1987). The improvement over previous methods was the incorporation of the Coulomb failure criterion into the calculations. This allows the cohesion and coefficient of friction to be constrained for the fault populations and uses a linear inversion to calculate a stress tensor rather than Angelier's much more complicated non-linear one.

I obtained a compiled version of Reches' program from Kenneth Hardcastle of the University of Massachusetts at Amherst in August, 1989. The program was written by Hardcastle in Microsoft BASIC version 5.60 for an IBM PC or compatible computer with an 80287 math coprocessor. Using this program, Hardcastle performed paleostress analyses on fault data from eastern Vermont and western New Hampshire (Hardcastle, 1989).

I determined that this program was operating correctly by examining several published fault populations for which Reches' method paleostress tensors were given and comparing my results to the published ones (Angelier, 1984; Reches, 1987). This done, I began to evaluate the performance of Reches' method using artificial fault populations.

7.1 Program Assumptions

Reches' method of paleostress analysis is based upon the following three assumptions (Reches, 1987).

1. Faults are assumed to slip in the direction of the maximum resolved shear stress within the fault plane (*i.e.* at right angles to the direction of zero shear stress).

2. The magnitudes of the shear and normal stresses acting upon a fault plane satisfy the Coulomb failure criterion ($\sigma_s > C_0 + \mu \sigma_n$). This assumption implies that faults will slip under geologically-realistic conditions.
3. Slip on a fault occurs within a relatively static stress field and the coefficient of friction μ and cohesion C_0 terms for a fault may be represented by their mean values.

7.2 Theory

The mathematics in this section roughly follows the derivations given in Reches (1987).

For each fault plane in the population to test, the following items of information are known -- the orientation of the normal vector to the fault plane, the orientation of the fault's slip vector, and the fault's sense of slip. Assuming a geographic coordinate system with X_1 northward, X_2 eastward, and X_3 downward, the two unit vectors representing the normal and slip directions may be represented by

$$\langle N_1, N_2, N_3 \rangle \tag{1}$$

and

$$\langle S_1, S_2, S_3 \rangle \tag{2}$$

where N_i and S_i are the direction cosines for the normal and slip vectors and the 1, 2, and 3 subscripts refer to the north, east, and down directions respectively.

The direction cosines in equations (1) and (2) satisfy the following identities:

$$N_1^2 + N_2^2 + N_3^2 = 1 \quad (3)$$

$$S_1^2 + S_2^2 + S_3^2 = 1 \quad (4)$$

$$N_1S_1 + N_2S_2 + N_3S_3 = 0 \quad (5)$$

Given that S_i represents the components of the fault's slip vector, N_i represents the components of the fault's normal vector, and B_i represents the components of the vector orthogonal to both \mathbf{S} and \mathbf{N} (*i.e.* \mathbf{B} is the normal vector to the movement plane), then

$$\mathbf{B} = \mathbf{N} \times \mathbf{S} \quad (6)$$

where the symbol \times represents the operation of determining the cross product of two vectors (Marsden and Tromba, 1981, p. 25).

Assumption 1 in section 7.1 states that the resolved shear stress parallel to vector \mathbf{B} (*i.e.* at right angles to vector \mathbf{S}) is equal to zero. Resolving the stresses parallel to \mathbf{B} (Jaeger and Cook, 1979, p. 17-24), denoting nine components of the stress tensor as $\sigma_{i,j}$ (where $i = 1, 2,$ or 3 and $j = 1, 2,$ or 3), and using the identities in equations (3), (4), and (5) allows one to set up the following relationship:

$$\begin{aligned} N_1B_1 (\sigma_{1,1} - \sigma_{3,3}) + N_2B_2 (\sigma_{2,2} - \sigma_{3,3}) + (N_2B_3 + B_2N_3) \sigma_{2,3} + \\ (N_1B_3 + B_1N_3) \sigma_{1,3} + (N_1B_2 + B_1N_2) \sigma_{1,2} = 0 \end{aligned} \quad (7)$$

In a similar manner, the stresses may be resolved parallel to the vector \mathbf{N} (which is the fault's normal stress σ_n)

$$\begin{aligned} \sigma_n = & [N_1^2 (\sigma_{1,1} - \sigma_{3,3}) + N_2^2 (\sigma_{2,2} - \sigma_{3,3}) + \sigma_{3,3} + N_2 N_3 2\sigma_{2,3} + \\ & N_1 N_3 2\sigma_{1,3} + N_1 N_3 2\sigma_{1,3} + N_1 N_2 2\sigma_{1,2}] \end{aligned} \quad (8)$$

and the vector \mathbf{S} (the fault's shear stress σ_s).

$$\begin{aligned} \sigma_s = & N_1 S_1 (\sigma_{1,1} - \sigma_{3,3}) + N_2 S_2 (\mu_{2,2} - \mu_{3,3}) + (N_2 S_3 + S_2 N_3) \mu_{2,3} + \\ & (N_1 S_3 + S_1 N_3) \sigma_{1,3} + (N_1 S_2 + S_1 N_2) \sigma_{1,2} \end{aligned} \quad (9)$$

Assumption 2 in section 7.1 states that a fault must satisfy the Coulomb failure criterion.

$$\sigma_s = C_0 + \mu \sigma_n \quad (10)$$

Substituting equations (8) and (9) into equation (10) yields¹

$$\begin{aligned} & N_1 S_1 (\sigma_{1,1} - \sigma_{3,3}) + N_2 S_2 (\sigma_{2,2} - \sigma_{3,3}) + (N_2 S_3 + S_2 N_3) \sigma_{2,3} + \\ & (N_1 S_3 + S_1 N_3) \sigma_{1,3} + (N_1 S_2 + S_1 N_2) \sigma_{1,2} = \\ & C_0 + \mu [N_1^2 (\sigma_{1,1} - \sigma_{3,3}) + N_2^2 (\sigma_{2,2} - \sigma_{3,3}) + \sigma_{3,3} + N_2 N_3 2\sigma_{2,3} + \\ & N_1 N_3 2\sigma_{1,3} + N_1 N_3 2\sigma_{1,3} + N_1 N_2 2\sigma_{1,2}] \end{aligned} \quad (11)$$

Equation (11) may be rewritten as

¹ Equation (3) in Reches' (1987) paper is incorrect with $\mu_{2,2}$, $\mu_{3,3}$, and $\mu_{2,3}$ representing what should be $\sigma_{2,2}$, $\sigma_{3,3}$, and $\tau_{2,3}$ respectively. This error has been corrected for equation (11).

$$\begin{aligned}
& [(N_1 S_1 - \mu N_1^2) (\sigma_{1,1} - \sigma_{3,3})] + [(N_2 S_2 - \mu N_2^2) (\sigma_{2,2} - \sigma_{3,3})] + \\
& [(N_2 S_3 + S_2 N_3 - 2\mu N_2 N_3) \sigma_{2,3}] + [(N_1 S_3 + S_1 N_3 - 2\mu N_1 N_3) \sigma_{1,3}] + \\
& [(N_1 S_2 + S_1 N_2 - 2\mu N_1 N_2) \sigma_{1,2}] = C_0 + \mu \sigma_{3,3}
\end{aligned} \tag{12}$$

Equations (7) and (12) may be written for each fault in a population of n faults resulting in a total of $2n$ equations. Thus, for a given fault population, the left sides of the two equations (*i.e.* the sides which are equal to 0 and $C_0 + \mu \sigma_{3,3}$ respectively) may be used to create a $2n \times 5$ matrix of the form

$$\begin{bmatrix}
[N_1 B_1]_1 & [N_2 B_2]_1 & [(N_2 B_3 + B_2 N_3)]_1 & [(N_1 B_3 + B_1 N_3)]_1 & [(N_1 B_2 + B_1 N_2)]_1 \\
\dots & \dots & \dots & \dots & \dots \\
[N_1 B_1]_n & [N_2 B_2]_n & [(N_2 B_3 + B_2 N_3)]_n & [(N_1 B_3 + B_1 N_3)]_n & [(N_1 B_2 + B_1 N_2)]_n \\
[N_1 S_1 - \mu N_1^2]_1 & [N_2 S_2 - \mu N_2^2]_1 & [N_2 S_3 + S_2 N_3 - 2\mu N_2 N_3]_1 & [N_1 S_3 + S_1 N_3 - 2\mu N_1 N_3]_1 & [N_1 S_2 + S_1 N_2 - 2\mu N_1 N_2]_1 \\
\dots & \dots & \dots & \dots & \dots \\
[N_1 S_1 - \mu N_1^2]_n & [N_2 S_2 - \mu N_2^2]_n & [N_2 S_3 + S_2 N_3 - 2\mu N_2 N_3]_n & [N_1 S_3 + S_1 N_3 - 2\mu N_1 N_3]_n & [N_1 S_2 + S_1 N_2 - 2\mu N_1 N_2]_n
\end{bmatrix} \tag{13}$$

where the subscripts 1 through n indicate the parameters associated with each of the n faults.

Denoting the matrix in equation (13) as \mathbf{A} , the following relationship may be set up

$$\mathbf{A} \times \mathbf{D} = \mathbf{F} \tag{14}$$

where \mathbf{D} is the vector

$$\langle (\sigma_{1,1} - \sigma_{3,3}), (\sigma_{2,2} - \sigma_{3,3}), \sigma_{2,3}, \sigma_{1,3}, \sigma_{1,2} \rangle \quad (15)$$

of the unknown stresses to be solved for and \mathbf{F} is the vector

$$\langle [0]_1, \dots, [0]_n, [C_0 + \mu \sigma_{3,3}]_1, \dots, [C_0 + \mu \sigma_{3,3}]_n \rangle \quad (16)$$

where the first n terms are zero and the last n terms are $(C_0 + \mu \sigma_{3,3})$ thus satisfying assumptions number 1 and 2 described in section 7.1.

Equation (14) is an overdetermined linear system (*i.e.* there are more equations than unknowns) in which the tensor \mathbf{A} is determined from the measured fault normal and slip vector orientations and the vector \mathbf{F} represents the chosen values for μ and C_0 . The stress vector \mathbf{D} is determined by using a standard least-squares linear inversion method (Schied, 1968; Anton, 1981, p. 315-327; Fröberg, 1985, p. 155-157, 250-254). Since \mathbf{D} yields the paleostress tensor $\sigma_{i,j}$, the magnitudes and orientations of the principal stresses σ_1 , σ_2 , and σ_3 may thus be determined.

7.3 Program Input

The program utilizing Reches' method of paleostress analysis requires six items of information to run -- the fault's strike ($0^\circ \rightarrow 360^\circ$), the fault's dip angle ($0^\circ \rightarrow 90^\circ$), the trend of a slickenline on the fault surface ($0^\circ \rightarrow 360^\circ$), the plunge of that slickenline ($0^\circ \rightarrow 90^\circ$), the rotation sense of the fault as viewed down the plunge of the rotation axis (1 = clockwise and 2 = counterclockwise), and the confidence level of the fault (1 = excellent \rightarrow 4 = poor).

This information must be in an ASCII data file where each fault datum is written on a single line as integers separated by blank spaces.

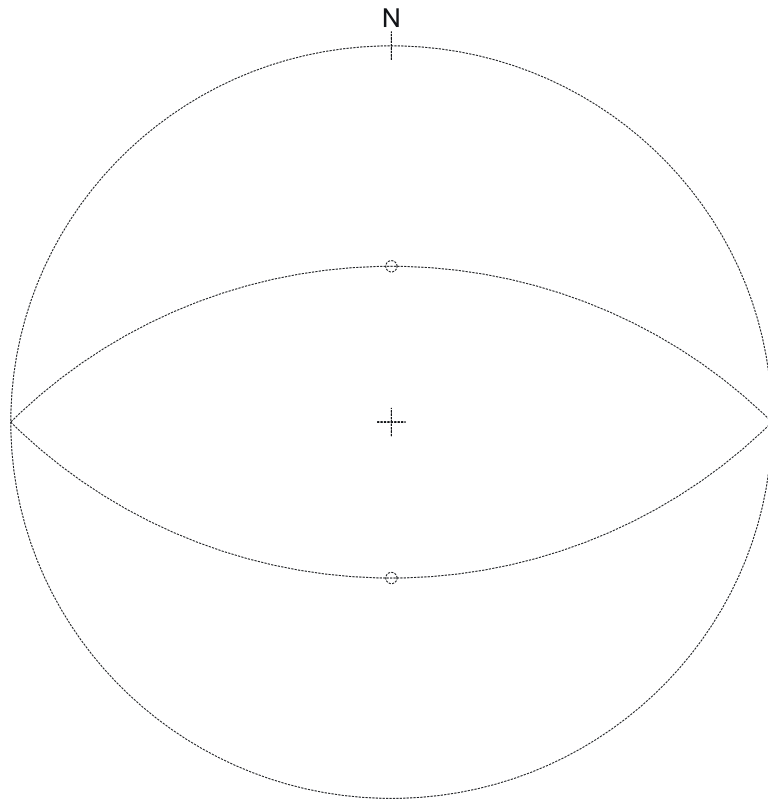


Figure 7-1 - Lower-hemisphere stereographic projection showing a conjugate set of two normal faults with an east-west strike and a dip of 45°

As an example, a conjugate set of two normal faults with an east-west strike and a dip of 45° (figure 7-1) would be written to the input file as

090	45	180	45	2	1
270	45	000	45	2	1

since the first fault has a strike of 090°, a dip of 45°, a slickenline with a trend of 180° and a plunge of 45°, a counterclockwise (2) rotation sense, and a confidence level of 1 (excellent). The second fault has a strike of 270°, a dip of 45°, a slickenline with a trend of 000° and a plunge of 45°, a counterclockwise (2) rotation sense, and a confidence level of 1 (excellent).

Once the ASCII data file has been read into the program, the user is asked to supply values for the coefficient of friction μ , the cohesion C_0 , and the fluid pressure P_{H_2O} on the fault. The fluid pressure term simply results in a lower effective normal stress on the fault and was set to zero for all tests of the program. The coefficient of friction and cohesion were normally set equal to the values used when creating the artificial fault populations with the slip vector calculation program (chapter 5).

7.4 Program Procedures

When all of the data has been entered into the program, the direction cosines of the normal and slip vectors (equations 1 and 2) are calculated. Using equation (6), the components of vector **B** orthogonal to vectors **N** and **S** are determined. Next, the coefficients of matrix **A** (equation 13) and vector **F** are calculated using N_i , S_i , B_i , μ , and C_0 .

The overdetermined system $\mathbf{A} \times \mathbf{D} = \mathbf{F}$ (equation 14) must now be solved for **D** by using standard linear algebra methods for determining a least-squares linear inversion of **A** (Schied, 1968; Anton, 1981, p. 315-327; Fröberg, 1985, p. 155-157,250-254) such that

$$\mathbf{D} = \mathbf{A}^{-1} \times \mathbf{F} \quad (17)$$

When the five components of vector \mathbf{D} are calculated, the vertical stress $\sigma_{3,3}$ is set equal to 1.0 and scales the magnitudes of $\sigma_{1,1}$ and $\sigma_{2,2}$ since the first two components of vector \mathbf{D} are $(\sigma_{1,1} - \sigma_{3,3})$ and $(\sigma_{2,2} - \sigma_{3,3})$.

The components of vector \mathbf{D} contain all of the $\sigma_{i,j}$ components of the stress tensor σ which may, in turn, be used to determine the magnitudes and orientations of the three principal stress axes σ_1 , σ_2 , and σ_3 . The three eigenvalues and eigenvectors of the 3 x 3 stress tensor σ correspond to the magnitudes and orientations of the three principal stress axes respectively. These eigenvalues and eigenvectors may be calculated using standard linear algebra techniques (Anton, 1981, p. 261-284; Fröberg, 1985, p. 22-26).

The stress tensor components $\sigma_{i,j}$ are now substituted into equation (11) for each fault. The program calculates, for each of the n faults, the normal stress σ_n , shear stress in the slip direction σ_s , coefficient of friction μ , and the misfit angle. The misfit angle, or angular divergence, is the angle between the observed slip direction (given by slickenlines on the fault plane and the fault's shear sense) and the expected slip direction determined by the calculated paleostress tensor. The mean angular divergence and coefficient of friction are also calculated for the population.

The goal of Reches' method is to find a geologically-reasonable coefficient of friction μ which will result in a paleostress tensor which yields the lowest average angular divergence.

7.5 Program Output

The program results, along with the initial data, are displayed on the computer's screen

```

File.....PH20.....Friction.....Cohesion.....N
C:\fault.dat.....0.00.....0.65.....0.....12
-----
Sigma 1.....Sigma 2.....Sigma 3.....S2-S3/S1-S2.....Confidence Weighting
-----
194;82.....97;1.....7;8.....1;2;3;4
1.015.....0.475.....0.212.....0.327
-----
Field Data:.....Predicted Values
-----
Fault Fault Slicks Con Fault Fault Slicks Anglr Normal Shear Coeff
No. Str,Dip Az,Plg fdnc Class Class Az,Plg Dvrgnc Stress Stress Frct'n
-----
1 282;44 1;42 1 N N 9;44 6 0.736 0.382 0.52
2 104;64 163;59 1 N N 179;62 8 0.303 0.250 0.82
3 115;38 186;36 1 N N 193;37 6 0.615 0.394 0.64
4 61;49 180;45 1 N N 183;44 2 0.527 0.356 0.68
5 56;51 181;45 1 N N 182;45 1 0.523 0.342 0.65
6 113;67 152;56 1 N N 161;60 6 0.286 0.210 0.72
7 103;55 174;54 1 N N 186;55 7 0.382 0.226 0.85
8 70;65 204;57 1 N N 211;53 5 0.336 0.246 0.72
9 69;59 193;54 1 N N 199;52 4 0.391 0.299 0.76
10 301;52 358;47 1 N N 19;51 14 0.644 0.383 0.59
11 126;35 193;33 1 N N 198;34 4 0.673 0.381 0.57
12 144;50 193;42 1 N N 198;44 4 0.547 0.323 0.61
-----
Averages:.....6.....0.497.....0.325.....0.68
-----

```

Figure 7-2 - Figure showing the graphical output from Reches' method of paleostress analysis using Kenneth Hardcastle's (1989) program. This is an analysis from a population of 12 artificially generated faults. See text for an explanation of the header abbreviations used.

in the format shown in figure 7-2.

The output data consists of -- the file name containing the original fault population input data; the fluid pressure P_{H_2O} , coefficient of friction μ , and cohesion C_0 values chosen by the user; the number (N) of faults in the population; the trend and plunge in degrees of the three principal stress axes σ_1 , σ_2 , and σ_3 and their relative magnitudes; the stress ratio Φ (denoted by S1-S3/S2-S3); the entered strike and dip in degrees (Str,Dip) of each fault; the entered trend and plunge in degrees (Az,Plg) of the slickenlines for each fault; the entered confidence level (Confduc) for each fault; the fault class obtained from the entered rotation sense for each fault; the predicted fault class for each fault; the predicted trend and plunge in degrees (Az,Plg) of the slickenlines for each fault; the angular divergence in degrees (Anglr Dvrgnc) between the entered slickenline orientations and the predicted slickenline orientations for each fault; the calculated normal and shear stresses on each fault; the calculated coefficient of friction (Coeff. Frct'n) for each fault; and the averages of the calculated angular divergences, normal stresses, shear stresses, and coefficients of friction for the fault population.

After the data has been displayed, the user has the option of saving the data to an ASCII data file and/or running the same population again for a different set of fluid pressure, coefficient of friction, and cohesion values. The data for each paleostress analysis I obtained was plotted on lower-hemisphere stereographic projections by a Turbo Pascal version 3.01 program I wrote for that purpose (Appendix D). The program read the fault population data and the predicted principal stress axes orientations and created AutoCAD script files for plotting stereonet via AutoCAD.

7.6 Discussion

Reches' method of paleostress analysis was chosen for testing for several reasons. I had

a user-friendly copy of the program which worked correctly, the program was written for an IBM PC or compatible computer, the use of a non-linear inversion allows the program to perform calculations for reasonably-sized fault populations in short amounts of time (less than 1 minute for most populations), the program is claimed to be an improvement over Angelier's computational method of paleostress analysis since it takes into account the Coulomb failure criterion, and the method has been used in several published field studies (Reches, 1987; Hardcastle, 1989).

CHAPTER 8

PALEOSTRESS ANALYSIS TEST DATA

The artificial fault populations used for testing the two paleostress analysis programs were created with four specific questions in mind:

1. How accurate are paleostress analysis programs given a geologically-realistic population of faults?
2. How do the paleostress analysis programs react to special types of fault populations?
3. How sensitive are paleostress analysis programs to errors in the initial fault population data?
4. How do the results of paleostress analysis programs compare to one another for the same initial population of faults?

To answer these questions, the fault populations discussed in the following sections were created.

8.1 Creating the Artificial Fault Populations

For creating the artificial fault populations, a standard stress field was defined. This allowed for easy comparison between the results of the paleostress analyses and did not significantly constrain the tests in any way. The slip vector calculation program requires the user to specify the orientations for the principal stress axes σ_1 and σ_3 , the relative magnitudes

for the most compressive σ_1 and the least compressive σ_3 principal stress axes, and values for the coefficient of friction μ and cohesion C_0 acting upon the fault planes (chapter 5). For all of the artificial fault populations discussed in this chapter, the above values were set such that σ_1 had a plunge and trend of 90/000 (up) with a relative magnitude of +1.0, σ_3 had a plunge and trend of 00/000 (north) with a relative magnitude of -1.0, the coefficient of friction μ was set to 0.85 (Barton and Choubey, 1977; Byerlee, 1978), and the cohesion C_0 was set to 0.0. Note that the orientations of σ_1 and σ_3 imply that σ_2 has an orientation of 00/090 (east). The magnitude of σ_2 is dependant upon the stress ratio Φ which is $[(\sigma_1 - \sigma_3) / (\sigma_2 - \sigma_3)]$.

For each fault-slip datum generated by the slip vector calculation program, the shear stress to normal stress ratio was examined. If this ratio was too low, the fault could not be expected to slip under any realistic geological conditions. Only those faults with a sufficiently high shear stress to normal stress ratio were used in all of the analyses.

The fault orientation data (the plunge and trend of the fault's normal vector and the pitch angle of the slip vectors) for the fault planes in each population discussed in this chapter are listed in Appendix B.

8.2 Random Fault-Slip Populations

To test the accuracy of the paleostress analysis programs, three random pole fault-slip populations were created in the following manner:

1. A standard stress field was decided upon (section 8.1).
2. A Turbo Pascal version 3.01 program was written to randomly return two numbers -- one between 0 and 89 inclusive and one between 0 and 359 inclusive. The random

numbers were chosen through Turbo Pascal's RANDOM function.

3. The two numbers generated were taken to be the plunge and trend respectively of a pole (normal vector) to a fault plane.
4. The pole to this fault plane was entered into the slip vector calculation program (chapter 5) and the calculated pitch angles of the slip vector in the fault plane and the shear stress to normal stress ratios acting upon the fault plane were returned for five values of Φ ($\Phi = 0.00$, $\Phi = 0.25$, $\Phi = 0.50$, $\Phi = 0.75$, and $\Phi = 1.00$).
5. If the shear stress to normal stress ratios for each value of Φ acting upon the fault plane were all above a cutoff value of 1.0, the fault could be expected to slip under realistic geological conditions and the fault plane was included into the random pole fault population. If one or more of the ratios were below the cutoff value, the fault was not included in the population.
6. Steps 2 through 5 were repeated until three populations of 18 fault planes each were created.

While the fault planes in the random-pole fault populations were randomly chosen, it is important to remember that they do not necessarily have a random spatial distribution. In addition, only those randomly-chosen faults which satisfied a failure criteria for the standard stress field (section 8.1) were included in each population. The purpose of randomly choosing a plunge and trend for each fault plane was not to insure a random spatial distribution of faults, but to insure that any bias in selecting faults to include in each population was eliminated.

Three populations of random-pole faults (labelled RP-01, RP-02, and RP-03), for five values of Φ each, yields a total of 15 fault populations (figures 8-1 → 8-15) to test for each of the two paleostress analysis program used. By comparing the results of these tests to the original standard stress field (section 8.1), the accuracy of the paleostress programs was evaluated.

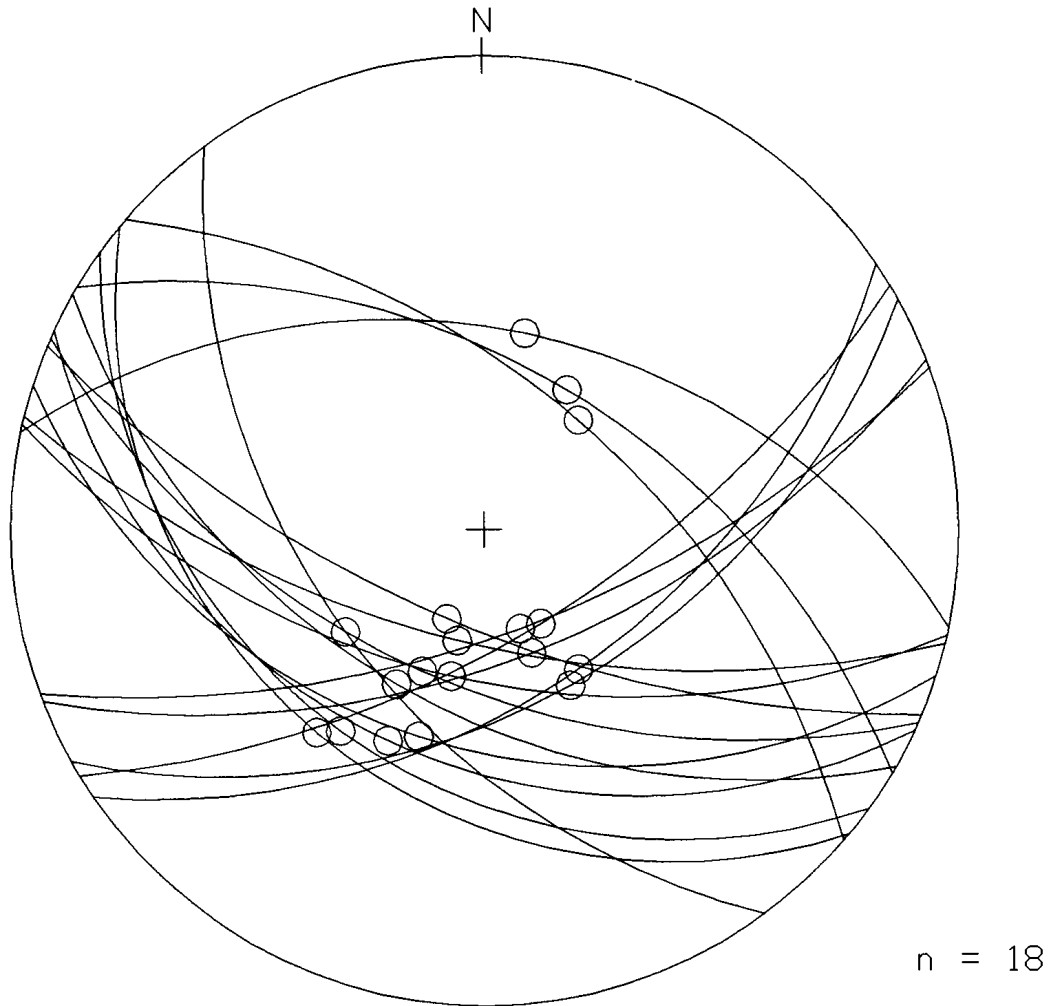


Figure 8-1 - Lower-hemisphere stereographic projection of fault population RP-01 showing 18 normal faults and their associated slip vectors (circles) for a $\bar{\Phi}$ value of 0.00 (RP-01-00). The orientations of the three principal stress axes σ_1 , σ_2 , and σ_3 are up, east, and north respectively.

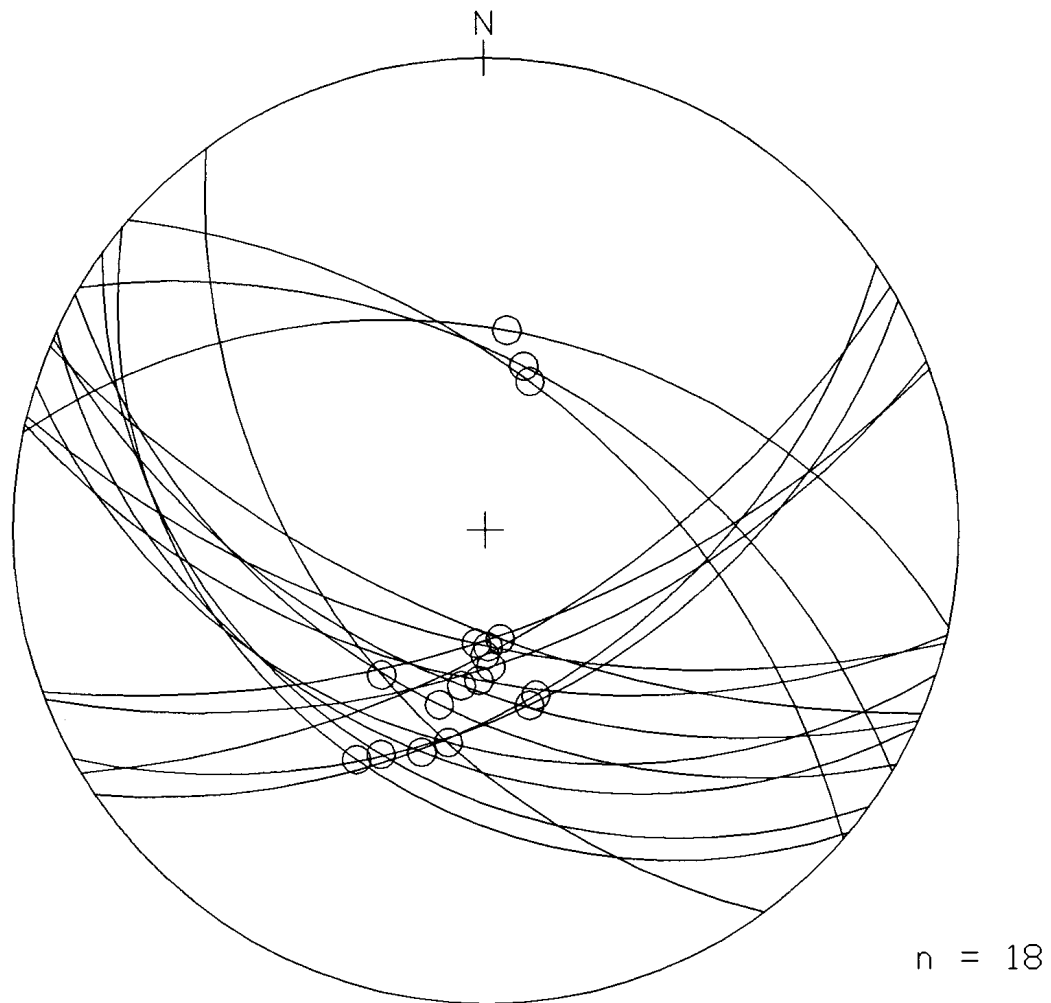


Figure 8-2 - Lower-hemisphere stereographic projection of fault population RP-01 showing 18 normal faults and their associated slip vectors (circles) for a Φ value of 0.25 (RP-01-25). The orientations of the three principal stress axes σ_1 , σ_2 , and σ_3 are up, east, and north respectively.

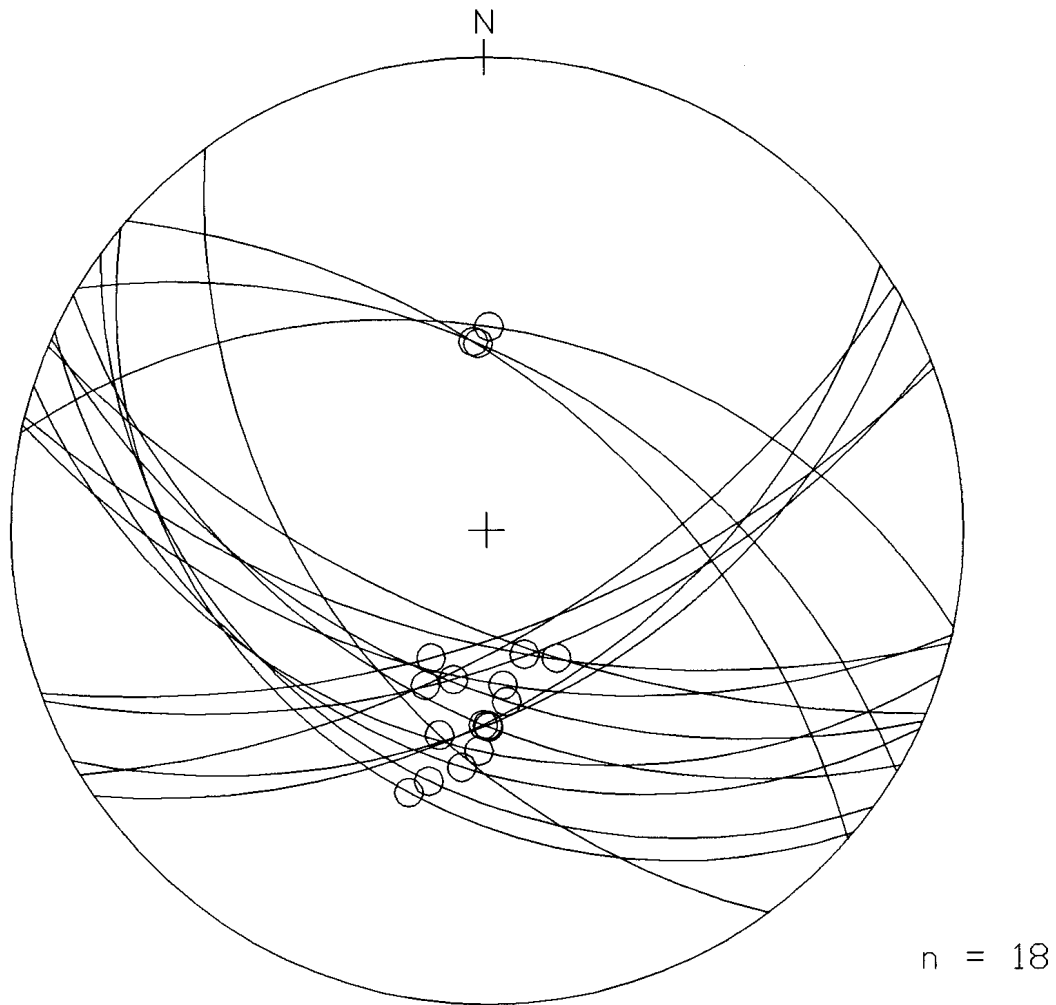


Figure 8-3 - Lower-hemisphere stereographic projection of fault population RP-01 showing 18 normal faults and their associated slip vectors (circles) for a Φ value of 0.50 (RP-01-50). The orientations of the three principal stress axes σ_1 , σ_2 , and σ_3 are up, east, and north respectively.

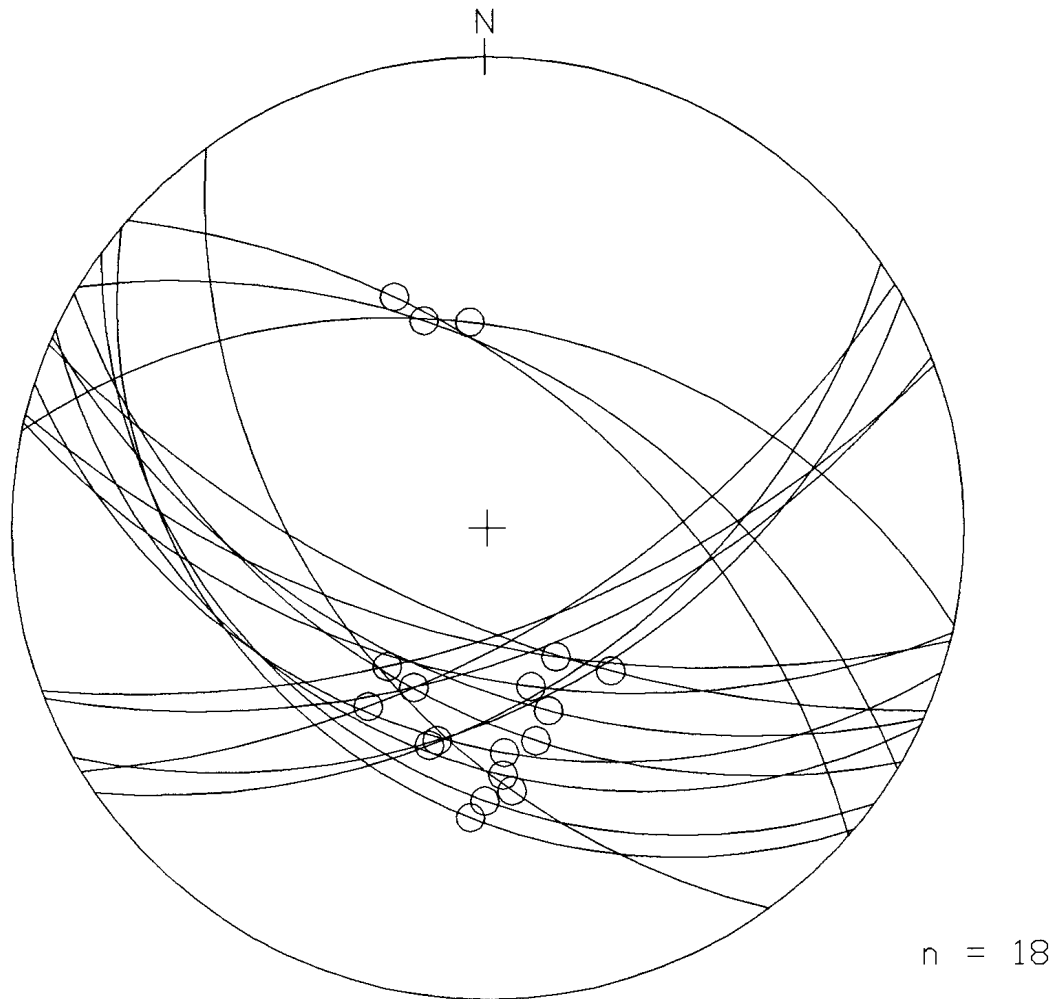


Figure 8-4 - Lower-hemisphere stereographic projection of fault population RP-01 showing 18 normal faults and their associated slip vectors (circles) for a Φ value of 0.75 (RP-01-75). The orientations of the three principal stress axes σ_1 , σ_2 , and σ_3 are up, east, and north respectively.

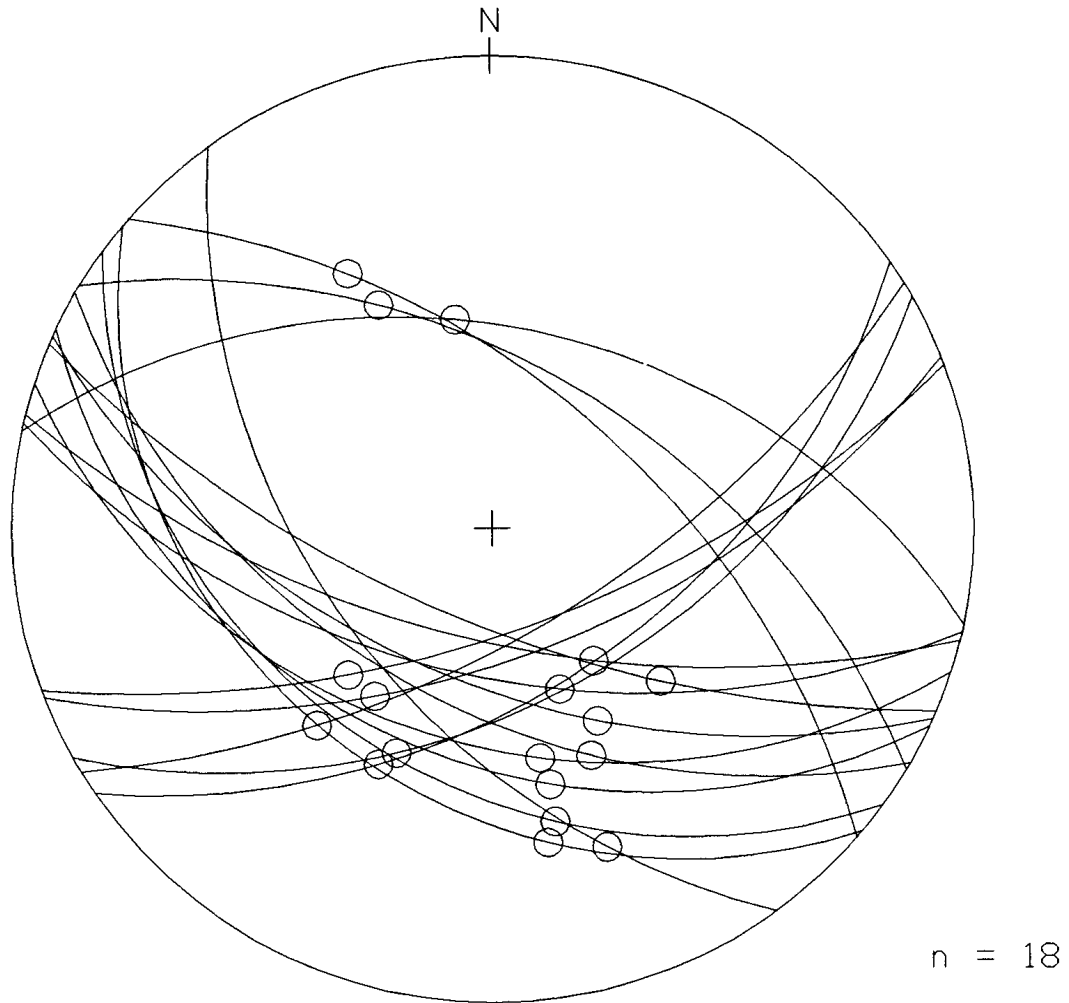


Figure 8-5 - Lower-hemisphere stereographic projection of fault population RP-01 showing 18 normal faults and their associated slip vectors (circles) for a Φ value of 1.00 (RP-01-10). The orientations of the three principal stress axes σ_1 , σ_2 , and σ_3 are up, east, and north respectively.

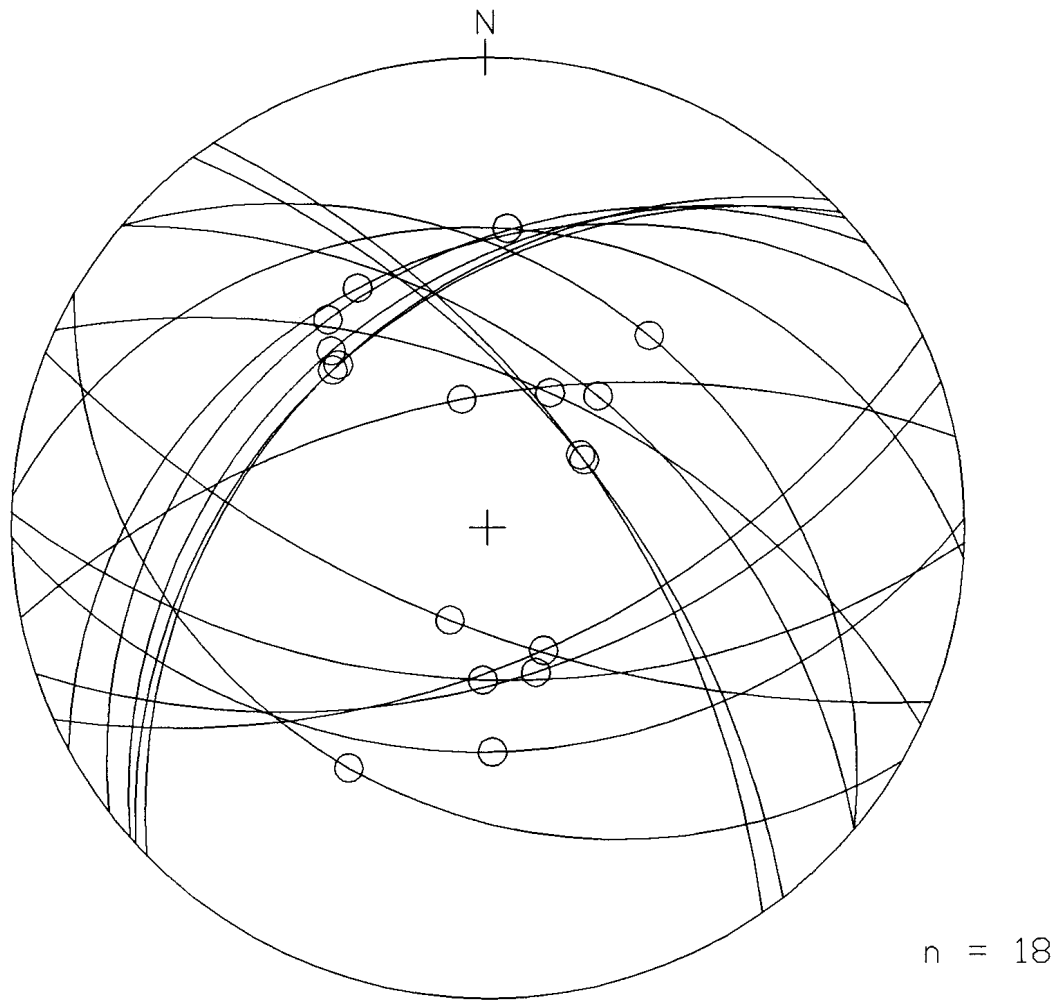


Figure 8-6 - Lower-hemisphere stereographic projection of fault population RP-02 showing 18 normal faults and their associated slip vectors (circles) for a Φ value of 0.00 (RP-02-00). The orientations of the three principal stress axes σ_1 , σ_2 , and σ_3 are up, east, and north respectively.

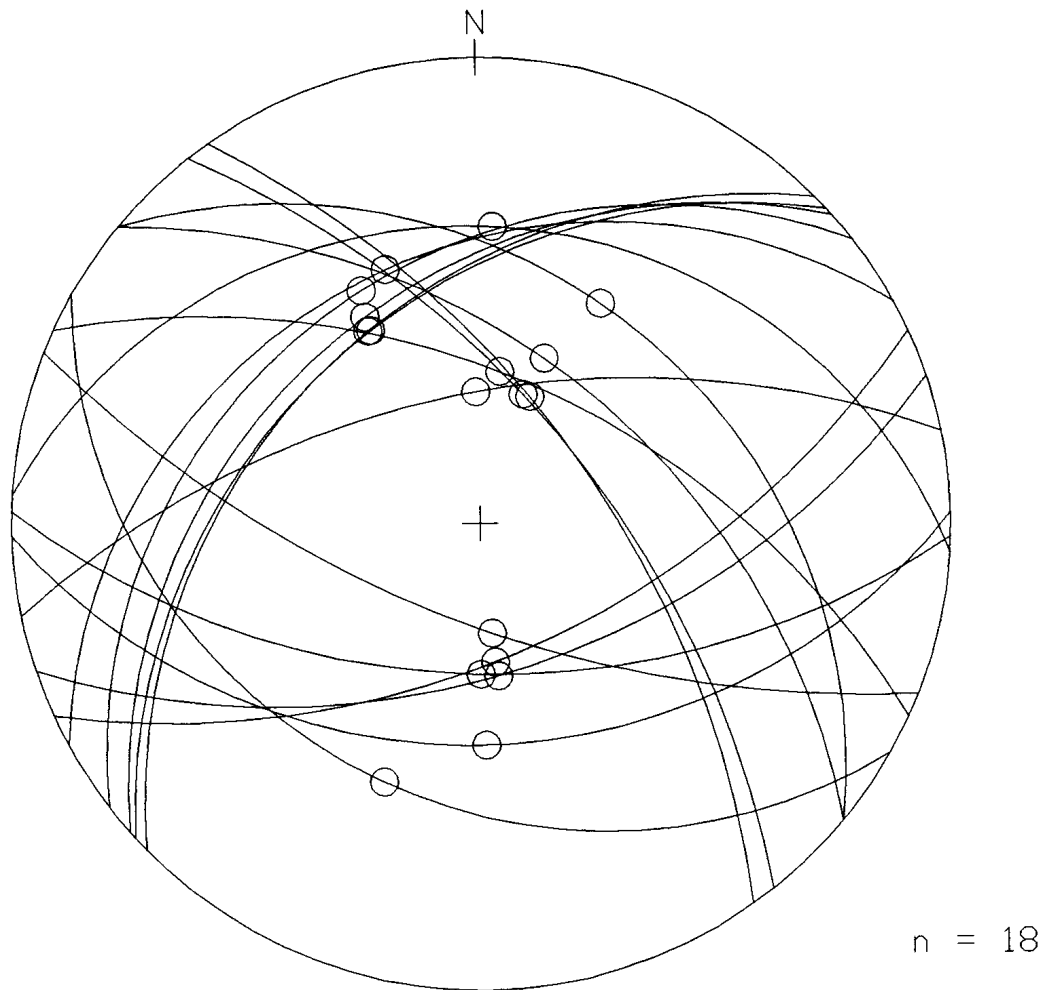


Figure 8-7 - Lower-hemisphere stereographic projection of fault population RP-02 showing 18 normal faults and their associated slip vectors (circles) for a Φ value of 0.25 (RP-02-25). The orientations of the three principal stress axes σ_1 , σ_2 , and σ_3 are up, east, and north respectively.

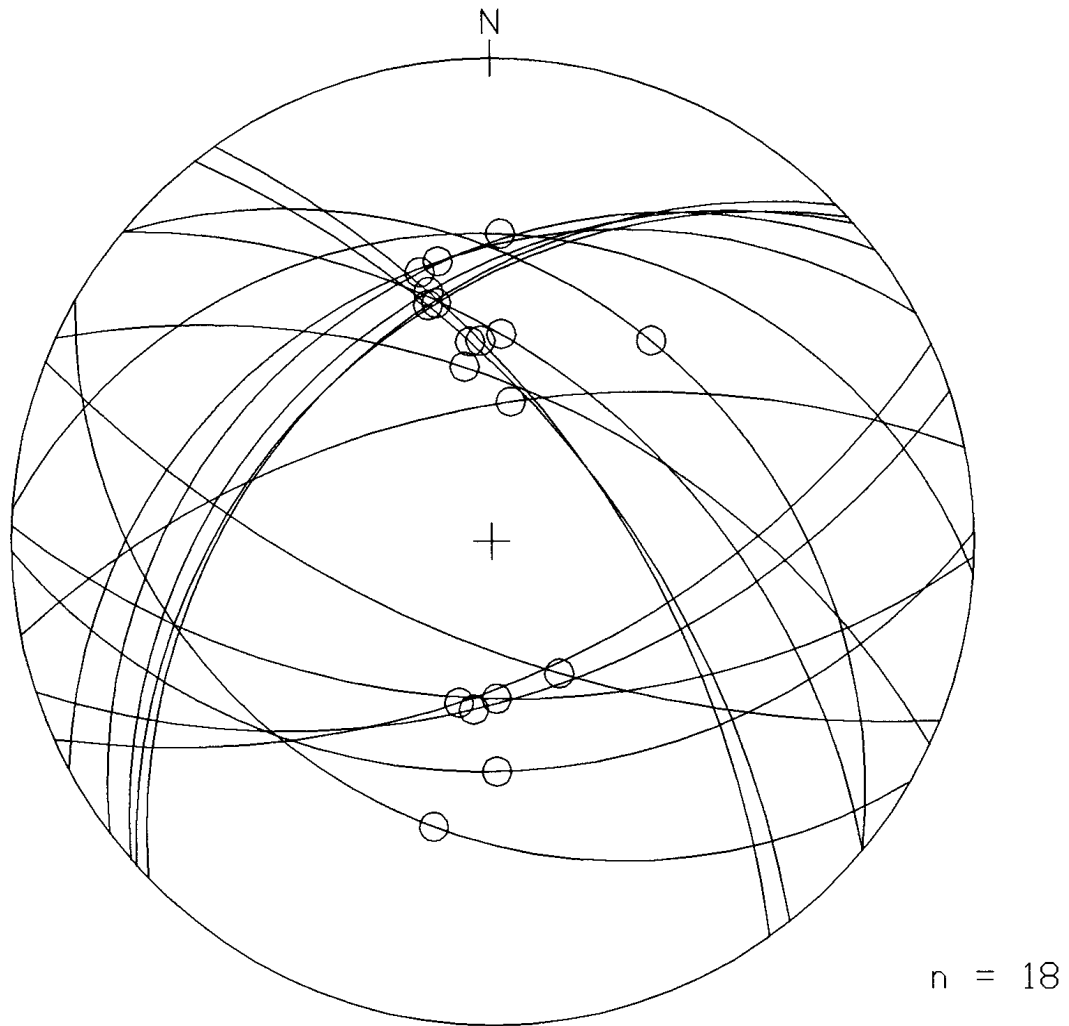


Figure 8-8 - Lower-hemisphere stereographic projection of fault population RP-02 showing 18 normal faults and their associated slip vectors (circles) for a $\bar{\Phi}$ value of 0.50 (RP-02-50). The orientations of the three principal stress axes σ_1 , σ_2 , and σ_3 are up, east, and north respectively.

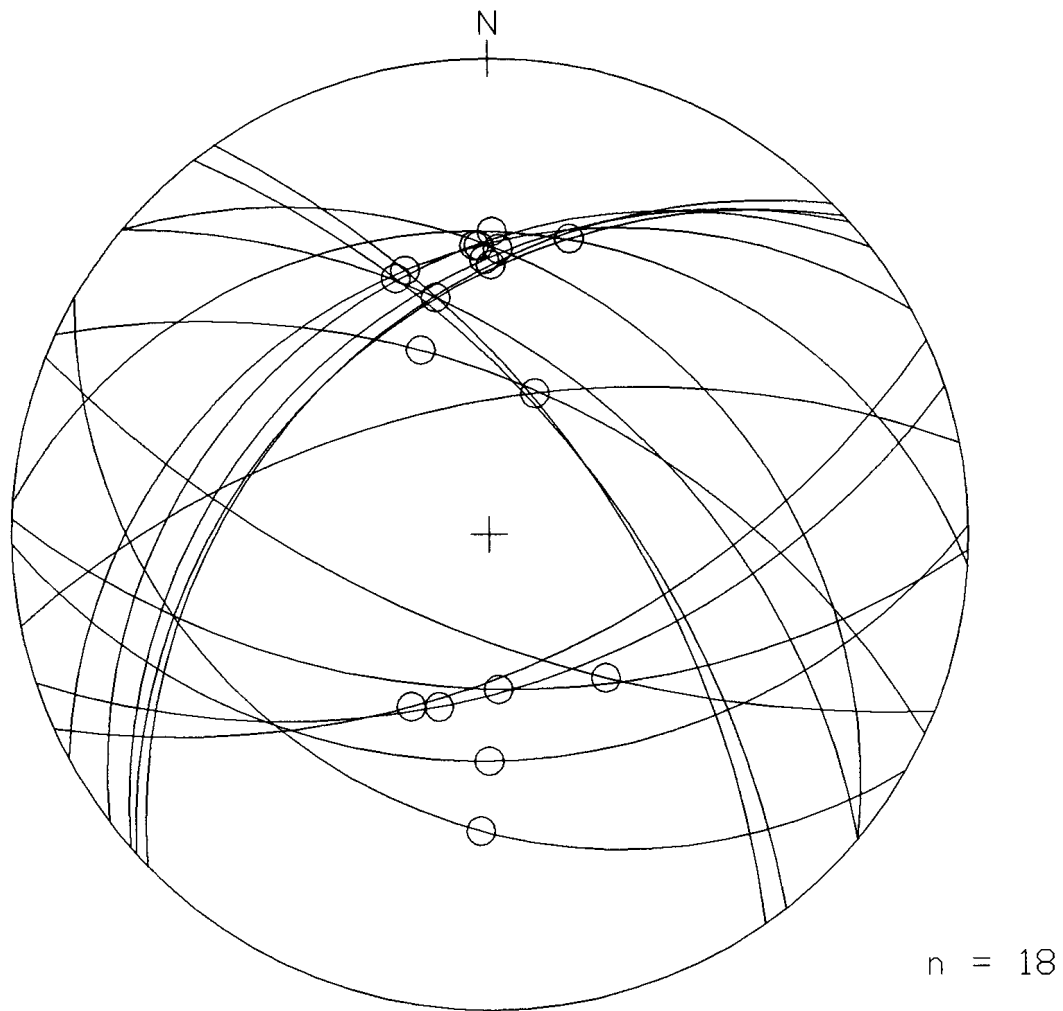


Figure 8-9 - Lower-hemisphere stereographic projection of fault population RP-02 showing 18 normal faults and their associated slip vectors (circles) for a Φ value of 0.75 (RP-02-75). The orientations of the three principal stress axes σ_1 , σ_2 , and σ_3 are up, east, and north respectively.

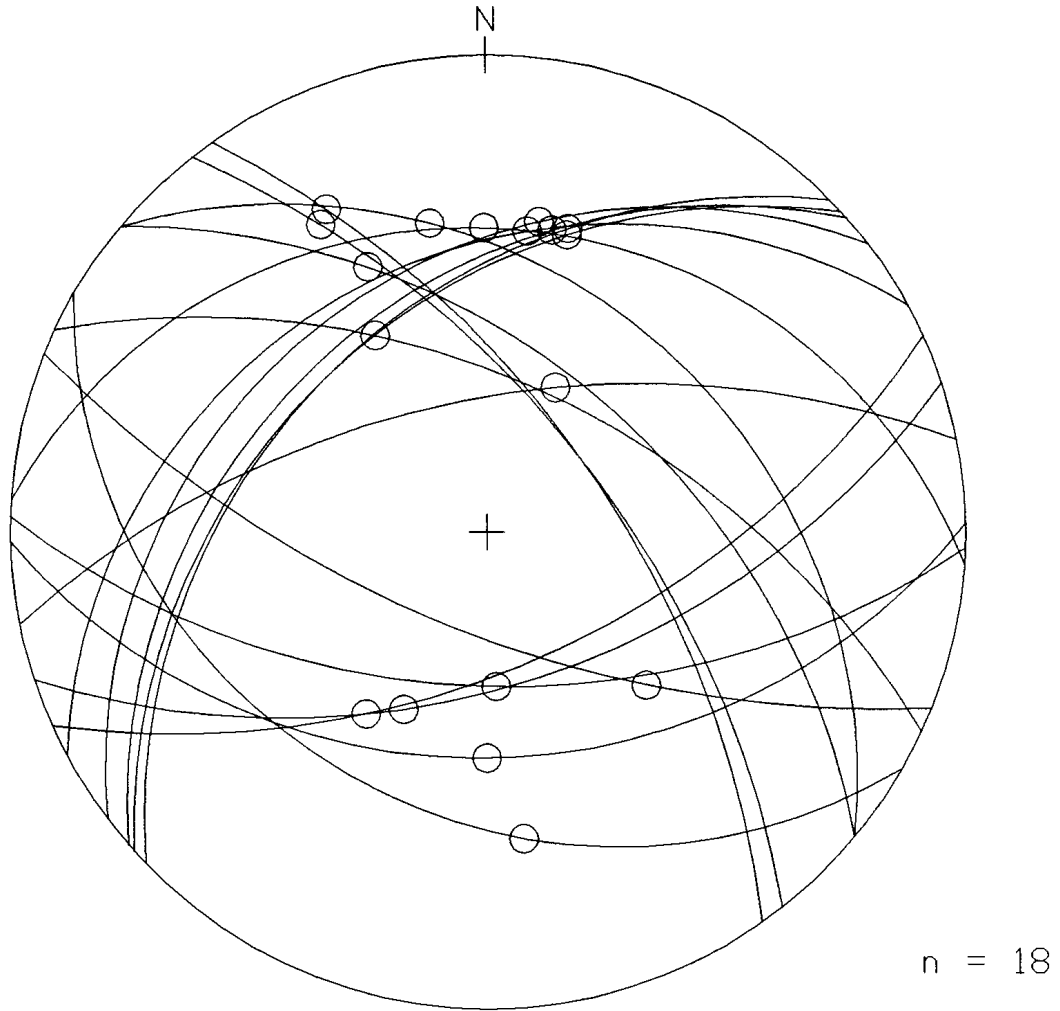


Figure 8-10 - Lower-hemisphere stereographic projection of fault population RP-02 showing 18 normal faults and their associated slip vectors (circles) for a Φ value of 1.00 (RP-02-10). The orientations of the three principal stress axes σ_1 , σ_2 , and σ_3 are up, east, and north respectively.

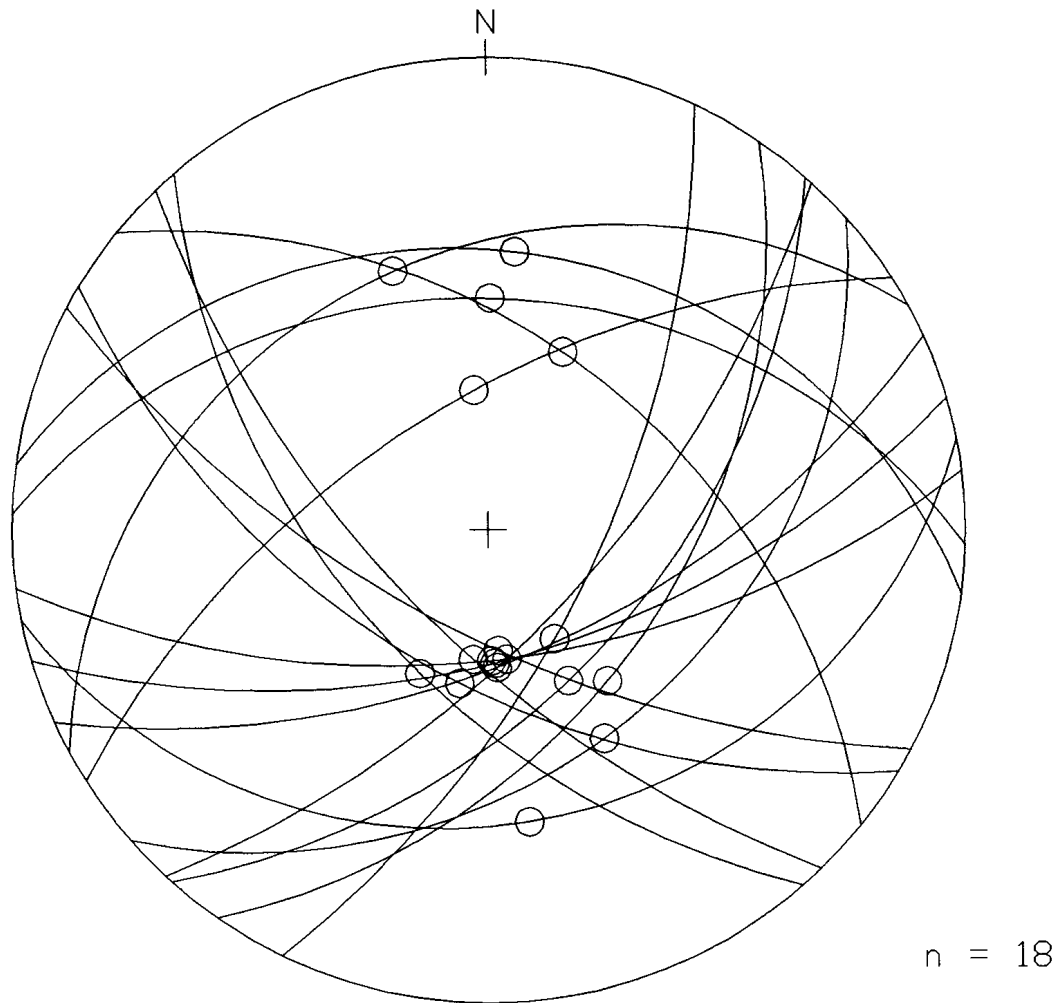


Figure 8-11 - Lower-hemisphere stereographic projection of fault population RP-03 showing 18 normal faults and their associated slip vectors (circles) for a Φ value of 0.00 (RP-03-00). The orientations of the three principal stress axes σ_1 , σ_2 , and σ_3 are up, east, and north respectively.

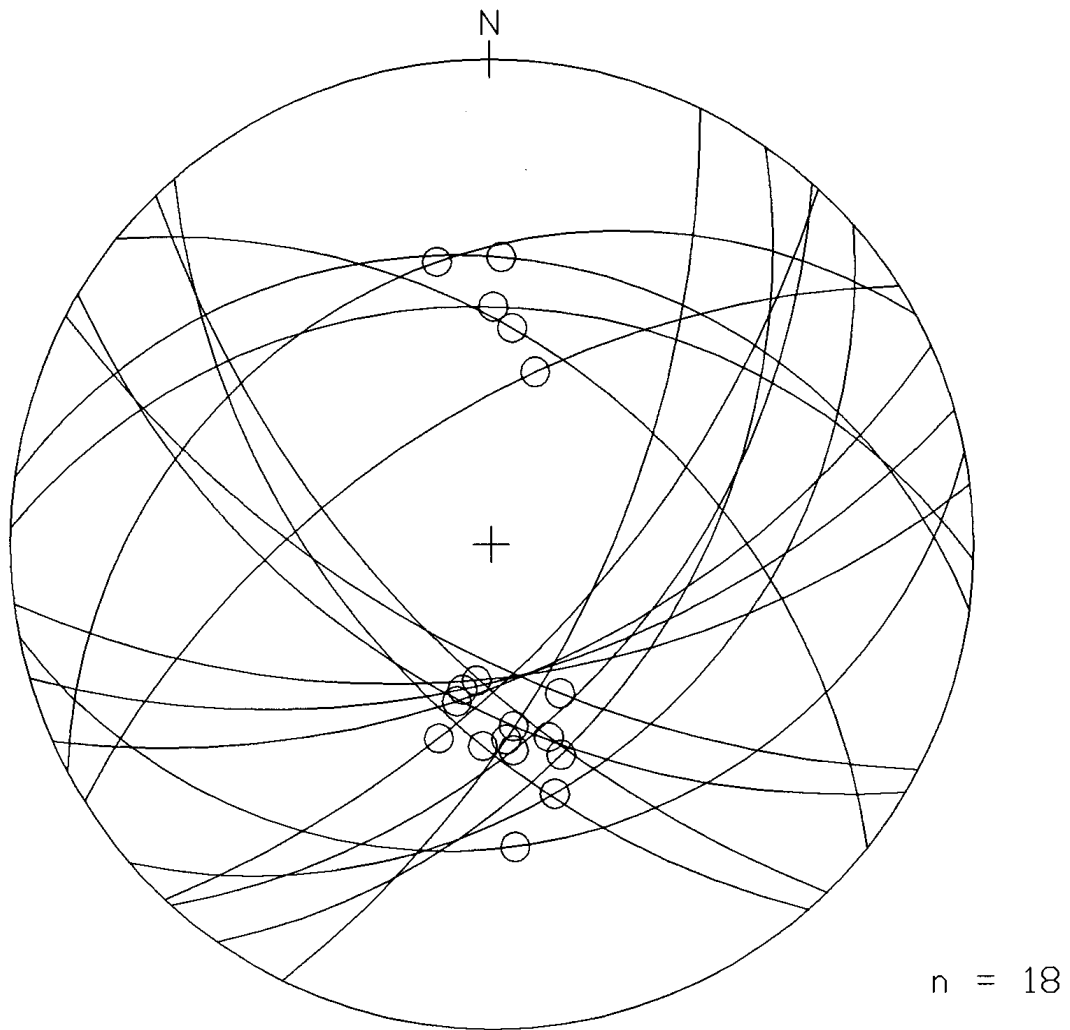


Figure 8-12 - Lower-hemisphere stereographic projection of fault population RP-03 showing 18 normal faults and their associated slip vectors (circles) for a Φ value of 0.25 (RP-03-25). The orientations of the three principal stress axes σ_1 , σ_2 , and σ_3 are up, east, and north respectively.

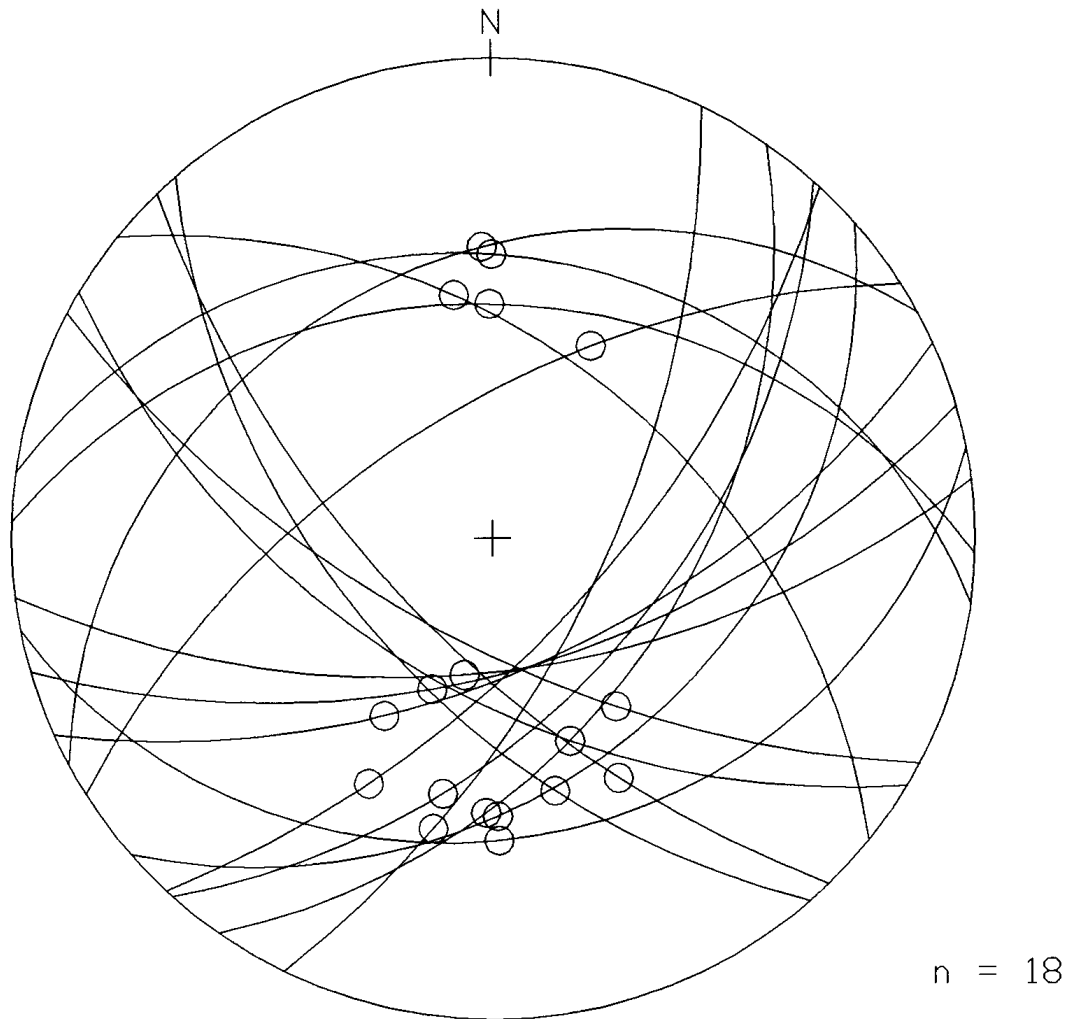


Figure 8-13 - Lower-hemisphere stereographic projection of fault population RP-03 showing 18 normal faults and their associated slip vectors (circles) for a $\bar{\Phi}$ value of 0.50 (RP-03-50). The orientations of the three principal stress axes σ_1 , σ_2 , and σ_3 are up, east, and north respectively.

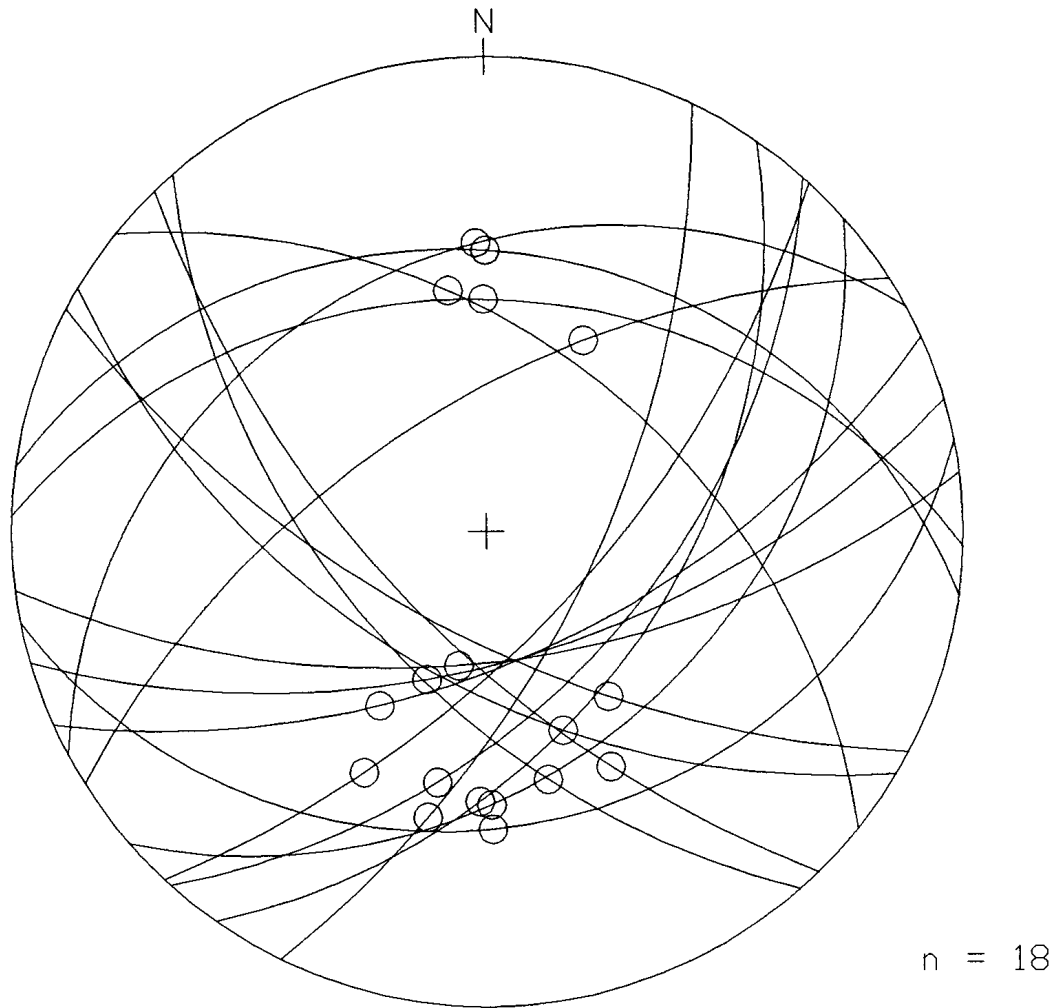


Figure 8-14 - Lower-hemisphere stereographic projection of fault population RP-03 showing 18 normal faults and their associated slip vectors (circles) for a Φ value of 0.75 (RP-03-75). The orientations of the three principal stress axes σ_1 , σ_2 , and σ_3 are up, east, and north respectively.

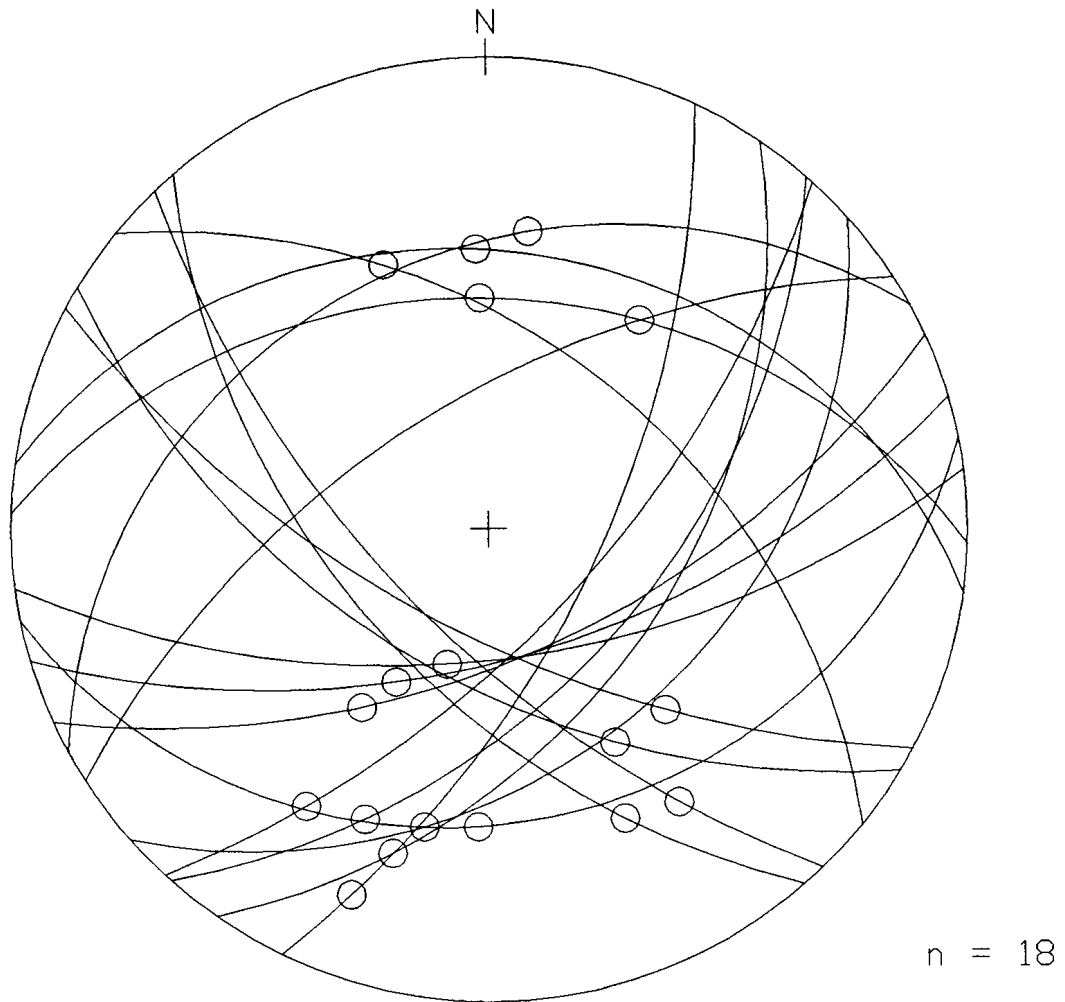


Figure 8-15 - Lower-hemisphere stereographic projection of fault population RP-03 showing 18 normal faults and their associated slip vectors (circles) for a Φ value of 1.00 (RP-03-10). The orientations of the three principal stress axes σ_1 , σ_2 , and σ_3 are up, east, and north respectively.

8.3 Creating Special-Case Fault Populations

The behavior of paleostress analysis programs to special-case fault populations was next examined. Hardcastle (1990) claimed that Reches' method (chapter 7) returned inconsistent results with simple conjugate fault populations and Allmendinger (1989) indicated that Gephart and Forsyth's method (chapter 3) gave inconsistent results for thrust faults when they were all of a very similar orientation. Given the mathematics involved in calculating paleostress tensors from fault data, faults which have orientations close to the principal stress planes (the planes normal to the three principal stress axes) may influence the calculations adversely.

With these thoughts in mind, several special-case fault populations were created -- simple Andersonian conjugate faults, orthorhombic symmetry faults, radial symmetry faults, and faults which all have approximately the same orientation.

8.4 Andersonian Conjugate Fault Populations

Conjugate fault sets are commonly found in the field and used to estimate paleostress orientations (Davis, 1984, p. 306; Ragan, 1985, p. 135; Suppe, 1985, p. 292; Rowland, 1986, p. 134; Dennis, 1987, p. 236; Marshak and Mitra, 1988, p. 261; Spencer, 1988, p. 199). Using Anderson's (1951) theory of faulting (section 2.1), it is a trivial matter to assign possible principal stress axis orientations for a conjugate fault population. The most compressive principal stress axis σ_1 bisects the acute angle of the conjugate faults, the intermediate principal stress axis σ_2 is parallel to the intersection of the conjugate faults, and the least compressive principal stress axis σ_3 bisects the obtuse angle of the conjugate faults. Two conjugate fault populations were chosen for testing to see if the paleostress analysis programs returned the same principal stress axes as Anderson's theory.

The first conjugate fault population (AC-01), was created such that the strikes of all of the faults were either parallel, or subparallel ($\pm 5^\circ$), to the principal plane for the σ_3 axis with their acute angle being bisected by σ_1 (figures 8-16 → 8-20). This population is consistent with Anderson's theory given the standard stress field of up, east, and north for σ_1 , σ_2 , and σ_3 respectively.

The second conjugate fault population (AC-02), was created such that all of the faults were oriented at 45° from the principal planes for the σ_2 and σ_3 axes with their acute angle being bisected by σ_1 (figures 8-21 → 8-25). This population is **not** consistent with Anderson's theory since σ_2 and σ_3 are oriented at 45° from their predicted positions.

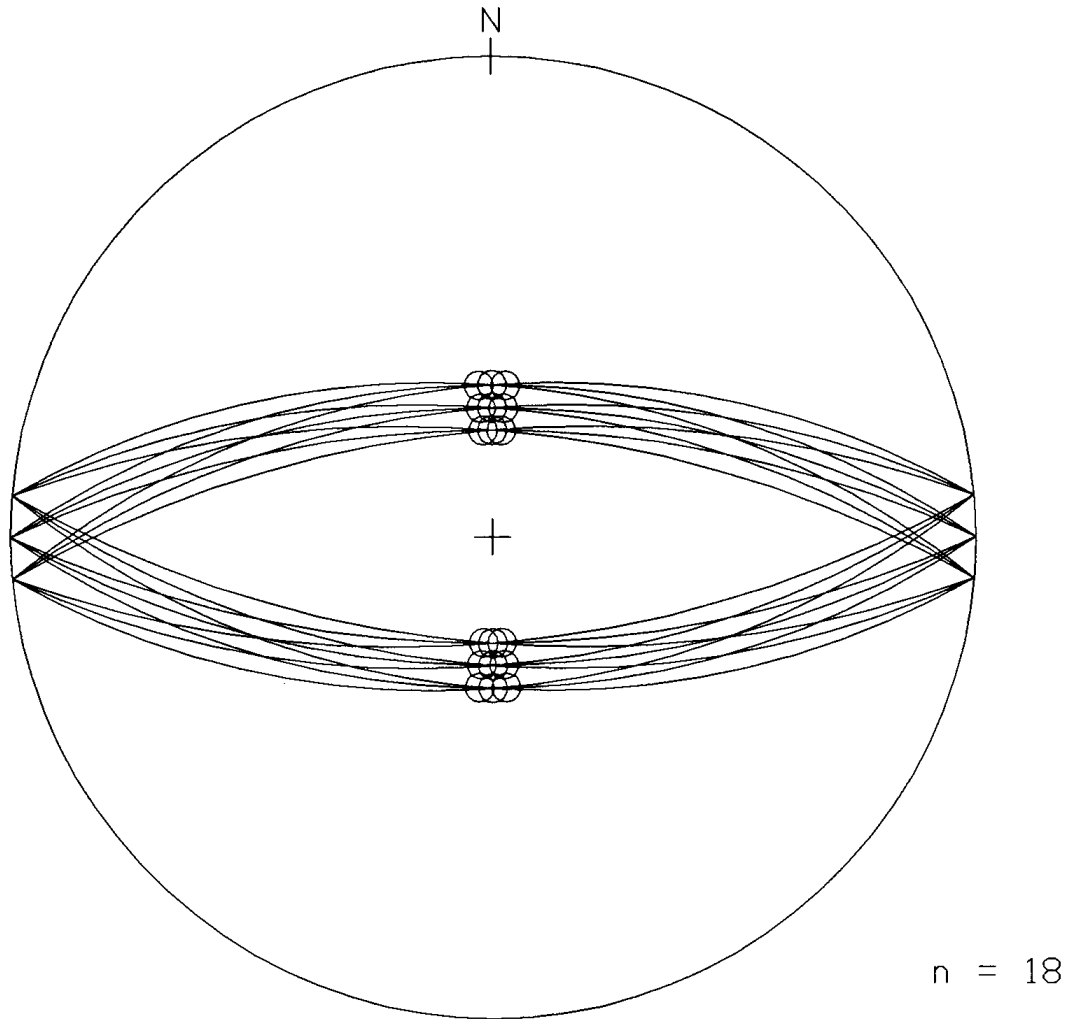


Figure 8-16 - Lower-hemisphere stereographic projection of fault population AC-01 showing 18 normal faults and their associated slip vectors (circles) for a Φ value of 0.00 (AC-01-00). The orientations of the three principal stress axes σ_1 , σ_2 , and σ_3 are up, east, and north respectively.

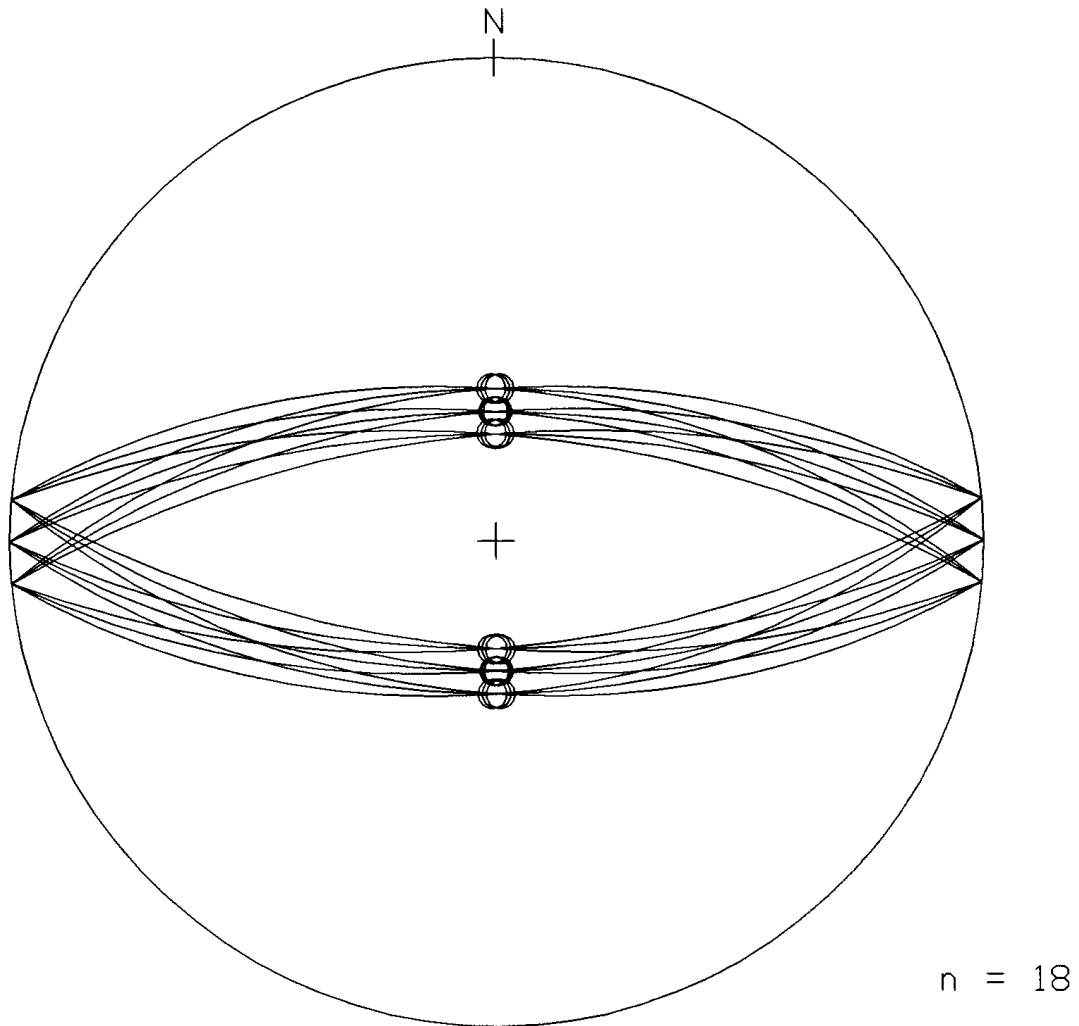


Figure 8-17 - Lower-hemisphere stereographic projection of fault population AC-01 showing 18 normal faults and their associated slip vectors (circles) for a Φ value of 0.25 (AC-01-25). The orientations of the three principal stress axes σ_1 , σ_2 , and σ_3 are up, east, and north respectively.

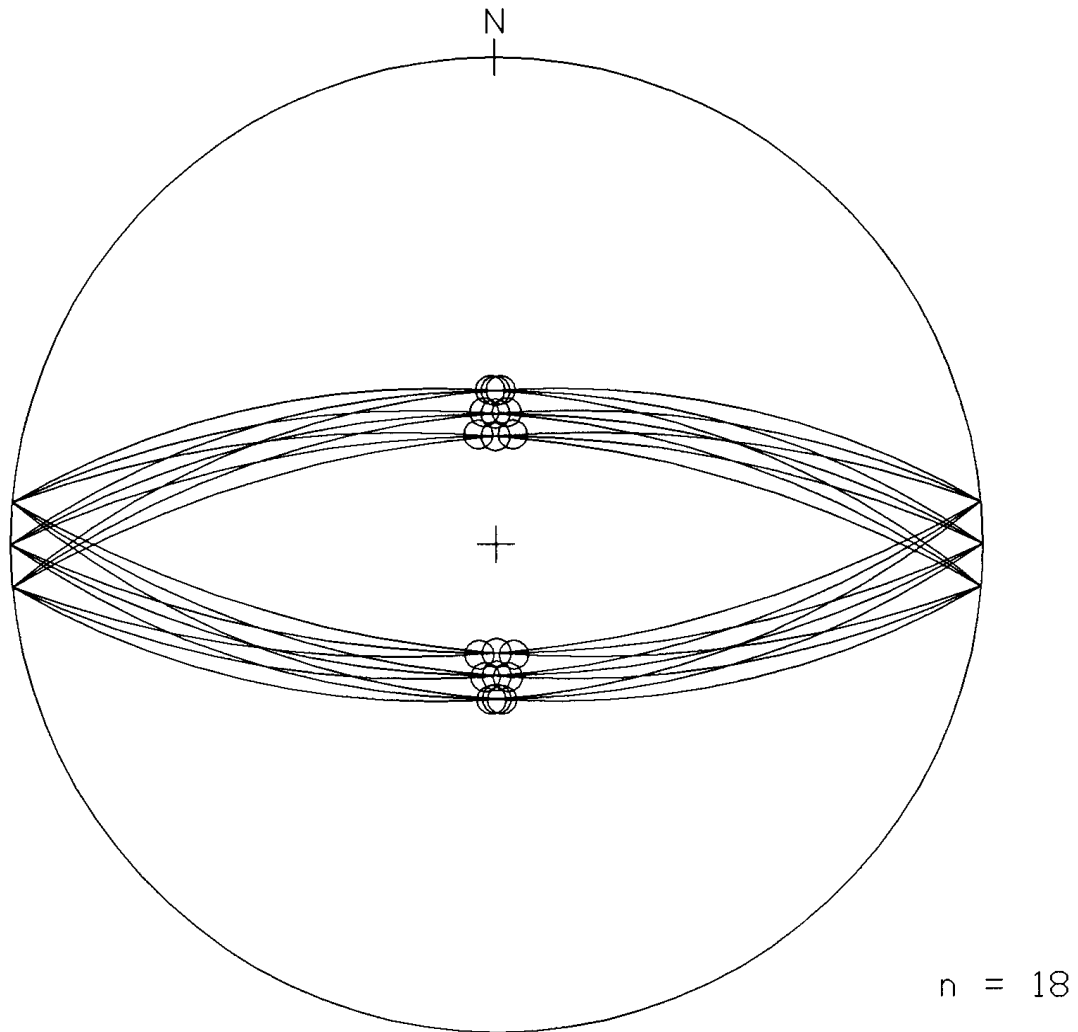


Figure 8-18 - Lower-hemisphere stereographic projection of fault population AC-01 showing 18 normal faults and their associated slip vectors (circles) for a Φ value of 0.50 (AC-01-50). The orientations of the three principal stress axes σ_1 , σ_2 , and σ_3 are up, east, and north respectively.

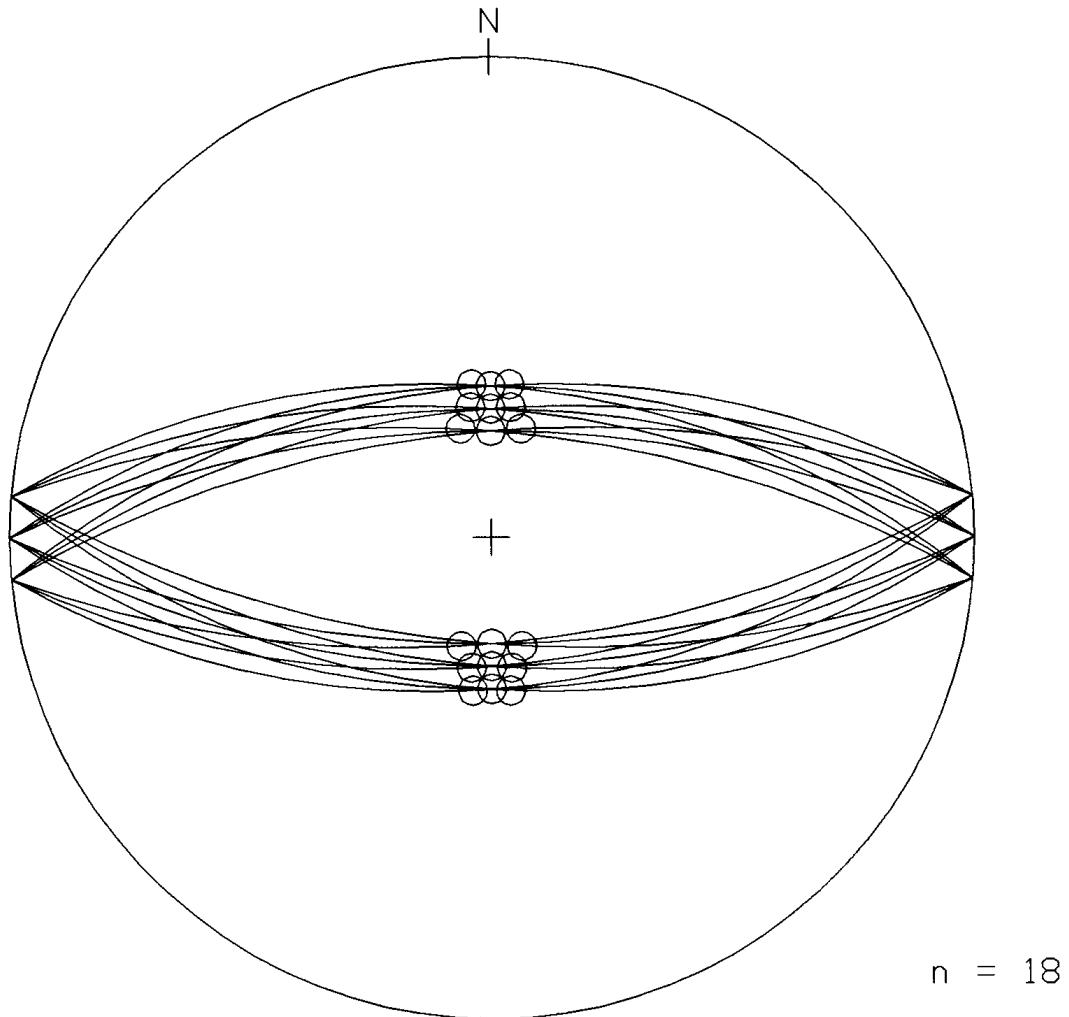


Figure 8-19 - Lower-hemisphere stereographic projection of fault population AC-01 showing 18 normal faults and their associated slip vectors (circles) for a Φ value of 0.75 (AC-01-75). The orientations of the three principal stress axes σ_1 , σ_2 , and σ_3 are up, east, and north respectively.

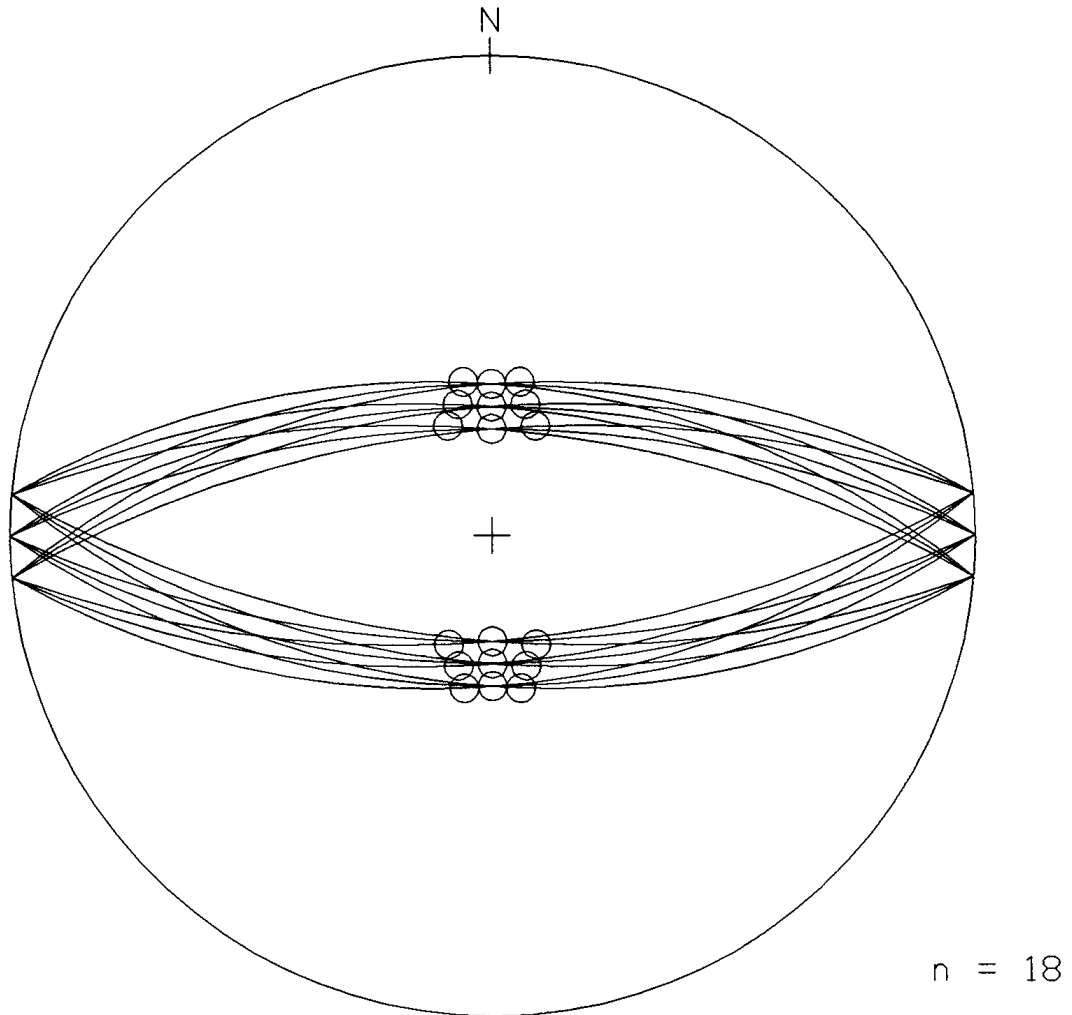


Figure 8-20 - Lower-hemisphere stereographic projection of fault population AC-01 showing 18 normal faults and their associated slip vectors (circles) for a Φ value of 1.00 (AC-01-10). The orientations of the three principal stress axes σ_1 , σ_2 , and σ_3 are up, east, and north respectively.

8.5 Orthorhombic Fault Populations

Orthorhombic, or rhombohedral, fault patterns have been described in several areas (Aydin and Reches, 1982; Krantz, 1986; Krantz, 1989). These faults are termed orthorhombic since they are arranged in an orthorhombic symmetry about the principal strain axes and usually consist of two sets of conjugate normal faults. The occurrence of these faults is not well explained by conjugate faulting theory and Krantz (1989) suggested that orthorhombic fault patterns represent the general, three-dimensional strain case (the odd-axis model) and conjugate faults are thus relegated to the special case of plane strain.

An orthorhombic fault population consisting of 20 faults was created for testing the paleostress analysis programs (OS-01). The 20 faults of the population formed five distinct sets of orthorhombic faults with $\pm 5^\circ$ offsets in strike and dip from the two conjugate sets at 45° from the σ_2 and σ_3 principal planes. For all of the conjugate fault sets in the population, σ_1 bisected their acute angle and σ_2 or σ_3 bisected their obtuse angles (figures 8-26 → 8-30).

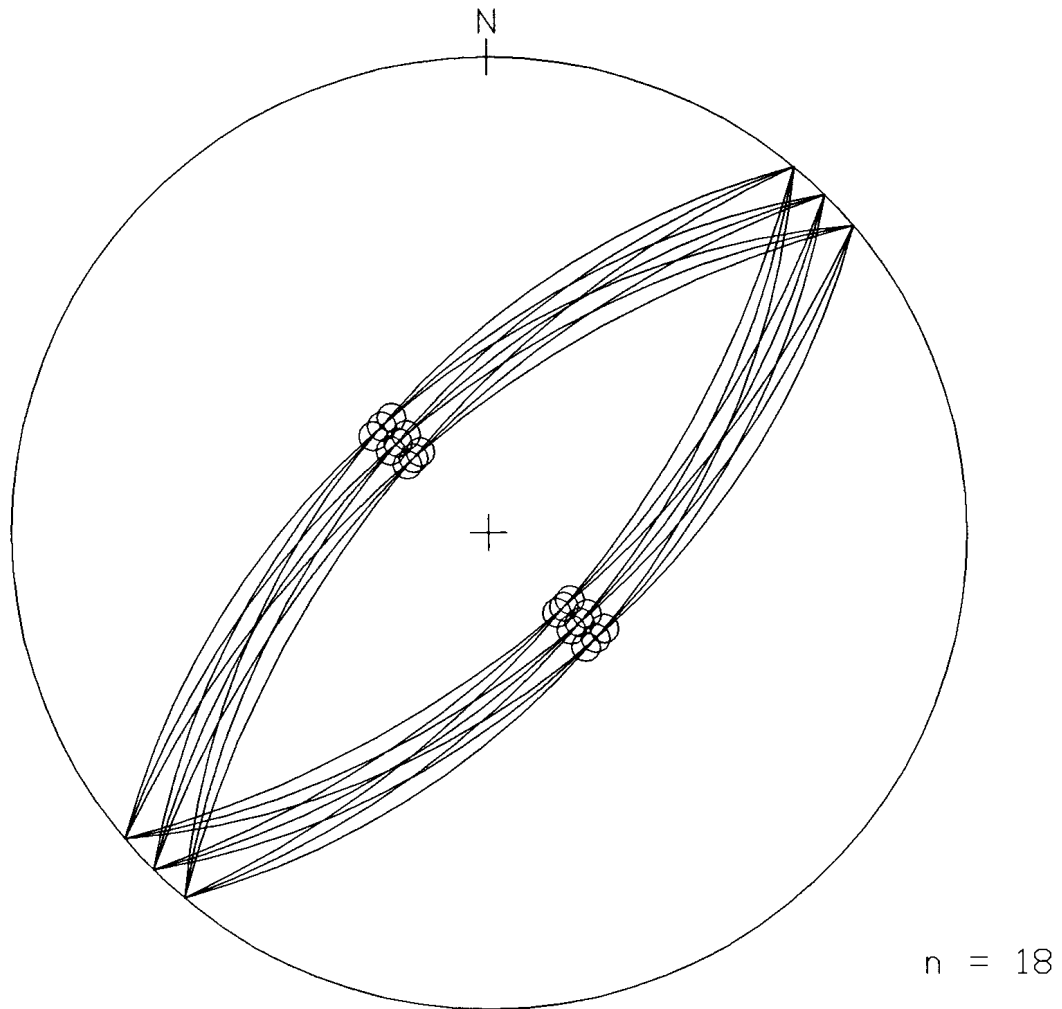


Figure 8-21 - Lower-hemisphere stereographic projection of fault population AC-02 showing 18 normal faults and their associated slip vectors (circles) for a Φ value of 0.00 (AC-02-00). The orientations of the three principal stress axes σ_1 , σ_2 , and σ_3 are up, east, and north respectively.

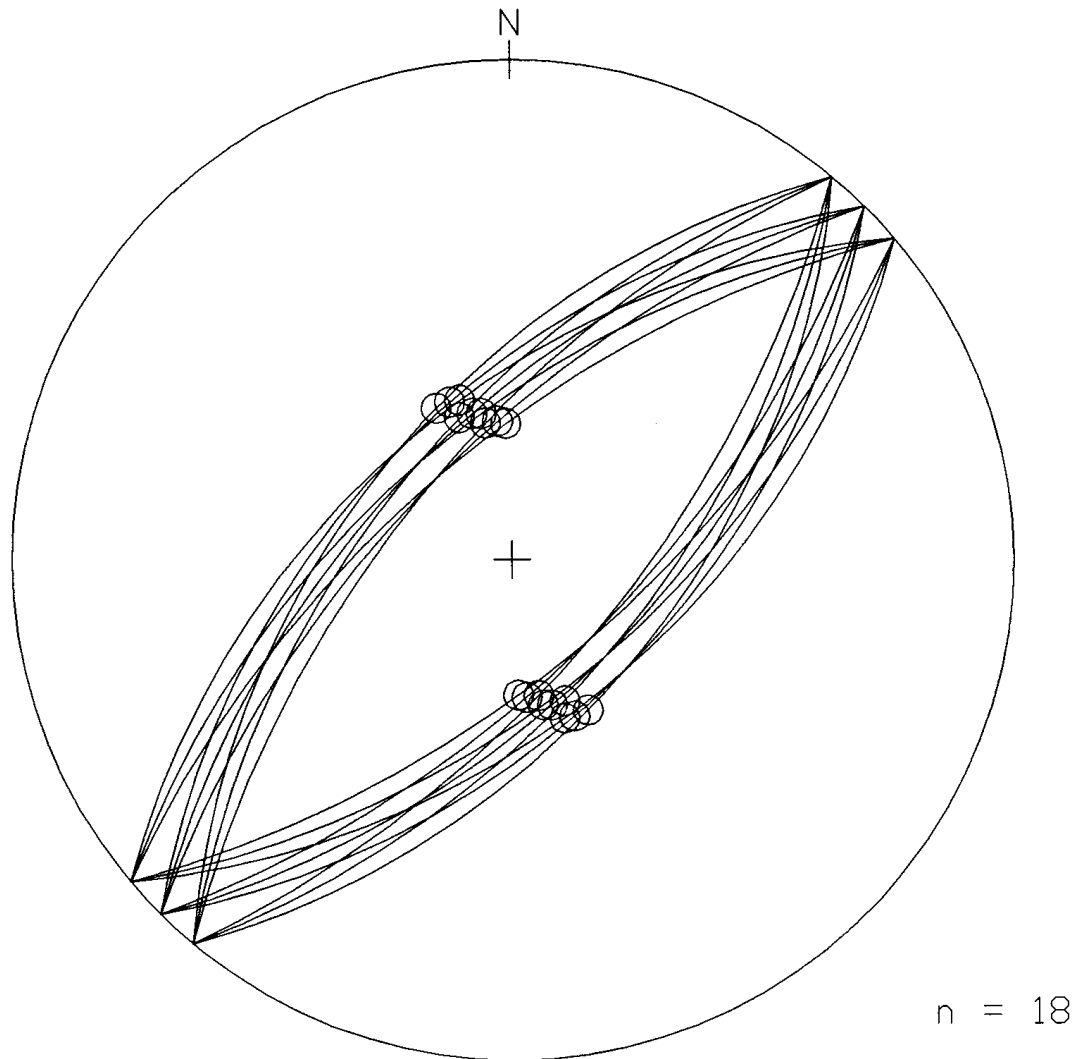


Figure 8-22 - Lower-hemisphere stereographic projection of fault population AC-02 showing 18 normal faults and their associated slip vectors (circles) for a Φ value of 0.25 (AC-02-25). The orientations of the three principal stress axes σ_1 , σ_2 , and σ_3 are up, east, and north respectively.

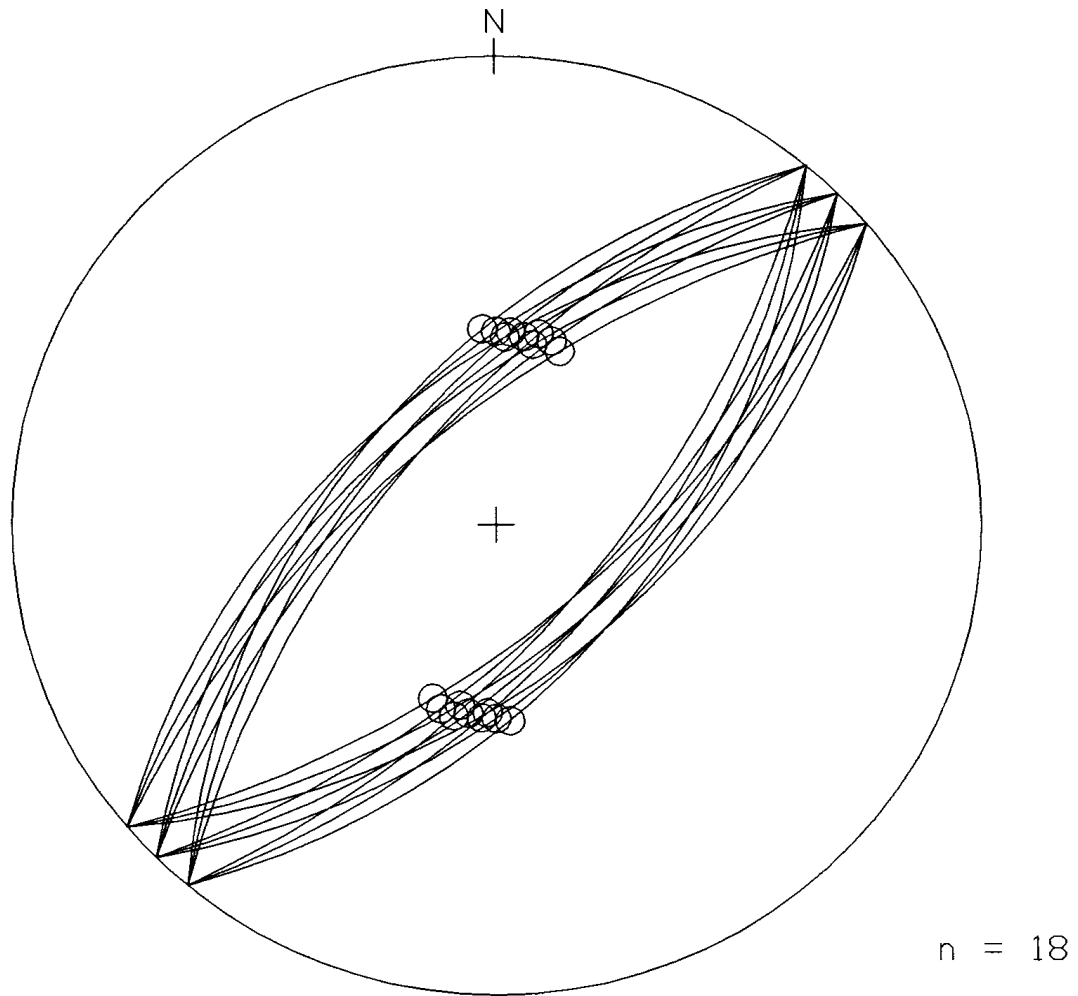


Figure 8-23 - Lower-hemisphere stereographic projection of fault population AC-02 showing 18 normal faults and their associated slip vectors (circles) for a Φ value of 0.50 (AC-02-50). The orientations of the three principal stress axes σ_1 , σ_2 , and σ_3 are up, east, and north respectively.

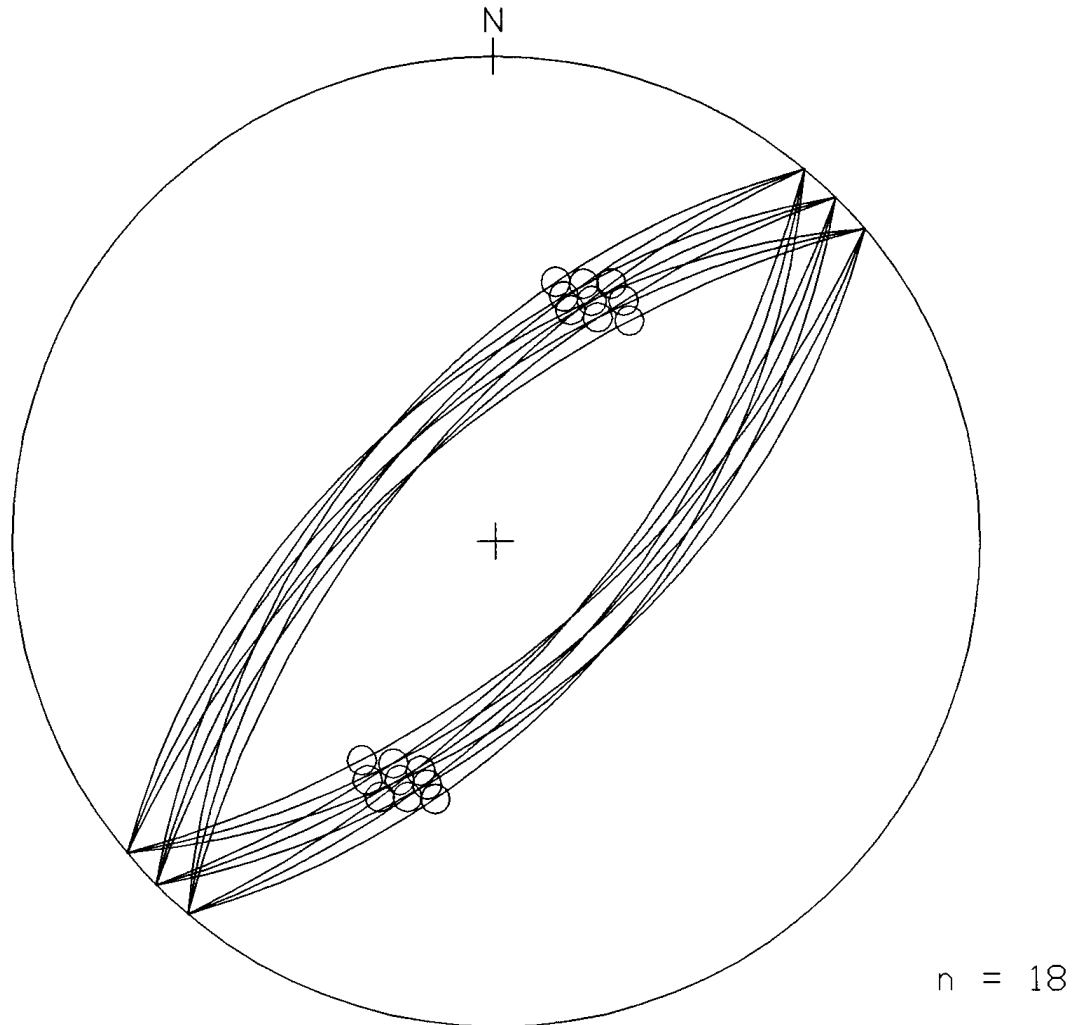


Figure 8-24 - Lower-hemisphere stereographic projection of fault population AC-02 showing 18 normal faults and their associated slip vectors (circles) for a Φ value of 0.75 (AC-02-75). The orientations of the three principal stress axes σ_1 , σ_2 , and σ_3 are up, east, and north respectively.

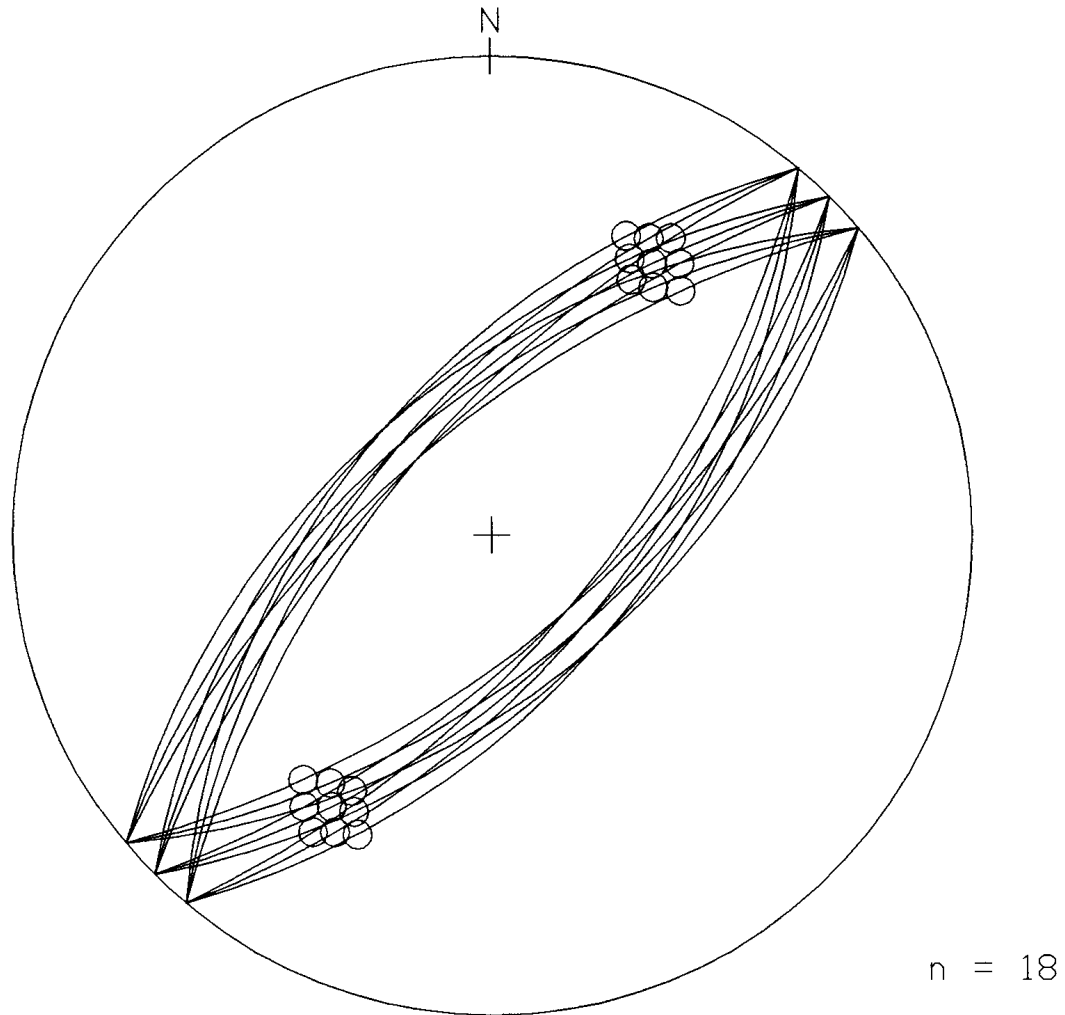


Figure 8-25 - Lower-hemisphere stereographic projection of fault population AC-02 showing 18 normal faults and their associated slip vectors (circles) for a Φ value of 1.00 (AC-02-10). The orientations of the three principal stress axes σ_1 , σ_2 , and σ_3 are up, east, and north respectively.

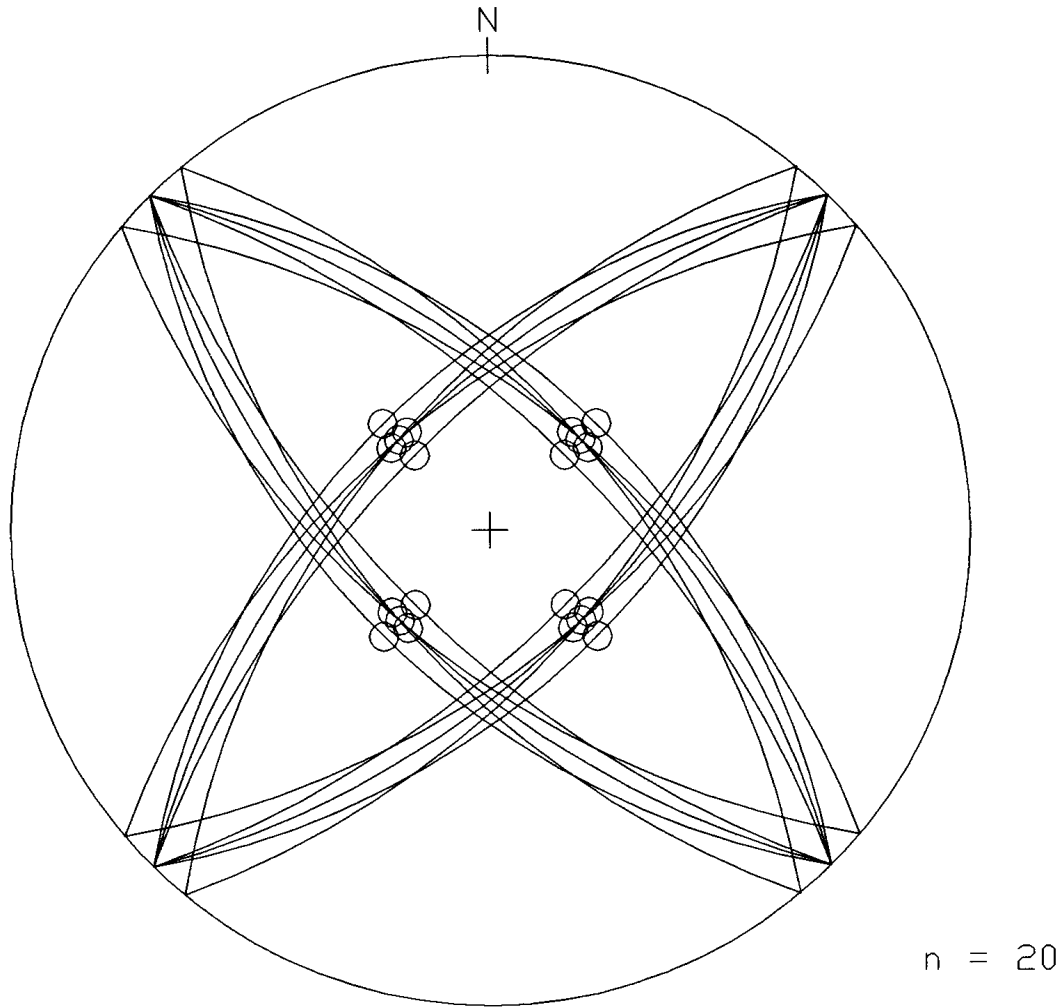


Figure 8-26 - Lower-hemisphere stereographic projection of fault population OS-01 showing 20 orthorhombic normal faults and their associated slip vectors (circles) for a Φ value of 0.00 (OS-01-00). The orientations of the three principal stress axes σ_1 , σ_2 , and σ_3 are up, east, and north respectively.

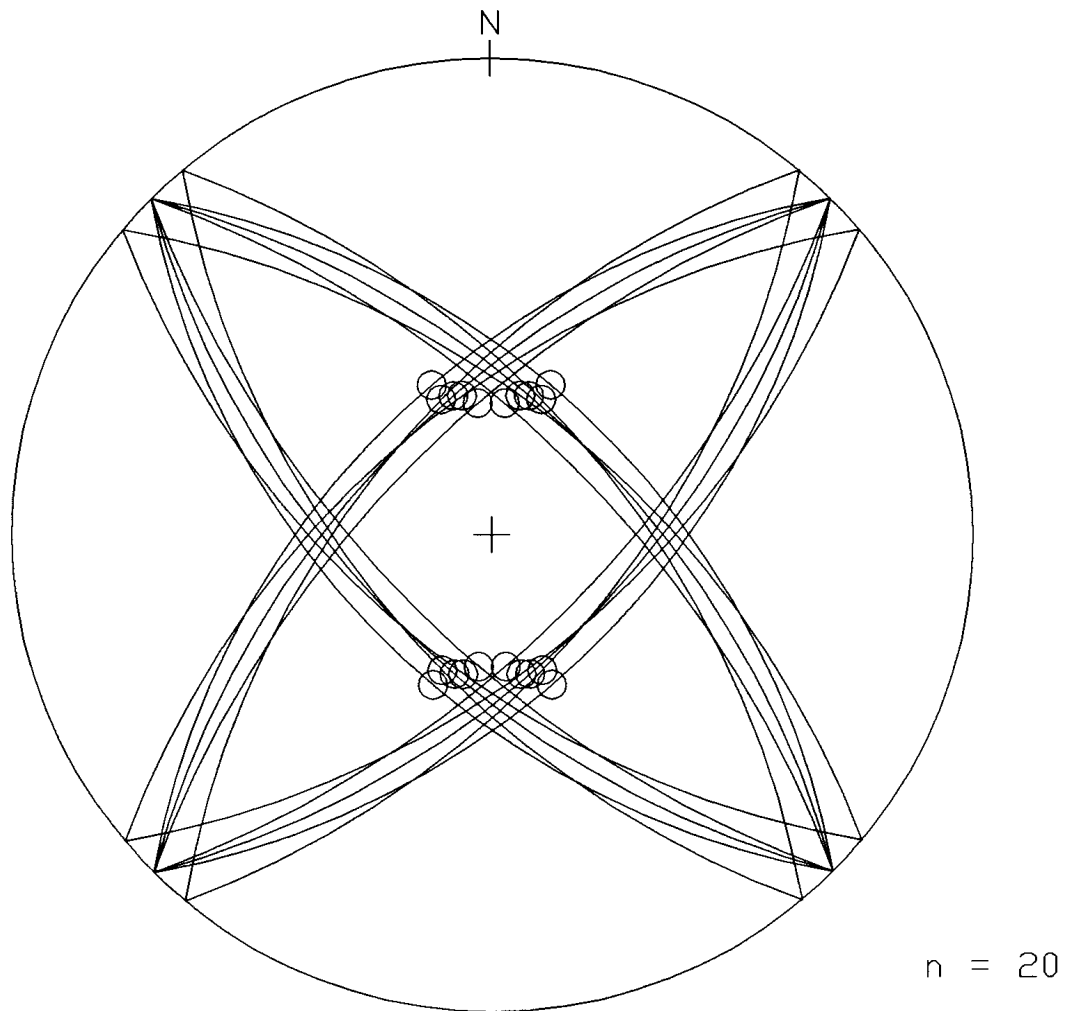


Figure 8-27 - Lower-hemisphere stereographic projection of fault population OS-01 showing 20 orthorhombic normal faults and their associated slip vectors (circles) for a Φ value of 0.25 (OS-01-25). The orientations of the three principal stress axes σ_1 , σ_2 , and σ_3 are up, east, and north respectively.

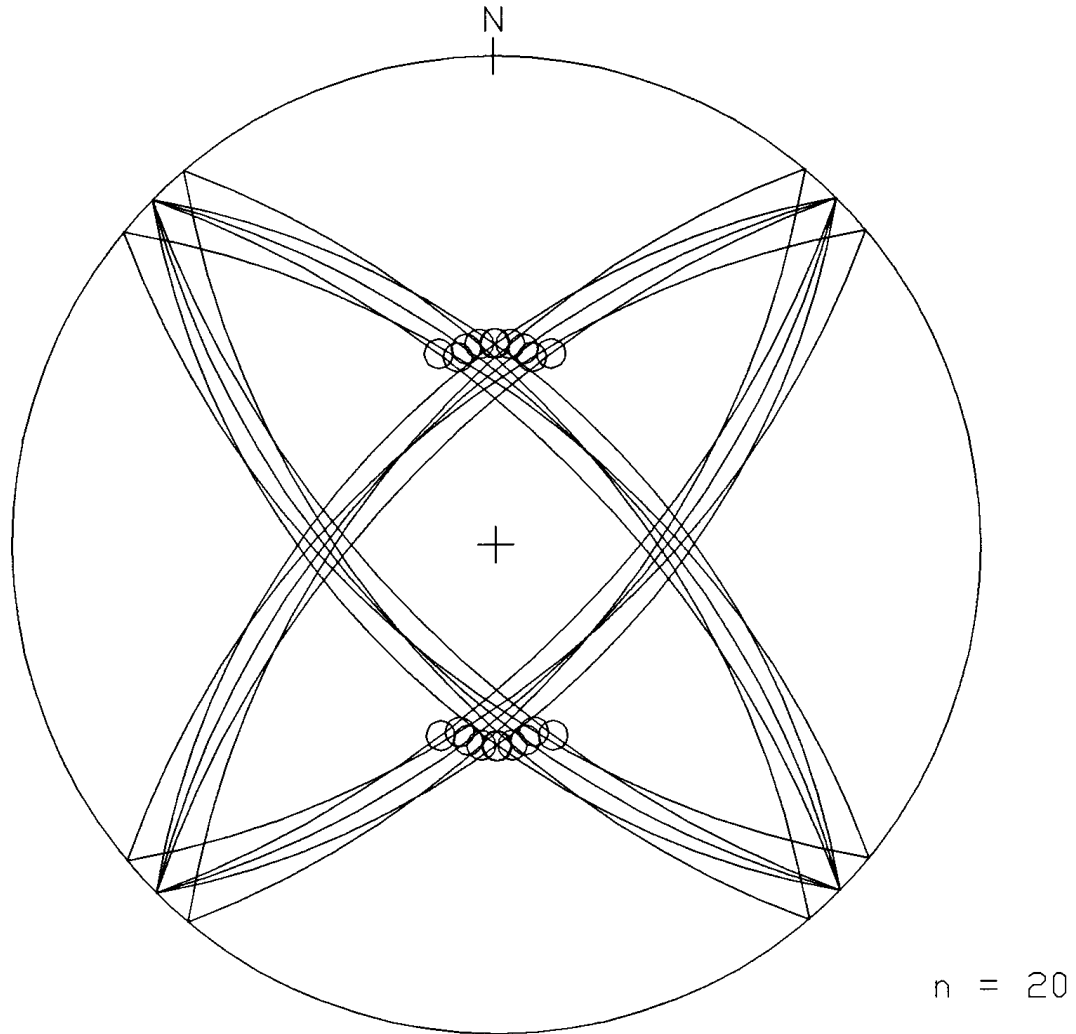


Figure 8-28 - Lower-hemisphere stereographic projection of fault population OS-01 showing 20 orthorhombic normal faults and their associated slip vectors (circles) for a Φ value of 0.50 (OS-01-50). The orientations of the three principal stress axes σ_1 , σ_2 , and σ_3 are up, east, and north respectively.

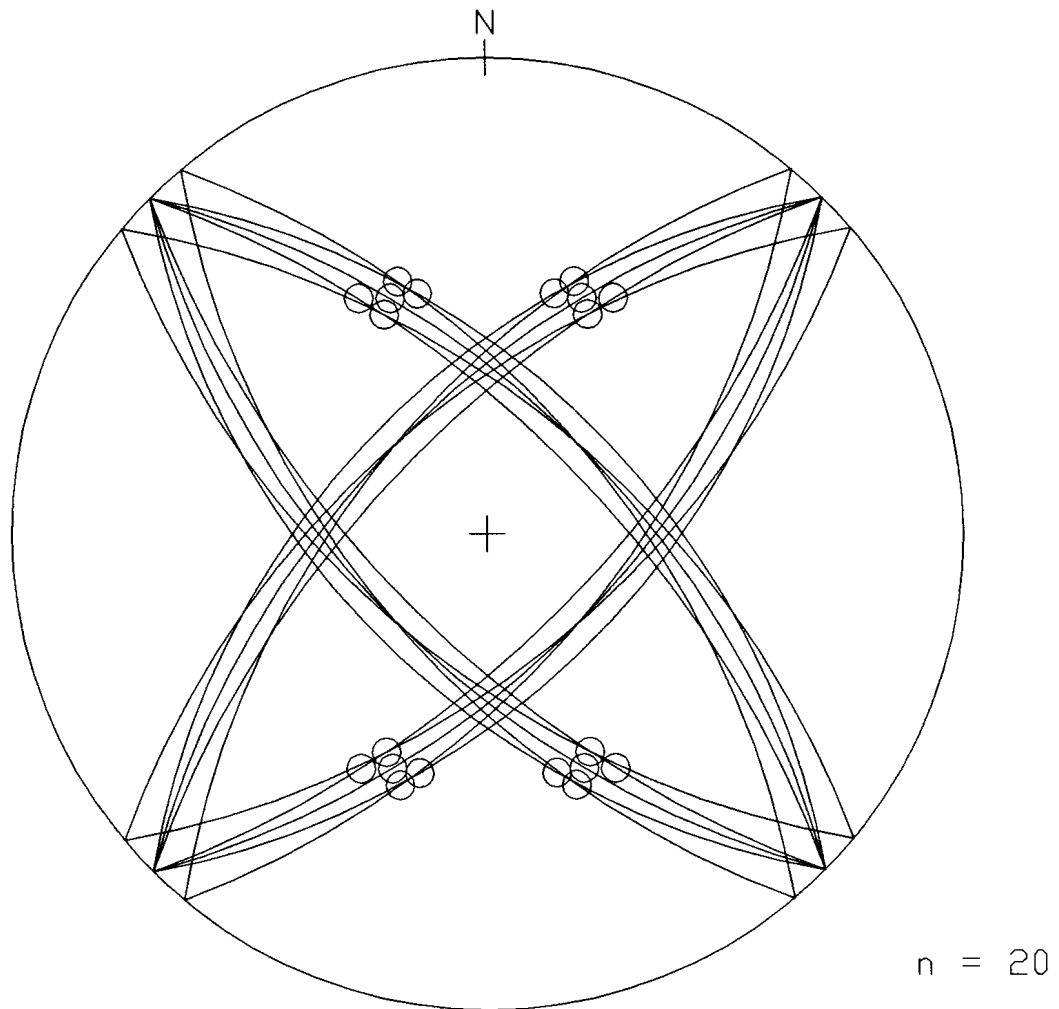


Figure 8-29 - Lower-hemisphere stereographic projection of fault population OS-01 showing 20 orthorhombic normal faults and their associated slip vectors (circles) for a Φ value of 0.75 (OS-01-75). The orientations of the three principal stress axes σ_1 , σ_2 , and σ_3 are up, east, and north respectively.

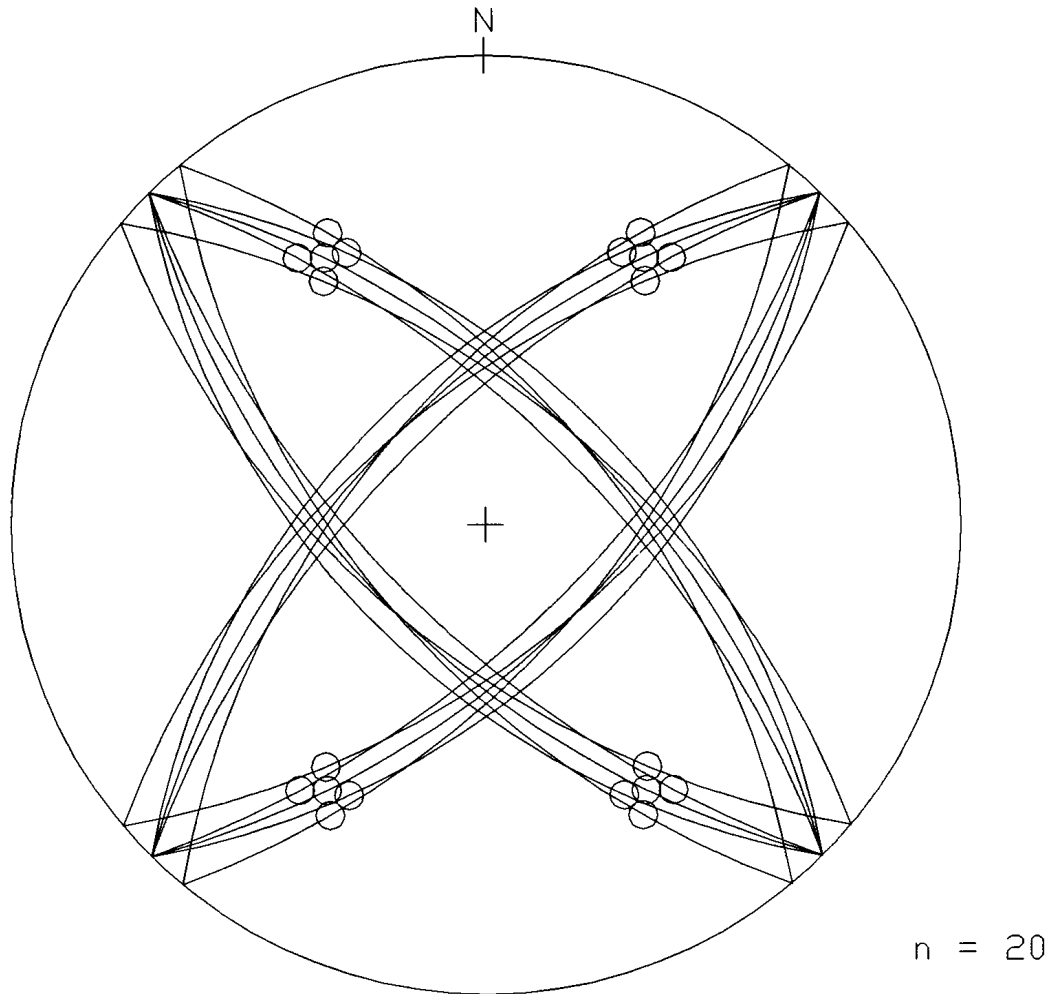


Figure 8-30 - Lower-hemisphere stereographic projection of fault population OS-01 showing 20 orthorhombic normal faults and their associated slip vectors (circles) for a Φ value of 1.00 (OS-01-10). The orientations of the three principal stress axes σ_1 , σ_2 , and σ_3 are up, east, and north respectively.

8.6 Radial Symmetry Fault Populations

While creating the conjugate and orthorhombic fault populations, I noticed that conjugate normal fault sets oriented at a wide range of strike directions would experience slip in my standard stress field (section 8.1). The only exceptions were those conjugate sets with a strike of less than 30° from the σ_1 principal stress direction. I therefore created a radial symmetry fault population (RS-01) consisting of 10 normal faults with strikes of 30° , 60° , 90° , 120° , and 150° for each of the five conjugate sets. Their acute angles were bisected by σ_1 (figures 8-31 → 8-35). While this may not be a geologically-reasonable fault population, it does satisfy all of the initial paleostress assumptions and should be solvable by the analysis programs. For this reason, the population was included in the study.

8.7 Fault Populations of a Similar Orientation

Finally, three special-case fault populations were created such that all of the faults in each population had a very similar orientation (SO-01, SO-02, and SO-03). This is a type of fault population which may reasonably be expected to form.

The first population (SO-01) of 15 normal faults was created such that the strikes were parallel, and subparallel ($\pm 3^\circ$ and $\pm 6^\circ$), to the σ_3 principal plane. All of the faults were also oriented such that they made an angle of 30° ($\pm 5^\circ$) from the σ_1 principal stress direction (figures 8-36 → 8-40).

The second population (SO-02) of 15 normal faults was created such that their strikes were oriented at 30° ($\pm 3^\circ$ and $\pm 6^\circ$) from the σ_2 direction. All of the faults were also oriented such that they made an angle of 30° ($\pm 5^\circ$) from the σ_1 principal stress direction (figures 8-41 → 8-45).

The third population (SO-03) of 15 normal faults was created such that their strikes were oriented at 45° ($\pm 3^\circ$ and $\pm 6^\circ$) from the σ_2 and σ_3 directions. All of the faults were also oriented such that they made an angle of 30° ($\pm 5^\circ$) from the σ_1 principal stress direction (figures 8-46 → 8-50).

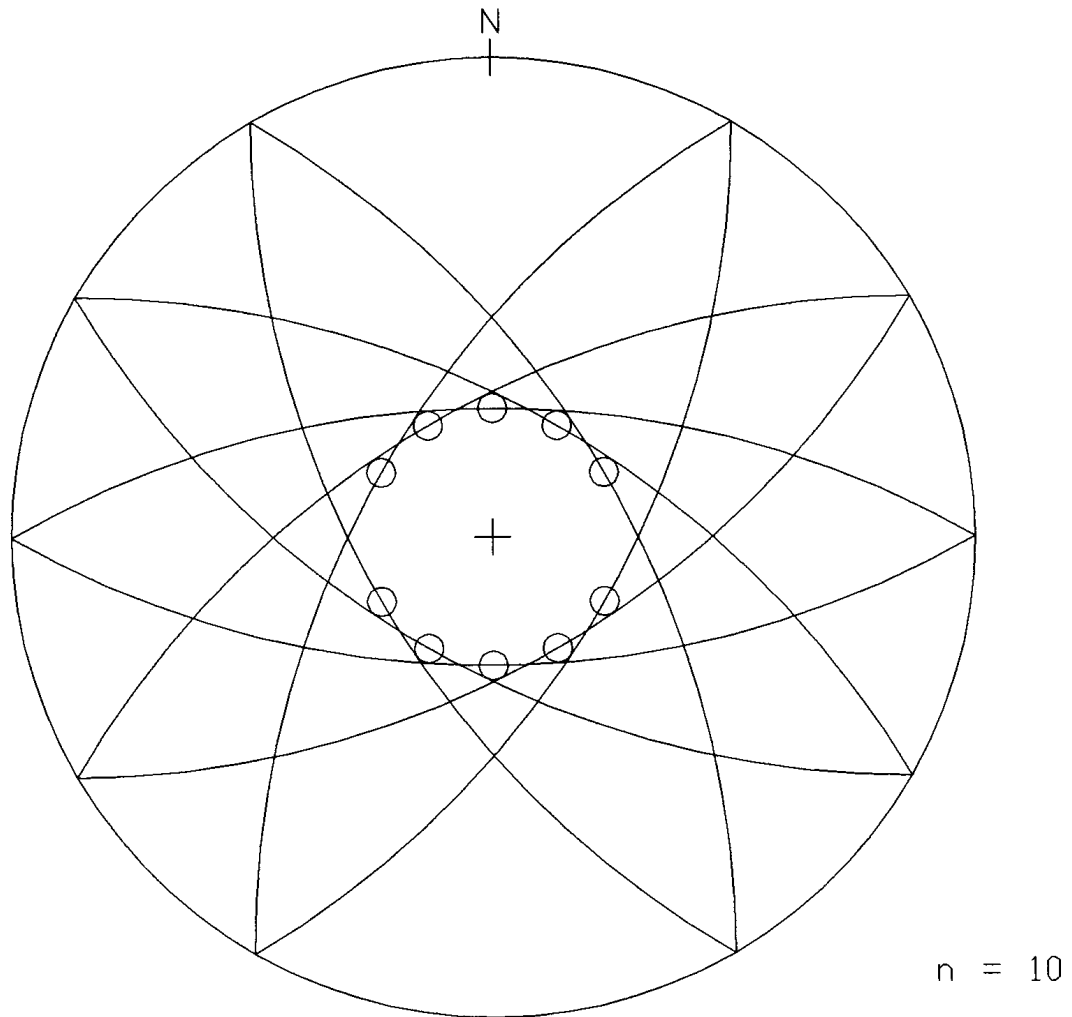


Figure 8-31 - Lower-hemisphere stereographic projection of fault population RS-01 showing 10 radial symmetry normal faults and their associated slip vectors (circles) for a Φ value of 0.00 (RS-01-00). The orientations of the three principal stress axes σ_1 , σ_2 , and σ_3 are up, east, and north respectively.

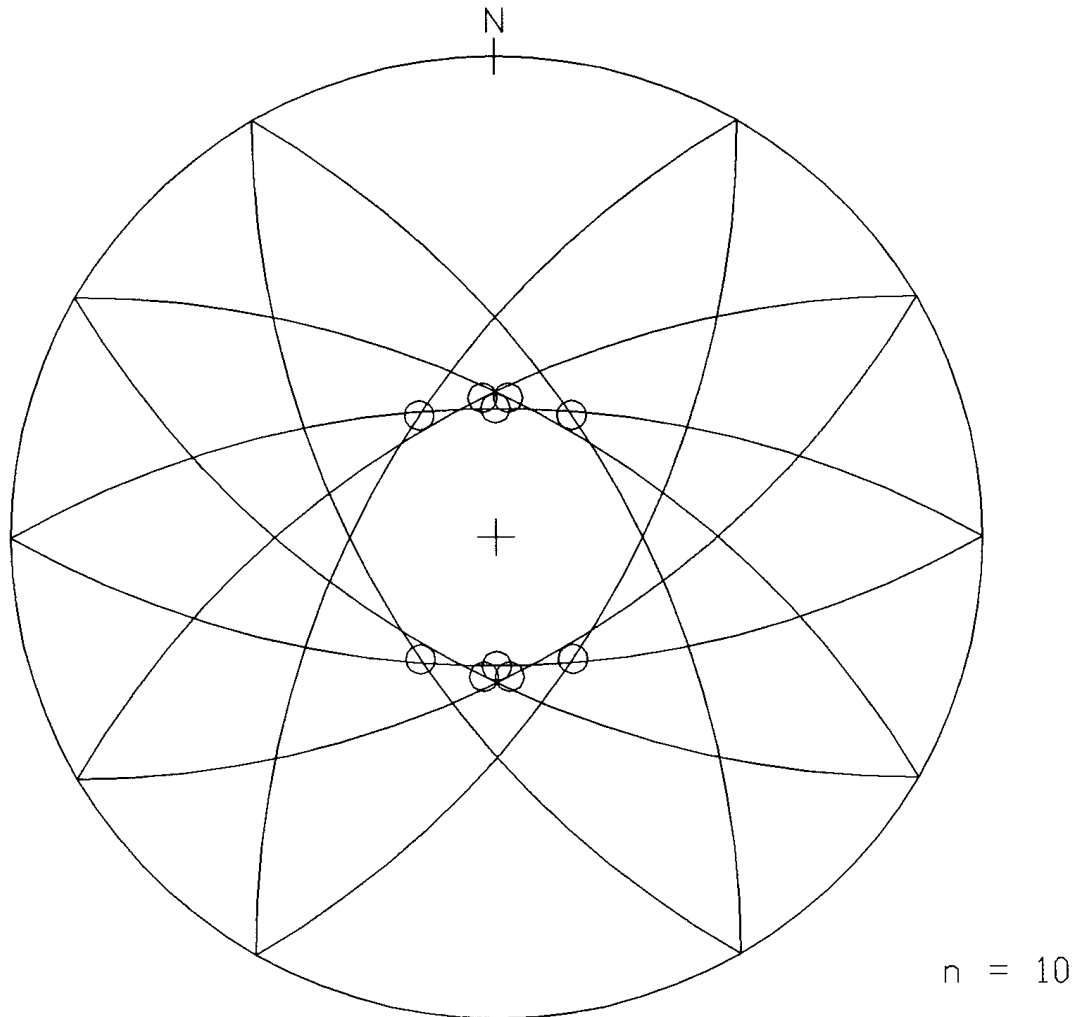


Figure 8-32 - Lower-hemisphere stereographic projection of fault population RS-01 showing 10 radial symmetry normal faults and their associated slip vectors (circles) for a Φ value of 0.25 (RS-01-25). The orientations of the three principal stress axes σ_1 , σ_2 , and σ_3 are up, east, and north respectively.

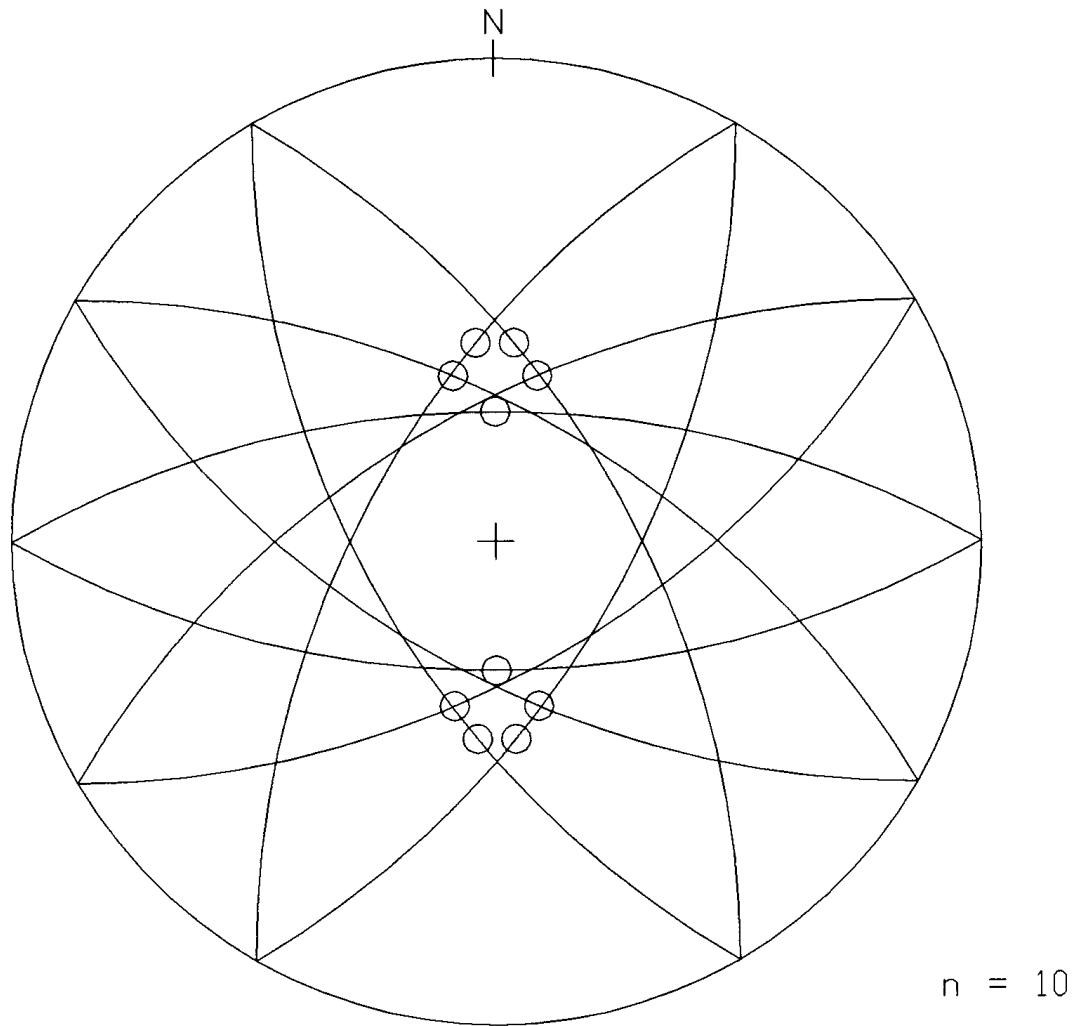


Figure 8-33 - Lower-hemisphere stereographic projection of fault population RS-01 showing 10 radial symmetry normal faults and their associated slip vectors (circles) for a Φ value of 0.50 (RS-01-50). The orientations of the three principal stress axes σ_1 , σ_2 , and σ_3 are up, east, and north respectively.

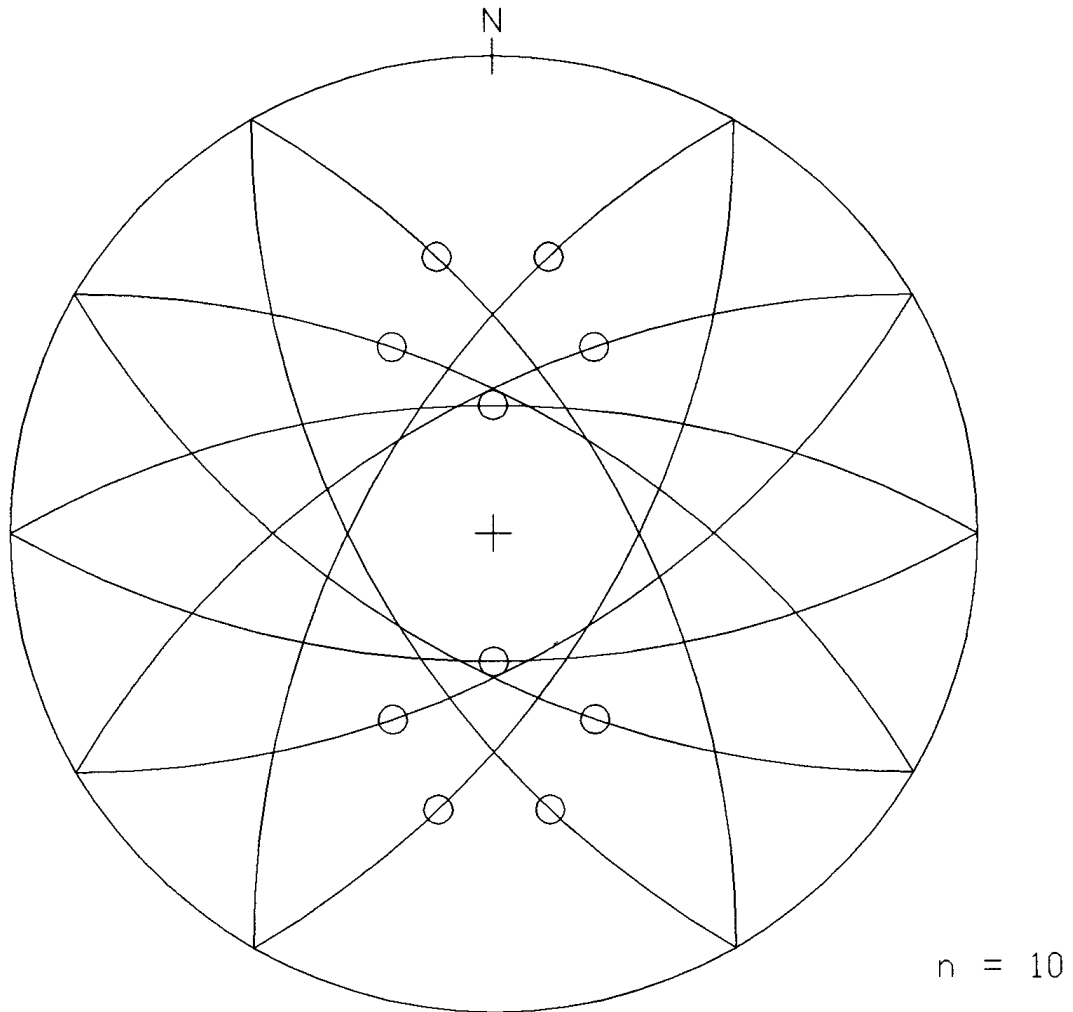


Figure 8-34 - Lower-hemisphere stereographic projection of fault population RS-01 showing 10 radial symmetry normal faults and their associated slip vectors (circles) for a Φ value of 0.75 (RS-01-75). The orientations of the three principal stress axes σ_1 , σ_2 , and σ_3 are up, east, and north respectively.

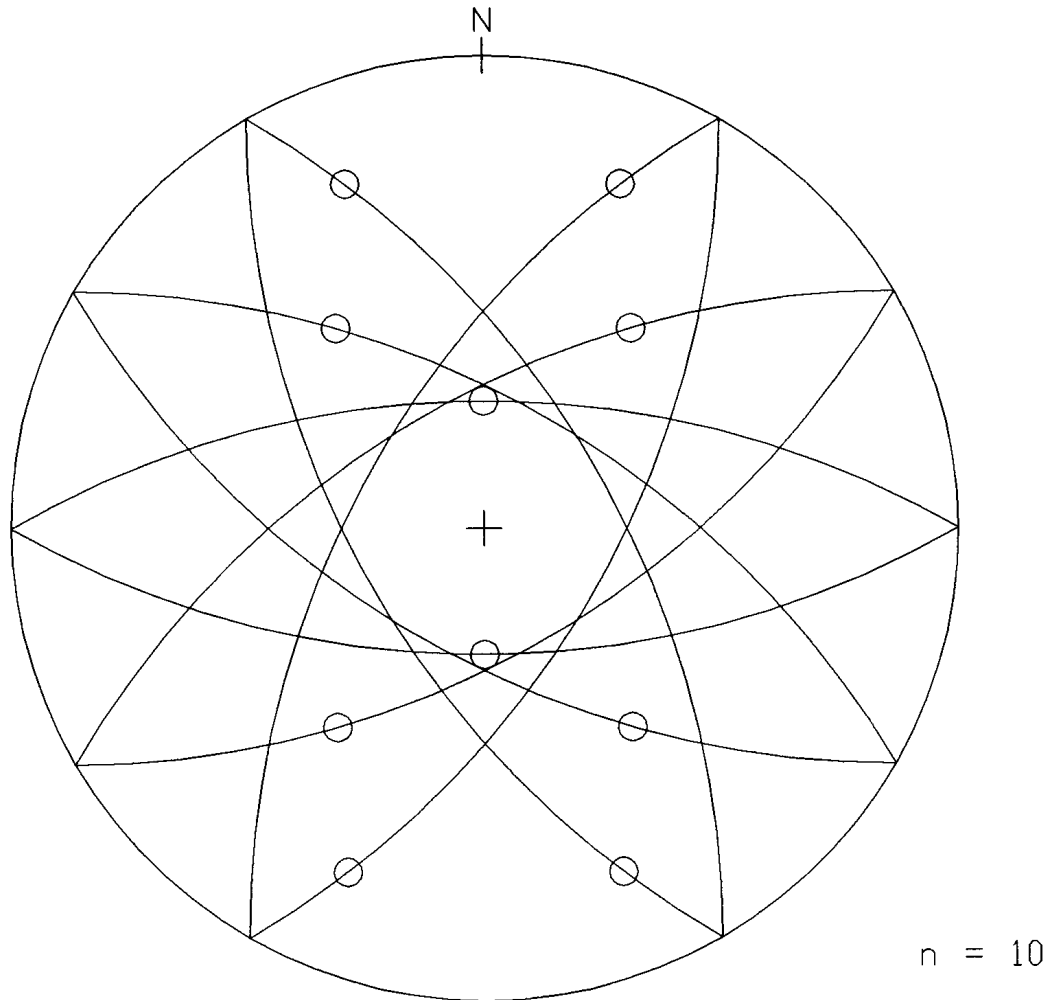


Figure 8-35 - Lower-hemisphere stereographic projection of fault population RS-01 showing 10 radial symmetry normal faults and their associated slip vectors (circles) for a Φ value of 1.00 (RS-01-10). The orientations of the three principal stress axes σ_1 , σ_2 , and σ_3 are up, east, and north respectively.

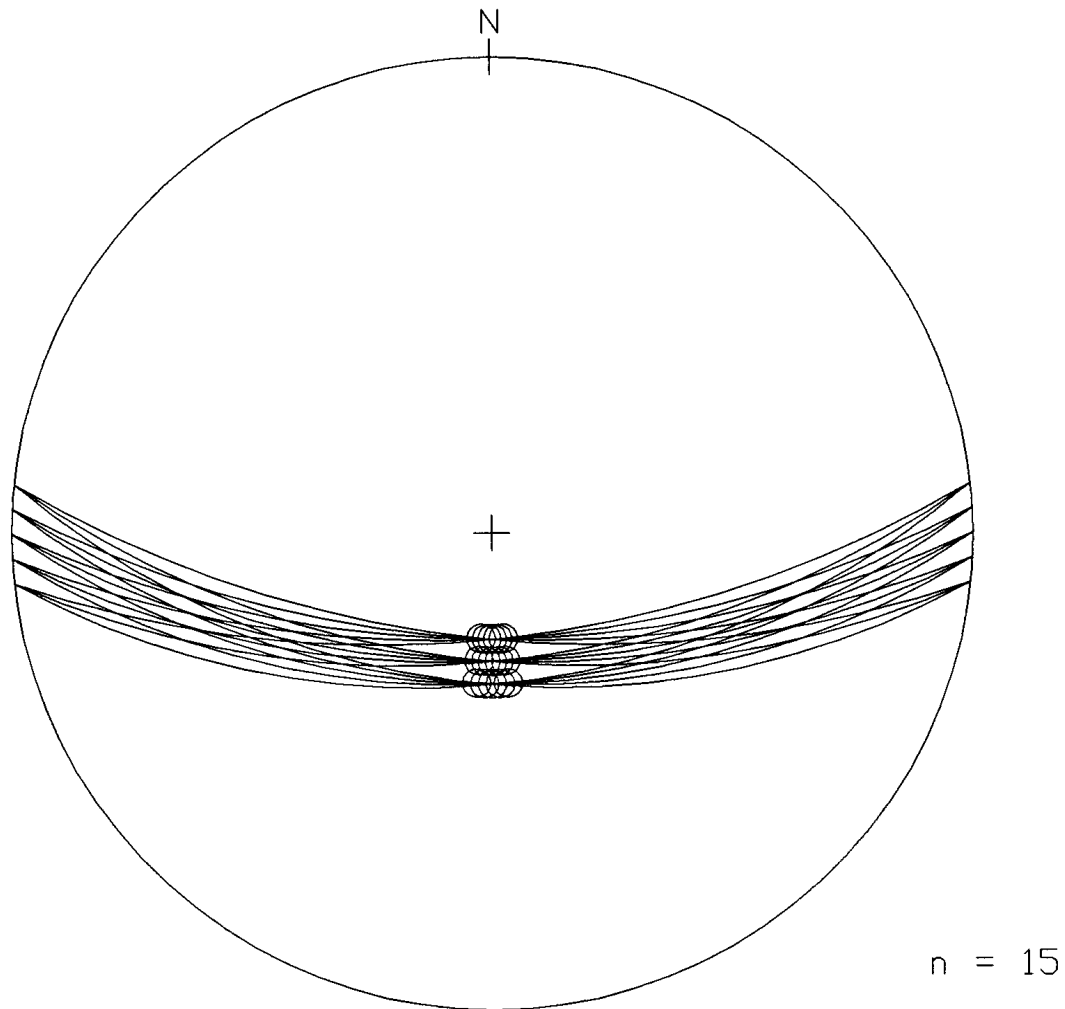


Figure 8-36 - Lower-hemisphere stereographic projection of fault population SO-01 showing 15 normal faults of approximately the same orientation and their associated slip vectors (circles) for a Φ value of 0.00 (SO-01-00). The orientations of the three principal stress axes σ_1 , σ_2 , and σ_3 are up, east, and north respectively.

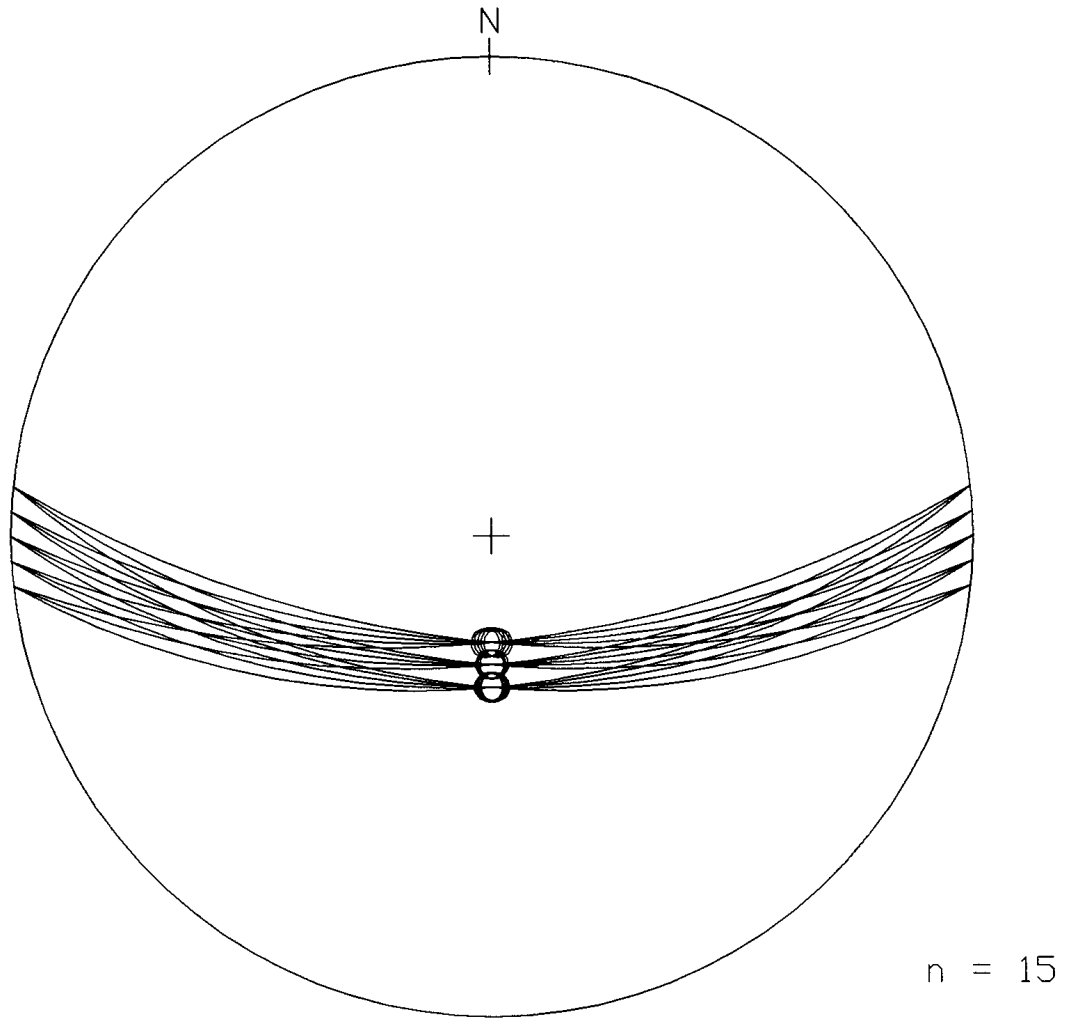


Figure 8-37 - Lower-hemisphere stereographic projection of fault population SO-01 showing 15 normal faults of approximately the same orientation and their associated slip vectors (circles) for a Φ value of 0.25 (SO-01-25). The orientations of the three principal stress axes σ_1 , σ_2 , and σ_3 are up, east, and north respectively.

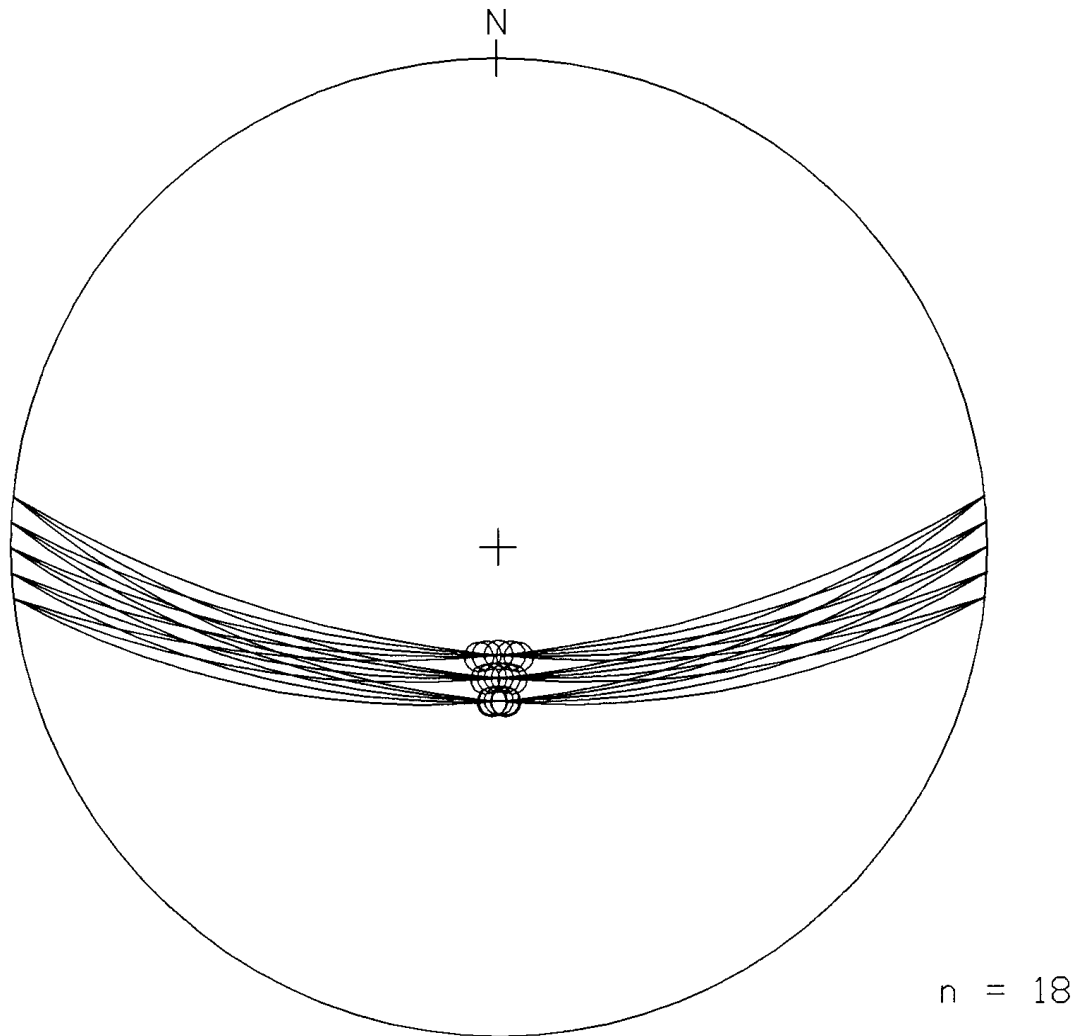


Figure 8-38 - Lower-hemisphere stereographic projection of fault population SO-01 showing 15 normal faults of approximately the same orientation and their associated slip vectors (circles) for a Φ value of 0.50 (SO-01-50). The orientations of the three principal stress axes σ_1 , σ_2 , and σ_3 are up, east, and north respectively.

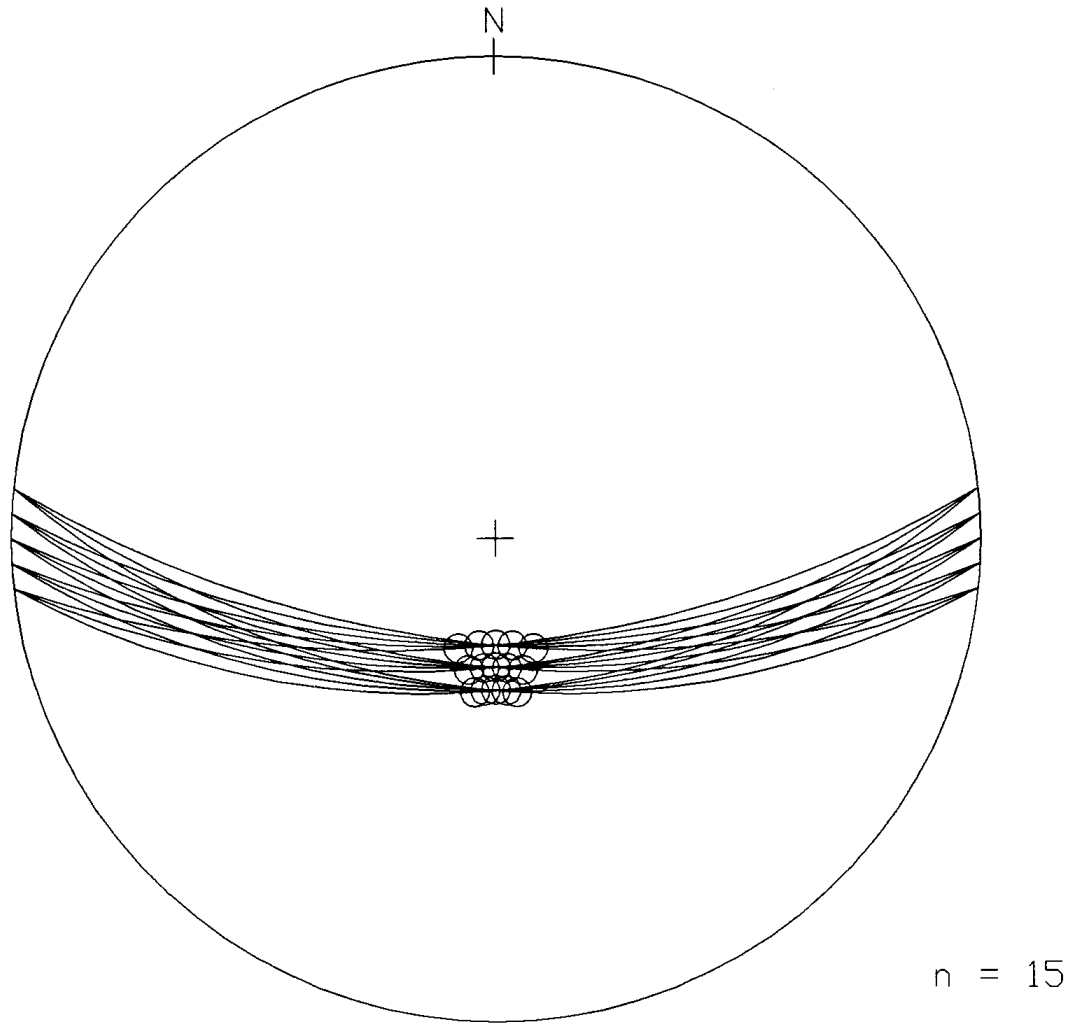


Figure 8-39 - Lower-hemisphere stereographic projection of fault population SO-01 showing 15 normal faults of approximately the same orientation and their associated slip vectors (circles) for a Φ value of 0.75 (SO-01-75). The orientations of the three principal stress axes σ_1 , σ_2 , and σ_3 are up, east, and north respectively.

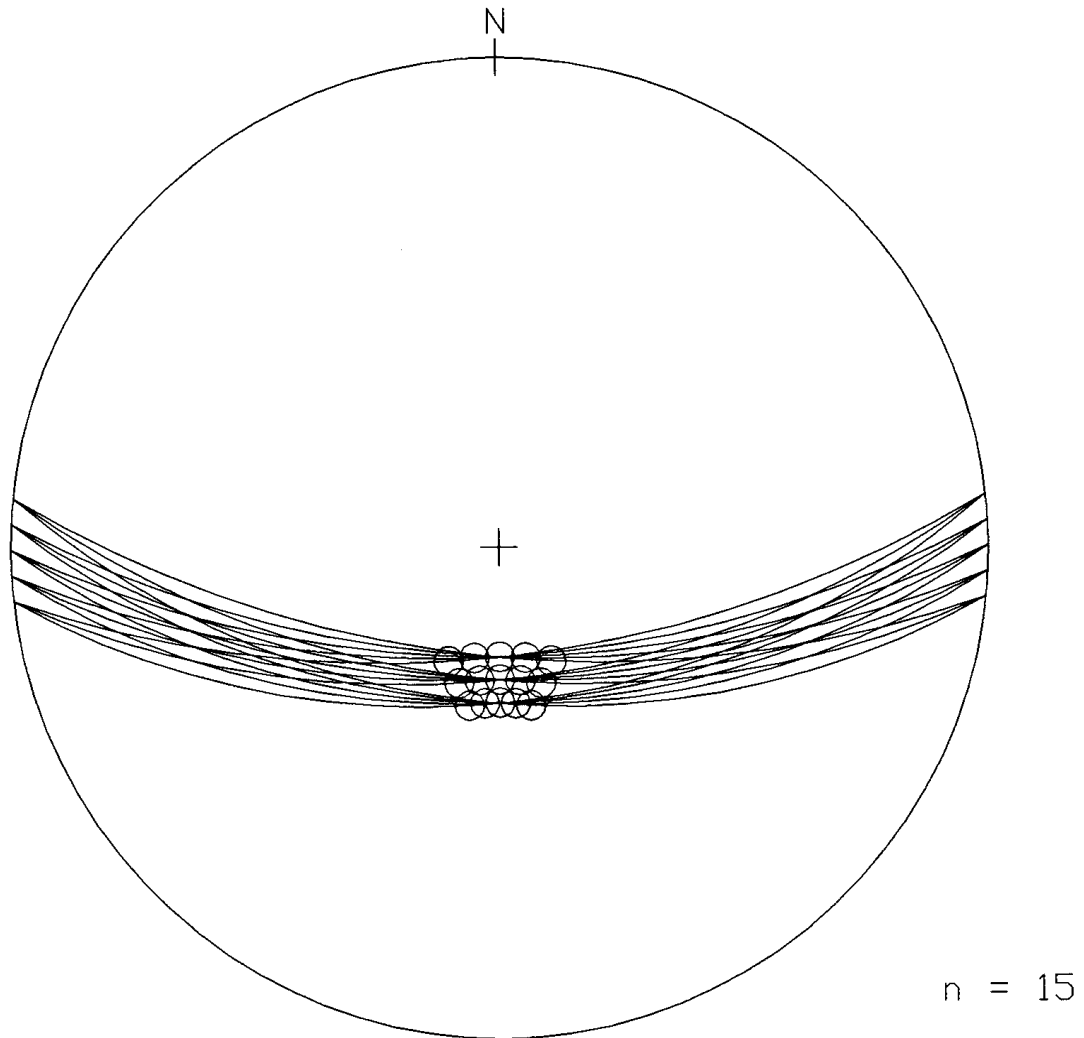


Figure 8-40 - Lower-hemisphere stereographic projection of fault population SO-01 showing 15 normal faults of approximately the same orientation and their associated slip vectors (circles) for a Φ value of 1.00 (SO-01-10). The orientations of the three principal stress axes σ_1 , σ_2 , and σ_3 are up, east, and north respectively.

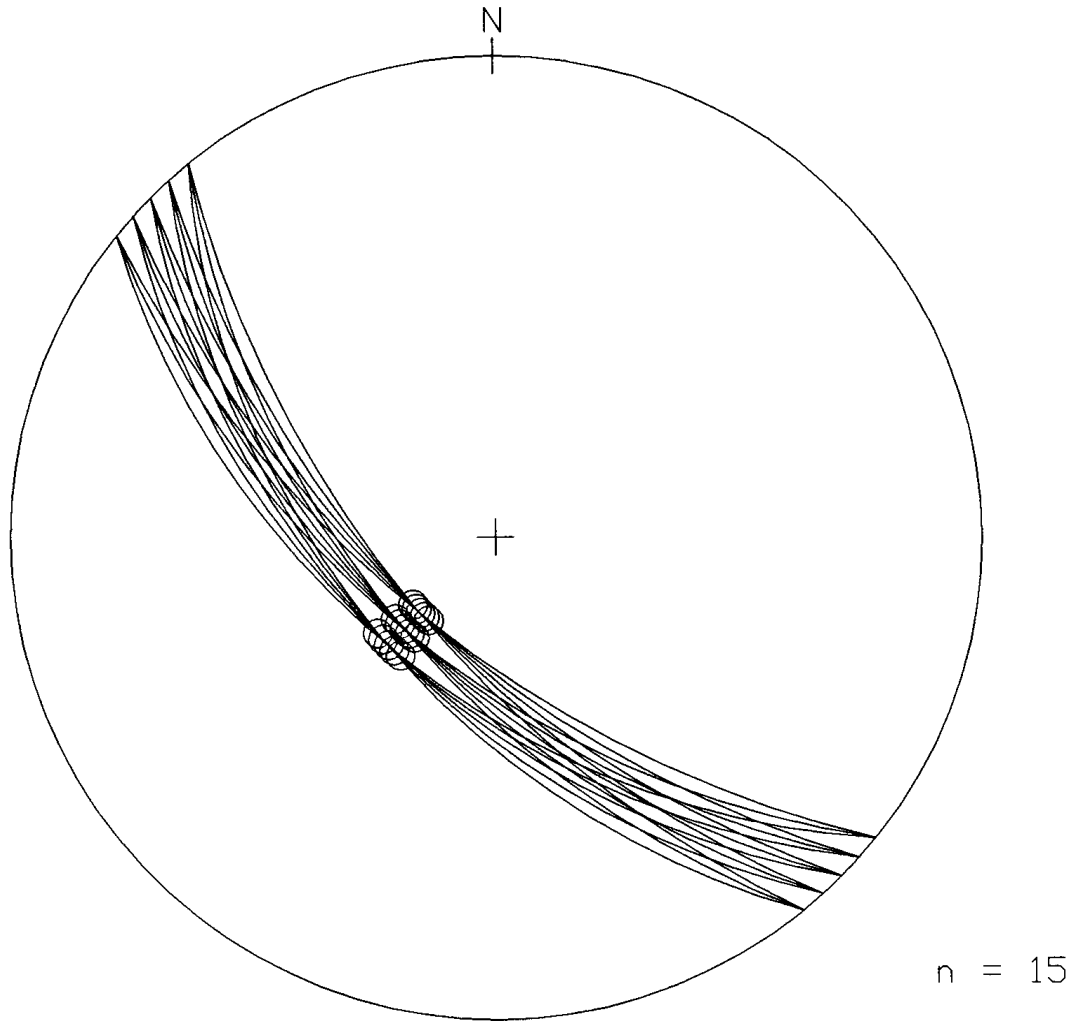


Figure 8-41 - Lower-hemisphere stereographic projection of fault population SO-02 showing 15 normal faults of approximately the same orientation and their associated slip vectors (circles) for a Φ value of 0.00 (SO-02-00). The orientations of the three principal stress axes σ_1 , σ_2 , and σ_3 are up, east, and north respectively.

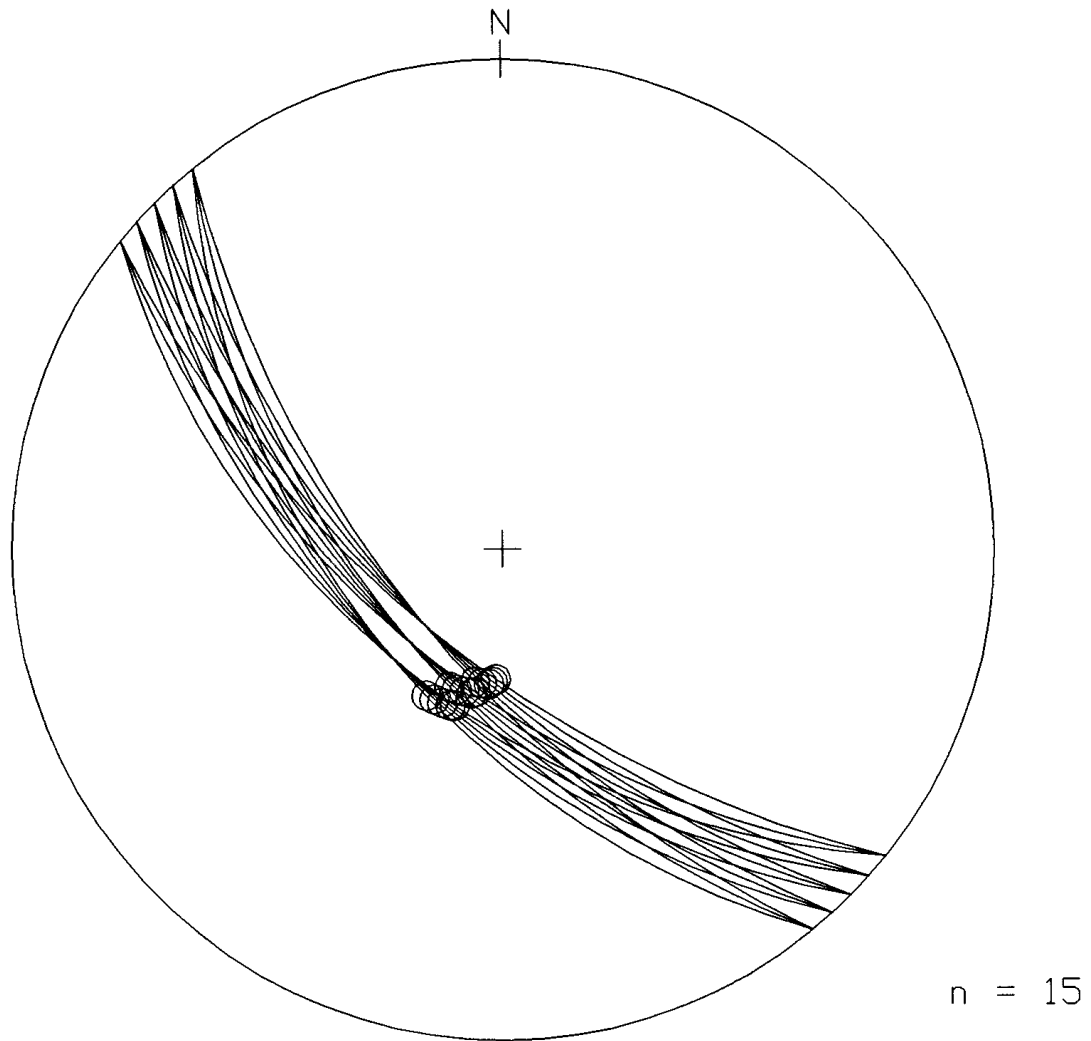


Figure 8-42 - Lower-hemisphere stereographic projection of fault population SO-02 showing 15 normal faults of approximately the same orientation and their associated slip vectors (circles) for a Φ value of 0.25 (SO-02-25). The orientations of the three principal stress axes σ_1 , σ_2 , and σ_3 are up, east, and north respectively.

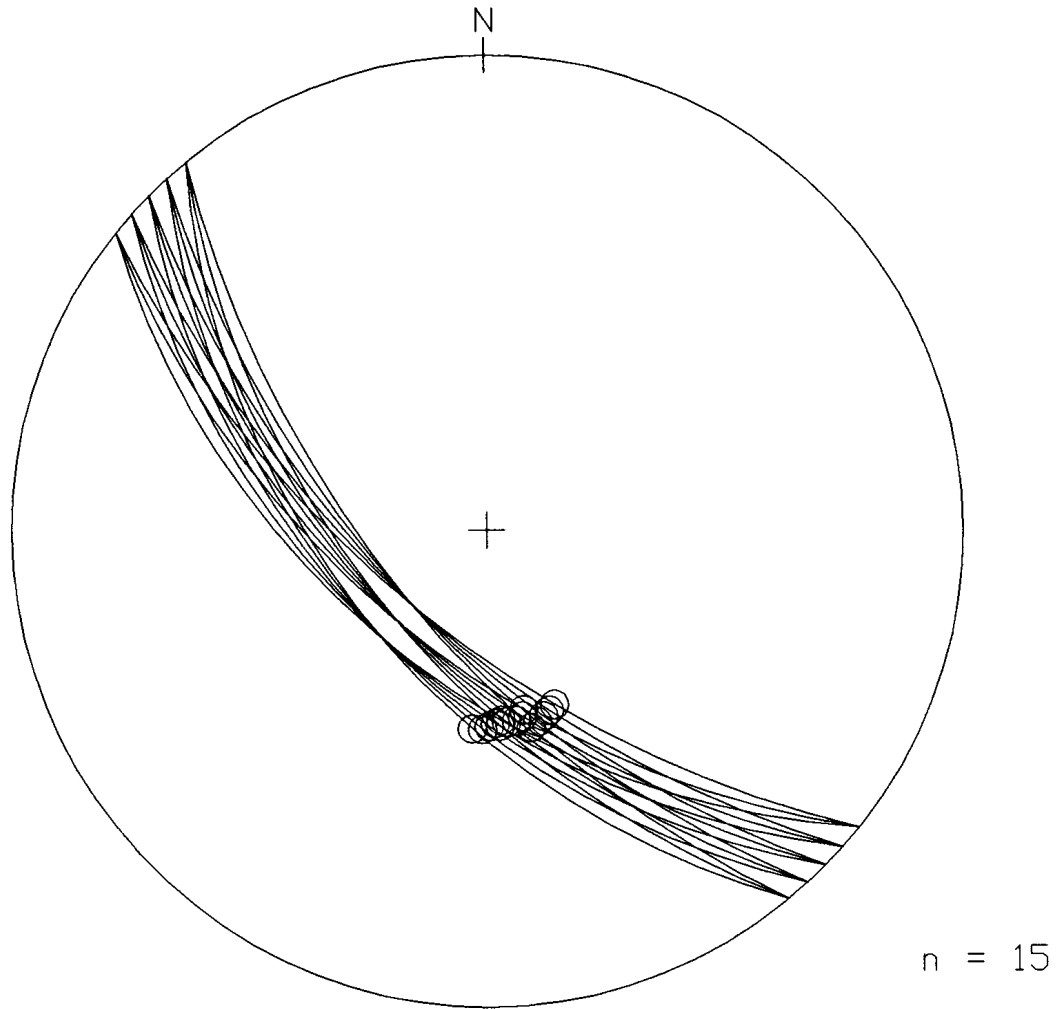


Figure 8-43 - Lower-hemisphere stereographic projection of fault population SO-02 showing 15 normal faults of approximately the same orientation and their associated slip vectors (circles) for a Φ value of 0.50 (SO-02-50). The orientations of the three principal stress axes σ_1 , σ_2 , and σ_3 are up, east, and north respectively.

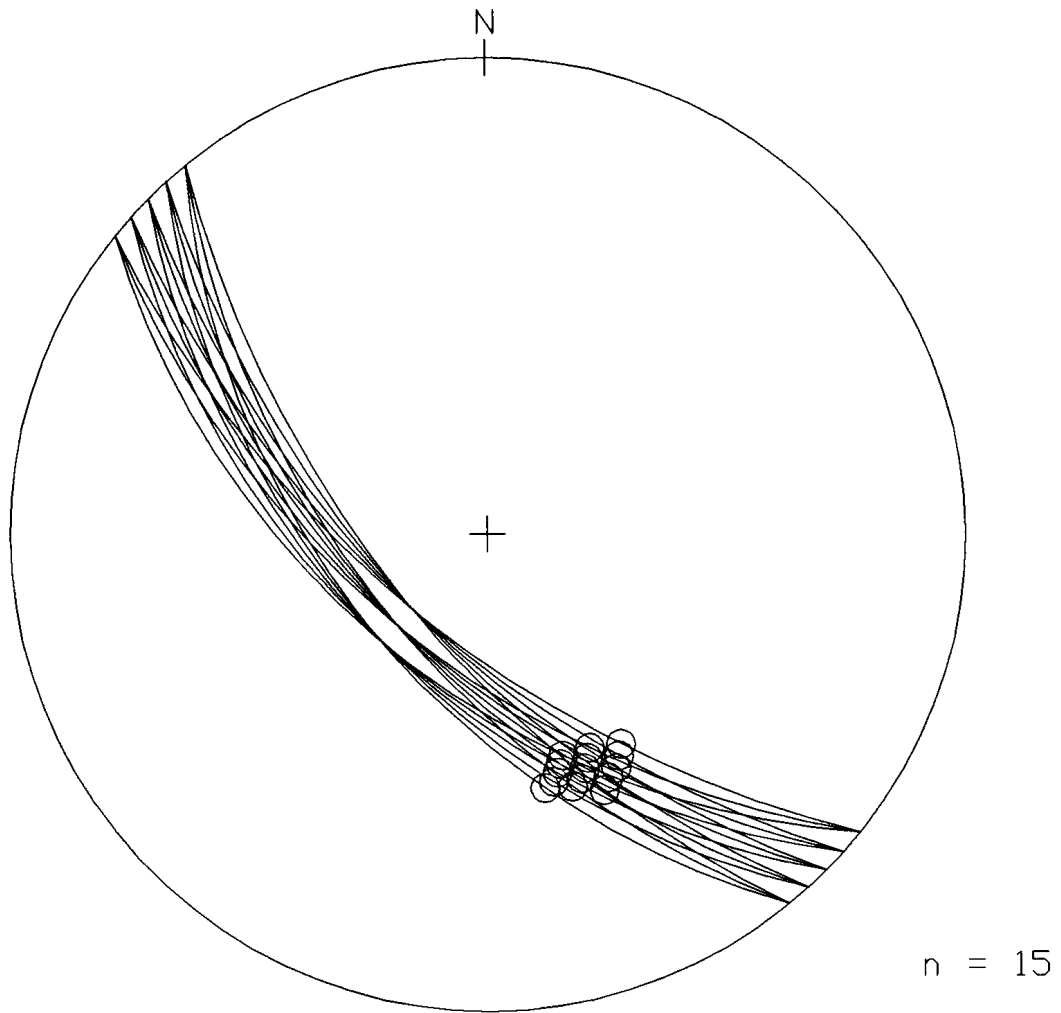


Figure 8-44 - Lower-hemisphere stereographic projection of fault population SO-02 showing 15 normal faults of approximately the same orientation and their associated slip vectors (circles) for a Φ value of 0.75 (SO-02-75). The orientations of the three principal stress axes σ_1 , σ_2 , and σ_3 are up, east, and north respectively.

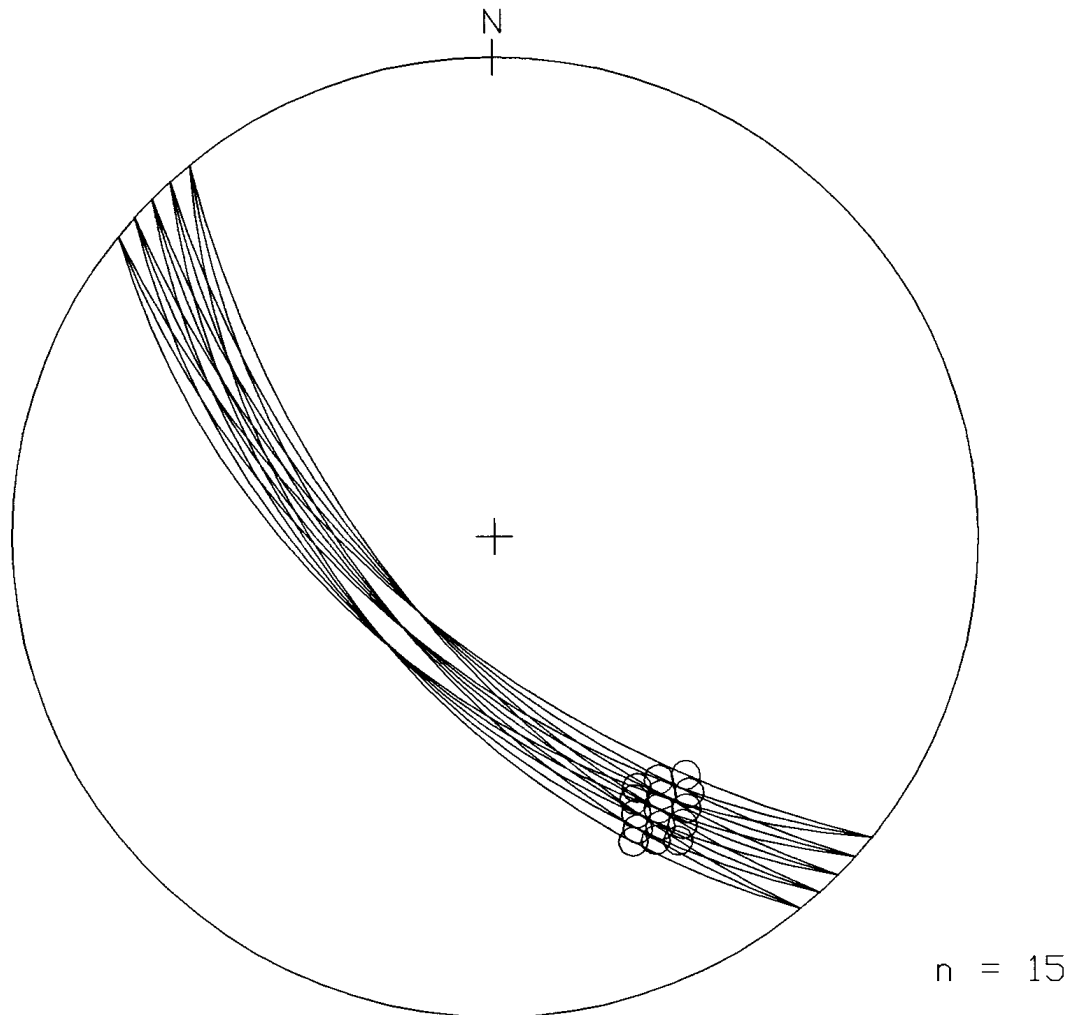


Figure 8-45 - Lower-hemisphere stereographic projection of fault population SO-02 showing 15 normal faults of approximately the same orientation and their associated slip vectors (circles) for a Φ value of 1.00 (SO-02-10). The orientations of the three principal stress axes σ_1 , σ_2 , and σ_3 are up, east, and north respectively.

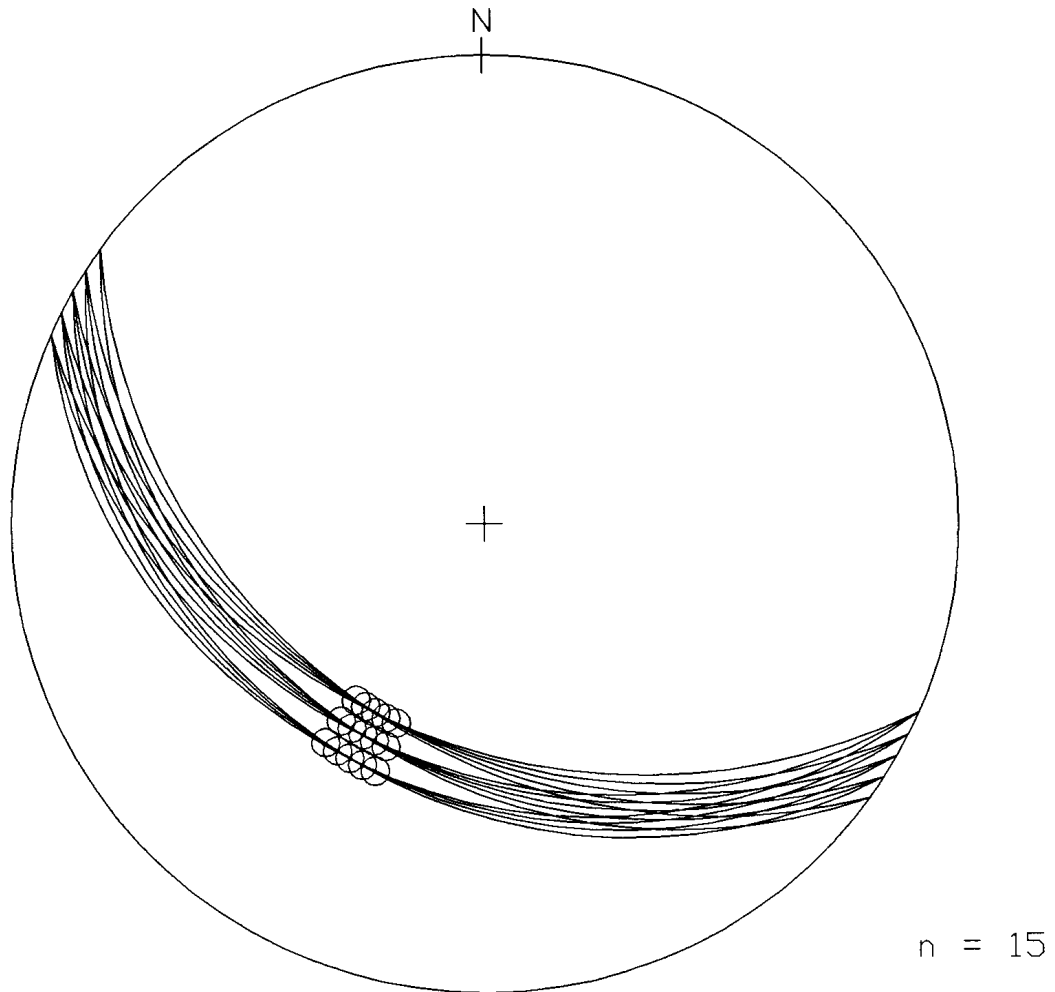


Figure 8-46 - Lower-hemisphere stereographic projection of fault population SO-03 showing 15 normal faults of approximately the same orientation and their associated slip vectors (circles) for a Φ value of 0.00 (SO-03-00). The orientations of the three principal stress axes σ_1 , σ_2 , and σ_3 are up, east, and north respectively.

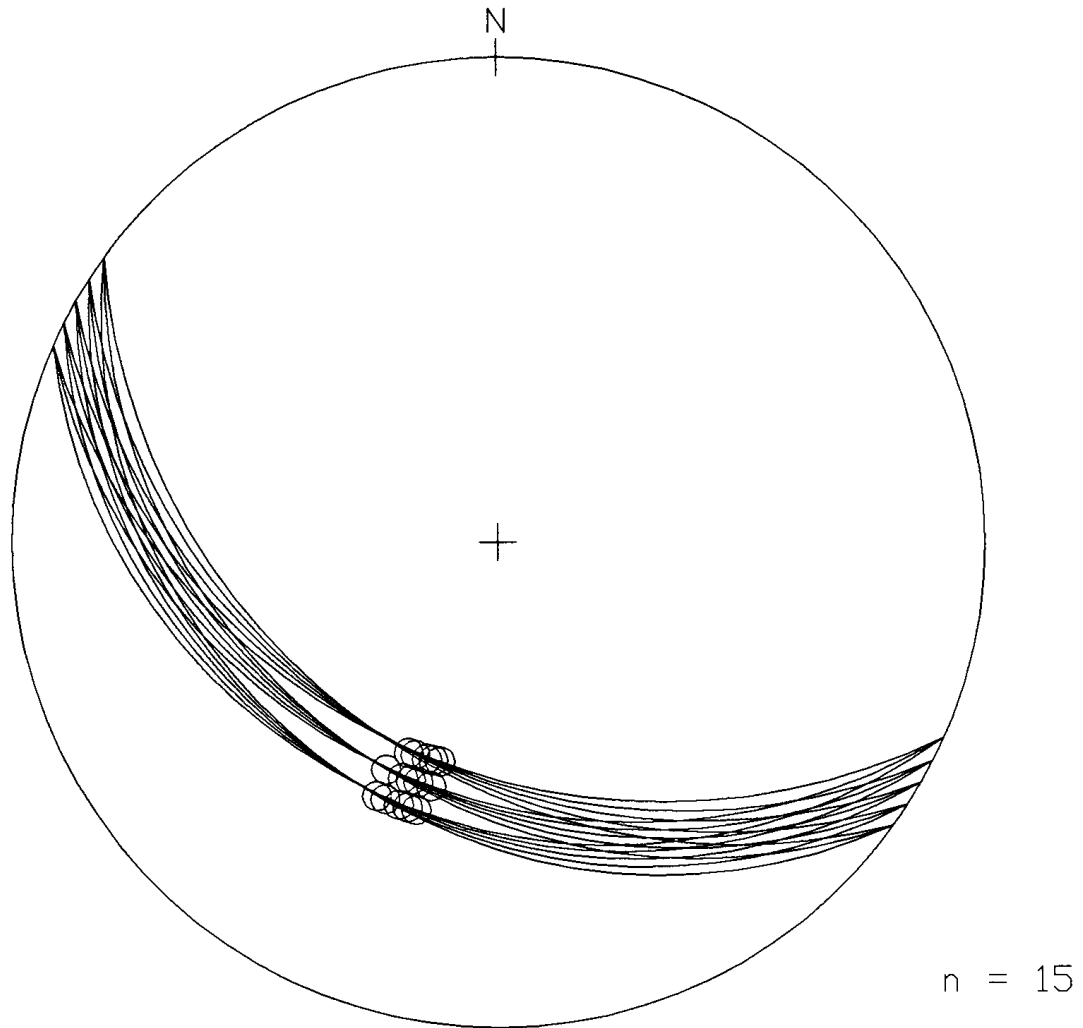


Figure 8-47 - Lower-hemisphere stereographic projection of fault population SO-03 showing 15 normal faults of approximately the same orientation and their associated slip vectors (circles) for a Φ value of 0.25 (SO-03-25). The orientations of the three principal stress axes σ_1 , σ_2 , and σ_3 are up, east, and north respectively.

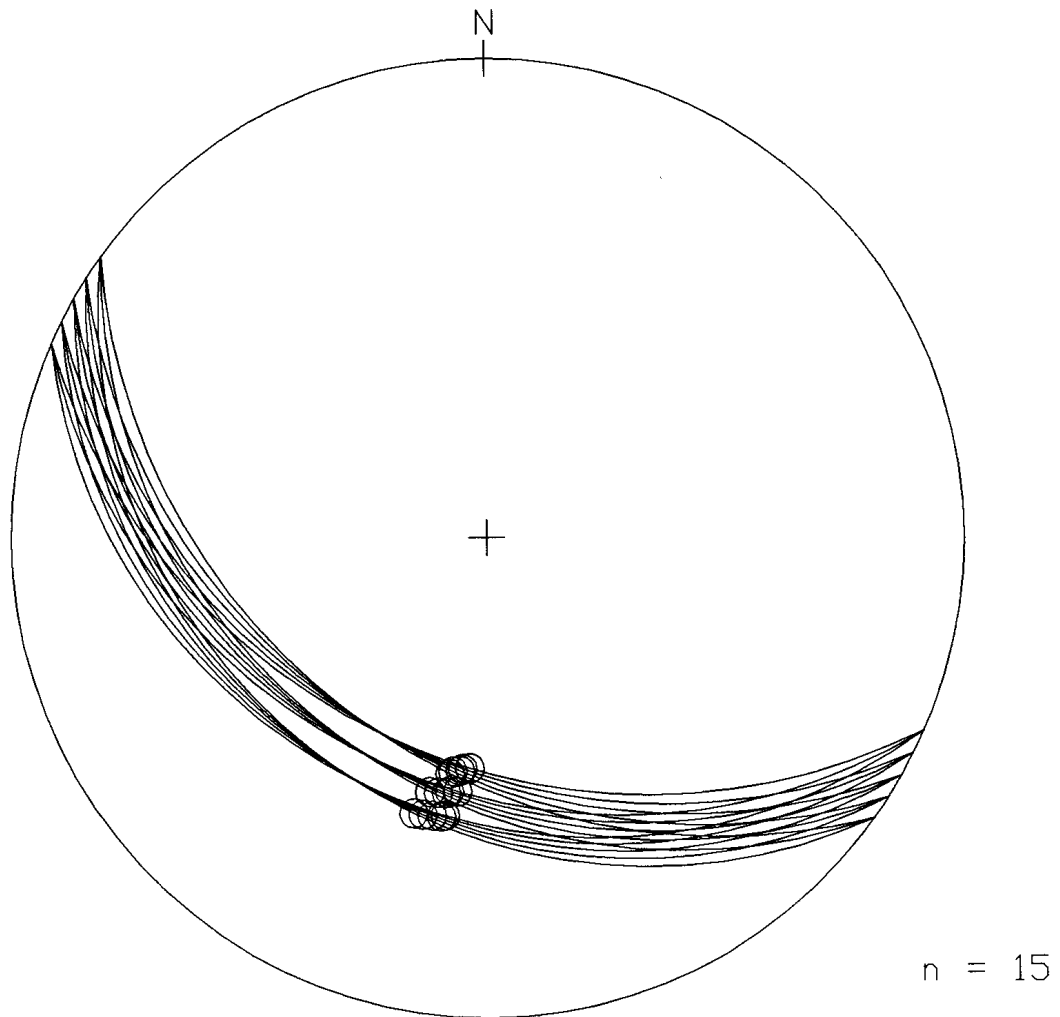


Figure 8-48 - Lower-hemisphere stereographic projection of fault population SO-03 showing 15 normal faults of approximately the same orientation and their associated slip vectors (circles) for a Φ value of 0.50 (SO-03-50). The orientations of the three principal stress axes σ_1 , σ_2 , and σ_3 are up, east, and north respectively.

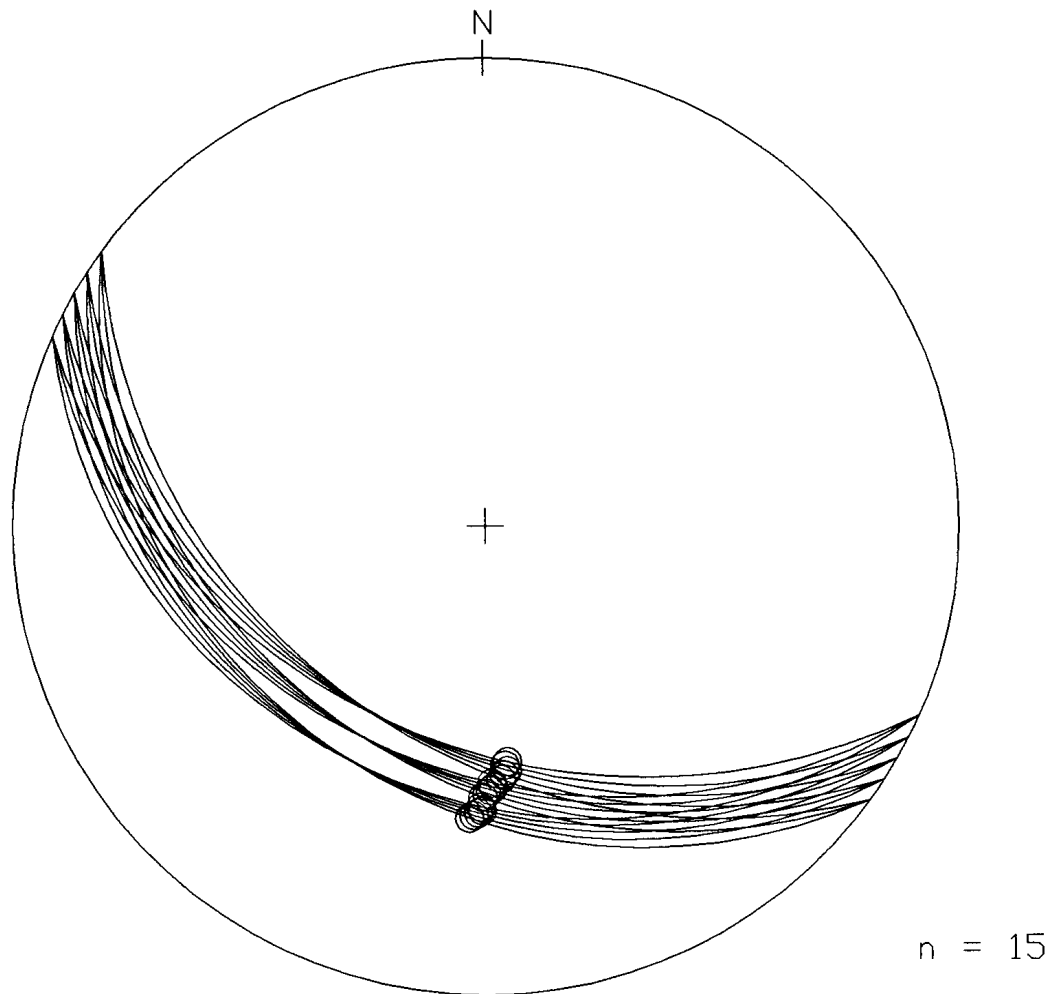


Figure 8-49 - Lower-hemisphere stereographic projection of fault population SO-03 showing 15 normal faults of approximately the same orientation and their associated slip vectors (circles) for a Φ value of 0.75 (SO-03-75). The orientations of the three principal stress axes σ_1 , σ_2 , and σ_3 are up, east, and north respectively.

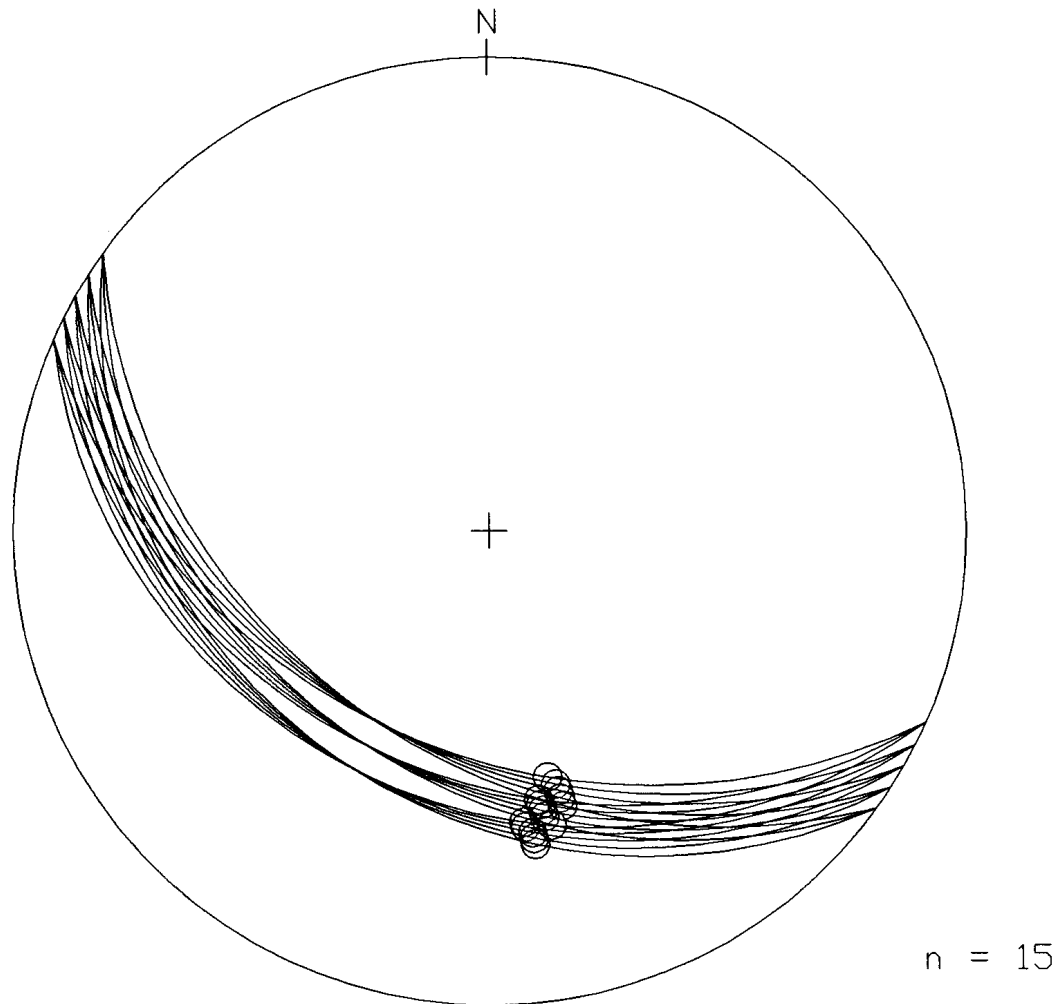


Figure 8-50 - Lower-hemisphere stereographic projection of fault population SO-03 showing 15 normal faults of approximately the same orientation and their associated slip vectors (circles) for a Φ value of 1.00 (SO-03-10). The orientations of the three principal stress axes σ_1 , σ_2 , and σ_3 are up, east, and north respectively.

8.8 Final Fault Population Tests

To test the sensitivity of the paleostress analysis programs, the following steps were performed to the random-pole fault populations (RP-01, RP-02, and RP-03):

1. Randomly removing one or more planes from the population and observing the change in the calculated paleostress tensor.
2. Randomly adding one or more planes to the populations and observing the change in the calculated paleostress tensor.
3. Giving a random $\pm 5^\circ$ variability in plunge and trend of the fault normal vectors and giving a $\pm 5^\circ$ variability in the pitch angles of the slip vectors for each fault datum in the population.

In this way, the sensitivity of the two paleostress analysis programs to insufficient data, extraneous data, and measurement errors was evaluated.

Angelier's (1979) field data (FD-01) of 38 Neogene age normal faults from Central Crete, Greece (figure 8-51 and table 8-1) were also run through the paleostress analysis programs. This data population has become an unofficial standard against which other paleostress analysis methods are tested to see if they yield the same results as Angelier (Gephart and Forsyth, 1984; Michael, 1984; Reches, 1987) and is only used for a comparison here -- I did not worry about whether the results were geologically-reasonable or not.

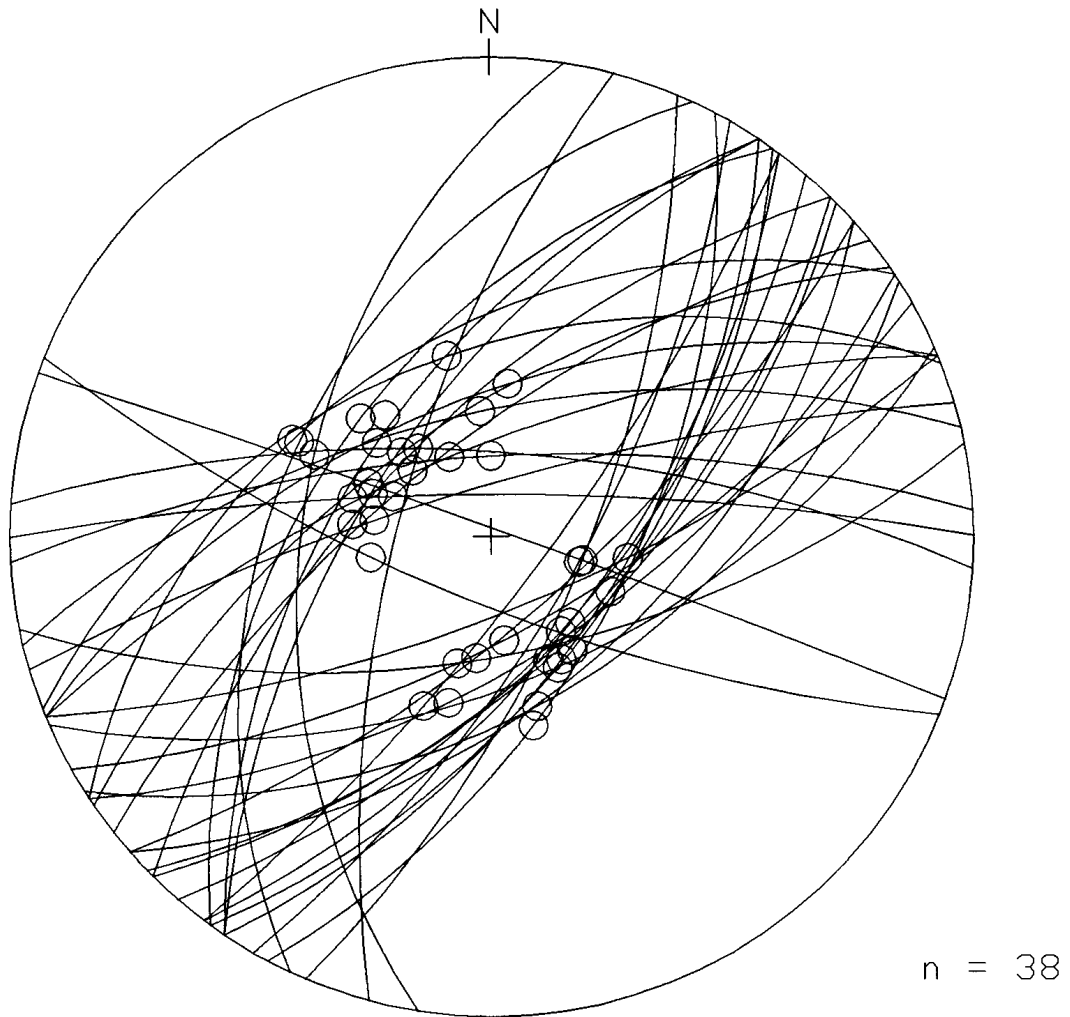


Figure 8-51 - Lower-hemisphere stereographic projection of fault population FD-01 showing 38 normal faults from Central Crete, Greece (Angelier, 1979) and their associated slip vectors.

FaultPlane		Slickenline	
Strike	Dip	Trend	Plunge
045°	61°	115°	59°
036°	59°	145°	58°
270°	80°	286°	57°
232°	68°	292°	65°
225°	63°	290°	61°
290°	88°	293°	59°
254°	78°	278°	62°
046°	60°	155°	59°
257°	61°	355°	61°
067°	56°	153°	56°
049°	70°	187°	61°
216°	50°	312°	50°
058°	51°	165°	50°
079°	62°	195°	59°
236°	62°	313°	61°
214°	61°	275°	58°
034°	60°	151°	57°
037°	63°	138°	63°
068°	72°	099°	58°
049°	53°	139°	90°
189°	47°	295°	46°
237°	45°	296°	41°
112°	74°	260°	61°
205°	42°	296°	42°
214°	56°	309°	56°
037°	77°	202°	48°
057°	61°	195°	51°
248°	58°	006°	55°
061°	67°	173°	65°
028°	58°	168°	46°
030°	69°	106°	68°
041°	63°	144°	62°
023°	68°	105°	68°
249°	48°	346°	48°
248°	69°	332°	69°
195°	68°	310°	66°
274°	70°	320°	63°
267°	71°	000°	71°

Table 8-1 - A listing of the orientations for Angelier's (1979) population of 38 normal faults from Central Crete, Greece.

CHAPTER 9

TESTING PROCEDURES AND RESULTS

In this chapter, the results of the tests on the artificial fault populations by the two paleostress analysis program (Reches' method and Angelier's method) are presented.

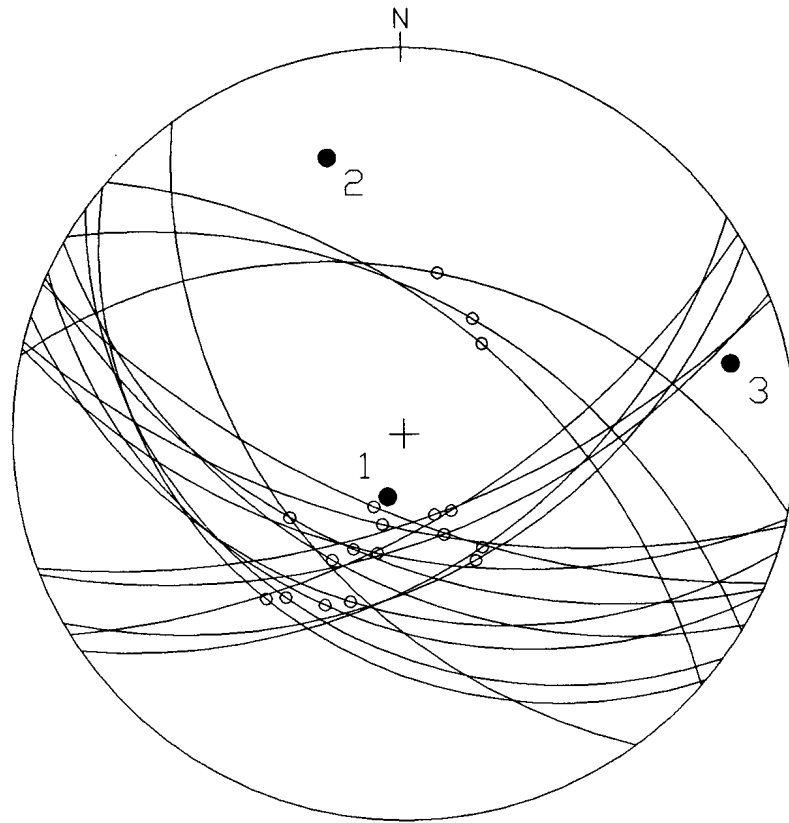
9.1 Testing Procedures

The testing procedures used were very straightforward. The artificial fault populations shown in chapter 8 and listed in appendix B, were created in the manner discussed in chapter 5. The fault-slip data for each population at each of the five values of Φ examined (0.00, 0.25, 0.50, 0.75, and 1.00) were manually converted into input formats compatible with the two programs. This new fault data was then read into the paleostress analysis programs and results were obtained. The angles between the known and the calculated orientations of the principal stress axes σ_1 , σ_2 , and σ_3 were determined using the program listed in appendix E.

These results were carefully examined to see if they were consistent with the initial assumptions used to create the artificial fault populations. If they were not the same, the reasons why were ascertained (or at least surmised).

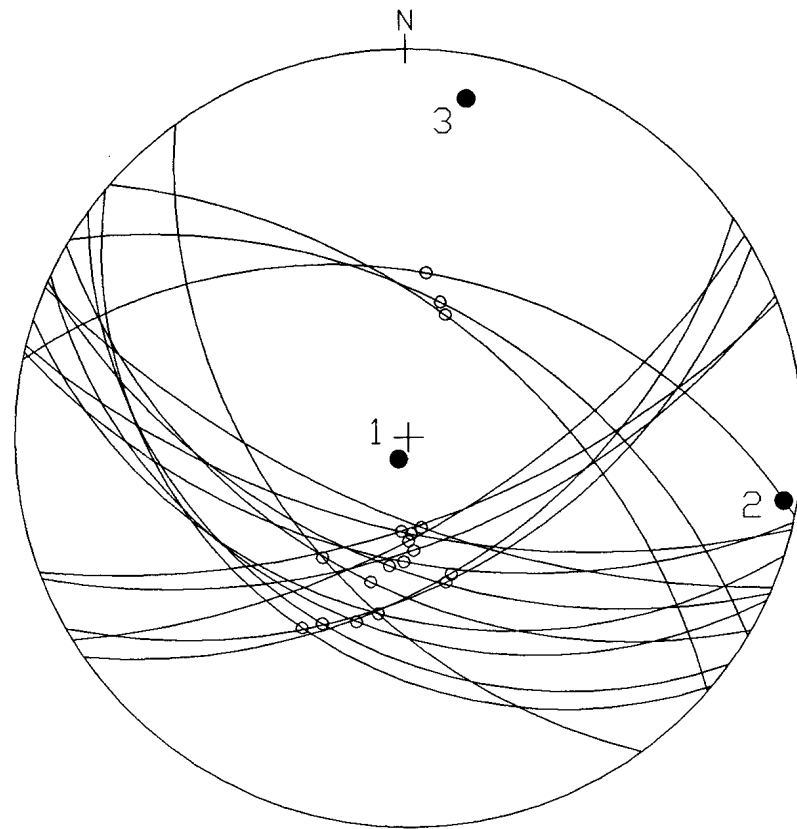
9.2 Random-Pole Fault Population Results

The three random-pole fault populations RP-01, RP-02, and RP-03 were the first to be examined. The results of this examination are shown in figures 9-1 through 9-15 for Reches' method and figures 9-16 through 9-30 for Angelier's method. Comparisons of the results of Reches' and Angelier's methods are given in tables 9-1 through 9-3.



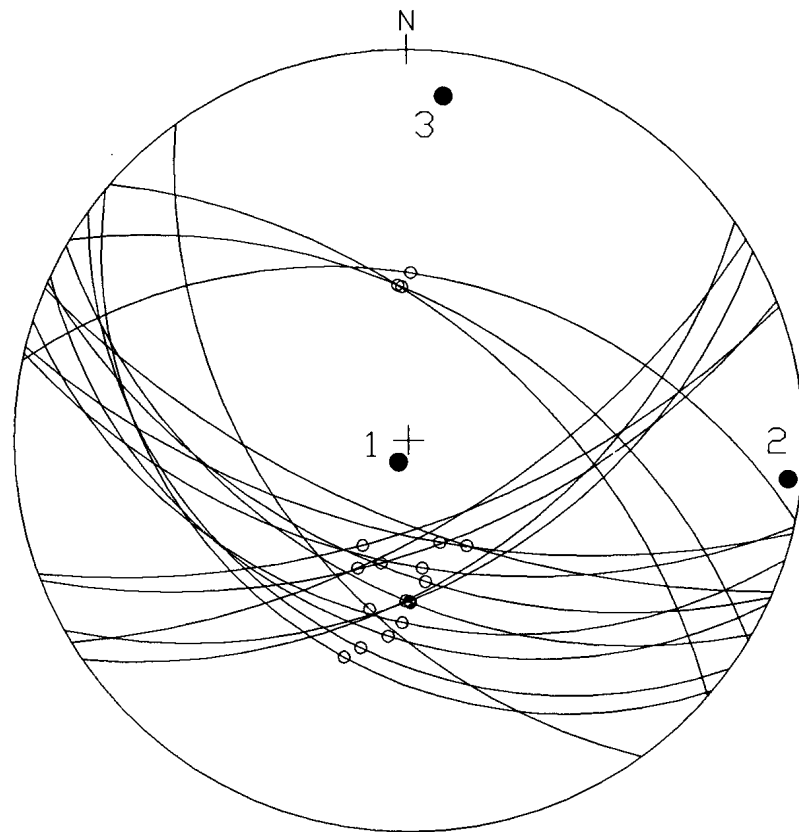
	Known	Program	Error
σ_1	90/000	71/195	19.0°
σ_2	00/090	17/345	75.7°
σ_3	00/000	09/078	78.1°
Φ	0.00	0.069	0.069

Figure 9-1 - Lower-hemisphere stereographic projection and table demonstrating the differences between the known and calculated principal stress axes σ_1 , σ_2 , and σ_3 and the value of Φ for fault population RP-01-00 using Reches' method of paleostress analysis. In the stereographic projection, the known principal stress axes σ_1 , σ_2 , and σ_3 are oriented up, east, and north respectively and the calculated principal stress axes are denoted by the filled circles labelled 1, 2, and 3.



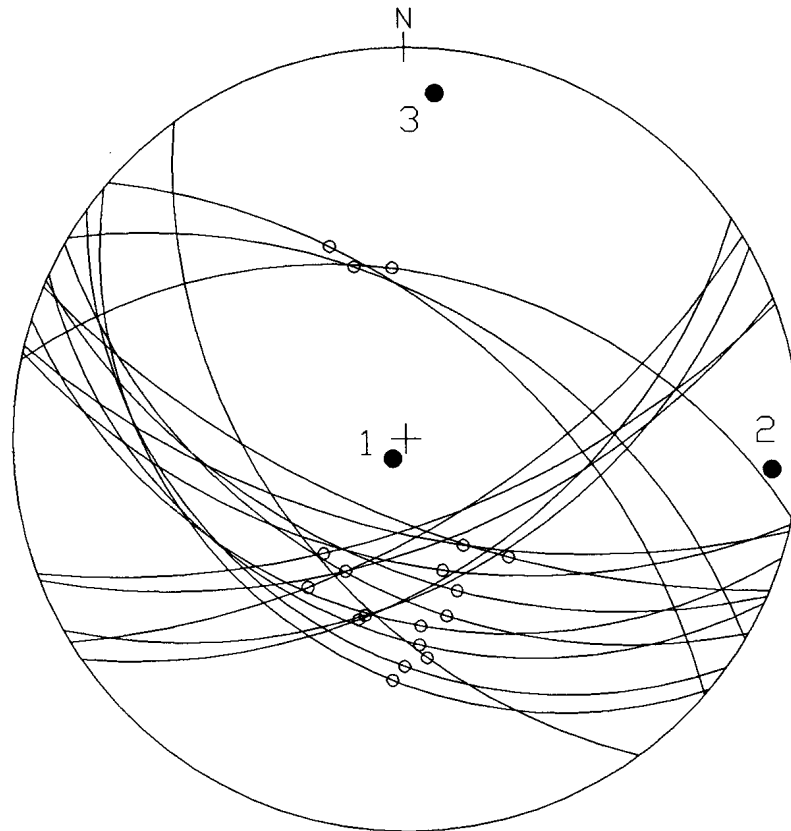
	Known	Program	Error
σ_1	90/000	83/205	7.0°
σ_2	00/090	02/100	10.2°
σ_3	00/000	07/010	12.2°
Φ	0.25	0.131	0.119

Figure 9-2 - Lower-hemisphere stereographic projection and table demonstrating the differences between the known and calculated principal stress axes σ_1 , σ_2 , and σ_3 and the value of Φ for fault population RP-01-25 using Reches' method of paleostress analysis. In the stereographic projection, the known principal stress axes σ_1 , σ_2 , and σ_3 are oriented up, east, and north respectively and the calculated principal stress axes are denoted by the filled circles labelled 1, 2, and 3.



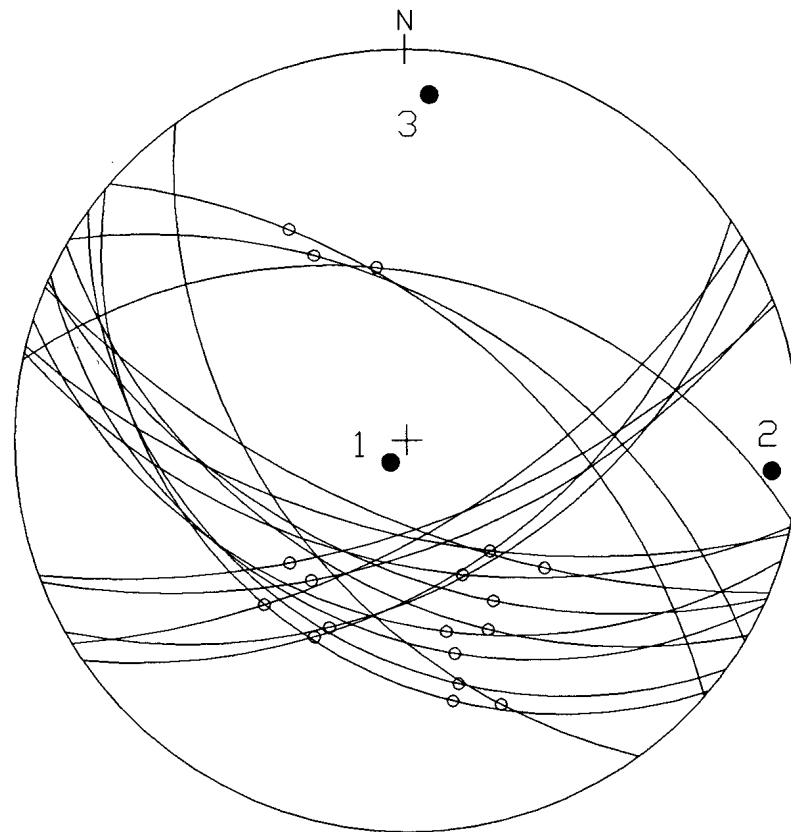
	Known	Program	Error
σ_1	90/000	83/205	7.0°
σ_2	00/090	02/096	6.3°
σ_3	00/000	07/006	9.2°
Φ	0.50	0.387	0.113

Figure 9-3 - Lower-hemisphere stereographic projection and table demonstrating the differences between the known and calculated principal stress axes σ_1 , σ_2 , and σ_3 and the value of Φ for fault population RP-01-50 using Reches' method of paleostress analysis. In the stereographic projection, the known principal stress axes σ_1 , σ_2 , and σ_3 are oriented up, east, and north respectively and the calculated principal stress axes are denoted by the filled circles labelled 1, 2, and 3.



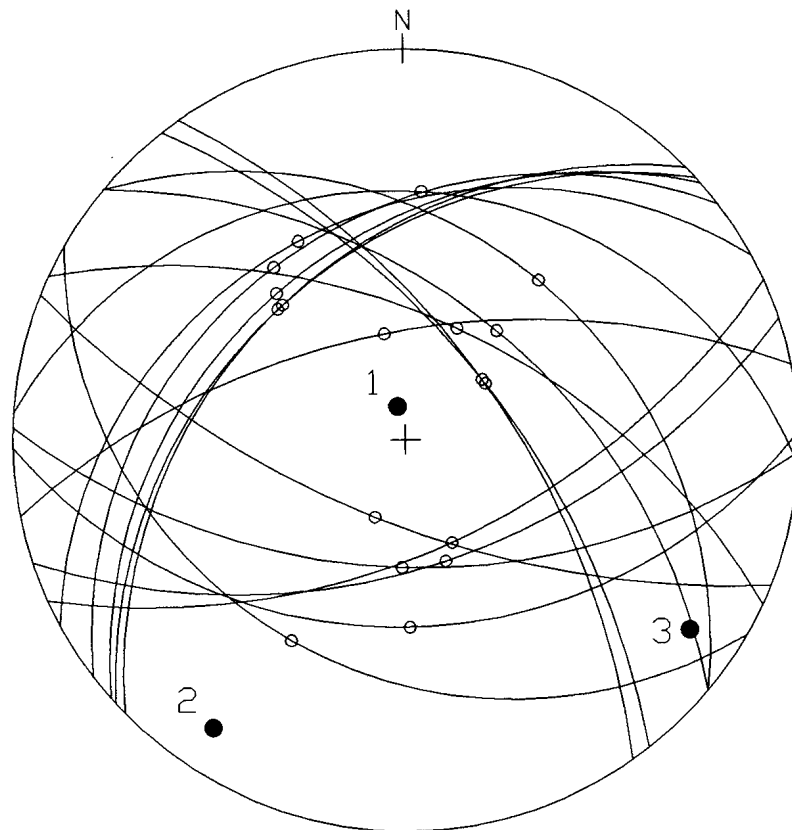
	Known	Program	Error
σ_1	90/000	83/214	7.0°
σ_2	00/090	04/095	6.4°
σ_3	00/000	07/005	8.6°
Φ	0.75	0.683	0.112

Figure 9-4 - Lower-hemisphere stereographic projection and table demonstrating the differences between the known and calculated principal stress axes σ_1 , σ_2 , and σ_3 and the value of Φ for fault population RP-01-75 using Reches' method of paleostress analysis. In the stereographic projection, the known principal stress axes σ_1 , σ_2 , and σ_3 are oriented up, east, and north respectively and the calculated principal stress axes are denoted by the filled circles labelled 1, 2, and 3.



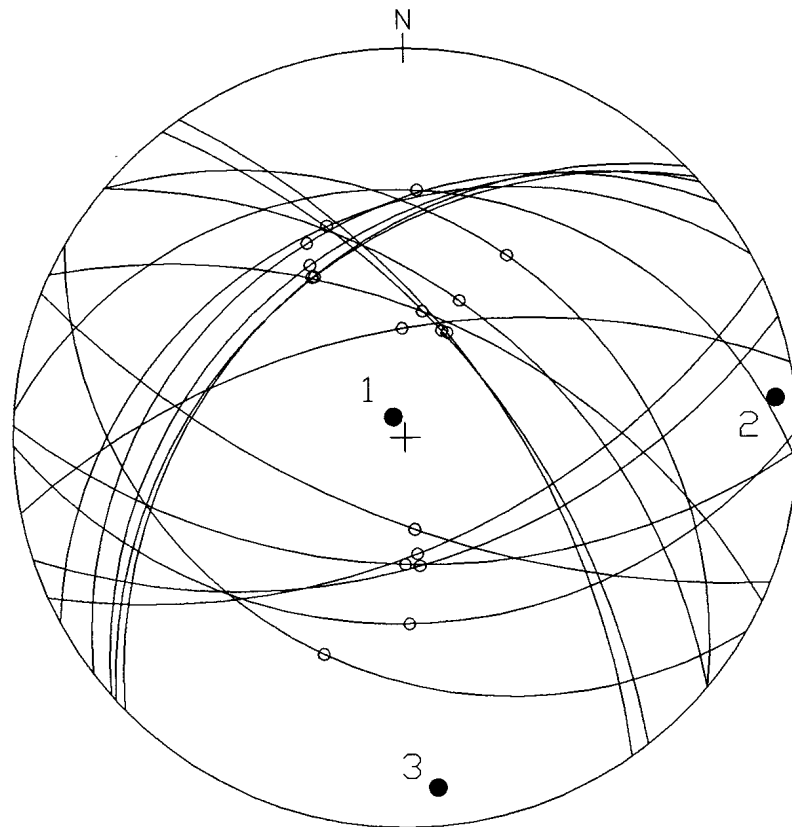
	Known	Program	Error
σ_1	90/000	82/217	8.0°
σ_2	00/090	04/095	6.4°
σ_3	00/000	07/004	8.1°
Φ	1.00	0.903	0.097

Figure 9-5 - Lower-hemisphere stereographic projection and table demonstrating the differences between the known and calculated principal stress axes σ_1 , σ_2 , and σ_3 and the value of Φ for fault population RP-01-10 using Reches' method of paleostress analysis. In the stereographic projection, the known principal stress axes σ_1 , σ_2 , and σ_3 are oriented up, east, and north respectively and the calculated principal stress axes are denoted by the filled circles labelled 1, 2, and 3.



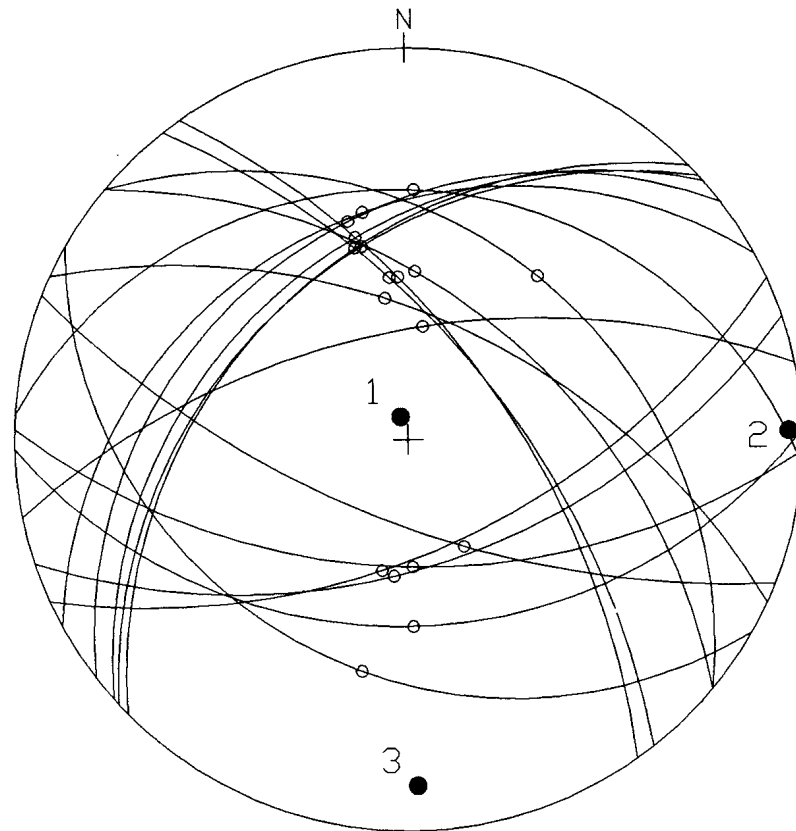
	Known	Program	Error
σ_1	90/000	80/347	10.0°
σ_2	00/090	07/214	56.3°
σ_3	00/000	08/124	56.4°
Φ	0.00	0.178	0.178

Figure 9-6 - Lower-hemisphere stereographic projection and table demonstrating the differences between the known and calculated principal stress axes σ_1 , σ_2 , and σ_3 and the value of Φ for fault population RP-02-00 using Reches' method of paleostress analysis. In the stereographic projection, the known principal stress axes σ_1 , σ_2 , and σ_3 are oriented up, east, and north respectively and the calculated principal stress axes are denoted by the filled circles labelled 1, 2, and 3.



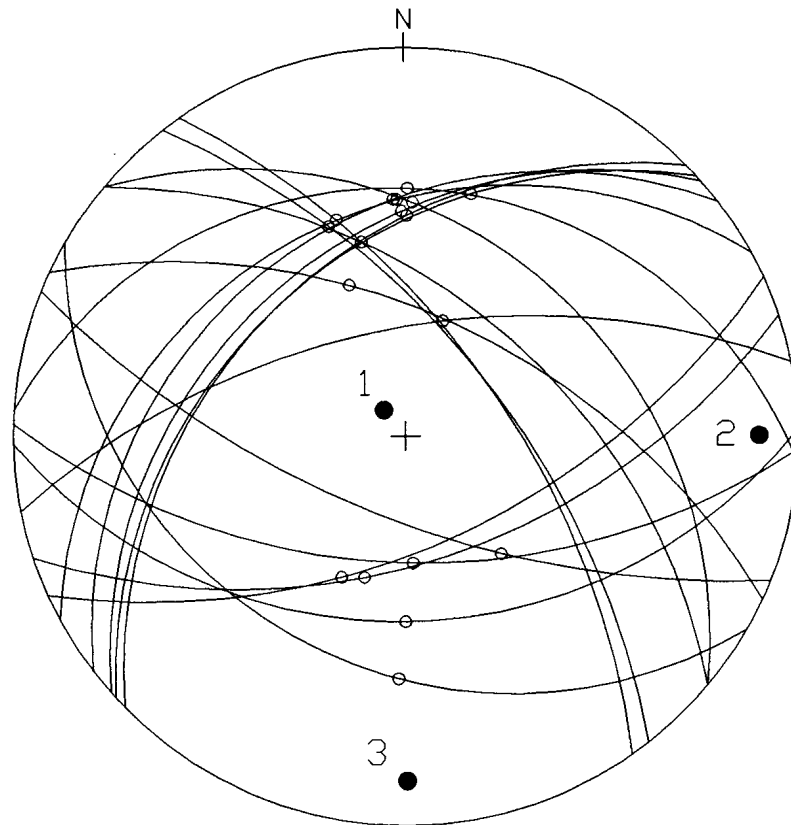
	Known	Program	Error
σ_1	90/000	83/330	7.0°
σ_2	00/090	03/084	6.7°
σ_3	00/000	06/175	7.8°
Φ	0.25	0.178	0.072

Figure 9-7 - Lower-hemisphere stereographic projection and table demonstrating the differences between the known and calculated principal stress axes σ_1 , σ_2 , and σ_3 and the value of Φ for fault population RP-02-25 using Reches' method of paleostress analysis. In the stereographic projection, the known principal stress axes σ_1 , σ_2 , and σ_3 are oriented up, east, and north respectively and the calculated principal stress axes are denoted by the filled circles labelled 1, 2, and 3.



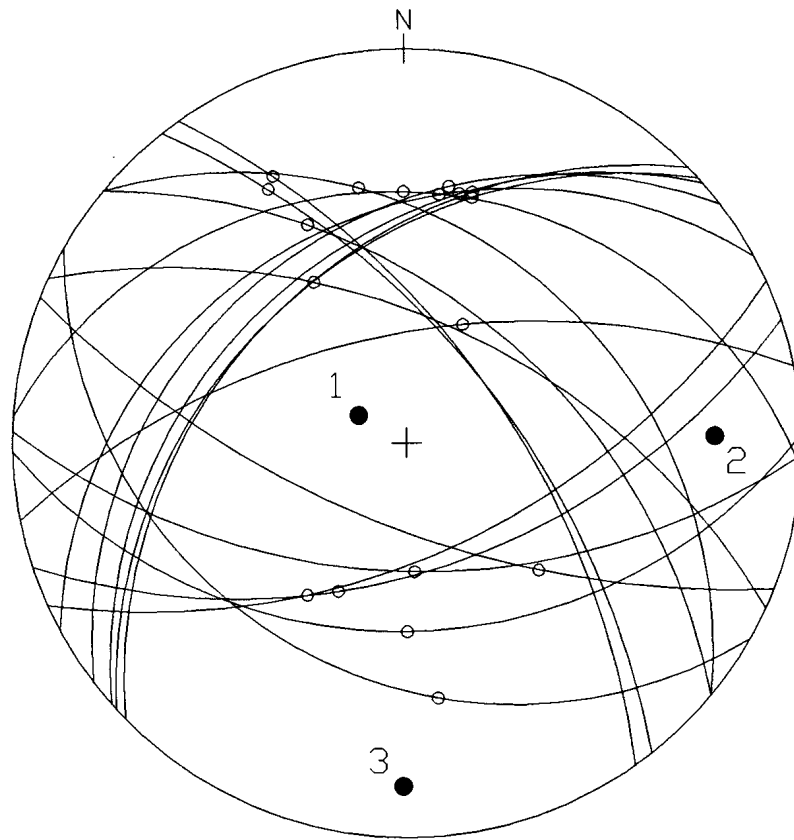
	Known	Program	Error
σ_1	90/000	83/342	7.0°
σ_2	00/090	02/089	2.2°
σ_3	00/000	07/179	7.1°
Φ	0.50	0.351	0.149

Figure 9-8 - Lower-hemisphere stereographic projection and table demonstrating the differences between the known and calculated principal stress axes σ_1 , σ_2 , and σ_3 and the value of Φ for fault population RP-02-50 using Reches' method of paleostress analysis. In the stereographic projection, the known principal stress axes σ_1 , σ_2 , and σ_3 are oriented up, east, and north respectively and the calculated principal stress axes are denoted by the filled circles labelled 1, 2, and 3.



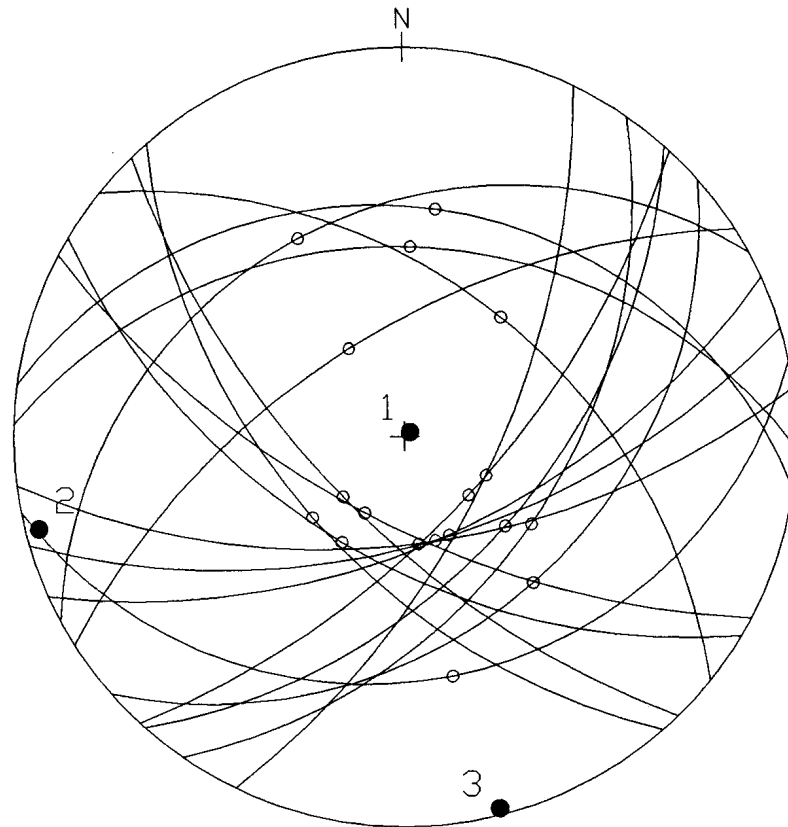
	Known	Program	Error
σ_1	90/000	80/321	10.0°
σ_2	00/090	06/090	6.0°
σ_3	00/000	07/180	7.0°
Φ	0.75	0.637	0.113

Figure 9-9 - Lower-hemisphere stereographic projection and table demonstrating the differences between the known and calculated principal stress axes σ_1 , σ_2 , and σ_3 and the value of Φ for fault population RP-02-75 using Reches' method of paleostress analysis. In the stereographic projection, the known principal stress axes σ_1 , σ_2 , and σ_3 are oriented up, east, and north respectively and the calculated principal stress axes are denoted by the filled circles labelled 1, 2, and 3.



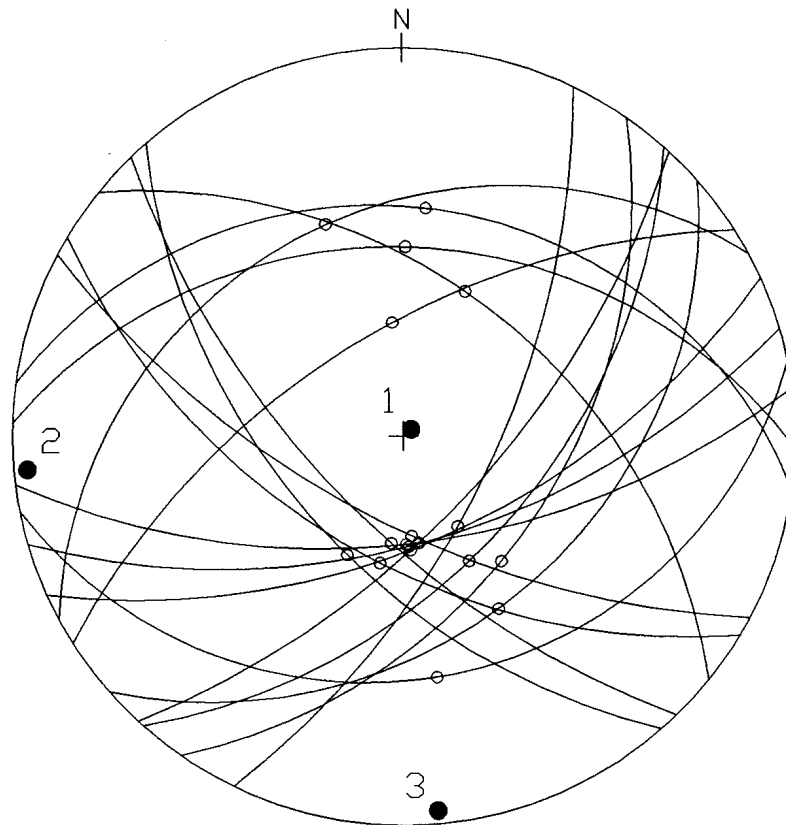
	Known	Program	Error
σ_1	90/000	74/300	16.0°
σ_2	00/090	14/089	14.0°
σ_3	00/000	08/181	8.1°
Φ	1.00	0.903	0.128

Figure 9-10 - Lower-hemisphere stereographic projection and table demonstrating the differences between the known and calculated principal stress axes σ_1 , σ_2 , and σ_3 and the value of Φ for fault population RP-02-10 using Reches' method of paleostress analysis. In the stereographic projection, the known principal stress axes σ_1 , σ_2 , and σ_3 are oriented up, east, and north respectively and the calculated principal stress axes are denoted by the filled circles labelled 1, 2, and 3.



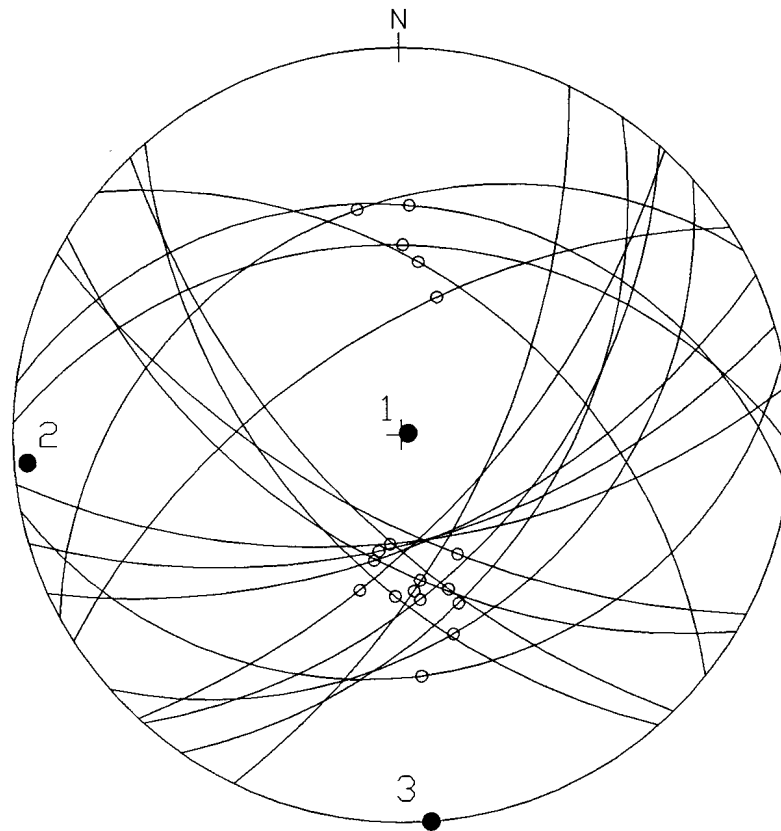
	Known	Program	Error
σ_1	90/000	88/049	2.0°
σ_2	00/090	02/256	14.1°
σ_3	00/000	01/156	14.0°
Φ	0.00	0.070	0.070

Figure 9-11 - Lower-hemisphere stereographic projection and table demonstrating the differences between the known and calculated principal stress axes σ_1 , σ_2 , and σ_3 and the value of Φ for fault population RP-03-00 using Reches' method of paleostress analysis. In the stereographic projection, the known principal stress axes σ_1 , σ_2 , and σ_3 are oriented up, east, and north respectively and the calculated principal stress axes are denoted by the filled circles labelled 1, 2, and 3.



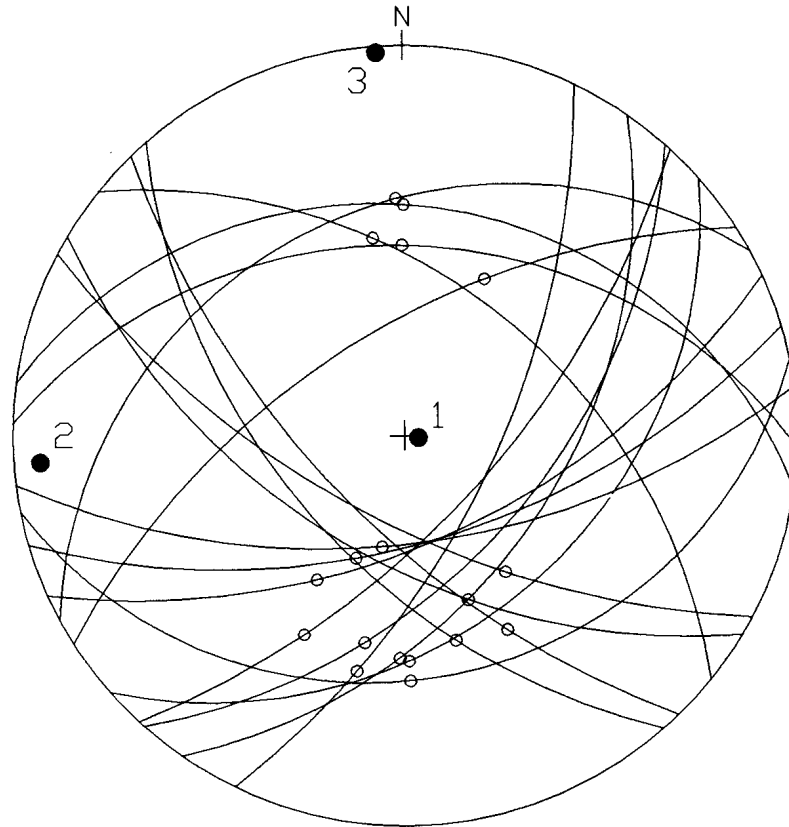
	Known	Program	Error
σ_1	90/000	87/047	3.0°
σ_2	00/090	02/265	5.4°
σ_3	00/000	02/175	5.4°
Φ	0.25	0.252	0.002

Figure 9-12 - Lower-hemisphere stereographic projection and table demonstrating the differences between the known and calculated principal stress axes σ_1 , σ_2 , and σ_3 and the value of Φ for fault population RP-03-25 using Reches' method of paleostress analysis. In the stereographic projection, the known principal stress axes σ_1 , σ_2 , and σ_3 are oriented up, east, and north respectively and the calculated principal stress axes are denoted by the filled circles labelled 1, 2, and 3.



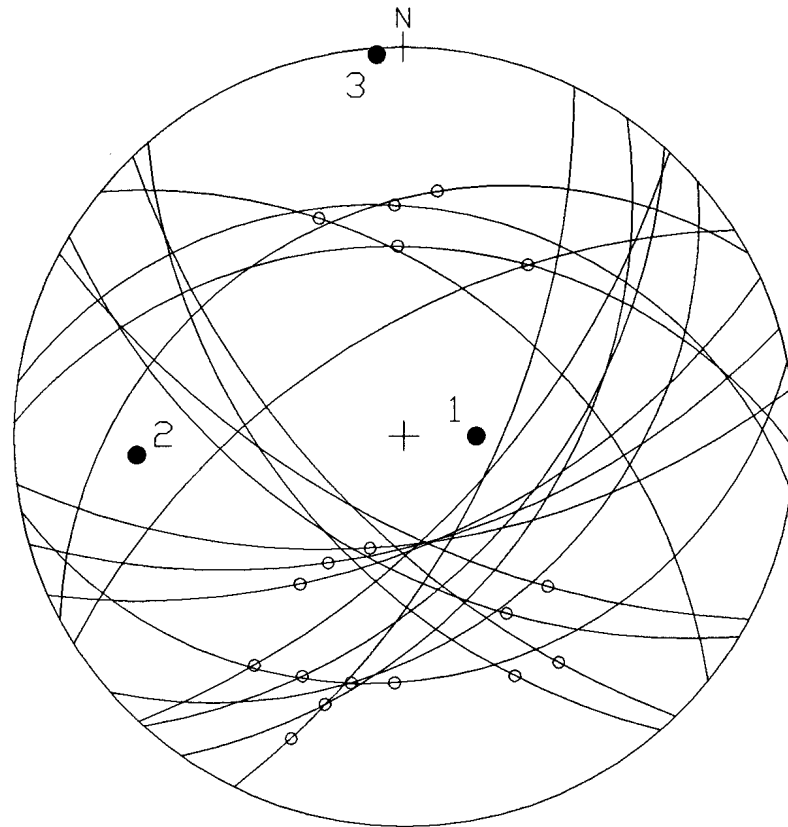
	Known	Program	Error
σ_1	90/000	88/076	2.0°
σ_2	00/090	02/266	4.5°
σ_3	00/000	00/176	4.0°
Φ	0.50	0.437	0.063

Figure 9-13 - Lower-hemisphere stereographic projection and table demonstrating the differences between the known and calculated principal stress axes σ_1 , σ_2 , and σ_3 and the value of Φ for fault population RP-03-50 using Reches' method of paleostress analysis. In the stereographic projection, the known principal stress axes σ_1 , σ_2 , and σ_3 are oriented up, east, and north respectively and the calculated principal stress axes are denoted by the filled circles labelled 1, 2, and 3.



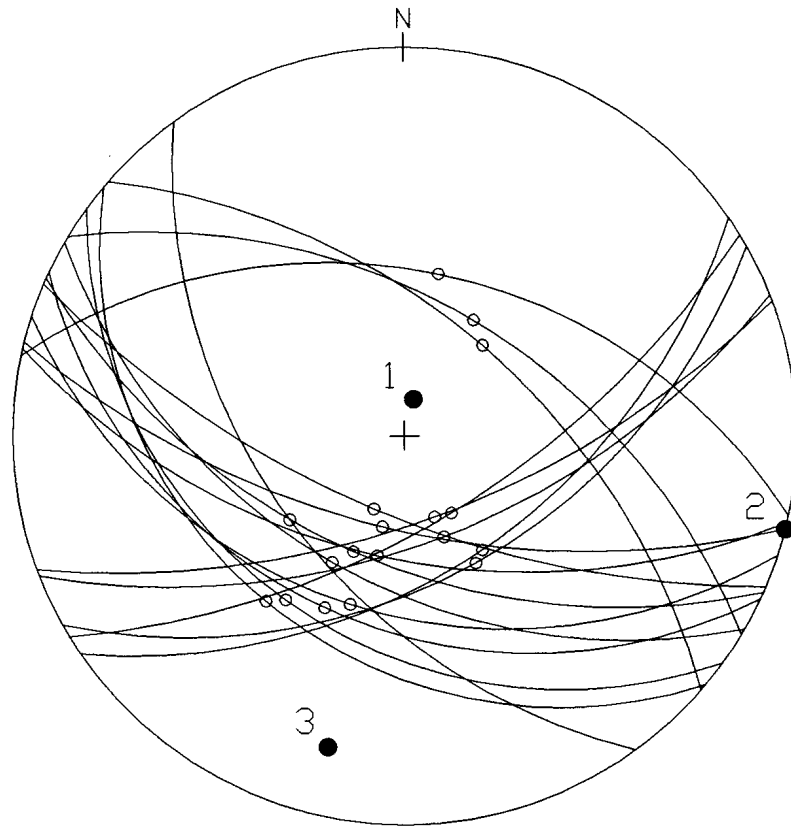
	Known	Program	Error
σ_1	90/000	86/098	4.0°
σ_2	00/090	04/26	5.7°
σ_3	00/000	01/356	4.1°
Φ	0.75	0.658	0.092

Figure 9-14 - Lower-hemisphere stereographic projection and table demonstrating the differences between the known and calculated principal stress axes σ_1 , σ_2 , and σ_3 and the value of Φ for fault population RP-03-75 using Reches' method of paleostress analysis. In the stereographic projection, the known principal stress axes σ_1 , σ_2 , and σ_3 are oriented up, east, and north respectively and the calculated principal stress axes are denoted by the filled circles labelled 1, 2, and 3.



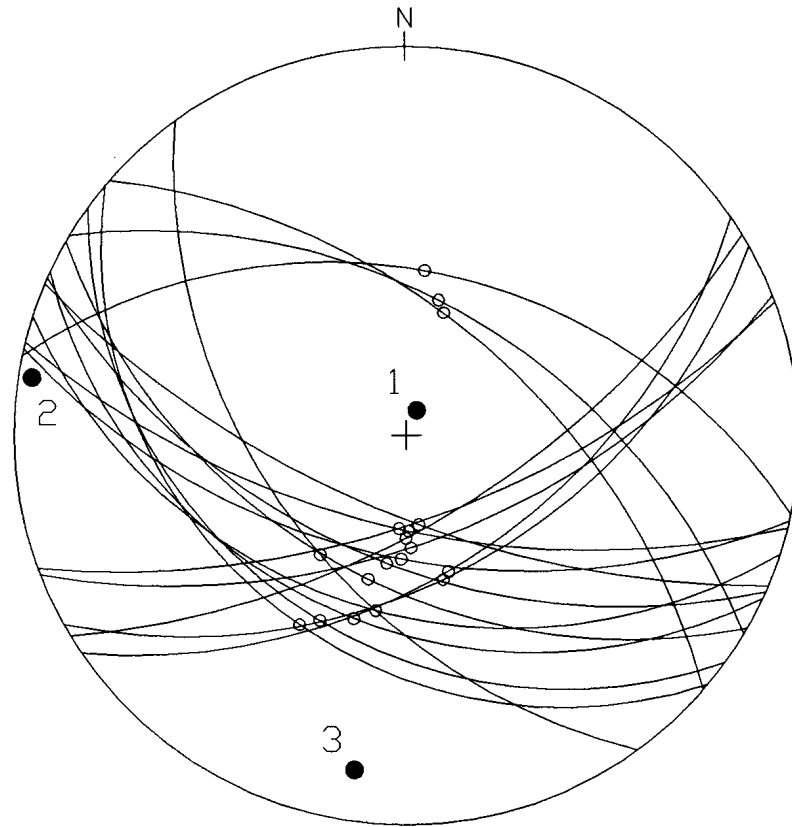
	Known	Program	Error
σ_1	90/000	69/090	21.0°
σ_2	00/090	21/266	21.4°
σ_3	00/000	01/356	4.1°
Φ	1.00	0.880	0.120

Figure 9-15 - Lower-hemisphere stereographic projection and table demonstrating the differences between the known and calculated principal stress axes σ_1 , σ_2 , and σ_3 and the value of Φ for fault population RP-03-10 using Reches' method of paleostress analysis. In the stereographic projection, the known principal stress axes σ_1 , σ_2 , and σ_3 are oriented up, east, and north respectively and the calculated principal stress axes are denoted by the filled circles labelled 1, 2, and 3.



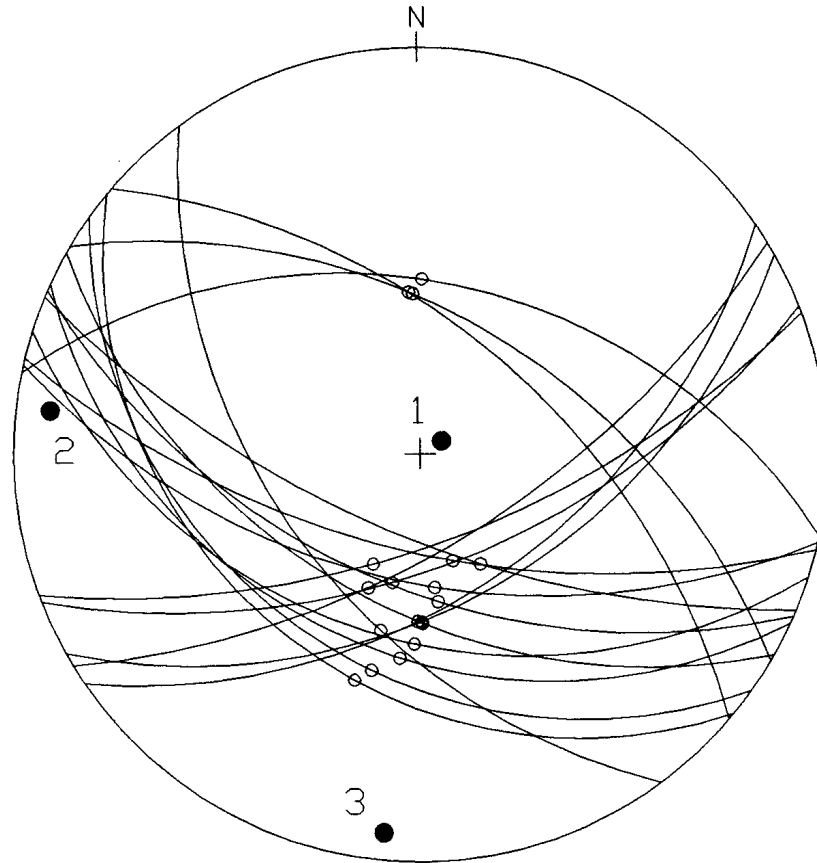
	Known	Program	Error
σ_1	90/000	79/014	11.0°
σ_2	00/090	00/104	14.0°
σ_3	00/000	11/194	17.7°
Φ	0.00	0.236	0.236

Figure 9-16 - Lower-hemisphere stereographic projection and table demonstrating the differences between the known and calculated principal stress axes σ_1 , σ_2 , and σ_3 and the value of Φ for fault population RP-01-00 using Angelier's method of paleostress analysis. In the stereographic projection, the known principal stress axes σ_1 , σ_2 , and σ_3 are oriented up, east, and north respectively and the calculated principal stress axes are denoted by the filled circles labelled 1, 2, and 3.



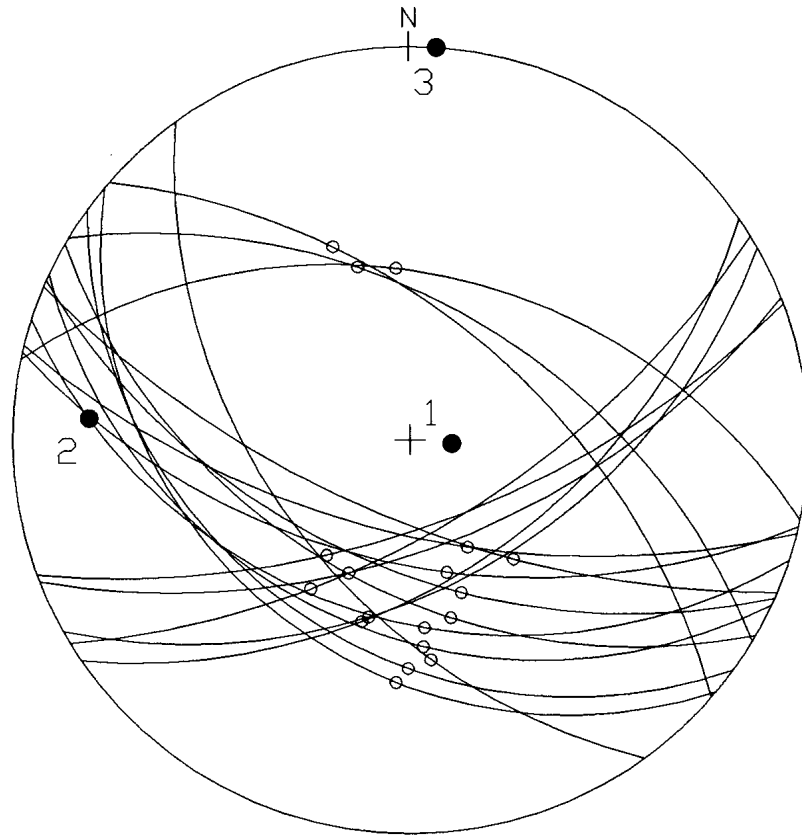
	Known	Program	Error
σ_1	90/000	82/022	8.0°
σ_2	00/090	02/279	9.2°
σ_3	00/000	08/189	12.0°
Φ	0.25	0.390	0.140

Figure 9-17 - Lower-hemisphere stereographic projection and table demonstrating the differences between the known and calculated principal stress axes σ_1 , σ_2 , and σ_3 and the value of Φ for fault population RP-01-25 using Angelier's method of paleostress analysis. In the stereographic projection, the known principal stress axes σ_1 , σ_2 , and σ_3 are oriented up, east, and north respectively and the calculated principal stress axes are denoted by the filled circles labelled 1, 2, and 3.



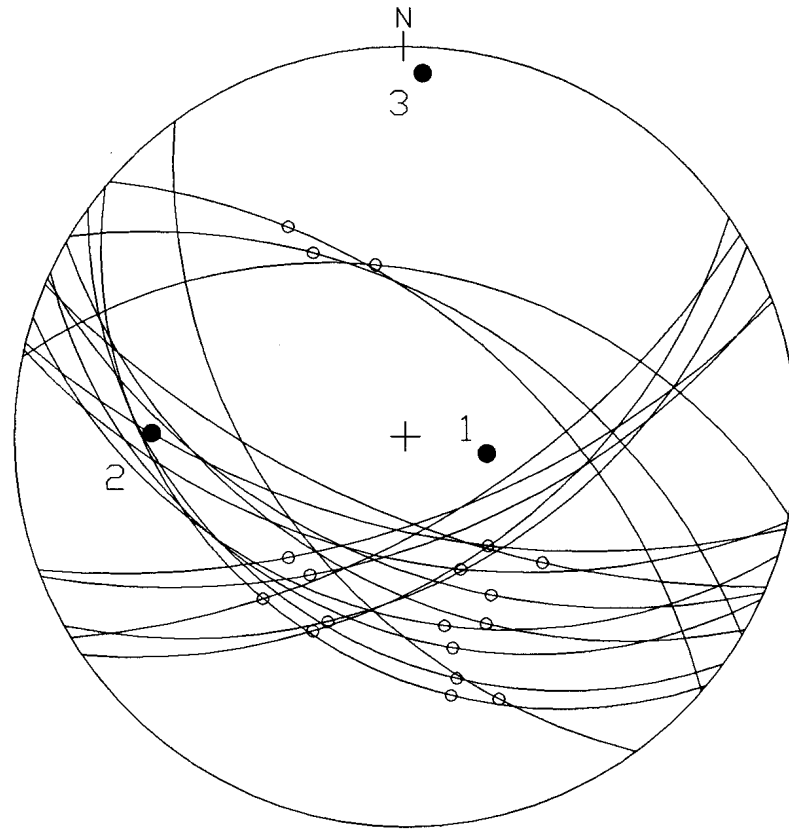
	Known	Program	Error
σ_1	90/000	83/059	7.0°
σ_2	00/090	05/277	8.6°
σ_3	00/000	04/186	7.2°
Φ	0.50	0.550	0.050

Figure 9-18 - Lower-hemisphere stereographic projection and table demonstrating the differences between the known and calculated principal stress axes σ_1 , σ_2 , and σ_3 and the value of Φ for fault population RP-01-50 using Angelier's method of paleostress analysis. In the stereographic projection, the known principal stress axes σ_1 , σ_2 , and σ_3 are oriented up, east, and north respectively and the calculated principal stress axes are denoted by the filled circles labelled 1, 2, and 3.



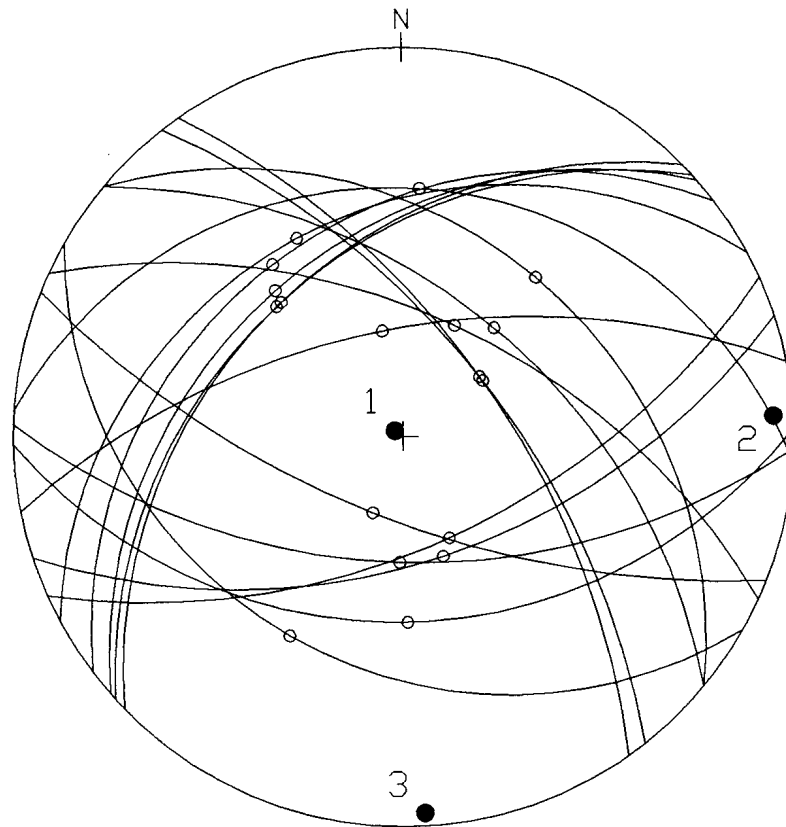
	Known	Program	Error
σ_1	90/000	78/095	12.0°
σ_2	00/090	12/274	12.6°
σ_3	00/000	00/004	4.0°
Φ	0.75	0.694	0.056

Figure 9-19 - Lower-hemisphere stereographic projection and table demonstrating the differences between the known and calculated principal stress axes σ_1 , σ_2 , and σ_3 and the value of Φ for fault population RP-01-75 using Angelier's method of paleostress analysis. In the stereographic projection, the known principal stress axes σ_1 , σ_2 , and σ_3 are oriented up, east, and north respectively and the calculated principal stress axes are denoted by the filled circles labelled 1, 2, and 3.



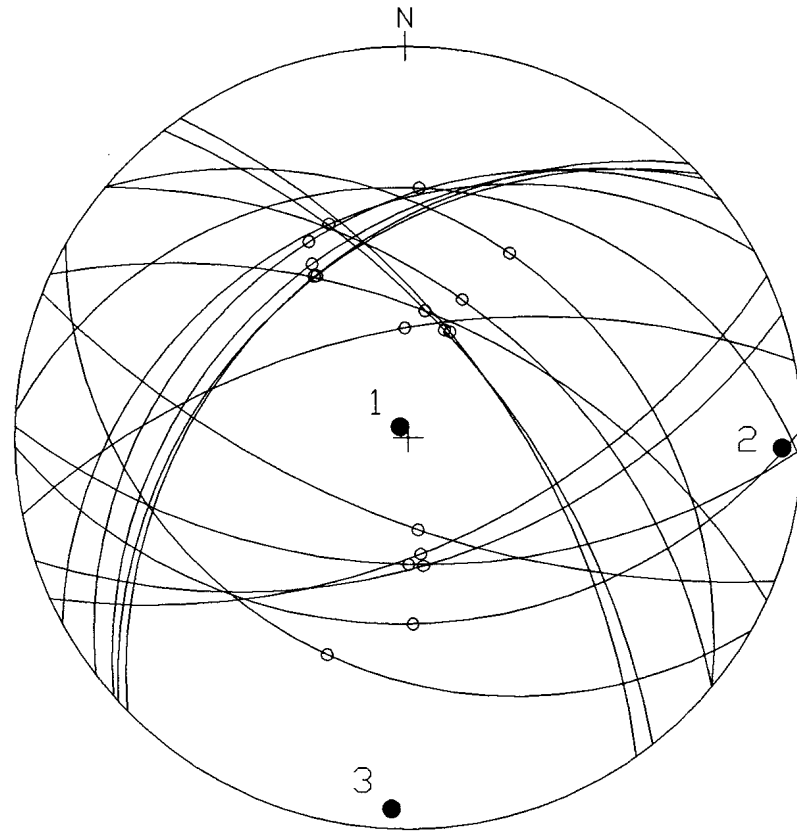
	Known	Program	Error
σ_1	90/000	66/102	24.0°
σ_2	00/090	24/271	24.0°
σ_3	00/000	04/003	5.0°
Φ	1.00	0.796	0.204

Figure 9-20 - Lower-hemisphere stereographic projection and table demonstrating the differences between the known and calculated principal stress axes σ_1 , σ_2 , and σ_3 and the value of Φ for fault population RP-01-10 using Angelier's method of paleostress analysis. In the stereographic projection, the known principal stress axes σ_1 , σ_2 , and σ_3 are oriented up, east, and north respectively and the calculated principal stress axes are denoted by the filled circles labelled 1, 2, and 3.



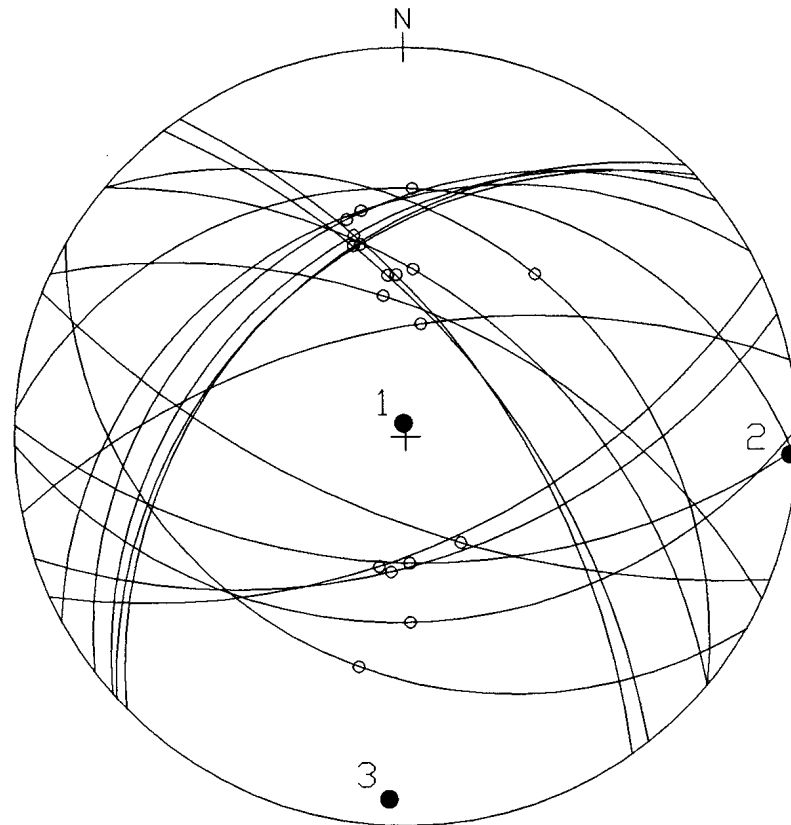
	Known	Program	Error
σ_1	90/000	87/304	3.0°
σ_2	00/090	03/087	4.2°
σ_3	00/000	02/177	3.6°
Φ	0.00	0.077	0.077

Figure 9-21 - Lower-hemisphere stereographic projection and table demonstrating the differences between the known and calculated principal stress axes σ_1 , σ_2 , and σ_3 and the value of Φ for fault population RP-02-00 using Angelier's method of paleostress analysis. In the stereographic projection, the known principal stress axes σ_1 , σ_2 , and σ_3 are oriented up, east, and north respectively and the calculated principal stress axes are denoted by the filled circles labelled 1, 2, and 3.



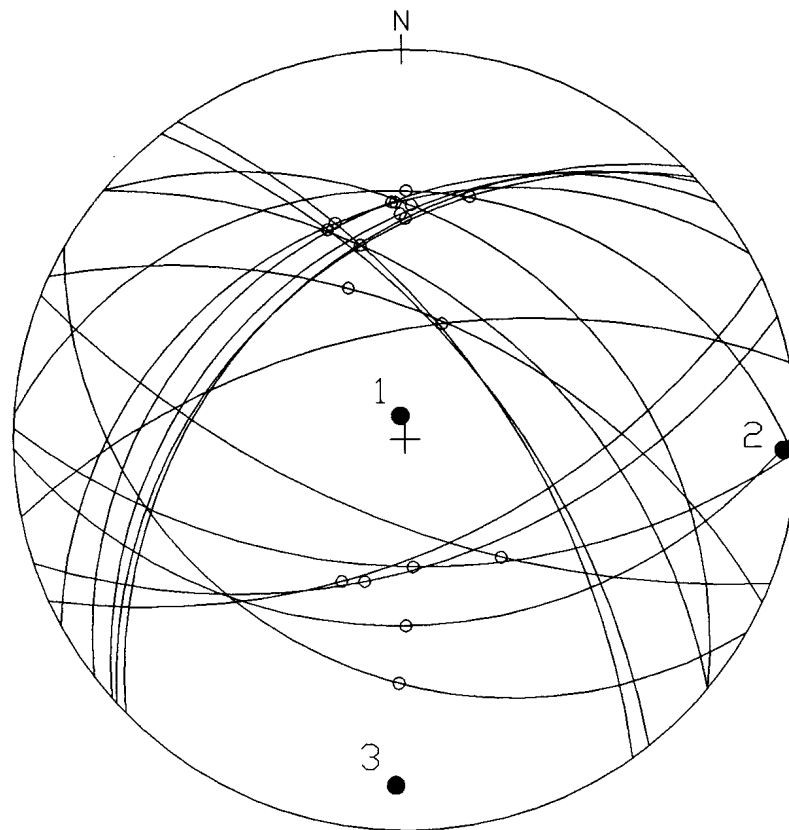
	Known	Program	Error
σ_1	90/000	86/323	4.0°
σ_2	00/090	03/092	3.6°
σ_3	00/000	03/183	4.2°
Φ	0.25	0.253	0.003

Figure 9-22 - Lower-hemisphere stereographic projection and table demonstrating the differences between the known and calculated principal stress axes σ_1 , σ_2 , and σ_3 and the value of Φ for fault population RP-02-25 using Angelier's method of paleostress analysis. In the stereographic projection, the known principal stress axes σ_1 , σ_2 , and σ_3 are oriented up, east, and north respectively and the calculated principal stress axes are denoted by the filled circles labelled 1, 2, and 3.



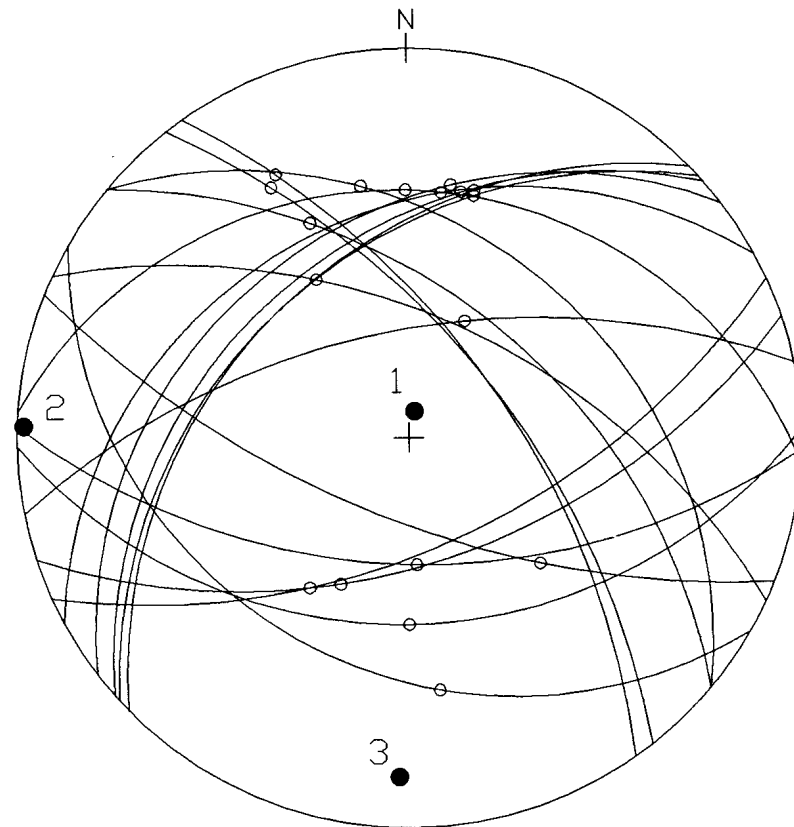
	Known	Program	Error
σ_1	90/000	86/351	4.0°
σ_2	00/090	01/093	3.2°
σ_3	00/000	04/183	5.0°
Φ	0.50	0.443	0.060

Figure 9-23 - Lower-hemisphere stereographic projection and table demonstrating the differences between the known and calculated principal stress axes σ_1 , σ_2 , and σ_3 and the value of Φ for fault population RP-02-50 using Angelier's method of paleostress analysis. In the stereographic projection, the known principal stress axes σ_1 , σ_2 , and σ_3 are oriented up, east, and north respectively and the calculated principal stress axes are denoted by the filled circles labelled 1, 2, and 3.



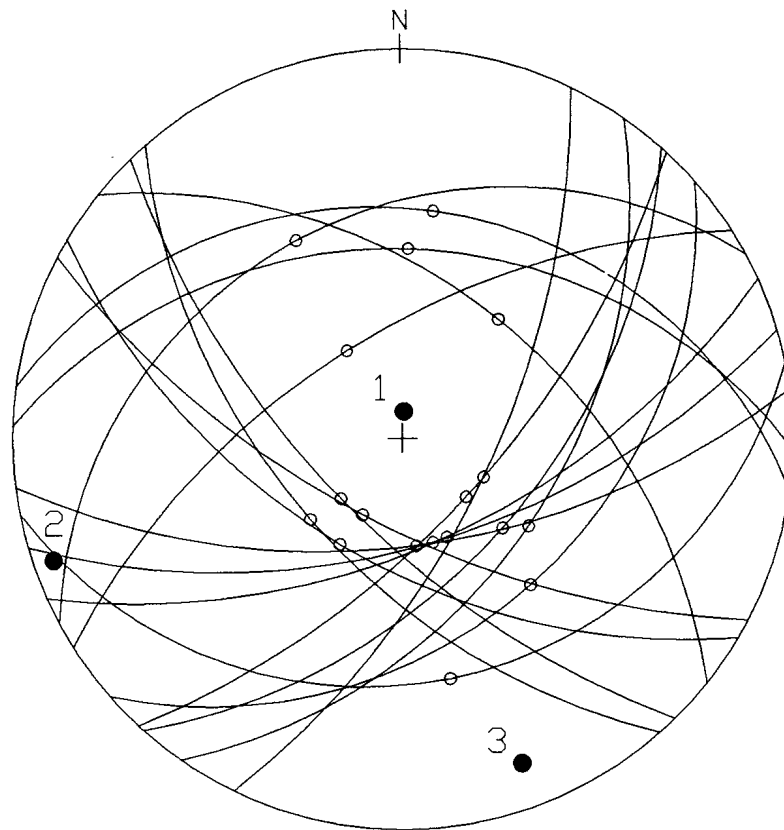
	Known	Program	Error
σ_1	90/000	83/349	7.0°
σ_2	00/090	02/092	2.8°
σ_3	00/000	07/182	7.3°
Φ	0.75	0.675	0.075

Figure 9-24 - Lower-hemisphere stereographic projection and table demonstrating the differences between the known and calculated principal stress axes σ_1 , σ_2 , and σ_3 and the value of Φ for fault population RP-02-75 using Angelier's method of paleostress analysis. In the stereographic projection, the known principal stress axes σ_1 , σ_2 , and σ_3 are oriented up, east, and north respectively and the calculated principal stress axes are denoted by the filled circles labelled 1, 2, and 3.



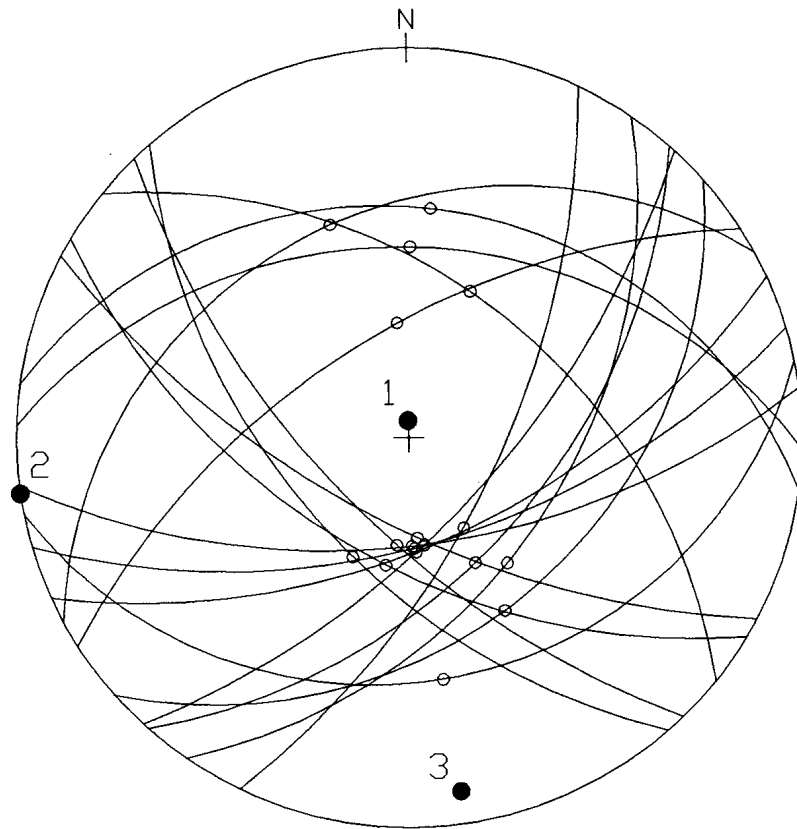
	Known	Program	Error
σ_1	90/000	82/012	8.0°
σ_2	00/090	01/272	2.2°
σ_3	00/000	08/182	8.2°
Φ	1.00	0.846	0.154

Figure 9-25 - Lower-hemisphere stereographic projection and table demonstrating the differences between the known and calculated principal stress axes σ_1 , σ_2 , and σ_3 and the value of Φ for fault population RP-02-10 using Anglier's method of paleostress analysis. In the stereographic projection, the known principal stress axes σ_1 , σ_2 , and σ_3 are oriented up, east, and north respectively and the calculated principal stress axes are denoted by the filled circles labelled 1, 2, and 3.



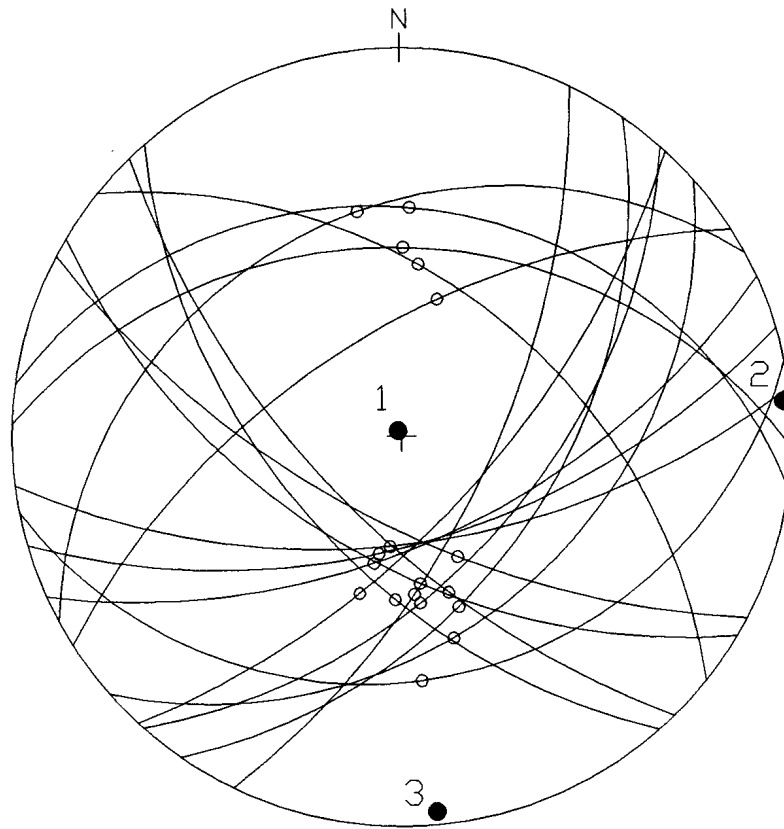
	Known	Program	Error
σ_1	90/000	82/003	8.0°
σ_2	00/090	03/251	19.2°
σ_3	00/000	07/160	21.1°
Φ	0.00	0.149	0.149

Figure 9-26 - Lower-hemisphere stereographic projection and table demonstrating the differences between the known and calculated principal stress axes σ_1 , σ_2 , and σ_3 and the value of Φ for fault population RP-03-00 using Angelier's method of paleostress analysis. In the stereographic projection, the known principal stress axes σ_1 , σ_2 , and σ_3 are oriented up, east, and north respectively and the calculated principal stress axes are denoted by the filled circles labelled 1, 2, and 3.



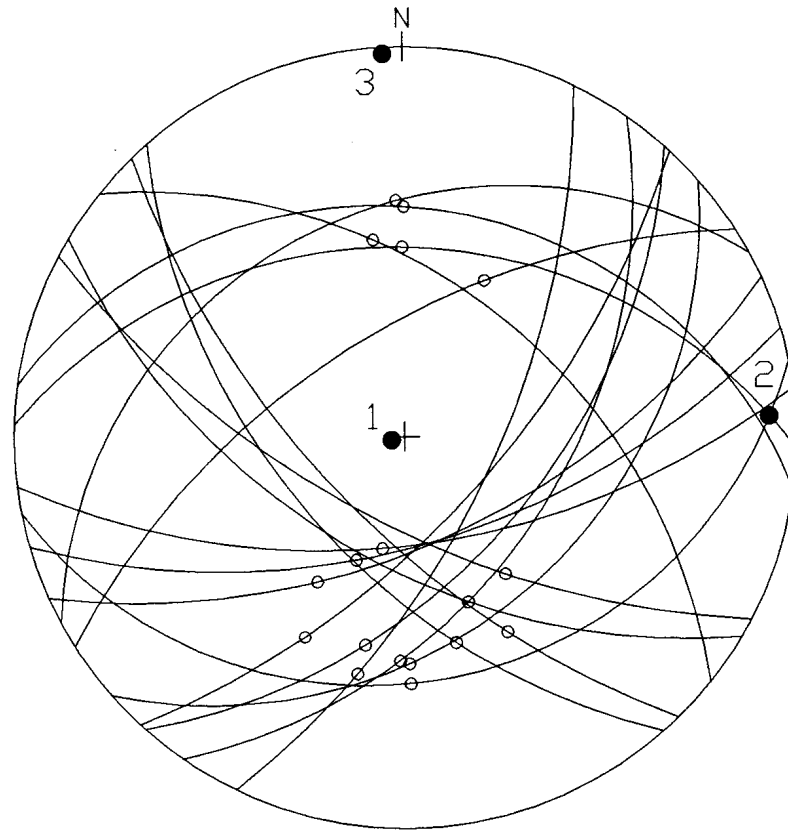
	Known	Program	Error
σ_1	90/000	85/357	5.0°
σ_2	00/090	00/262	8.0°
σ_3	00/000	05/172	9.4°
Φ	0.25	0.326	0.076

Figure 9-27 - Lower-hemisphere stereographic projection and table demonstrating the differences between the known and calculated principal stress axes σ_1 , σ_2 , and σ_3 and the value of Φ for fault population RP-03-25 using Angelier's method of paleostress analysis. In the stereographic projection, the known principal stress axes σ_1 , σ_2 , and σ_3 are oriented up, east, and north respectively and the calculated principal stress axes are denoted by the filled circles labelled 1, 2, and 3.



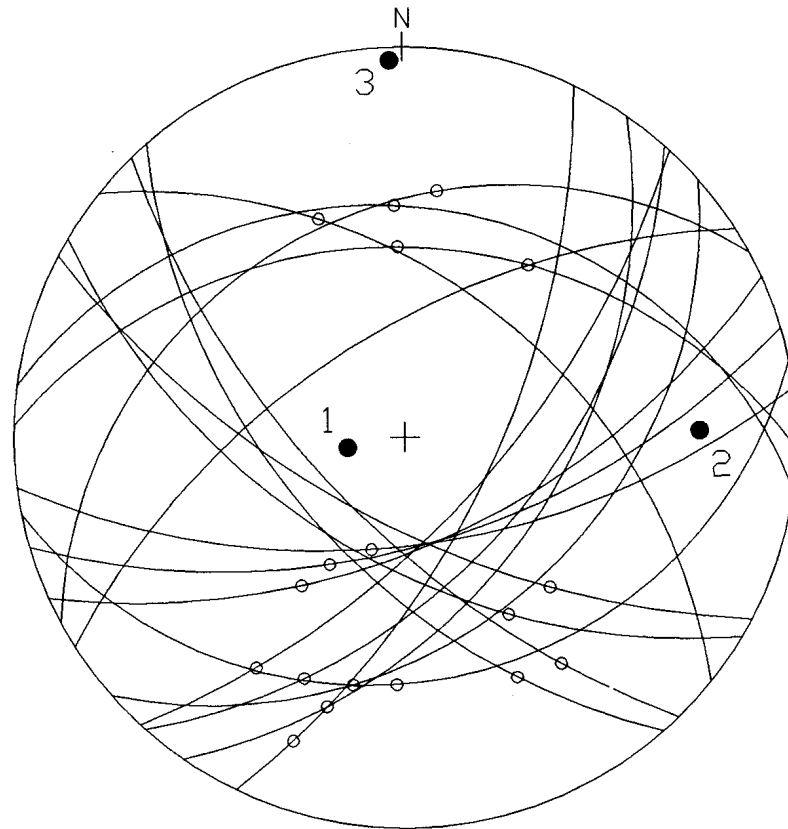
	Known	Program	Error
σ_1	90/000	88/329	2.0°
σ_2	00/090	01/085	5.1°
σ_3	00/000	02/175	5.4°
Φ	0.50	0.528	0.028

Figure 9-28 - Lower-hemisphere stereographic projection and table demonstrating the differences between the known and calculated principal stress axes σ_1 , σ_2 , and σ_3 and the value of Φ for fault population RP-03-50 using Angelier's method of paleostress analysis. In the stereographic projection, the known principal stress axes σ_1 , σ_2 , and σ_3 are oriented up, east, and north respectively and the calculated principal stress axes are denoted by the filled circles labelled 1, 2, and 3.



	Known	Program	Error
σ_1	90/000	86/256	4.0°
σ_2	00/090	04/087	5.0°
σ_3	00/000	01/357	3.2°
Φ	0.75	0.728	0.022

Figure 9-29 - Lower-hemisphere stereographic projection and table demonstrating the differences between the known and calculated principal stress axes σ_1 , σ_2 , and σ_3 and the value of Φ for fault population RP-03-75 using Angelier's method of paleostress analysis. In the stereographic projection, the known principal stress axes σ_1 , σ_2 , and σ_3 are oriented up, east, and north respectively and the calculated principal stress axes are denoted by the filled circles labelled 1, 2, and 3.



	Known	Program	Error
σ_1	90/000	73/260	17.0°
σ_2	00/090	16/089	16.0°
σ_3	00/000	02/358	2.8°
Φ	1.00	0.901	0.099

Figure 9-30 - Lower-hemisphere stereographic projection and table demonstrating the differences between the known and calculated principal stress axes σ_1 , σ_2 , and σ_3 and the value of Φ for fault population RP-03-10 using Angelier's method of paleostress analysis. In the stereographic projection, the known principal stress axes σ_1 , σ_2 , and σ_3 are oriented up, east, and north respectively and the calculated principal stress axes are denoted by the filled circles labelled 1, 2, and 3.

For fault population RP-01, Reches' method returned the largest principal stress orientation errors for an initial Φ value of 0.00 where the orientations of σ_2 and σ_3 were reversed. The orientation errors were all less than 15° for an initial Φ value of 0.25 and all less than 10° for initial Φ values of 0.50, 0.75, and 1.00. The errors in magnitude between the initial and calculated values of Φ were all less than 0.15 (fiFigures 9-1 through 9-5).

For fault population RP-02, Reches' method returned the largest principal stress orientation errors for an initial Φ value of 0.00 with the largest errors in the orientations of σ_2 and σ_3 . The orientation errors were all 10° or less for all other initial Φ values. The errors in magnitude between the initial and calculated values of Φ were all less than 0.18 (fiFigures 9-6 through 9-10).

For fault population RP-03, Reches' method returned the largest principal stress orientation errors for an initial Φ value of 1.00 with the largest errors in the orientations of σ_1 and σ_2 . The orientation errors were all less than 15° for an initial Φ value of 0.00 and all less than 10° for initial Φ values of 0.25, 0.50, and 0.75. The errors in magnitude between the initial and calculated values of Φ were all 0.12 or less (fiFigures 9-11 through 9-15).

For fault population RP-01, Angelier's method returned the largest principal stress orientation errors for an initial Φ value of 1.00 with the largest errors in the orientations of σ_1 and σ_2 . The orientation errors were all 20° or less for all other initial Φ values. The errors in magnitude between the initial and calculated values of Φ were all less than 0.24 (fiFigures 9-16 through 9-20).

For fault population RP-02, Angelier's method returned principal stress orientation errors of less than 10° for all initial Φ values. The errors in magnitude between the initial and calculated values of Φ were all less than 0.16 for an initial Φ value of 1.00 and less than

0.08 for initial Φ values of 0.25, 0.50, 0.75, and 1.00 (fiFigures 9-21 through 9-25).

For fault population RP-03, Angelier's method returned the largest principal stress orientation errors for initial Φ values of 0.00 and 1.00 with the largest errors in the orientations of σ_2 and σ_3 for an initial Φ value of 0.00 and σ_2 and σ_3 for an initial Φ value of 1.00. The orientation errors were all 10° or less for all other Φ values. The errors in magnitude between the initial and calculated values of Φ were all less than 0.15 (fiFigures 9-26 through 9-30).

As a general observation, the calculated orientations of some of the principal stress axes σ_1 , σ_2 , and σ_3 seem to be displaced from their true orientations such that they are roughly subparallel local concentrations of slip vectors. Figure 9-1 displays this well with the orientation of σ_1 .

Tables 9-1, 9-2, and 9-3 compare the results of Reches' and Angelier's methods for each of the three random-pole fault populations RP-01, RP-02, and RP-03 respectively.

Table 9-1 shows Reches' and Angelier's methods to poorly correspond for fault population RP-01 given initial Φ values of 0.00 and 1.00 with a 20° or less angular deviation for intermediate initial Φ values. Table 9-2 shows Reches' and Angelier's methods to similarly poorly correspond given initial Φ values of 0.00 and 1.00 with a 10° or less angular deviation for intermediate initial Φ values. Table 9-3 shows Reches' and Angelier's methods to poorly correspond given an initial Φ value of 1.00 with a 10° or less angular deviation for all other initial Φ values. The errors in magnitude between Reches' and Angelier's methods for the initial and calculated values of Φ were 2.25 or less for fault population RP-01 and 0.10 or less for fault populations RP-02 and RP-3.

These results generally indicate that both Reches' and Angelier's methods return reasonable ($\pm 20^\circ$) principal stress axis orientation results for intermediate initial Φ values

(0.25, 0.50, and 0.75) but may not perform well given initial Φ values of 0.00 or 1.00 (plane strain). This is most likely due to the fact that for an initial Φ value of 0.00, σ_2 is equal in magnitude to σ_3 and for an initial Φ value of 1.00, σ_2 is equal in magnitude to σ_1 and the programs have difficulty in assigning the proper orientations for these stress axes.

		Reches'	Angelier's	Deviation
Known Φ of 0.00	σ_1	71/195	79/014	30.0°
	σ_2	17/345	00/104	62.4°
	σ_3	09/078	11/194	66.7°
	Φ	0.069	0.236	0.167
Known Φ of 0.25	σ_1	83/205	82/022	15.0°
	σ_2	02/100	02/279	4.1°
	σ_3	07/010	08/189	15.0°
	Φ	0.165	0.390	0.225
Known Φ of 0.50	σ_1	83/205	83/059	13.4°
	σ_2	02/096	05/277	7.1°
	σ_3	07/006	04/186	11.0°
	Φ	0.378	0.550	0.172
Known Φ of 0.75	σ_1	83/214	78/095	16.5°
	σ_2	04/095	12/274	16.0°
	σ_3	07/005	00/004	7.1°
	Φ	0.638	0.694	0.056
Known Φ of 1.00	σ_1	82/217	66/102	28.3°
	σ_2	04/095	24/271	28.3°
	σ_3	07/004	04/003	3.2°
	Φ	0.903	0.796	0.107

Table 9-1 - Table demonstrating the deviation for the orientations of the σ_1 , σ_2 , and σ_3 principal stress axes and the principal stress magnitude ratio Φ between Reches' and Angelier's methods of paleostress analysis on fault population RP-01 at five different values of Φ .

		Reches'	Angelier's	Deviation
Known Φ of 0.00	σ_1	80/347	87/304	8.1°
	σ_2	07/214	03/087	53.8°
	σ_3	08/124	02/177	53.1°
	Φ	0.178	0.077	0.101
Known Φ of 0.25	σ_1	83/330	86/323	3.1°
	σ_2	03/084	03/092	8.0°
	σ_3	06/175	03/183	8.5°
	Φ	0.178	0.253	0.075
Known Φ of 0.50	σ_1	83/342	86/351	3.1°
	σ_2	02/089	01/093	4.1°
	σ_3	07/179	04/183	5.0°
	Φ	0.351	0.443	0.092
Known Φ of 0.75	σ_1	80/321	83/349	5.0°
	σ_2	06/090	02/092	4.5°
	σ_3	07/180	07/182	2.0°
	Φ	0.637	0.675	0.038
Known Φ of 1.00	σ_1	74/300	82/012	15.5°
	σ_2	14/087	01/272	15.8°
	σ_3	08/081	08/182	80.3°
	Φ	0.872	0.846	0.026

Table 9-2 - Table demonstrating the deviation for the orientations of the σ_1 , σ_2 , and σ_3 principal stress axes and the principal stress magnitude ratio Φ between Reches' and Angelier's methods of paleostress analysis on fault population RP-02 at five known values of Φ .

		Reches'	Angelier's	Deviation
Known Φ of 0.00	σ_1	88/049	82/003	6.8°
	σ_2	02/256	03/251	5.1°
	σ_3	01/166	07/160	8.5°
	Φ	0.070	0.149	0.079
Known Φ of 0.25	σ_1	87/047	85/357	5.6°
	σ_2	02/265	00/262	3.6°
	σ_3	02/175	05/172	4.2°
	Φ	0.252	0.326	0.074
Known Φ of 0.50	σ_1	88/076	88/329	3.2°
	σ_2	02/266	01/085	3.2°
	σ_3	00/176	02/175	2.2°
	Φ	0.437	0.528	0.091
Known Φ of 0.75	σ_1	86/098	86/256	7.9°
	σ_2	04/266	04/087	8.1°
	σ_3	01/356	01/357	1.0°
	Φ	0.658	0.728	0.070
Known Φ of 1.00	σ_1	69/090	73/260	37.9°
	σ_2	21/266	16/089	37.1°
	σ_3	01/356	02/358	2.2°
	Φ	0.880	0.901	0.021

Table 9-3 - Table demonstrating the deviation for the orientations of the σ_1 , σ_2 , and σ_3 principal stress axes and the principal stress magnitude ratio Φ between Reches' and Angelier's methods of paleostress analysis on fault population RP-03 at five different values of Φ .

9.3 Special-Case Fault Population Results

The first special-case fault populations to be tested were the two conjugate fault populations AC-01 and AC-02. In conjugate fault population AC-01, the conjugate fault set was parallel to the principal stress axis σ_3 and perpendicular to the principal stress axes σ_1 and σ_2 . In conjugate fault population AC-02, the conjugate fault set was at 45° to both σ_2 and σ_3 and perpendicular to the principal stress axis σ_1 .

Utilizing Reches' method, conjugate population AC-01 returned surprising results (figures 9-31 through 9-35). The Φ values returned were the opposite of what one would expect. A Φ of 1.00 was returned for an initial Φ of 0.00, a Φ of 0.70 was returned for an initial Φ of 0.25, a Φ of 0.49 was returned for an initial Φ of 0.50 (which is quite good), a Φ of 0.27 was returned for an initial Φ of 0.75, and a Φ of 0.09 was returned for an initial Φ of 1.00. This is most likely related to the fact that the σ_1 and σ_3 principal stress axes were switched and had opposite orientations from what was expected (*i.e.* σ_1 had the proper orientation for σ_2 and vice versa). This is obviously a systematic error arising within the program algorithms.

Angelier's method produced an exact match between the initial and calculated orientations of the three principal stress axes for conjugate population AC-01 (figures 9-36 through 9-41). The errors in magnitude between the initial and calculated values of Φ however, were quite large (approaching 0.5) for initial Φ values of 0.00 and 1.00 and smallest (0.004) for an initial Φ value of 0.50.

Conjugate fault population AC-02 also returned surprising result since Reches' method was totally unable to deal with this set of faults (figures 9-41 through 9-45). The σ_1 and σ_3 orientations were once again switched and, more importantly, the values for Φ ranged from

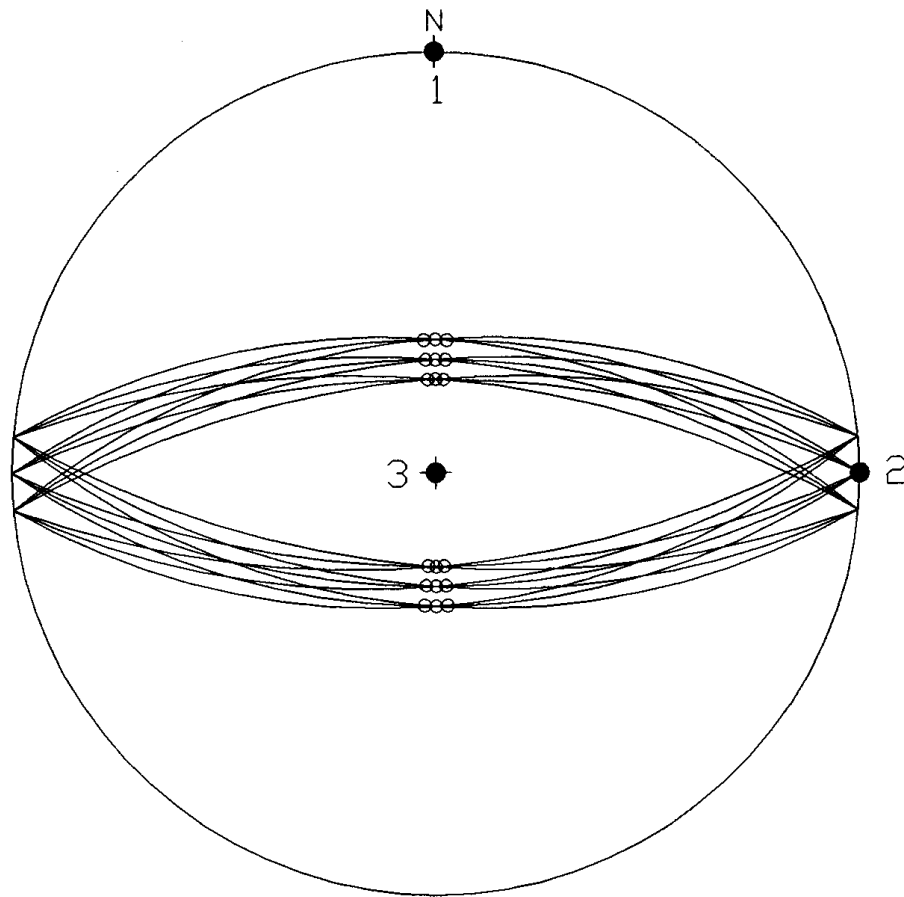
1.00 to 6.13. The ratio Φ , by definition, ranges from 0.0 to 1.0 only. This implies that the program is apparently confusing the σ_1 and σ_3 magnitudes with each other. When the σ_1 and σ_3 orientations are switched, however, the solution is correct. This is a reasonable result since most structural geology textbooks would graphically assign σ_2 to be parallel to the intersection of the conjugate set (which it isn't in this case).

Angelier's method also returned wildly inaccurate results for conjugate fault population AC-02 (figures 9-46 through 9-50). At low initial Φ values (0.00, 0.25, and 0.50), the program confused the orientations of σ_2 and σ_3 and at larger initial Φ values (0.75 and 1.00), the program confused the orientations of σ_1 and σ_2 . The error in magnitude between the initial and calculated values for Φ ranged from a low of 0.155 to a high of 0.479 which is unacceptable.

Comparing the results of Reches' and Angelier's methods for conjugate fault population AC-01 (table 9-4) shows the 90° error in the orientations of the σ_1 and σ_3 principal stress axes for Reches' method. The deviations in magnitude between the initial and calculated values for Φ ranged from a low of 0.019 to a high of 0.648.

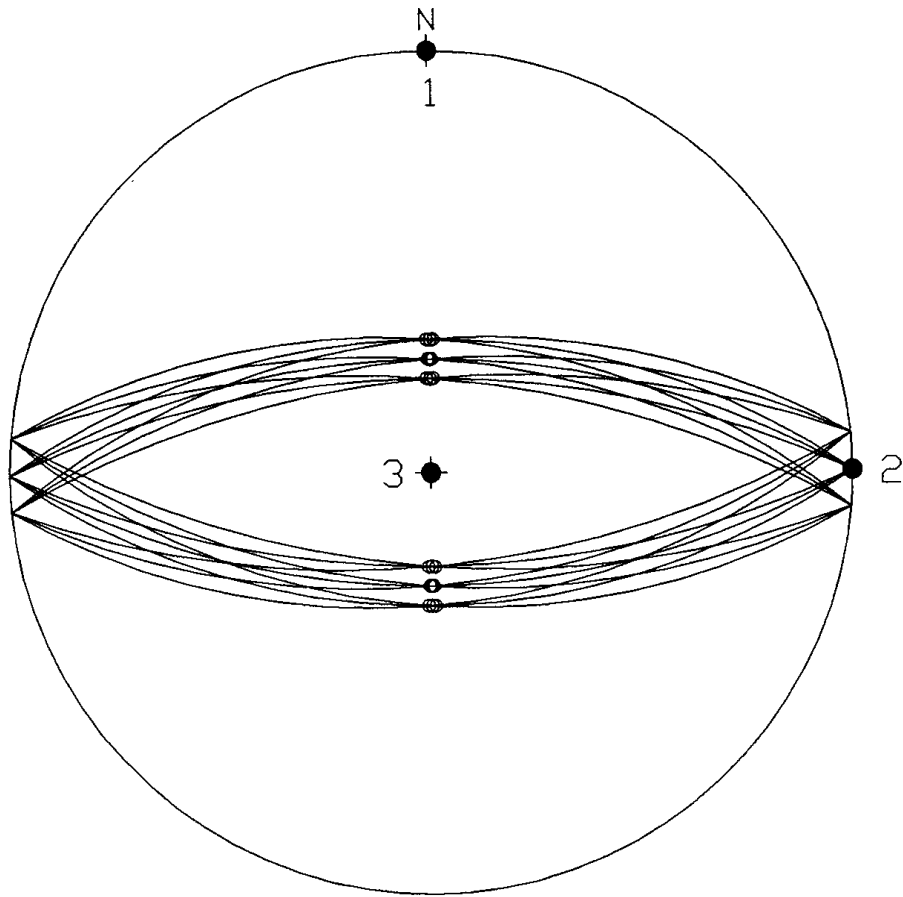
Comparing the results of Reches' and Angelier's methods for conjugate fault population AC-02 (table 9-5) shows large deviations in the orientations of the σ_1 , σ_2 , and σ_3 principal stress axes for initial Φ values of 0.00, 0.25, and 0.50 and large deviations in the orientations of the σ_2 and σ_3 principal stress axes for initial Φ values of 0.75 and 1.00. The deviations in magnitude between the initial and calculated values for Φ were large (0.521) for an initial Φ value of 0.00 and undefined for all other initial Φ values.

A general observation seems to be that both Angelier's and Reches' methods of paleostress analysis return more reasonable results for conjugate fault sets which parallel principal stress axes.



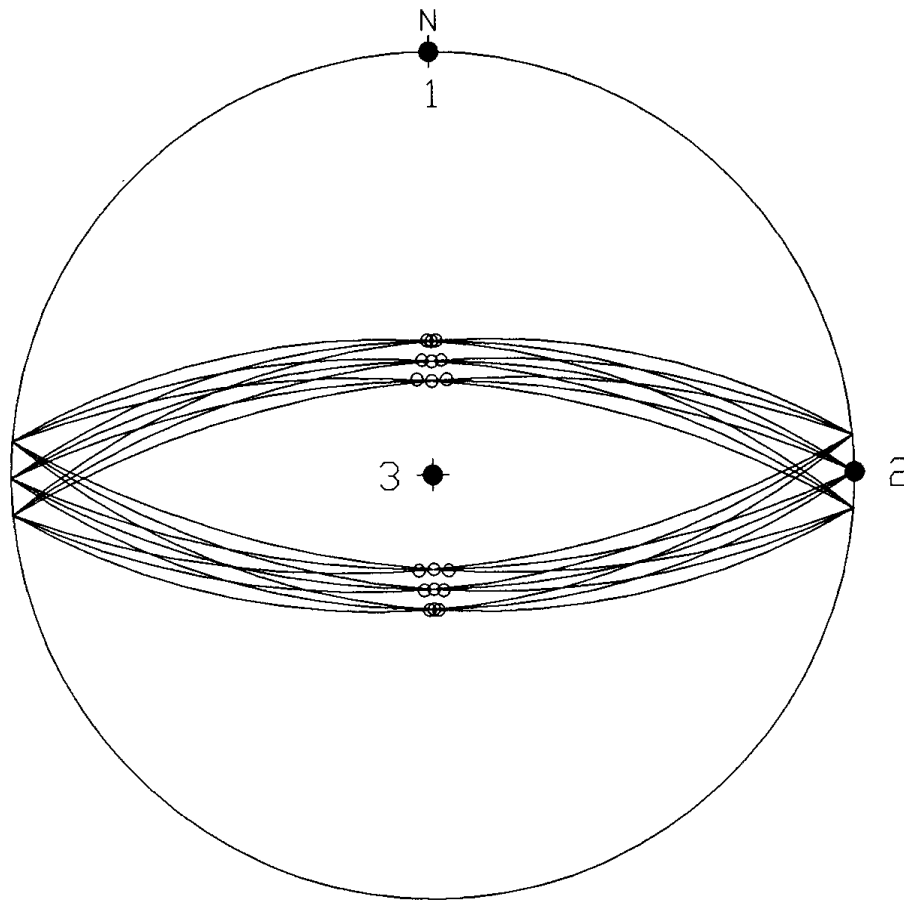
	Known	Program	Error
σ_1	90/000	00/000	90.0°
σ_2	00/090	00/090	0.0°
σ_3	00/000	90/270	90.0°
Φ	0.00	1.000	1.000

Figure 9-31 - Lower-hemisphere stereographic projection and table demonstrating the differences between the known and calculated principal stress axes σ_1 , σ_2 , and σ_3 and the value of Φ for fault population AC-01-00 using Reches' method of paleostress analysis. In the stereographic projection, the known principal stress axes σ_1 , σ_2 , and σ_3 are oriented up, east, and north respectively and the calculated principal stress axes are denoted by the filled circles labelled 1, 2, and 3.



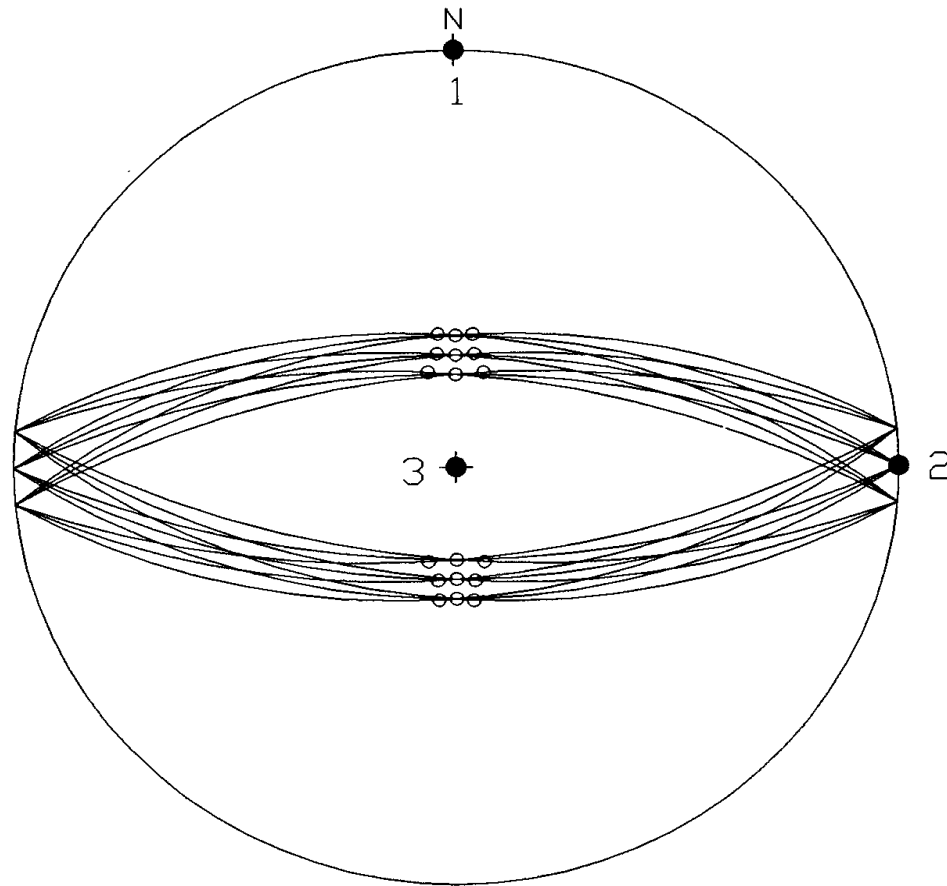
	Known	Program	Error
σ_1	90/000	00/000	90.0°
σ_2	00/090	00/090	0.0°
σ_3	00/000	90/270	90.0°
Φ	0.25	0.695	0.305

Figure 9-32 - Lower-hemisphere stereographic projection and table demonstrating the differences between the known and calculated principal stress axes σ_1 , σ_2 , and σ_3 and the value of Φ for fault population AC-01-25 using Reches' method of paleostress analysis. In the stereographic projection, the known principal stress axes σ_1 , σ_2 , and σ_3 are oriented up, east, and north respectively and the calculated principal stress axes are denoted by the filled circles labelled 1, 2, and 3.



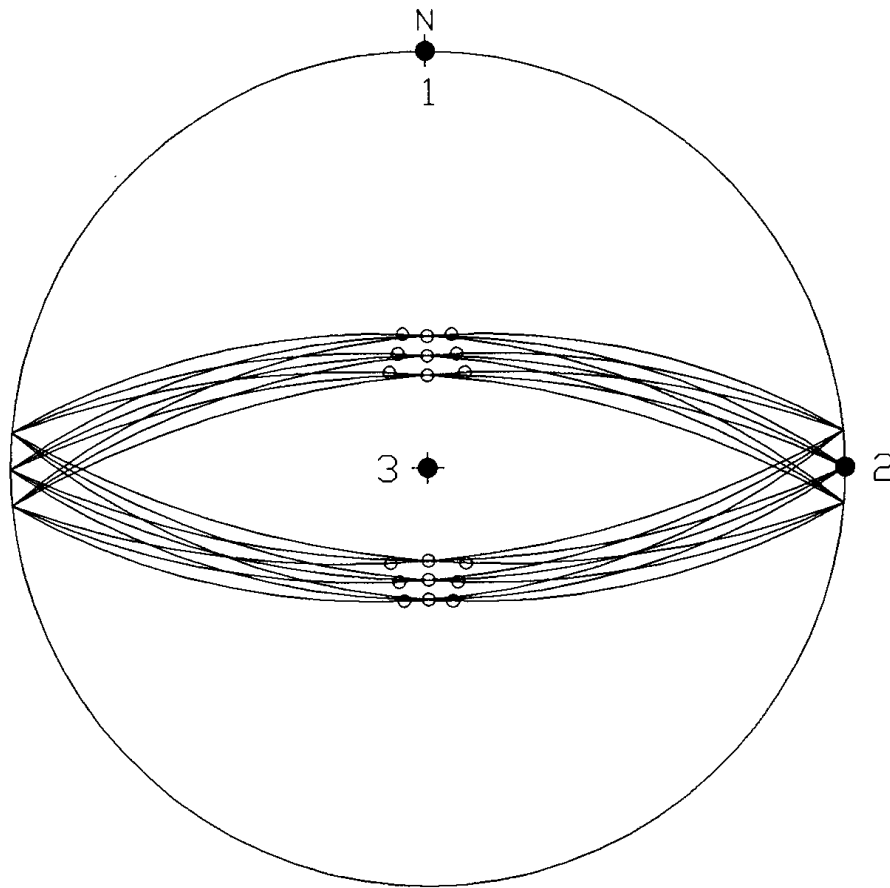
	Known	Program	Error
σ_1	90/000	00/000	90.0°
σ_2	00/090	00/090	0.0°
σ_3	00/000	90/270	90.0°
Φ	0.50	0.485	0.515

Figure 9-33 - Lower-hemisphere stereographic projection and table demonstrating the differences between the known and calculated principal stress axes σ_1 , σ_2 , and σ_3 and the value of Φ for fault population AC-01-50 using Reches' method of paleostress analysis. In the stereographic projection, the known principal stress axes σ_1 , σ_2 , and σ_3 are oriented up, east, and north respectively and the calculated principal stress axes are denoted by the filled circles labelled 1, 2, and 3.



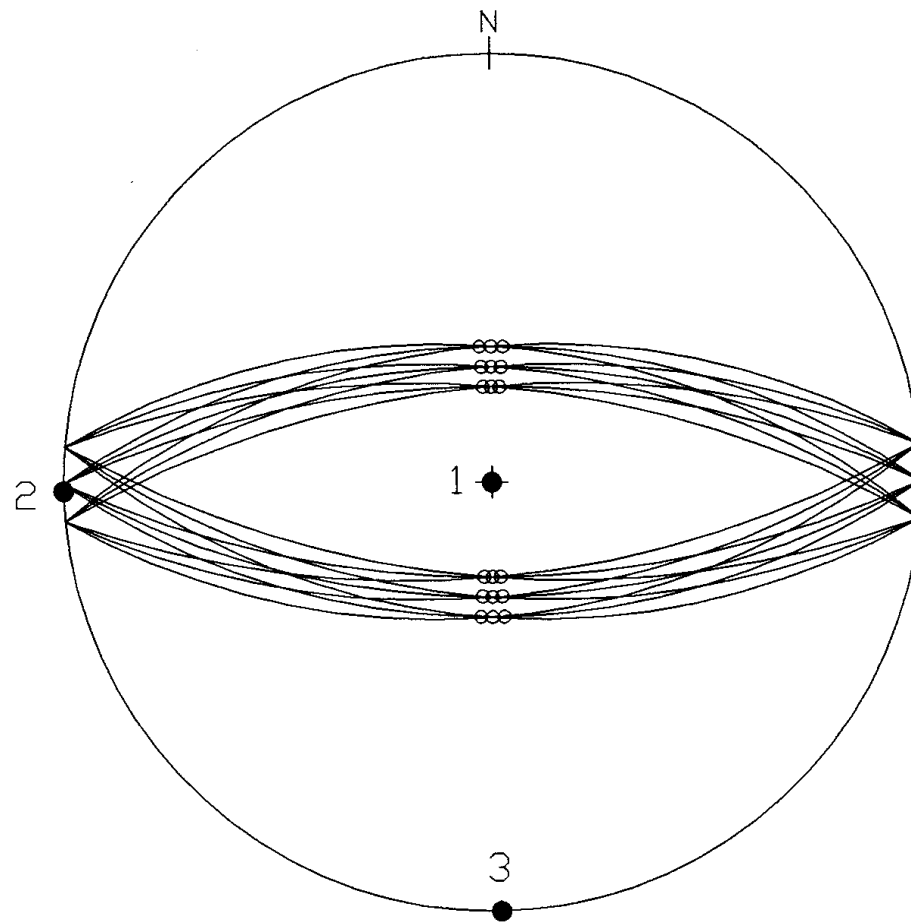
	Known	Program	Error
σ_1	90/000	00/000	90.0°
σ_2	00/090	00/090	0.0°
σ_3	00/000	90/270	90.0°
Φ	0.75	0.274	0.726

Figure 9-34 - Lower-hemisphere stereographic projection and table demonstrating the differences between the known and calculated principal stress axes σ_1 , σ_2 , and σ_3 and the value of Φ for fault population AC-01-75 using Reches' method of paleostress analysis. In the stereographic projection, the known principal stress axes σ_1 , σ_2 , and σ_3 are oriented up, east, and north respectively and the calculated principal stress axes are denoted by the filled circles labelled 1, 2, and 3.



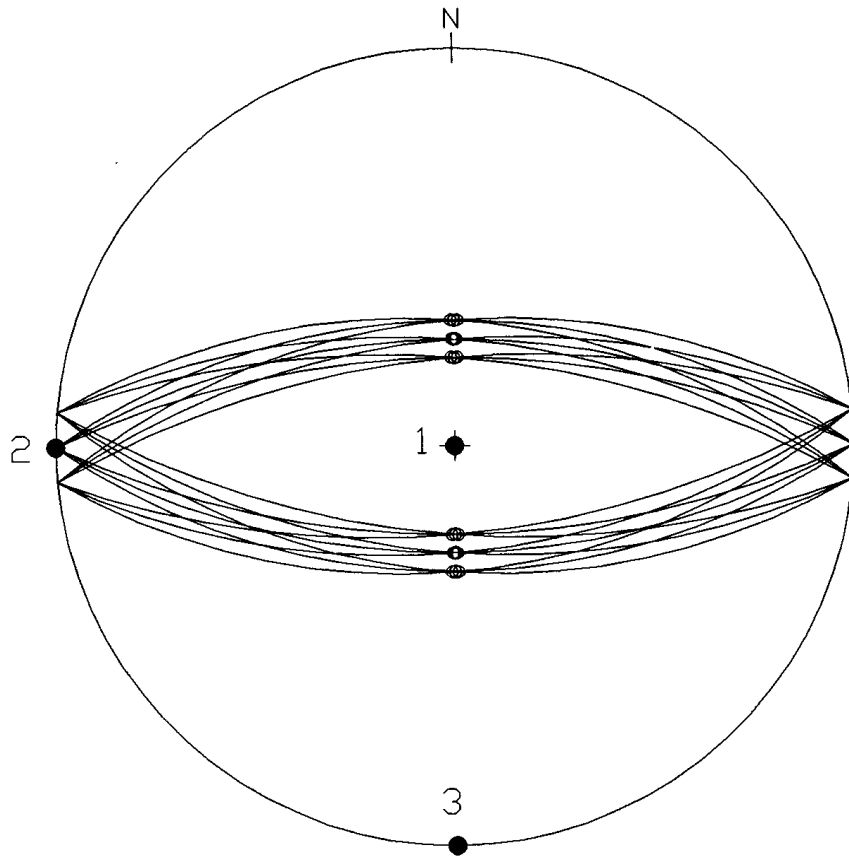
	Known	Program	Error
σ_1	90/000	00/000	90.0°
σ_2	00/090	00/090	0.0°
σ_3	00/000	90/270	90.0°
Φ	1.00	0.089	0.911

Figure 9-35 - Lower-hemisphere stereographic projection and table demonstrating the differences between the known and calculated principal stress axes σ_1 , σ_2 , and σ_3 and the value of Φ for fault population AC-01-10 using Reches' method of paleostress analysis. In the stereographic projection, the known principal stress axes σ_1 , σ_2 , and σ_3 are oriented up, east, and north respectively and the calculated principal stress axes are denoted by the filled circles labelled 1, 2, and 3.



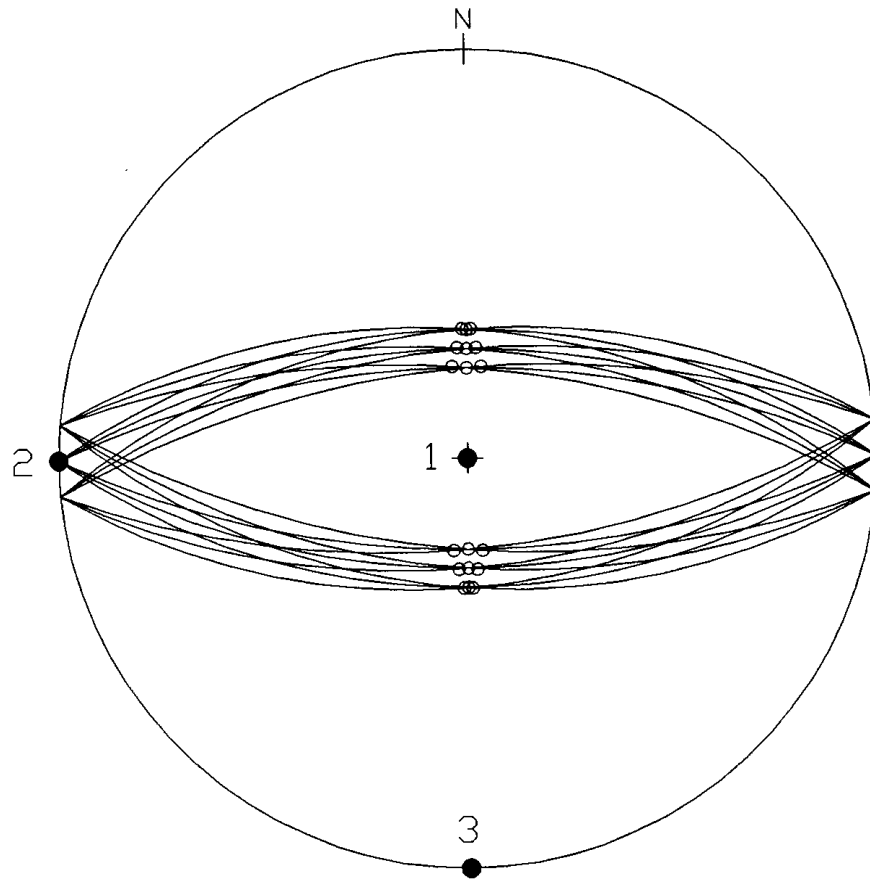
	Known	Program	Error
σ_1	90/000	90/051	0.0°
σ_2	00/090	00/269	1.0°
σ_3	00/000	00/179	1.0°
Φ	0.00	0.453	0.453

Figure 9-36 - Lower-hemisphere stereographic projection and table demonstrating the differences between the known and calculated principal stress axes σ_1 , σ_2 , and σ_3 and the value of Φ for fault population AC-01-00 using Angelier's method of paleostress analysis. In the stereographic projection, the known principal stress axes σ_1 , σ_2 , and σ_3 are oriented up, east, and north respectively and the calculated principal stress axes are denoted by the filled circles labelled 1, 2, and 3.



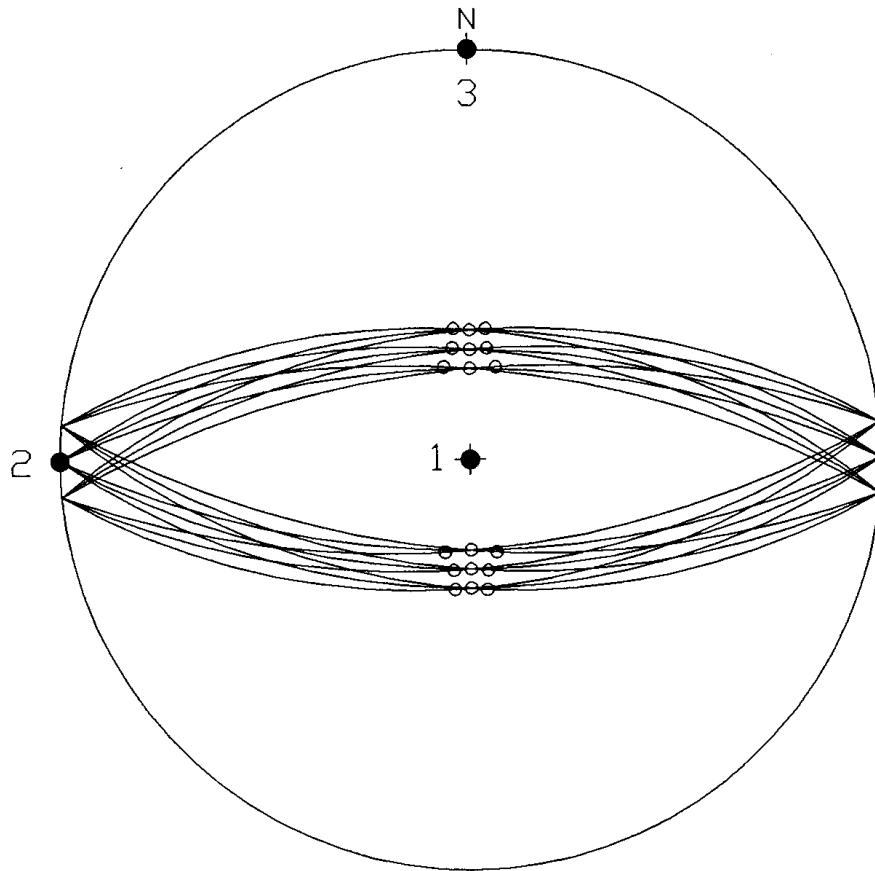
	Known	Program	Error
σ_1	90/000	90/076	0.0°
σ_2	00/090	00/270	0.0°
σ_3	00/000	00/180	0.0°
Φ	0.25	0.477	0.227

Figure 9-37 - Lower-hemisphere stereographic projection and table demonstrating the differences between the known and calculated principal stress axes σ_1 , σ_2 , and σ_3 and the value of Φ for fault population AC-01-25 using Angelier's method of paleostress analysis. In the stereographic projection, the known principal stress axes σ_1 , σ_2 , and σ_3 are oriented up, east, and north respectively and the calculated principal stress axes are denoted by the filled circles labelled 1, 2, and 3.



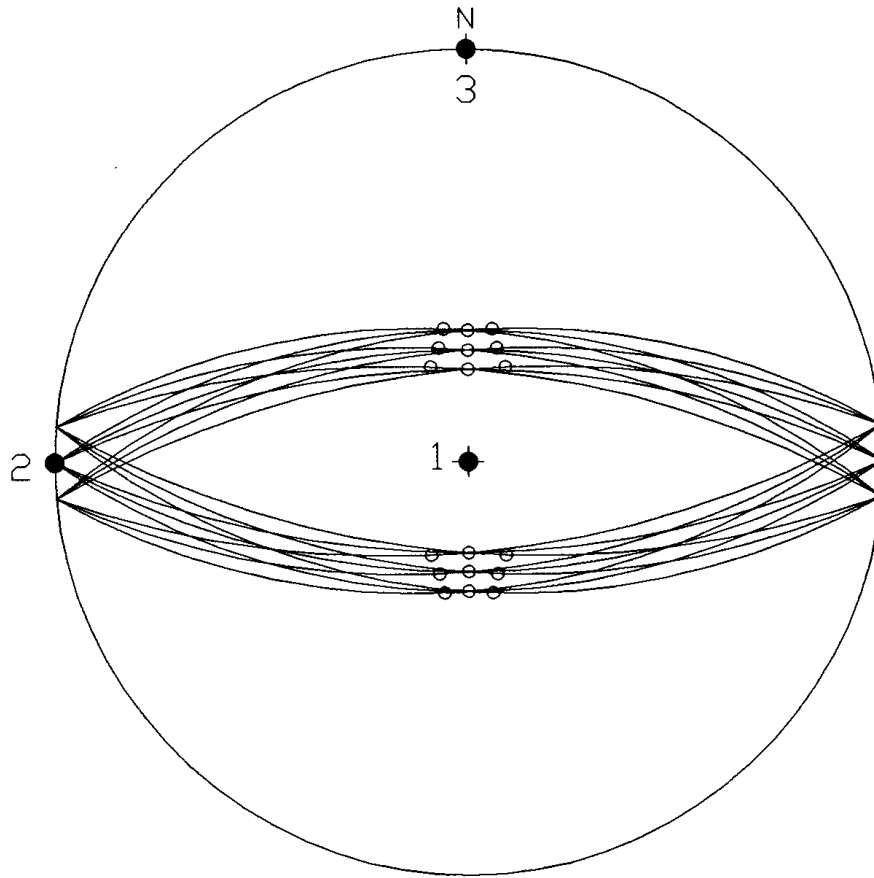
	Known	Program	Error
σ_1	90/000	90/050	0.0°
σ_2	00/090	00/270	0.0°
σ_3	00/000	00/180	0.0°
Φ	0.50	0.504	0.004

Figure 9-38 - Lower-hemisphere stereographic projection and table demonstrating the differences between the known and calculated principal stress axes σ_1 , σ_2 , and σ_3 and the value of Φ for fault population AC-01-50 using Angelier's method of paleostress analysis. In the stereographic projection, the known principal stress axes σ_1 , σ_2 , and σ_3 are oriented up, east, and north respectively and the calculated principal stress axes are denoted by the filled circles labelled 1, 2, and 3.



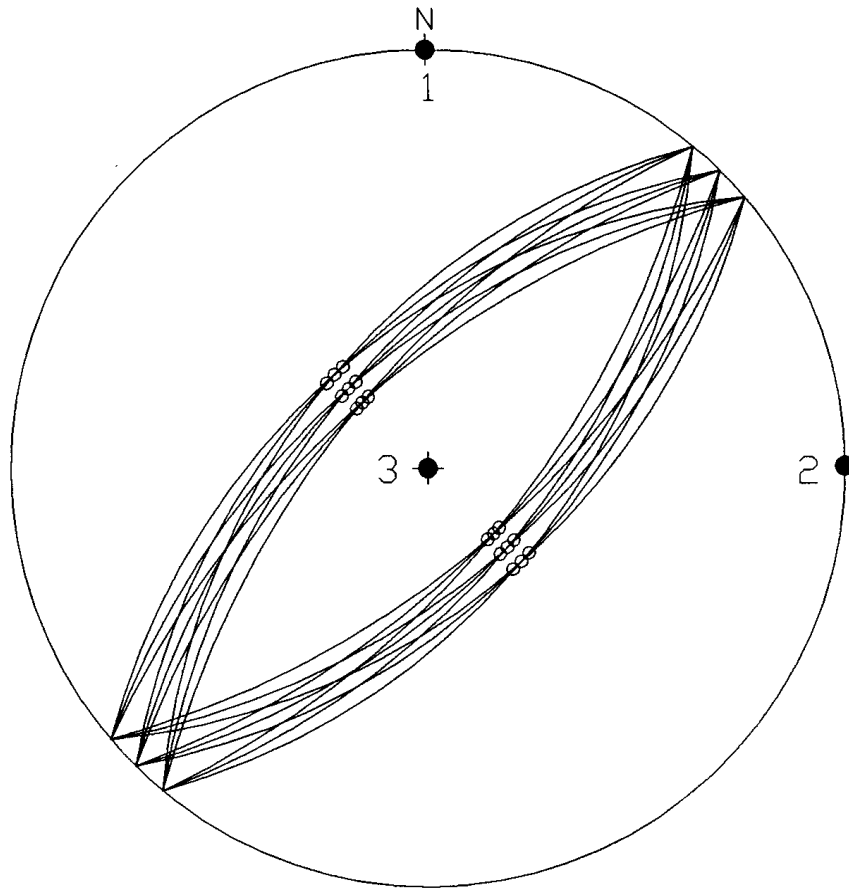
	Known	Program	Error
σ_1	90/000	90/130	0.0°
σ_2	00/090	00/270	0.0°
σ_3	00/000	00/360	0.0°
Φ	0.75	0.531	0.219

Figure 9-39 - Lower-hemisphere stereographic projection and table demonstrating the differences between the known and calculated principal stress axes σ_1 , σ_2 , and σ_3 and the value of Φ for fault population AC-01-75 using Angelier's method of paleostress analysis. In the stereographic projection, the known principal stress axes σ_1 , σ_2 , and σ_3 are oriented up, east, and north respectively and the calculated principal stress axes are denoted by the filled circles labelled 1, 2, and 3.



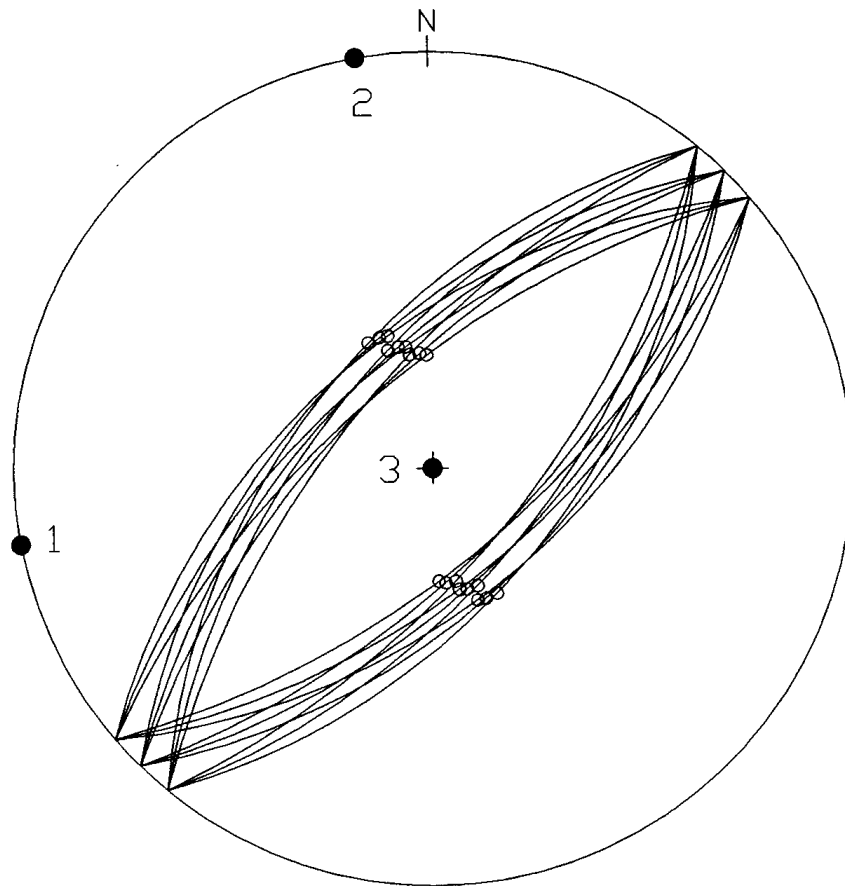
	Known	Program	Error
σ_1	90/000	90/102	0.0°
σ_2	00/090	00/270	0.0°
σ_3	00/000	00/360	0.0°
Φ	1.00	0.559	0.441

Figure 9-40 - Lower-hemisphere stereographic projection and table demonstrating the differences between the known and calculated principal stress axes σ_1 , σ_2 , and σ_3 and the value of Φ for fault population AC-01-10 using Angelier's method of paleostress analysis. In the stereographic projection, the known principal stress axes σ_1 , σ_2 , and σ_3 are oriented up, east, and north respectively and the calculated principal stress axes are denoted by the filled circles labelled 1, 2, and 3.



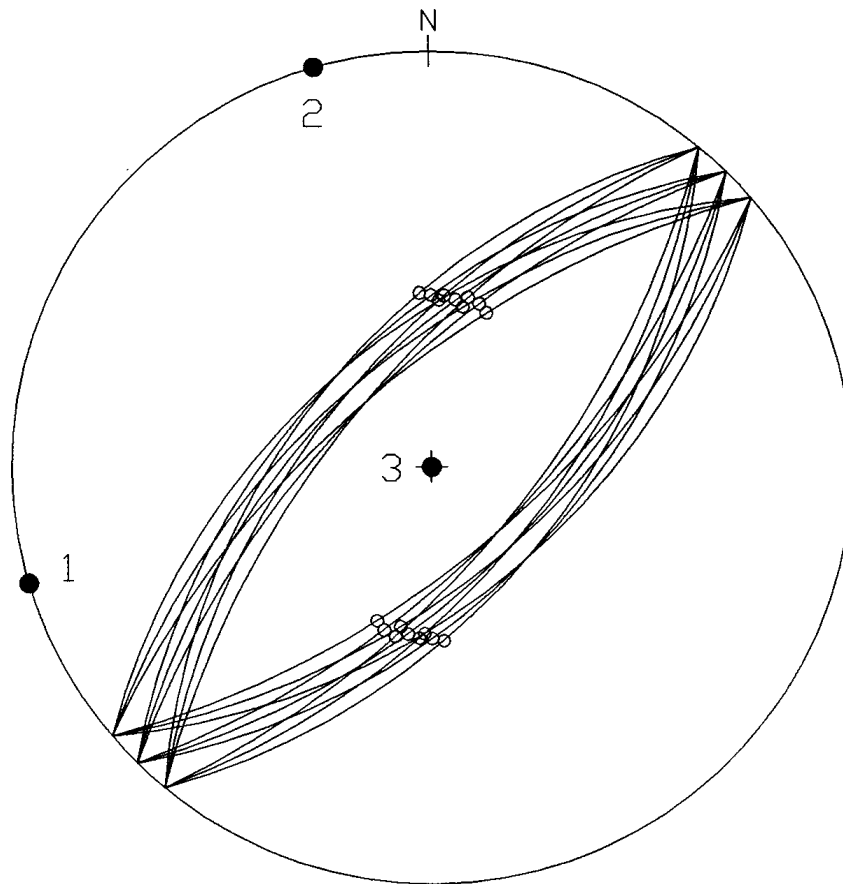
	Known	Program	Error
σ_1	90/000	00/000	90.0°
σ_2	00/090	00/090	0.0°
σ_3	00/000	90/270	90.0°
Φ	0.00	1.000	1.000

Figure 9-41 - Lower-hemisphere stereographic projection and table demonstrating the differences between the known and calculated principal stress axes σ_1 , σ_2 , and σ_3 and the value of Φ for fault population AC-02-00 using Reches' method of paleostress analysis. In the stereographic projection, the known principal stress axes σ_1 , σ_2 , and σ_3 are oriented up, east, and north respectively and the calculated principal stress axes are denoted by the filled circles labelled 1, 2, and 3.



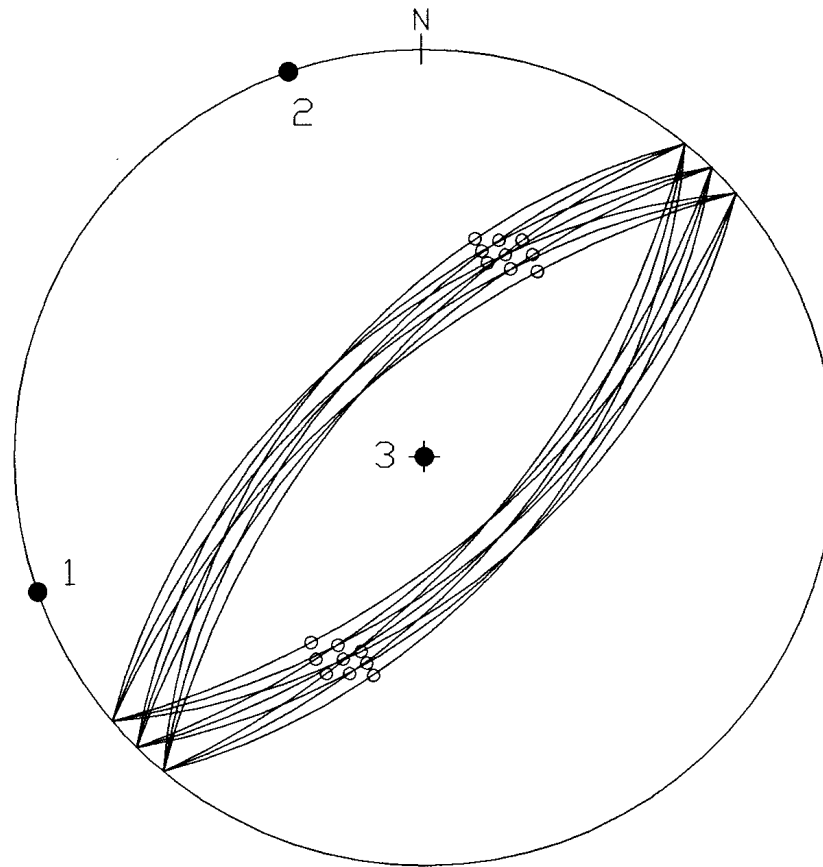
	Known	Program	Error
σ_1	90/000	00/260	90.0°
σ_2	00/090	00/350	80.0°
σ_3	00/000	90/270	90.0°
Φ	0.25	1.358	?

Figure 9-42 - Lower-hemisphere stereographic projection and table demonstrating the differences between the known and calculated principal stress axes σ_1 , σ_2 , and σ_3 and the value of Φ for fault population AC-02-25 using Reches' method of paleostress analysis. In the stereographic projection, the known principal stress axes σ_1 , σ_2 , and σ_3 are oriented up, east, and north respectively and the calculated principal stress axes are denoted by the filled circles labelled 1, 2, and 3.



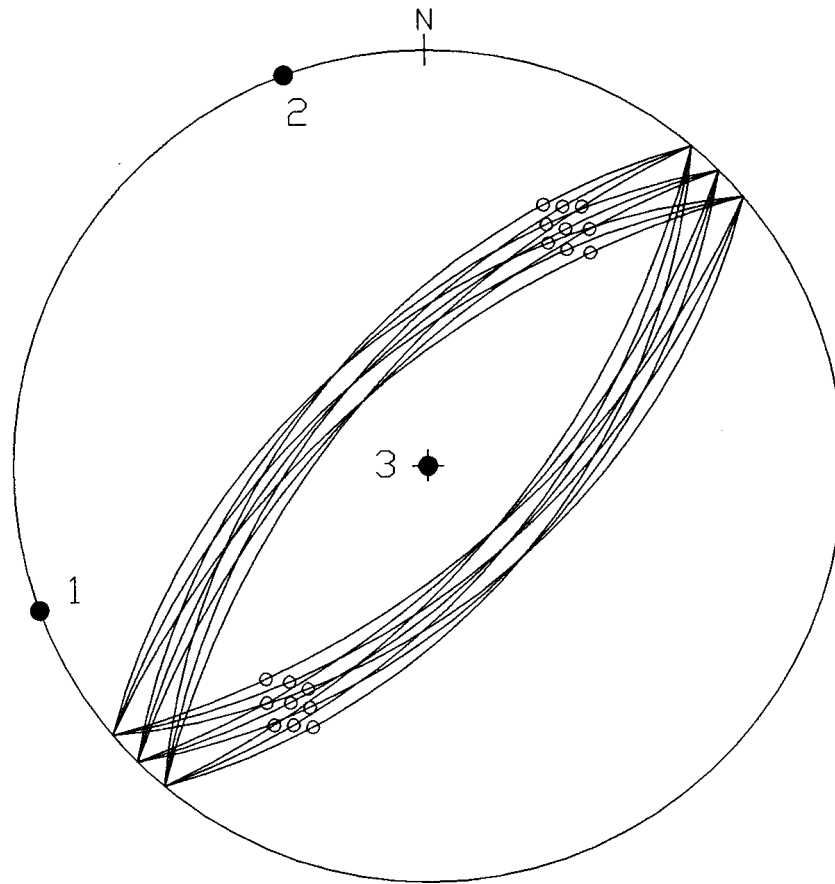
	Known	Program	Error
σ_1	90/000	00/254	90.0°
σ_2	00/090	00/344	74.0°
σ_3	00/000	90/270	90.0°
Φ	0.50	2.732	?

Figure 9-43 - Lower-hemisphere stereographic projection and table demonstrating the differences between the known and calculated principal stress axes σ_1 , σ_2 , and σ_3 and the value of Φ for fault population AC-02-50 using Reches' method of paleostress analysis. In the stereographic projection, the known principal stress axes σ_1 , σ_2 , and σ_3 are oriented up, east, and north respectively and the calculated principal stress axes are denoted by the filled circles labelled 1, 2, and 3.



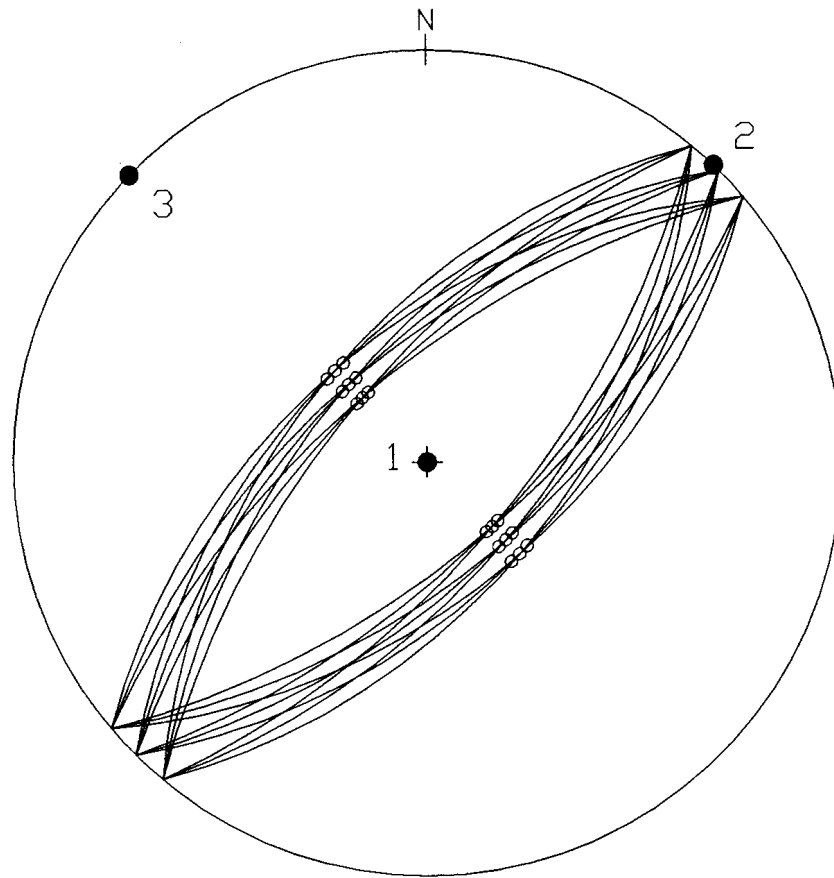
	Known	Program	Error
σ_1	90/000	00/251	90.0°
σ_2	00/090	00/341	71.0°
σ_3	00/000	90/270	90.0°
Φ	0.75	6.133	?

Figure 9-44 - Lower-hemisphere stereographic projection and table demonstrating the differences between the known and calculated principal stress axes σ_1 , σ_2 , and σ_3 and the value of Φ for fault population AC-02-75 using Reches' method of paleostress analysis. In the stereographic projection, the known principal stress axes σ_1 , σ_2 , and σ_3 are oriented up, east, and north respectively and the calculated principal stress axes are denoted by the filled circles labelled 1, 2, and 3.



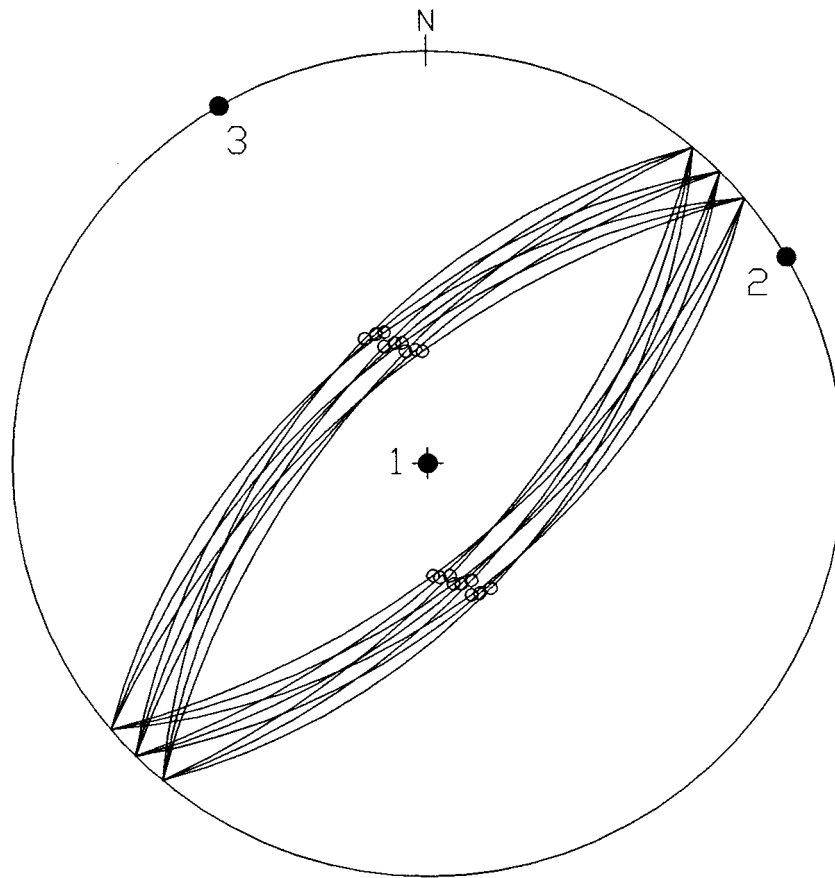
	Known	Program	Error
σ_1	90/000	00/250	90.0°
σ_2	00/090	00/340	70.0°
σ_3	00/000	90/270	90.0°
Φ	1.00	1.312	?

Figure 9-45 - Lower-hemisphere stereographic projection and table demonstrating the differences between the known and calculated principal stress axes σ_1 , σ_2 , and σ_3 and the value of Φ for fault population AC-02-10 using Reches' method of paleostress analysis. In the stereographic projection, the known principal stress axes σ_1 , σ_2 , and σ_3 are oriented up, east, and north respectively and the calculated principal stress axes are denoted by the filled circles labelled 1, 2, and 3.



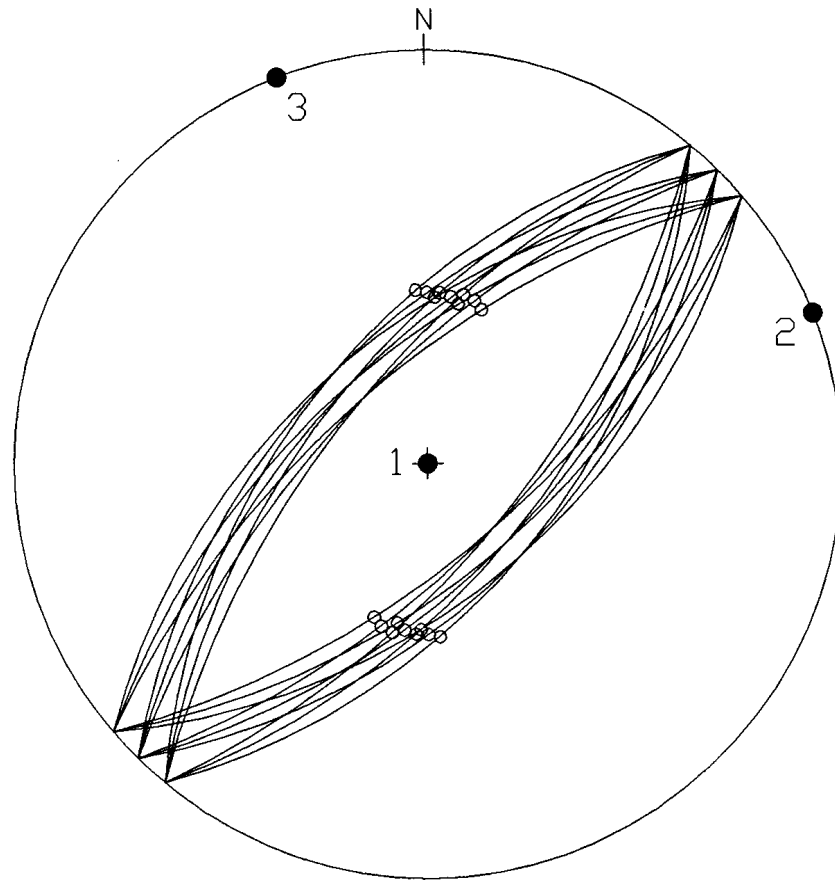
	Known	Program	Error
σ_1	90/000	90/179	0.0°
σ_2	00/090	00/0	46.0°
σ_3	00/000	90/314	46.0°
Φ	0.00	0.479	0.479

Figure 9-46 - Lower-hemisphere stereographic projection and table demonstrating the differences between the known and calculated principal stress axes σ_1 , σ_2 , and σ_3 and the value of Φ for fault population AC-02-00 using Angelier's method of paleostress analysis. In the stereographic projection, the known principal stress axes σ_1 , σ_2 , and σ_3 are oriented up, east, and north respectively and the calculated principal stress axes are denoted by the filled circles labelled 1, 2, and 3.



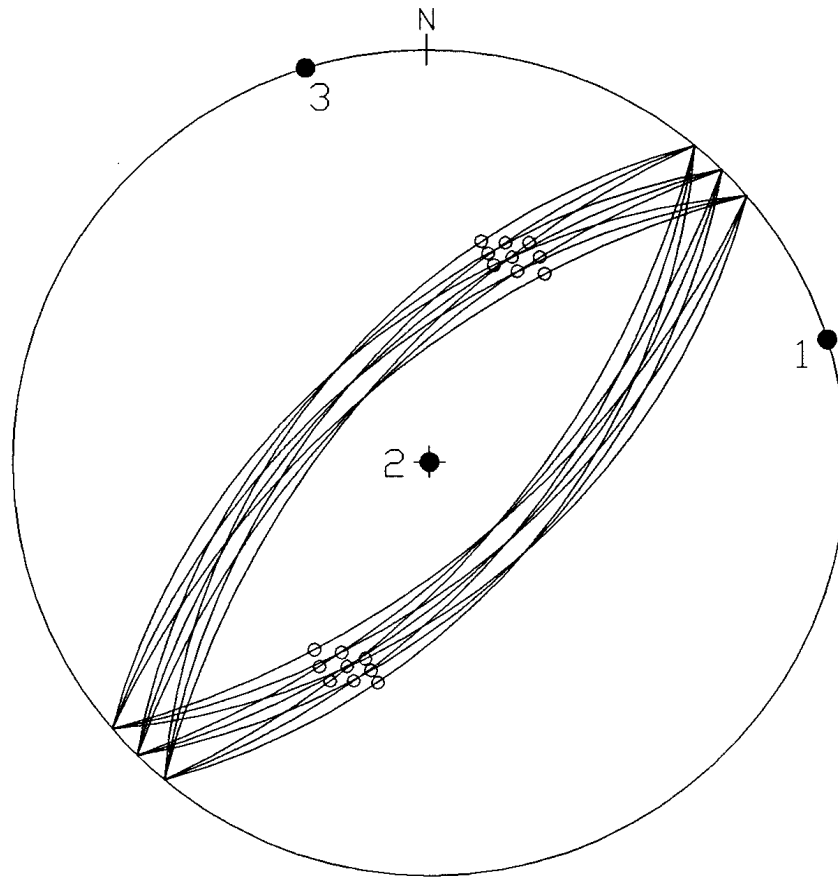
	Known	Program	Error
σ_1	90/000	90/192	0.0°
σ_2	00/090	00/060	30.0°
σ_3	00/000	00/330	30.0°
Φ	0.25	0.557	0.307

Figure 9-47 - Lower-hemisphere stereographic projection and table demonstrating the differences between the known and calculated principal stress axes σ_1 , σ_2 , and σ_3 and the value of Φ for fault population AC-02-25 using Angelier's method of paleostress analysis. In the stereographic projection, the known principal stress axes σ_1 , σ_2 , and σ_3 are oriented up, east, and north respectively and the calculated principal stress axes are denoted by the filled circles labelled 1, 2, and 3.



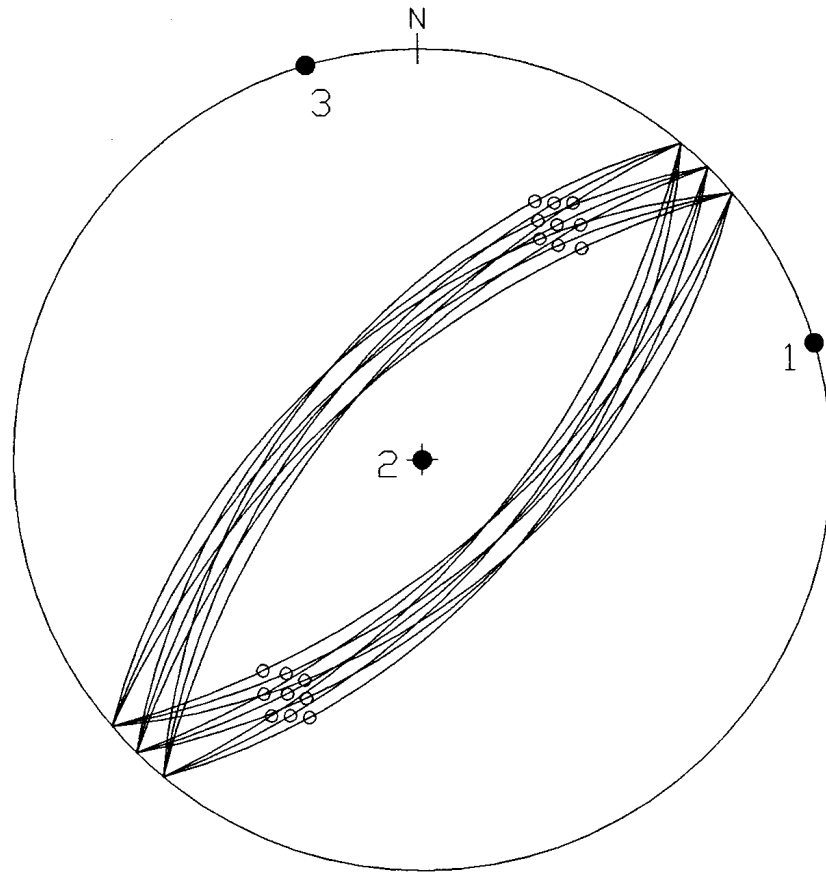
	Known	Program	Error
σ_1	90/000	90/170	0.0°
σ_2	00/090	00/069	21.0°
σ_3	00/000	90/339	21.0°
Φ	0.50	0.772	0.272

Figure 9-48 - Lower-hemisphere stereographic projection and table demonstrating the differences between the known and calculated principal stress axes σ_1 , σ_2 , and σ_3 and the value of Φ for fault population AC-02-50 using Angelier's method of paleostress analysis. In the stereographic projection, the known principal stress axes σ_1 , σ_2 , and σ_3 are oriented up, east, and north respectively and the calculated principal stress axes are denoted by the filled circles labelled 1, 2, and 3.



	Known	Program	Error
σ_1	90/000	00/073	90.0°
σ_2	00/090	90/184	90.0°
σ_3	00/000	00/343	17.0°
Φ	0.75	0.905	0.155

Figure 9-49 - Lower-hemisphere stereographic projection and table demonstrating the differences between the known and calculated principal stress axes σ_1 , σ_2 , and σ_3 and the value of Φ for fault population AC-02-75 using Angelier's method of paleostress analysis. In the stereographic projection, the known principal stress axes σ_1 , σ_2 , and σ_3 are oriented up, east, and north respectively and the calculated principal stress axes are denoted by the filled circles labelled 1, 2, and 3.



	Known	Program	Error
σ_1	90/000	00/074	90.0°
σ_2	00/090	90/167	90.0°
σ_3	00/000	00/344	17.0°
Φ	1.00	0.676	0.324

Figure 9-50 - Lower-hemisphere stereographic projection and table demonstrating the differences between the known and calculated principal stress axes σ_1 , σ_2 , and σ_3 and the value of Φ for fault population AC-02-10 using Angelier's method of paleostress analysis. In the stereographic projection, the known principal stress axes σ_1 , σ_2 , and σ_3 are oriented up, east, and north respectively and the calculated principal stress axes are denoted by the filled circles labelled 1, 2, and 3.

		Reches'	Angelier's	Deviation
Known Φ of 0.00	σ_1	00/000	90/051	90.0°
	σ_2	00/090	00/269	1.0°
	σ_3	90/270	00/179	90.0°
	Φ	1.000	0.453	0.547
Known Φ of 0.25	σ_1	00/000	90/076	90.0°
	σ_2	00/090	00/270	0.0°
	σ_3	90/270	00/180	90.0°
	Φ	0.695	0.477	0.218
Known Φ of 0.50	σ_1	00/000	90/050	90.0°
	σ_2	00/090	00/270	0.0°
	σ_3	90/270	00/180	90.0°
	Φ	0.485	0.504	0.019
Known Φ of 0.75	σ_1	00/000	90/130	90.0°
	σ_2	00/090	00/270	0.0°
	σ_3	90/270	00/360	90.0°
	Φ	0.274	0.531	0.257
Known Φ of 1.00	σ_1	00/000	90/102	90.0°
	σ_2	00/090	00/270	0.0°
	σ_3	90/270	00/360	90.0°
	Φ	0.089	0.559	0.648

Table 9-4 - Table demonstrating the deviation for the orientations of the σ_1 , σ_2 , and σ_3 principal stress axes and the principal stress magnitude ratio Φ between Reches' and Angelier's methods of paleostress analysis on fault population AC-01 at five different values of Φ .

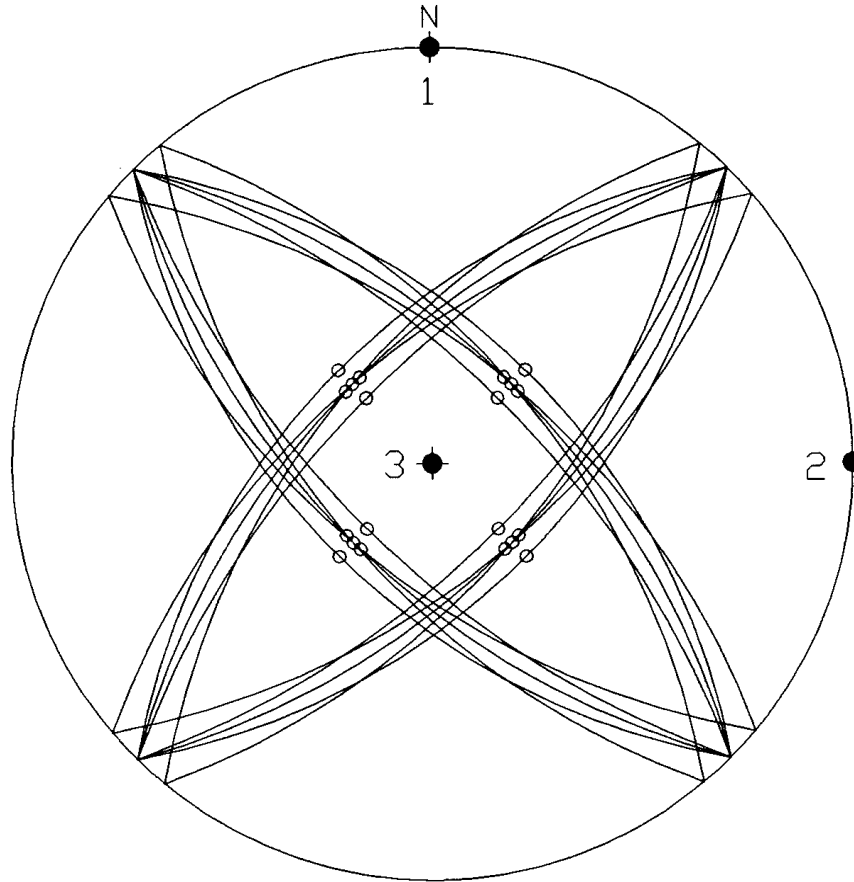
		Reches'	Angelier's	Deviation
Known Φ of 0.00	σ_1	00/000	90/179	90.0°
	σ_2	00/090	00/044	46.0°
	σ_3	90/270	00/314	90.0°
	Φ	1.000	0.479	0.521
Known Φ of 0.25	σ_1	00/260	90/192	90.0°
	σ_2	00/350	00/060	70.0°
	σ_3	90/270	00/330	90.0°
	Φ	1.358	0.557	?
Known Φ of 0.50	σ_1	00/254	90/170	90.0°
	σ_2	00/344	00/069	85.0°
	σ_3	90/270	00/339	90.0°
	Φ	2.372	0.772	?
Known Φ of 0.75	σ_1	00/251	00/073	2.0°
	σ_2	00/341	90/184	90.0°
	σ_3	90/270	00/343	90.0°
	Φ	6.133	0.905	?
Known Φ of 1.00	σ_1	00/250	00/074	4.0°
	σ_2	00/340	90/167	90.0°
	σ_3	90/270	00/344	90.0°
	Φ	1.312	0.676	?

Table 9-5 - Table demonstrating the deviation for the orientations of the σ_1 , σ_2 , and σ_3 principal stress axes and the principal stress magnitude ratio Φ between Reches' and Angelier's methods of paleostress analysis on fault population AC-02 at five different values of Φ .

The next special-case fault population to be examined was the orthorhombic symmetry population OS-01. The orthorhombic symmetry faults created a situation very similar to the conjugate fault population AC-01. For Reches' method (figures 9-51 through 9-55), the Φ values returned, once again, seemed to be the opposite of what one would expect. A Φ of 1.00 was returned for an initial Φ of 0.00, a Φ of 0.76 was returned for an initial Φ of 0.25, a Φ of 0.51 was returned for an initial Φ of 0.50 (which is quite good), a Φ of 0.26 was returned for an initial Φ of 0.75, and a Φ of 0.02 was returned for an initial Φ of 1.00. Not surprisingly, the σ_1 and σ_3 were once again switched and a correct solution results if they are changed.

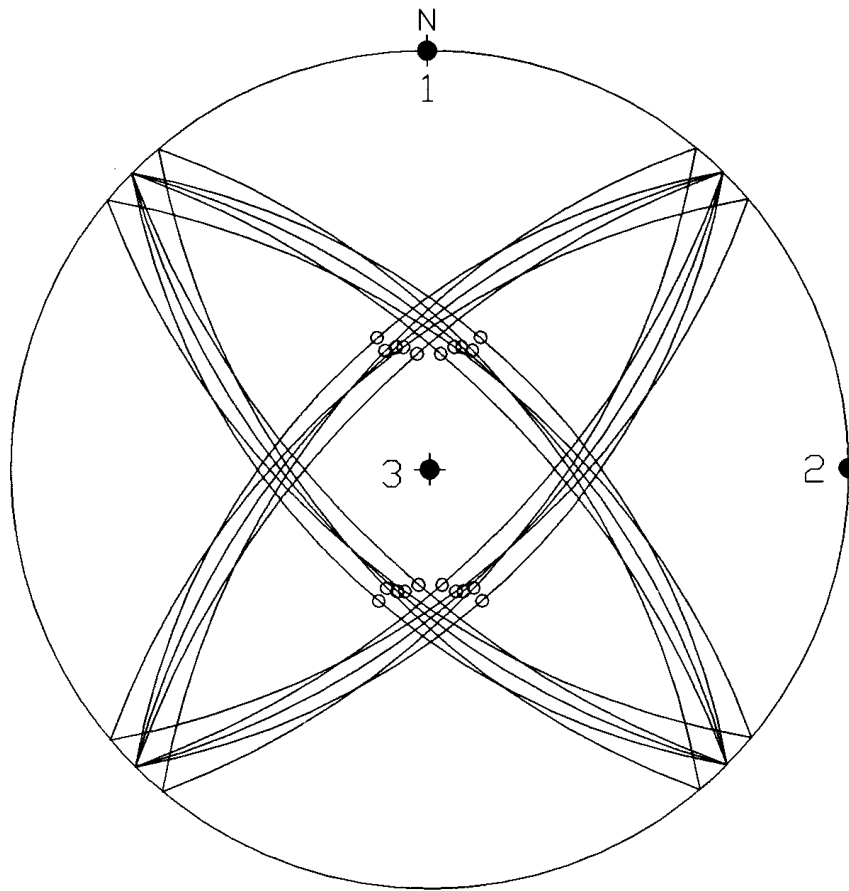
Using Angelier's method (figures 9-56 through 9-60), the orientations of the principal stress axes σ_1 , σ_2 , and σ_3 were exactly matched for initial Φ values of 0.25, 0.50, and 0.75. For an initial Φ value of 0.00, however, the orientations of σ_2 and σ_3 were reversed and for an initial Φ value of 1.00, the orientations of σ_1 and σ_2 were reversed. The errors in magnitude for the calculated value of Φ were all less than 0.050 for each initial Φ value.

Comparing the results of Reches' to Angelier's methods for orthorhombic fault population OS-01 (table 9-6) shows large deviations in the orientations of the principal stress axes and in the calculated values for Φ but this is primarily due to the inaccuracy of Reche's method given this type of fault population.



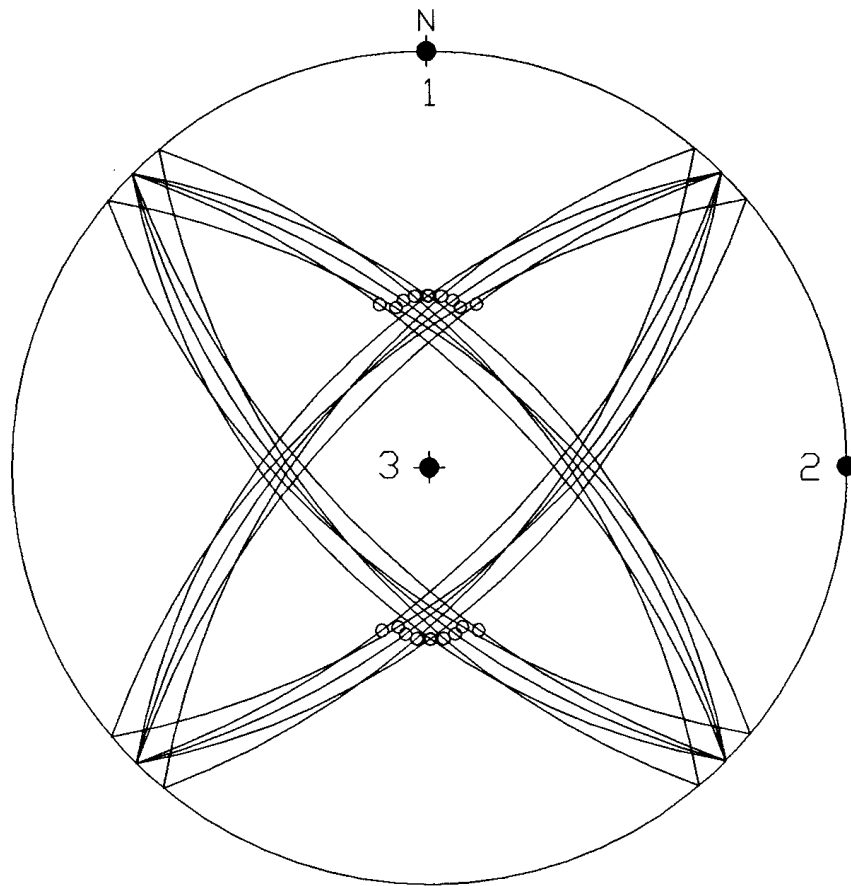
	Known	Program	Error
σ_1	90/000	00/000	90.0°
σ_2	00/090	00/090	0.0°
σ_3	00/000	90/270	90.0°
Φ	0.00	1.000	1.000

Figure 9-51 - Lower-hemisphere stereographic projection and table demonstrating the differences between the known and calculated principal stress axes σ_1 , σ_2 , and σ_3 and the value of Φ for fault population OS-01-00 using Reches' method of paleostress analysis. In the stereographic projection, the known principal stress axes σ_1 , σ_2 , and σ_3 are oriented up, east, and north respectively and the calculated principal stress axes are denoted by the filled circles labelled 1, 2, and 3.



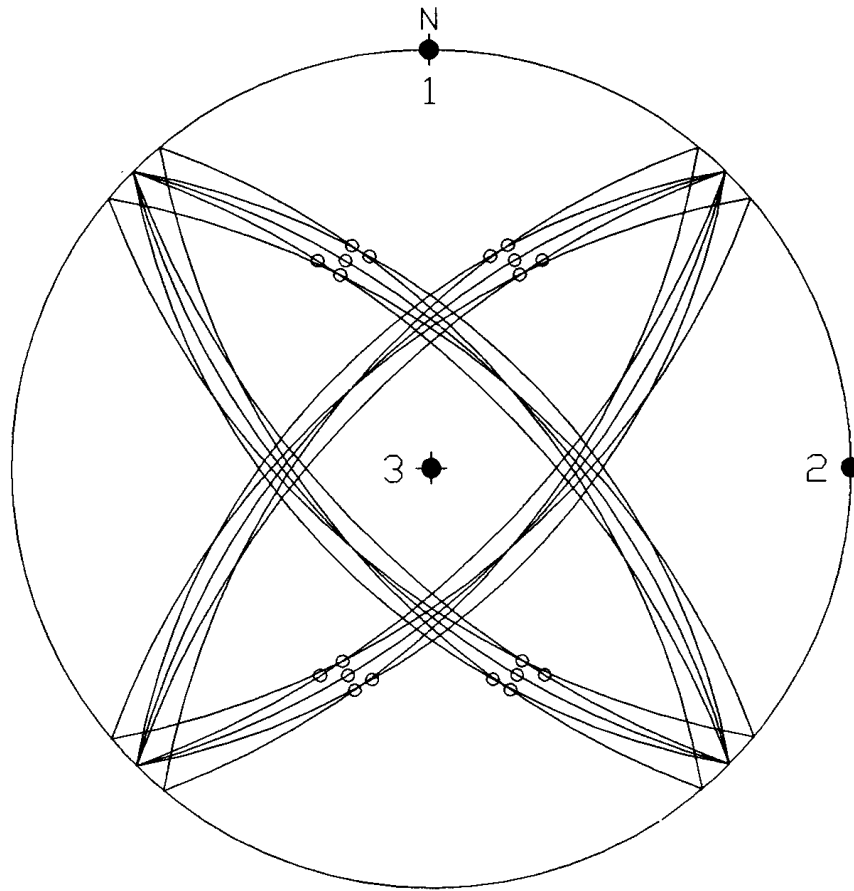
	Known	Program	Error
σ_1	90/000	00/000	90.0°
σ_2	00/090	00/090	0.0°
σ_3	00/000	90/270	90.0°
Φ	0.25	0.755	0.505

Figure 9-52 - Lower-hemisphere stereographic projection and table demonstrating the differences between the known and calculated principal stress axes σ_1 , σ_2 , and σ_3 and the value of Φ for fault population OS-01-25 using Reches' method of paleostress analysis. In the stereographic projection, the known principal stress axes σ_1 , σ_2 , and σ_3 are oriented up, east, and north respectively and the calculated principal stress axes are denoted by the filled circles labelled 1, 2, and 3.



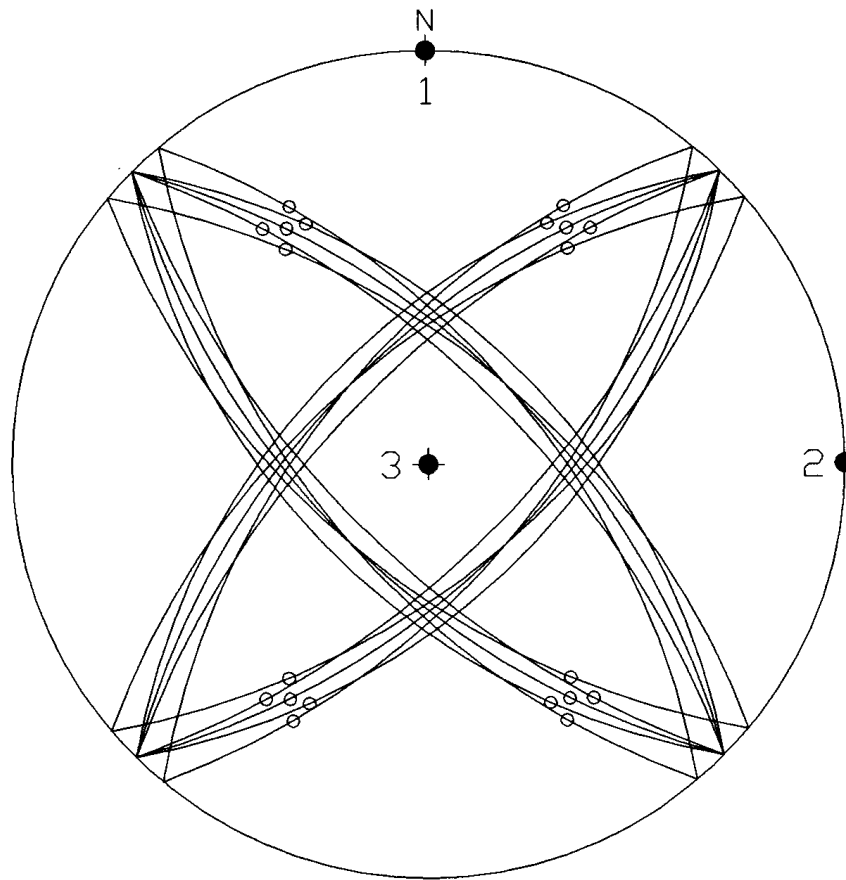
	Known	Program	Error
σ_1	90/000	00/000	90.0°
σ_2	00/090	00/090	0.0°
σ_3	00/000	90/270	90.0°
Φ	0.50	0.502	0.002

Figure 9-53 - Lower-hemisphere stereographic projection and table demonstrating the differences between the known and calculated principal stress axes σ_1 , σ_2 , and σ_3 and the value of Φ for fault population OS-01-50 using Reches' method of paleostress analysis. In the stereographic projection, the known principal stress axes σ_1 , σ_2 , and σ_3 are oriented up, east, and north respectively and the calculated principal stress axes are denoted by the filled circles labelled 1, 2, and 3.



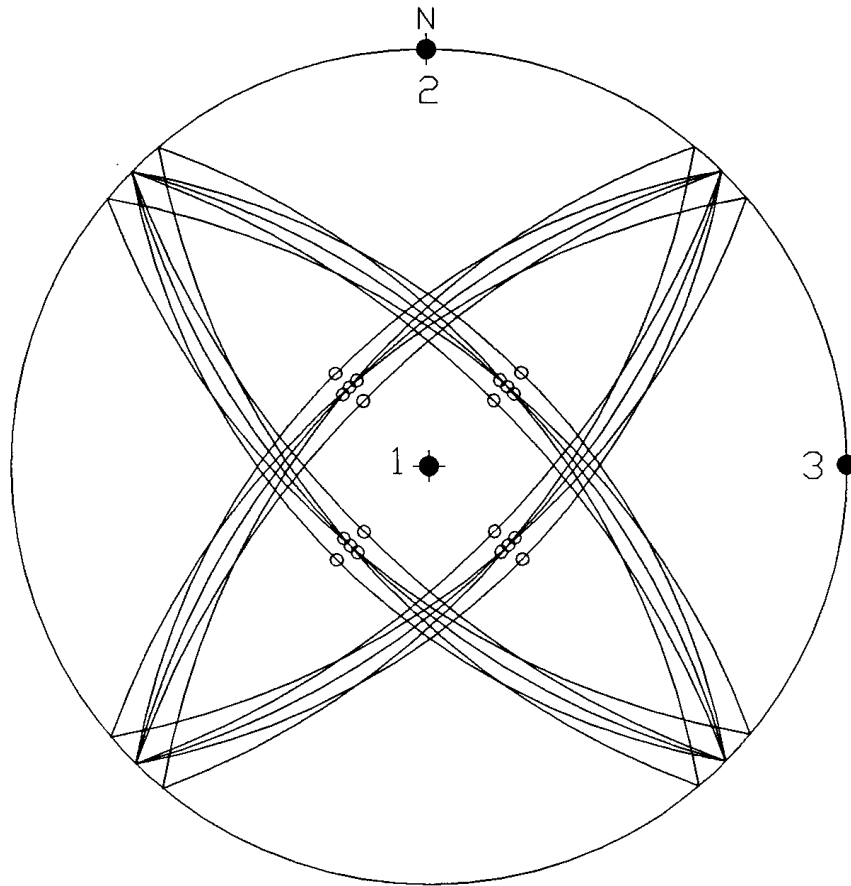
	Known	Program	Error
σ_1	90/000	00/000	90.0°
σ_2	00/090	00/090	0.0°
σ_3	00/000	90/270	90.0°
Φ	0.75	0.261	0.489

Figure 9-54 - Lower-hemisphere stereographic projection and table demonstrating the differences between the known and calculated principal stress axes σ_1 , σ_2 , and σ_3 and the value of Φ for fault population OS-01-75 using Reches' method of paleostress analysis. In the stereographic projection, the known principal stress axes σ_1 , σ_2 , and σ_3 are oriented up, east, and north respectively and the calculated principal stress axes are denoted by the filled circles labelled 1, 2, and 3.



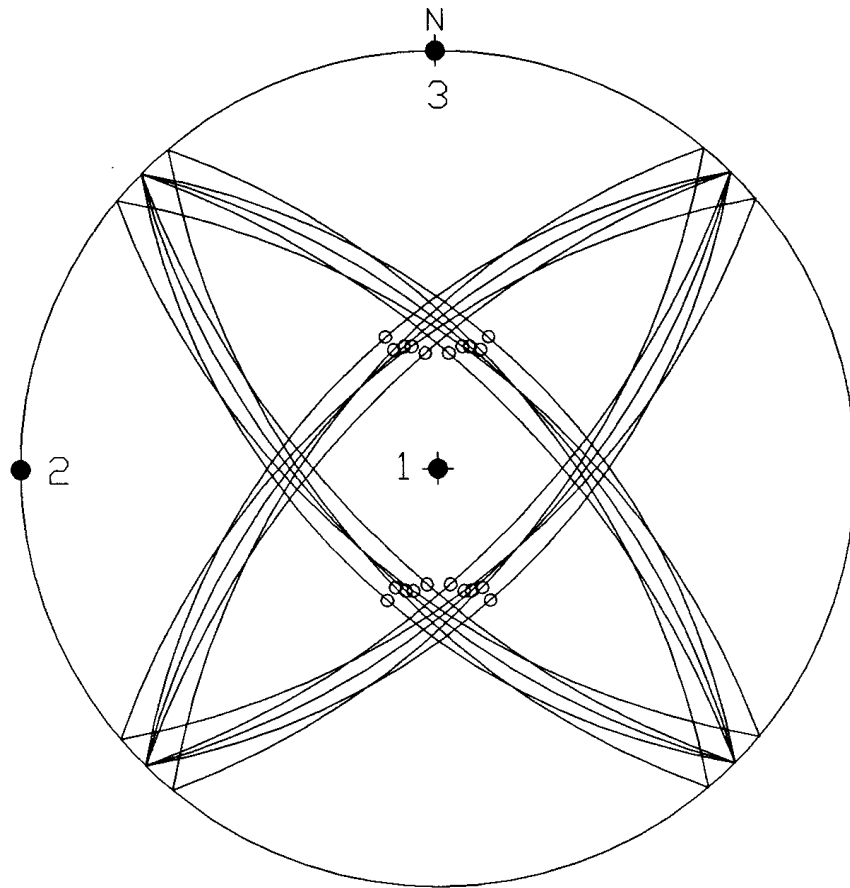
	Known	Program	Error
σ_1	90/000	00/000	90.0°
σ_2	00/090	00/090	0.0°
σ_3	00/000	90/270	90.0°
Φ	1.00	0.015	0.985

Figure 9-55 - Lower-hemisphere stereographic projection and table demonstrating the differences between the known and calculated principal stress axes σ_1 , σ_2 , and σ_3 and the value of Φ for fault population OS-01-10 using Reches' method of paleostress analysis. In the stereographic projection, the known principal stress axes σ_1 , σ_2 , and σ_3 are oriented up, east, and north respectively and the calculated principal stress axes are denoted by the filled circles labelled 1, 2, and 3.



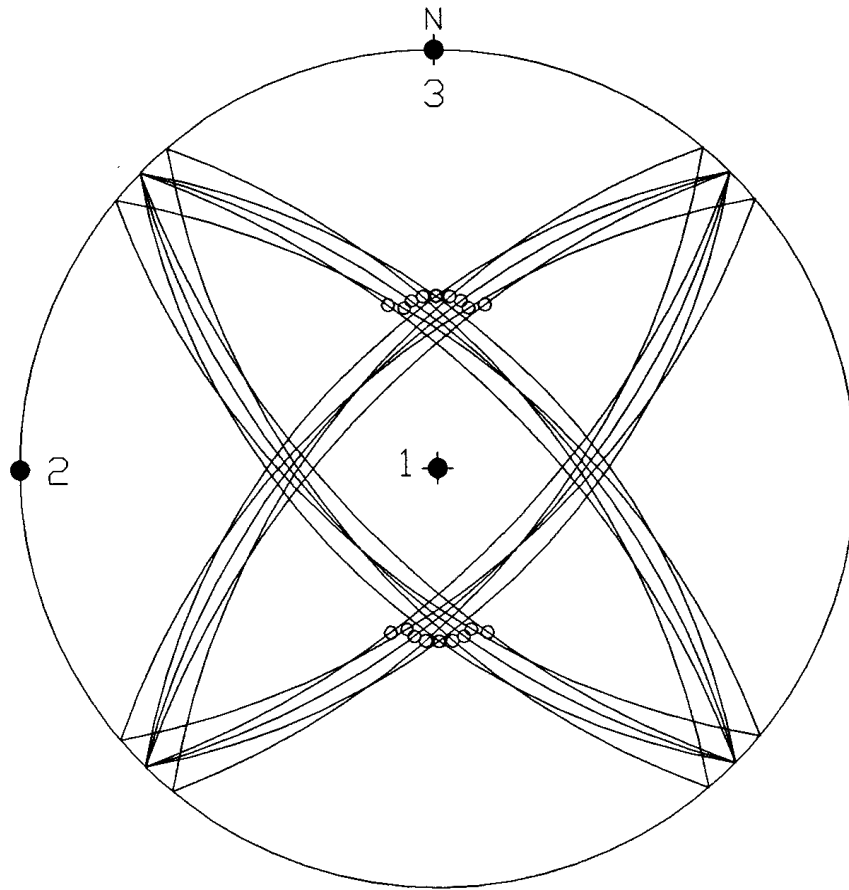
	Known	Program	Error
σ_1	90/000	90/196	0.0°
σ_2	00/090	00/360	90.0°
σ_3	00/000	00/090	90.0°
Φ	0.00	0.000	0.000

Figure 9-56 - Lower-hemisphere stereographic projection and table demonstrating the differences between the known and calculated principal stress axes σ_1 , σ_2 , and σ_3 and the value of Φ for fault population OS-01-00 using Angelier's method of paleostress analysis. In the stereographic projection, the known principal stress axes σ_1 , σ_2 , and σ_3 are oriented up, east, and north respectively and the calculated principal stress axes are denoted by the filled circles labelled 1, 2, and 3.



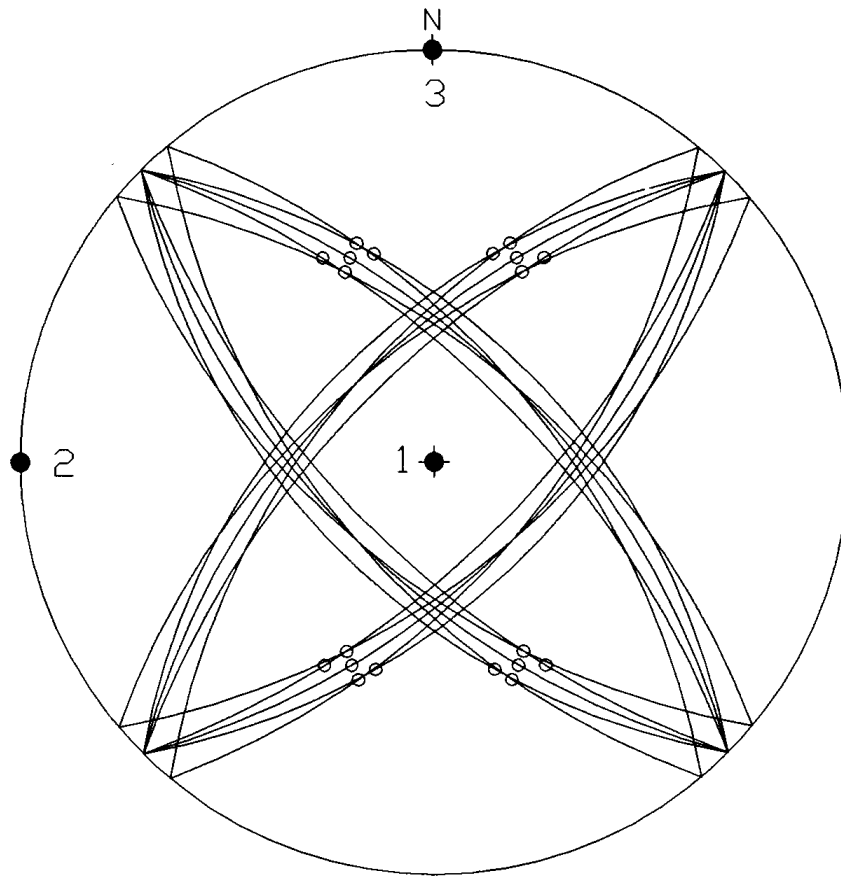
	Known	Program	Error
σ_1	90/000	90/131	0.0°
σ_2	00/090	00/270	0.0°
σ_3	00/000	00/000	0.0°
Φ	0.25	0.266	0.016

Figure 9-57 - Lower-hemisphere stereographic projection and table demonstrating the differences between the known and calculated principal stress axes σ_1 , σ_2 , and σ_3 and the value of Φ for fault population OS-01-25 using Angelier's method of paleostress analysis. In the stereographic projection, the known principal stress axes σ_1 , σ_2 , and σ_3 are oriented up, east, and north respectively and the calculated principal stress axes are denoted by the filled circles labelled 1, 2, and 3.



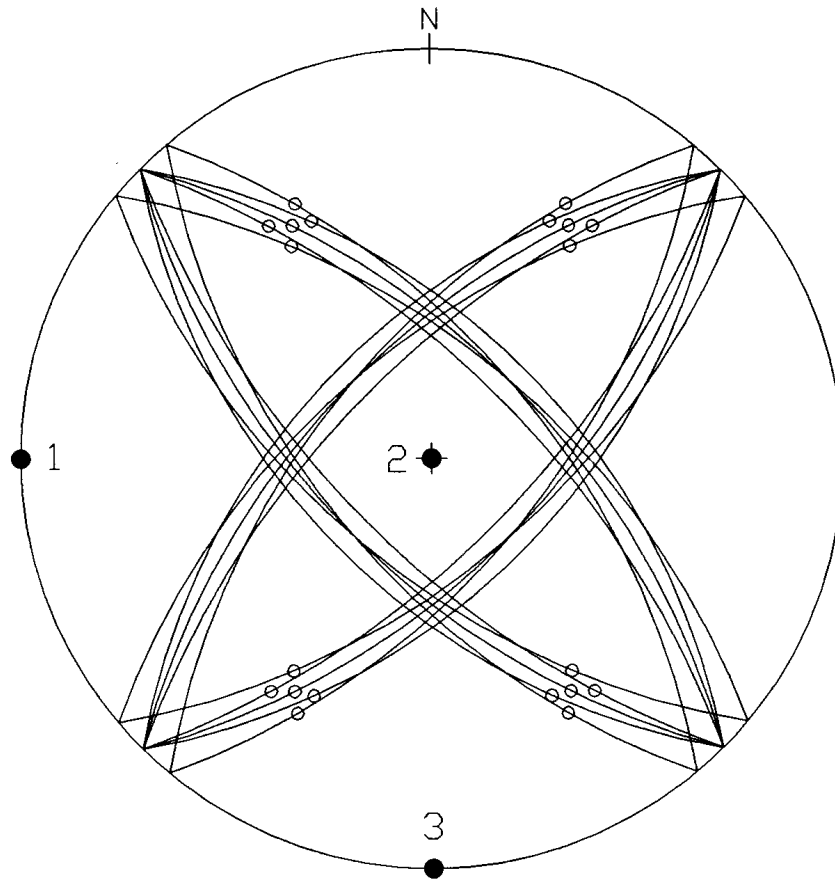
	Known	Program	Error
σ_1	90/000	90/126	0.0°
σ_2	00/090	00/270	0.0°
σ_3	00/000	00/000	0.0°
Φ	0.50	0.525	0.025

Figure 9-58 - Lower-hemisphere stereographic projection and table demonstrating the differences between the known and calculated principal stress axes σ_1 , σ_2 , and σ_3 and the value of Φ for fault population OS-01-50 using Angelier's method of paleostress analysis. In the stereographic projection, the known principal stress axes σ_1 , σ_2 , and σ_3 are oriented up, east, and north respectively and the calculated principal stress axes are denoted by the filled circles labelled 1, 2, and 3.



	Known	Program	Error
σ_1	90/000	90/098	0.0°
σ_2	00/090	00/270	0.0°
σ_3	00/000	00/360	0.0°
Φ	0.75	0.776	0.026

Figure 9-59 - Lower-hemisphere stereographic projection and table demonstrating the differences between the known and calculated principal stress axes σ_1 , σ_2 , and σ_3 and the value of Φ for fault population OS-01-75 using Angelier's method of paleostress analysis. In the stereographic projection, the known principal stress axes σ_1 , σ_2 , and σ_3 are oriented up, east, and north respectively and the calculated principal stress axes are denoted by the filled circles labelled 1, 2, and 3.



	Known	Program	Error
σ_1	90/000	00/270	90.0°
σ_2	00/090	90/090	90.0°
σ_3	00/000	00/180	0.0°
Φ	1.00	0.981	0.019

Figure 9-60 - Lower-hemisphere stereographic projection and table demonstrating the differences between the known and calculated principal stress axes σ_1 , σ_2 , and σ_3 and the value of Φ for fault population OS-01-10 using Angelier's method of paleostress analysis. In the stereographic projection, the known principal stress axes σ_1 , σ_2 , and σ_3 are oriented up, east, and north respectively and the calculated principal stress axes are denoted by the filled circles labelled 1, 2, and 3.

		Reches'	Angelier's	Deviation
Known Φ of 0.00	σ_1	00/000	90/196	90.0°
	σ_2	00/090	00/360	90.0°
	σ_3	90/270	00/090	90.0°
	Φ	1.000	0.000	1.000
Known Φ of 0.25	σ_1	00/000	90/131	90.0°
	σ_2	00/090	00/270	0.0°
	σ_3	90/270	00/000	90.0°
	Φ	0.755	0.266	0.489
Known Φ of 0.50	σ_1	00/000	90/126	90.0°
	σ_2	00/090	00/270	0.0°
	σ_3	90/270	00/000	90.0°
	Φ	0.502	0.525	0.023
Known Φ of 0.75	σ_1	00/000	90/098	90.0°
	σ_2	00/090	00/270	0.0°
	σ_3	90/270	00/000	90.0°
	Φ	0.261	0.776	0.515
Known Φ of 1.00	σ_1	00/000	00/270	90.0°
	σ_2	00/090	90/090	0.0°
	σ_3	90/270	00/180	90.0°
	Φ	0.015	0.981	0.966

Table 9-6 - Table demonstrating the deviation for the orientations of the σ_1 , σ_2 , and σ_3 principal stress axes and the principal stress magnitude ratio Φ between Reches' and Angelier's methods of paleostress analysis on fault population OS-01 at five different values of Φ .

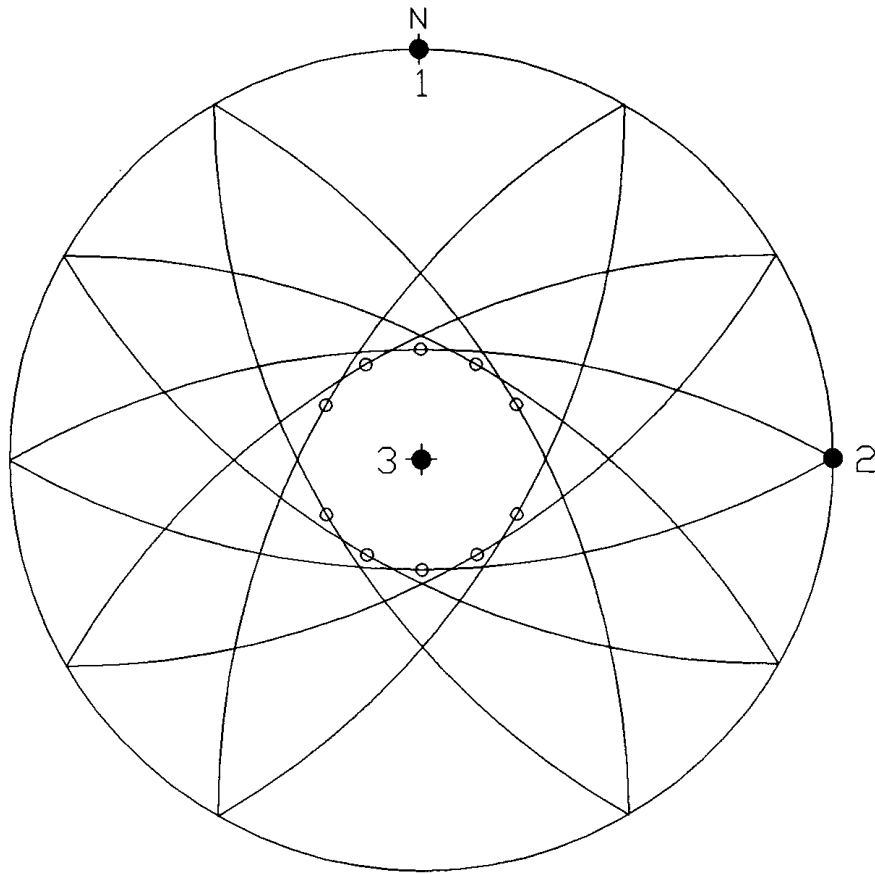
The radial symmetry fault population RS-01 was also very similar to the conjugate fault population AC-01. The Φ values returned by Reches' method (figures 9-61 through 9-65), once again, seemed to be the opposite of what one would expect. A Φ of 1.00 was returned for an initial Φ of 0.00, a Φ of 0.75 was returned for an initial Φ of 0.25, a Φ of 0.58 was returned for an initial Φ of 0.50 (which is quite good), a Φ of 0.39 was returned for an initial Φ of 0.75, and a Φ of 0.18 was returned for an initial Φ of 1.00. Not surprisingly, the σ_1 and σ_3 were once again switched and a correct solution results if they are changed.

Using Angelier's method (figures 9-66 through 9-70), the orientations of the principal stress axes σ_1 , σ_2 , and σ_3 were exactly matched for initial Φ values of 0.50, 0.75, and 1.00. For initial Φ values of 0.00 and 0.25, the orientations of σ_2 and σ_3 were still quite small. The errors in magnitude for the calculated value of Φ were all less than 0.050 for each initial Φ value.

Comparing the results of Reches' to Angelier's methods for radial symmetry fault population RS-01 (table 9-7) shows large deviations in the orientations of the principal stress axes and in the calculated values for Φ but this is primarily due to the inaccuracy of Reche's method given this type of fault population.

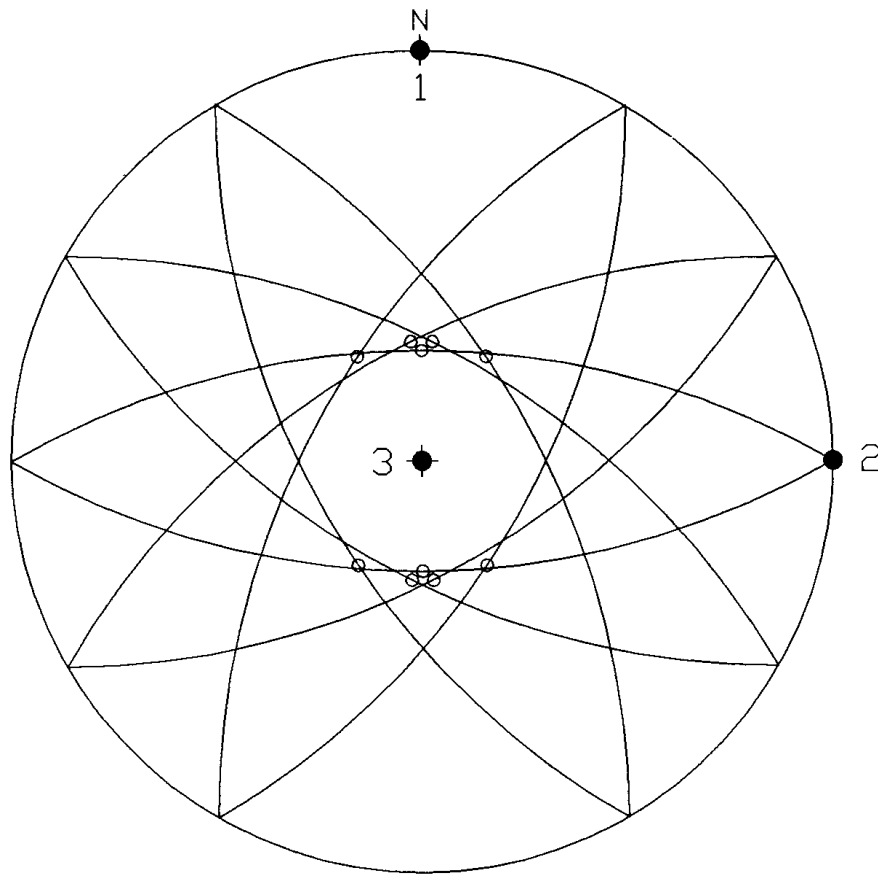
It seems that for conjugate-type fault sets (the orthorhombic and the radial symmetry fault populations are both types of conjugate fault sets), Reches' method paleostress analysis program reversed the orientations of the σ_1 and σ_3 axes and calculated Φ values based on that switch. This seems to be a result of the mathematical algorithms used to calculate the paleostress axes. Otherwise, the programs do return the correct orientations for the paleostress axes and would yield a correct solution. The Φ values returned likewise are only somewhat incorrect. The Φ value returned for an initial Φ of 0.50 is essentially 0.50. For Reches' method, the Φ value returned for 0.25 is essentially 0.75 (and vice versa), and the Φ value

returned for 0.0 is exactly 1.0 (and vice versa). For Angelier's method, the Φ values returned are essentially correct.



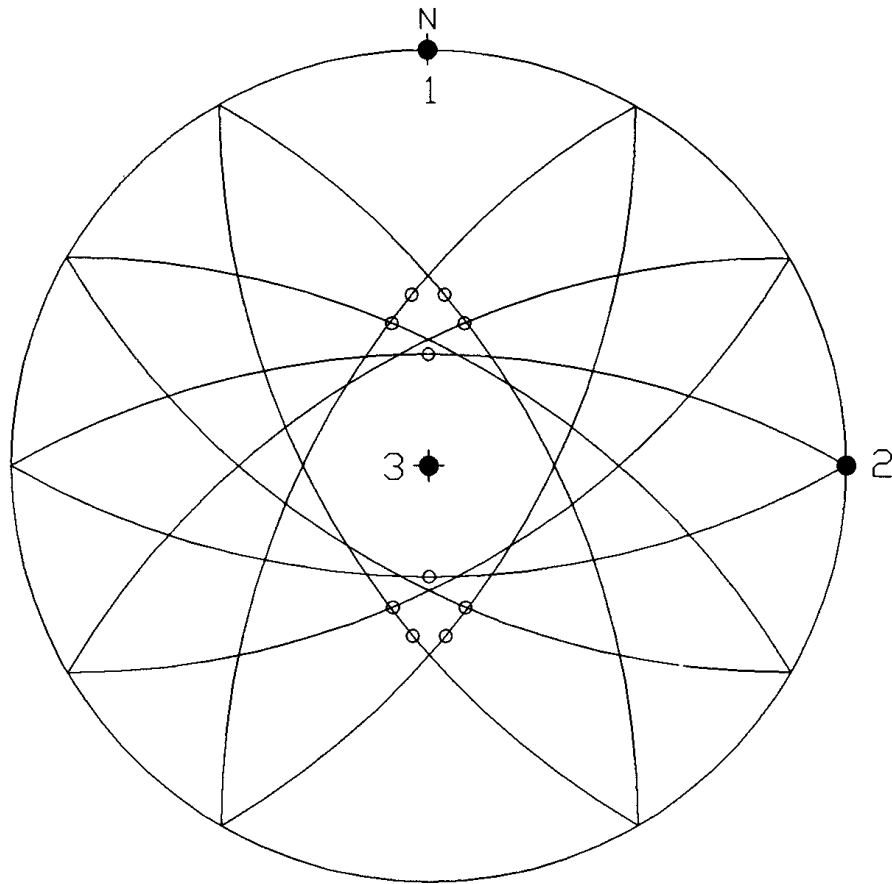
	Known	Program	Error
σ_1	90/000	00/000	90.0°
σ_2	00/090	00/090	0.0°
σ_3	00/000	90/270	90.0°
Φ	0.00	1.000	1.000

Figure 9-61 - Lower-hemisphere stereographic projection and table demonstrating the differences between the known and calculated principal stress axes σ_1 , σ_2 , and σ_3 and the value of Φ for fault population RS-01-00 using Reches' method of paleostress analysis. In the stereographic projection, the known principal stress axes σ_1 , σ_2 , and σ_3 are oriented up, east, and north respectively and the calculated principal stress axes are denoted by the filled circles labelled 1, 2, and 3.



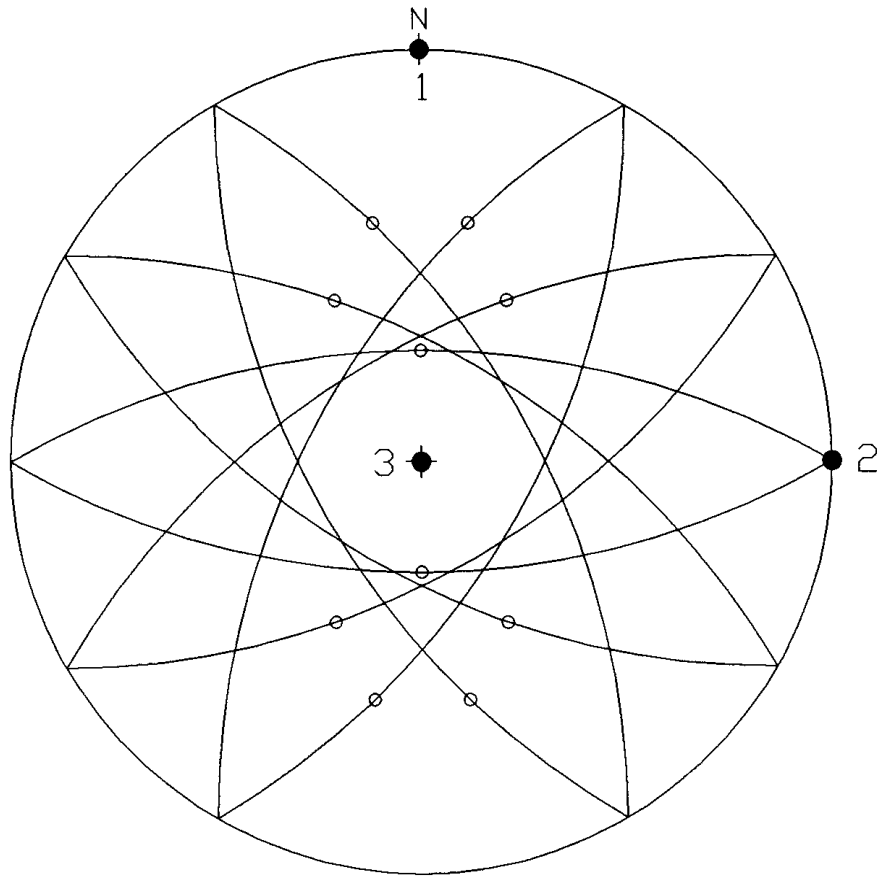
	Known	Program	Error
σ_1	90/000	00/000	90.0°
σ_2	00/090	00/090	0.0°
σ_3	00/000	90/270	90.0°
Φ	0.25	0.746	0.496

Figure 9-62 - Lower-hemisphere stereographic projection and table demonstrating the differences between the known and calculated principal stress axes σ_1 , σ_2 , and σ_3 and the value of Φ for fault population RS-01-25 using Reches' method of paleostress analysis. In the stereographic projection, the known principal stress axes σ_1 , σ_2 , and σ_3 are oriented up, east, and north respectively and the calculated principal stress axes are denoted by the filled circles labelled 1, 2, and 3.



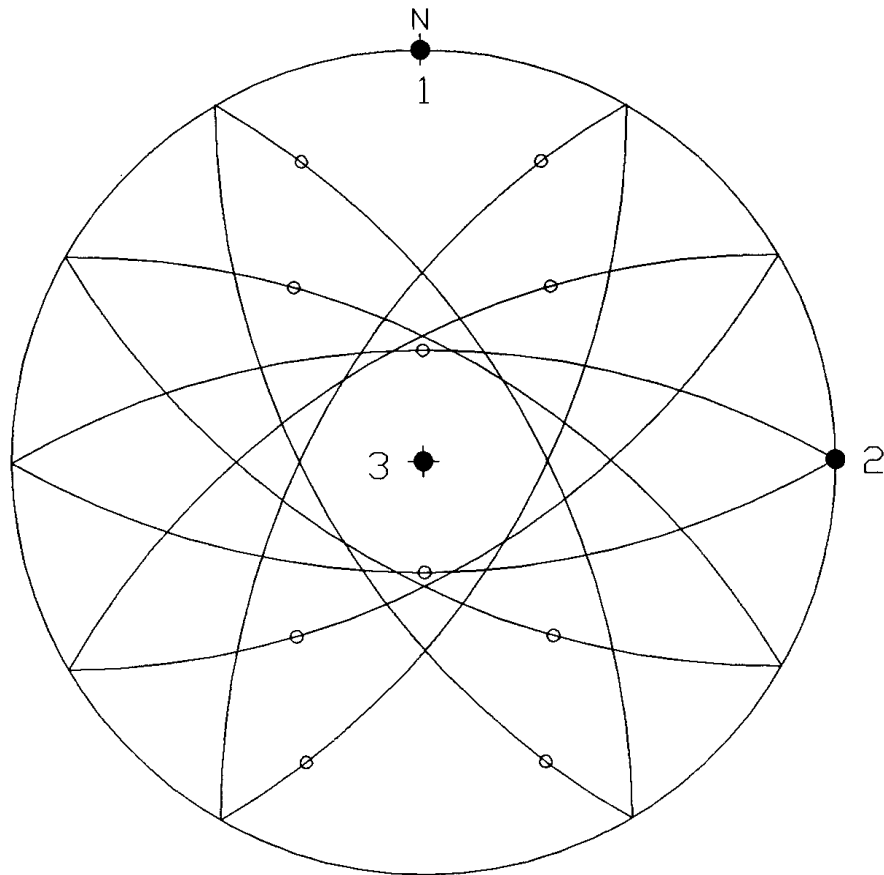
	Known	Program	Error
σ_1	90/000	00/000	90.0°
σ_2	00/090	00/090	0.0°
σ_3	00/000	90/270	90.0°
Φ	0.50	0.583	0.083

Figure 9-63 - Lower-hemisphere stereographic projection and table demonstrating the differences between the known and calculated principal stress axes σ_1 , σ_2 , and σ_3 and the value of Φ for fault population RS-01-50 using Reches' method of paleostress analysis. In the stereographic projection, the known principal stress axes σ_1 , σ_2 , and σ_3 are oriented up, east, and north respectively and the calculated principal stress axes are denoted by the filled circles labelled 1, 2, and 3.



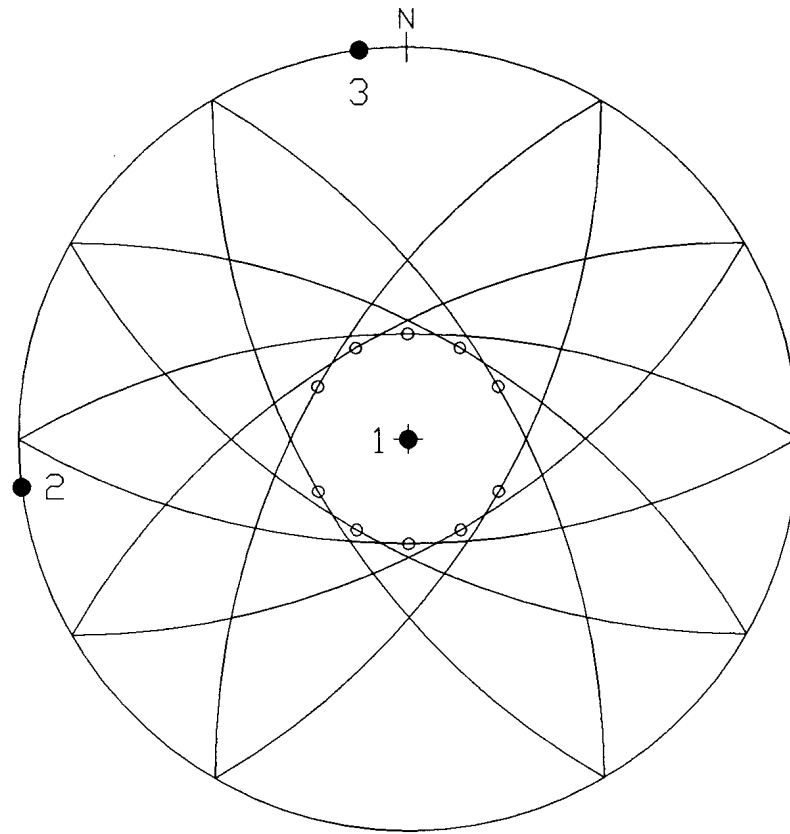
	Known	Program	Error
σ_1	90/000	00/000	90.0°
σ_2	00/090	00/090	0.0°
σ_3	00/000	90/270	90.0°
Φ	0.75	0.392	0.358

Figure 9-64 - Lower-hemisphere stereographic projection and table demonstrating the differences between the known and calculated principal stress axes σ_1 , σ_2 , and σ_3 and the value of Φ for fault population RS-01-75 using Reches' method of paleostress analysis. In the stereographic projection, the known principal stress axes σ_1 , σ_2 , and σ_3 are oriented up, east, and north respectively and the calculated principal stress axes are denoted by the filled circles labelled 1, 2, and 3.



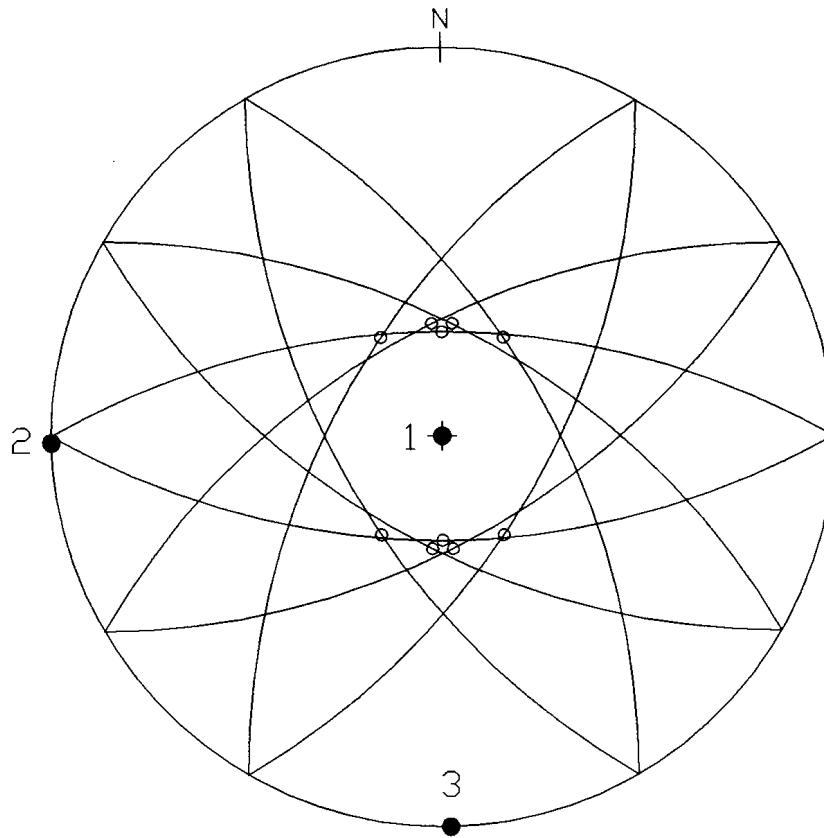
	Known	Program	Error
σ_1	90/000	00/000	90.0°
σ_2	00/090	00/090	0.0°
σ_3	00/000	90/270	90.0°
Φ	1.00	0.184	0.816

Figure 9-65 - Lower-hemisphere stereographic projection and table demonstrating the differences between the known and calculated principal stress axes σ_1 , σ_2 , and σ_3 and the value of Φ for fault population RS-01-10 using Reches' method of paleostress analysis. In the stereographic projection, the known principal stress axes σ_1 , σ_2 , and σ_3 are oriented up, east, and north respectively and the calculated principal stress axes are denoted by the filled circles labelled 1, 2, and 3.



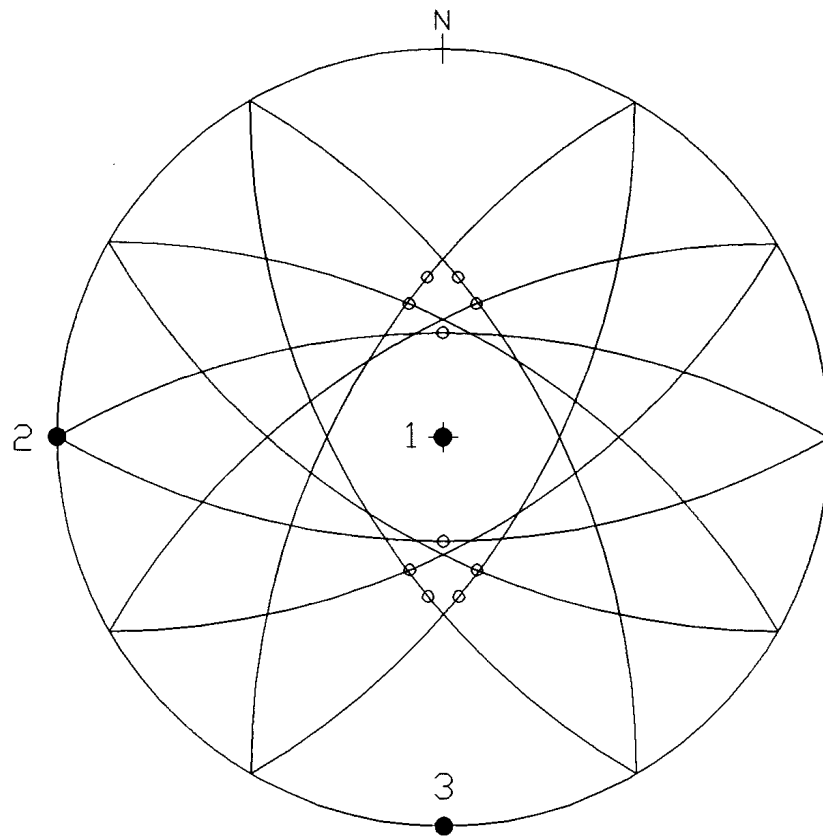
	Known	Program	Error
σ_1	90/000	90/102	0.0°
σ_2	00/090	00/263	7.0°
σ_3	00/000	00/353	7.0°
Φ	0.00	0.036	0.036

Figure 9-66 - Lower-hemisphere stereographic projection and table demonstrating the differences between the known and calculated principal stress axes σ_1 , σ_2 , and σ_3 and the value of Φ for fault population RS-01-00 using Angelier's method of paleostress analysis. In the stereographic projection, the known principal stress axes σ_1 , σ_2 , and σ_3 are oriented up, east, and north respectively and the calculated principal stress axes are denoted by the filled circles labelled 1, 2, and 3.



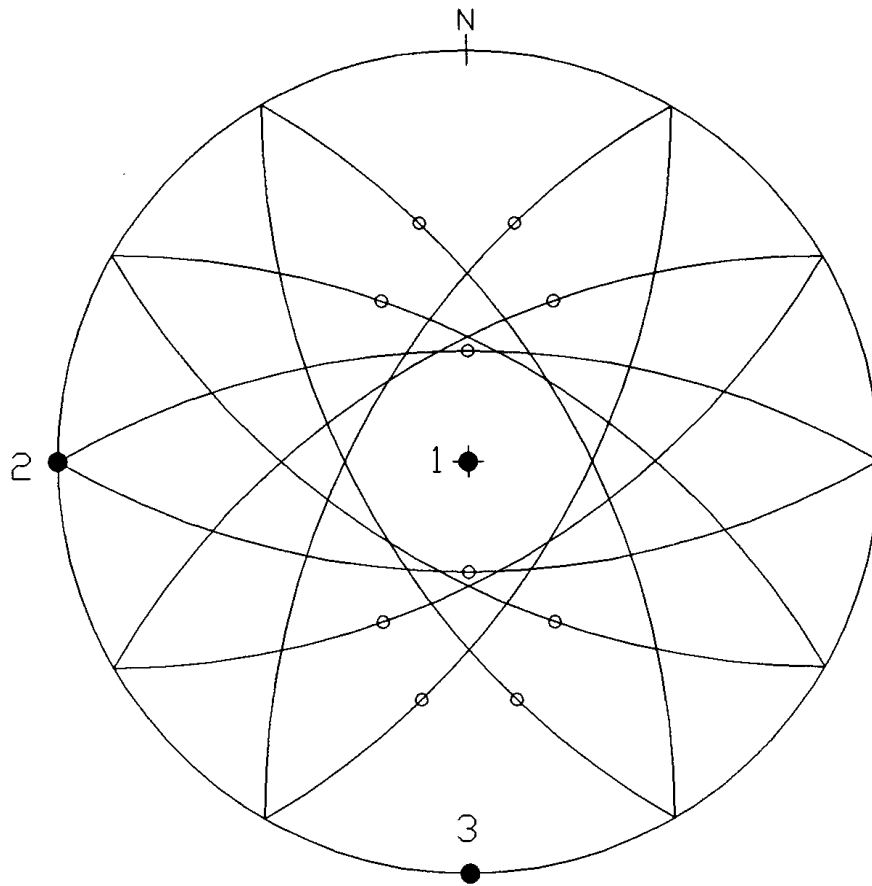
	Known	Program	Error
σ_1	90/000	90/012	0.0°
σ_2	00/090	00/269	1.0°
σ_3	00/000	00/179	1.0°
Φ	0.25	0.252	0.002

Figure 9-67 - Lower-hemisphere stereographic projection and table demonstrating the differences between the known and calculated principal stress axes σ_1 , σ_2 , and σ_3 and the value of Φ for fault population RS-01-25 using Angelier's method of paleostress analysis. In the stereographic projection, the known principal stress axes σ_1 , σ_2 , and σ_3 are oriented up, east, and north respectively and the calculated principal stress axes are denoted by the filled circles labelled 1, 2, and 3.



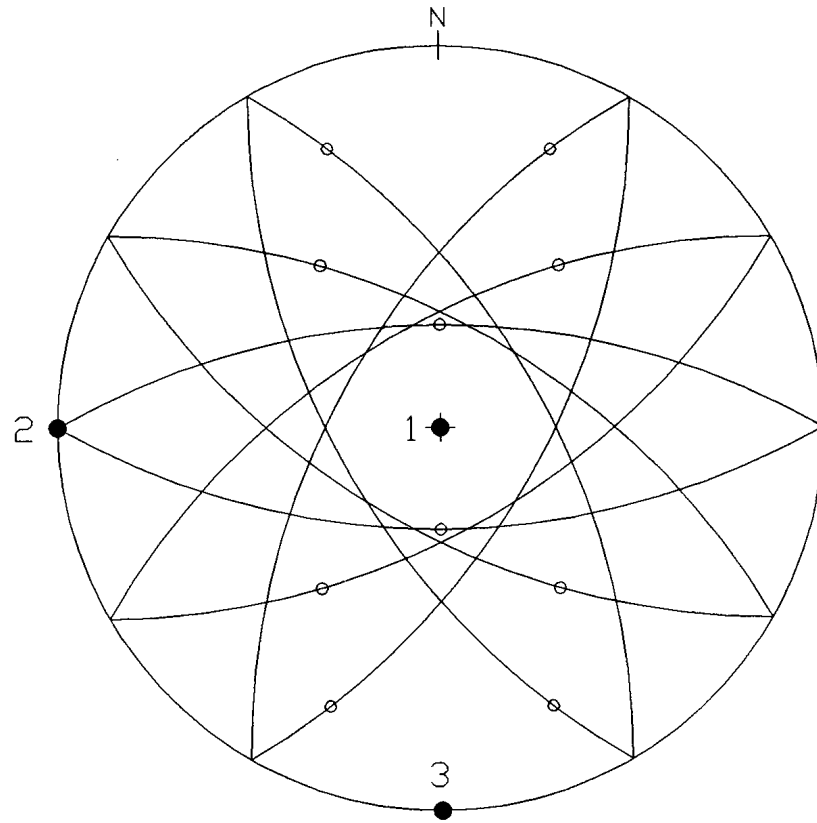
	Known	Program	Error
σ_1	90/000	90/081	0.0°
σ_2	00/090	00/270	0.0°
σ_3	00/000	00/180	0.0°
Φ	0.50	0.493	0.007

Figure 9-68 - Lower-hemisphere stereographic projection and table demonstrating the differences between the known and calculated principal stress axes σ_1 , σ_2 , and σ_3 and the value of Φ for fault population RS-01-50 using Angelier's method of paleostress analysis. In the stereographic projection, the known principal stress axes σ_1 , σ_2 , and σ_3 are oriented up, east, and north respectively and the calculated principal stress axes are denoted by the filled circles labelled 1, 2, and 3.



	Known	Program	Error
σ_1	90/000	90/085	0.0°
σ_2	00/090	90/270	0.0°
σ_3	00/000	00/180	0.0°
Φ	0.75	0.742	0.008

Figure 9-69 - Lower-hemisphere stereographic projection and table demonstrating the differences between the known and calculated principal stress axes σ_1 , σ_2 , and σ_3 and the value of Φ for fault population RS-01-75 using Angelier's method of paleostress analysis. In the stereographic projection, the known principal stress axes σ_1 , σ_2 , and σ_3 are oriented up, east, and north respectively and the calculated principal stress axes are denoted by the filled circles labelled 1, 2, and 3.



	Known	Program	Error
σ_1	90/000	00/090	0.0°
σ_2	00/090	90/270	0.0°
σ_3	00/000	00/180	0.0°
Φ	1.00	0.997	0.003

Figure 9-70 - Lower-hemisphere stereographic projection and table demonstrating the differences between the known and calculated principal stress axes σ_1 , σ_2 , and σ_3 and the value of Φ for fault population RS-01-10 using Angelier's method of paleostress analysis. In the stereographic projection, the known principal stress axes σ_1 , σ_2 , and σ_3 are oriented up, east, and north respectively and the calculated principal stress axes are denoted by the filled circles labelled 1, 2, and 3.

		Reches'	Angelier's	Deviation
Known Φ of 0.00	σ_1	00/000	90/102	90.0°
	σ_2	00/090	00/263	7.0°
	σ_3	90/270	00/353	90.0°
	Φ	1.000	0.036	0.964
Known Φ of 0.25	σ_1	00/000	90/012	90.0°
	σ_2	00/090	00/269	1.0°
	σ_3	90/270	00/179	90.0°
	Φ	0.746	0.252	0.494
Known Φ of 0.50	σ_1	00/000	90/081	90.0°
	σ_2	00/090	00/270	0.0°
	σ_3	90/270	00/180	90.0°
	Φ	0.583	0.493	0.090
Known Φ of 0.75	σ_1	00/000	90/085	90.0°
	σ_2	00/090	00/270	0.0°
	σ_3	90/270	00/180	90.0°
	Φ	0.392	0.742	0.350
Known Φ of 1.00	σ_1	00/000	00/090	90.0°
	σ_2	00/090	90/270	90.0°
	σ_3	90/270	00/180	90.0°
	Φ	0.184	0.997	0.813

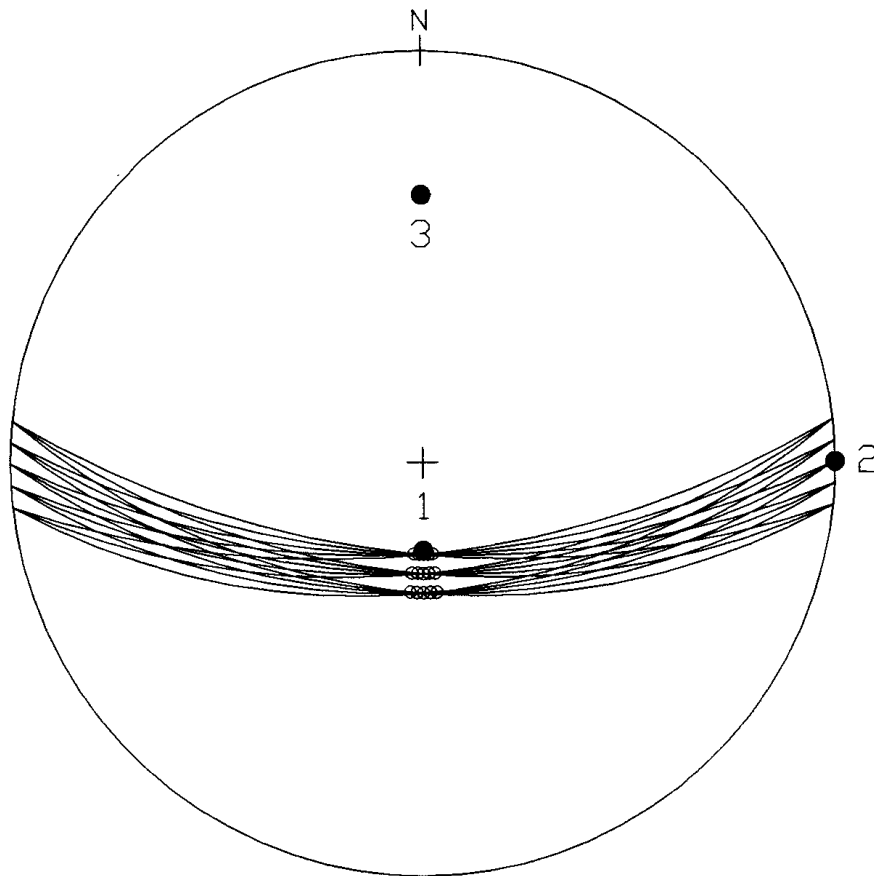
Table 9-7 - Table demonstrating the deviation for the orientations of the σ_1 , σ_2 , and σ_3 principal stress axes and the principal stress magnitude ratio Φ between Reches' and Angelier's methods of paleostress analysis on fault population RS-01 at five different values of Φ .

Finally, the three fault populations SO-01, SO-02, and SO-03 consisting of fault planes of similar orientations were tested. These faults also gave somewhat unexpected results which were a bit different from the results given for the other special-case fault populations tested.

First, consider the results for Reches' method on fault population SO-01 (figures 9-71 through 9-75). The orientations for the σ_2 principal stress axes are correct, which is not too surprising considering that the faults are all parallel to the east-west axis, but the σ_1 and σ_3 axes are quite a bit off ($\pm 18^\circ$). The Φ values returned by the program are also very odd. The Φ value returned for an initial Φ of 0.00 is negative and the Φ values returned for initial Φ values of 0.75 and 1.00 are both greater than 1.0. Since Φ is defined as being between 0.0 and 1.0 inclusive, these values are obviously in error. In this case, however, switching the axes will not help.

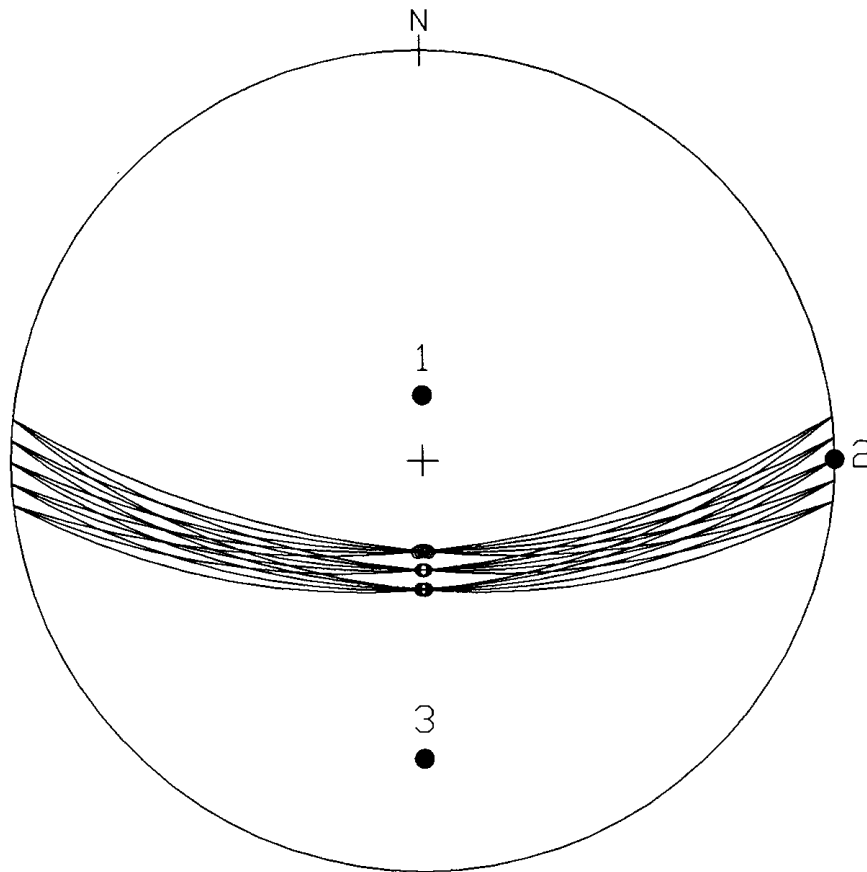
For Angelier's method, in a similar fashion, the orientations for the σ_2 principal stress axes are essentially correct and the σ_1 and σ_3 axes are quite a bit off ($\pm 16^\circ$). The errors in magnitude for the calculated values of Φ were largest (almost 0.4) at an initial Φ value of 0.50 and somewhat smaller for larger and smaller initial Φ values.

Comparing the results of Reches' to Angelier's methods for similar orientation fault population SO-01 (table 9-8) shows large deviations ($\pm 36^\circ$) in the orientations of the principal stress axes σ_1 , σ_2 , and σ_3 for an initial Φ value of 0.00 but rather small deviations (less than 10°) for all of the principal stress axis orientations at initial Φ values of 0.25, 0.50, 0.75, and 1.00.



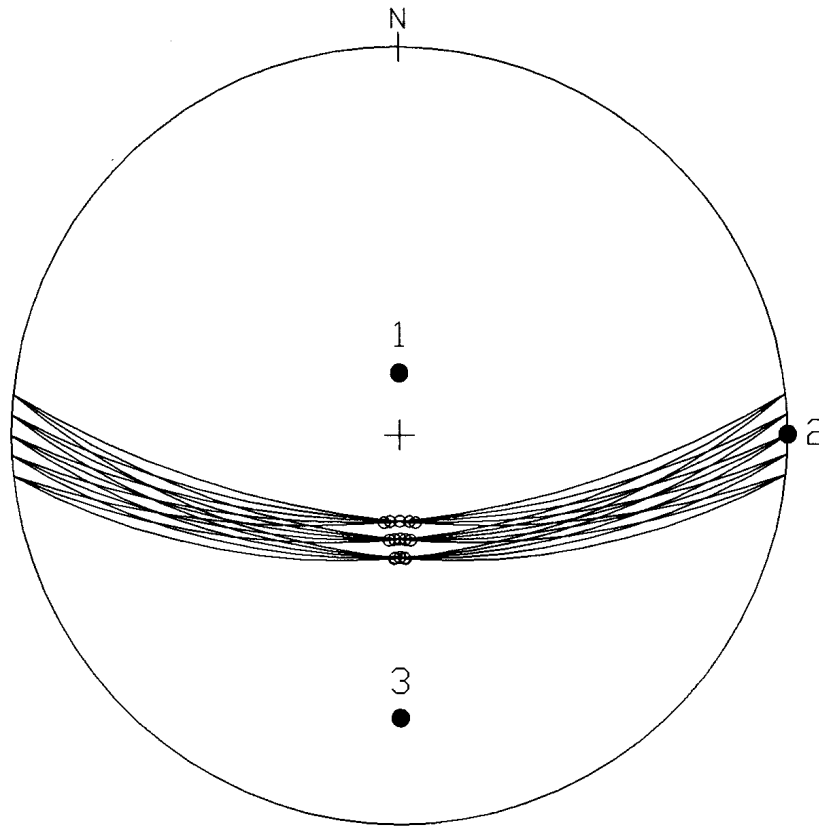
	Known	Program	Error
σ_1	90/000	66/180	24.0°
σ_2	00/090	00/090	0.0°
σ_3	00/000	24/000	24.0°
Φ	0.00	-0.047	?

Figure 9-71 - Lower-hemisphere stereographic projection and table demonstrating the differences between the known and calculated principal stress axes σ_1 , σ_2 , and σ_3 and the value of Φ for fault population SO-01-00 using Reches' method of paleostress analysis. In the stereographic projection, the known principal stress axes σ_1 , σ_2 , and σ_3 are oriented up, east, and north respectively and the calculated principal stress axes are denoted by the filled circles labelled 1, 2, and 3.



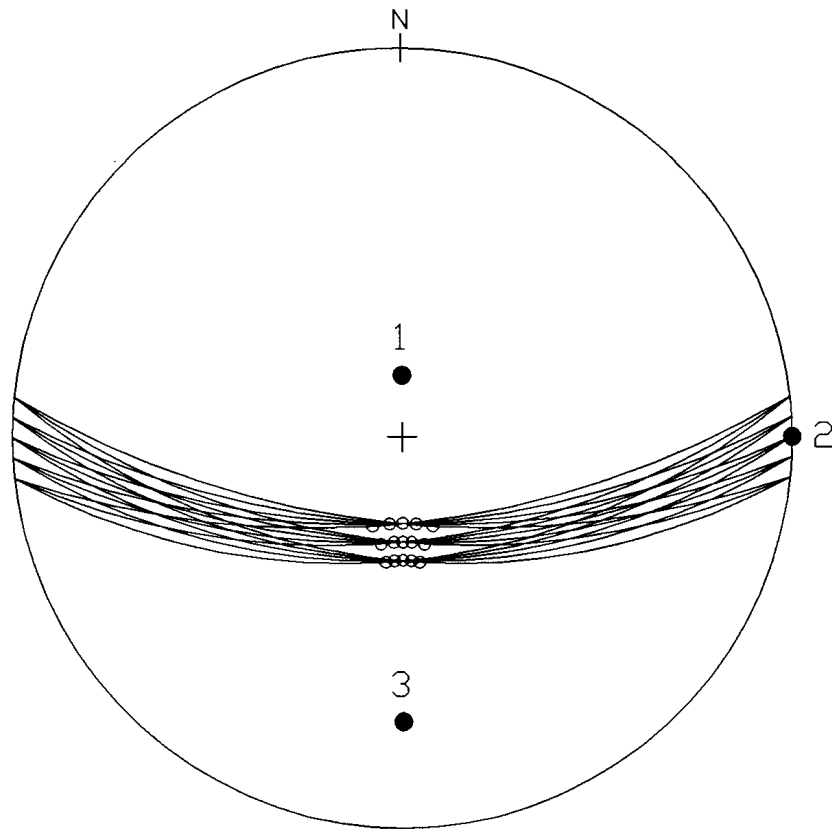
	Known	Program	Error
σ_1	90/000	72/000	18.0°
σ_2	00/090	00/090	0.0°
σ_3	00/000	18/180	18.0°
Φ	0.25	0.581	0.331

Figure 9-72 - Lower-hemisphere stereographic projection and table demonstrating the differences between the known and calculated principal stress axes σ_1 , σ_2 , and σ_3 and the value of Φ for fault population SO-01-25 using Reches' method of paleostress analysis. In the stereographic projection, the known principal stress axes σ_1 , σ_2 , and σ_3 are oriented up, east, and north respectively and the calculated principal stress axes are denoted by the filled circles labelled 1, 2, and 3.



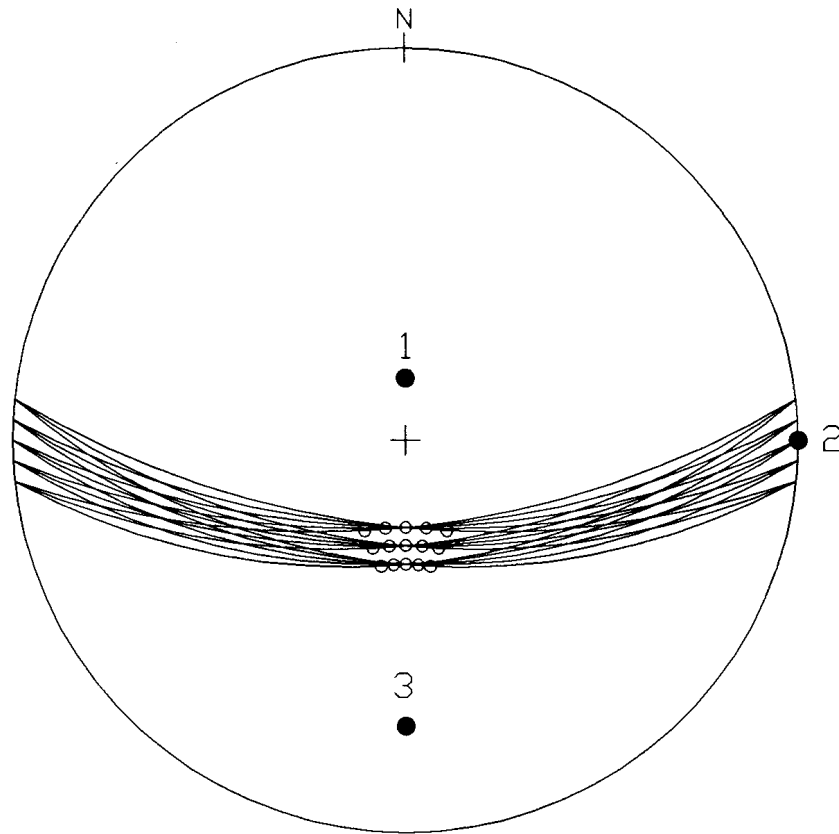
	Known	Program	Error
σ_1	90/000	72/000	18.0°
σ_2	00/090	00/090	0.0°
σ_3	00/000	18/180	18.0°
Φ	0.50	0.847	0.347

Figure 9-73 - Lower-hemisphere stereographic projection and table demonstrating the differences between the known and calculated principal stress axes σ_1 , σ_2 , and σ_3 and the value of Φ for fault population SO-01-50 using Reches' method of paleostress analysis. In the stereographic projection, the known principal stress axes σ_1 , σ_2 , and σ_3 are oriented up, east, and north respectively and the calculated principal stress axes are denoted by the filled circles labelled 1, 2, and 3.



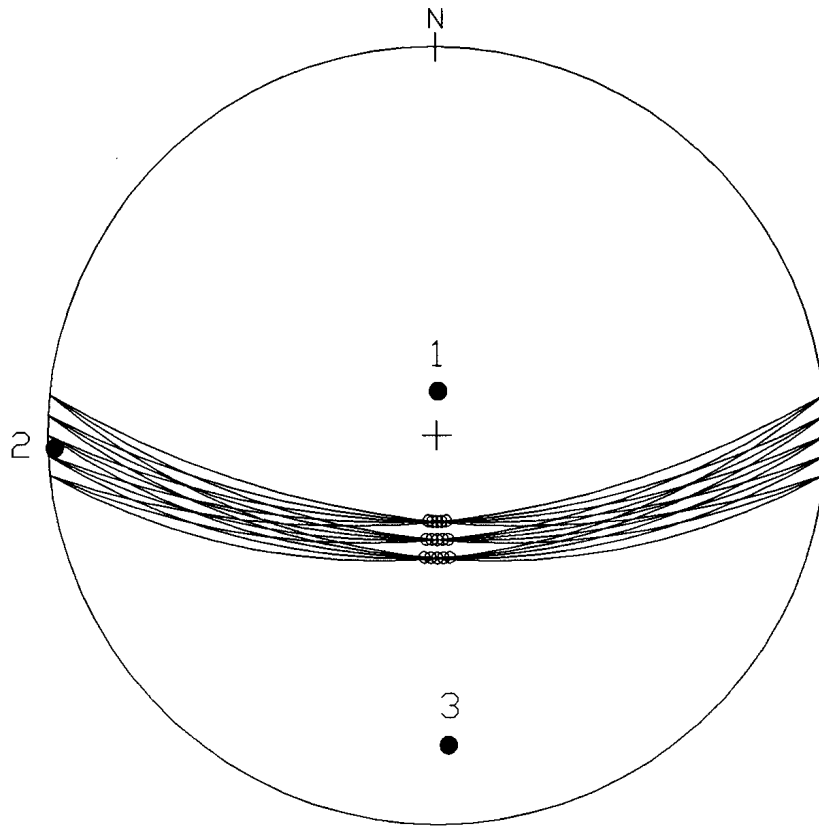
	Known	Program	Error
σ_1	90/000	72/000	18.0°
σ_2	00/090	00/090	0.0°
σ_3	00/000	18/180	18.0°
Φ	0.75	1.125	?

Figure 9-74 - Lower-hemisphere stereographic projection and table demonstrating the differences between the known and calculated principal stress axes σ_1 , σ_2 , and σ_3 and the value of Φ for fault population SO-01-75 using Reches' method of paleostress analysis. In the stereographic projection, the known principal stress axes σ_1 , σ_2 , and σ_3 are oriented up, east, and north respectively and the calculated principal stress axes are denoted by the filled circles labelled 1, 2, and 3.



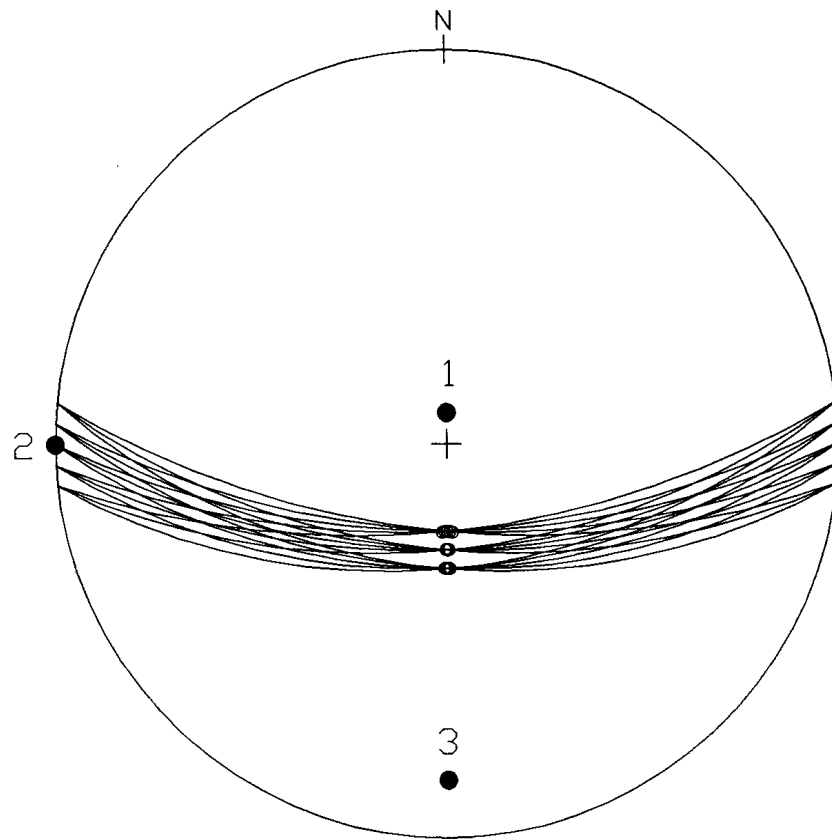
	Known	Program	Error
σ_1	90/000	72/000	18.0°
σ_2	00/090	00/090	0.0°
σ_3	00/000	18/180	18.0°
Φ	1.00	1.364	1.000

Figure 9-75 - Lower-hemisphere stereographic projection and table demonstrating the differences between the known and calculated principal stress axes σ_1 , σ_2 , and σ_3 and the value of Φ for fault population SO-01-10 using Reches' method of paleostress analysis. In the stereographic projection, the known principal stress axes σ_1 , σ_2 , and σ_3 are oriented up, east, and north respectively and the calculated principal stress axes are denoted by the filled circles labelled 1, 2, and 3.



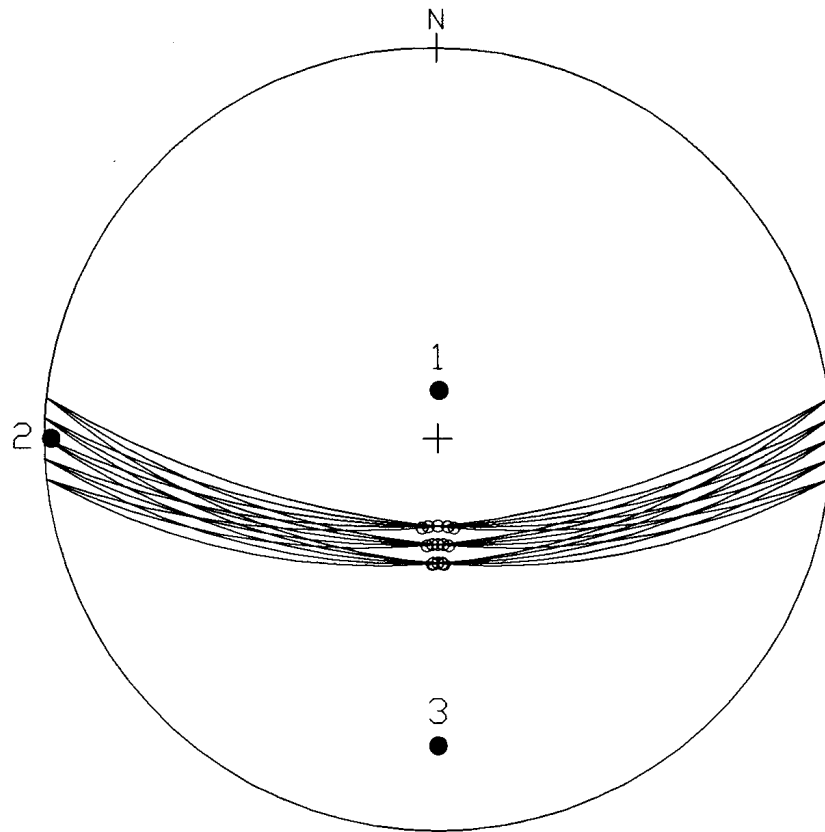
	Known	Program	Error
σ_1	90/000	77/002	13.0°
σ_2	00/090	01/268	2.2°
σ_3	00/000	13/178	13.2°
Φ	0.00	0.136	0.136

Figure 9-76 - Lower-hemisphere stereographic projection and table demonstrating the differences between the known and calculated principal stress axes σ_1 , σ_2 , and σ_3 and the value of Φ for fault population SO-01-00 using Angelier's method of paleostress analysis. In the stereographic projection, the known principal stress axes σ_1 , σ_2 , and σ_3 are oriented up, east, and north respectively and the calculated principal stress axes are denoted by the filled circles labelled 1, 2, and 3.



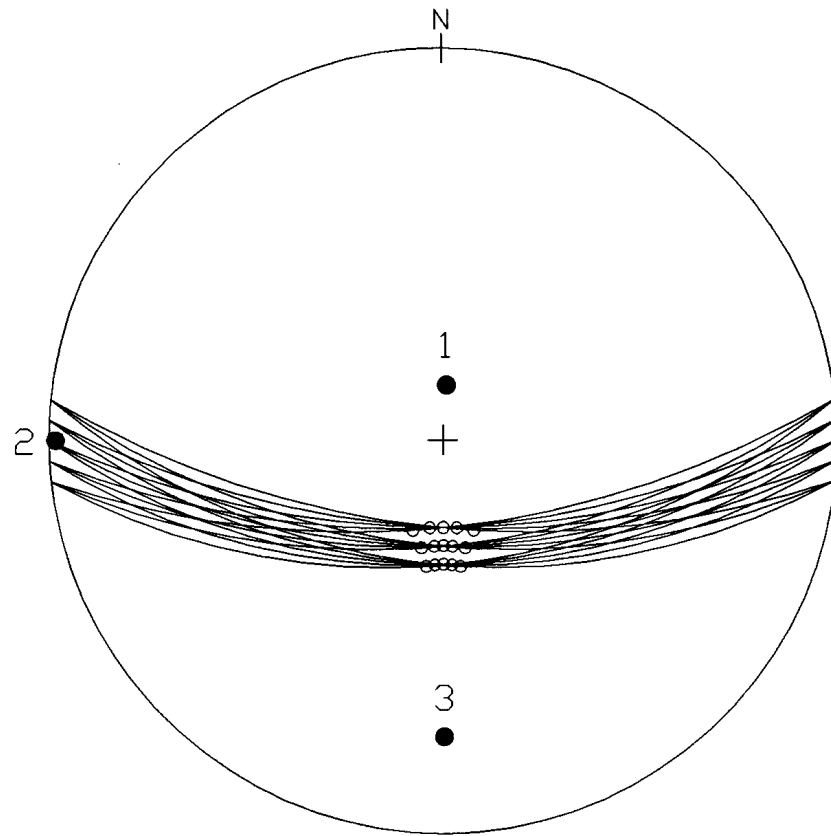
	Known	Program	Error
σ_1	90/000	81/000	9.0°
σ_2	00/090	00/270	0.0°
σ_3	00/000	09/180	9.0°
Φ	0.25	0.334	0.084

Figure 9-77 - Lower-hemisphere stereographic projection and table demonstrating the differences between the known and calculated principal stress axes σ_1 , σ_2 , and σ_3 and the value of Φ for fault population SO-01-25 using Angelier's method of paleostress analysis. In the stereographic projection, the known principal stress axes σ_1 , σ_2 , and σ_3 are oriented up, east, and north respectively and the calculated principal stress axes are denoted by the filled circles labelled 1, 2, and 3.



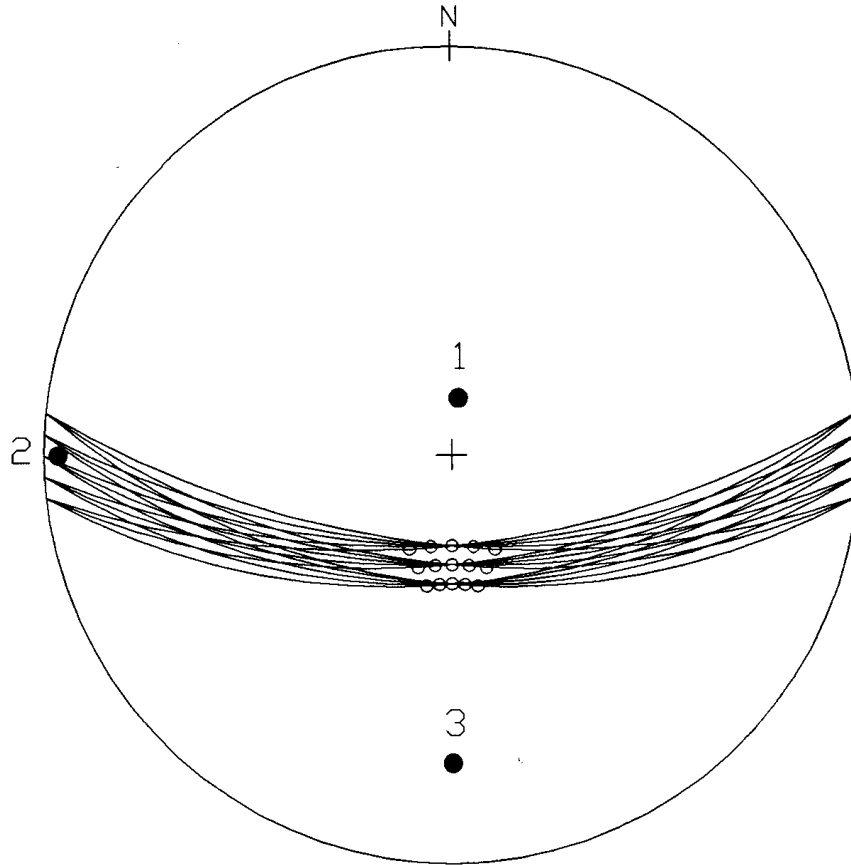
	Known	Program	Error
σ_1	90/000	76/002	14.0°
σ_2	00/090	01/270	1.0°
σ_3	00/000	14/180	14.0°
Φ	0.50	0.880	0.380

Figure 9-78 - Lower-hemisphere stereographic projection and table demonstrating the differences between the known and calculated principal stress axes σ_1 , σ_2 , and σ_3 and the value of Φ for fault population SO-01-50 using Angelier's method of paleostress analysis. In the stereographic projection, the known principal stress axes σ_1 , σ_2 , and σ_3 are oriented up, east, and north respectively and the calculated principal stress axes are denoted by the filled circles labelled 1, 2, and 3.



	Known	Program	Error
σ_1	90/000	74/004	16.0°
σ_2	00/090	01/270	1.0°
σ_3	00/000	16/180	16.0°
Φ	0.75	0.939	0.189

Figure 9-79 - Lower-hemisphere stereographic projection and table demonstrating the differences between the known and calculated principal stress axes σ_1 , σ_2 , and σ_3 and the value of Φ for fault population SO-01-75 using Angelier's method of paleostress analysis. In the stereographic projection, the known principal stress axes σ_1 , σ_2 , and σ_3 are oriented up, east, and north respectively and the calculated principal stress axes are denoted by the filled circles labelled 1, 2, and 3.



	Known	Program	Error
σ_1	90/000	74/007	16.0°
σ_2	00/090	02/270	2.0°
σ_3	00/000	16/180	16.0°
Φ	1.00	0.967	0.033

Figure 9-80 - Lower-hemisphere stereographic projection and table demonstrating the differences between the known and calculated principal stress axes σ_1 , σ_2 , and σ_3 and the value of Φ for fault population SO-01-10 using Angelier's method of paleostress analysis. In the stereographic projection, the known principal stress axes σ_1 , σ_2 , and σ_3 are oriented up, east, and north respectively and the calculated principal stress axes are denoted by the filled circles labelled 1, 2, and 3.

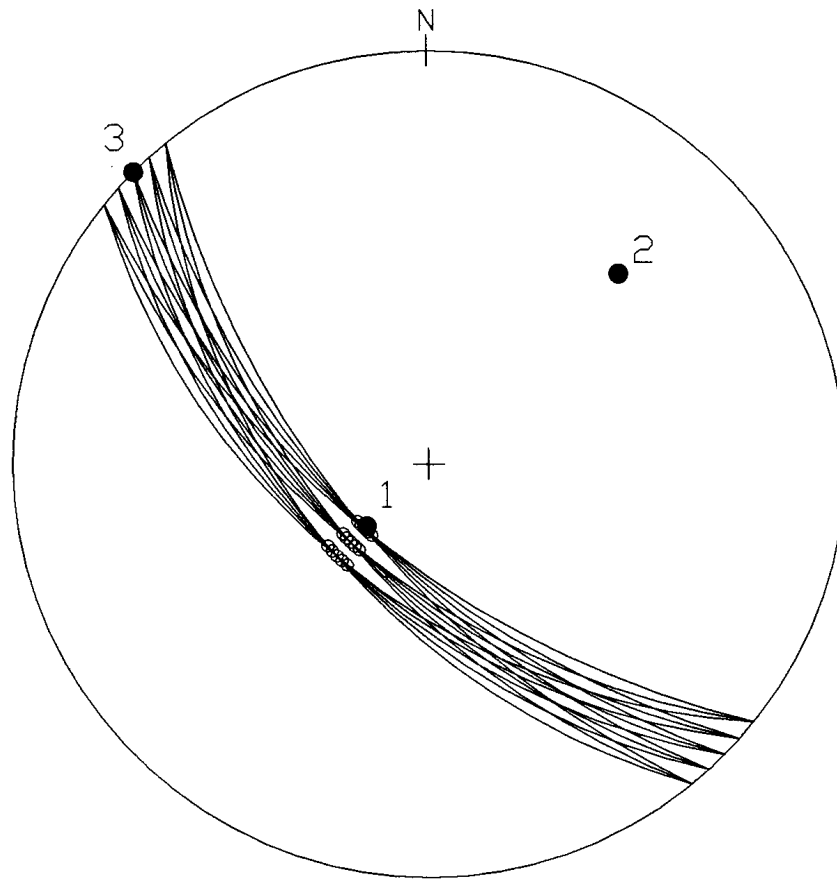
		Reches'	Angelier's	Deviation
Known Φ of 0.00	σ_1	66/180	77/002	37.0°
	σ_2	00/090	01/268	2.2°
	σ_3	24/000	13/178	37.1°
	Φ	-0.047	0.136	?
Known Φ of 0.25	σ_1	72/000	81/000	9.0°
	σ_2	00/090	00/270	0.0°
	σ_3	18/180	09/180	9.0°
	Φ	0.581	0.334	0.218
Known Φ of 0.50	σ_1	72/000	76/002	4.0°
	σ_2	00/090	01/270	1.0°
	σ_3	18/180	14/180	4.0°
	Φ	0.847	0.880	0.019
Known Φ of 0.75	σ_1	72/000	74/004	2.3°
	σ_2	00/090	01/270	1.0°
	σ_3	18/180	16/000	2.0°
	Φ	1.125	0.939	?
Known Φ of 1.00	σ_1	72/000	74/007	2.9°
	σ_2	00/090	02/270	2.0°
	σ_3	18/180	16/180	2.0°
	Φ	1.364	0.967	?

Table 9-8 - Table demonstrating the deviation for the orientations of the σ_1 , σ_2 , and σ_3 principal stress axes and the principal stress magnitude ratio Φ between Reches' and Angelier's methods of paleostress analysis on fault population SO-01 at five different values of Φ .

The results from Reches' method (figures 9-81 through 9-85) and Angelier's method (figures 9-86 through 9-90) for similar orientation fault population SO-02 are even worse than those for SO-01. None of the three principal stress axes are correct and none of the Φ values are even close to being what they should be. Comparing Reches' to Angelier's method (table 9-9) shows that, while both incorrect, they are also both consistent.

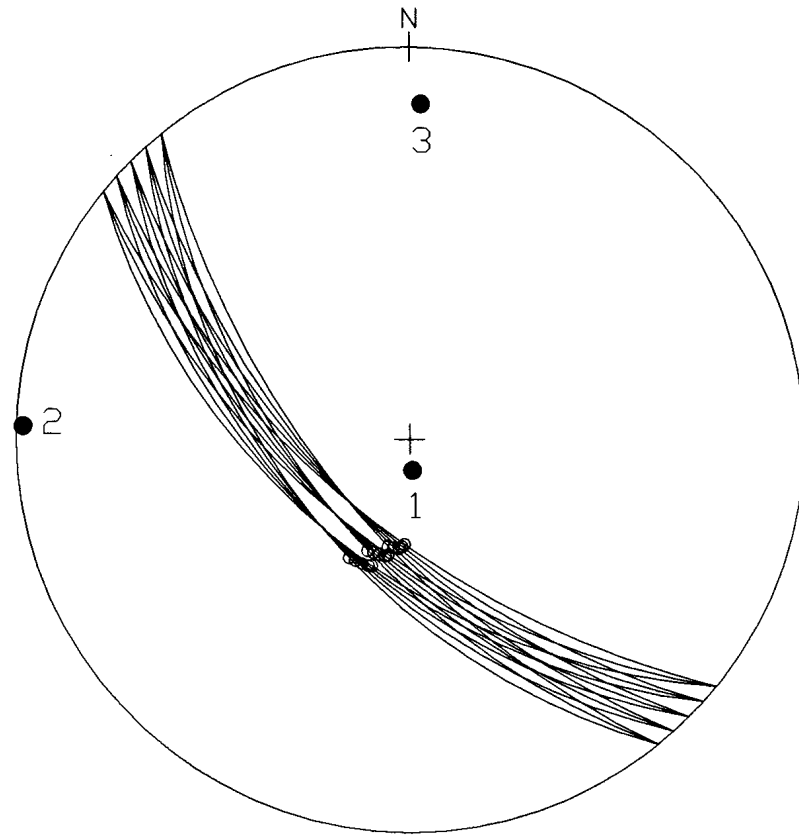
The results from Reches' method (figures 9-90 through 9-95) and Angelier's method (figures 9-96 through 9-100) for similar orientation fault population SO-03 has a similar problem. None of the three principal stress axes are correct and none of the Φ values are even close to being what they should be. Comparing Reches' to Angelier's method (table 9-10) shows that these results are also consistent.

I am not able to give a satisfactory explanation of why these two fault populations should be so far off. It is probably due to the fact that when you have a population of faults where all of them are of a similar orientation, there is not enough of a constraint upon the location of the principal stress axes. The rationale behind a negative Φ value being returned for SO-02 when Φ is initially 0.00 is a mystery. I was not able to ascertain why negative Φ values should be returned. The reason is undoubtedly contained within the source code of the programs and simple error checking should have been able to constrain Φ to be between 0.0 and 1.0 inclusive. A value outside of that range should not be allowed.



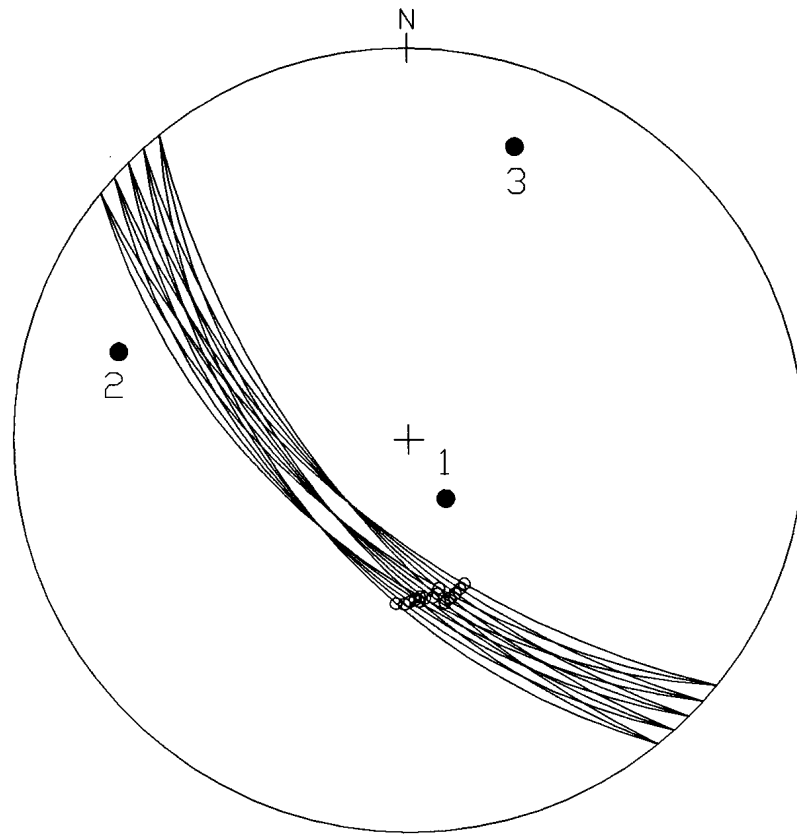
	Known	Program	Error
σ_1	90/000	66/225	24.0°
σ_2	00/090	24/045	49.8°
σ_3	00/000	00/315	45.0°
Φ	0.00	0.045	0.045

Figure 9-81 - Lower-hemisphere stereographic projection and table demonstrating the differences between the known and calculated principal stress axes σ_1 , σ_2 , and σ_3 and the value of Φ for fault population SO-02-00 using Reches' method of paleostress analysis. In the stereographic projection, the known principal stress axes σ_1 , σ_2 , and σ_3 are oriented up, east, and north respectively and the calculated principal stress axes are denoted by the filled circles labelled 1, 2, and 3.



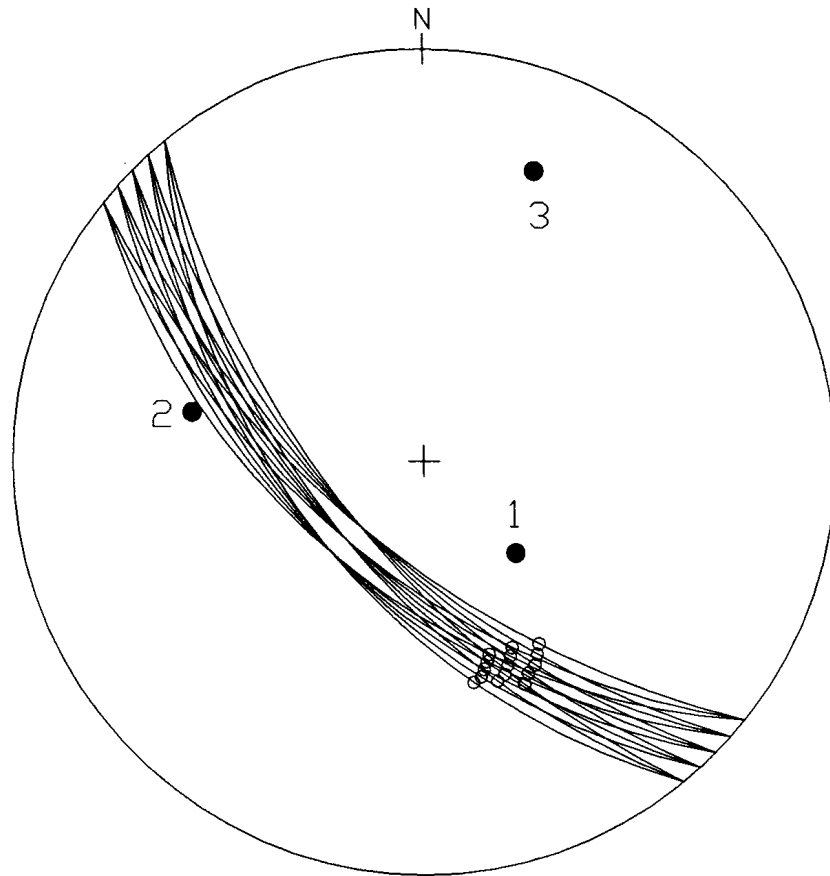
	Known	Program	Error
σ_1	90/000	81/175	9.0°
σ_2	00/090	01/272	2.2°
σ_3	00/000	09/002	9.2°
Φ	0.25	0.110	0.140

Figure 9-82 - Lower-hemisphere stereographic projection and table demonstrating the differences between the known and calculated principal stress axes σ_1 , σ_2 , and σ_3 and the value of Φ for fault population SO-02-25 using Reches' method of paleostress analysis. In the stereographic projection, the known principal stress axes σ_1 , σ_2 , and σ_3 are oriented up, east, and north respectively and the calculated principal stress axes are denoted by the filled circles labelled 1, 2, and 3.



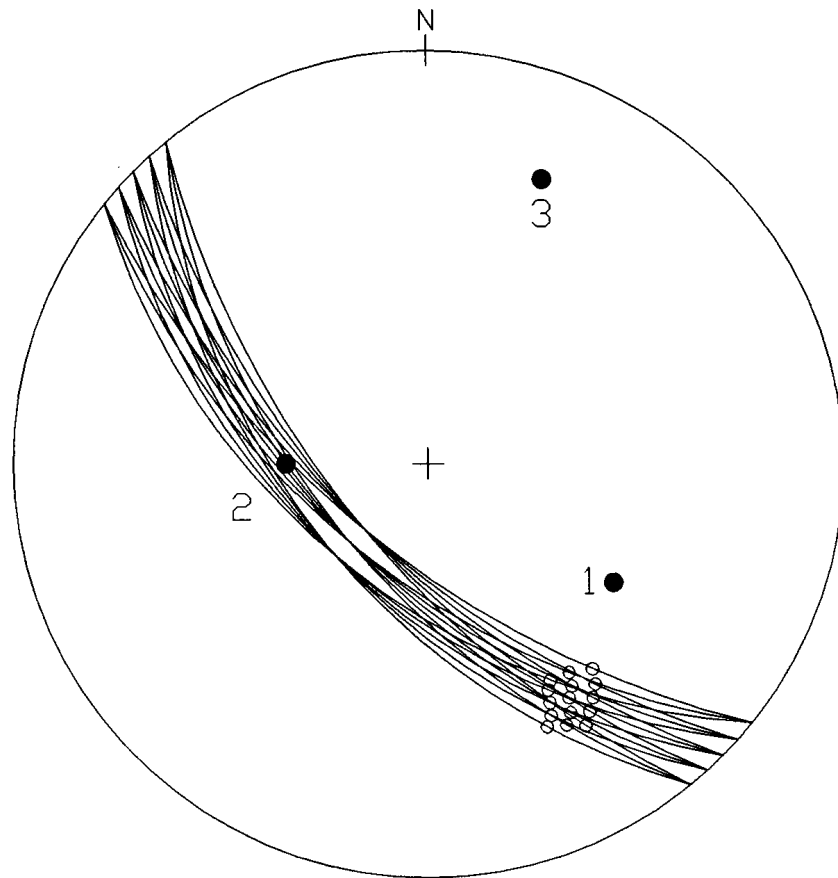
	Known	Program	Error
σ_1	90/000	70/148	20.0°
σ_2	00/090	15/287	22.5°
σ_3	00/000	13/020	23.7°
Φ	0.50	0.275	0.225

Figure 9-83 - Lower-hemisphere stereographic projection and table demonstrating the differences between the known and calculated principal stress axes σ_1 , σ_2 , and σ_3 and the value of Φ for fault population SO-02-50 using Reches' method of paleostress analysis. In the stereographic projection, the known principal stress axes σ_1 , σ_2 , and σ_3 are oriented up, east, and north respectively and the calculated principal stress axes are denoted by the filled circles labelled 1, 2, and 3.



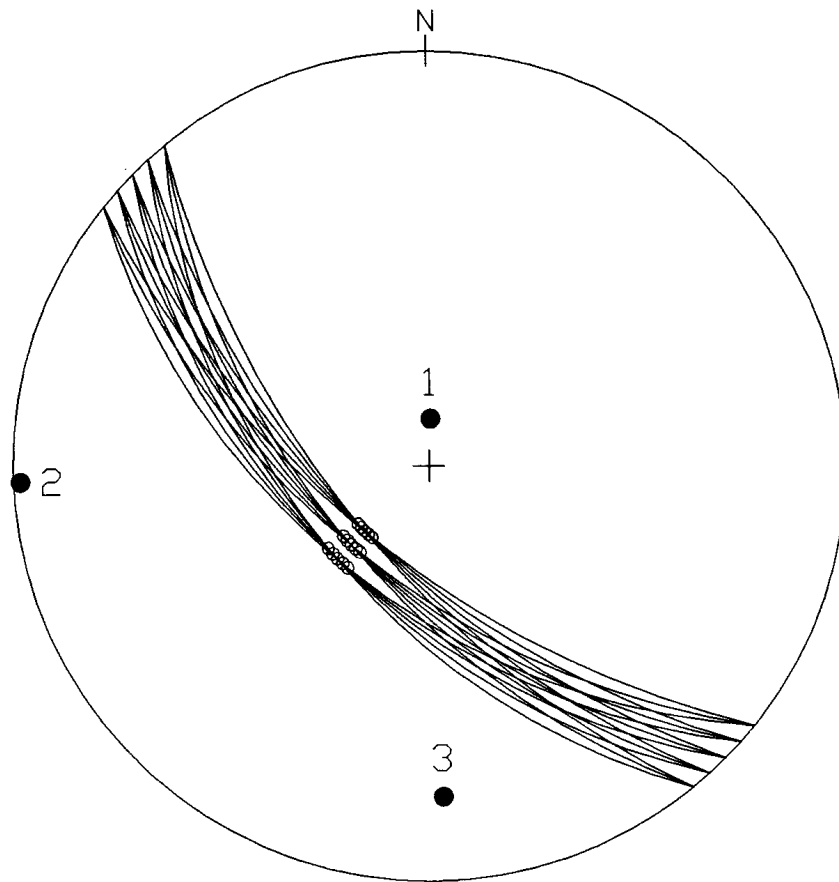
	Known	Program	Error
σ_1	90/000	55/135	35.0°
σ_2	00/090	30/282	32.1°
σ_3	00/000	16/021	26.2°
Φ	0.75	0.464	0.286

Figure 9-84 - Lower-hemisphere stereographic projection and table demonstrating the differences between the known and calculated principal stress axes σ_1 , σ_2 , and σ_3 and the value of Φ for fault population SO-02-75 using Reches' method of paleostress analysis. In the stereographic projection, the known principal stress axes σ_1 , σ_2 , and σ_3 are oriented up, east, and north respectively and the calculated principal stress axes are denoted by the filled circles labelled 1, 2, and 3.



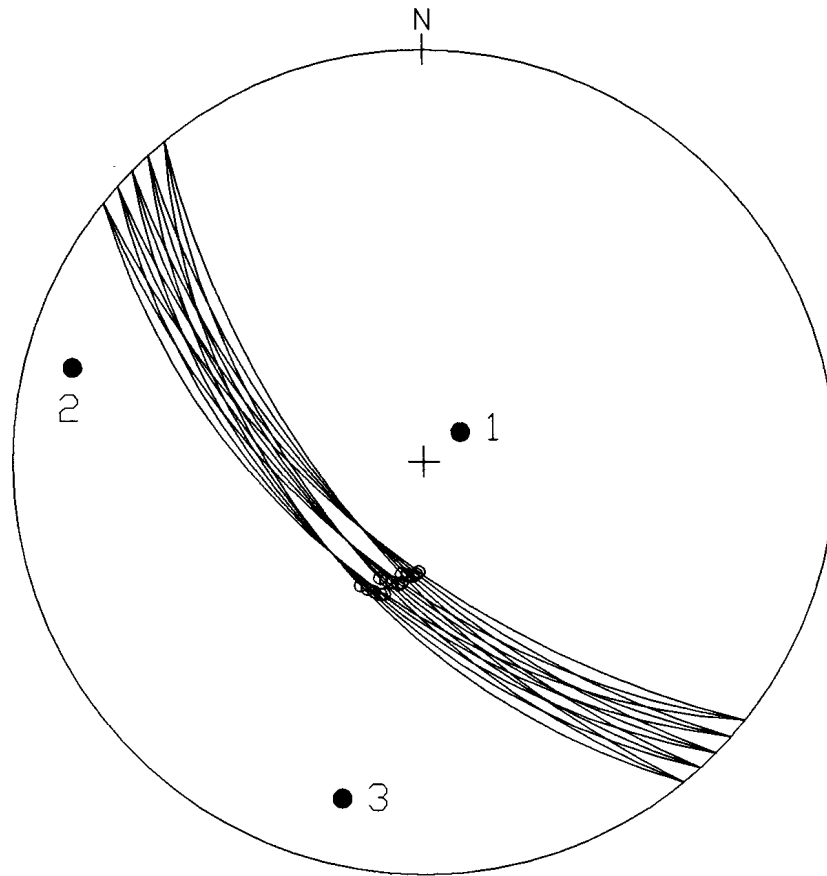
	Known	Program	Error
σ_1	90/000	34/123	56.0°
σ_2	00/090	52/270	52.0°
σ_3	00/000	17/022	27.5°
Φ	1.00	0.469	0.531

Figure 9-85 - Lower-hemisphere stereographic projection and table demonstrating the differences between the known and calculated principal stress axes σ_1 , σ_2 , and σ_3 and the value of Φ for fault population SO-02-10 using Reches' method of paleostress analysis. In the stereographic projection, the known principal stress axes σ_1 , σ_2 , and σ_3 are oriented up, east, and north respectively and the calculated principal stress axes are denoted by the filled circles labelled 1, 2, and 3.



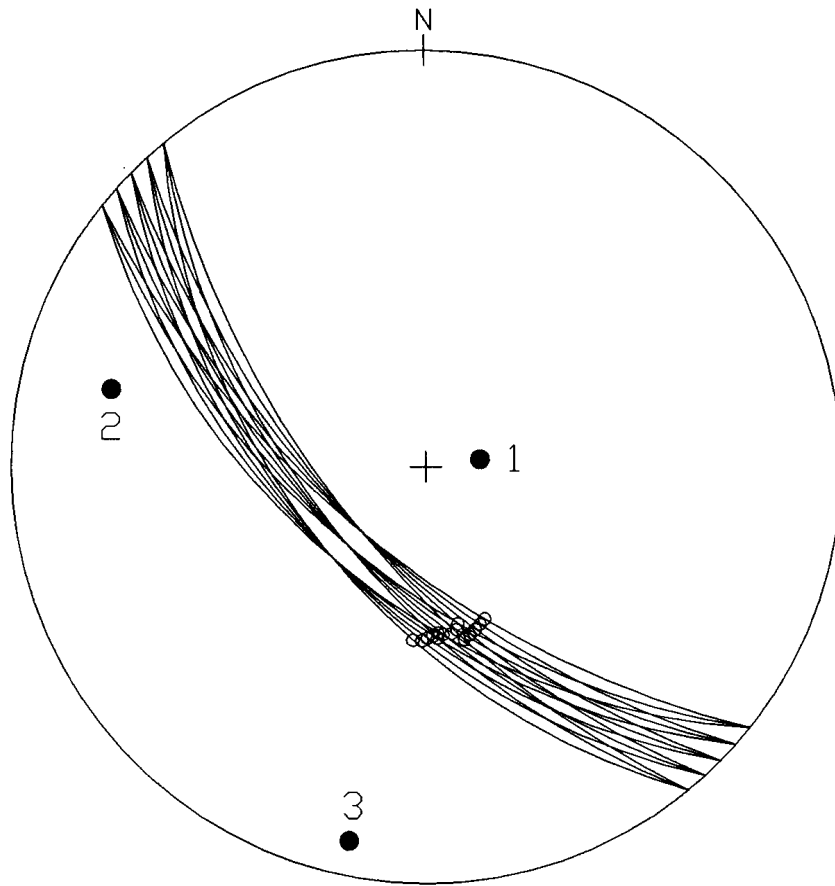
	Known	Program	Error
σ_1	90/000	7/047	13.0°
σ_2	00/090	01/313	43.0°
σ_3	00/000	13/223	44.6°
Φ	0.00	0.130	0.130

Figure 9-86 - Lower-hemisphere stereographic projection and table demonstrating the differences between the known and calculated principal stress axes σ_1 , σ_2 , and σ_3 and the value of Φ for fault population SO-02-00 using Angelier's method of paleostress analysis. In the stereographic projection, the known principal stress axes σ_1 , σ_2 , and σ_3 are oriented up, east, and north respectively and the calculated principal stress axes are denoted by the filled circles labelled 1, 2, and 3.



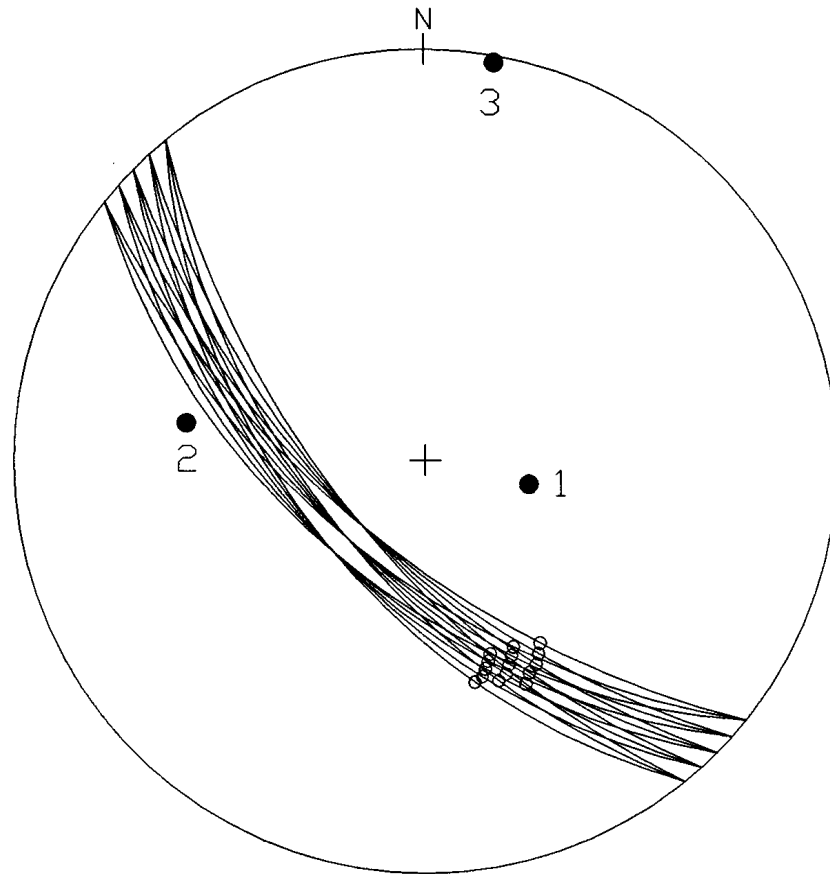
	Known	Program	Error
σ_1	90/000	77/051	13.0°
σ_2	00/090	07/285	16.5°
σ_3	00/000	10/194	17.1°
Φ	0.25	0.252	0.002

Figure 9-87 - Lower-hemisphere stereographic projection and table demonstrating the differences between the known and calculated principal stress axes σ_1 , σ_2 , and σ_3 and the value of Φ for fault population SO-02-25 using Angelier's method of paleostress analysis. In the stereographic projection, the known principal stress axes σ_1 , σ_2 , and σ_3 are oriented up, east, and north respectively and the calculated principal stress axes are denoted by the filled circles labelled 1, 2, and 3.



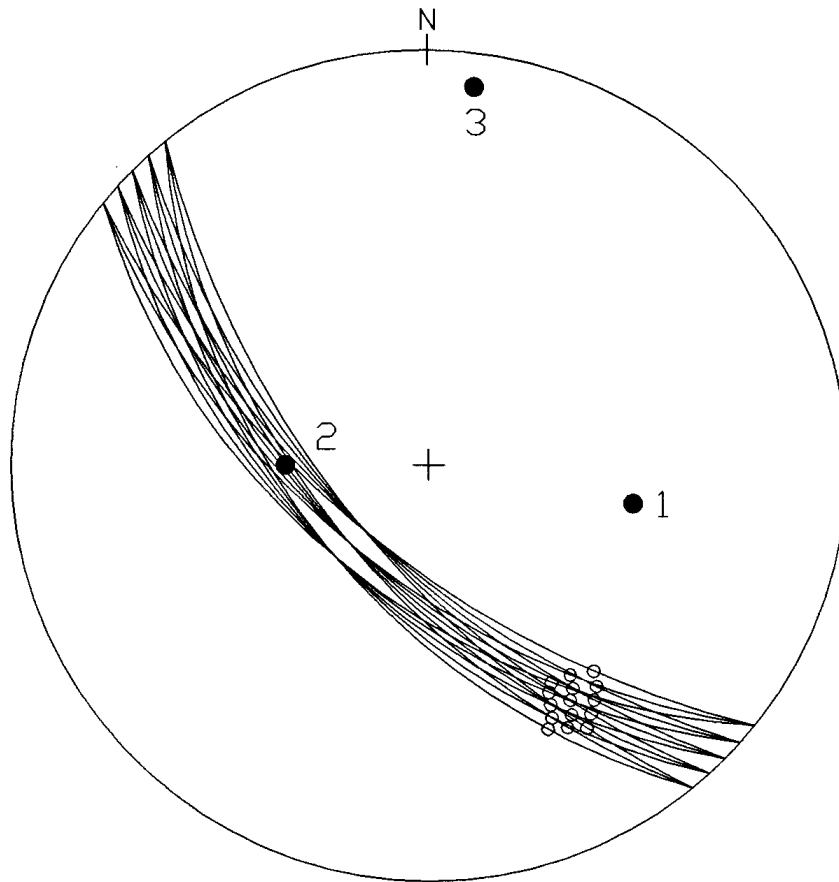
	Known	Program	Error
σ_1	90/000	75/082	15.0°
σ_2	00/090	14/284	19.7°
σ_3	00/000	05/192	13.0°
Φ	0.50	0.615	0.015

Figure 9-88 - Lower-hemisphere stereographic projection and table demonstrating the differences between the known and calculated principal stress axes σ_1 , σ_2 , and σ_3 and the value of Φ for fault population SO-02-50 using Angelier's method of paleostress analysis. In the stereographic projection, the known principal stress axes σ_1 , σ_2 , and σ_3 are oriented up, east, and north respectively and the calculated principal stress axes are denoted by the filled circles labelled 1, 2, and 3.



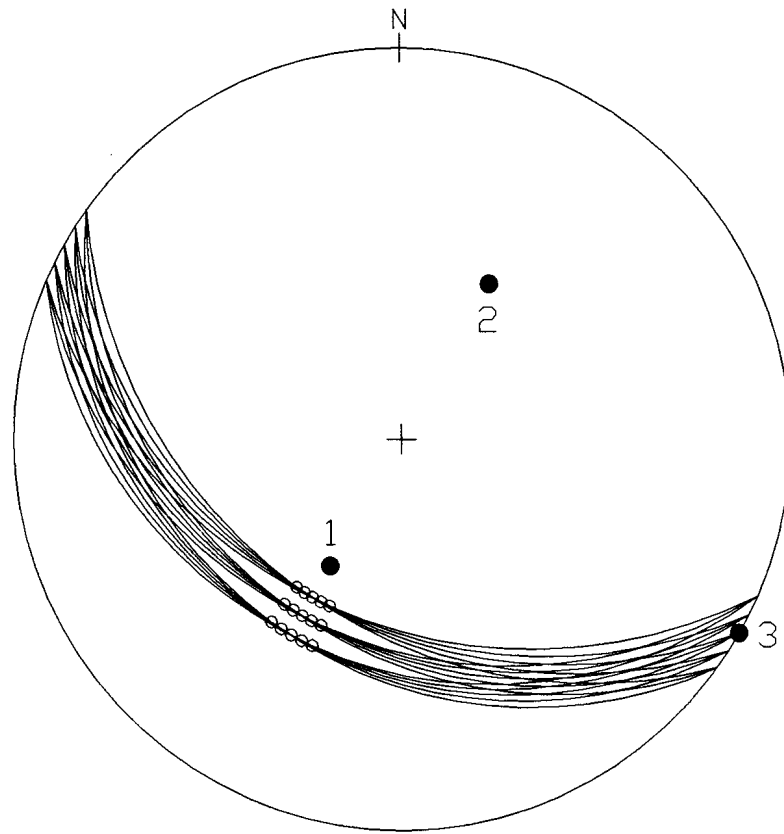
	Known	Program	Error
σ_1	90/000	61/103	29.0°
σ_2	00/090	29/279	30.2°
σ_3	00/000	01/010	10.0°
Φ	0.75	0.746	0.004

Figure 9-89 - Lower-hemisphere stereographic projection and table demonstrating the differences between the known and calculated principal stress axes σ_1 , σ_2 , and σ_3 and the value of Φ for fault population SO-02-75 using Angelier's method of paleostress analysis. In the stereographic projection, the known principal stress axes σ_1 , σ_2 , and σ_3 are oriented up, east, and north respectively and the calculated principal stress axes are denoted by the filled circles labelled 1, 2, and 3.



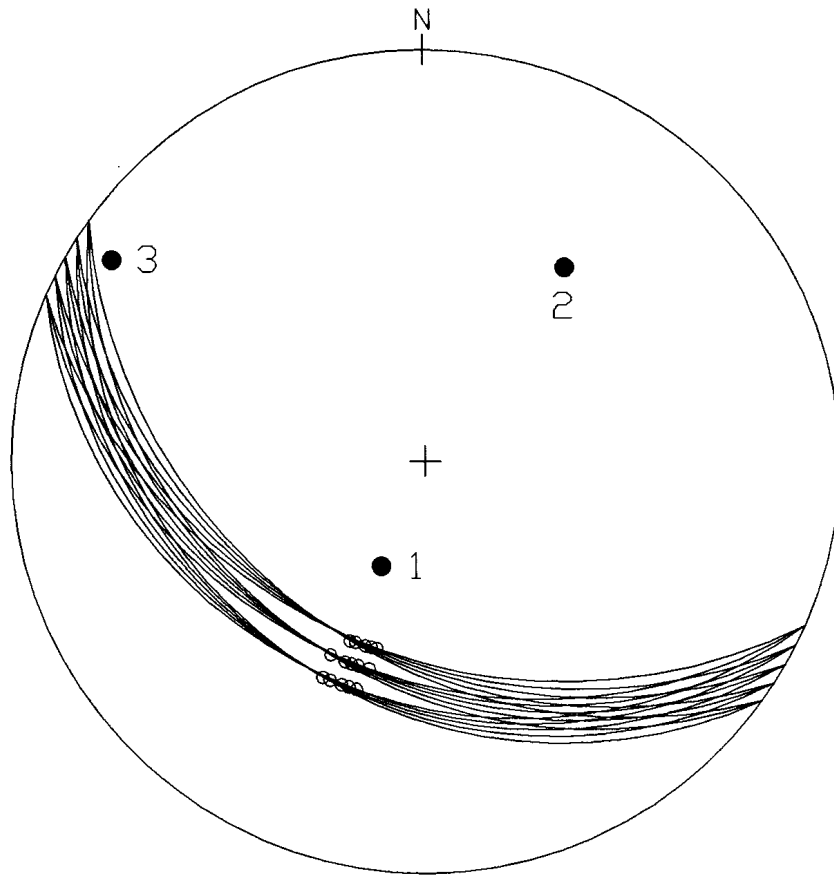
	Known	Program	Error
σ_1	90/000	37/101	53.0°
σ_2	00/090	52/270	52.0°
σ_3	00/000	05/0070	8.6°
Φ	1.00	0.786	0.214

Figure 9-90 - Lower-hemisphere stereographic projection and table demonstrating the differences between the known and calculated principal stress axes σ_1 , σ_2 , and σ_3 and the value of Φ for fault population SO-02-10 using Angelier's method of paleostress analysis. In the stereographic projection, the known principal stress axes σ_1 , σ_2 , and σ_3 are oriented up, east, and north respectively and the calculated principal stress axes are denoted by the filled circles labelled 1, 2, and 3.



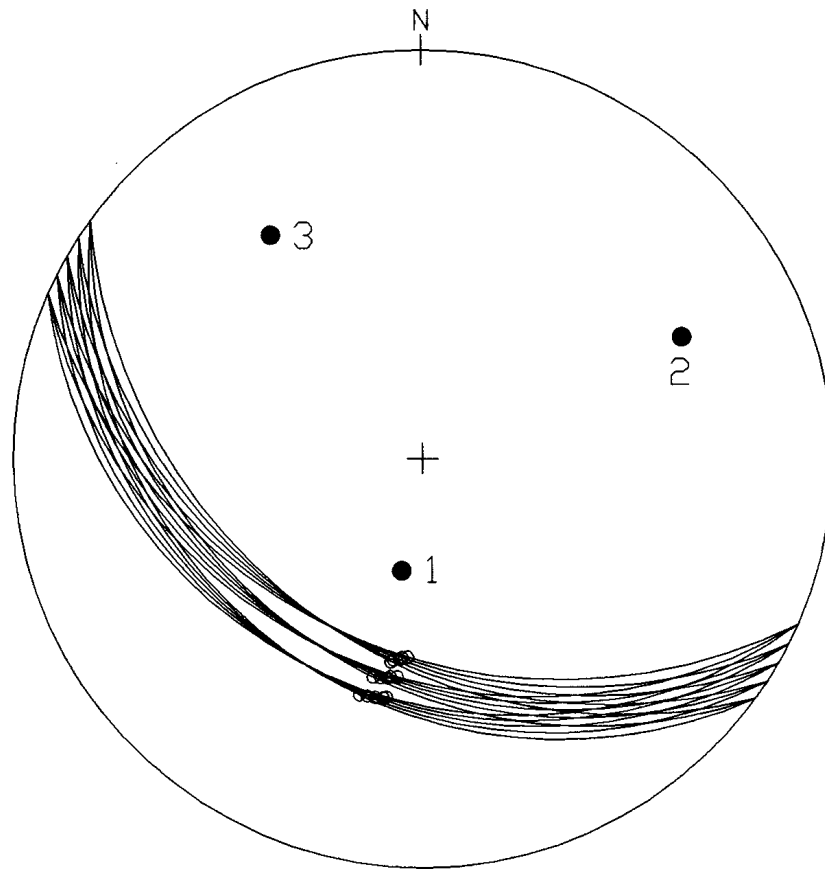
	Known	Program	Error
σ_1	90/000	49/210	41.0°
σ_2	00/090	41/030	67.8°
σ_3	00/000	00/120	60.0°
Φ	0.00	0.202	0.202

Figure 9-91 - Lower-hemisphere stereographic projection and table demonstrating the differences between the known and calculated principal stress axes σ_1 , σ_2 , and σ_3 and the value of Φ for fault population SO-03-00 using Reches' method of paleostress analysis. In the stereographic projection, the known principal stress axes σ_1 , σ_2 , and σ_3 are oriented up, east, and north respectively and the calculated principal stress axes are denoted by the filled circles labelled 1, 2, and 3.



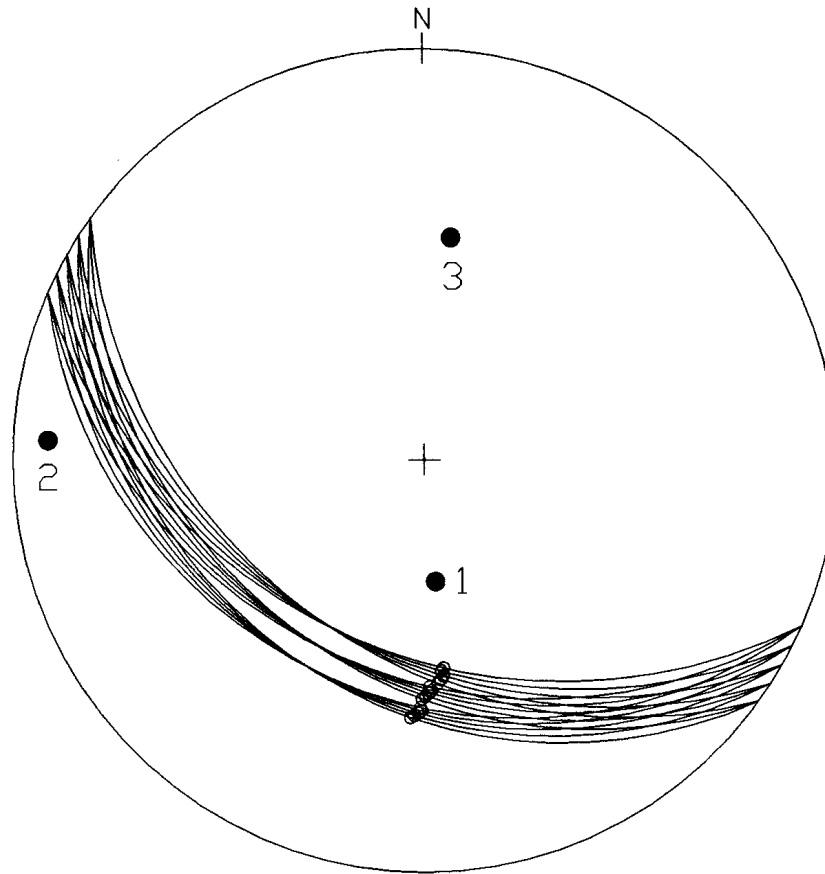
	Known	Program	Error
σ_1	90/000	59/203	31.0°
σ_2	00/090	30/036	59.4°
σ_3	00/000	06/303	57.2°
Φ	0.25	0.191	0.059

Figure 9-92 - Lower-hemisphere stereographic projection and table demonstrating the differences between the known and calculated principal stress axes σ_1 , σ_2 , and σ_3 and the value of Φ for fault population SO-03-25 using Reches' method of paleostress analysis. In the stereographic projection, the known principal stress axes σ_1 , σ_2 , and σ_3 are oriented up, east, and north respectively and the calculated principal stress axes are denoted by the filled circles labelled 1, 2, and 3.



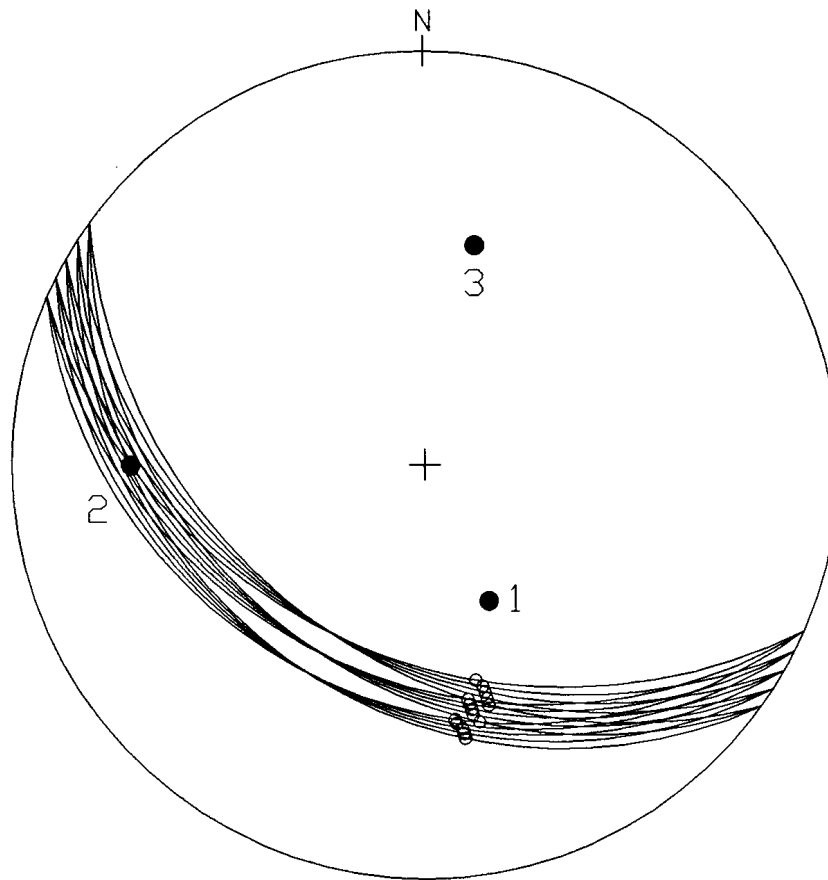
	Known	Program	Error
σ_1	90/000	59/191	31.0°
σ_2	00/090	20/065	31.6°
σ_3	00/000	23/326	40.3°
Φ	0.50	0.082	0.418

Figure 9-93 - Lower-hemisphere stereographic projection and table demonstrating the differences between the known and calculated principal stress axes σ_1 , σ_2 , and σ_3 and the value of Φ for fault population SO-03-50 using Reches' method of paleostress analysis. In the stereographic projection, the known principal stress axes σ_1 , σ_2 , and σ_3 are oriented up, east, and north respectively and the calculated principal stress axes are denoted by the filled circles labelled 1, 2, and 3.



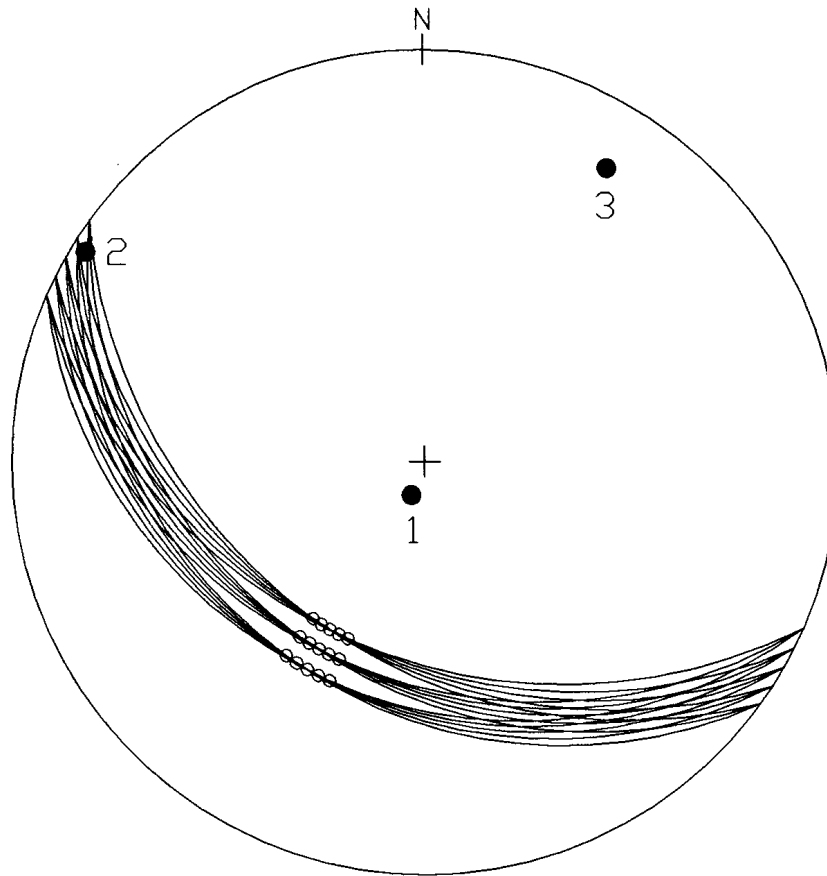
	Known	Program	Error
σ_1	90/000	57/175	33.0°
σ_2	00/090	05/273	5.8°
σ_3	00/000	33/007	33.7°
Φ	0.75	0.207	0.543

Figure 9-94 - Lower-hemisphere stereographic projection and table demonstrating the differences between the known and calculated principal stress axes σ_1 , σ_2 , and σ_3 and the value of Φ for fault population SO-03-75 using Reches' method of paleostress analysis. In the stereographic projection, the known principal stress axes σ_1 , σ_2 , and σ_3 are oriented up, east, and north respectively and the calculated principal stress axes are denoted by the filled circles labelled 1, 2, and 3.



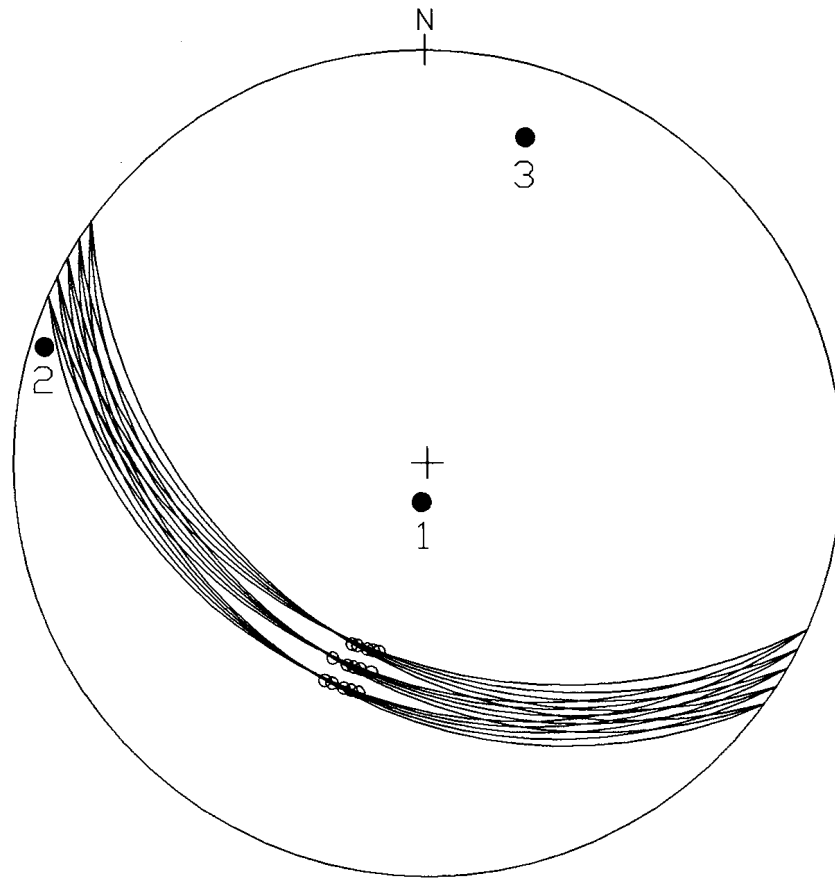
	Known	Program	Error
σ_1	90/000	50/155	40.0°
σ_2	00/090	19/270	19.0°
σ_3	00/000	33/013	35.2°
Φ	1.00	0.408	0.592

Figure 9-95 - Lower-hemisphere stereographic projection and table demonstrating the differences between the known and calculated principal stress axes σ_1 , σ_2 , and σ_3 and the value of Φ for fault population SO-03-10 using Reches' method of paleostress analysis. In the stereographic projection, the known principal stress axes σ_1 , σ_2 , and σ_3 are oriented up, east, and north respectively and the calculated principal stress axes are denoted by the filled circles labelled 1, 2, and 3.



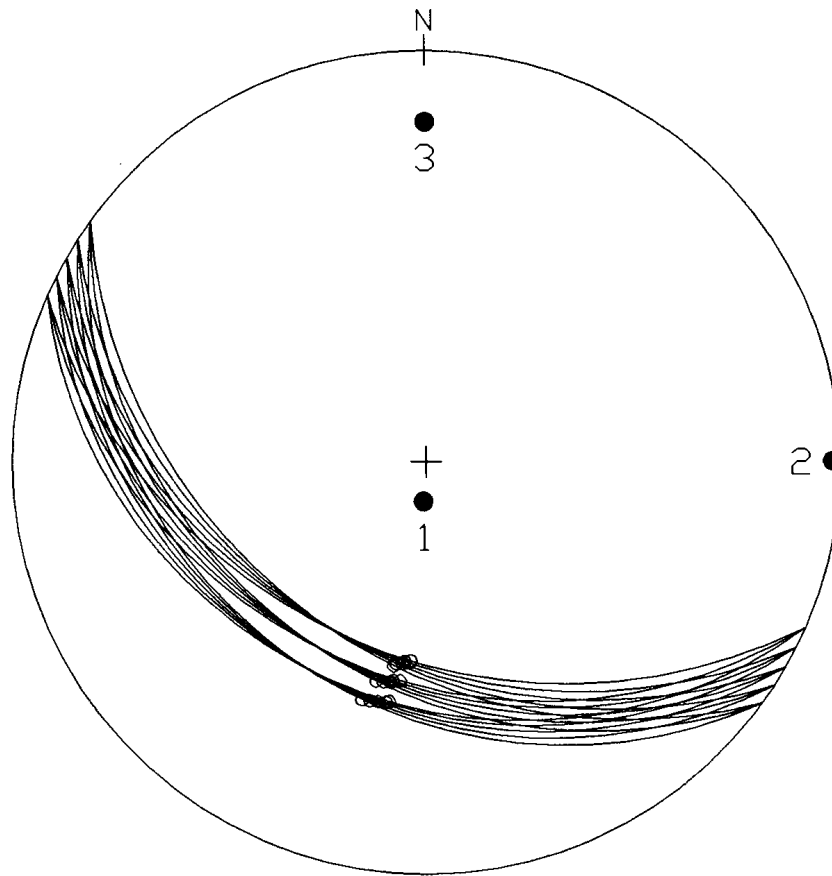
	Known	Program	Error
σ_1	90/000	80/202	10.0°
σ_2	00/090	02/302	32.1°
σ_3	00/000	10/032	33.4°
Φ	0.00	0.000	0.000

Figure 9-96 - Lower-hemisphere stereographic projection and table demonstrating the differences between the known and calculated principal stress axes σ_1 , σ_2 , and σ_3 and the value of Φ for fault population SO-03-00 using Angelier's method of paleostress analysis. In the stereographic projection, the known principal stress axes σ_1 , σ_2 , and σ_3 are oriented up, east, and north respectively and the calculated principal stress axes are denoted by the filled circles labelled 1, 2, and 3.



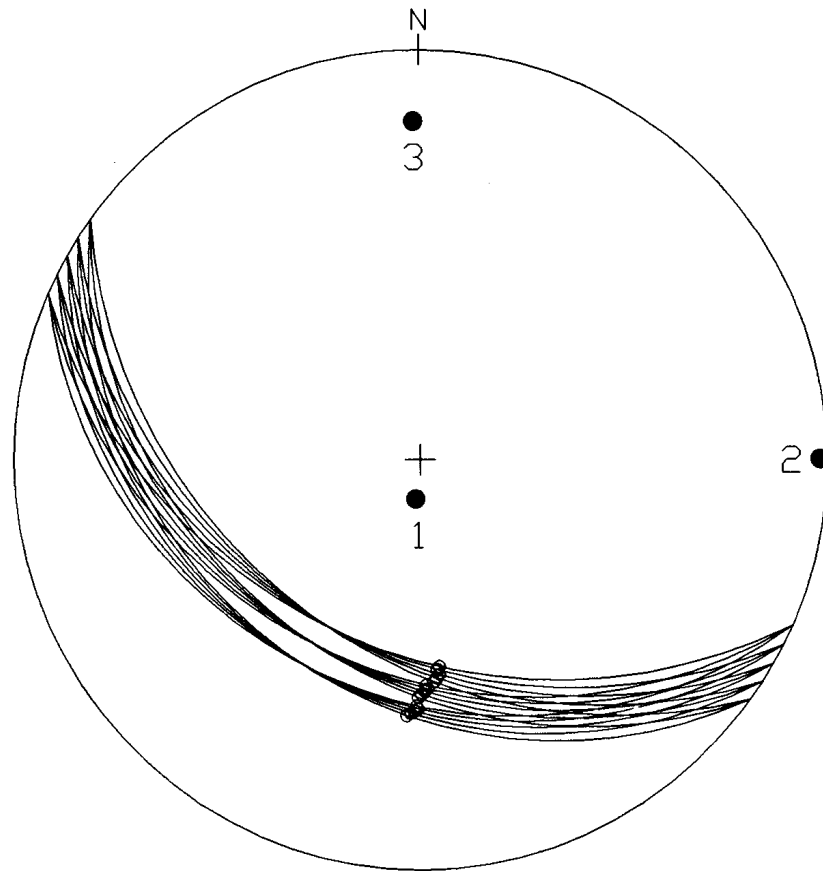
	Known	Program	Error
σ_1	90/000	79/189	11.0°
σ_2	00/090	02/287	17.1°
σ_3	00/000	11/017	20.2°
Φ	0.25	0.190	0.060

Figure 9-97 - Lower-hemisphere stereographic projection and table demonstrating the differences between the known and calculated principal stress axes σ_1 , σ_2 , and σ_3 and the value of Φ for fault population SO-03-25 using Angelier's method of paleostress analysis. In the stereographic projection, the known principal stress axes σ_1 , σ_2 , and σ_3 are oriented up, east, and north respectively and the calculated principal stress axes are denoted by the filled circles labelled 1, 2, and 3.



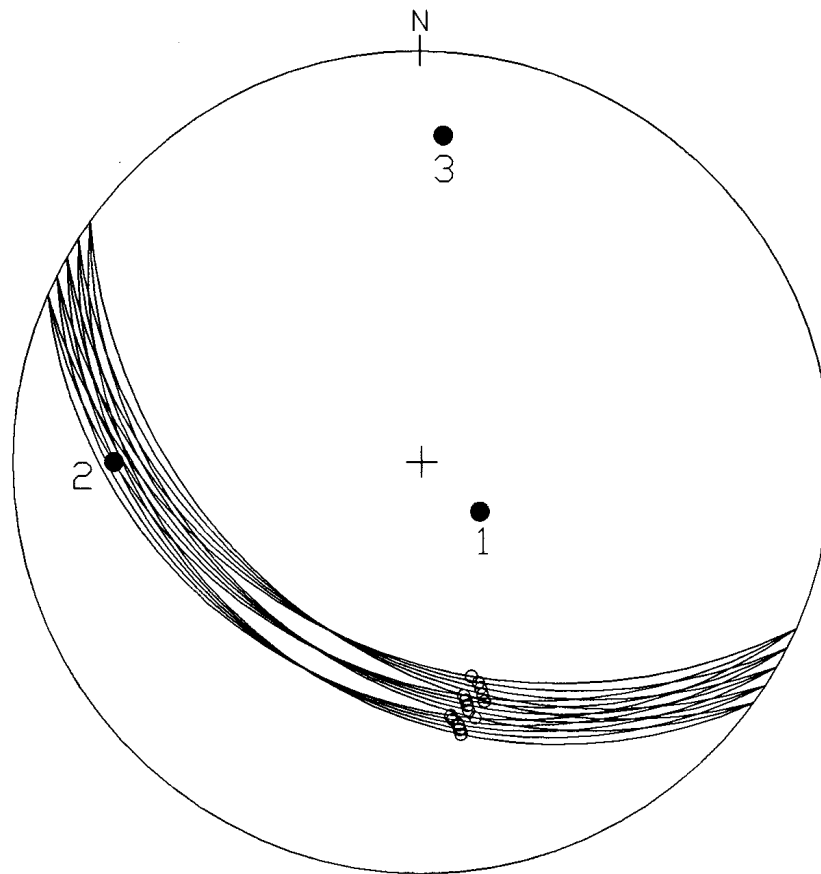
	Known	Program	Error
σ_1	90/000	79/184	11.0°
σ_2	00/090	01/090	1.0°
σ_3	00/000	11/360	11.0°
Φ	0.50	0.299	0.201

Figure 9-98 - Lower-hemisphere stereographic projection and table demonstrating the differences between the known and calculated principal stress axes σ_1 , σ_2 , and σ_3 and the value of Φ for fault population SO-03-50 using Angelier's method of paleostress analysis. In the stereographic projection, the known principal stress axes σ_1 , σ_2 , and σ_3 are oriented up, east, and north respectively and the calculated principal stress axes are denoted by the filled circles labelled 1, 2, and 3.



	Known	Program	Error
σ_1	90/000	79/187	11.0°
σ_2	00/090	01/090	1.0°
σ_3	00/000	11/359	11.0°
Φ	0.75	0.584	0.166

Figure 9-99 - Lower-hemisphere stereographic projection and table demonstrating the differences between the known and calculated principal stress axes σ_1 , σ_2 , and σ_3 and the value of Φ for fault population SO-03-75 using Angelier's method of paleostress analysis. In the stereographic projection, the known principal stress axes σ_1 , σ_2 , and σ_3 are oriented up, east, and north respectively and the calculated principal stress axes are denoted by the filled circles labelled 1, 2, and 3.



	Known	Program	Error
σ_1	90/000	69/130	21.0°
σ_2	00/090	16/270	16.0°
σ_3	00/000	13/004	13.6°
Φ	1.00	0.865	0.135

Figure 9-100 - Lower-hemisphere stereographic projection and table demonstrating the differences between the known and calculated principal stress axes σ_1 , σ_2 , and σ_3 and the value of Φ for fault population SO-03-10 using Angelier's method of paleostress analysis. In the stereographic projection, the known principal stress axes σ_1 , σ_2 , and σ_3 are oriented up, east, and north respectively and the calculated principal stress axes are denoted by the filled circles labelled 1, 2, and 3.

		Reches'	Angelier's	Deviation
Known Φ of 0.00	σ_1	66/225	77/047	37.0°
	σ_2	24/045	01/313	88.6°
	σ_3	00/315	13/223	88.1°
	Φ	0.045	0.130	0.085
Known Φ of 0.25	σ_1	81/175	77/051	19.5°
	σ_2	01/272	07/285	14.3°
	σ_3	09/002	10/194	22.4°
	Φ	0.110	0.252	0.142
Known Φ of 0.50	σ_1	70/148	75/082	19.3°
	σ_2	15/287	14/284	3.1°
	σ_3	13/020	05/192	19.7°
	Φ	0.275	0.615	0.340
Known Φ of 0.75	σ_1	55/135	61/103	17.8°
	σ_2	30/282	29/279	2.8°
	σ_3	16/021	01/010	18.5°
	Φ	0.464	0.746	0.282
Known Φ of 1.00	σ_1	34/123	37/101	18.1°
	σ_2	52/270	52/270	0.0°
	σ_3	17/022	05/007	19.0°
	Φ	0.469	0.786	0.317

Table 9-9 - Table demonstrating the deviation for the orientations of the σ_1 , σ_2 , and σ_3 principal stress axes and the principal stress magnitude ratio Φ between Reches' and Angelier's methods of paleostress analysis on fault population SO-02 at five different values of Φ .

		Reches'	Angelier's	Deviation
Known Φ of 0.00	σ_1	49/210	80/202	36.1°
	σ_2	41/030	02/302	87.2°
	σ_3	00/120	10/032	88.0°
	Φ	0.202	0.000	0.202
Known Φ of 0.25	σ_1	59/203	79/189	20.5°
	σ_2	30/036	02/287	74.7°
	σ_3	06/303	11/017	73.2°
	Φ	0.191	0.190	0.001
Known Φ of 0.50	σ_1	59/191	79/184	20.1°
	σ_2	20/065	01/090	31.0°
	σ_3	23/326	11/360	34.5°
	Φ	0.082	0.299	0.217
Known Φ of 0.75	σ_1	57/175	79/187	22.3°
	σ_2	05/273	01/090	6.7°
	σ_3	33/007	11/359	23.2°
	Φ	0.202	0.584	0.382
Known Φ of 1.00	σ_1	50/155	69/130	22.5°
	σ_2	19/270	16/270	3.0°
	σ_3	33/013	13/004	21.6°
	Φ	0.408	0.865	0.457

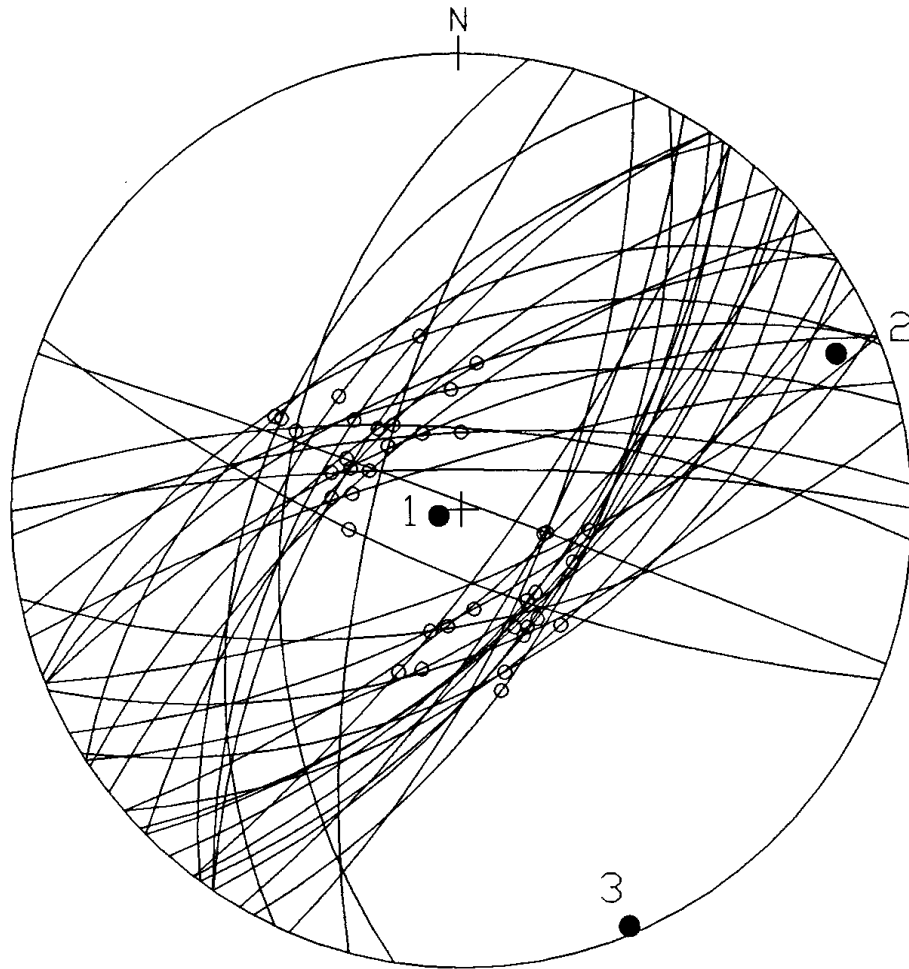
Table 9-10 - Table demonstrating the deviation for the orientations of the σ_1 , σ_2 , and σ_3 principal stress axes and the principal stress magnitude ratio Φ between Reches' and Angelier's methods of paleostress analysis on fault population SO-01 at five different values of Φ .

9.4 Other Test Results

The paleostress analysis programs were next checked for their sensitivity to a variability in the orientations of the fault planes and in the pitch angles of the slip vectors. This was done by arbitrarily changing the orientations of one or more of the fault datums and then recalculating the paleostress tensor for that population. These tests were done with the RP-01, RP-02, and RP-03 fault populations. The preliminary results indicate that the programs are not very sensitive to minor changes ($\pm 5^\circ$) in either the strike, dip, or pitch angles of the fault data.

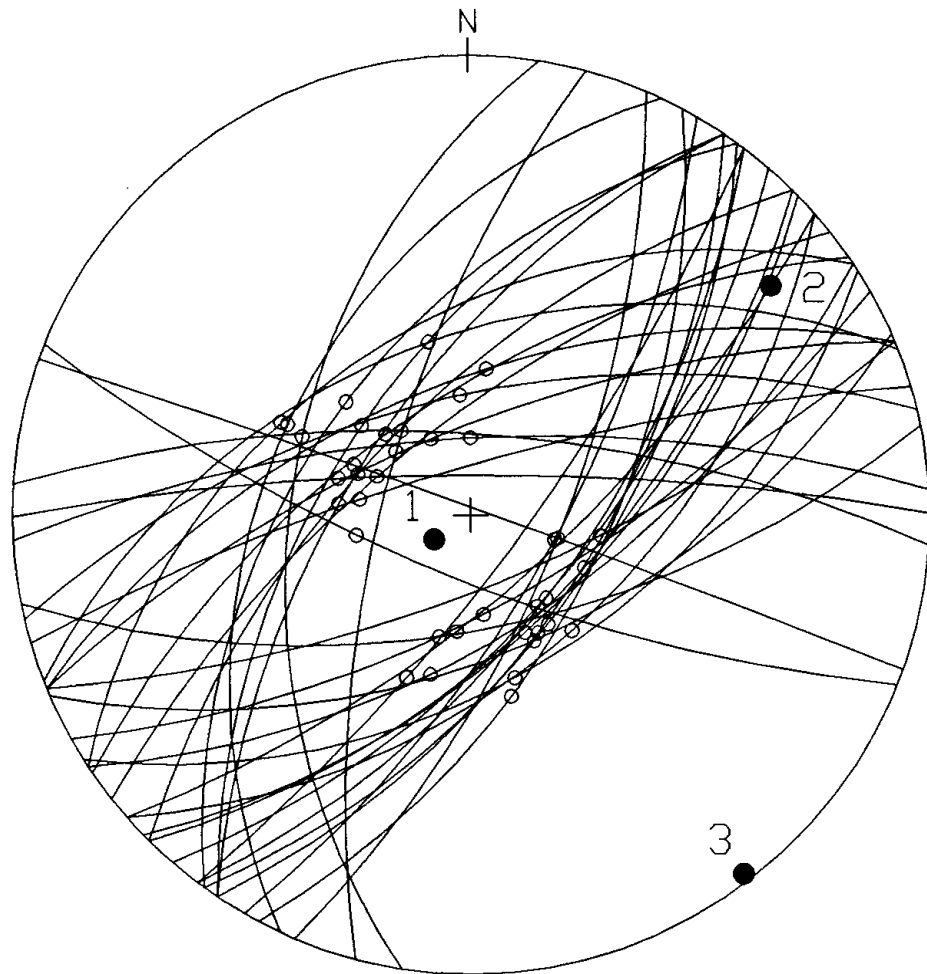
The paleostress analysis programs were also checked for their sensitivity for randomly inserting or removing a fault plane from the population. These tests were performed on all of the fault populations discussed. Adding or removing a fault plane from a population usually had little effect except in cases where the fault planes were parallel to one of the principal planes or if they were the only fault planes at some specific orientation which was sufficiently far from the other fault planes.

In general, the two paleostress analysis programs tested returned consistent results (with some notable exceptions). This is important since if two separate programs return widely differing results, then one or both of them are wrong.



	Known	Program	Error
σ_1	?	84/255	?
σ_2	?	06/068	?
σ_3	?	01/158	?
Φ	?	0.050	?

Figure 9-101 - Lower-hemisphere stereographic projection and table showing the calculated principal stress axes σ_1 , σ_2 , and σ_3 and the value of Φ for fault population FD-01-00 using Reches' method of paleostress analysis. [38 Neogene-age normal faults from central Crete (Angelier, 1979); see p. 173, and Table 8-1, p. 175]



	Known	Program	Error
σ_1	?	79/237	?
σ_2	?	11/053	?
σ_3	?	01/143	?
Φ	?	0.225	?

Figure 9-102 - Lower-hemisphere stereographic projection and table showing the calculated principal stress axes σ_1 , σ_2 , and σ_3 and the value of Φ for fault population FD-01-00 using Angelier's method of paleostress analysis. [38 Neogene-age normal faults from central Crete (Angelier, 1979); see p. 173, and Table 8-1, p. 175]

CHAPTER 10

CONCLUSIONS

Now that the rationale for the tests, the testing procedures, and the test results have been explained, it is time to put it all together.

10.1 What do the Results Mean?

One may draw several conclusions from the data presented in chapter 9.

1. The two methods of paleostress analysis examined seem to work fairly well for fault populations with moderately-scattered faults such as those in populations RP-01, RP-02, and RP-03. A population of faults with some scatter evidently acts to constrain the possible positions of the principal stress axes. With such fault populations, the programs seemed to return better stress axes orientations and better calculated values of Φ for cases where Φ was not equal to 0.0 or 1.0. This is reasonable since it is impossible to distinguish between two of the stress axes when they have the same magnitudes (*i.e.* at $\Phi = 0.0$, $\sigma_2 = \sigma_3$ and at $\Phi = 1.0$, $\sigma_2 = \sigma_1$).
2. The two methods of paleostress analysis examined seemed not to work very well for special-case fault populations. This is most-likely due to the fact that such populations can not well-constrain the paleostress axes (chapter 2). While such special-case populations would probably never be used for a paleostress analysis, more work is needed to determine if conjugate or orthorhombic fault sets within moderately-scattered fault populations would have an adverse effect.

3. The two methods of paleostress analysis examined seemed to be fairly immune to mild measurement errors and a small amount of extraneous data. Much of the sensitivity is a result of exactly which planes are removed or added and more work is needed to quantify this. This is needed in order for people who use paleostress analysis programs to realize what type of accuracy their results have. The calculation of error cones around the returned principal stress axes would be a useful addition to paleostress programs.

4. Finally, the two paleostress analysis programs examined seemed to compare to one another fairly well. The results returned for most populations were close enough for either program to be used with approximately equal accuracy. The exceptions to this were when one or the other of the programs "blew up" (as in the case of conjugate fault sets) and returned totally incorrect data. More work is needed to see if these favorable comparisons hold up with additional tests.

In most regards, Reches' and Angelier's methods of paleostress analysis seemed to perform fairly well. Caution must be used when applying these methods, however, and more systematic tests are needed to further outline the two program's limitations for certain types of fault populations.

10.2 Practical Problems in Evaluating Paleostress Analysis Programs

There are several important practical problems which may arise when attempting to compare and evaluate paleostress analysis programs. A few of them are listed below.

1. When using a program written by someone else for performing paleostress analysis

techniques, one must be sure that the program does what it's supposed to do. It is virtually impossible to test a program such that one will have 100% confidence in its performance. Therefore, it is usually advisable to carefully check the program's source code for any possible errors. This may be an extremely difficult and time-consuming project since programmers may not write their source code in a clear and consistent manner. Poorly documented programs may be almost impossible to read and understand since the source code for paleostress analysis programs may easily run into hundreds of printed pages. There is also the problem of programmers who will **not** allow you to see their source code (such as Angelier). One must then make a decision as to whether or not to use their program. Since published field studies have made use of Angelier's method "as is", I chose to test it even though I had no access to the original source code. A possible way around this problem might be to write your own paleostress analysis programs based upon their published mathematical algorithms. Since such programs would often use similar procedures, a modular and highly-structured programming language such as C would be preferable to most others since that would allow the sharing of many subroutines by several different programs. A drawback of this solution, however, is that it would be very time-consuming and also somewhat frustrating since published descriptions of the mathematical algorithms used by paleostress analysis programs are not always clear and easy to follow. It is obviously a less-appealing prospect than obtaining a working (and presumably tested) program from someone else.

2. Closely related to the above problem is that paleostress analysis programs are written in many different computer languages for several different types of computers. I have programs written in FORTRAN for an IBM PC, BASIC for an IBM PC, FORTRAN for a Macintosh II, FORTRAN for a VAX-8650 mainframe, and a

paleostress analysis program called ROMSA from Lisle (1988) in an odd version of BASIC that does not seem to run correctly on any computer I've used. When comparing programs written in different languages for different machines, it is difficult to determine if an error is due to the mathematical algorithm used, the language used, or the machine used. Different languages and machines will have their own ways of truncating numbers, rounding-off numbers, and error handling.

3. When a paleostress analysis program returns an incorrect result, it is difficult to evaluate the source of that error. Is the error a mechanical error (a plus sign where there should be a minus sign in the program) or the result of an inherent flaw in the technique? Did the error arise as a result of the mathematical techniques used or because the initial assumptions underlying the whole concept are incorrect. These are very difficult problems to address and only by thorough testing can they be evaluated.
4. Another problem faced when attempting to compare various methods of paleostress analysis is that most of them, based upon personal experience, require their initial fault-slip data to be formatted in different ways. Should the fault orientation data be entered as a strike, dip, and dip direction for each fault plane or as a strike and dip for each fault plane where the strike is assumed to follow a right-hand rule (the strike is the trend of the fault's pole + 90°) or simply as a plunge and trend for the pole to each fault plane? Should the orientations of the striations on the fault plane be entered as pitch angles or as plunge and trend values or simply as a trend (since the plunge will be constrained by the fault's orientation)? Should the fault's sense of slip be given as up, down, left, or right or should it be specified by the pitch angle of the striations or should it be given as a clockwise or counterclockwise rotation about some axis? Finally, should the fault data be assigned some type of weighting scheme?

Everyone writing paleostress analysis programs has their own preferences and, unfortunately, they never seem to correspond. A way around this mess would be to write all of the analysis programs yourself and use a consistent scheme for entering the data -- this option has the drawbacks listed in number 1 above. Another possible solution is to write a program to do the conversions and then write the converted data to an input file for each type of analysis program used. Such a program would have the advantage of receiving data in any format you were comfortable with and automatically converting it for you. Doing all of the conversions by hand for several different paleostress analysis methods can be extremely time-consuming and is obviously more prone to random errors than is an automated conversion system.

5. Using programs written by someone else has other problems as well. I've received paleostress analysis programs with several pages of fairly clear documentation, I've received programs with several pages of documentation in French, and I've received programs with absolutely no documentation whatsoever. Attempting to use undocumented programs is a "trial and error" procedure which involves much wasted time and effort. Angelier's program (chapter 6) is probably the worst in that regard. I found his program to be exceedingly difficult to use -- even after having experience with several other methods of paleostress analysis. It was an undocumented, compiled program with unclear and misleading interactive prompts and I found it to be very counter-intuitive in the way it worked. The program using Reches' method of paleostress analysis which was written by Kenneth Hardcastle (chapter 7), on the other hand, was very easy to use. Most paleostress analysis programs lie between those two extremes.

6. Some methods of paleostress analysis are very computationally-intensive. Gephart and

Forsyth's method (1984) was not examined in my study for the simple reason that a population of 20 faults takes a full 24-hour day to run! Testing dozens of such faults (especially without owning an appropriate computer) is a major project. Testing non-linear inversion methods, such as Angelier's, may also be very time-intensive for large fault populations. As faults are added to the populations arithmetically, the time needed to perform an analysis increases exponentially due to the mathematics involved in performing matrix inversions (where the matrices may have a rank of $2n$ where n is the number of faults in the population examined).

7. Since most of the pioneers in paleostress analysis are French, many of the important papers and even some of the program documentation is written in that language. If one does not possess a reading knowledge of French, it is difficult to learn all that one should about paleostress analysis techniques. I was fortunate in having access to someone (Debra Lenard of SUNY Albany) who was able to translate French technical papers into English without too much difficulty. The process did, however, take some time and effort.

8. Finally, it is very difficult to choose artificial fault populations for testing the various methods of paleostress analysis. Since an infinite variety of populations may be created, careful thought must go into the problem. Obviously, it is desirable to test special-cases (*e.g.* a population containing a fault plane parallel to one of the principal stress axes) and geologically-realistic fault populations (*e.g.* orthorhombic symmetry fault sets). Every possible type of fault population can not be tested, however, so the best one may hope for is to be able to formulate general rules or guidelines for using paleostress analysis techniques (*e.g.* stating that method A is better for testing small populations of faults while method B is better for larger ones or method C can not be

used for fault populations containing conjugate sets of faults, etc.).

Anticipating the obligatory question "If you had to do it all over again, what would you do differently?", I would reply as follows. If I had to do it all over again, I would first take the time to write my own computer programs -- in a language such as C and for an IBM PC -- to perform several different methods of paleostress analysis. The programs would read the data from a single type of ASCII fault-slip data file and write the results in a standardized format. Once this were done (not a trivial task), the testing of these methods would be much easier than it is by using other people's programs. I had no way of knowing this, however, before I began this study.

10.3 Suggestions for Future Work

There is a great need for more work on the problems of paleostress analysis. As more people use paleostress analysis programs, such as those written by Angelier, a greater need exists for people to evaluate their effectiveness. While Angelier may be aware of the limitations of his method, those who use his program may not be. I realize that this thesis study is only a beginning in the systematic examination of paleostress analysis, but at least it's a beginning. Since the obvious time constraints for my thesis defense have prevented me from including much more of the preliminary data I've gathered, I plan to continue with the analyses of these paleostress programs (possibly with the addition of one or two more such as Etchecopar's method and/or Gephart and Forsyth's method) with the goal of sending the results for publication before the summer of 1991.

The major suggestion I would leave for anyone (including myself) planning to further examine paleostress analysis techniques, is to do what I outlined in the previous section. Write the programs yourself and standardize them. I would also suggest quantifying graphical

methods of paleostress analysis such as Lisle's (1988) so that they may be run on a computer as well. Finally, the comparison of the dynamic paleostress analysis techniques to the various kinematic analysis techniques which have been proposed (Marrett and Allmendinger, 1990) is sure to yield some fruitful insights into the mechanics of faulting and the relationships between stress and strain.

APPENDIX A
GLOSSARY OF SYMBOLS

The following is a list of mathematical symbols used in this thesis. The symbols are listed in alphabetical order with the Latin alphabet listed before the Greek alphabet. Arbitrary constants are not listed and in cases where the same symbol has been used in two different contexts, both are listed separately.

C_0	=	Cohesion term of the Coulomb failure criterion
d	=	Trend of a fault plane's dip direction
F_N	=	Normal force acting upon a plane
F_S	=	Shear force acting upon a plane
F_T	=	Total force acting upon a plane
i	=	Pitch angle of a fault plane's slip vector
l_i	=	Direction cosine where $i = 1, 2, \text{ or } 3$
l	=	Direction cosine equivalent to l_1
l_e	=	Direction cosine between a fault normal and east
l_n	=	Direction cosine between a fault normal and north
l_u	=	Direction cosine between a fault normal and the vertical axis
m	=	Direction cosine equivalent to l_2
N	=	Normal force acting upon a plane
\mathbf{N}	=	Normal vector to a fault plane
n	=	Normal force acting upon a plane
n	=	Direction cosine equivalent to l_3
\mathbf{O}	=	Normal vector to a movement plane
p	=	A fault plane's dip angle

R	=	Ratio of the principal stress axes
r	=	Pitch of a slip vector on a plane
S	=	Shear force acting upon a plane
S	=	Slip vector in a fault plane
s	=	Shear force acting upon a plane
T	=	Total stress vector acting upon a plane
T_i	=	Total stress vector component i where i = 1, 2, or 3
t₁	=	A positive constant
t₂	=	A positive constant
α	=	The shear stress term $\sigma_{1,2}$ or $\sigma_{2,1}$
β	=	The shear stress term $\sigma_{2,3}$ or $\sigma_{3,2}$
γ	=	The shear stress term $\sigma_{1,3}$ or $\sigma_{3,1}$
δ	=	Tensor aspect ratio of the principal stress axes
δ	=	Dip angle of a plane
ε	=	Measurement error
ε₀	=	Difference between average strike and true strike
ε_S	=	Strike measurement error
ε_T	=	Trend measurement error
μ	=	Coefficient of friction term of the Coulomb failure criterion
σ^x	=	The standard deviation of a variable x
σ	=	The geologic stress tensor
σ'	=	The reduced geologic stress tensor
σ₁	=	Most compressive principal stress axis
σ₂	=	Intermediate principal stress axis

σ_3	=	Least compressive principal stress axis
σ_{ij}	=	Stress tensor component (i,j) where i and j = 1, 2, or 3
σ_n	=	Normal stress acting upon a plane
σ_s	=	Shear stress acting upon a plane
σ_x	=	Principal stress axis in the X-direction
σ_y	=	Principal stress axis in the Y-direction
σ_z	=	Principal stress axis in the Z-direction
Φ	=	Ratio of the principal stress axes
ψ	=	Angular measure modulo 2π

APPENDIX B

ARTIFICIAL FAULT POPULATION DATA

This is a listing of all the artificial fault population data shown in stereographic projection in chapter 8. The change in slip vector orientations is shown for each of the five values of Φ examined (0.00, 0.25, 0.50, 0.75, 1.00) and the format for each fault datum is:

46 192 86

where 46° is the plunge of the fault's normal vector, 192° is the trend of the fault's normal vector, and 86° is the pitch of the slip vector. The pitch angle is the angle, in the plane of the fault, between the strike vector and the slip vector. The strike vector points in the direction defined by the trend of the fault plane's normal vector + 90° (*i.e.* 282°). A pitch is negative if the angle is measured from the opposite side of the strike vector (*i.e.* the trend of the fault plane's normal vector - 90°). All of the faults are normal faults so no additional information is needed regarding sense-of-slip.

RP-01 FAULT POPULATION

$\Phi = 0.00$	$\Phi = 0.25$	$\Phi = 0.50$	$\Phi = 0.75$	$\Phi = 1.00$
46 192 90	46 192 86	46 192 82	46 192 78	46 192 74
27 014 90	27 014 83	27 014 75	27 014 68	27 014 61
52 025 90	52 025 83	52 025 75	52 025 67	52 025 59
41 331 90	41 331 -80	41 331 -70	41 331 -59	41 331 -50
39 326 90	39 326 -79	39 326 -66	39 326 -54	39 326 -43
23 023 90	23 023 77	23 023 64	23 023 52	23 023 43
35 013 90	35 013 84	35 013 79	35 013 73	35 013 68
25 340 90	25 340 -79	25 340 -68	25 340 -58	25 340 -49
31 339 90	31 339 -80	31 339 -71	31 339 -62	31 339 -53
38 211 90	38 211 79	38 211 68	38 211 56	38 211 46
55 036 90	55 036 81	55 036 71	55 036 60	55 036 48
40 054 90	40 054 78	40 054 61	40 054 43	40 054 25
49 018 90	49 018 84	49 018 78	49 018 73	49 018 67
34 221 90	34 221 76	34 221 61	34 221 43	34 221 33
58 040 90	58 040 81	58 040 70	58 040 58	58 040 45
36 024 90	36 024 81	36 024 71	36 024 62	36 024 53
41 030 90	41 030 80	41 030 69	41 030 59	41 030 49
26 329 90	26 329 -75	26 329 -60	26 329 -47	26 329 -36

RP-02 FAULT POPULATION

$\Phi = 0.00$	$\Phi = 0.25$	$\Phi = 0.50$	$\Phi = 0.75$	$\Phi = 1.00$
36 002 90	36 002 89	36 002 88	36 002 87	36 002 87
24 022 90	24 022 78	24 022 65	24 022 54	24 022 45
58 143 90	58 143 -81	58 143 -71	58 143 -60	58 143 -48
61 030 90	61 030 82	61 030 74	61 030 65	61 030 57
28 232 90	28 232 73	28 232 53	28 232 35	28 232 20
51 359 90	51 359 90	51 359 90	51 359 -89	51 359 -89
56 220 90	56 220 81	56 220 89	56 220 57	56 220 45
35 205 90	35 205 80	35 205 69	35 205 60	35 205 51
65 184 90	65 184 89	65 184 88	65 184 87	65 184 86
40 220 90	40 220 78	40 220 64	40 220 50	40 220 37
60 152 90	60 152 -83	60 152 -75	60 152 -67	60 152 -58
36 342 90	36 342 -83	36 342 -75	36 342 -68	36 342 -61
32 336 90	32 336 -80	32 336 -69	32 336 -59	32 336 -50
50 136 90	50 136 -79	50 136 -67	50 136 -53	50 136 -38
31 169 90	31 169 -85	31 169 -80	31 169 -74	31 169 -69
53 139 90	53 139 -80	53 139 -68	53 139 -56	53 139 -43
28 235 90	28 235 73	28 235 53	28 235 34	28 235 18
50 138 90	50 138 -80	50 138 -67	50 138 -40	50 138 -40

RP-03 FAULT POPULATION

$\Phi = 0.00$	$\Phi = 0.25$	$\Phi = 0.50$	$\Phi = 0.75$	$\Phi = 1.00$
25 028 90	25 028 75	25 028 61	25 028 49	25 028 38
38 312 90	38 312 -77	38 312 -61	38 312 -44	38 312 -29
35 031 90	35 031 78	35 031 66	35 031 54	35 031 44
64 349 90	64 349 -87	64 349 -84	64 349 -81	64 349 -78
25 313 90	25 313 -71	25 313 -51	25 313 -34	25 313 -22
60 152 90	60 152 -83	60 152 -75	60 152 -67	60 152 -58
31 344 90	31 344 -83	31 344 -75	31 344 -68	31 344 -61
52 182 90	52 182 89	52 182 89	52 182 88	52 182 87
30 148 90	30 148 -76	30 148 -62	30 148 -50	30 148 -39
43 219 90	43 219 79	43 219 66	43 219 53	43 219 40
53 319 90	53 319 -80	53 319 -68	53 319 -56	53 319 -43
25 046 90	25 046 71	25 046 51	25 046 35	25 046 22
35 049 90	35 049 76	35 049 59	35 049 42	35 049 27
61 188 90	61 188 88	61 188 85	61 188 83	61 188 81
43 305 90	43 305 -78	43 305 -63	43 305 -44	43 305 -26
31 336 90	31 336 -79	31 336 -69	31 336 -53	31 336 -49
31 353 90	31 353 -87	31 353 -83	31 353 -80	31 353 -77
26 296 90	26 296 -74	26 296 -53	26 296 -30	26 296 -12

AC-01 FAULT POPULATION

$\Phi = 0.00$	$\Phi = 0.25$	$\Phi = 0.50$	$\Phi = 0.75$	$\Phi = 1.00$
30 000 90	30 000 90	30 000 90	30 000 90	30 000 90
30 005 90	30 005 88	30 005 85	30 005 83	30 005 80
30 355 90	30 355 -88	30 355 -85	30 355 -83	30 355 -80
30 180 90	30 180 90	30 180 90	30 180 90	30 180 90
30 175 90	30 175 -88	30 175 -85	30 175 -83	30 175 -80
30 185 90	30 185 88	30 185 85	30 185 83	30 185 80
25 000 90	25 000 90	25 000 90	25 000 90	25 000 90
25 005 90	25 005 87	25 005 84	25 005 81	25 005 78
25 355 90	25 355 -87	25 355 -84	25 355 -81	25 355 -78
25 180 90	25 180 90	25 180 90	25 180 90	25 180 90
25 175 90	25 175 -87	25 175 -84	25 175 -81	25 175 -78
25 185 90	25 185 87	25 185 84	25 185 81	25 185 78
35 000 90	35 000 90	35 000 90	35 000 90	35 000 90
35 005 90	35 005 88	35 005 86	35 005 83	35 005 81
35 355 90	35 355 -88	35 355 -86	35 355 -83	35 355 -81
35 180 90	35 180 90	35 180 90	35 180 90	35 180 90
35 175 90	35 175 -88	35 175 -86	35 175 -83	35 175 -81
35 185 90	35 185 88	35 185 86	35 185 83	35 185 81

AC-02 FAULT POPULATION

$\Phi = 0.00$	$\Phi = 0.25$	$\Phi = 0.50$	$\Phi = 0.75$	$\Phi = 1.00$
30 135 90	30 135 -74	30 135 -56	30 135 -40	30 135 -27
30 140 90	30 140 -75	30 140 -58	30 140 -43	30 140 -31
30 130 90	30 130 -74	30 130 -55	30 130 -37	30 130 -23
30 315 90	30 315 -74	30 315 -56	30 315 -40	30 315 -27
30 310 90	30 310 -74	30 310 -55	30 310 -37	30 310 -23
30 320 90	30 320 -75	30 320 -58	30 320 -43	30 320 -31
25 135 90	25 135 -71	25 135 -52	25 135 -35	25 135 -23
25 140 90	25 140 -72	25 140 -54	25 140 -38	25 140 -27
25 130 90	25 130 -71	25 130 -51	25 130 -33	25 130 -20
25 315 90	25 315 -71	25 315 -52	25 315 -35	25 315 -23
25 310 90	25 310 -71	25 310 -51	25 310 -33	25 310 -20
25 320 90	25 320 -72	25 320 -54	25 320 -38	25 320 -27
35 135 90	35 135 -76	35 135 -60	35 135 -44	35 135 -30
35 140 90	35 140 -77	35 140 -62	35 140 -47	35 140 -34
35 130 90	35 130 -76	35 130 -59	35 130 -41	35 130 -26
35 315 90	35 315 -76	35 315 -60	35 315 -44	35 315 -30
35 310 90	35 310 -76	35 310 -59	35 310 -41	35 310 -26
35 320 90	35 320 -77	35 320 -62	35 320 -47	35 320 -34

OS-01 FAULT POPULATION

$\Phi = 0.00$	$\Phi = 0.25$	$\Phi = 0.50$	$\Phi = 0.75$	$\Phi = 1.00$
30 045 90	30 045 74	30 045 56	30 045 40	30 045 27
30 135 90	30 135 -74	30 135 -56	30 135 -40	30 135 -27
30 225 90	30 225 74	30 225 56	30 225 40	30 225 27
30 315 90	30 315 -74	30 315 -56	30 315 -40	30 315 -27
30 050 90	30 050 74	30 050 55	30 050 37	30 050 23
30 040 90	30 040 75	30 040 58	30 040 43	30 040 31
25 045 90	25 045 71	25 045 52	25 045 35	25 045 23
35 045 90	35 045 76	35 045 60	35 045 44	35 045 30
30 130 90	30 130 -74	30 130 -55	30 130 -37	30 130 -23
30 140 90	30 140 -75	30 140 -58	30 140 -43	30 140 -31
25 135 90	25 135 -71	25 135 -52	25 135 -35	25 135 -23
35 135 90	35 135 -76	35 135 -60	35 135 -44	35 135 -30
30 220 90	30 220 75	30 220 58	30 220 43	30 220 31
30 230 90	30 230 74	30 230 55	30 230 37	30 230 23
25 225 90	25 225 71	25 225 52	25 225 35	25 225 23
35 225 90	35 225 76	35 225 60	35 225 44	35 225 30
30 310 90	30 310 -74	30 310 -55	30 310 -37	30 310 -23
30 320 90	30 320 -75	30 320 -58	30 320 -43	30 320 -31
25 315 90	25 315 -71	25 315 -52	25 315 -35	25 315 -23
35 315 90	35 315 -76	35 315 -60	35 315 -44	35 315 -30

RS-01 FAULT POPULATION

$\Phi = 0.00$	$\Phi = 0.25$	$\Phi = 0.50$	$\Phi = 0.75$	$\Phi = 1.00$
30 000 90	30 000 90	30 000 90	30 000 90	30 000 90
30 030 90	30 030 77	30 030 64	30 030 51	30 030 41
30 060 90	30 060 75	30 060 55	30 060 34	30 060 16
30 120 90	30 120 -75	30 120 -55	30 120 -34	30 120 -16
30 150 90	30 150 -77	30 150 -64	30 150 -51	30 150 -41
30 180 90	30 180 90	30 180 90	30 180 90	30 180 90
30 210 90	30 210 77	30 210 64	30 210 51	30 210 41
30 240 90	30 240 75	30 240 55	30 240 34	30 240 16
30 300 90	30 300 -75	30 300 -55	30 300 -34	30 300 -16
30 330 90	30 330 -77	30 330 -64	30 330 -51	30 330 -41

SO-01 FAULT POPULATION

$\Phi = 0.00$	$\Phi = 0.25$	$\Phi = 0.50$	$\Phi = 0.75$	$\Phi = 1.00$
30 000 90	30 000 90	30 000 90	30 000 90	30 000 90
35 000 90	35 000 90	35 000 90	35 000 90	35 000 90
25 000 90	25 000 90	25 000 90	25 000 90	25 000 90
30 006 90	30 006 87	30 006 84	30 006 81	30 006 78
35 006 90	35 006 87	35 006 85	35 006 82	35 006 80
25 006 90	25 006 86	25 006 83	25 006 79	25 006 76
30 354 90	30 354 -87	30 354 -84	30 354 -81	30 354 -78
35 354 90	35 354 -87	35 354 -85	35 354 -82	35 354 -80
25 354 90	25 354 -86	25 354 -83	25 354 -79	25 354 -76
30 003 90	30 003 89	30 003 87	30 003 86	30 003 84
35 003 90	35 003 89	35 003 87	35 003 86	35 003 85
25 003 90	25 003 88	25 003 86	25 003 85	25 003 83
30 357 90	30 357 -89	30 357 -87	30 357 -86	30 357 -84
35 357 90	35 357 -89	35 357 -87	35 357 -86	35 357 -85
25 357 90	25 357 -88	25 357 -86	25 357 -85	25 357 -83

SO-02 FAULT POPULATION

$\Phi = 0.00$	$\Phi = 0.25$	$\Phi = 0.50$	$\Phi = 0.75$	$\Phi = 1.00$
55 030 90	55 030 82	55 030 73	55 030 64	55 030 55
50 030 90	50 030 81	50 030 72	50 030 62	50 030 53
60 030 90	60 030 82	60 030 74	60 030 65	60 030 56
55 033 90	55 033 81	55 033 72	55 033 62	55 033 52
50 033 90	50 033 81	50 033 71	50 033 60	50 033 50
60 033 90	60 033 82	60 033 73	60 033 63	60 033 53
55 036 90	55 036 82	55 036 71	55 036 60	55 036 48
50 036 90	50 036 80	50 036 69	50 036 58	50 036 47
60 036 90	60 036 81	60 036 72	60 036 61	60 036 50
55 027 90	55 027 83	55 027 75	55 027 66	55 027 58
50 027 90	50 027 82	50 027 74	50 027 65	50 027 56
60 027 90	60 027 83	60 027 75	60 027 67	60 027 60
55 024 90	55 024 83	55 024 76	55 024 69	55 024 61
50 024 90	50 024 83	50 024 75	50 024 67	50 024 60
60 024 90	60 024 84	60 024 77	60 024 70	60 024 63

SO-03 FAULT POPULATION

$\Phi = 0.00$	$\Phi = 0.25$	$\Phi = 0.50$	$\Phi = 0.75$	$\Phi = 1.00$
30 045 90	30 045 74	30 045 56	30 045 40	30 045 27
25 045 90	25 045 71	25 045 52	25 045 35	25 045 23
35 045 90	35 045 76	35 045 60	35 045 44	35 045 30
30 048 90	30 048 74	30 048 56	30 048 38	30 048 24
25 048 90	25 048 71	25 048 51	25 048 34	25 048 21
35 048 90	35 048 76	35 048 59	35 048 42	35 048 27
30 051 90	30 051 74	30 051 55	30 051 37	30 051 22
25 051 90	25 051 71	25 051 50	25 051 32	25 051 19
35 051 90	35 051 76	35 051 59	35 051 41	35 051 25
30 042 90	30 042 74	30 042 57	30 042 42	30 042 29
25 042 90	25 042 72	25 042 63	25 042 37	25 042 25
35 042 90	35 042 76	35 042 61	35 042 46	35 042 33
30 039 90	30 039 75	30 039 59	30 039 44	30 039 32
25 039 90	25 039 73	25 039 54	25 039 39	25 039 28
35 039 90	35 039 76	35 039 62	35 039 48	35 039 35

APPENDIX C

SLIP VECTOR CALCULATION PROGRAM

Complete listing of the slip vector calculation program discussed in chapter five. The program consists of three files -- the main program SLIP.PAS, the include file DXF.INC which contains AutoCAD DXF file creation procedures, and the help file SLIP.TXT. The program is written in Turbo Pascal version 3.01 for an IBM PC or compatible computer.

program Slip;

```
{ ***** }
{
{   This is a program to calculate the slip vector and stress ratios   }
{ on planes of random orientations in a stress field given the mean   }
{ and deviatoric stresses. Read the help file SLIP.TXT to learn more  }
{ about this program.                                                }
{ ***** }
{
{                               SLIP.PAS - Version 2.0                }
{
{   Copyright (C) 1989 -- Steven H. Schimmrich                       }
{   For educational and research purposes only                       }
{   All commercial rights reserved                                   }
{
{   Steven H. Schimmrich                                             }
{   Department of Geological Sciences                                }
{   State University of New York at Albany                           }
{   Albany, New York 12222                                          }
{ ***** }
{ ***** }
```

```
{ Initializations }
```

label 1;

const

```
HELPPFILE      = 'SLIP.TXT';
PAGES          = 5;
PI             = 3.1415927;
```

type

```
RegisterList   =
record
```

```

    AX,BX,CX,DX,BP,SI,DI,DS,ES,Flags : integer;
end;
linarray2d = array[1..3,1..51] of real;
chararray3 = array[1..3] of string[5];
linarray51 = array[1..51] of real;
linarray3 = array[1..3] of real;
string12 = string[12];
string78 = string[78];

var
Sigma1, Sigma3, Mu, Cohesion,
Plunge, Trend, CutOff : real;
DMin, DMax : char;
Choice, Intervals : integer;
Cosines : linarray3;
Sigma : chararray3;
Stresses, SlipVector : linarray2d;
Ratios, SlipAngle : linarray51;
QuitIt, IsThereData : boolean;
FileName : string12;

{ General program functions }

function Exists(FileName : string12): boolean;
{ Checks to see if a file exists on the disk }
var
Name : file;
begin
Assign(Name,FileName);
{$I-}
Reset(Name);
{$I+}
Exists := (IOResult = 0);
end;

function Zero(Value : real): boolean;
{ Checks to see if a value is essentially 0.0 }
begin
if (abs(Value) < 0.00001)
then Zero := true
else Zero := false;
end;

function DegToRad(DegreeMeasure : real): real;
{ Converts an angle in degrees to one in radians }
begin
DegToRad := ((DegreeMeasure * PI) / 180.0);
end;

function RadToDeg(RadianMeasure : real): real;
{ Converts an angle in radians to one in degrees }
begin

```

```

RadToDeg := ((RadianMeasure * 180.0) / PI);
end;

function Tan(Angle : real): real;
  { Returns the tangent of an angle }
begin
  Tan := sin(Angle) / cos(Angle);
end;

function ArcCos(AValue : real): real;
  { Returns the arccosine of a value }
var
  X, Y : real;
begin
  if (AValue = 0.0)
  then ArcCos := (PI / 2.0)
  else if (AValue = 1.0)
  then ArcCos := 0.0
  else if (AValue = -1.0)
  then ArcCos := PI
  else
  begin
    X := (AValue / sqrt(1.0 - sqr(AValue)));
    Y := arctan(abs(1.0 / X));
    if (X > 0.0)
    then ArcCos := Y
    else ArcCos := (PI - Y);
  end;
end;

function ArcSin(AValue : real): real;
  { Returns the arcsine of a value }
var
  X, Y : real;
begin
  if (AValue = 0.0)
  then ArcSin := 0.0
  else
  if (AValue = 1.0)
  then ArcSin := (PI / 2.0)
  else
  if (AValue = -1.0)
  then ArcSin := (-PI / 2.0)
  else
  begin
    X := (AValue / sqrt(1.0 - sqr(AValue)));
    if (X = 0.0)
    then ArcSin := 0.0
    else
    begin
      Y := arctan(abs(X));
      if (X > 0.0)

```

```

        then ArcSin := Y
        else ArcSin := -Y;
    end;
end;
end;

{ General program procedures }

procedure Alarm;
    { Sounds an alarm }
var
    Count : integer;
begin
    for Count := 1 to 4 do
    begin
        sound(880);
        delay(50);
        sound(0);
        delay(50);
        nosound;
    end;
end;

procedure Beep;
    { Sounds a beep }
begin
    sound(880);
    delay(50);
    nosound;
end;

procedure HoldScreen(var QuitIt : boolean);
    { Holds the screen until any key is pressed }
var
    Key : char;
begin
    write(' Press any ');
    textcolor(12);
    write('key');
    textcolor(14);
    write(' to continue (');
    textcolor(12);
    write('Q');
    textcolor(14);
    write(' to quit)...');
    read(kbd,Key);
    if (upcase(Key) = 'Q')
    then QuitIt := true
    else QuitIt := false;
end;

procedure EndGraphics;

```

```

    { Ends a graphics display }
begin
  Beep;
  repeat until (keypressed);
  textmode;
  textcolor(11);
  clrscr;
end;

procedure Cursor(On : boolean);
  { Turns cursor on and off }
var
  Register : RegisterList;
begin
  if (On)
  then
    then
      if (mem[0:$449] = 7)
      then
        Register.CX := $0C0D
      else
        Register.CX := $0607
      else
        Register.CX := $2000;
  Register.AX := $0100;
  intr($10,Register);
end;

procedure DrawBox(ULX, ULY, LRX, LRY : integer);
  { Draws a box around text in text mode }
var
  X, Y, XDistance : integer;
begin
  gotoxy(ULX,ULY);
  write(#201);
  XDistance := LRX - ULX - 1;
  for X := 1 to XDistance do
    write(#205);
  write(#187);
  for Y := (ULY + 1) to (LRY - 1) do
  begin
    gotoxy(LRX,Y);
    write(#186);
    gotoxy(ULX,Y);
    write(#186);
  end;
  gotoxy(ULX,LRY);
  write(#200);
  for X := 1 to XDistance do
    write(#205);
  write(#188);
end;

```

```

{ Error display procedure }

procedure ShowError(ErrorType : integer);
  { Displays appropriate error messages }
begin
  clrscr;
  Alarm;
  gotoxy(28,2);
  textcolor(12);
  writeln('Slip Vector Plotting Program');
  gotoxy(37,10);
  textcolor(28);
  writeln('* ERROR *');
  textcolor(11);
  case (ErrorType) of
    1 : begin
      gotoxy(21,14);
      write('File ',HELPPFILE,' does not exist on the disk');
      end;
    2 : begin
      gotoxy(22,14);
      writeln('σ1 and σ3 must be between -100 and +100');
      end;
    3 : begin
      gotoxy(30,14);
      writeln('σ3 must be less than σ1');
      end;
    4 : begin
      gotoxy(26,14);
      writeln('μ must be between 0.0 and 100.0');
      end;
    5 : begin
      gotoxy(26,14);
      writeln('C must be between 0.0 and 100.0');
      end;
    6 : begin
      gotoxy(20,14);
      writeln('The plunge must be between 0 and 90 degrees');
      end;
    7 : begin
      gotoxy(20,14);
      writeln('The trend must be between 0 and 360 degrees');
      end;
    8 : begin
      gotoxy(20,14);
      writeln('Can only examine between 2 and 50 intervals');
      end;
    9 : begin
      gotoxy(19,14);
      writeln('Do not specify an extension for the filename');
      end;
    10 : begin

```

```

    gotoxy(23,14);
    writeln('That file already exists on this disk');
end;
11 : begin
    gotoxy(29,14);
    writeln('Data must be entered first');
end;
12 : begin
    gotoxy(18,14);
    writeln('The number entered must be a positive real value');
end;
13 : begin
    gotoxy(21,14);
    writeln('σ1 and σ3 cannot have the same orientation');
end;
end;
gotoxy(30,15);
write('Recheck and try again...');
delay(5000);
end;

```

```

{ Informational page display procedures }

```

```

procedure IntroPage;
{ Displays an introduction page }
begin
    textmode;
    clrscr;
    cursor(false);
    textcolor(12);
    DrawBox(20,9,61,18);
    textcolor(11);
    gotoxy(27,10);
    writeln('Slip Vector Plotting Program');
    gotoxy(32,12);
    writeln('Program written by');
    gotoxy(31,14);
    writeln('Steven H. Schimmrich');
    gotoxy(24,15);
    writeln('Department of Geological Sciences');
    gotoxy(22,16);
    writeln('State University of New York at Albany');
    gotoxy(30,17);
    writeln('Albany, New York 12222');
    textcolor(11);
    delay(5000);
    cursor(true);
end;

```

```

procedure Working;
{ Displays a message that the program is working }
begin

```

```

clrscr;
Cursor(false);
textcolor(12);
DrawBox(26,10,57,16);
textcolor(11);
gotoxy(28,11);
writeln('Slip Vector Plotting Program');
gotoxy(36,13);
writeln('Don"t Panic!');
gotoxy(33,15);
writeln('I"m working on it');
delay(1000);
end;

procedure Writing(FileName : string12);
{ Displays a message that the program is writing to a file }
var
  Len1, Len2 : integer;
begin
  clrscr;
  Len1 := length(FileName);
  Len2 := trunc((12 - Len1) / 2);
  cursor(false);
  textcolor(12);
  DrawBox((21 + Len2),9,(50 + Len1 + Len2),15);
  textcolor(11);
  gotoxy(28,10);
  writeln('Slip Vector Plotting Program');
  gotoxy(36,12);
  writeln('Don"t Panic!');
  gotoxy((23 + Len2),14);
  write('Writing data to disk file ');
  textcolor(12);
  write(FileName);
  textcolor(11);
  delay(1000);
end;

procedure CreatePage(FileName : string12);
{ Displays a page that DXF is being created for AutoCAD }
var
  Len1, Len2 : integer;
begin
  clrscr;
  Len1 := length(FileName);
  Len2 := trunc((12 - Len1) / 2);
  cursor(false);
  textcolor(12);
  DrawBox((18 + Len2),9,(52 + Len1 + Len2),15);
  textcolor(11);
  gotoxy(28,10);
  writeln('Slip Vector Plotting Program');

```

```

gotoxy(36,12);
writeln('Don"t Panic!');
gotoxy((20 + Len2),14);
write('Writing data to AutoCAD DXFile ');
textcolor(12);
write(FileName);
textcolor(11);
delay(1000);
end;

procedure ExitPage;
  { Displays an exit page }
begin
  textmode;
  clrscr;
  cursor(false);
  textcolor(12);
  DrawBox(26,10,57,16);
  textcolor(11);
  gotoxy(28,11);
  writeln('Slip Vector Plotting Program');
  gotoxy(35,13);
  writeln('POET Software');
  gotoxy(33,14);
  writeln('Copyright (C) 1989');
  gotoxy(32,15);
  writeln('Steven H. Schimmrich');
  delay(5000);
  cursor(true);
  textmode;
  clrscr;
end;

  { Main menu procedures }

procedure MainMenuChoice(var Choice : integer);
  { Returns the number of the menu item selected }
var
  Key : char;
begin
  repeat
    read(kbd,Key);
    Choice := ord(Key) - 48;
    if (not(Choice in [1..7]))
      then Beep;
    until (Choice in [1..7]);
end;

procedure MainMenu(var Choice : integer);
  { Displays main operations menu }
var
  Count : integer;

```

```

begin
  clrscr;
  textcolor(12);
  DrawBox(25,2,56,4);
  textcolor(11);
  gotoxy(27,3);
  writeln('Slip Vector Plotting Program');
  gotoxy(2,9);
  writeln('What do you wish to do ?');
  writeln;
  for Count := 1 to 7 do
  begin
    textcolor(12);
    write(' ',Count);
    textcolor(11);
    case (Count) of
      1 : writeln(' - Learn more about the program');
      2 : writeln(' - Perform the slip vector calculations');
      3 : writeln(' - Display a graph of the results');
      4 : writeln(' - Display a stereonet of the results');
      5 : writeln(' - Display a listing of the results');
      6 : writeln(' - Print the results');
      7 : writeln(' - Exit the program');
    end;
  end;
  writeln;
  write(' Press the ');
  textcolor(12);
  write('number');
  textcolor(11);
  write(' of you choice...');
  MainMenuChoice(Choice);
end;

{ Main menu option # 1 - Help pages display }

```

```

procedure HelpPages;
  { Sequentially displays help file }
label 1;
var
  Line      :      string78;
  Page, Row :      integer;
  Key       :      char;
  DataFile  :      text[1024];
begin
  assign(DataFile,HELPPFILE);
  reset(DataFile);
  for Row := 1 to 5 do
    readln(DataFile,Line);
  for Page := 1 to PAGES do
  begin
    clrscr;

```

```

for Row := 1 to 23 do
begin
  readln(DataFile,Line);
  if (copy(Line,1,1) = '*')
  then
  begin
    textcolor(12);
    delete(Line,1,1);
  end;
  writeln(Line);
  textcolor(11);
end;
write(' Press any ');
textcolor(12);
write('key');
textcolor(11);
write(' to continue (');
textcolor(12);
write('Q');
textcolor(11);
write(' to quit)...');
read(kbd,Key);
if (upcase(Key) = 'Q')
  then goto 1;
end;
1:close(DataFile);
end;

{ Main menu option # 2 - Perform calculations }

procedure AskData(var Sigma : chararray3; var Sigma1, Sigma3, Mu, Cohesion, Plunge,
  Trend : real; var DMin, DMax : char; var Intervals : integer);
{ Asks for user supplied data }
label 1;
begin
1:{Continue}
  clrscr;
  textcolor(12);
  DrawBox(25,1,56,3);
  gotoxy(27,2);
  textcolor(11);
  writeln('Slip Vector Plotting Program');
  gotoxy(2,5);
  writeln('What is the orientation of the maximum compressive');
  gotoxy(2,6);
  write('principal stress axis  $\sigma_1$  (');
  textcolor(12);
  write('N');
  textcolor(11);
  write('orth, ');
  textcolor(12);
  write('E');

```

```

textcolor(11);
write('ast, or ');
textcolor(12);
write('U');
textcolor(11);
write('p) ? ');
repeat
  read(kbd,DMax);
  if (not(uppercase(DMax) in ['N','E','U']))
    then Beep;
until (uppercase(DMax) in ['N','E','U']);
gotoxy(50,6);
textcolor(12);
writeln(uppercase(DMax));
textcolor(11);
gotoxy(2,8);
writeln('What is the orientation of the minimum compressive');
gotoxy(2,9);
write('principal stress axis  $\sigma_3$  (');
textcolor(12);
write('N');
textcolor(11);
write('orth, ');
textcolor(12);
write('E');
textcolor(11);
write('ast, or ');
textcolor(12);
write('U');
textcolor(11);
write('p) ? ');
repeat
  read(kbd,DMin);
  if (not(uppercase(DMin) in ['N','E','U']))
    then Beep;
until (uppercase(DMin) in ['N','E','U']);
gotoxy(50,9);
textcolor(12);
writeln(uppercase(DMin));
textcolor(11);
if (uppercase(Dmax) = uppercase(DMin))
  then
  begin
    ShowError(13);
    goto 1;
  end;
case (uppercase(DMax)) of
  'N' : Sigma[1] := 'North';
  'U' : Sigma[1] := ' Up';
  'E' : Sigma[1] := ' East';
end;
case (uppercase(DMin)) of

```

```

'N' : Sigma[3] := 'North';
'U' : Sigma[3] := ' Up';
'E' : Sigma[3] := ' East';
end;
if ((not(uppercase(DMin) in ['N'])) and (not(uppercase(DMax) in ['N'])))
  then Sigma[2] := 'North';
if ((not(uppercase(DMin) in ['U'])) and (not(uppercase(DMax) in ['U'])))
  then Sigma[2] := ' Up';
if ((not(uppercase(DMin) in ['E'])) and (not(uppercase(DMax) in ['E'])))
  then Sigma[2] := ' East';
gotoxy(2,11);
write('Enter the value for  $\sigma_1$  : ');
Sigma1 := -999.9;
textcolor(12);
readln(Sigma1);
textcolor(11);
if ((Sigma1 < -100.0) or (Sigma1 > 100.0))
  then
  begin
  ShowError(2);
  goto 1;
  end;
gotoxy(2,12);
write('Enter the value for  $\sigma_3$  : ');
Sigma3 := -999.9;
textcolor(12);
readln(Sigma3);
textcolor(11);
if ((Sigma3 < -100.0) or (Sigma3 > 100.0))
  then
  begin
  ShowError(2);
  goto 1;
  end;
if (Sigma3 > Sigma1)
  then
  begin
  ShowError(3);
  goto 1;
  end;
gotoxy(2,14);
write('Enter the coefficient of friction ( $\mu$ ) : ');
textcolor(12);
Mu := -999.9;
readln(Mu);
textcolor(11);
if ((Mu < 0.0) or (Mu > 100.0))
  then
  begin
  ShowError(4);
  goto 1;
  end;

```

```

gotoxy(2,15);
write('Enter the cohesion (C) : ');
textcolor(12);
Cohesion := -999.9;
readln(Cohesion);
textcolor(11);
if ((Cohesion < 0.0) or (Cohesion > 100.0))
  then
  begin
    ShowError(5);
    goto 1;
  end;
gotoxy(2,17);
writeln('Now enter the plunge and trend of the normal');
writeln(' vector to the fault plane you wish to examine');
gotoxy(2,20);
write('Enter the plunge : ');
Plunge := -999.9;
textcolor(12);
readln(Plunge);
textcolor(11);
if ((Plunge < 0.0) or (Plunge >= 90.0))
  then
  begin
    ShowError(6);
    goto 1;
  end;
gotoxy(2,21);
write('Enter the trend : ');
Trend := -999.9;
textcolor(12);
readln(Trend);
textcolor(11);
if ((Trend < 0.0) or (Trend >= 360.0))
  then
  begin
    ShowError(7);
    goto 1;
  end;
if (Trend = 360.0)
  then Trend := Trend - 360.0;
gotoxy(2,23);
write('How many values of  $\sigma_2$  between  $\sigma_1$  and  $\sigma_3$  do you wish to examine ? ');
Intervals := -9;
textcolor(12);
readln(Intervals);
textcolor(11);
if ((Intervals < 2) or (Intervals > 50))
  then
  begin
    ShowError(8);
    goto 1;
  end;

```

```

    end;
end;

procedure DirCosines(Plunge, Trend : real; DMin, DMax : char; var Cosines : linarray3);
  { Returns the direction cosines of the normal vector }
begin
  Plunge := DegToRad(Plunge);
  Trend := DegToRad(Trend);
  if ((uppercase(DMax) = 'N') and (uppercase(DMin) = 'E'))
  then
    begin
      Cosines[1] := (cos(Plunge) * cos(Trend));
      Cosines[2] := sin(Plunge);
      Cosines[3] := (cos(Plunge) * sin(Trend));
    end;
  if ((uppercase(DMax) = 'N') and (uppercase(DMin) = 'U'))
  then
    begin
      Cosines[1] := (cos(Plunge) * cos(Trend));
      Cosines[2] := (cos(Plunge) * sin(Trend));
      Cosines[3] := sin(Plunge);
    end;
  if ((uppercase(DMax) = 'E') and (uppercase(DMin) = 'N'))
  then
    begin
      Cosines[1] := (cos(Plunge) * sin(Trend));
      Cosines[2] := sin(Plunge);
      Cosines[3] := (cos(Plunge) * cos(Trend));
    end;
  if ((uppercase(DMax) = 'E') and (uppercase(DMin) = 'U'))
  then
    begin
      Cosines[1] := (cos(Plunge) * sin(Trend));
      Cosines[2] := (cos(Plunge) * cos(Trend));
      Cosines[3] := sin(Plunge);
    end;
  if ((uppercase(DMax) = 'U') and (uppercase(DMin) = 'N'))
  then
    begin
      Cosines[1] := sin(Plunge);
      Cosines[2] := (cos(Plunge) * sin(Trend));
      Cosines[3] := (cos(Plunge) * cos(Trend));
    end;
  if ((uppercase(DMax) = 'U') and (uppercase(DMin) = 'E'))
  then
    begin
      Cosines[1] := sin(Plunge);
      Cosines[2] := (cos(Plunge) * cos(Trend));
      Cosines[3] := (cos(Plunge) * sin(Trend));
    end;
end;
end;

```

```

procedure Cauchy(Intervals : integer; Sigma1, Sigma3 : real; Cosines : linarray3;
                 var Stresses : linarray2d);
  { Uses Cauchy's Formula to calculate the total stress components }
var
  Count, Value           : integer;
  Sigma2, Step, Temp, Deviator : real;
begin
  Deviator := (Sigma1 - Sigma3);
  Step := (Deviator / Intervals);
  Sigma2 := Sigma3;
  for Count := 1 to (Intervals + 1) do
    begin
      Stresses[1,Count] := Sigma1 * Cosines[1];
      Stresses[2,Count] := Sigma2 * Cosines[2];
      Stresses[3,Count] := Sigma3 * Cosines[3];
      Sigma2 := Sigma2 + Step;
    end;
  end;

procedure CalculateStresses(Intervals : integer; Mu, Cohesion, Trend, Plunge : real;
                             Cosines : linarray3; Stresses : linarray2d;
                             var SlipVector : linarray2d; DMin, DMax : char;
                             var SlipAngle, Ratios : linarray51);
  { Calculates slip vector and shear to normal stress ratio for each phi }
var
  Count : integer;
  DotProduct, StressVectorNormalized, Angle,
  ShearStress, NormalStress, Phi, Sigma1,
  Sigma2, Sigma3, Beta, Strike : real;
begin
  for Count := 1 to (Intervals + 1) do
    begin
      StressVectorNormalized := (sqrt(sqr(Stresses[1,Count]) + sqr(Stresses[2,Count]) +
                                     sqr(Stresses[3,Count])));
      DotProduct := ((Cosines[1] * Stresses[1,Count]) + (Cosines[2] * Stresses[2,Count]) +
                    (Cosines[3] * Stresses[3,Count]));
      Angle := (ArcCos(DotProduct / StressVectorNormalized));
      ShearStress := (abs(StressVectorNormalized * sin(Angle)));
      NormalStress := (abs(StressVectorNormalized * cos(Angle)));
      if (((Zero(NormalStress)) or (Zero(Mu))) and (Zero(Cohesion)))
        then Ratios[Count] := 0.0
        else Ratios[Count] := (ShearStress / ((NormalStress * Mu) + Cohesion));
      if (Cosines[1] <> 0.0)
        then Sigma1 := Stresses[1,Count] / Cosines[1]
        else Sigma1 := 0.0;
      if (Cosines[2] <> 0.0)
        then Sigma2 := Stresses[2,Count] / Cosines[2]
        else Sigma2 := 0.0;
      if (Cosines[3] <> 0.0)
        then Sigma3 := Stresses[3,Count] / Cosines[3]
        else Sigma3 := 0.0;
      if ((upcase(DMax) = 'N') and (upcase(DMin) = 'E'))
    end;
  end;

```

```

then
begin
Phi := ((Sigma2 - Sigma3) / (Sigma1 - Sigma3));
if (Zero(Cosines[2]))
then SlipAngle[Count] := 0.0;
if (Zero(Cosines[1]))
then SlipAngle[Count] := 0.0;
if (Zero(Cosines[3]))
then SlipAngle[Count] := (PI / 2.0);
if ((not(Zero(Cosines[1]))) and (not(Zero(Cosines[2]))) and
(not(Zero(Cosines[3])))
then SlipAngle[Count] := arctan(((sqr(Cosines[1]) * Cosines[2]) - (Phi * Cosines[2]) +
(Phi * sqr(Cosines[2] * Cosines[2])) / (Cosines[3] * Cosines[1]));
end;
if ((upcase(DMax) = 'N') and (upcase(DMin) = 'U'))
then
begin
if (Sigma1 = Sigma2)
then SlipAngle[Count] := (PI / 2.0)
else
begin
Phi := ((Sigma3 - Sigma2) / (Sigma1 - Sigma2));
if (Zero(Cosines[3]))
then SlipAngle[Count] := 0.0;
if (Zero(Cosines[1]))
then SlipAngle[Count] := 0.0;
if (Zero(Cosines[2]))
then SlipAngle[Count] := (PI / 2.0);
if ((not(Zero(Cosines[1]))) and (not(Zero(Cosines[2]))) and
(not(Zero(Cosines[3])))
then SlipAngle[Count] := arctan(((sqr(Cosines[1]) * Cosines[3]) - (Phi * Cosines[3])
+ (Phi * sqr(Cosines[3]) * Cosines[3])) /
(Cosines[2] * Cosines[1]));
end;
end;
if ((upcase(DMax) = 'U') and (upcase(DMin) = 'N'))
then
begin
if (Sigma3 = Sigma2)
then SlipAngle[Count] := (PI / 2.0)
else
begin
Phi := ((Sigma1 - Sigma2) / (Sigma3 - Sigma2));
if (Zero(Cosines[1]))
then SlipAngle[Count] := (PI / 2.0);
if (Zero(Cosines[2]))
then SlipAngle[Count] := (PI / 2.0);
if (Zero(Cosines[3]))
then SlipAngle[Count] := (PI / 2.0);
if ((not(Zero(Cosines[1]))) and (not(Zero(Cosines[2]))) and
(not(Zero(Cosines[3])))
then SlipAngle[Count] := arctan(((sqr(Cosines[3]) * Cosines[1]) - (Phi * Cosines[1])

```

```

+ (Phi * sqrt(Cosines[1]) * Cosines[1]) /
(Cosines[2] * Cosines[3]));

end;
end;
if ((upcase(DMax) = 'U') and (upcase(DMin) = 'E'))
then
begin
if (Sigma2 = Sigma3)
then SlipAngle[Count] := (PI / 2.0)
else
begin
Phi := ((Sigma1 - Sigma3) / (Sigma2 - Sigma3));
if (Zero(Cosines[1]))
then SlipAngle[Count] := (PI / 2.0);
if (Zero(Cosines[2]))
then SlipAngle[Count] := (PI / 2.0);
if (Zero(Cosines[3]))
then SlipAngle[Count] := (PI / 2.0);
if ((not(Zero(Cosines[1]))) and (not(Zero(Cosines[2]))) and
(not(Zero(Cosines[3]))))
then SlipAngle[Count] := arctan(((sqrt(Cosines[2]) * Cosines[1]) - (Phi * Cosines[1])
+ (Phi * sqrt(Cosines[1]) * Cosines[1])) /
(Cosines[3] * Cosines[2]));

end;
end;
if ((upcase(DMax) = 'E') and (upcase(DMin) = 'U'))
then
begin
if (Sigma1 = Sigma2)
then SlipAngle[Count] := (PI / 2.0)
else
begin
Phi := ((Sigma3 - Sigma1) / (Sigma2 - Sigma1));
if (Zero(Cosines[3]))
then SlipAngle[Count] := 0.0;
if (Zero(Cosines[1]))
then SlipAngle[Count] := 0.0;
if (Zero(Cosines[2]))
then SlipAngle[Count] := (PI / 2.0);
if ((not(Zero(Cosines[1]))) and (not(Zero(Cosines[2]))) and
(not(Zero(Cosines[3]))))
then SlipAngle[Count] := arctan(((sqrt(Cosines[2]) * Cosines[3]) - (Phi * Cosines[3])
+ (Phi * sqrt(Cosines[3]) * Cosines[3])) /
(Cosines[1] * Cosines[2]));

end;
end;
if ((upcase(DMax) = 'E') and (upcase(DMin) = 'N'))
then
begin
Phi := ((Sigma2 - Sigma1) / (Sigma3 - Sigma1));
if (Zero(Cosines[2]))
then SlipAngle[Count] := 0.0;

```

```

if (Zero(Cosines[1]))
  then SlipAngle[Count] := 0.0;
if (Zero(Cosines[3]))
  then SlipAngle[Count] := (PI / 2.0);
if ((not(Zero(Cosines[1]))) and (not(Zero(Cosines[2]))) and (not(Zero(Cosines[3])))
  then SlipAngle[Count] := arctan(((sqr(Cosines[3]) * Cosines[2]) - (Phi * Cosines[2]) +
    (Phi * sqr(Cosines[2]) * Cosines[2])) /
    (Cosines[1] * Cosines[3]));

end;
SlipAngle[Count] := RadToDeg(SlipAngle[Count]);
if (not(Zero(SlipAngle[Count])))
  then Beta := RadToDeg(arctan(cos(DegToRad(90 - Plunge)) *
    Tan(DegToRad(SlipAngle[Count])))
  else Beta := 0.0;
Strike := Trend + 90.0;
if (Strike > 360.0)
  then Strike := Strike - 180.0;
SlipVector[2,Count] := Strike + Beta;
if (not(Zero(abs(Beta) - 90.0)))
  then SlipVector[1,Count] := RadToDeg(ArcCos(cos(DegToRad(SlipAngle[Count])) /
    cos(DegToRad(Beta))))
  else SlipVector[1,Count] := 90.0 - Plunge;
if ((SlipAngle[Count] < 0.0) or (SlipAngle[Count] = 90.0))
  then SlipVector[2,Count] := SlipVector[2,Count] + 180.0;
if (Trend > 270)
  then SlipVector[2,Count] := SlipVector[2,Count] + 180.0;
if (SlipVector[2,Count] > 360.0)
  then SlipVector[2,Count] := SlipVector[2,Count] - 360.0;
end;
end;

```

{ Main menu option # 3 - Examine a graph of the results }

```

procedure Circle(XVal, YVal : integer; Radius : real);
  { Draws a circle of a given radius about a given center point }
var
  Angle, X, Y      :      integer;
  Radian           :      real;
begin
  for Angle := 0 to 180 do
    begin
      Radian := (((Angle * 2.0) * PI) / 180.0);
      Y := round(YVal - (Radius * cos(Radian)));
      X := round(XVal + (Radius * (sin(Radian) / 0.416)));
      plot(X,Y,1);
    end;
  end;
end;

```

```

procedure AskCutOff(var CutOff : real);
  { Asks cutoff value for the shear to normal stress ratios }
begin
  repeat

```

```

    clrscr;
    textcolor(12);
    DrawBox(25,1,56,3);
    textcolor(11);
    gotoxy(27,2);
    writeln('Slip Vector Plotting Program');
    gotoxy(2,8);
    write('Enter minimum shear to normal stress ratio (default is 0.0) : ');
    textcolor(12);
    CutOff := 0.0;
    readln(CutOff);
    textcolor(11);
    if (CutOff < 0.0)
        then ShowError(12);
    until (CutOff >= 0.0);
end;

procedure DrawGraphAxes(CutOff, Trend, Plunge : real; Sigma : chararray3);
    { Draws the axes of the graph }
var
    IntPlunge, IntTrend : integer;
begin
    hires;
    palette(1);
    hirescolor(4);
    gotoxy(2,1);
    writeln('Slip Vector Plotting Program');
    gotoxy(2,2);
    IntPlunge := round(Plunge);
    IntTrend := round(Trend);
    writeln('Fault plane normal at ',IntPlunge:2,' / ',IntTrend:3);
    gotoxy(2,3);
    writeln('Cutoff value = ',CutOff:4:2);
    gotoxy(40,1);
    writeln('Fault Planes');
    Circle(318,11,2.0);
    gotoxy(42,2);
    writeln(' = Slipped');
    Circle(318,20,1.0);
    gotoxy(42,3);
    writeln(' = Locked');
    gotoxy(62,1);
    writeln('Sigma 1 = ',Sigma[1]);
    gotoxy(62,2);
    writeln('Sigma 2 = ',Sigma[2]);
    gotoxy(62,3);
    writeln('Sigma 3 = ',Sigma[3]);
    draw(71,115,590,115,1);
    gotoxy(2,24);
    writeln('Phi');
    gotoxy(9,24);
    writeln('0.0');

```

```

draw(178,113,178,117,1);
gotoxy(22,24);
writeln('0.2');
draw(281,113,281,117,1);
gotoxy(35,24);
writeln('0.4');
draw(384,113,384,117,1);
gotoxy(48,24);
writeln('0.6');
draw(487,113,487,117,1);
gotoxy(61,24);
writeln('0.8');
draw(590,113,590,117,1);
gotoxy(74,24);
writeln('1.0');
draw(75,180,75,50,1);
gotoxy(2,5);
writeln('Pitch');
draw(79,180,71,180,1);
gotoxy(6,23);
writeln('-90');
draw(79,147,71,147,1);
gotoxy(6,19);
writeln('-45');
draw(79,115,71,115,1);
gotoxy(8,15);
writeln('0');
draw(79,83,71,83,1);
gotoxy(7,11);
writeln('45');
draw(79,50,71,50,1);
gotoxy(7,7);
writeln('90');
end;

```

```

procedure PlotPoints(Intervals : integer; CutOff, Sigma1, Sigma3 : real; Ratios,
                    SlipAngle : linarray51);
{ Plots the phi versus pitch points }
var
  Count, XVal, YVal      : integer;
  Deviator, Phi, Step, Sigma2 : real;
begin
  Deviator := (Sigma1 - Sigma3);
  Step := (Deviator / Intervals);
  Sigma2 := Sigma3;
  for Count := 1 to (Intervals + 1) do
  begin
    Phi := ((Sigma2 - Sigma3) / (Sigma1 - Sigma3));
    XVal := round(75.0 + (Phi * 515.0));
    YVal := round(115.0 - ((SlipAngle[Count] * 130.0) / 180.0));
    if (Ratios[Count] >= CutOff)
    then Circle(XVal,YVal,2.0)
  end;
end;

```

```

    else Circle(XVal,YVal,1.0);
if (abs(abs(SlipAngle[Count]) - 90.0) < 0.0001)
  then
  begin
    YVal := round(115.0 - ((abs(SlipAngle[Count]) * 130.0) / 180.0));
    if (Ratios[Count] >= CutOff)
      then Circle(XVal,YVal,2.0)
      else Circle(XVal,YVal,1.0);
    YVal := round(115.0 - ((-abs(SlipAngle[Count]) * 130.0) / 180.0));
    if (Ratios[Count] >= CutOff)
      then Circle(XVal,YVal,2.0)
      else Circle(XVal,YVal,1.0);
    end;
    Sigma2 := Sigma2 + Step;
  end;
end;

{ Main menu option # 4 - Display a stereonet of the results }

procedure DrawStereonet(CutOff, Plunge, Trend : real; Sigma : chararray3);
  { Draws stereonet on the screen }
var
  Angle, X, Y, IntPlunge, IntTrend :      integer;
  Radian                             :      real;
begin
  hires;
  palette(1);
  hirescolor(4);
  IntPlunge := round(Plunge);
  IntTrend := round(Trend);
  for Angle := 0 to 3600 do
  begin
    Radian := DegToRad(Angle / 10.0);
    X := round(315.0 + (90.0 * (sin(Radian) / 0.416)));
    Y := round(102.0 - (90.0 * cos(Radian)));
    plot(X,Y,1);
  end;
  draw(315,100,315,104,1);
  draw(313,102,317,102,1);
  draw(315,14,315,10,1);
  gotoxy(40,1);
  writeln('N');
  gotoxy(3,2);
  writeln('Slip Vector');
  gotoxy(3,3);
  writeln('Plotting Program');
  gotoxy(3,4);
  writeln('Fault Plane Normal');
  gotoxy(3,5);
  writeln('at ',IntPlunge:2,' / ',IntTrend:3);
  gotoxy(63,2);
  writeln('Lower-Hemisphere');

```

```

gotoxy(66,3);
writeln('Stereographic');
gotoxy(69,4);
writeln('Projection');
gotoxy(63,22);
writeln('Sigma 1 = ',Sigma[1]);
gotoxy(63,23);
writeln('Sigma 2 = ',Sigma[2]);
gotoxy(63,24);
writeln('Sigma 3 = ',Sigma[3]);
gotoxy(5,22);
writeln('= Slip');
gotoxy(5,23);
writeln('= Locked');
gotoxy(3,24);
writeln('Cutoff Value = ',CutOff:4:2);
circle(18,170,2.0);
circle(18,179,1.0);
end;

procedure DrawFaultPlane(Plunge, Trend, Radius : real);
  { Draws a great circle on a Wulff net }
var
  Step, XVal, YVal          : integer;
  Strike, Dip, ApparentDip, Distance, Beta : real;
begin
  if (Plunge = 0.0)
    then Plunge := Plunge + 0.0001;
  Dip := DegToRad(90.0 - Plunge);
  if ((Trend >= 90.0) and (Trend < 270.0))
    then Strike := Trend - 90.0
    else Strike := Trend + 90.0;
  if (Strike >= 360.0)
    then Strike := Strike - 360.0;
  for Step := 0 to 1800 do
  begin
    Beta := DegToRad(Step / 10.0);
    ApparentDip := arctan(Tan(Dip) * sin(Beta));
    Distance := Radius * Tan((PI / 4.0) - (ApparentDip / 2.0));
    if (Distance < 1.0)
      then
      begin
        Distance := RadToDeg(Beta);
        if (Distance > 90.0)
          then Distance := 90.0 - Distance;
        Beta := DegToRad(Strike);
        Beta := (((5.0 * PI) / 2.0) - Beta);
        if (Beta >= (2.0 * PI))
          then Beta := (Beta - (2.0 * PI));
        if (Beta < 0.0)
          then Beta := (Beta + (2.0 * PI));
      end
    end
  end
end

```

```

else
begin
  if ((Trend >= 90.0) and (Trend < 270.0))
    then Beta := DegToRad(Strike) - Beta
    else Beta := DegToRad(Strike) + Beta;
  if (Beta >= (2.0 * PI))
    then Beta := (Beta - (2.0 * PI));
  if (Beta < 0.0)
    then Beta := (Beta + (2.0 * PI));
  Beta := (((5.0 * PI) / 2.0) - Beta);
  if (Beta >= (2.0 * PI))
    then Beta := (Beta - (2.0 * PI));
  if (Beta < 0.0)
    then Beta := (Beta + (2.0 * PI));
end;
XVal := round(315.0 + ((Distance * cos(Beta)) / 0.416));
YVal := round(102.0 - (Distance * sin(Beta)));
plot(XVal,YVal,1);
end;
end;

procedure DataPlot(Intervals : integer; CutOff, Trend : real; Cosines : linarray3;
                  SlipVector : linarray2d; Ratios : linarray51);
  { Plots slip vectors on the fault plane }
var
  Count, XVal, YVal      : integer;
  Distance, Theta, ZeroTrend : real;
begin
  for Count := 1 to (Intervals + 1) do
  begin
    Distance := (90.0 * Tan((PI / 4.0) - (DegToRad(SlipVector[1,Count]) / 2.0)));
    if (SlipVector[1,Count] = 0.0)
    then
    begin
      ZeroTrend := (SlipVector[2,Count] + 180.0);
      if (ZeroTrend >= 360.0)
      then ZeroTrend := ZeroTrend - 360.0;
      Theta := (((5.0 * PI) / 2.0) - DegToRad(ZeroTrend));
      XVal := round(315.0 + ((Distance * cos(Theta)) / 0.416));
      YVal := round(102.0 - (Distance * sin(Theta)));
      if (Ratios[Count] >= CutOff)
      then Circle(XVal,YVal,2.0)
      else Circle(XVal,YVal,1.0);
    end;
    Theta := (((5.0 * PI) / 2.0) - DegToRad(SlipVector[2,Count]));
    XVal := round(315.0 + ((Distance * cos(Theta)) / 0.416));
    YVal := round(102.0 - (Distance * sin(Theta)));
    if (Ratios[Count] >= CutOff)
    then Circle(XVal,YVal,2.0)
    else Circle(XVal,YVal,1.0);
  end;
  if ((Count = 1) and (not(Zero(Cosines[1]))) and (not(Zero(Cosines[2]))) and
    (not(zero(Cosines[3]))))

```

```

then
begin
  if ((Trend > 337.5) or (Trend <= 22.5))
    then gotoxy(round(XVal/8),round((YVal-15)*3/25));
  if ((Trend > 22.5) and (Trend <= 67.5))
    then gotoxy(round((XVal+30)/8),round((Yval-15)*3/25));
  if ((Trend > 67.5) and (Trend <= 112.5))
    then gotoxy(round((XVal+30)/8),round(YVal*3/25));
  if ((Trend > 112.5) and (Trend <= 157.5))
    then gotoxy(round((XVal+30)/8),round((Yval+15)*3/25));
  if ((Trend > 157.5) and (Trend <= 202.5))
    then gotoxy(round(XVal/8),round((YVal+15)*3/25));
  if ((Trend > 202.5) and (Trend <= 247.5))
    then gotoxy(round((XVal-30)/8),round((Yval+15)*3/25));
  if ((Trend > 247.5) and (Trend <= 292.5))
    then gotoxy(round((XVal-30)/8),round(YVal*3/25));
  if ((Trend > 292.5) and (Trend <= 337.5))
    then gotoxy(round((XVal-30)/8),round((Yval-15)*3/25));
  writeln(chr(232),' 0');
end;
if ((Count = (Intervals + 1)) and (not(Zero(Cosines[1]))) and
(not(Zero(Cosines[2]))) and (not(Zero(Cosines[3]))))
then
begin
  if ((Trend > 337.5) or (Trend <= 22.5))
    then gotoxy(round(XVal/8),round((YVal-15)*3/25));
  if ((Trend > 22.5) and (Trend <= 67.5))
    then gotoxy(round((XVal+30)/8),round((Yval-15)*3/25));
  if ((Trend > 67.5) and (Trend <= 112.5))
    then gotoxy(round((XVal+30)/8),round(YVal*3/25));
  if ((Trend > 112.5) and (Trend <= 157.5))
    then gotoxy(round((XVal+30)/8),round((Yval+15)*3/25));
  if ((Trend > 157.5) and (Trend <= 202.5))
    then gotoxy(round(XVal/8),round((YVal+15)*3/25));
  if ((Trend > 202.5) and (Trend <= 247.5))
    then gotoxy(round((XVal-30)/8),round((Yval+15)*3/25));
  if ((Trend > 247.5) and (Trend <= 292.5))
    then gotoxy(round((XVal-30)/8),round(YVal*3/25));
  if ((Trend > 292.5) and (Trend <= 337.5))
    then gotoxy(round((XVal-30)/8),round((Yval-15)*3/25));
  writeln(chr(232),' 1');
end;
end;
end;

{ Main menu option # 5 - Display a numerical listing of the results }

procedure WriteList(Intervals : integer; Sigma1, Sigma3, Trend, Plunge : real;
  SlipAngle, Ratios : linarray51; Sigma : chararray3);
{ Displays a numerical listing of the results }
label 1;
var

```

```

Count, IntPlunge, IntTrend, Page :      integer;
Deviator, Step, Sigma2, Pages, Phi    :      real;
begin
Sigma2 := Sigma3;
Pages := ((Intervals + 1.0) / 12.0);
if ((Pages - trunc(Pages)) > 0.00001) then Pages := Pages + 1.0;
for Page := 0 to (trunc(Pages) - 1) do
begin
clrscr;
writeln;
textcolor(12);
writeln('      Slip Vector Plotting Program Results');
textcolor(11);
writeln;
write(' Data for a plane with a normal oriented at : ');
IntPlunge := round(Plunge);
IntTrend := round(Trend);
writeln(IntPlunge:2, ' / ', IntTrend:3);
writeln;
write(' Sigma 1 = ', Sigma[1], ' Sigma 2 = ', Sigma[2]);
writeln(' Sigma 3 = ', Sigma[3]);
writeln;
writeln(' Sigma 1 Sigma 2 Sigma 3 Phi Pitch Shear/Normal');
writeln;
Deviator := (Sigma1 - Sigma3);
Step := (Deviator / Intervals);
for Count := ((Page * 12) + 1) to ((Page * 12) + 12) do
begin
Phi := ((Sigma2 - Sigma3) / (Sigma1 - Sigma3));
if (Count > (Intervals + 1)) then goto 1;
write(Sigma1:6:2, ' ', Sigma2:6:2, ' ', Sigma3:6:2, ' ');
writeln(Phi:6:2, ' ', SlipAngle[Count]:6:2, ' ', Ratios[Count]:6:2);
Sigma2 := Sigma2 + Step;
1: end;
gotoxy(2,24);
write('Press any ');
textcolor(12);
write('key');
textcolor(11);
write(' to continue...');
repeat until (keypressed);
end;
end;

{ Main menu option # 6 - Procedures to print the results }

procedure AskDiskFileName(var FileName : String12);
{ Asks for the name of a disk data file }
var
FileLength, Count      :      integer;
Extension              :      boolean;
Key                   :      char;

```

```

begin
  repeat
    clrscr;
    textcolor(12);
    DrawBox(25,1,56,3);
    textcolor(11);
    gotoxy(27,2);
    writeln('Slip Vector Plotting Program');
    gotoxy(2,10);
    write('Enter a filename (');
    textcolor(12);
    write('.DAT');
    textcolor(11);
    write(') : ');
    textcolor(12);
    readln(FileName);
    textcolor(11);
    FileLength := length(FileName);
    Extension := false;
    for Count := 1 to FileLength do
      if (copy(FileName,Count,1) = '.')
        then
          Extension := true;
    FileName := FileName + '.dat';
    if ((Exists(FileName)) or (Extension))
      then
        if (Extension)
          then
            ShowError(9)
          else
            ShowError(10);
    until ((not(Exists(FileName))) and (not(Extension)));
end;

procedure AskAcadFileName(var FileName : String12);
  { Asks for the name of a disk data file }
var
  FileLength, Count      :      integer;
  Extension              :      boolean;
  Key                   :      char;
begin
  repeat
    clrscr;
    textcolor(12);
    DrawBox(25,1,56,3);
    textcolor(11);
    gotoxy(27,2);
    writeln('Slip Vector Plotting Program');
    gotoxy(2,10);
    write('Enter a filename (');
    textcolor(12);
    write('.DXF');

```

```

textcolor(11);
write(') : ');
textcolor(12);
readln(FileName);
textcolor(11);
FileLength := length(FileName);
Extension := false;
for Count := 1 to FileLength do
  if (copy(FileName,Count,1) = '.')
  then
    Extension := true;
FileName := FileName + '.dxf';
if ((Exists(FileName)) or (Extension))
then
  if (Extension)
  then
    ShowError(9)
  else
    ShowError(10);
until ((not(Exists(FileName))) and (not(Extension)));
end;

procedure PrintMenuChoice(var Choice : integer);
  { Returns the number of the print menu item selected }
var
  Key : char;
begin
  repeat
    read(kbd,Key);
    Choice := ord(Key) - 48;
    if (not(Choice in [1..4]))
    then Beep;
  until (Choice in [1..4]);
end;

procedure PrintMenu(var Choice : integer);
  { Displays the print menu }
var
  Count : integer;
begin
  clrscr;
  textcolor(12);
  DrawBox(25,2,56,4);
  textcolor(11);
  gotoxy(27,3);
  writeln('Slip Vector Plotting Program');
  gotoxy(2,10);
  writeln('What do you wish to do?');
  writeln;
  for Count := 1 to 4 do
  begin
    textcolor(12);

```

```

write(' ',Count);
textcolor(11);
case (Count) of
  1 : writeln(' - Write the numerical results to a disk file');
  2 : writeln(' - Create a DXFile of the stereonet for AutoCAD');
  3 : writeln(' - Create a DXFile of the graph for AutoCAD');
  4 : writeln(' - Return to the main menu');
end;
end;
writeln;
write(' Press the ');
textcolor(12);
write('number');
textcolor(11);
write(' of you choice...');
MainMenuChoice(Choice);
end;

{ Procedure to write the results to a disk file }

procedure WriteFile(Intervals : integer; Sigma1, Sigma3, Mu, Cohesion, Trend,
                   Plunge : real; SlipAngle, Ratios : linarray51;
                   FileName : string12; Sigma : chararray3);
{ Writes a disk data file of the results }
var
  Count, IntPlunge, IntTrend      : integer;
  Deviator, Phi, Step, Sigma2    : real;
  DataFile                       : text;
begin
  assign(DataFile,FileName);
  rewrite(DataFile);
  writeln(DataFile,' ');
  writeln(DataFile,' ');
  writeln(DataFile,' ');
  writeln(DataFile,'                Slip Vector Plotting Program');
  writeln(DataFile,' ');
  writeln(DataFile,' ');
  writeln(DataFile,' ');
  write(DataFile,' Data for a plane with a normal oriented at : ');
  IntPlunge := round(Plunge);
  IntTrend := round(Trend);
  writeln(DataFile,IntPlunge:2,' / ',IntTrend:3);
  writeln(DataFile,' ');
  writeln(DataFile,' ');
  write(DataFile,' Sigma 1 = ',Sigma[1],'   Sigma 1 = ',Sigma1:5:2);
  writeln(DataFile,'   Coefficient of friction = ',Mu:5:2);
  write(DataFile,' Sigma 2 = ',Sigma[2],'   Sigma 3 = ',Sigma3:5:2);
  writeln(DataFile,'   Cohesion           = ',Cohesion:5:2);
  write(DataFile,' Sigma 3 = ',Sigma[3]);
  writeln(DataFile,' ');
  writeln(DataFile,' ');
  writeln(DataFile,' ');

```

```

write(DataFile,' Sigma 1 Sigma 2 Sigma 3 Phi');
writeln(DataFile,' Pitch Stress ratio');
writeln(DataFile,' ');
Deviator := (Sigma1 - Sigma3);
Step := (Deviator / Intervals);
Sigma2 := Sigma3;
for Count := 1 to (Intervals + 1) do
begin
Phi := ((Sigma2 - Sigma3) / (Sigma1 - Sigma3));
write(DataFile,Sigma1:6:2,' ',Sigma2:6:2,' ',Sigma3:6:2,' ');
write(DataFile,Phi:6:2,' ',SlipAngle[Count]:6:2,' ');
writeln(DataFile,Ratios[Count]:6:2);
Sigma2 := Sigma2 + Step;
end;
writeln(DataFile,' ');
close(DataFile);
end;

{ AutoCAD DXFile creation procedures }

{$I DXF.INC}

{ Main Program }

begin
QuitIt := false;
IsThereData := false;
IntroPage;
repeat
MainMenu(Choice);
case (Choice) of
1 : HelpPages;
2 : begin
AskData(Sigma,Sigma1,Sigma3,Mu,Cohesion,Plunge,Trend,DMin,DMax,Intervals);
Working;
DirCosines(Plunge,Trend,Dmin,DMax,Cosines);
Cauchy(Intervals,Sigma1,Sigma3,Cosines,Stresses);
CalculateStresses(Intervals,Mu,Cohesion,Trend,Plunge,Cosines,
Stresses,SlipVector,DMin,DMax,SlipAngle,Ratios);
Cursor(true);
IsThereData := true;
Beep;
end;
3 : begin
if (IsThereData)
then
begin
AskCutOff(CutOff);
DrawGraphAxes(CutOff,Trend,Plunge,Sigma);
PlotPoints(Intervals,CutOff,Sigma1,Sigma3,Ratios,SlipAngle);
EndGraphics;
end
end
end

```

```

    else
        ShowError(11);
    end;
4 : begin
    if (IsThereData)
    then
        begin
            AskCutOff(CutOff);
            DrawStereonet(CutOff,Plunge,Trend,Sigma);
            DrawFaultPlane(Plunge,Trend,90.0);
            DataPlot(Intervals,CutOff,Trend,Cosines,SlipVector,Ratios);
            EndGraphics;
        end
    else
        ShowError(11);
    end;
5 : begin
    if (IsThereData)
    then
        WriteList(Intervals,Sigma1,Sigma3,Trend,
            Plunge,SlipAngle,Ratios,Sigma)
    else
        ShowError(11);
    end;
6 : begin
    if (IsThereData)
    then
        begin
            Printmenu(Choice);
            case (Choice) of
                1 : begin
                    AskDiskFileName(FileName);
                    Writing(FileName);
                    WriteFile(Intervals,Sigma1,Sigma3,Mu,Cohesion,Trend,
                        Plunge,SlipAngle,Ratios,FileName,Sigma);
                    Cursor(true);
                    Beep;
                end;
                2 : begin
                    AskCutOff(CutOff);
                    AskAcadFileName(FileName);
                    CreatePage(FileName);
                    DXFileNet(Intervals,CutOff,Plunge,Trend,Cosines,
                        SlipVector,Ratios,FileName,Sigma);
                    Cursor(true);
                    Beep;
                end;
                3 : begin
                    AskCutOff(CutOff);
                    AskAcadFileName(FileName);
                    CreatePage(FileName);
                    DXFileGraph(Intervals,CutOff,Plunge,Trend,Sigma1,

```

```
                                Sigma3,Ratios,SlipAngle,FileName);
        Cursor(true);
        Beep;
    end;
    4 : {Continue}
    end;
end
else
    ShowError(11);
end;
7 : QuitIt := true;
end;
Until (QuitIt);
ExitPage;
end.
```

Listing of the include file DXF.INC which creates AutoCAD DXF files.

```

{ **** }
{
{
{ DXF.INC
{
{ Procedures to create AutoCAD DXFiles for SLIP.PAS
{
{ **** }
{
{ Procedures available:
{
{ DXFileNet - Creates an AutoCAD DXfile for the stereonet
{ DXFileGraph - Creates an AutoCAD DXFile for the graph
{
{ **** }
}
}
}
}
}
}
}
}

procedure DXFileNet(Intervals : integer; CutOff, Plunge, Trend : real;
                   Cosines : linarray3; SlipVector : linarray2d;
                   Ratios : linarray51; FileName : string12;
                   Sigma : chararray3);
{ Creates an AutoCAD DXFile for the stereonet }
var
  Count, IntPlunge, IntTrend           : integer;
  Strike, Dip, ApparentDip, Theta,
  Distance, Beta, XVA1, YVA1, ZeroTrend : real;
  DataFile                             : text;
begin
  IntPlunge := round(Plunge);
  IntTrend := round(Trend);
  assign(DataFile,FileName);
  rewrite(DataFile);
  writeln(DataFile,'0');
  writeln(DataFile,'SECTION');
  writeln(DataFile,'2');
  writeln(DataFile,'HEADER');
  writeln(DataFile,'9');
  writeln(DataFile,'$TEXTSTYLE');
  writeln(DataFile,'7');
  writeln(DataFile,'SIMPLEX');
  writeln(DataFile,'0');
  writeln(DataFile,'ENDSEC');
  writeln(DataFile,'0');
  writeln(DataFile,'SECTION');
  writeln(DataFile,'2');
  writeln(DataFile,'ENTITIES');
  writeln(DataFile,'0');
  writeln(DataFile,'CIRCLE');
  writeln(DataFile,'8');
  writeln(DataFile,'0');

```

```
writeln(DataFile,'10');
writeln(DataFile,'7.500');
writeln(DataFile,'20');
writeln(DataFile,'4.500');
writeln(DataFile,'40');
writeln(DataFile,'4.000');
writeln(DataFile,'0');
writeln(DataFile,'LINE');
writeln(DataFile,'8');
writeln(DataFile,'0');
writeln(DataFile,'10');
writeln(DataFile,'7.350');
writeln(DataFile,'20');
writeln(DataFile,'4.500');
writeln(DataFile,'11');
writeln(DataFile,'7.650');
writeln(DataFile,'21');
writeln(DataFile,'4.500');
writeln(DataFile,'0');
writeln(DataFile,'LINE');
writeln(DataFile,'8');
writeln(DataFile,'0');
writeln(DataFile,'10');
writeln(DataFile,'7.500');
writeln(DataFile,'20');
writeln(DataFile,'4.350');
writeln(DataFile,'11');
writeln(DataFile,'7.500');
writeln(DataFile,'21');
writeln(DataFile,'4.650');
writeln(DataFile,'0');
writeln(DataFile,'LINE');
writeln(DataFile,'8');
writeln(DataFile,'0');
writeln(DataFile,'10');
writeln(DataFile,'7.500');
writeln(DataFile,'20');
writeln(DataFile,'8.350');
writeln(DataFile,'11');
writeln(DataFile,'7.500');
writeln(DataFile,'21');
writeln(DataFile,'8.650');
writeln(DataFile,'0');
writeln(DataFile,'TEXT');
writeln(DataFile,'8');
writeln(DataFile,'0');
writeln(DataFile,'10');
writeln(DataFile,'7.45');
writeln(DataFile,'20');
writeln(DataFile,'8.800');
writeln(DataFile,'40');
writeln(DataFile,'0.20');
```

```
writeln(DataFile,'1');
writeln(DataFile,'N');
writeln(DataFile,'0');
writeln(DataFile,'TEXT');
writeln(DataFile,'8');
writeln(DataFile,'0');
writeln(DataFile,'10');
writeln(DataFile,'0.500');
writeln(DataFile,'20');
writeln(DataFile,'8.300');
writeln(DataFile,'40');
writeln(DataFile,'0.20');
writeln(DataFile,'1');
writeln(DataFile,'Slip Vector');
writeln(DataFile,'0');
writeln(DataFile,'TEXT');
writeln(DataFile,'8');
writeln(DataFile,'0');
writeln(DataFile,'10');
writeln(DataFile,'0.500');
writeln(DataFile,'20');
writeln(DataFile,'7.900');
writeln(DataFile,'40');
writeln(DataFile,'0.20');
writeln(DataFile,'1');
writeln(DataFile,'Plotting Program');
writeln(DataFile,'0');
writeln(DataFile,'TEXT');
writeln(DataFile,'8');
writeln(DataFile,'0');
writeln(DataFile,'10');
writeln(DataFile,'0.500');
writeln(DataFile,'20');
writeln(DataFile,'7.500');
writeln(DataFile,'40');
writeln(DataFile,'0.20');
writeln(DataFile,'1');
writeln(DataFile,'Fault Plane Normal');
writeln(DataFile,'0');
writeln(DataFile,'TEXT');
writeln(DataFile,'8');
writeln(DataFile,'0');
writeln(DataFile,'10');
writeln(DataFile,'0.500');
writeln(DataFile,'20');
writeln(DataFile,'7.100');
writeln(DataFile,'40');
writeln(DataFile,'0.20');
writeln(DataFile,'1');
writeln(DataFile,'at ',IntPlunge:2,' / ',IntTrend:3);
writeln(DataFile,'0');
writeln(DataFile,'TEXT');
```

```
writeln(DataFile,'8');
writeln(DataFile,'0');
writeln(DataFile,'10');
writeln(DataFile,'11.000');
writeln(DataFile,'20');
writeln(DataFile,'8.300');
writeln(DataFile,'40');
writeln(DataFile,'0.20');
writeln(DataFile,'1');
writeln(DataFile,'Lower-Hemisphere');
writeln(DataFile,'0');
writeln(DataFile,'TEXT');
writeln(DataFile,'8');
writeln(DataFile,'0');
writeln(DataFile,'10');
writeln(DataFile,'11.600');
writeln(DataFile,'20');
writeln(DataFile,'7.900');
writeln(DataFile,'40');
writeln(DataFile,'0.20');
writeln(DataFile,'1');
writeln(DataFile,'Stereographic');
writeln(DataFile,'0');
writeln(DataFile,'TEXT');
writeln(DataFile,'8');
writeln(DataFile,'0');
writeln(DataFile,'10');
writeln(DataFile,'12.200');
writeln(DataFile,'20');
writeln(DataFile,'7.500');
writeln(DataFile,'40');
writeln(DataFile,'0.20');
writeln(DataFile,'1');
writeln(DataFile,'Projection');
writeln(DataFile,'0');
writeln(DataFile,'TEXT');
writeln(DataFile,'8');
writeln(DataFile,'0');
writeln(DataFile,'10');
writeln(DataFile,'11.200');
writeln(DataFile,'20');
writeln(DataFile,'1.300');
writeln(DataFile,'40');
writeln(DataFile,'0.20');
writeln(DataFile,'1');
writeln(DataFile,'Sigma 1 = ',Sigma[1]);
writeln(DataFile,'0');
writeln(DataFile,'TEXT');
writeln(DataFile,'8');
writeln(DataFile,'0');
writeln(DataFile,'10');
writeln(DataFile,'11.200');
```

```
writeln(DataFile,'20');
writeln(DataFile,'0.900');
writeln(DataFile,'40');
writeln(DataFile,'0.20');
writeln(DataFile,'1');
writeln(DataFile,'Sigma 2 = ',Sigma[2]);
writeln(DataFile,'0');
writeln(DataFile,'TEXT');
writeln(DataFile,'8');
writeln(DataFile,'0');
writeln(DataFile,'10');
writeln(DataFile,'11.200');
writeln(DataFile,'20');
writeln(DataFile,'0.500');
writeln(DataFile,'40');
writeln(DataFile,'0.20');
writeln(DataFile,'1');
writeln(DataFile,'Sigma 3 = ',Sigma[3]);
writeln(DataFile,'0');
writeln(DataFile,'TEXT');
writeln(DataFile,'8');
writeln(DataFile,'0');
writeln(DataFile,'10');
writeln(DataFile,'0.800');
writeln(DataFile,'20');
writeln(DataFile,'1.300');
writeln(DataFile,'40');
writeln(DataFile,'0.20');
writeln(DataFile,'1');
writeln(DataFile,' = Slip');
writeln(DataFile,'0');
writeln(DataFile,'TEXT');
writeln(DataFile,'8');
writeln(DataFile,'0');
writeln(DataFile,'10');
writeln(DataFile,'0.800');
writeln(DataFile,'20');
writeln(DataFile,'0.900');
writeln(DataFile,'40');
writeln(DataFile,'0.20');
writeln(DataFile,'1');
writeln(DataFile,' = Locked');
writeln(DataFile,'0');
writeln(DataFile,'TEXT');
writeln(DataFile,'8');
writeln(DataFile,'0');
writeln(DataFile,'10');
writeln(DataFile,'0.500');
writeln(DataFile,'20');
writeln(DataFile,'0.500');
writeln(DataFile,'40');
writeln(DataFile,'0.20');
```

```

writeln(DataFile,'1');
writeln(DataFile,'Cutoff Value = ',CutOff:4:2);
writeln(DataFile,'0');
writeln(DataFile,'CIRCLE');
writeln(DataFile,'8');
writeln(DataFile,'0');
writeln(DataFile,'10');
writeln(DataFile,'0.600');
writeln(DataFile,'20');
writeln(DataFile,'1.400');
writeln(DataFile,'40');
writeln(DataFile,'0.150');
writeln(DataFile,'0');
writeln(DataFile,'CIRCLE');
writeln(DataFile,'8');
writeln(DataFile,'0');
writeln(DataFile,'10');
writeln(DataFile,'0.600');
writeln(DataFile,'20');
writeln(DataFile,'1.000');
writeln(DataFile,'40');
writeln(DataFile,'0.050');
if (Plunge = 0.0)
  then Plunge := Plunge + 0.0001;
Dip := DegToRad(90.0 - Plunge);
if ((Trend >= 90.0) and (Trend < 270.0))
  then Strike := Trend - 90.0
  else Strike := Trend + 90.0;
if (Strike >= 360.0)
  then Strike := Strike - 360.0;
for Count := 0 to 1800 do
begin
  Beta := DegToRad(Count / 10.0);
  ApparentDip := arctan(Tan(Dip) * sin(Beta));
  Distance := 4.000 * Tan((PI / 4.0) - (ApparentDip / 2.0));
  if (Distance < 0.05)
  then
  begin
    Distance := (RadToDeg(Beta) * (2.0 / 45.0));
    if (Distance > 4.000)
    then Distance := 4.000 - Distance;
    Beta := DegToRad(Strike);
    Beta := (((5.0 * PI) / 2.0) - Beta);
    if (Beta >= (2.0 * PI))
    then Beta := (Beta - (2.0 * PI));
    if (Beta < 0.0)
    then Beta := (Beta + (2.0 * PI));
  end
  else
  begin
    if ((Trend >= 90.0) and (Trend < 270.0))
    then Beta := DegToRad(Strike) - Beta

```

```

    else Beta := DegToRad(Strike) + Beta;
  if (Beta >= (2.0 * PI))
    then Beta := (Beta - (2.0 * PI));
  if (Beta < 0.0)
    then Beta := (Beta + (2.0 * PI));
  Beta := (((5.0 * PI) / 2.0) - Beta);
  if (Beta >= (2.0 * PI))
    then Beta := (Beta - (2.0 * PI));
  if (Beta < 0.0)
    then Beta := (Beta + (2.0 * PI));
end;
XVal := (7.500 + (Distance * cos(Beta)));
YVal := (4.500 + (Distance * sin(Beta)));
writeln(DataFile,'0');
writeln(DataFile,'POINT');
writeln(DataFile,'8');
writeln(DataFile,'0');
writeln(DataFile,'10');
writeln(DataFile,XVAL);
writeln(DataFile,'20');
writeln(DataFile,YVAL);
end;
for Count := 1 to (Intervals + 1) do
begin
  Distance := (4.000 * Tan((PI / 4.0) - (DegToRad(SlipVector[1,Count]) / 2.0)));
  if (SlipVector[1,Count] = 0.0)
    then
      begin
        ZeroTrend := (SlipVector[2,Count] + 180.0);
        if (ZeroTrend >= 360.0)
          then ZeroTrend := ZeroTrend - 360.0;
        Theta := (((5.0 * PI) / 2.0) - DegToRad(ZeroTrend));
        XVal := (7.500 + (Distance * cos(Theta)));
        YVal := (4.500 + (Distance * sin(Theta)));
        writeln(DataFile,'0');
        writeln(DataFile,'CIRCLE');
        writeln(DataFile,'8');
        writeln(DataFile,'0');
        writeln(DataFile,'10');
        writeln(DataFile,XVAL);
        writeln(DataFile,'20');
        writeln(DataFile,YVAL);
        writeln(DataFile,'40');
        if (Ratios[Count] >= CutOff)
          then writeln(DataFile,'0.150')
          else writeln(DataFile,'0.050');
        end;
        Theta := (((5.0 * PI) / 2.0) - DegToRad(SlipVector[2,Count]));
        XVal := (7.500 + (Distance * cos(Theta)));
        YVal := (4.500 + (Distance * sin(Theta)));
        writeln(DataFile,'0');
        writeln(DataFile,'CIRCLE');

```

```

writeln(DataFile,'8');
writeln(DataFile,'0');
writeln(DataFile,'10');
writeln(DataFile,XVAL);
writeln(DataFile,'20');
writeln(DataFile,YVAL);
writeln(DataFile,'40');
if (Ratios[Count] >= CutOff)
  then writeln(DataFile,'0.150')
  else writeln(DataFile,'0.050');
if ((Count = 1) and (not(Zero(Cosines[1]))) and (not(Zero(Cosines[2])))
  and (not(Zero(Cosines[3])))
  then
  begin
  writeln(DataFile,'0');
  writeln(DataFile,'TEXT');
  writeln(DataFile,'8');
  writeln(DataFile,'0');
  if ((Trend > 337.5) or (Trend <= 22.5))
    then
    begin
    writeln(DataFile,'10');
    writeln(DataFile,(XVAL));
    writeln(DataFile,'20');
    writeln(DataFile,(YVAL+0.50));
    end;
  if ((Trend > 22.5) and (Trend <= 67.5))
    then
    begin
    writeln(DataFile,'10');
    writeln(DataFile,(XVAL+0.50));
    writeln(DataFile,'20');
    writeln(DataFile,(YVAL+0.50));
    end;
  if ((Trend > 67.5) and (Trend <= 112.5))
    then
    begin
    writeln(DataFile,'10');
    writeln(DataFile,(XVAL+0.50));
    writeln(DataFile,'20');
    writeln(DataFile,(YVAL));
    end;
  if ((Trend > 112.5) and (Trend <= 157.5))
    then
    begin
    writeln(DataFile,'10');
    writeln(DataFile,(XVAL+0.50));
    writeln(DataFile,'20');
    writeln(DataFile,(YVAL-0.50));
    end;
  if ((Trend > 157.5) and (Trend <= 202.5))
    then

```

```

begin
  writeln(DataFile,'10');
  writeln(DataFile,(XVAL));
  writeln(DataFile,'20');
  writeln(DataFile,(YVAL-0.50));
end;
if ((Trend > 202.5) and (Trend <= 247.5))
then
begin
  writeln(DataFile,'10');
  writeln(DataFile,(XVAL-0.50));
  writeln(DataFile,'20');
  writeln(DataFile,(YVAL-0.50));
end;
if ((Trend > 247.5) and (Trend <= 292.5))
then
begin
  writeln(DataFile,'10');
  writeln(DataFile,(XVAL-0.50));
  writeln(DataFile,'20');
  writeln(DataFile,(YVAL));
end;
if ((Trend > 292.5) and (Trend <= 337.5))
then
begin
  writeln(DataFile,'10');
  writeln(DataFile,(XVAL-0.50));
  writeln(DataFile,'20');
  writeln(DataFile,(YVAL+0.50));
end;
writeln(DataFile,'40');
writeln(DataFile,'0.15');
writeln(DataFile,'1');
writeln(DataFile,'Phi = 0');
end;
if ((Count = (Intervals + 1)) and (not(Zero(Cosines[1]))) and
(not(Zero(Cosines[2]))) and (not(Zero(Cosines[3]))))
then
begin
  writeln(DataFile,'0');
  writeln(DataFile,'TEXT');
  writeln(DataFile,'8');
  writeln(DataFile,'0');
  if ((Trend > 337.5) or (Trend <= 22.5))
  then
  begin
    writeln(DataFile,'10');
    writeln(DataFile,(XVAL));
    writeln(DataFile,'20');
    writeln(DataFile,(YVAL+0.50));
  end;
  if ((Trend > 22.5) and (Trend <= 67.5))

```

```
then
begin
  writeln(DataFile,'10');
  writeln(DataFile,(XVAL+0.50));
  writeln(DataFile,'20');
  writeln(DataFile,(YVAL+0.50));
end;
if ((Trend > 67.5) and (Trend <= 112.5))
then
begin
  writeln(DataFile,'10');
  writeln(DataFile,(XVAL+0.50));
  writeln(DataFile,'20');
  writeln(DataFile,(YVAL));
end;
if ((Trend > 112.5) and (Trend <= 157.5))
then
begin
  writeln(DataFile,'10');
  writeln(DataFile,(XVAL+0.50));
  writeln(DataFile,'20');
  writeln(DataFile,(YVAL-0.50));
end;
if ((Trend > 157.5) and (Trend <= 202.5))
then
begin
  writeln(DataFile,'10');
  writeln(DataFile,(XVAL));
  writeln(DataFile,'20');
  writeln(DataFile,(YVAL-0.50));
end;
if ((Trend > 202.5) and (Trend <= 247.5))
then
begin
  writeln(DataFile,'10');
  writeln(DataFile,(XVAL-0.50));
  writeln(DataFile,'20');
  writeln(DataFile,(YVAL-0.50));
end;
if ((Trend > 247.5) and (Trend <= 292.5))
then
begin
  writeln(DataFile,'10');
  writeln(DataFile,(XVAL-0.50));
  writeln(DataFile,'20');
  writeln(DataFile,(YVAL));
end;
if ((Trend > 292.5) and (Trend <= 337.5))
then
begin
  writeln(DataFile,'10');
  writeln(DataFile,(XVAL-0.50));
```

```

        writeln(DataFile,'20');
        writeln(DataFile,(YVAL+0.50));
    end;
    writeln(DataFile,'40');
    writeln(DataFile,'0.15');
    writeln(DataFile,'1');
    writeln(DataFile,'Phi = 1');
end;
end;
writeln(DataFile,'0');
writeln(DataFile,'ENDSEC');
writeln(DataFile,'0');
writeln(DataFile,'EOF');
close(DataFile);
end;

procedure DXFileGraph(Intervals : integer; CutOff, Plunge, Trend, Sigma1, Sigma3 : real;
                      Ratios, SlipAngle : linarray51; FileName : string12);
{ Creates an AutoCAD DXFile for the graph }
var
    Count, IntPlunge, IntTrend           : integer;
    Deviator, Phi, Step, Sigma2, XVal, YVal : real;
    DataFile                             : text;
begin
    assign(DataFile,FileName);
    rewrite(DataFile);
    writeln(DataFile,'0');
    writeln(DataFile,'SECTION');
    writeln(DataFile,'2');
    writeln(DataFile,'HEADER');
    writeln(DataFile,'9');
    writeln(DataFile,'$TEXTSTYLE');
    writeln(DataFile,'7');
    writeln(DataFile,'SIMPLEX');
    writeln(DataFile,'0');
    writeln(DataFile,'ENDSEC');
    writeln(DataFile,'0');
    writeln(DataFile,'SECTION');
    writeln(DataFile,'2');
    writeln(DataFile,'ENTITIES');
    writeln(DataFile,'0');
    writeln(DataFile,'LINE');
    writeln(DataFile,'8');
    writeln(DataFile,'0');
    writeln(DataFile,'10');
    writeln(DataFile,'3.000');
    writeln(DataFile,'20');
    writeln(DataFile,'2.000');
    writeln(DataFile,'11');
    writeln(DataFile,'3.000');
    writeln(DataFile,'21');
    writeln(DataFile,'7.000');
end;

```

```

writeln(DataFile,'0');
writeln(DataFile,'LINE');
writeln(DataFile,'8');
writeln(DataFile,'0');
writeln(DataFile,'10');
writeln(DataFile,'3.000');
writeln(DataFile,'20');
writeln(DataFile,'4.5');
writeln(DataFile,'11');
writeln(DataFile,'13.000');
writeln(DataFile,'21');
writeln(DataFile,'4.5');
for Count := 0 to 5 do
begin
  XVal := ((2.0 * Count) + 3.000);
  writeln(DataFile,'0');
  writeln(DataFile,'LINE');
  writeln(DataFile,'8');
  writeln(DataFile,'0');
  writeln(DataFile,'10');
  writeln(DataFile,XVAL);
  writeln(DataFile,'20');
  writeln(DataFile,'4.35');
  writeln(DataFile,'11');
  writeln(DataFile,XVAL);
  writeln(DataFile,'21');
  writeln(DataFile,'4.65');
  writeln(DataFile,'0');
  writeln(DataFile,'TEXT');
  writeln(DataFile,'8');
  writeln(DataFile,'0');
  writeln(DataFile,'10');
  writeln(DataFile,(XVal - 0.20));
  writeln(DataFile,'20');
  writeln(DataFile,'1.600');
  writeln(DataFile,'40');
  writeln(DataFile,'0.20');
  writeln(DataFile,'1');
  writeln(DataFile,(Count * 0.2):2:1);
end;
for Count := 0 to 4 do
begin
  YVal := ((1.25 * Count) + 2.000);
  writeln(DataFile,'0');
  writeln(DataFile,'LINE');
  writeln(DataFile,'8');
  writeln(DataFile,'0');
  writeln(DataFile,'10');
  writeln(DataFile,'2.850');
  writeln(DataFile,'20');
  writeln(DataFile,YVAL);
  writeln(DataFile,'11');

```

```

writeln(DataFile,'3.150');
writeln(DataFile,'21');
writeln(DataFile,YVAL);
writeln(DataFile,'0');
writeln(DataFile,'TEXT');
writeln(DataFile,'8');
writeln(DataFile,'0');
writeln(DataFile,'10');
writeln(DataFile,'2.05');
writeln(DataFile,'20');
writeln(DataFile,(YVal - 0.1));
writeln(DataFile,'40');
writeln(DataFile,'0.20');
writeln(DataFile,'1');
case (Count) of
  0 : writeln(DataFile,'-90');
  1 : writeln(DataFile,'-45');
  2 : writeln(DataFile,' 0');
  3 : writeln(DataFile,' 45');
  4 : writeln(DataFile,' 90');
end;
end;
writeln(DataFile,'0');
writeln(DataFile,'TEXT');
writeln(DataFile,'8');
writeln(DataFile,'0');
writeln(DataFile,'10');
writeln(DataFile,'1.800');
writeln(DataFile,'20');
writeln(DataFile,'8.800');
writeln(DataFile,'40');
writeln(DataFile,'0.20');
writeln(DataFile,'1');
writeln(DataFile,'Slip Vector Plotting Program');
IntPlunge := round(Plunge);
IntTrend := round(Trend);
writeln(DataFile,'0');
writeln(DataFile,'TEXT');
writeln(DataFile,'8');
writeln(DataFile,'0');
writeln(DataFile,'10');
writeln(DataFile,'1.800');
writeln(DataFile,'20');
writeln(DataFile,'8.500');
writeln(DataFile,'40');
writeln(DataFile,'0.20');
writeln(DataFile,'1');
writeln(DataFile,'Fault Plane Normal at ',IntPlunge:2,' / ',IntTrend:3);
writeln(DataFile,'0');
writeln(DataFile,'TEXT');
writeln(DataFile,'8');
writeln(DataFile,'0');

```

```
writeln(DataFile,'10');
writeln(DataFile,'1.800');
writeln(DataFile,'20');
writeln(DataFile,'8.200');
writeln(DataFile,'40');
writeln(DataFile,'0.20');
writeln(DataFile,'1');
writeln(DataFile,'Cutoff Value = ',CutOff:4:2);
writeln(DataFile,'0');
writeln(DataFile,'TEXT');
writeln(DataFile,'8');
writeln(DataFile,'0');
writeln(DataFile,'10');
writeln(DataFile,'1.800');
writeln(DataFile,'20');
writeln(DataFile,'7.600');
writeln(DataFile,'40');
writeln(DataFile,'0.20');
writeln(DataFile,'1');
writeln(DataFile,'Pitch');
writeln(DataFile,'0');
writeln(DataFile,'TEXT');
writeln(DataFile,'8');
writeln(DataFile,'0');
writeln(DataFile,'10');
writeln(DataFile,'8.000');
writeln(DataFile,'20');
writeln(DataFile,'8.800');
writeln(DataFile,'40');
writeln(DataFile,'0.20');
writeln(DataFile,'1');
writeln(DataFile,'Fault Plane');
writeln(DataFile,'0');
writeln(DataFile,'TEXT');
writeln(DataFile,'8');
writeln(DataFile,'0');
writeln(DataFile,'10');
writeln(DataFile,'8.200');
writeln(DataFile,'20');
writeln(DataFile,'8.500');
writeln(DataFile,'40');
writeln(DataFile,'0.20');
writeln(DataFile,'1');
writeln(DataFile,' = Slip');
writeln(DataFile,'0');
writeln(DataFile,'TEXT');
writeln(DataFile,'8');
writeln(DataFile,'0');
writeln(DataFile,'10');
writeln(DataFile,'8.200');
writeln(DataFile,'20');
writeln(DataFile,'8.200');
```

```
writeln(DataFile,'40');
writeln(DataFile,'0.20');
writeln(DataFile,'1');
writeln(DataFile,' = Locked');
writeln(DataFile,'0');
writeln(DataFile,'CIRCLE');
writeln(DataFile,'8');
writeln(DataFile,'0');
writeln(DataFile,'10');
writeln(DataFile,'8.000');
writeln(DataFile,'20');
writeln(DataFile,'8.550');
writeln(DataFile,'40');
writeln(DataFile,'0.150');
writeln(DataFile,'0');
writeln(DataFile,'CIRCLE');
writeln(DataFile,'8');
writeln(DataFile,'0');
writeln(DataFile,'10');
writeln(DataFile,'8.000');
writeln(DataFile,'20');
writeln(DataFile,'8.250');
writeln(DataFile,'40');
writeln(DataFile,'0.050');
writeln(DataFile,'0');
writeln(DataFile,'TEXT');
writeln(DataFile,'8');
writeln(DataFile,'0');
writeln(DataFile,'10');
writeln(DataFile,'11.000');
writeln(DataFile,'20');
writeln(DataFile,'8.800');
writeln(DataFile,'40');
writeln(DataFile,'0.20');
writeln(DataFile,'1');
writeln(DataFile,'Sigma 1 = ',Sigma[1]);
writeln(DataFile,'0');
writeln(DataFile,'TEXT');
writeln(DataFile,'8');
writeln(DataFile,'0');
writeln(DataFile,'10');
writeln(DataFile,'11.000');
writeln(DataFile,'20');
writeln(DataFile,'8.500');
writeln(DataFile,'40');
writeln(DataFile,'0.20');
writeln(DataFile,'1');
writeln(DataFile,'Sigma 2 = ',Sigma[2]);
writeln(DataFile,'0');
writeln(DataFile,'TEXT');
writeln(DataFile,'8');
writeln(DataFile,'0');
```

```

writeln(DataFile,'10');
writeln(DataFile,'11.000');
writeln(DataFile,'20');
writeln(DataFile,'8.200');
writeln(DataFile,'40');
writeln(DataFile,'0.20');
writeln(DataFile,'1');
writeln(DataFile,'Sigma 3 = ',Sigma[3]);
writeln(DataFile,'0');
writeln(DataFile,'TEXT');
writeln(DataFile,'8');
writeln(DataFile,'0');
writeln(DataFile,'10');
writeln(DataFile,'7.800');
writeln(DataFile,'20');
writeln(DataFile,'1.000');
writeln(DataFile,'40');
writeln(DataFile,'0.20');
writeln(DataFile,'1');
writeln(DataFile,'Phi');
Deviator := (Sigma1 - Sigma3);
Step := (Deviator / Intervals);
Sigma2 := Sigma3;
for Count := 1 to (Intervals + 1) do
begin
  Phi := ((Sigma2 - Sigma3) / (Sigma1 - Sigma3));
  XVal := (3.000 + (Phi * 10.0));
  YVal := (4.500 + ((SlipAngle[Count] * 5.0) / 180.0));
  writeln(DataFile,'0');
  writeln(DataFile,'CIRCLE');
  writeln(DataFile,'8');
  writeln(DataFile,'0');
  writeln(DataFile,'10');
  writeln(DataFile,XVAL);
  writeln(DataFile,'20');
  writeln(DataFile,YVAL);
  writeln(DataFile,'40');
  if (Ratios[Count] >= CutOff)
  then writeln(DataFile,'0.150')
  else writeln(DataFile,'0.050');
  if (abs(abs(SlipAngle[Count]) - 90.0) < 0.0001)
  then
  begin
    YVal := (4.500 + ((SlipAngle[Count] * 5.0) / 180.0));
    writeln(DataFile,'0');
    writeln(DataFile,'CIRCLE');
    writeln(DataFile,'8');
    writeln(DataFile,'0');
    writeln(DataFile,'10');
    writeln(DataFile,XVAL);
    writeln(DataFile,'20');
    writeln(DataFile,YVAL);
  end
end

```

```
writeln(DataFile,'40');
if (Ratios[Count] >= CutOff)
  then writeln(DataFile,'0.150')
  else writeln(DataFile,'0.050');
YVal := (4.500 - ((SlipAngle[Count] * 5.0) / 180.0));
writeln(DataFile,'0');
writeln(DataFile,'CIRCLE');
writeln(DataFile,'8');
writeln(DataFile,'0');
writeln(DataFile,'10');
writeln(DataFile,XVAL);
writeln(DataFile,'20');
writeln(DataFile,YVAL);
writeln(DataFile,'40');
if (Ratios[Count] >= CutOff)
  then writeln(DataFile,'0.150')
  else writeln(DataFile,'0.050');
end;
Sigma2 := Sigma2 + Step;
end;
writeln(DataFile,'0');
writeln(DataFile,'ENDSEC');
writeln(DataFile,'0');
writeln(DataFile,'EOF');
close(DataFile);
end;
```

Listing of the help file SLIP.TXT called by SLIP.PAS, the program listed above.

SLIP.TXT - A 6 page help file for the program SLIP.PAS

An asterisk before a line causes it to be highlighted when the help option is chosen in the program. The first five lines of this file are not read.

1.

* Slip Vector Plotting Program

This is a program to calculate the slip vector and the stress ratios acting upon a fault plane of any arbitrary orientation with a varying magnitude of σ_2 given fixed magnitudes for σ_1 and σ_3 where the principal stress axes may be oriented either north/south, east/west, or vertical at your choosing. The results of this program are then displayed as a graph of the ratio of the principal stresses versus the pitch of the slip vector from the strike of the fault plane, as a lower-hemisphere stereographic projection of the fault plane and the slip vectors resulting from differing values of σ_2 , or as a numerical listing of the values of σ_1 , σ_2 , and σ_3 and the pitch of the slip vectors and the stress ratios which are associated with them. The stress ratios are defined as $[\sigma_s / (\mu\sigma_n + C)]$ where σ_s is the shear stress, σ_n is the normal stress, μ is the coefficient of friction, and C is the cohesion.

The idea for this program came from a paper in volume 96 of Geological Magazine by M. H. P. Bott entitled "The Mechanics of Oblique Slip Faulting" published in 1959. Bott showed that the position of the slip vector in the fault plane is dependant upon the ratios of the three principal stresses.

2.

* Slip Vector Plotting Program

When you begin program execution, you will be asked to provide a value for σ_1 and σ_3 . The program will accept any positive real numbers as valid values provided, of course, that the value for σ_1 is greater than that for σ_3 . A value for the coefficient of friction (μ) and the cohesion must then be supplied. Next, the values of the plunge and trend of the normal to the fault plane you wish to examine must be entered. The plunge may be any real number between 0 and 89.9 inclusive and the trend may be any real number between 0 and 359.9 inclusive. The program will then ask for the number of intervals of σ_2 you wish to examine as σ_2 varies between σ_3 and σ_1 in however many increments you specify. The program will accept any integer between 2 and 50 inclusive for this value.

Although the program will accept any real numbers greater than or equal to zero for the values of σ_1 , σ_3 , μ , and C, it must be kept in mind that there are many values which could be entered which may not have any real geological significance. Always try to keep in mind as to what might be realistic values for the deviatoric stress ($\sigma_1 - \sigma_3$) and for the isotropic stress $[(\sigma_1 + \sigma_2 + \sigma_3) / 3.0]$.

3.

* Slip Vector Plotting Program

After this program has run, you may examine the data in several ways. First, you may examine a graph plotting Φ versus the pitch of the slip vector from the strike direction. Φ is defined as $[(\sigma_2 - \sigma_3) / (\sigma_1 - \sigma_3)]$ and the pitch varies from -90.0 to +90.0 degrees as an angle from the strike direction which is always between 0.0 and 180.0 degrees inclusive. Second, a lower-hemisphere stereograph projection may be examined which plots the fault plane and the positions of the different slip vectors on it for the differing values of σ_2 . Third, the numerical values of σ_1 , σ_2 , and σ_3 may be written along with the values for the pitch of the slip vectors and the ratio of the shear to normal stresses associated with them. This data may also be printed by writing it to a disk data file and then using the DOS command:

* PRINT filename.ext

The graph and the stereonet may also be written to an AutoCAD drawing interchange file (DXF).

4.

* Slip Vector Plotting Program

To create and print an AutoCAD drawing interchange file, first write the data to a file with the extension .DXF and then read that file into AutoCAD using the DXFIN command. Once in AutoCAD, changes may be made if desired and the drawing may then be plotted using a laser printer or pen plotter.

Before creating the graph or stereonet plots, the program will ask for a cutoff value for the shear to normal stress ratio. When a value greater than 0.0 is specified, any slip vector with a stress ratio above the cutoff will be plotted as a circle and any slip vector with a value below the cutoff will be plotted as a square. The rationale for doing this is that faulting will occur only when the stress ratio exceeds a certain value. When a geologically reasonable value is entered, it may be assumed that any vector plotting as a circle may initiate slip while any vector plotting as a square will leave the fault remaining locked.

The main purpose of this program is to generate a data set of known fault orientations and their slip directions given a specified stress field. This data will then be used to test and evaluate different computer methods for determining principal stress orientations from faults and their slip vectors.

5.

* Slip Vector Plotting Program

This program was written by Steven H. Schimmrich in Turbo Pascal (Borland, Inc. - registered trademark) for an IBM AT personal computer with a numeric

coprocessor, 512 K memory, and color graphics capabilities. The program may not run properly on other machines. Version 1.0 of this program was written in April of 1988, version 2.0 in July of 1988. This help file that you are reading is called SLIP.TXT and must be on the same disk as the main program SLIP.PAS is. The compiled version of this program is called SLIP.COM and may be run from the DOS level by simply typing SLIP at the DOS prompt.

If at any time during the program execution it becomes "stuck" or the keyboard freezes, pressing the Ctrl key and the C letter key at the same time will usually return you to the DOS level. If that fails try pressing the Ctrl, Alt, and Del keys all at the same time to reboot the computer.

* SLIP.PAS
* Copyright (C) 1988
* Steven H. Schimmrich

APPENDIX D

FAULT PLANE PLOTTING PROGRAM

Complete listing of the fault plane plotting program discussed in chapters six and seven. The program FPLANE.PAS is written in Turbo Pascal version 3.01 for an IBM PC or compatible computer.

```
program FPlane;
```

```
{ **** }
{
  This is a program to create an AutoCAD script file of planes and
  their associated slip directions for plotting on a lower-hemisphere
  equal-angle stereographic projection.
}
{ **** }
```

```
      FPLANE.PAS - Version 1.0
```

```
      Copyright (C) 1989 -- Steven H. Schimmrich
      For educational and research purposes only
      All commercial rights reserved
```

```
      Steven H. Schimmrich
      Department of Geological Sciences
      State University of New York at Albany
      Albany, New York 12222
```

```
{ Initializations }
```

```
type
```

```
RegisterList      =
  record
    AX,BX,CX,DX,BP,SI,DI,DS,ES,Flags : integer;
  end;
RArr              = array[1..100] of real;
String25          = string[25];
```

```
var
```

```
Plunge, Trend, Pitch : RArr;
Number                : integer;
FileName              : String25;
```

```

{General program functions }

function Exists(FileName : String25): boolean;
  { Checks to see if a file exists on the disk }
var
  Name : file;
begin
  Assign(Name,FileName);
  {$I-}
  Reset(Name);
  {$I+}
  Exists := (IOResult = 0);
end;

procedure Cursor(On : boolean);
  { Turns cursor on and off }
var
  Register : RegisterList;
begin
  if (On)
  then
    if (mem[0:$449] = 7)
    then
      Register.CX := $0C0D
    else
      Register.CX := $0607
    else
      Register.CX := $2000;
  Register.AX := $0100;
  intr($10,Register);
end;

function Zero(Value : real): boolean;
  { Checks to see if a value is essentially 0.0 }
begin
  if (abs(Value) < 0.00001)
  then Zero := true
  else Zero := false;
end;

function DegToRad(DegreeMeasure : real): real;
  { Converts an angle in degrees to one in radians }
begin
  DegToRad := ((DegreeMeasure * PI) / 180.0);
end;

function RadToDeg(RadianMeasure : real): real;
  { Converts an angle in radians to one in degrees }
begin
  RadToDeg := ((RadianMeasure * 180.0) / PI);
end;

```

```

function Tan(Angle : real): real;
  { Returns the tangent of an angle }
begin
  Tan := sin(Angle) / cos(Angle);
end;

function ArcCos(AValue : real): real;
  { Returns the arccosine of a value }
var
  X, Y : real;
begin
  if (AValue = 0.0)
  then ArcCos := (PI / 2.0)
  else if (AValue = 1.0)
  then ArcCos := 0.0
  else if (AValue = -1.0)
  then ArcCos := PI
  else
  begin
    X := (AValue / sqrt(1.0 - sqr(AValue)));
    Y := arctan(abs(1.0 / X));
    if (X > 0.0)
    then ArcCos := Y
    else ArcCos := (PI - Y);
  end;
end;

{ General program procedures }

procedure DrawBox(ULX, ULY, LRX, LRY : integer);
  { Draws a box around text in text mode }
var
  X, Y, XDistance : integer;
begin
  gotoxy(ULX,ULY);
  write(#201);
  XDistance := LRX - ULX - 1;
  for X := 1 to XDistance do
    write(#205);
  write(#187);
  for Y := (ULY + 1) to (LRY - 1) do
  begin
    gotoxy(LRX,Y);
    write(#186);
    gotoxy(ULX,Y);
    write(#186);
  end;
  gotoxy(ULX,LRY);
  write(#200);
  for X := 1 to XDistance do
    write(#205);
  write(#188);

```

```

end;

procedure DisplayPage;
  { Displays an introduction page }
begin
  textmode;
  clrscr;
  cursor(false);
  textcolor(12);
  DrawBox(20,9,61,18);
  textcolor(11);
  gotoxy(27,10);
  writeln('Fault Plane Plotting Program');
  gotoxy(32,12);
  writeln('Program written by');
  gotoxy(31,14);
  writeln('Steven H. Schimmrich');
  gotoxy(24,15);
  writeln('Department of Geological Sciences');
  gotoxy(22,16);
  writeln('State University of New York at Albany');
  gotoxy(30,17);
  writeln('Albany, New York 12222');
  delay(5000);
  cursor(true);
  clrscr;
end;

procedure IntroPage;
  { Displays a short introduction to the program }
var
  Key : char;
begin
  gotoxy(27,2);
  textcolor(12);
  writeln('Fault Plane Plotting Program');
  textcolor(11);
  writeln;
  writeln;
  writeln(' This is a quick and dirty program to plot fault planes and their associated');
  writeln(' slip directions onto an equal-angle stereographic projection using an AutoCAD');
  writeln(' SCRipt file. This program was written because the RockWare stereonet program');
  writeln(' on this computer can not plot planes as great circles easily. ');
  writeln(' This program first asks for a filename of a disk file containing the fault');
  writeln(' data. This data must have the following format : ');
  writeln;
  textcolor(12);
  writeln(' 25 125 13');
  textcolor(11);
  writeln;
  writeln(' where 25 is the plunge and 125 is the trend of the fault plane normal and 13');
  writeln(' is the pitch of the slip vector within the fault plane. The pitch is the angle');

```

```

writeln(' between the strike (the trend of the normal + 90 degrees) and the slip vector');
writeln(' which varies from -90 to 90 degrees. If you do not wish to plot the slip');
writeln(' vectors, enter a 99 for the pitch. Entering a 999 for the pitch will treat');
writeln(' the plunge and trend values as an axis and plot a circle. ');
write(' The program will then create an AutoCAD file named FPLANE.SCR ');
writeln('overwriting');
writeln(' any old versions of FPLANE.SCR if they exist on the disk. The file may then');
writeln(' be read into AutoCAD and plotted using the laser printer. If any text is');
writeln(' desired, it may be added while in AutoCAD. ');
writeln;
gotoxy(2,25);
write('Press any ');
textcolor(12);
write('key');
textcolor(11);
write(' to continue... ');
read(kbd,Key);
clrscr;
end;

```

```

procedure AskFileName(var FileName : String25);
  { Asks for the name of the data file }
begin
  gotoxy(27,2);
  textcolor(12);
  writeln('Fault Plane Plotting Program');
  textcolor(11);
  writeln;
  writeln;
  writeln(' The program now needs the name of the disk file');
  writeln(' containing the fault normals and slip directions. ');
  repeat
    writeln;
    write(' Enter the name of the data file : ');
    textcolor(12);
    readln(FileName);
    textcolor(11);
    if (not(Exists(FileName)))
      then
        begin
          sound(880);
          delay(50);
          nosound;
          writeln;
          textcolor(12);
          writeln(' * ERROR * That file does not exist on this disk');
          textcolor(11);
        end;
    until (Exists(FileName));
  clrscr;
end;

```

```

procedure ReadData(FileName : String25; var Number : integer;
                  var Plunge, Trend, Pitch : RArr);
  { Reads in the data from a disk file }
var
  DataFile : text;
begin
  Number := 0;
  gotoxy(27,2);
  textcolor(12);
  writeln('Fault Plane Plotting Program');
  textcolor(11);
  gotoxy(2,8);
  write('Creating AutoCAD file...');
  assign(DataFile,FileName);
  reset(DataFile);
  while (not(EOF(DataFile))) do
  begin
    Number := Number + 1;
    readln(DataFile,Plunge[Number],Trend[Number],Pitch[Number]);
  end;
  close(DataFile);
end;

procedure CreatePlot(var Number : integer; var Plunge, Trend, Pitch : RArr);
  { Creates the AutoCAD plot of data }
label 1;
label 2;
const
  ACADFILE = 'FPLANE.SCR';
var
  Strike, Dip, ApparentDip, Theta,
  Distance, Beta, XVal, YVal, XVal1,
  Yval1, XVal2, YVal2, XVal3, YVal3,
  ZeroTrend, SlipTrend, SlipPlunge      :      real;
  Count, Counter                        :      integer;
  DataFile                               :      text;
begin
  assign(DataFile,ACADFILE);
  rewrite(DataFile);
  writeln(DataFile,'CIRCLE');
  writeln(DataFile,'7.500,4.500');
  writeln(DataFile,'4.000');
  writeln(DataFile,'LINE');
  writeln(DataFile,'7.350,4.500');
  writeln(DataFile,'7.650,4.500');
  writeln(DataFile,' ');
  writeln(DataFile,'LINE');
  writeln(DataFile,'7.500,4.350');
  writeln(DataFile,'7.500,4.650');
  writeln(DataFile,' ');
  writeln(DataFile,'LINE');
  writeln(DataFile,'7.500,8.350');

```

```

writeln(DataFile,'7.500,8.650');
writeln(DataFile,' ');
writeln(DataFile,'TEXT');
writeln(DataFile,'MIDDLE');
writeln(DataFile,'7.500,8.800');
writeln(DataFile,'0.200');
writeln(DataFile,'0');
writeln(DataFile,'N');
for Count := 1 to Number do
begin
  if (Pitch[Count] = 999.0) then goto 1;
  if (Plunge[Count] = 0.0)
  then Plunge[Count] := Plunge[Count] + 0.0001;
  Dip := DegToRad(90.0 - Plunge[Count]);
  if ((Trend[Count] >= 90.0) and (Trend[Count] < 270.0))
  then Strike := Trend[Count] - 90.0
  else Strike := Trend[Count] + 90.0;
  if (Strike >= 360.0)
  then Strike := Strike - 360.0;
  for Counter := 0 to 2 do
  begin
    Beta := DegToRad(Counter * 90.0);
    ApparentDip := arctan(Tan(Dip) * sin(Beta));
    Distance := 4.000 * Tan((PI / 4.0) - (ApparentDip / 2.0));
    if (Distance < 0.05)
    then
    begin
      Distance := (RadToDeg(Beta) * (2.0 / 45.0));
      if (Distance > 4.000)
      then Distance := 4.000 - Distance;
      Beta := DegToRad(Strike);
      Beta := (((5.0 * PI) / 2.0) - Beta);
      if (Beta >= (2.0 * PI))
      then Beta := (Beta - (2.0 * PI));
      if (Beta < 0.0)
      then Beta := (Beta + (2.0 * PI));
    end
  else
  begin
    if ((Trend[Count] >= 90.0) and (Trend[Count] < 270.0))
    then Beta := DegToRad(Strike) - Beta
    else Beta := DegToRad(Strike) + Beta;
    if (Beta >= (2.0 * PI))
    then Beta := (Beta - (2.0 * PI));
    if (Beta < 0.0)
    then Beta := (Beta + (2.0 * PI));
    Beta := (((5.0 * PI) / 2.0) - Beta);
    if (Beta >= (2.0 * PI))
    then Beta := (Beta - (2.0 * PI));
    if (Beta < 0.0)
    then Beta := (Beta + (2.0 * PI));
  end;
end;

```

```

XVal := (7.500 + (Distance * cos(Beta)));
YVal := (4.500 + (Distance * sin(Beta)));
case (Counter) of
  0 : begin
    XVal1 := XVal;
    YVal1 := YVal;
  end;
  1 : begin
    XVal2 := XVal;
    YVal2 := YVal;
  end;
  2 : begin
    XVal3 := XVal;
    YVal3 := YVal;
  end;
end;
end;
if ((abs(XVal1 - XVal2) >= 0.01) or (abs(YVal1 - YVal2) >= 0.001))
then
begin
  writeln(DataFile,'ARC');
  writeln(DataFile,XVal1:5:3,',',YVal1:5:3);
  writeln(DataFile,XVal2:5:3,',',YVal2:5:3);
  writeln(DataFile,XVal3:5:3,',',YVal3:5:3);
end
else
begin
  writeln(DataFile,'LINE');
  writeln(DataFile,XVal1:5:3,',',YVal1:5:3);
  writeln(DataFile,XVal3:5:3,',',YVal3:5:3);
  writeln(DataFile,' ');
end;
if (Pitch[Count] = 99.0) then goto 2;
if (not(Zero(Pitch[Count])))
then Beta := RadToDeg(arctan(cos(DegToRad(90 - Plunge[Count])) *
Tan(DegToRad(Pitch[Count]))))
else Beta := 0.0;
Strike := Trend[Count] + 90.0;
if (Strike > 360.0)
then Strike := Strike - 180.0;
SlipTrend := Strike + Beta;
if (not(Zero(abs(Beta) - 90.0)))
then SlipPlunge := RadToDeg(ArcCos(cos(DegToRad(Pitch[Count])) /
cos(DegToRad(Beta))))
else SlipPlunge := 90.0 - Plunge[Count];
if ((Pitch[Count] < 0.0) or (Pitch[Count] = 90.0))
then SlipTrend := SlipTrend + 180.0;
if (Trend[Count] > 270)
then SlipTrend := SlipTrend + 180.0;
if (SlipTrend > 360.0)
then SlipTrend := SlipTrend - 360.0;
Distance := (4.000 * Tan((PI / 4.0) - (DegToRad(SlipPlunge) / 2.0)));

```

```

if (SlipPlunge = 0.0)
  then
  begin
    ZeroTrend := (SlipTrend + 180.0);
    if (ZeroTrend >= 360.0)
      then ZeroTrend := ZeroTrend - 360.0;
    Theta := (((5.0 * PI) / 2.0) - DegToRad(ZeroTrend));
    XVal := (7.500 - (Distance * cos(Theta)));
    YVal := (4.500 - (Distance * sin(Theta)));
    writeln(DataFile,'CIRCLE');
    writeln(DataFile,XVAL:5:3,',',YVAL:5:3);
    writeln(DataFile,'0.060');
  end;
Theta := (((5.0 * PI) / 2.0) - DegToRad(SlipTrend));
if (Pitch[Count] = 90.0)
  then
  begin
    XVal := (7.500 - (Distance * cos(Theta)));
    YVal := (4.500 - (Distance * sin(Theta)));
  end
  else
  begin
    XVal := (7.500 + (Distance * cos(Theta)));
    YVal := (4.500 + (Distance * sin(Theta)));
  end;
writeln(DataFile,'CIRCLE');
writeln(DataFile,XVAL:5:3,',',YVAL:5:3);
writeln(DataFile,'0.060');
goto 2;
1: {continue};
  Distance := (4.000 * Tan((PI / 4.0) - (DegToRad(Plunge[Count]) / 2.0)));
  Theta := (((5.0 * PI) / 2.0) - DegToRad(Trend[Count]));
  XVal := (7.500 + (Distance * cos(Theta)));
  YVal := (4.500 + (Distance * sin(Theta)));
  writeln(DataFile,'CIRCLE');
  writeln(DataFile,XVAL:5:3,',',YVAL:5:3);
  writeln(DataFile,'0.090');
2: {continue};
end;
writeln(DataFile,'REGEN');
close(DataFile);
gotoxy(2,12);
write('AutoCAD file ');
textcolor(12);
write('FPLANE.SCR');
textcolor(11);
write(' created...');
sound(880);
delay(50);
nosound;
delay(5000);
end;

```

```
{ Main program }  
  
begin  
  DisplayPage;  
  IntroPage;  
  AskFileName(FileName);  
  ReadData(FileName,Number,Plunge,Trend,Pitch);  
  CreatePlot(Number,Plunge,Trend,Pitch);  
  DisplayPage;  
end.
```

APPENDIX E

VECTOR ANGLE CALCULATION PROGRAM

Complete listing of the vector angle calculation program discussed in chapter nine. The program ANGLE.PAS is written in Turbo Pascal version 3.01 for an IBM PC or compatible computer.

```
program Angle;
```

```
{ ***** }
{
{   This is a program to calculate the angles between two vectors
{   given their stereographic plunges and trends in degrees.
{
{ ***** }
{
{           ANGLE.PAS - Version 1.0
{
{   Copyright (C) 1989 -- Steven H. Schimmrich
{   For educational and research purposes only
{   All commercial rights reserved
{
{           Steven H. Schimmrich
{           Department of Geological Sciences
{           State University of New York at Albany
{           Albany, New York 12222
{
{ ***** }
```

```
{ Initializations }
```

```
var
```

```
  Plunge1, Plunge2, Trend1, Trend2           :   integer;
  Angle, DotProduct, X1, Y1, Z1, X2, Y2, Z2   :   real;
  Loop                                         :   boolean;
  Key                                          :   char;
```

```
function DegtoRad(DegreeMeasure : real): real;
{ Converts an angle in degrees to one in radians }
begin
  DegtoRad := ((DegreeMeasure * PI) / 180.0);
end;
```

```
function RadtoDeg(RadianMeasure : real): real;
{ Converts an angle in radians to one in degrees }
```

```

begin
  RadtoDeg := ((RadianMeasure * 180.0) / PI);
end;

function ArcCos(AValue : real): real;
{ Returns the arccosine of a value }
var
  X, Y : real;
begin
  if (AValue = 0.0)
  then ArcCos := (PI / 2.0)
  else if (AValue = 1.0)
  then ArcCos := 0.0
  else if (AValue = -1.0)
  then ArcCos := PI
  else
  begin
    X := (AValue / sqrt(1.0 - sqr(AValue)));
    Y := arctan(abs(1.0 / X));
    if (X > 0.0)
    then ArcCos := Y
    else ArcCos := (PI - Y);
  end;
end;

{ Main program }

begin
  Loop := true;
  while (Loop) do
  begin
    clrscr;
    textcolor(12);
    writeln('          Angle Calculation Program');
    textcolor(14);
    writeln;
    writeln;
    writeln('  Given the plunge and trend values in degrees of two');
    writeln('vectors, this program will calculate the angle between');
    writeln('them in degrees. ');
    writeln;
    writeln;
    write('Vector');
    textcolor(12);
    writeln(' 1');
    textcolor(14);
    writeln;
    write(' Enter the plunge : ');
    textcolor(12);
    readln(Plunge1);
    textcolor(14);
    write(' Enter the trend : ');

```

```

textcolor(12);
readln(Trend1);
textcolor(14);
writeln;
write('Vector');
textcolor(12);
writeln(' 2');
textcolor(14);
writeln;
write(' Enter the plunge : ');
textcolor(12);
readln(Plunge2);
textcolor(14);
write(' Enter the trend : ');
textcolor(12);
readln(Trend2);
textcolor(14);
if ((Plunge1 > 90) or (Plunge1 < 0) or (Plunge2 > 90) or (Plunge2 < 0)
    or (Trend1 > 360) or (Trend1 < 0) or (Trend2 > 360) or (Trend2 < 0))
then
begin
    writeln;
    writeln;
    sound(880);
    delay(100);
    nosound;
    textcolor(12);
    write('ERROR');
    textcolor(14);
    writeln(' - An incorrect plunge or trend has been entered!');
    exit;
end;
X1 := (cos(DegtoRad(Plunge1)) * cos(DegtoRad(Trend1)));
Y1 := (sin(DegtoRad(Plunge1)));
Z1 := (cos(DegtoRad(Plunge1)) * sin(DegtoRad(Trend1)));
X2 := (cos(DegtoRad(Plunge2)) * cos(DegtoRad(Trend2)));
Y2 := (sin(DegtoRad(Plunge2)));
Z2 := (cos(DegtoRad(Plunge2)) * sin(DegtoRad(Trend2)));
DotProduct := ((X1 * X2) + (Y1 * Y2) + (Z1 * Z2));
Angle := (RadtoDeg(ArcCos(DotProduct)));
if (Angle > 90.0)
    then Angle := 180.0 - Angle;
writeln;
writeln;
write('The angle between vectors');
textcolor(12);
write(' 1');
textcolor(14);
write(' and');
textcolor(12);
write(' 2');
textcolor(14);

```

```
write(' is');
textcolor(12);
write(Angle:6:1);
textcolor(14);
writeln(' degrees. ');
writeln;
writeln;
write('Do another calculation ( ');
textcolor(12);
write('Y');
textcolor(14);
write(' or');
textcolor(12);
write(' N');
textcolor(14);
write(') ? ');
read(kbd,Key);
if (Key in ['y','Y'])
  then Loop := true
  else Loop := false;
end;
clrscr;
end.
```

REFERENCES

- Aleksandrowski, P. 1985. Graphical determination of principal stress directions for slickenside lineation populations: An attempt to modify Arthaud's method. *Journal of Structural Geology*. **7**:73-82.
- Allmendinger, R. W. 1989. Personal communication with Richard Allmendinger of Cornell University.
- Anderson, E. M. 1951. *The Dynamics of Faulting and Dyke Formation with Applications to Britain*. 2nd edition. Oliver and Boyd: Edinburgh. 206 pages.
- Angelier, J. 1975. Sur l'analyse de mesures recueillies dans des sites faillés: L'utilité d'une confrontation entre les méthodes dynamiques et cinématiques. *Comptes Rendus Hebdomadaires de L'Académie des Sciences France, Série D*. **281**:1805-1808.
- Angelier, J. and Mechler, P. 1977. Sur une méthode graphique de recherche des contraintes également utilisable en tectonique et en séismologie: La méthode des dièdres droits. *Bulletin de la Société Géologique de France*. **19**:1309-1318.
- Angelier, J. 1979. Determination of the mean principal directions of stresses for a given fault population. *Tectonophysics*. **56**:T17-T26.
- Angelier, J. and Goguel, J. 1979. Sur une méthode simple de détermination des axes principaux des contraintes pour une population de failles. *Comptes Rendus Hebdomadaires de L'Académie des Sciences France, Série D*. **288**:307-310.
- Angelier, J. and Manoussis, S. 1980. Classification automatique et distinction des phases superposées en tectonique de failles. *Comptes Rendus Hebdomadaires de L'Académie des Sciences France, Série D*. **290**:651-654.
- Angelier, J., Tarantola, A., Valette, B., and Manoussis, S. 1982. Inversion of field data in fault tectonics to obtain the regional stress. I. Single phase fault populations: A new method of computing the stress tensor. *Geophysical Journal of the Royal Astronomical*

- Society*. **69**:607-621.
- Angelier, J. 1984. Tectonic analysis of fault slip data sets. *Journal of Geophysical Research*. **89**:5835-5848.
- Angelier, J., Colletta, B., and Anderson, R. E. 1985. Neogene paleostress changes in the Basin and Range: A case study at Hoover Dam, Nevada-Arizona. *Geological Society of America Bulletin*. **96**:347-361.
- Angelier, J. 1989. From orientation to magnitudes in paleostress determinations using fault slip data. *Journal of Structural Geology*. **11**:37-50.
- Armijo, R. and Cisternas, A. 1978. Un problème inverse en microtectonique cassante. *Comptes Rendus Hebdomadaires de L'Académie des Sciences France, Série D*. **287**:595-598.
- Armijo, R., Carey, E., and Cisternas, A. 1982. The inverse problem in microtectonics and the separation of tectonic phases. *Tectonophysics*. **82**:145-160.
- Athaud, F. 1969. Méthode de détermination graphique des directions de raccourcissement, d'allongement et intermédiaire d'une population de failles. *Bulletin de la Société Géologique de France*. **11**:729-737.
- Arthaud, F. and Mattauer, M. 1969. Exemples de stylolites d'origine tectonique dans le Languedoc, leurs relations avec la tectonique cassante. *Bulletin de la Société Géologique de France*. **11**:738-744.
- Aydin, A. 1977. Faulting in Sandstone. Ph.D. dissertation. Stanford University.
- Aydin, A. 1980. Determination of the orientation of the principal stresses from three or more sets of contemporaneous faults (abstract). *EOS: Transactions of the American Geophysical Union*. **61**:1117.
- Aydin, A. and Reches, Z. 1982. Number and orientation of fault sets in the field and in experiments. *Geology*. **10**:107-112.
- Bahat, D. and Rabinovich, A. 1988. Paleostress determination in a rock by a fractographic

- method. *Journal of Structural Geology*. **10**:193-199.
- Barton, N. and Choubey, V. 1977. The shear strength of rocks in theory and practice. *Rock Mechanics*. **10**:1-54.
- Berger, A. R. 1971. Dynamic analysis using dykes with oblique internal foliations. *Geological Society of America Bulletin*. **82**:781-786.
- Billings, M. P. 1972. *Structural Geology*. 3rd edition. Prentice-Hall: Englewood Cliffs, NJ. 606 pages.
- Borradaile, G. J. 1986. The internal tectonic fabric of minor intrusions and their potential as regional paleostress indicators. *Geological Magazine*. **123**:665-671.
- Bott, M. H. P. 1959. The mechanics of oblique-slip faulting. *Geological Magazine*. **96**:109-117.
- Brace, W. F. and Kohlstedt, D. L. 1980. Limits on lithospheric stress imposed by laboratory experiments. *Journal of Geophysical Research*. **85**:6248-6252.
- Brown, S. R. and Scholz, C. H. 1985. Broad bandwidth study of the topography of natural rock surfaces. *Journal of Geophysical Research*. **90**:12,575-12,582.
- Buchner, F. 1981. Rhinegraben: Horizontal stylolites indicating stress regimes of earlier states of rifting. *Tectonophysics*. **73**:113-118.
- Beutner, E. C. 1972. Reverse gravitational movement on earlier overthrusts, Lemhi Range, Idaho. *Geological Society of America Bulletin*. **83**:839-847
- Byerlee, J. D. 1968. Brittle-ductile transition in rocks. *Journal of Geophysical Research*. **73**:4741-4750.
- Byerlee, J. D. 1978. Friction of rocks. *Pure and Applied Geophysics*. **116**:615-626.
- Byerlee, J. D., Mjachkin, V., Summers, R., and Voevoda, O. 1978. Structures developed in fault gouge during stable sliding and stick-slip. *Tectonophysics*. **44**:161-171.
- Caputo, M. and Caputo, R. 1988. Structural analysis: New analytical approach and applications. *Annales Tectonicæ*. **2**:84-89.

- Carey, E. and Brunier, B. 1974. Analyse théorique et numérique d'un modèle mécanique élémentaire appliqué à l'étude d'une population de failles. *Comptes Rendus Hebdomadaires de L'Académie des Sciences France, Série D.* **279**:891-894.
- Carey, E. 1976. Analyse numérique d'un modèle mécanique élémentaire appliqué à l'étude d'une population de failles: Calcul d'un tenseur moyen des contraintes a partir de stries de glissement. Thèse 3ème cycle. Université de Paris Sud.
- Carter, N. L. and Raleigh, C. B. 1969. Principal stress directions from plastic flow in crystals. *Geological Society of America Bulletin.* **80**:1231-1264.
- Célérier, B. 1988. How much does slip on a reactivated fault plane constrain the stress tensor? *Tectonics.* **7**:1257-1278.
- Cheaney, R. F. 1983. *Statistical Methods in Geology.* George Allen & Unwin: London. 169 pages.
- Compton, R. R. 1962. *Manual of Field Geology.* John Wiley: New York, NY. 378 pages.
- Coulomb, C. A. 1776. Sur une application des règles de maximis et minimis à quelques problèmes de statique, relatifs à l'architecture. *Academie Royale des Sciences, Paris. Memoires de Mathematique et de Physique.* **7**:343-382.
- Cox, A. and Hart, R. B. 1986. *Plate Tectonics: How it Works.* Blackwell Scientific: Palo Alto, CA. 392 pages.
- Davidson, L. M. and Park, R. G. 1978. Late Nagssugtoqidian stress orientation derived from deformed granodiorite dykes north of Holsteinsborg, West Greenland. *Journal of the Geological Society of London.* **135**:283-289.
- Davis, G. H. 1984. *Structural Geology of Rocks and Regions.* John Wiley & Sons: New York, NY. 492 pages.
- Dennis, J. G. 1987. *Structural Geology: An Introduction.* Wm. C. Brown: Dubuque, Iowa. 448 pages.
- Dieterich, J. H. and Carter, N. L. 1969. Stress-history of folding. *American Journal of*

- Science*. **267**:129-154.
- Donath, F. A. 1962. Analysis of Basin-Range structure. *Geological Society of America Bulletin*. **73**:1-16.
- Donath, F. A. 1964. Strength variation and deformational behavior in anisotropic rock. In Judd, W. R. 1964. *State of Stress in the Earth's Crust*. American Elsevier: New York, NY. Pages 281-299.
- Durney, D. W. and Ramsay, J. G. 1973. Incremental strains measured by syntectonic crystal growths. In De Jong, K. A. and Scholten, R. 1973. *Gravity and Tectonics*. Pages 67-96.
- Edelman, S. H. 1989. Limitations on the concept of stress in structural analysis. *Journal of Geological Education*. **37**:102-106.
- Ellsworth, W. L. and Zhonghuai, X. 1980. Determination of the stress tensor from focal mechanism data (abstract). *EOS: Transactions of the American Geophysical Union*. **61**:1117.
- Engelder, T. and Geiser, P. 1980. On the use of regional joint sets as trajectories of paleostress fields during the development of the Appalachian Plateau, New York. *Journal of Geophysical Research*. **85**:6319-6341.
- Engelder, T. 1982. Is there a genetic relationship between selected regional joints and contemporary stress within the lithosphere of North America? *Tectonics*. **1**:161-177.
- Etchecopar, A., Vasseur, G., and Daignieres, M. 1981. An inverse problem in microtectonics for the determination of stress tensors from fault striation analysis. *Journal of Structural Geology*. **3**:51-65.
- Fleuty, M. J. 1975. Slickensides and slickenlines. *Geological Magazine*. **112**:319-322.
- Friedman, M. 1964. Petrofabric techniques for the determination of the principal stress directions in rocks. In Judd, W. R. 1964. *State of Stress in the Earth's Crust*. American Elsevier: New York, NY. Pages 451-550.

- Frizzell, V. A. and Zoback, M. L. 1987. Stress orientation determined from fault slip data in Hampel Wash area, Nevada, and its relation to contemporary regional stress field. *Tectonics*. **6**:89-98.
- Fröberg, C. E. 1985. *Numerical Mathematics: Theory and Computer Applications*. Benjamin/Cummings: Meno Park, CA. 436 pages.
- Galindo-Zaldivar, J. and Gonzalez-Lodeiro, F. 1988. Fault phase differentiation by means of computer search on a grid pattern. *Annales Tectonicæ*. **2**:90-97.
- Gamond, J. F. 1983. Displacement features associated with fault zones: A comparison between observed examples and experimental models. *Journal of Structural Geology*. **5**:33-45.
- Gamond, J. F. 1987. Bridge structures as sense of displacement criteria in brittle fault zones. *Journal of Structural Geology*. **9**:609-620.
- Gay, N. C. 1970. The formation of step structures on slickensided shear surfaces. *Journal of Geology*. **78**:523-532.
- Gay, N. L. and Weiss, L. E. 1974. The relationship between principal stress direction and the geometry of kinks in foliated rocks. *Tectonophysics*. **21**:287-300.
- Gephart, J. W. and Forsyth, D. W. 1984. An improved method for determining the regional stress tensor using earthquake focal mechanism data: Application to the San Fernando earthquake sequence. *Journal of Geophysical Research*. **89**:9305-9320.
- Gephart, J. W. 1990. Personal communication with John Gephart of Cornell University.
- Hafner, W. 1951. Stress distributions and faulting. *Geological Society of America Bulletin*. **62**:373-398.
- Hancock, P. L. 1985. Brittle microtectonics: Principles and practice. *Journal of Structural Geology*. **7**:437-457.
- Hancock, P. L., Al-Kahdi, A., Barka, A. A., and Bevan, T. G. 1987. Aspects of analyzing brittle structures. *Annales Tectonicæ*. **1**:5-19.

- Handin, J. 1969. On the Coulomb-Mohr failure criterion. *Journal of Geophysical Research*, **74**:5343-5348.
- Hansen, K. M. and Mount, V. S. 1990. Smoothing and extrapolation of crustal stress orientation measurements. *Journal of Geophysical Research*, **95**:1155-1165
- Hardcastle, K. C. 1989. Possible paleostress tensor configurations derived from fault-slip data in eastern Vermont and western New Hampshire. *Tectonics*, **8**:265-284.
- Hardcastle, K. C. 1990. Personal communication with Kenneth Hardcastle of the University of Massachusetts at Amherst.
- Hartmann. 1896. *Distribution des Déformations dans les Métaux Soumis à des Efforts*. Berger-Leurault: Paris.
- Hatzor, Y. and Reches, Z. 1990. Structure and paleostresses in the Gilboa region, western margins of the Dead Sea transform. *Tectonophysics*, **180**:87-100.
- Hobbs, B. E., Means, W. D., and Williams, P. F. 1976. *An Outline of Structural Geology*. John Wiley: New York, NY. 571 pages.
- Huang, Q. and Angelier, J. 1987. Les systèmes de failles conjuguées: Un méthode d'identification, de séparation et de calcul des axes de contraint. *Comptes Rendus Hebdomadaires de L'Académie des Sciences France, Série 2*, **304**:465-468.
- Huang, Q. 1988. Computer-based method to separate heterogeneous sets of fault-slip data into sub-sets. *Journal of Structural Geology*, **10**:297-299.
- Jaeger, J. C. 1960. Shear failure of anisotropic rocks. *Geological Magazine*, **97**:65-72.
- Jaeger, J. C. 1969. *Elasticity, Fracture and Flow with Engineering and Geological Applications*. 3rd edition. Methuen: London. 268 pages.
- Jaeger, J. C. and Cook, N. G. W. 1979. *Fundamentals of Rock Mechanics*. 3rd edition. Chapman and Hall: London. 593 pages.
- Jang, B., Wang, H. F., Ren, X., and Kowallis, B. J. 1989. Precambrian paleostress from microcracks and fluid inclusions in the Wolf River batholith of central Wisconsin.

- Geological Society of America Bulletin*. **101**:1457-1464.
- Jaroszewski, W. 1984. *Fault and Fold Tectonics*. John Wiley, New York, NY. 565 pages.
- Jones, L. 1988. Focal mechanisms and the state of stress on the San Andreas fault in southern California. *Journal of Geophysical Research*. **93**:8869-8891.
- Julien, P. and Cornet, F. 1987. Stress determination from aftershocks of the Campania-Lucania earthquake of November 23, 1980. *Annales Geophysicæ*. **5B**:289-300.
- Kowallis, B. J., Wang, H. F., and Jang, B. 1987. Healed microcrack orientations in granite from Illinois borehole UPH-3 and their relationship to the rock's stress history. *Tectonophysics*. **135**:297-306.
- Krantz, R. W. 1986. Orthorhombic fault patterns and three-dimensional strain analysis, northern San Rafael Swell, Utah (abstract). *Geological Society of America Abstracts with Programs*. **18**:125.
- Krantz, R. W. 1988. Multiple fault sets and three-dimensional strain: Theory and application. *Journal of Structural Geology*. **10**:225-237.
- Krantz, R. W. 1989. Orthorhombic fault patterns: The odd axis model and slip vector orientations. *Tectonics*. **8**:483-495.
- Larroque, J. M. and Laurent, P. 1988. Evolution of the stress field pattern in the south of the Rhine Graben from the Eocene to the present. *Tectonophysics*. **148**:41-58.
- Laubach, S. E. 1989. Paleostress directions from the preferred orientation of closed microfractures (fluid-inclusion planes) in sandstone, East Texas basin, U.S.A. *Journal of Structural Geology*. **11**:603-611.
- Laurent, P., Bernard, P., Vasseur, G., and Etchecopar, A. 1981. Stress tensor determination from the study of e-twins in calcite: A linear programming method. *Tectonophysics*. **78**:651-660.
- Lee, Y. J. 1990. Slickenside petrography: Sense-of-slip indicators (abstract). *Geological Society of America Abstracts with Programs*. **22**:A182.

- Lespinasse, M. and Pêcher, A. 1986. Microfracturing and regional stress field: A study of the preferred orientations of fluid inclusion planes in a granite from the Massif Central, France. *Journal of Structural Geology*. **8**:169-180.
- Lisle, R. J. 1987. Principal stress orientations from faults: An additional constraint. *Annales Tectonicæ*. **1**:155-158.
- Lisle, R. J. 1988. ROMSA: A BASIC program for paleostress analysis using fault-striation data. *Computers & Geosciences*. **14**:255-259.
- Lisle, R. J. 1989. Paleostress analysis from sheared dike sets. *Geological Society of America Bulletin*. **101**:968-972.
- Mandal, N. and Charaborty, C. 1989. Fault motion and curved slickenlines: A theoretical analysis. *Journal of Structural Geology*. **11**:497-501.
- Mandelbrot, B. B. 1977. *Fractals: Form, Chance and Dimension*. W. H. Freeman: San Francisco, CA. 365 pages.
- Mandelbrot, B. B. 1983. *The Fractal Geometry of Nature*. W. H. Freeman: New York, NY. 468 pages.
- Mandl, G. 1987. Discontinuous fault zones. *Journal of Structural Geology*. **9**:105-110.
- Mandl, G. 1988. *Mechanics of Tectonic Faulting*. Elsevier: Amsterdam. 407 pages.
- Manning, A. H. and de Boer, J. Z. 1989. Deformation of Mesozoic dikes in New England. *Geology*. **17**:1016-1019.
- Marrett, R. and Allmendinger, R. W. 1990. Kinematic analysis of fault-slip data. *Journal of Structural Geology*. **12**:973-986.
- Marsden, J. E. and Tromba, A. J. 1981. *Vector Calculus*. W. H. Freeman: San Francisco, CA. 591 pages.
- Marshak, S. and Mitra, G. 1988. *Basic Methods of Structural Geology*. Prentice-Hall: Englewood Cliffs, NJ. 446 pages.
- McBride, J. H. Remarks on the derivation of the paleostress system from inferred faults on

- deep seismic reflection records. *Tectonophysics*. **168**:275-282.
- McKenzie, D. P. 1969. The relationship between fault plane solutions for earthquakes and the directions of the principal stresses. *Seismological Society of America Bulletin*. **59**:591-601.
- Means, W. D. 1976. *Stress and Strain*. Springer-Verlag: New York, NY. 339 pages.
- Means, W. D. 1987. A newly recognized type of slickenside striation. *Journal of Structural Geology*. **9**:585-590.
- Michael, A. J. 1984. Determination of stress from slip data: Faults and folds. *Journal of Geophysical Research*. **89**:11,517-11,526.
- Michael, A. J. 1987a. Use of focal mechanisms to determine stress: A control study. *Journal of Geophysical Research*. **92**:357-368.
- Michael, A. J. 1987b. Stress rotation during the Coalinga aftershock sequence. *Journal of Geophysical Research*. **92**:7963-7979.
- Muller, O. H. and Pollard, D. D. 1977. The stress state near Spanish Peaks, Colorado, determined from a dike pattern. *Pure and Applied Geophysics*. **115**:69-86.
- Norris, D. K. and Barron, K. 1969. Structural analysis of features on natural and artificial faults. In Baer, A. J. and Norris, D. K. 1969. *Research in Tectonics: Geological Survey of Canada Paper 68-52*. pages 136-157.
- Oertel, G. 1965. The mechanics of faulting in clay experiments. *Tectonophysics*. **2**:343-393.
- Okubo, P. G. and Aki, K. 1987. Fractal geometry in the San Andreas fault system. *Journal of Geophysical Research*. **92**:345-355.
- Paterson, M. S. 1958. Experimental deformation and faulting in Wombeyan marble. *Geological Society of America Bulletin*. **69**:465-476.
- Pêcher, A., Lespinasse, M., and Leroy, J. 1985. Relations between fluid inclusion trails and regional stress field: A tool for fluid chronology - An example of an intragranitic

- uranium ore deposit (northwest Massif Central, France). *Lithos*. **18**:229-237.
- Pershing, J. C. 1989. Modelling discontinuum rock mass behavior: A test of paleostress analysis (abstract). *Geological Society of America Abstracts with Programs*. **21**:A265.
- Petit, J. P., Proust, F., and Tapponnier, P. 1983. Critères de sens de mouvement sur les miroirs de failles en roches non calcaires. *Bulletin de la Société Géologique de France*. **25**:589-608.
- Petit, J. P. 1987. Criteria for the sense of movement on fault surfaces in brittle rocks. *Journal of Structural Geology*. **9**:597-608.
- Pfiffner, O. A. and Burkhard, M. 1987. Determination of paleo-stress axes orientations from fault, twin and earthquake data. *Annales Tectonicæ*. **1**:48-57.
- Plumb, R. A., Engelder, T., and Yale, D. 1984. Near surface *in situ* stress correlation with microcrack fabric within the New Hampshire granites. *Journal of Geophysical Research*. **89**:9350-9364.
- Plumb, R. A. and Cox, J. W. 1986. Stress directions in eastern North America determined to 4.5 km from borehole elongation measurements. *Journal of Geophysical Research*. **92**:4805-4816.
- Pollard, D. 1990. Personal communication with David Pollard of Stanford University.
- Power, W. L., Tullis, T. E., Brown, S. R., Boitnott, G. N., and Scholz, C. H. 1987. Roughness of natural fault surfaces. *Geophysical Research Letters*. **14**:29-32.
- Price, N. J. 1966. *Fault and Joint Development in Brittle and Semi-Brittle Rock*. Pergamon: Oxford. 176 pages.
- Ragan, D. M. 1985. *Structural Geology: An Introduction to Geometrical Techniques*. 3rd edition. John Wiley & Sons: New York, NY. 393 pages.
- Reches, Z. and Dieterich, J. H. 1983. Faulting of rocks in three-dimensional strain fields, I. Failure of rocks in polyaxial servo-controlled experiments. *Tectonophysics*. **95**:111-132.

- Reches, Z. 1987. Determination of the tectonic stress tensor from slip along faults that obey the Coulomb yield condition. *Tectonics*. **6**:849-861.
- Rice, A. H. N. 1986. Structures associated with superimposed inhomogeneous shearing of basic dykes from Finnmark, Norway. *Tectonophysics*. **128**:61-75.
- Riecker, R. E. 1965. Fault plane features: An alternative explanation. *Journal of Sedimentary Petrology*. **35**:746-748.
- Rod, E. 1966. A discussion of the paper: "Fault plane features: An alternate explanation" by R. E. Riecker. *Journal of Sedimentary Petrology*. **36**:1163-1165.
- Rowland, S. M. 1986. *Structural Analysis and Synthesis: A Laboratory Course in Structural Geology*. Blackwell Scientific: Palo Alto, CA. 208 pages.
- Sassi, W. and Carey-Gailhardis, E. 1987. Interprétation mécanique de glissement sur les failles: Introduction d'un critère de frottement. *Annales Tectonicae*. **1**:139-154.
- Schied, F. J. 1968. *Schaum's Outline of Theory and Problems of Numerical Analysis*. McGraw-Hill: New York, NY. 422 pages.
- Schimmrich, S. H. 1990. A Pascal program for determining slip-vector orientations on fault planes. *Journal of Geological Education*. **38**:284-287.
- Scholz, C. H. and Aviles, C. A. 1986. The fractal geometry of faults and faulting. In Das, S., Boatwright, J., and Scholz, C. H. 1986. *Earthquake Source Mechanics*. American Geophysical Union: Washington, D. C. Pages 147-155.
- Scholz, C. H. 1990. *The Mechanics of Earthquakes and Faulting*. Cambridge University Press: Cambridge. 439 pages.
- Scott, W. H., Hansen, E., and Twiss, R. J. 1965. Stress analysis of quartz deformation lamellae in a minor fold. *American Journal of Science*. **263**:729-746.
- Segall, P. and Pollard, D. D. 1980. Mechanics of discontinuous faults. *Journal of Geophysical Research*. **85**:4337-4350.
- Shepard, T. J. 1990. Geological link between fluid inclusions, dilatant microcracks, and

- paleostress field. *Journal of Geophysical Research*. **95**:11,115-11,120.
- Spang, J. H. 1972. Numerical method for dynamic analysis of calcite twin lamellae. *Geological Society of America Bulletin*. **83**:467-472.
- Spang, J. H. and Van Der Lee, J. 1975. Numerical dynamic analysis of quartz deformation lamellae and calcite and dolomite twin lamellae. *Geological Society of America Bulletin*. **86**:1266-1272.
- Spencer, E. W. 1988. *Introduction to the Structure of the Earth*. 3rd edition. McGraw-Hill: New York, NY. 551 pages.
- Suppe, J. 1985. *Principles of Structural Geology*. Prentice-Hall: Englewood Cliffs, NJ. 537 pages.
- Suter, M. 1986. Orientation data on the state of stress in northeastern Mexico as inferred from stress-induced borehole elongations. *Journal of Geophysical Research*. **92**:2617-2626.
- Tchalenko, J. S. 1970. Similarity between shear zones of different magnitude. *Geological Society of America Bulletin*. **81**:1625-1640.
- Thorpe, W. 1969. Reduction v. organicism. *New Scientist*. **43**:635-638.
- Tjia, H. D. 1964. Slickensides and fault movements. *Geological Society of America Bulletin*. **75**:683-686.
- Tjia, H. D. 1967. Sense of fault displacements. *Geologie en Mijnbouw*. **46**:392-396.
- Tjia, H. D. 1972. Fault movement, reoriented stress field and subsidiary structures. *Pacific Geology*. **5**:49-70.
- Twiss, R. J. and Gefell, M. J. 1990. Curved slickenfibers: A new brittle shear sense indicator with application to a sheared serpentinite. *Journal of Structural Geology*. **12**:471-481.
- Umhoefer, P. J. 1990. Fault-striation analysis near the NW Yalakom fault, Tyaughton basin, British Columbia: Strike slip structures overprinting mid-Cretaceous thrust structures.

- Geological Society of America Abstracts with Programs*. **22**:A95.
- Vasseur, G., Etchecopar, A., and Philip, H. 1983. Stress state inferred from multiple focal mechanisms. *Annales Geophysicæ*. **1**:291-298.
- Wahlstrom, R. 1987. Focal mechanisms of earthquakes in southern Quebec, southeastern Ontario, and northeastern New York with implications for regional seismotectonics and stress field characteristics. *Seismological Society of America*. **77**:891-924.
- Wallace, R. E. 1951. Geometry of shearing stress and relation to faulting. *Journal of Geology*. **59**:118-130.
- Wallace, R. E. 1973. Surface fracture patterns along the San Andreas fault. In Kovach, R. and Nur, A. 1973. *Proceedings of the Conference on Tectonic Problems of the San Andreas Fault System: Special Publication 13*. Stanford University Press: Palo Alto, CA. pages 248-250.
- Wallbrecher, E. and Fritz, H. 1989. Quantitative evaluation of the shape factor and the orientation of a paleo-stress ellipsoid from the distribution of slickenside striations. *Annales Tectonicæ*. **3**:110-122.
- White, S. H. 1979. Difficulties associated with paleo-stress estimates. *Bulletin de Minéralogie*. **102**:210-215.
- Woodcock, N. H. 1976. The accuracy of structural field measurements. *Journal of Geology*. **84**:350-355.
- Zoback, M. D. and Zoback, M. L. 1980. State of stress in the conterminous United States. *Journal of Geophysical Research*. **85**:6113-6156.